ASSESSMENT OF THE EFFECTS OF GROUND MOTION MODIFICATION ON GROUND MOTIONS AND SEISMIC RESPONSE OF GEOTECHNICAL SYSTEMS

by

Clinton Pierce Carlson

A dissertation submitted in partial fulfillment
of the requirements for the degree of
Doctor of Philosophy
(Civil Engineering)
in The University of Michigan
2014

Doctoral Committee:

Associate Professor Dimitrios P. Zekkos, Chair
Assistant Professor Adda G. Athanasopoulos-Zekkos
Associate Professor Edward L. Ionides
Associate Professor Jason P. McCormick

DEDICATION

This thesis is dedicated to all who have helped me along the way including my friends, fellow students, professors, family, but most importantly, my parents, who inspired me from a young age to push myself to do great things.

ACKNOWLEDGEMENTS

First of all, I would like to thank my parents. They have raised me to be a very self-motivated individual (for the most part). However, I always know that if I fail at something they will be there to pick me back up and support me through my next endeavor. I love you mom and dad.

To my sister Corissa, thank you for the words of encouragement during my research. I can now give you advice as you follow in my footsteps and earn your PhD. To my brothers Kris and Rejean, thank you for the guidance in life. To my grandparents, aunts, uncles, cousins, nephews, nieces, etc., thank you for the encouragement during my studies and "making buildings so they don't fall down during earthquakes." I don't know if I will make as much money as all of you seem to think I will, but I guess I can try. I love my family and I'm glad they are in my life. I also want to thank my friends. Even the small things you did like calling me up at 1 in the morning, visiting me from out-of-town, or sending me a text to ask, "r u done yet? :)," was greatly appreciated as it took my mind off work.

The other person that I owe a lot to in completing this PhD is Prof. Dimitrios Zekkos. I can say without a doubt he is the hardest working person I've met. Through his guidance and dedication to my success and the success of my research project, I matured from a coursework-focused undergraduate student into a critical-thinking graduate student. He stuck with me through some very unproductive semesters and terrible presentations to produce the following thesis. I'm not going to say that I love Prof. Zekkos, because that would be weird; however, I have a lot of respect for Prof. Zekkos because of his *insane* work ethic and dedication to his students.

I would also like to thank the other professors on my committee. To Prof. Adda Zekkos and Prof. Jason McCormick, thank you for being available to meet to discuss parts of my research and provide valuable input. To Prof. Edward Ionides, thank you for being willing to meet with me after I did not contact you for about two years and greatly helping me with the development of the regression equations.

I've earned my bachelor's, master's, and doctoral degrees from the University of Michigan, so I would also like to thank the other professors that I have interacted with during my time here. Prof. Jerry Lynch, thank you for acting like an advisor to me during my undergraduate degree and encouraging me to pursue a graduate degree. I also want to thank the other professors in structural and geotechnical engineering for the help in the courses I took with you. I was absolutely terrified to go to some of your office hours, but when I did, you were willing to help me understand the problem and the concepts behind the problem. I also can't forget to thank the lab technicians that helped aid me during my time as a graduate student instructor, specifically Bob Fischer.

I'm very glad I did my PhD at the University of Michigan because there is a great sense of community among the graduate students. It was very helpful knowing that I could talk to other graduate students about any problems I was having in classes, with research, or with professors. It was also a lot of fun spending time with everybody; from barbecues to fantasy football. I would like to thank Jon and Will for directly helping me with some analysis and proofreading for my thesis. I would like to thank Andhika and Fei for being helpful group members. To all the current and former graduate students in the Civil Engineering Department, thanks for just being an awesome group of people to be around.

Finally, I must thank the agencies that helped fund this research. This research was conducted with partial funding from the Earthquake Engineering Research Institute (EERI) and the Federal Emergency Management Agency (FEMA) through the EERI/FEMA NEHRP Graduate Fellowship and the United States Society on Dams (USSD) through the USSD 2011 Scholarship. I would also like to thank the University of Michigan. I'm glad that I was able to earn all three of my degrees at this prestigious university. Now that I'm leaving, maybe the football team will improve.

So, thank you to those of you who have helped me along the way in any capacity and enjoy reading (browsing) my thesis.

TABLE OF CONTENTS

LIST OF TABLES

TABLE

LIST OF FIGURES

FIGURE

LIST OF APPENDICES

APPENDIX

ABSTRACT

Dynamic analyses are typically required as part of the seismic design of critical infrastructure. Recorded ground motions from earthquake events with characteristics that are consistent to the design earthquake event are typically selected and used as input to perform dynamic analyses. However, for certain regions or design earthquakes, limited appropriate recorded ground motions are available for selection. An alternative approach is ground motion modification, which is executed either with time or frequency domain techniques. Ground motion modification alters the intensity and frequency content of the acceleration time history of a seed ground motion so that its acceleration response spectrum matches a target response spectrum. Despite this benefit, ground motion modification has been criticized for producing ground motions with unrealistic amounts of energy or unrealistic time histories. However, there is limited research on the effects of ground motion modification on the seed motion to support or discourage its use in practice.

This research investigates the impact of time and frequency domain modification techniques on ground motion characteristics and time histories and on the response metrics considered in subsequent site response analyses. The effects of modification on three sets of approximately 100 motions selected for three different earthquake scenarios and for each scenario matched to five alternative target spectra are examined along with the effects of modification on site response analyses when these modified motions are used as input to two sites.

One of the major findings of this research is that the effects of time domain and frequency domain modification on the characteristics of the seed motion are strongly correlated to the mismatch between the acceleration response spectrum of the original motion and the target response spectrum. This finding allows the engineer to predict the ground motion characteristics of the resulting modified ground motion prior to performing spectral matching and use that information to select the most appropriate ground motions and technique for modification. The

effects of modification on the responses for geotechnical dynamic analyses appear to be related to the impact of modification on the ground motion characteristics.

CHAPTER 1
Introduction

1.1 Background and Motivation

In the seismic design of critical infrastructure, dynamic analyses are conducted to quantify the response of geotechnical and structural systems when subjected to a design earthquake event (CEN 2005, ASCE 2010, NIST 2011, FEMA 2005, 2009, 2012). For these analyses, three (e.g., FEMA 2005, NIST 2011) to fourteen (e.g., FEMA 2012) ground motions recorded from previous earthquake events that are consistent with the design earthquake scenario (i.e., magnitude, source-to-site distance, spectral shape, etc.) are required by the design codes. Typically, the ground motions must be selected such that their average acceleration response spectrum is equal to or greater than a target design response spectrum. Given the impact the motions have on the results of the response analyses, the selection of appropriate ground motions is a critical step in the design process (Bray and Travasarou 2007, Haselton 2009, Rathje et al. 2010, Athanasopoulos-Zekkos and Saadi 2012).

In regions where few or no recorded ground motions consistent with the design scenario are available, the selection process becomes more problematic, usually requiring the selection criteria to be relaxed (Bommer and Acevedo 2004). Additionally, running time history response analyses can be computationally intensive, so it is desirable to use a smaller suite of ground motions that have response spectra that are similar in shape and amplitude to the target spectrum. Other codes (e.g., ASCE 2005, AASHTO 2010) require that motions used for the seismic response analyses are simulated to match the target response spectrum. For all of these issues, ground motion modification presents a viable alternative.

Ground motion modification, or spectral matching, is used to alter the intensity and frequency content of a seed acceleration time history from a recorded earthquake until its acceleration response spectrum matches a target design response spectrum. For ground motion modification, the seed motion is modified using time domain, frequency domain, or other

techniques. It has also been suggested that the selection of the original set of motions becomes less critical when using ground motion modification since the response spectra of the motions are matched to the target response spectrum (Hancock et al. 2008). For a suite of ground motions, spectral matching produces a response spectrum for a modified ground motion that is nearly identical to the target spectrum and has limited variability, reducing the number of ground motions required to perform response history analyses (Hancock et al. 2008, Bazzuro and Luco 2006). Also, it is almost necessary to use ground motion modification for three-dimensional dynamic analyses as there are essentially no earthquake recordings with three components of motion (i.e., two perpendicular horizontal components and a vertical component of motion) that have response spectra consistent with target spectra developed for each direction of motion. Other benefits of ground motion modification are discussed in Zekkos et al. (2012).

Despite its use in numerous projects (e.g., Ostadan et al. 1996, Hancock and Bommer 2007, Grant and Diaferia 2013), ground motion modification is still criticized for producing unrealistic motions. Matching a ground motion to a uniform hazard spectrum, which has contributions from multiple earthquake events, may cause the motion to produce an overly conservative system response. For example, Naeim and Lew (1995) observed that the frequency domain modification technique introduced unrealistic amounts of energy to the seed ground motion during the modification process, although other studies (e.g., Zekkos et al. 2012) have shown this is not always the case. Ground motion modification also matches the response spectra of motions to a smooth response spectrum, which is not typical of recorded ground motions. For these reasons, ground motion modification is commonly avoided in practice. Engineers that do utilize ground motion modification are typically biased towards one technique (e.g., time domain or frequency domain) and completely neglect using other techniques. However, the major issue with spectral matching is that its quantitative impact on the stationary (e.g., peak ground displacement) and non-stationary (e.g., displacement time history) characteristics of the seed ground motions and the subsequent seismic response analyses is largely unknown. Given the unknown quantitative effects of modification and the importance of input ground motions on the results of seismic analyses, it is necessary to evaluate the impact of ground motion modification on the original ground motions and the responses for subsequent dynamic analyses.

1.2 Scope

The goal of this research is to systematically investigate the impact of modification on the characteristics and time histories of the seed ground motion and the geotechnical dynamic response analyses for which the ground motions are used in order to provide a quantitative assessment of the impacts of spectral matching. This study examines the effects of time and frequency domain modification techniques on three different aspects of the seed ground motion.

A computer program was developed to aid this research. The computer program performs time and frequency domain modification to match a suite of scaled ground motions to a target response spectrum. Ground motion characteristics, time histories, and response spectra for the scaled and modified motions are calculated by the program and summarized in a one-page output file.

The first portion of this research quantifies the impact of modification on the ground motion characteristics of the seed motion. Ground motion characteristics (e.g., peak ground velocity) are commonly used in empirical equations to predict the seismic responses of geotechnical systems (e.g., Saygili and Rathje 2008, Athanasopoulos-Zekkos and Saadi 2012) in lieu of performing response history analyses; therefore, the impact of modification on these characteristics must be understood. Based on observations in earlier studies on the effects of ground motion modification (Carlson et al. 2014a), it is hypothesized that the mismatch between the response spectrum of the recorded ground motion and the target spectrum (i.e., spectral mismatch) has a significant impact on the effects of ground motion modification. For three very different earthquake scenarios (scenario I: shallow crustal event; scenario II: subduction zone event; scenario III: stable continental event), approximately one hundred ground motions were selected and scaled using three different factors and subsequently matched to five target spectra with varying intensities and frequency contents to examine the impact of modification and spectral mismatch on the ground motion characteristics of the seed ground motions.

The effects of ground motion modification on the time histories of the seed ground motions, as quantified by the goodness-of-fit between the scaled and modified time histories, are also examined in this study. Since the time histories are used as input in the response history analyses, it is important to understand how they are impacted by ground motion modification. Threshold values of goodness-of-fit are also established in this portion of the research to identify

modified motions with likely acceptable, possibly acceptable, and likely unacceptable time histories. This portion of the research assesses the impact of spectral mismatch on modification on the goodness-of-fit values using spectral mismatch. The relationship between the goodness-of-fit and modified-to-scaled ground motion characteristic ratios is examined for the different time histories in an attempt to establish goodness-of-fit limits for acceptable ground motions. Quantitative threshold values of goodness-of-fit between modified and scaled time histories are also established based on a visual examination of the scaled and modified time histories to identify acceptable modified motions.

Finally, the effects of modification on the responses of geotechnical dynamic analyses for two different soil profiles are examined for scenarios I and II. This assessment investigates whether modification systematically introduces bias in the responses for geotechnical dynamic analyses relative to the responses caused by scaled motions and if the ground motions modified by different modification techniques leads to different responses. Again, the impact of spectral mismatch on the effects of ground motion modification on the responses for geotechnical dynamic analyses is examined.

1.3 Outline of Thesis

This thesis is divided into seven chapters. **Chapter 1** presents the motivation for using ground motion modification, the motivation and scope for this research, and the organization of this thesis.

Chapter 2 reviews the process for selecting an appropriate set of ground motions and identifies alternatives for the selection process when few or no recorded ground motions are available, particularly ground motion modification. The methodology behind time domain and frequency domain modification techniques and programs that use these and other techniques are discussed. Finally, **Chapter 2** presents research that has been conducted to study the effects of modification on ground motion characteristics and responses for subsequent dynamic analyses to further show the need for the work presented in this thesis.

Details for a computer program developed as part of this study are provided in **Chapter 3**. The procedures used by the program to calculate ground motion characteristics, time histories, response spectra, and spectral mismatch and goodness-of-fit metrics are presented in this chapter.

Chapter 3 also discusses the steps used for the time domain and frequency domain modification subroutines within the program and provides the values used for input parameters in these subroutines. A one-page output file produced by the computer program is also shown and discussed. The end of **Chapter 3** discusses improvements that must be made to the computer program before it could potentially be made available for public use.

Chapter 4 presents the results of the study on the effects of modification on the ground motion characteristics. The process of developing target acceleration response spectra and selecting motions for three earthquake scenarios used in this study is provided at the beginning of **Chapter 4**. To investigate the impact of spectral mismatch on the effects of ground motion modification on the ground motion characteristics, ratios of the characteristics for the modified motions to those of the scaled ground motions are calculated and plotted versus spectral mismatch metrics for scenarios I and II in **Chapter 4**. Regression equations are developed for the relationships between the modified-to-scaled ratios and spectral mismatch for various ground motion characteristics. The resulting modified-to-scaled ground motion characteristic ratios for the motions in scenario III are then used to validate the general applicability of these regression equations. **Chapter 4** concludes with a summary of the major findings for the effects of modification on the ground motion characteristics and recommendations based on these findings.

Chapter 5 presents the results of the study on the effects of modification on the goodness-of-fit between the time histories of the scaled and modified motions. The goodness-of-fit values for the time histories are plotted against spectral mismatch and the modified-to-scaled ground motion characteristic ratios. Regression equations are developed for the relationships between the goodness-of-fit and the modified-to-scaled ground motion characteristic ratios using scenarios I and II. The results of the third scenario are compared to these regression equations to check their general applicability. A visual examination of acceleration, velocity, and displacement time histories of motions in scenarios I and II is also performed in **Chapter 5** to develop threshold values for the goodness-of-fit metric that identify modified motions that are likely acceptable, possibly acceptable, and likely unacceptable. Major findings for the effects of modification on the time histories of the ground motions and recommendations based on this study are presented at the end of **Chapter 5**.

Results for the impact of ground motion modification on the geotechnical dynamic analyses for two sites are presented in **Chapter 6**. The properties of the two sites developed for

the geotechnical seismic response analyses and the programs used to perform these analyses are presented at the beginning of this chapter. For both sites, median responses produced by the sets of scaled and modified motions from scenarios I and II are compared along with the modified-to-scaled ratios of these medians. Median cyclic stress ratio, maximum horizontal acceleration, and maximum shear strain profiles are normalized by the corresponding responses at the base of the soil profiles to examine how the scaled and modified motions are impacted by site effects. The ratios of the seismic responses produced by the modified motions to those produced by the scaled motions are then plotted versus the spectral mismatch in **Chapter 6** to study how the initial mismatch affects the responses produced by the modified ground motions. The end of **Chapter 6** presents major findings and recommendations on the effects of modification on the responses for geotechnical dynamic analyses.

Chapter 7 summarizes all of the findings from this study and provides recommendations for use in earthquake engineering practice. Future directions for this research topic are also presented in **Chapter 7**.

CHAPTER 2
Ground Motion Selection and Modification

2.1 Ground Motion Selection

For critical infrastructure or infrastructure in highly seismic regions, codes typically require dynamic analyses be performed using input time histories. Eurocode 8 (CEN 2005) requires a set of at least seven input time histories are used if the expected action of the earthquake event is modeled using input time histories. For dams, the Federal Emergency Management Agency (FEMA; 2005) requires three or more input time histories (more should be used for nonlinear analyses) that have an average response spectrum that is consistent with the target spectrum and individual response spectra that do not greatly exceed the target spectrum are used if dynamic analyses are necessary. These input time histories should be selected from previously recorded earthquake events with similar moment magnitudes, source-to-site distances, and fault types to the design scenario according to FEMA (2005). The American Society of Civil Engineers (ASCE; 2010) requires a suite of at least three ground motions with response spectra that are compatible with the target spectrum are used in linear and nonlinear response history analyses. Response history analyses are required by ASCE for buildings that are very tall or have certain irregularities for seismic design categories D, E, or F (see Table 12.6-1 in ASCE 2010). Seven to eleven pairs of ground motions are required for two-dimensional nonlinear response history analyses according to the Applied Technology Council (ATC; FEMA 2012). The ATC specifies that the pairs of ground motions are selected such that their average response spectrum is greater than the target spectrum for periods between 0.2 and 2 times the natural period of system (FEMA 2012). Consideration should also be given to the spectral shape of the ground motion and moment magnitude and source-to-site distance of the earthquake event in the selection process (FEMA 2012). The National Earthquake Hazard Reduction Program (NEHRP; NIST 2011) provides a summary of the selection process for input ground motions in response history analyses specified by current codes. NEHRP also points out the necessity to perform

nonlinear response history analyses for new infrastructure equipped with seismic isolators, designing seismic upgrades for existing infrastructure, designing nonconforming frames in new buildings, and assessing seismic performance of infrastructure (NIST 2011).

As specified in the codes, ground motions are typically selected from previously recorded earthquake events with properties consistent to the design scenario. The choice of what parameters (e.g., moment magnitude) to base this selection on and the range of acceptable values for those parameters is a critical part of the selection process (Bommer and Acevedo 2004). Additionally, the selection of motions can have a significant impact on the responses of dynamic analyses (Bray and Travasarou 2007, Haselton 2009, Rathje et al. 2010, Athanasopoulos-Zekkos and Saadi 2012). Recently, the selection of "appropriate" ground motions for the design scenario has been a major focus in the earthquake engineering community. Bommer and Acevedo (2004) provided comprehensive guidelines on the selection process for earthquake ground motions recorded from previous events including key parameters to consider in the selection process. Watson-Lamprey and Abrahamson (2006) showed that selecting motions based on parameters such as moment magnitude and source-to-site distance may not be critical for predicting Newmark-type slope displacements if ground motion characteristics such as Arias intensity (Arias 1970) and peak ground velocity are considered in the selection process. Haselton (2009) observed that motions selected from a similar magnitude event that had spectral shapes consistent to the conditional mean spectrum (Baker 2011) accurately predicted point-of-comparison median drift responses for four buildings. Catalán et al. (2010) observed it was important that the selected motions had response spectra consistent with the target spectrum at the natural period of the structural system for regions of low to moderate seismicity. A more comprehensive review of studies that have investigated the selection process for a suitable set of ground motions is provided by Katsanos et al. (2010). Overall, it is recommended that ground motions are selected from earthquake events with very similar moment magnitudes to the design scenario and that their average response spectrum is consistent with the target spectrum. Source-to-site distances, fault types, and ground motion characteristics are used as secondary considerations in the selection process when several ground motions are available for selection.

Another major consideration in the selection process is the number of motions required. Although codes require three to fourteen ground motions, studies by Shome et al. (1998) and Hancock et al. (2008) observe that significantly more ground motions may be required

depending on the response parameter of interest. For example, both Shome et al. (1998) and Hancock et al. (2008) observe that at least 50 motions are required to accurately predict the hysteretic energy absorbed by the structural system (i.e., within 10%) when ground motions are selected from previously recorded events. These studies also observe that the number of motions in the selection can generally be reduced if the ground motions have spectral shapes consistent with the shape of the target spectrum. Several programs have been developed (e.g., Kottke and Rathje 2008, Jayaram et al. 2011, Wang 2011) to aid the engineer in the selection of an optimal suite of ground motions that have spectral shapes consistent with the target spectrum. These programs also allow a desired variability to be matched by the selection of motions.

Despite the work done to assess how many and which ground motions to select, there are still design scenarios where limited ground motion recordings are available. This includes regions with limited seismic activity (e.g., Eastern United States) or regions that are anticipating much larger events than those previously recorded (e.g., Pacific Northwest United States). For such scenarios, four alternatives exist:

- Relax the criteria used in the selection process: The limits placed on parameters such as moment magnitude are relaxed so that motions from a larger pool of events are available for selection. However, the parameters that are relaxed and the amount of relaxation must be selected carefully (Bommer and Acevedo 2004).
- Generate synthetic ground motions that match the target spectrum: Mathematical procedures, including white noise functions (e.g., Housner and Jennings 1964, Sabetta and Pugliese 1996) and Green's function (e.g., Hartzell 1978, Joyner and Boore 1986), are used to produce synthetic ground motions that have response spectra identical to the target spectrum. SIMQKE (Gasparini and Vanmarcke 1979) is a commonly used program for the generation of synthetic ground motions. A more extensive list of programs that utilize mathematical procedures to generate synthetic ground motions can be found in Douglas and Aochi (2008). Use of synthetic ground motions in practice is limited due to the significant scientific and modeling uncertainties associated with the development of such time histories. Synthetic ground motions have also been accused of introducing many cycles with high energy content in the acceleration time history that are not representative of real ground motions (Bommer and Acevedo 2004). Synthetic ground motions are not a focus of this research.

- Scale ground motions to be more consistent with the target spectrum: A constant scaling factor is applied to the acceleration time history and response spectrum of the seed motion to alter its intensity. A ground motion can be scaled so that its response spectrum matches the target peak ground acceleration (Al Atik and Abrahamson 2010) or the target spectrum at the fundamental period of the system (Shome et al. 1998, Baker 2011) or to minimize the mismatch between the response spectrum of the scaled motion and the target spectrum (Mazzoni et al. 2012). Scaling is commonly used to produce a suite of ground motions from previously recorded earthquake events with an average response spectrum that is equal to or greater than the target spectrum for a period(s) of interest. Algorithms have been developed to select both an appropriate set of motions and appropriate scaling factors to apply to the selected motions in order to match or exceed the target spectrum (Kottke and Rathje 2008, Jayaram et al. 2011, Wang 2011). However, scaling the ground motion does not alter its spectral shape which may not be consistent with the target spectrum. Also, several scaled ground motions may be required to produce an average response spectrum that is approximately equal to the target spectrum. More rigorous modification of not only the intensity of the motion, but also its frequency content, must be used in such cases to alter the response spectra of previously recorded ground motions and match these spectra to the target spectrum.
- Modify existing ground motions to match a target spectrum: Ground motion modification, or spectral matching, can be used to alter the intensity and frequency content of previously recorded motions so that their response spectra match the target response spectrum. Since ground motion modification starts with a previously recorded acceleration time history, it is more likely to maintain realistic nonstationary characteristics (e.g., displacement time histories) than synthetic ground motions. **Figure 2.1** compares the original and modified displacement time history for an example ground motion to the displacement time history of a synthetic motion generated for the same earthquake scenario. Ground motion modification can be performed using time domain (e.g., Al Atik and Abrahamson 2010), frequency domain (e.g., Rizzo et al. 1975), or other (Suárez and Montejo 2005) modification techniques. The response spectra of selected ground motions can also be spectrally matched to plus and minus standard deviation target spectra to capture the variability of the design

scenario, but that process is not examined in this study. The process of ground motion modification is described in more detail in the following section.

2.2 Ground Motion Modification

2.2.1 Frequency Domain Modification

Frequency domain (FD) modification was proposed by Rizzo et al. (1975) and later used by Silva and Lee (1987) as part of the program RASCAL (RASCAL also uses random vibration theory and is not purely a FD modification program). FD modification applies scaling factors to the Fourier amplitude spectrum of a ground motion, thus altering its frequency content and intensity so that the acceleration response spectrum matches the target spectrum. Other FD modification algorithms exist (e.g., Preumont 1984, Karabalis et al. 2000), but the algorithm proposed by Rizzo et al. (1975) is examined in this study.

Figure 2.2 shows a diagram of the process used to perform FD modification. In the FD modification process, the acceleration time history of the seed motion is converted to the frequency domain by using a fast Fourier transform (FFT) to calculate a Fourier amplitude spectrum (*FAS*). Correction factors equal to the ratio of the target spectral acceleration to the spectral acceleration of the seed motion for different periods ($Sa_{tar}(T_i)$ / $Sa(T_i)$) are applied to the *FAS* of the seed motion at the corresponding frequencies to produce a modified *FAS*. The modified *FAS* is then transformed back into the time domain using an inverse FFT to produce a modified acceleration time history. This process is repeated until the response spectrum of the modified motion matches the target spectrum within a specified tolerance for all periods of interest or a maximum number of iterations is reached. In practice, approximately 100 periods that are evenly distributed logarithmically should be matched over the period range of interest.

Applying correction factors to the *FAS* affects the entire acceleration time history and response spectrum (Lilhanand and Tseng 1988). This may result in an unrealistic increase in the energy content of the seed ground motion during FD modification (Naeim and Lew 1995). Another effect of modifying the seed ground motion in the FD is the introduction of residual values in the velocity and displacement time histories. However, subsequent algorithms have been developed to prevent residual displacements from developing in the time histories during the FD modification process (e.g., Shahbazian and Pezeshk 2010).

2.2.2 Time Domain Modification

The time domain (TD) modification technique was introduced by Kaul (1978) and later extended to multiple damping values by Lilhanand and Tseng (1987, 1988). This method adds wavelets to the acceleration time history of the seed motion at targeted periods. This provides an improvement on the FD modification technique in that the entire time history is not affected during the TD modification process. The wavelets are calculated using the mismatch between the response spectrum of the seed motion and the target spectrum at periods of interest. RSPMatch was developed by Abrahamson (1992) to perform TD modification, but the wavelets used commonly introduced residual velocities and displacements in the time histories. RSPMatch05 (Hancock et al. 2006) and RSPMatch09 (Al Atik and Abrahamson 2010) subsequently improved the form of the adjustment wavelets in RSPMatch in order to prevent residual velocities and displacements from developing in the time histories during the TD modification process. The TD modification process used by RSPMatch09 is examined in this study; however, other algorithms have been proposed to perform spectral matching using TD modification (e.g., Spears 2008, Mazzoni et al. 2012, Gao et al. 2013).

This paragraph provides a summary of the mathematical procedure in RSPMatch09. More information on the mathematical procedure for TD modification can be found in Lilhanand and Tseng (1988) and Al Atik and Abrahamson (2010). A correction acceleration time history ($\delta a(t)$) and the adjustment to the response spectrum (δSa_i) are calculated using **Equations 2.1** and **2.2** (Al Atik and Abrahamson 2010), respectively.

$$\delta a(t) = \sum_{j=1}^{n_s} b_j f_j(t) \tag{2.1}$$

$$\delta Sa_i = \int_0^{\infty} \delta a(\tau) h_i(t_i - \tau) d\tau \tag{2.2}$$

Equations 2.1 and **2.2** are combined to form **Equation 2.3**.

$$\delta Sa_i = \sum_{j=1}^{N} b_j \int_0^{\infty} f_j(\tau) h_i(t_i - \tau) d\tau \tag{2.3}$$

$f_j(t)$ represents the time history adjustment wavelet; $h_i(t)$ represents the impulse response function for a given circular frequency (ω_i) and damping (λ_i); b_j represents the amplitudes of the adjustment wavelets; and n_s represents the number of spectral values matched. **Equation 2.4** (Al Atik and Abrahamson 2010) provides the equation for $h_i(t)$.

$$h_i(t) = \frac{-\omega_i}{\sqrt{1-\lambda_i^2}} \exp(-\omega_i \lambda_i t) \sin\left(\omega_i \sqrt{1-\lambda_i^2}\, t\right) \quad \textbf{(2.4)}$$

The $f_j(t)$ wavelets have an improved tapered cosine wavelet form, as shown in **Equation 2.5** (Al Atik and Abrahamson 2010), which integrates to zero for the velocity and displacement time histories, thus preventing the introduction of residual velocities and displacements in the time histories of the TD-modified motions.

$$f_j(t) = \cos\left[\omega_j \sqrt{1-\lambda_j^2}\left(t - t_j + \Delta t_j\right)\right] \exp\left[-\left(\frac{t - t_j + \Delta t_j}{\alpha_j}\right)\right] \quad \textbf{(2.5)}$$

The acceleration, velocity, and displacement time histories of the improved tapered cosine wavelet are shown in **Figure 2.3**. α_j represents an adjustment factor to the duration (**Equation 2.6**) that is used to ensure $f_j(t)$ has a smooth taper (Al Atik and Abrahamson 2010) and Δt_j represents the difference between the peak response time, t_j, and a reference time in the wavelet.

$$\alpha(\mathit{frequency}) = 1.178\, \mathit{frequency}^{-0.93} \quad \textbf{(2.6)}$$

The contribution of the adjustment wavelets added for other frequency and damping values on the amplitude of the adjustment wavelet for frequency and damping i can be represented by c_{ij} (**Equation 2.7**) (Al Atik and Abrahamson 2010).

$$c_{ij} = \int_0^{t_i} f_j(\tau) h_i(t_i - \tau)\, d\tau \quad \textbf{(2.7)}$$

The difference between the target spectrum and response spectrum of the seed ground motion for the periods that are matched is set to the vector δ**Sa** then the vector of amplitudes for the adjustment wavelets, **b**, is calculated using **Equation 2.8**.

$$\mathbf{b} = \mathbf{C}^{-1} \delta \mathbf{Sa} \quad \textbf{(2.8)}$$

C is a square matrix that contains the values for all c_{ij}. **b** is then used in **Equation 2.1** to calculate $\delta a(t)$. The modified acceleration time history is calculated by adding $\delta a(t)$ to the acceleration time history of the seed motion.

The improved tapered cosine wavelet integrates to zero velocity and displacement provided the peak response of the system for ω_i and λ_i does not occur near the beginning of the time history (Al Atik and Abrahamson 2010). The minimum time (t_{min}) at which the peak response can occur and still have no permanent velocity or displacement in the adjustment wavelet is calculated using **Equation 2.9** (Al Atik and Abrahamson 2010).

$$t_{\min} = 3.9223\, frequency_i^{-0.845} \quad (\mathbf{2.9})$$

If necessary, the beginning of the acceleration time history of the seed motion is padded with zeros in order to have the peak value of response occur at a time larger than t_{min}.

A diagram of the TD modification process is shown in **Figure 2.4**. TD modification is performed in multiple passes to match the target spectrum for an increasingly larger range of periods. The difference between the response spectrum of the seed motion and the target spectrum is calculated for the range of periods matched. The differences for different groups of spectral periods are used to calculate time history adjustment wavelets that are then added to the original acceleration time history. These wavelets are added to the acceleration time history over multiple iterations to produce a TD-modified acceleration time history with a response spectrum that matches the target spectrum in the specified period range. TD modification is repeated for an increasingly larger range of periods until the response spectrum of the modified motion matches the target spectrum within a specified tolerance for all periods of interest or the specified number of passes is reached. Approximately 100 periods that are evenly distributed logarithmically are matched during the TD modification process.

2.2.3 Other Modification Techniques

A more recent modification technique, the continuous wavelet transform method, was proposed by Mukherjee and Gupta (2002) and Suárez and Montejo (2005). This modification technique decomposes the acceleration time history of a seed motion into several time histories and scales these individual time histories until the response spectrum of the modified motion matches the target spectrum. Although the continuous wavelet transform method achieves matching and approximately maintains the duration of the seed motion, it is observed to significantly alter the acceleration time history (see Fig. 15 in Suárez and Montejo (2005)) (Hancock et al. 2006). Additional algorithms use the superposition of earthquake recordings and random processes (e.g., Cacciola and Deodatis 2011) or artificial neural network methods (e.g., Lin and Ghaboussi 2001) to perform ground motion modification. This study does not examine the effects of modification for these techniques.

2.3 Previous Research on the Effects of Ground Motion Modification

The suitability of modified ground motions for use in dynamic analyses for structural systems has recently been investigated. With conflicting results as to whether ground motion modification introduced bias in the responses of the structural dynamic analyses. Bazzurro and Luco (2006) and Huang et al. (2011) observed that motions modified using the TD technique produced smaller structural responses for nonlinear single degree-of-freedom systems than scaled ground motions. Similar observations were made by Iervolino et al. (2010) in regards to the peak responses produced by TD-modified motions and original recorded ground motions (i.e., smaller responses produced by TD-modified motions) for single degree-of-freedom systems that experienced nonlinear behavior, although this observation was not statistically significant. Naeim and Lew (1995) and Carballo (2000) observed that FD-modified motions had unrealistically large amounts of energy compared to those of the scaled ground motions. Hancock et al. (2008), Heo et al. (2011), and Grant and Diaferia (2013) did not observe biases between the structural responses caused by scaled motions and those caused by TD-modified motions when compared to median responses of numerical simulations for multiple degree-of-freedom systems. Also, Iervolino et al. (2010) did not observe any bias in the cyclic responses produced by the TD-modified motions with respect to the cyclic responses produced by the original recorded ground motions. The conflicting results of the suitability of modified motions for structural dynamic response analyses signify that a better understanding of the effects of modification is warranted. Additionally, the effects of modification on the geotechnical dynamic response analyses were not investigated in these studies.

Studies by the author's advisor and the author have examined the effects of ground motion modification on the ground motion characteristics and geotechnical seismic response analyses. The effects of TD and FD modification on the characteristics and geotechnical seismic response analyses for three soil profiles were examined for two different scenarios with approximately ten motions to provide an initial understanding of the effects of modification and the reasons behind these effects (Guisbert et al. 2010, Zekkos and Carlson 2011, Zekkos et al. 2012). Eight motions modified for a shallow crustal earthquake event (Zekkos et al. 2012) were observed to experience a slight increase in peak ground velocity and peak ground displacement (modified-to-scaled ratios of 1.1 and 1.4, respectively) when TD modification was employed, but

a slight decrease in these characteristics (modified-to-scaled ratios of 0.96 and 0.85, respectively) when FD modification was employed. Additionally, both modification techniques reduced the Arias intensities of the scaled motions for this scenario (modified-to-scaled ratios of 0.86 and 0.88 for TD and FD modification, respectively). For twelve motions selected for a subduction zone event (Guisbert et al. 2010, Zekkos et al. 2012), the modified motions generally had larger peak ground velocities, peak ground displacements, and Arias intensities than their scaled counterparts. **Table 2.1** compares the mean modified-to-scaled ground motion characteristic ratios for these two scenarios. For both of these scenarios, median maximum shear stresses produced by the TD- and FD-modified motions for soft and stiff sites were observed to be similar (Guisbert et al. 2010, Zekkos et al. 2012). The median maximum shear stresses produced by the TD-modified motions for the shallow crustal earthquake event for a municipal solid waste site were smaller than the median maximum shear stresses produced by the scaled motions (Zekkos and Carlson 2011). For the shallow crustal earthquake event and sliding masses of three different depths, the Newmark-type slope displacements produced by the TD-modified motions were equal to or slightly less than those produced by the scaled motions for the municipal solid waste site (Zekkos and Carlson 2011), but were generally larger than the Newmark-type displacements produced by the FD-modified motions for the stiff and soft sites (Zekkos et al. 2012). However, for the subduction zone earthquake event and all sliding depths investigated, the FD-modified motions generally produced larger Newmark-type slope displacements than their TD-modified counterparts for both sites likely as a result of the larger Arias intensities observed for the FD-modified motions (Guisbert et al. 2010, Zekkos et al. 2012). Overall, the scaled motions were observed to have larger response spectra than the target spectrum for the shallow crustal earthquake event, but smaller response spectra, particularly for longer periods, than the target spectrum for the subduction zone event which may have led to the observed results in the ground motion characteristics and geotechnical seismic responses. This study provided an initial insight into the effects of modification, but was limited because a very small set of ground motions was investigated.

A similar study was performed by the author and the author's advisor for a shallow crustal earthquake event using a more statistically significant set of ground motions (i.e., 28 ground motions) (Carlson et al. 2014a). The modified-to-scaled peak ground velocity and peak ground displacement ratios for both modification techniques were less than 1. However, the

modified-to-scaled ratios for Arias intensity for both TD and FD modification techniques were approximately equal to 1 likely as a result of selecting and scaling motions to minimize the mismatch between the response spectra of the selected motions and the target spectrum (Carlson et al. 2014a). The similarity between the response spectra of the selected motions and the target spectrum was also believed to be the reason the responses for the geotechnical dynamic analyses (e.g., cyclic stress ratio, Newmark-type slope displacements) produced by the scaled and modified motions were generally very similar. In a study on the effects of modification on structural dynamic response analyses for a single degree-of-freedom system with a bilinear elastic-plastic behavior (Carlson et al. 2014b), it was observed that the sets of scaled, TD-modified, and FD-modified motions produced similar median peak structural accelerations, velocities, and displacements. However, the modified ground motions in this study caused the structural system to absorb much larger amounts of energy than the scaled motions did. Although more ground motions were investigated in this study, a wider selection of motions, target spectra, and earthquake scenarios must be investigated to fully understand the effects of modification.

Results of these preliminary studies (Zekkos and Carlson 2011, Zekkos et al. 2012, Carlson et al. 2014a, 2014b) suggest that the effects of modification on the ground motions are affected by many factors, including the selection of ground motions, earthquake scenario, site conditions, and structural systems. However, it is hypothesized that the mismatch between the response spectrum of the seed motion and the target spectrum (i.e., spectral mismatch) may be the main factor contributing to these observed results. Therefore, it is necessary to examine the characteristics of hundreds of ground motions matched to several target spectra of varying shape and intensity for multiple earthquake scenarios and the responses of subsequent geotechnical dynamic analyses to further understand the effects of ground motion modification and the impact of spectral mismatch.

Table 2.1. Summary of the mean modified-to-scaled ground motion characteristic ratios observed in previous studies conducted by the author and the author's advisor.

	Shallow Crustal Event; 8 Motions (Zekkos et al. 2012)		Subduction Zone Event; 12 Motions (Zekkos et al. 2012)		Shallow Crustal Event; 28 Motions (Carlson et al. 2014a)*	
Ground Motion Characteristic	TD	FD	TD	FD	TD	FD
Peak ground velocity	1.10	0.96	1.61	1.54	0.93	0.81
Peak ground displacement	1.40	0.85	2.57	2.00	0.96	0.67
Arias intensity	1.00	1.05	1.00	1.10	0.98	0.97
Significant duration	0.86	0.88	1.03	1.41	1.00	1.15

* The median modified-to-scaled characteristic ratios are shown for this study.

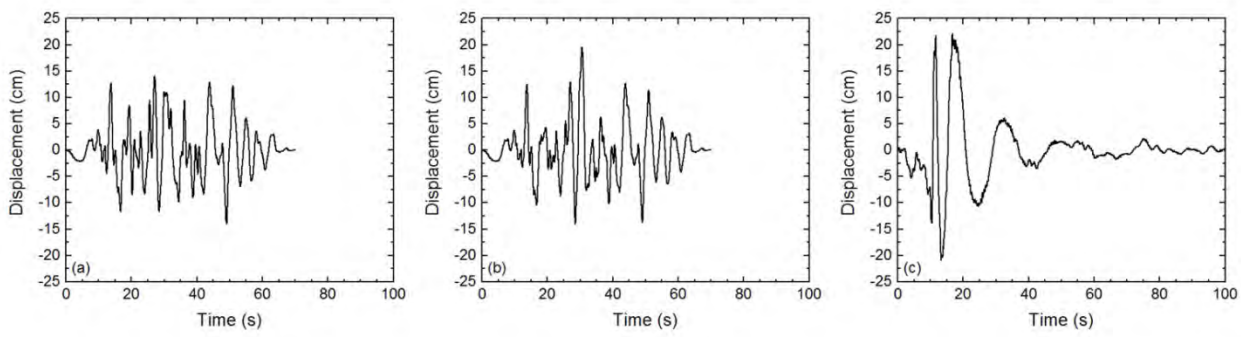

Figure 2.1. Displacement time histories of (a) a scaled ground motion, (b) its TD-modified counterpart, and (c) a synthetic ground motion generated for a similar earthquake event.

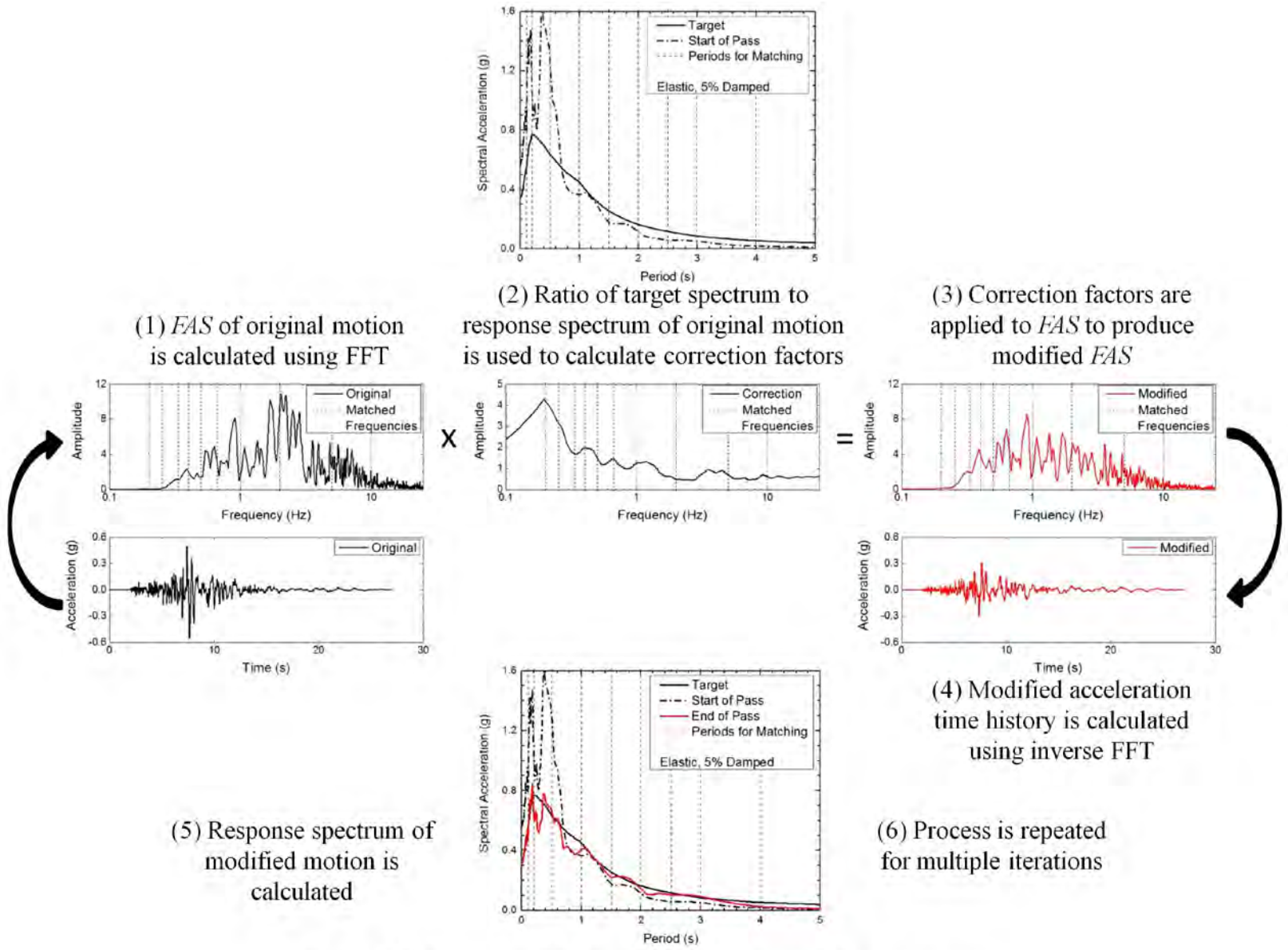

Figure 2.2. Diagram of the frequency domain modification process.

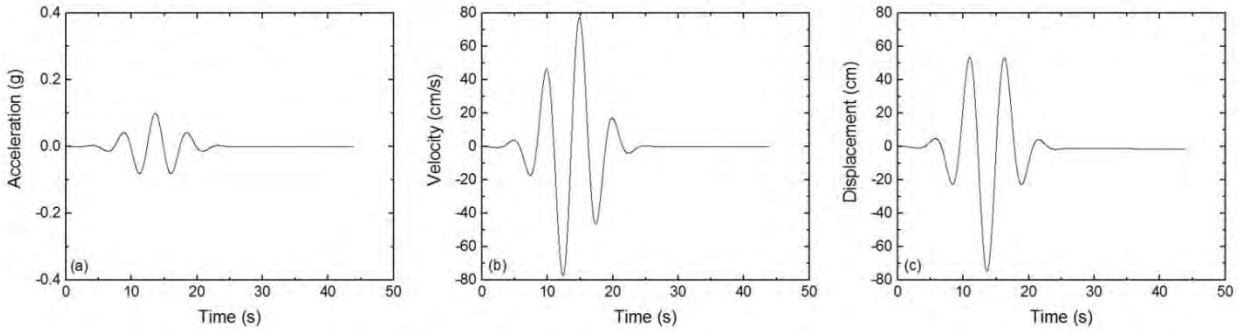

Figure 2.3. (a) Acceleration, (b) velocity, and (c) displacement time histories of the improved tapered cosine adjustment wavelet used by RSPMatch09 (Al Atik and Abrahamson 2010).

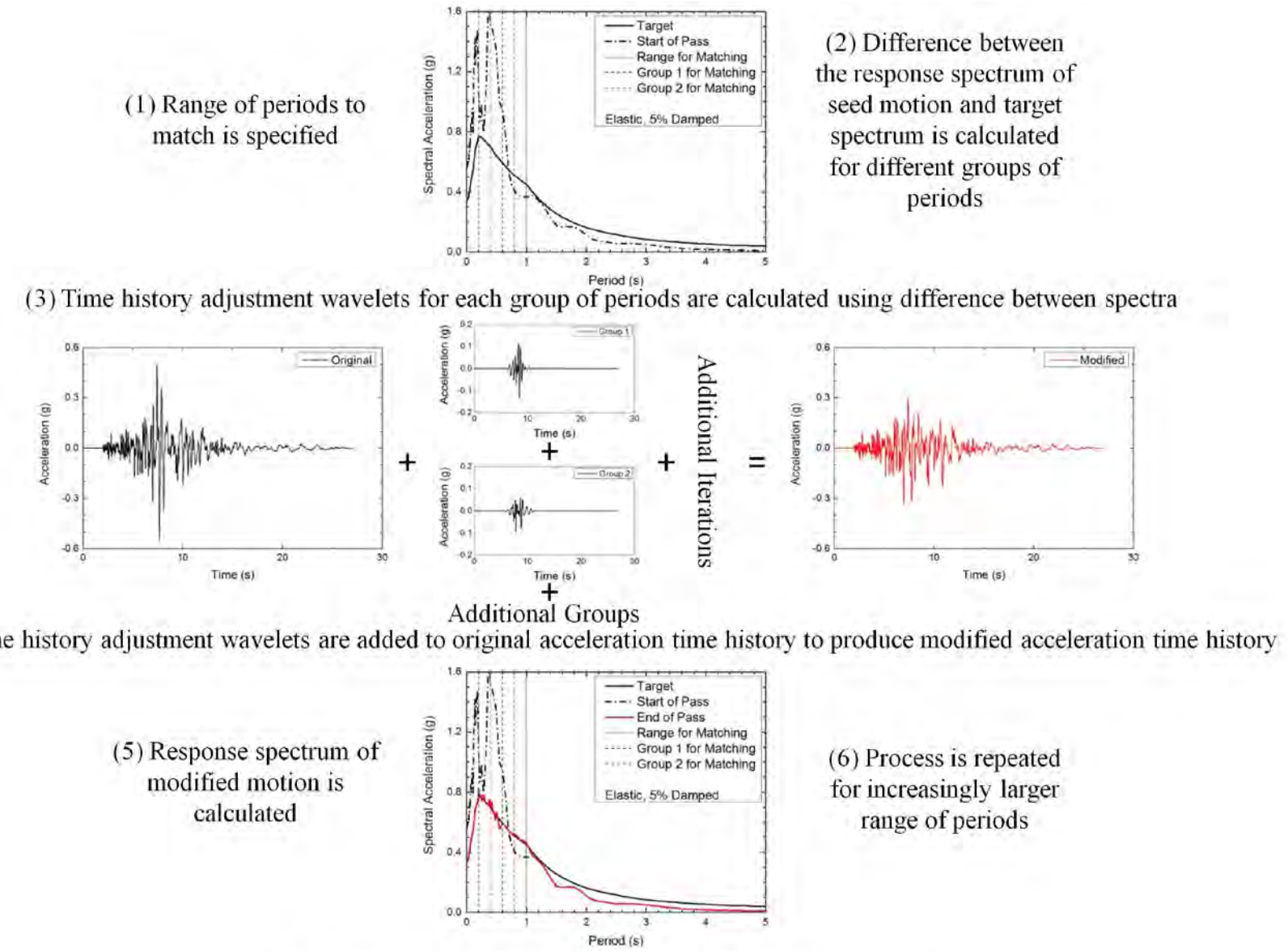

Figure 2.4. Diagram of the time domain modification process.

CHAPTER 3
Development of a Ground Motion Modification Program: GMM

3.1 Overview of the Program

GMM, a new ground motion modification program, was developed as part of this research project using MATLAB (The Mathworks, Inc. 2013). The program matches a suite of ground motions to multiple target spectra using TD and FD modification techniques and calculates the ground motion characteristics and time histories of the original, scaled, and modified ground motions. GMM also calculates the goodness-of-fit (*GOF*) between the modified and scaled time histories. A summary page is produced by GMM to outline the ground motion characteristics and time histories of the original, scaled, and modified ground motions. The step-by-step procedure for GMM is shown in **Figure 3.1**. The following sections describe each step of the program in more detail.

At the start of GMM, a list is generated containing the ground motion acceleration files with an .AT2 file extension within the same folder as GMM. The user then inputs the name of a text file containing the scaling factors to apply to the corresponding ground motions in the list and the target response spectrum to match during modification. The target spectrum file contains the number of spectral points used in matching (n_s) and the periods (T_i), frequencies (f_i), and spectral values ($Sa(T_i)$) of those points; the peak ground acceleration of the target spectrum (PGA_{tar}); and the number of damping values (n_d) for which the target spectrum is to be matched and the corresponding damping values (λ_i).

GMM then reads the ground motion acceleration files corresponding to the list of filenames one-by-one. The ground motion acceleration files must be in the format used in the Pacific Earthquake Engineering Research Center's (PEER) next generation attenuation (NGA) database (Chiou et al. 2008). Header lines in the ground motion acceleration files contain information such as the source of the file, the earthquake event, and the station name and location. The number of acceleration values recorded (n_t) and the time step (dt) of the values for

the acceleration time history in the ground motion file are also provided in the header. The remainder of the ground motion file contains the accelerations of the recording at each time step. Header lines are skipped and the n_t, dt, and acceleration values are read by GMM. Once the ground motions in the list have all been modified, the user has the option to input another set of text files for the target spectrum and the scaling factors or end the program.

For each ground motion, the ground motion characteristics, time histories, Arias intensity buildup (Husid 1969), Fourier amplitude spectrum, and response spectra of the original recording are calculated. Details on the calculations of the ground motion characteristics, time histories, and response spectra are provided in **Section 3.2**. The original ground motion is scaled then used as input to the TD and FD modification routines. Ground motion characteristics, time histories, Arias intensity buildups, Fourier amplitude spectra, and response spectra are calculated for the scaled, TD-modified, and FD-modified ground motions. The procedures in GMM used to perform TD and FD modification on the scaled ground motion are described in **Section 3.3**.

After calculating the ground motion characteristics and time histories of the original, scaled, and modified ground motions, spectral mismatch and *GOF* metrics are calculated. The spectral mismatch between the acceleration response spectrum of the scaled ground motion and the target spectrum and the *GOF* between the scaled and modified acceleration, velocity, and displacement time histories, Arias intensity buildups, and Fourier amplitude spectra are computed using different metrics. Details on the calculations of the metrics used for spectral mismatch and *GOF* are provided in **Section 3.4**.

Next, GMM saves the calculated characteristics and time histories of the original, scaled, TD-modified, and FD-modified ground motions in text files. The filenames of these text files include the name of the ground motion and the target spectrum to which it is matched. Separate text files are generated for the ground motion characteristics, time histories, Arias intensity buildups, Fourier amplitude spectra, response spectra, spectral mismatch and *GOF* metrics, *GOF* time histories, and coherence.

For each ground motion, a one page summary sheet, in .jpeg format, is produced by GMM containing plots and tables summarizing the characteristics and time histories of the original, scaled, TD-modified, and FD-modified motions. The output image file includes the ground motion characteristics and acceleration, velocity, and displacement time histories calculated for the original, scaled, TD-modified, and FD-modified motions along with the Arias

intensity buildup and acceleration response spectra calculated for the scaled and modified motions. More information on the output image files generated by GMM is provided in **Section 3.5**.

3.2 Calculation of Ground Motion Characteristics, Time Histories, and Response Spectra

For the original, scaled, TD-modified, and FD-modified ground motions, peak ground acceleration (*PGA*), peak ground velocity (*PGV*), peak ground displacement (*PGD*), Arias intensity (I_a) (Arias 1970), significant duration ($D_{5\text{-}95}$) (Trifunac and Brady 1975), cumulative absolute velocity (*CAV*) (EPRI 1988), and mean period (T_m) (Rathje et al. 1998) are calculated. The amplitudes (e.g., *PGV* or *PGD*), durations (e.g., $D_{5\text{-}95}$), frequency content (e.g., T_m), and energy (e.g., I_a or *CAV*) of the ground motions can be described using these characteristics. Non-stationary characteristics, including the acceleration ($a(t)$), velocity ($v(t)$), and displacement ($d(t)$) time histories, the I_a buildups ($I_a(t)$; Husid 1969), and the Fourier amplitude spectra (*FAS*), are also calculated for the ground motions. Time histories are used to calculate the *GOF* between the scaled and modified motions and the $a(t)$ of the scaled and modified ground motions are used as input in the seismic geotechnical analyses for this study.

The $a(t)$ of the original ground motion is read into the program from the ground motion file in units of the gravitational constant, g. The $a(t)$ of the scaled and modified ground motions are calculated using the processes described in **Section 3.3**. After converting the $a(t)$ to units of cm/s^2, trapezoidal integration is performed using **Equation 3.1** to calculate the $v(t)$ for each time step.

$$v(t)_{i+1} = dt * \frac{a(t)_{i+1} + a(t)_i}{2} + v(t)_i \tag{3.1}$$

Equation 3.1 is performed for $n_t - 1$ iterations. A second trapezoidal integration is performed using the $v(t)$ to calculate the $d(t)$. The initial values (i.e., $i = 1$) for $v(t)$ and $d(t)$ are assumed to be equal to 0. *PGA*, *PGV*, and *PGD* are the maximum absolute values of the $a(t)$, $v(t)$, and $d(t)$, respectively.

Equation 3.2 is used to calculate I_a, where g and $a(t)$ have the same units.

$$I_a = \frac{\pi}{2g} \int_0^{t_D} \left(a(t)\right)^2 dt \tag{3.2}$$

$I_a(t)$, in terms of percentage, is calculated by normalizing the cumulative I_a at each time step by the final value of I_a then multiplying by 100%. t_D represents the total duration of the time history. $D_{5\text{-}95}$ is taken as the time between the occurrences of 5% and 95% in the $I_a(t)$. *CAV* is calculated in a similar manner to I_a using **Equation 3.3**.

$$CAV = \int_0^{t_D} |a(t)| dt \tag{3.3}$$

A Fast Fourier Transform (FFT) is performed on the $a(t)$ to obtain the *FAS* and subsequently calculate T_m. FFTs are performed using the built-in function in MATLAB (The Mathworks, Inc. 2013) for this study. The *FAS* is calculated for a number of points, n_{FAS}, equal to the next power of 2 greater than n_t. The *FAS* are calculated for frequency values, f_i, in increments of $(1/dt)/(n_{FAS})$ with a range from $(1/dt)/(n_{FAS})$ to $1/dt$. The *FAS* is then used in **Equation 3.4** to calculate T_m.

$$T_m = \frac{\sum_{i=1}^{n_{FAS}} \frac{FAS(f_i)^2}{f_i}}{\sum_{i=1}^{n_{FAS}} FAS(f_i)^2} \tag{3.4}$$

Equation 3.4 is calculated using only f_i values between 0.25 and 20 Hz, which is the range used by Rathje et al. (1998).

Elastic acceleration, velocity, and displacement response spectra, *Sa*, *Sv*, and *Sd*, respectively, are calculated for the ground motion using Newmark's average acceleration method (Newmark 1959). The equations in Chopra (2007) for the Newmark average acceleration method are used by GMM to calculate the response spectra. Prior to calculating the spectral values for the modified motions at T_i and λ_i, the stability of the solution is checked. If dt/T_i is greater than 0.1, the *dt* for the $a(t)$ of the ground motion is decreased to satisfy this criterion and a new $a(t)$ is interpolated. *Sa* is calculated as a pseudo-acceleration response spectrum using **Equation 3.5**, but is referred to as the acceleration response spectrum in the remainder of the text.

$$Sa = \left(\frac{2\pi}{T_i}\right)^2 * Sd \tag{3.5}$$

The response spectra of the ground motions are used in the modification processes and calculations of spectral mismatch. In this study, response spectra with a damping value of 0.05

are calculated for 108 periods that are equally spaced, logarithmically, between 0.01 and 5 seconds.

3.3 Ground Motion Modification

3.3.1 Scaling

In this portion of GMM, the $a(t)$ of the original ground motion is multiplied by the corresponding scaling factor in the text file specified by the user. The ground motion characteristics, time histories, $I_a(t)$, *FAS*, and response spectra of the scaled ground motion are calculated. The $a(t)$ of the scaled ground motion is then modified using subroutines in GMM for the FD and TD techniques.

3.3.2 Frequency Domain Modification

The subroutine for FD modification in GMM is modeled after the work done by Rizzo et al. (1975). The flowchart in **Figure 3.2** illustrates the procedure for the FD modification subroutine within GMM.

First, the $a(t)$ of the scaled ground motion and the target response spectrum are read into the FD modification subroutine of GMM. The user then specifies the tolerance and the number of iterations to use for FD modification. Mismatch is calculated using **Equation 3.6** and compared to the specified tolerance to assess whether the match between the response spectrum of the ground motion and the target spectrum, Sa_{tar}, is satisfactory.

$$Mismatch(T_i) = \left| \frac{Sa_{tar}(T_i) - Sa(T_i)}{Sa_{tar}(T_i)} \right| \quad \textbf{(3.6)}$$

Mismatch is calculated for all periods in the target spectrum. For this study, the tolerance is set to 0.05 and the number of iterations is set to 4 for the FD modification subroutine. The user is then allowed to input a vector with a length equal to n_{FAS}, which contains scaling factors that are applied in the frequency domain to the correction factors calculated at each frequency during the iteration of the modification process. All the factors within the scaling vector are set to 1 for this study. If the user would like to scale the $a(t)$ of the input ground motion to match the PGA_{tar} prior to modification, the $a(t)$ is multiplied by a factor equal to the PGA_{tar} divided by the *PGA* of the input $a(t)$. Since this study aims to investigate the effects of modification for varying levels

of initial mismatch, the $a(t)$ of the ground motions are not scaled to PGA_{tar} prior to modification in the FD subroutine.

To begin the FD modification process, a FFT is used to put the $a(t)$ of the input ground motion into the frequency domain as a *FAS* with a length of n_{FAS}. The base 10 logarithms are calculated for each frequency in the target spectrum and the spectral values of the target spectrum and response spectrum of the input ground motion at each frequency. For frequency values, f_i, from the first frequency step, $(1/dt)/(n_{FAS})$, to $1/(2*dt)$, modification factors are calculated. The logarithmic $Sa_{tar}(f_i)$ and $Sa(f_i)$ are interpolated for each f_i then transformed back into arithmetic terms. Correction factors are calculated for each f_i using **Equation 3.7**.

$$Correction \quad Factor(f_i) = Sa_{tar}(f_i) / Sa(f_i) \tag{3.7}$$

If the mismatch between $Sa_{tar}(f_i)$ and $Sa(f_i)$, calculated using **Equation 3.6**, is within the specified tolerance, the correction factor at f_i is set to 1. The correction factors are then multiplied by the factors in the scaling vector specified by the user at the beginning of the FD modification subroutine to produce the amplitudes of modification for each f_i. Modification factors are calculated at each f_i as the complex pair, (-modification amplitude, 0). The conjugate pairs of the original *FAS* are multiplied by the modification factors to produce a modified *FAS*. After modifying the *FAS*, an inverse FFT is used to calculate the $a(t)$ of the FD-modified ground motion, which is then truncated to have a length of n_t. The new *PGA* and response spectrum are calculated for the FD-modified motion. The $a(t)$ and response spectrum of the FD-modified motion are then used in the next iteration of the modification process as the original values of $a(t)$ and response spectrum and the modification process is repeated for the specified number of iterations. Prior to the last iteration of the modification process, the entire $a(t)$ is scaled so that its *PGA* matches the PGA_{tar}.

At the end of the FD modification subroutine, the $a(t)$ of the modified ground motions undergo the following post-processing steps:

- Locally scale peak value(s) of $a(t)$ to PGA_{tar}: This step ensures that the FD-modified ground motion has a *PGA* equal to the target. The time step in the $a(t)$ of the FD-modified motion containing the *PGA* is increased or decreased to the target *PGA* value. If other points in the $a(t)$ of the FD-modified motion have accelerations greater than PGA_{tar}, those points are multiplied by the ratio of the *PGA* of the FD-modified motion to the PGA_{tar}. Only the time step containing the *PGA* is increased or decreased to match the PGA_{tar} to limit the impact on

the response spectrum of the FD-modified motion. However, this process can lead to the development of permanent displacements in the $d(t)$. **Figures 3.3a** and **3.3b** respectively show the process of increasing and decreasing the peak value(s) of the $a(t)$ to match the PGA_{tar} for two example FD-modified motions.

- Taper beginning and end of $a(t)$: Tapering is applied to the $a(t)$ of the modified motion to make sure it "ramps up" and "ramps down" like previously recorded $a(t)$. In this study, acceleration values for the first 1% and last 5% of the duration of the $a(t)$ of all the modified ground motions are tapered using the function given in **Equation 3.8**.

$$a(t_i)_{taper} = k * t_i^2 * a(t_i) \quad \textbf{(3.8)}$$

  k represents a coefficient with a value such that the tapered $a(t)$ equals the $a(t)$ at t_i equal to $0.01t_D$ and $0.95t_D$. The taper function for the end of the $a(t)$ also uses **Equation 3.8**, but the t_i^2 term is replaced with $(t_D\text{-}t_i)^2$. The process of tapering the $a(t)$ for an example FD-modified ground motion is shown in **Figure 3.4**.

- Baseline correct $a(t)$: The $a(t)$ of the modified ground motion is then baseline corrected to remove any residual displacements in the $d(t)$ that may have developed during the modification process or the other post-processing steps. A polynomial function, as shown in **Equation 3.9**, is fit to the $a(t)$ of the modified motion.

$$x_a(t_i) = \alpha_1 t_i^p + \alpha_2 t_i^{p-1} + \ldots + \alpha_p t_i + \alpha_{p+1} \quad \textbf{(3.9)}$$

  $x_a(t)$ represents the baseline correction function, the α_n values represent coefficients calculated for the function, and p represents the order of the polynomial for the function. The corrected $a(t)$ is calculated by subtracting $x_a(t)$ from $a(t)$. The $a(t)$, $v(t)$, and $d(t)$ of the modified ground motion are calculated and displayed for the user, who is allowed to increase the polynomial of the correction function until the time histories have a realistic shape (i.e., no residual displacements or sinusoidal behavior). A value between 1 (i.e., linear) and 9 (i.e., ninth order polynomial) must be specified by the user for the order of the polynomial for the correction function. The process and effects of baseline correcting the $a(t)$ of an example FD-modified ground motion is shown in **Figure 3.5**. For each ground motion and modification technique used in this study, the author selected the order of the polynomial in the baseline correction function based on a visual inspection of the $d(t)$. Admittedly, the selection of the polynomial order for the baseline correction function is a subjective process, but it should not

significantly affect the results of this study. However, the effects of baseline correction on the modified ground motions should be investigated.

3.3.3 Time Domain Modification

The TD modification subroutine in GMM is modeled after the most recent version of RSPMatch (Al Atik and Abrahamson 2010, Fouad and Rathje 2012). A flowchart illustrating the procedure for the TD modification subroutine is shown in **Figure 3.6**.

The $a(t)$ of the scaled ground motion and target spectrum are read into the TD modification subroutine of GMM. The user is asked to specify an input file containing the number of passes for which TD modification is performed. Each pass in the TD modification process matches the response spectrum of the input ground motion to the target spectrum over a specified range of periods. Multiple passes are generally used in the modification process to gradually match the response spectrum of the ground motion to the target spectrum for increasingly longer periods (Al Atik and Abrahamson 2010). In this study, TD modification is performed using three passes. The input file also contains names for files containing input parameters (e.g. number of iterations, tolerance) that are read in for each pass.

For each TD modification pass the parameters defined below are read into the subroutine from the corresponding input file. The input parameters for TD modification are described in more detail in Abrahamson (1998) and Fouad and Rathje (2012). Overall, the values recommended in Fouad and Rathje (2012) for the input parameters are used in this study.

- Maximum number of iterations to perform during each pass: For this study, a maximum of 20 iterations is used for all three passes.
- Tolerance for the mismatch between Sa and Sa_{tar}: The tolerance is set to 0.05 for all three passes.
- Convergence damping factor: This factor can be a fraction between 0 and 1. The convergence damping factor is applied to the correction acceleration time history (i.e., $\delta a(t)$) in each iteration to stabilize the convergence (Abrahamson 1998). In this study, a value of 1 is used for the convergence factor in all three passes.
- Scaling flag and period for scaling: The scaling flag is used to indicate if the user does not want to scale the $a(t)$ (0), scale the $a(t)$ prior to performing modification and after each iteration (1), or scale the $a(t)$ only prior to performing modification (2). Scaling is applied to

the $a(t)$ such that the response spectrum of the scaled ground motion and target spectrum have the same value at the specified period (i.e., $a(t)*Sa_{tar}(T_i)/Sa(T_i)$). Although it is recommended to scale the ground motion to match the target *PGA* prior to performing modification (Al Atik and Abrahamson 2010), one of the goals of this study is to investigate the effects of modification for varying levels of mismatch and thus, a scaling flag and period of 0 are used.

- Time step interpolation factor: This factor is used to decrease the *dt* of the $a(t)$. For example, a factor of 2 will reduce *dt* by half. This factor is set to 1 (i.e., no change in *dt*) for all three passes in this study.
- Maximum number of spectral values to include in each subgroup during modification: During modification, values for the target spectrum and response spectrum of the seed motion are split into smaller subgroups to increase the rate of convergence. Larger group sizes slow down convergence, but increase stability (Abrahamson 1998). For this study, the maximum group size is set to 30.
- Maximum frequency to which matching is performed: Values in the response spectrum of the seed motion and target spectrum with frequencies larger than this parameter are not read by the TD modification subroutine and thus, not directly matched during the modification process. In the author's experience, matching to frequencies above 35 Hz increases the possibility of numerical instabilities and errors developing in the resulting time histories; therefore, 35 Hz is used for the maximum frequency in each pass.
- Seed value and amplitude for randomization: These parameters are used to apply random variability to the target spectrum in the case that standard deviation is critical for the project. Both of these parameters are set to 0 for this study.
- Range of frequencies used in matching: Points in the response spectrum of the seed motion and target spectrum within this frequency range are read by the TD modification subroutine and matched for the pass. Al Atik and Abrahamson (2010) recommend matching the target at shorter periods (i.e., higher frequencies) in the first pass then extending the matching out to longer periods (i.e., smaller frequencies) in subsequent passes. For this study, the frequency ranges matched for passes 1, 2, and 3 are 1 to 35 Hz, 0.5 to 35 Hz, and 0.2 to 35 Hz, respectively.

Prior to modifying $a(t)$ in each pass, other initialization steps are performed. If it is not the first pass, the stored $a(t)$ from the previous pass that results in the smallest mismatch and the corresponding mismatch are used for the original $a(t)$ and smallest mismatch in the pass. Next, the target spectral values for the specified frequency range of the current pass are read into the TD modification subroutine. Though not used in this study and not shown in **Figure 3.6**, the next steps would interpolate $a(t)$ values for the new dt and randomize the target spectrum. The response spectrum of the seed motion and its mismatch with the target spectrum is then calculated for the frequency range of matching specified for the current pass. Mismatch in the TD modification subroutine is taken as the maximum value calculated using **Equation 3.6** over the frequency range of the current pass. If the user inputs 1 or 2 for the scaling flag, the $a(t)$ is then scaled so that the response spectrum of the scaled motion equals the target spectrum at the specified period. The $a(t)$ and the mismatch prior to the modification process are then stored as the case producing the smallest mismatch.

While the mismatch is greater than the specified tolerance and the iteration number is less than the maximum number of iterations specified, TD modification is performed for each damping value, λ_i. In this study, only a λ_i of 0.05 is used. The frequencies and spectral values for the target spectrum are split into subgroups that have the size specified in the input file for the current pass. For each subgroup, the $a(t)$ is padded if necessary based on the criterion described in **Section 2.2.3**. The response spectrum of the modified motion, along with its mismatch with the target spectrum, is calculated for the frequency range specified for the current pass. The mismatch between the response spectrum of the modified motion and the target spectrum is then used to calculate **C**, **b**, and $\delta a(t)$ using the process described in **Section 2.2.3**. $\delta a(t)$ is multiplied by the convergence damping factor then added to $a(t)$ to produce the modified $a(t)$ for the iteration. If the scaling flag in the input file is set to 1, the $a(t)$ is then scaled so that its response spectrum matches the target at the specified period. After each iteration, the response spectrum and mismatch of the modified $a(t)$ are recalculated and, if the mismatch for the modified $a(t)$ is less than that of the previous iteration, the modified $a(t)$ and the corresponding mismatch are stored as the case producing the smallest mismatch and used in the next iteration. Once the mismatch is less than the specified tolerance or the maximum number of iterations has been reached, the modified $a(t)$ that produces the response spectrum with the smallest mismatch and the corresponding mismatch are passed into the next pass in place of the original $a(t)$ and the

mismatch. The modification process is repeated for the specified number of passes and the modified $a(t)$ that produces the response spectrum with the smallest mismatch is saved.

Post-processing steps are performed on the modified $a(t)$ at the end of the TD modification subroutine. The peak value for the $a(t)$ of the TD-modified motion, and any other values larger than the PGA_{tar}, are scaled by the ratio of the *PGA* of the modified motion to the PGA_{tar}. Any points added to the $a(t)$ during the TD modification process for zero-padding are truncated. After trimming the $a(t)$ of the TD-modified motion, tapering and baseline correction functions are applied using the same procedure discussed for the FD-modified motion.

3.4 Mismatch/Goodness-of-Fit Metric Calculations

Several metrics are calculated by GMM to quantify the spectral mismatch between the response spectra of the scaled motions and target spectra and the *GOF* between the scaled and modified time histories. The equations for the metrics are presented here while **Chapters 4** and **5** provide the parameters used in these equations to calculate spectral mismatch and *GOF*. The metrics that are calculated by GMM include normalized error (*NE*), a tanh validation metric (*TVM*; Oberkampf and Trucano 2002, Green et al. 2011), an inverse modified root mean squared error (*imRMSE*; based on Kristeková et al. 2006), a complementary error function metric (*ERFCM*; Olsen and Mayhew 2010), Anderson's C1 and C10 metrics (*AC1* and *AC10*, respectively; Anderson 2004), and average coherence. The input time histories or response spectra (e.g., response spectra of the scaled motions) are compared to the reference time history or response spectrum (e.g., target response spectrum) in calculating these metrics.

NE is calculated using **Equation 3.10**.

$$NE = \frac{\sum_{i=1}^{n}\left(\frac{inp_i - ref_i}{ref_{peak}}\right)}{n} \quad \textbf{(3.10)}$$

ref and *inp* refer to the reference and input, respectively, time histories or response spectra. ref_{peak} refers to the peak value of the reference time history or the spectral value at some T_i. n represents the number of data points in the time histories or response spectra for which *GOF* or mismatch is calculated. Theoretically, *NE* approaches -1 when *ref* is much larger than *inp* and infinity when *inp* is much larger than *ref*. When *ref* and *inp* are equal, *NE* becomes 0. The benefit of using *NE*

is that its sign can be used to easily identify which of two time histories or response spectra is larger (i.e., positive *NE* means *inp* is larger and negative *NE* means *ref* is larger). The *NE* for each time step or T_i is also output by GMM.

Equation 3.11 shows the general form used to calculate *TVM*.

$$TVM = \frac{\sum_{i=1}^{n}\left[1-\tanh\left(\frac{|inp_i - ref_i|}{ref_i}\right)\right]}{n} \quad (\mathbf{3.11})$$

tanh refers to the hyperbolic tangent function, calculated using the built-in MATLAB function (The Mathworks, Inc. 2013). For *TVM*, the values at each time step or T_i are also output by GMM.

Equation 3.12 provides the calculation used for *imRMSE*. The square root term in **Equation 3.12** is a slightly modified version of *RMSE* (Kristeková et al. 2006). The exponential term and inverse are used to limit the *imRMSE* to values between 0 and 1 with poor matches represented by a value of 0.

$$imRMSE = \frac{1}{\exp\sqrt{\frac{\sum_{i=1}^{n}(inp_i - ref_i)^2}{\sum_{i=1}^{n} ref_i^{\,2}}}} \quad (\mathbf{3.12})$$

The calculation for *ERFCM* is provided in **Equation 3.13**. The erfc term refers to the complementary error function, calculated using the built-in function in MATLAB (The Mathworks, Inc. 2013).

$$ERFCM = \frac{\sum_{i=1}^{n}\left[erfc\left(\frac{2*|inp_i - ref_i|}{|inp_i| + |ref_i|}\right)\right]}{n} \quad (\mathbf{3.13})$$

TVM, *imRMSE*, and *ERFCM* equal 1 when *ref* and *inp* are equal and approximately 0 when *ref* and *inp* are significantly different. When *inp* is much larger than *ref*, *TVM*, *imRMSE*, and *ERFCM* theoretically approach 0. However, as a result of the equations used to calculate *TVM*, *imRMSE*, and *ERFCM*, the values approach 0.24, 0.37, and 0, respectively, when *ref* is much larger than *inp*. These metrics are used because they are bounded between 0 and 1.

The *AC1* and *AC10* metrics are calculated using **Equations 3.14** and **3.15**, respectively.

$$AC1 = \min_{i=1}^{n}\left(1 - \left|\frac{|inp_i| - |ref_i|}{ref_{peak}}\right|\right) \quad \textbf{(3.14)}$$

$$AC10 = \frac{\int_0^{t_D} inp(t) * ref(t) dt}{\sqrt{\int_0^{t_D} inp(t)^2 dt} * \sqrt{\int_0^{t_D} ref(t)^2 dt}} \quad \textbf{(3.15)}$$

The *AC1* metric is a single point value used to quantify the largest difference between *ref* and *inp* while the *AC10* metric roughly provides the cross-correlation between the *ref* and *inp* (Anderson 2004). The theoretical ranges for the values of *AC1* and *AC10* are negative infinity to 1 and approximately 0 to 1, respectively.

Coherence is calculated using the built-in function of MATLAB shown in **Equation 3.16** (The Mathworks, Inc. 2013).

$$Average \quad Coherence = \frac{\sum_{i=1}^{n_{FAS}} \frac{\left|P_{inp,ref}(f_i)\right|^2}{P_{inp}(f_i) * P_{ref}(f_i)}}{n_{FAS}} \quad \textbf{(3.16)}$$

$P_{inp}(f_i)$ and $P_{ref}(f_i)$ represent the power spectral density of *inp* and *ref*, respectively. $P_{inp,ref}(f_i)$ represents the cross-spectral density between *inp* and *ref*. Power spectral density describes the distribution of the power (or intensity) of the time history over different frequencies and cross-spectral density describes the contribution of multiple time histories to the power for different frequencies. A single point value of coherence is calculated using the average over all frequencies. Coherence between the *FAS* of the scaled and modified motions is not calculated.

For spectral mismatch, the metrics are calculated by GMM for different period ranges. Spectral mismatch is examined for different period ranges because some ground motion characteristics have been found to be better correlated to certain ranges of period (Chopra 2007, Riddell 2007). In addition to the entire range of periods for the target response spectrum, the metrics are also calculated for a short, intermediate, and long period range. The user can input to GMM the periods used to separate the different ranges. In this study, the spectral mismatch for the short, intermediate, and long period ranges are calculated for periods less than or equal to 0.5 seconds, periods between 0.5 and 3 seconds, and periods greater than or equal to 3 seconds, respectively.

3.5 One-Page Output Summary

A key output of GMM is a one-page summary of the results, in .jpeg format, for each ground motion matched to a target spectrum. An example of this one-page summary is shown in **Figure 3.7** for an example ground motion. The one-page summary aims to allow for an examination of the effects of modification on the ground motion and an objective decision to be made as to which modified ground motion (i.e., time domain or frequency domain) should be used. The header in this image displays the file name for the ground motion that is matched, the scaling factor that is applied to the ground motion, and the file containing the target spectrum to which the motion is matched. The percentages of tapering and the order of the polynomial for the baseline correction functions applied to the TD- and FD-modified motions in the post-processing steps are also shown in the header of the output image. Filenames for the output summaries contain the name of the ground motion acceleration file followed by the name of the file containing the target spectrum to which the motion is matched (e.g., 57_ORR021 targetCMS.jpeg). The $a(t)$, $v(t)$, and $d(t)$ of the original, scaled, TD-modified, and FD-modified ground motions are shown immediately below the header. A table is included to summarize the ground motion characteristics of the original, scaled, and modified motions. The build-up of normalized I_a of the scaled ground motion is compared to those of the TD- and FD-modified ground motions in the bottom left plot. The bottom right plot compares the response spectra of the scaled, TD-modified, and FD-modified ground motions and the target response spectrum.

3.6 Current State of Program and Future Improvements

GMM can be a useful tool for the practicing engineer in performing ground motion modification using the time domain and frequency domain techniques simultaneously and choosing the appropriate motions for a particular project. Several ground motions can be scaled and matched to multiple target spectra using both TD and FD modification then compared using one-page output summaries generated by GMM to select a set of scaled and/or modified motions with characteristics desirable for the project. Values for the *GOF* between the scaled and modified motions are also output by the program to quantify the changes to the non-stationary characteristics of the motion that occurred during modification. The following improvements are

planned to be incorporated in the near future by the author and his advisor so that it can be used in engineering practice:

- Add recommendations based on results of this study: Based on most of the results of this study, recommendations need to be incorporated as to which ground motions are appropriate for a given design scenario.
- Faster run time: The TD modification subroutine in GMM is more computationally intensive than the RSPMatch program since MATLAB code is used instead of FORTRAN code. The run time for GMM must be shortened to be used in practice.
- Add graphical user interface: Adding a graphical user interface to GMM will make it easier to use and understand.
- Add more error checks: GMM is currently designed for use in research. More error checks must be added to GMM to prevent users from entering values that could lead to erroneous results.

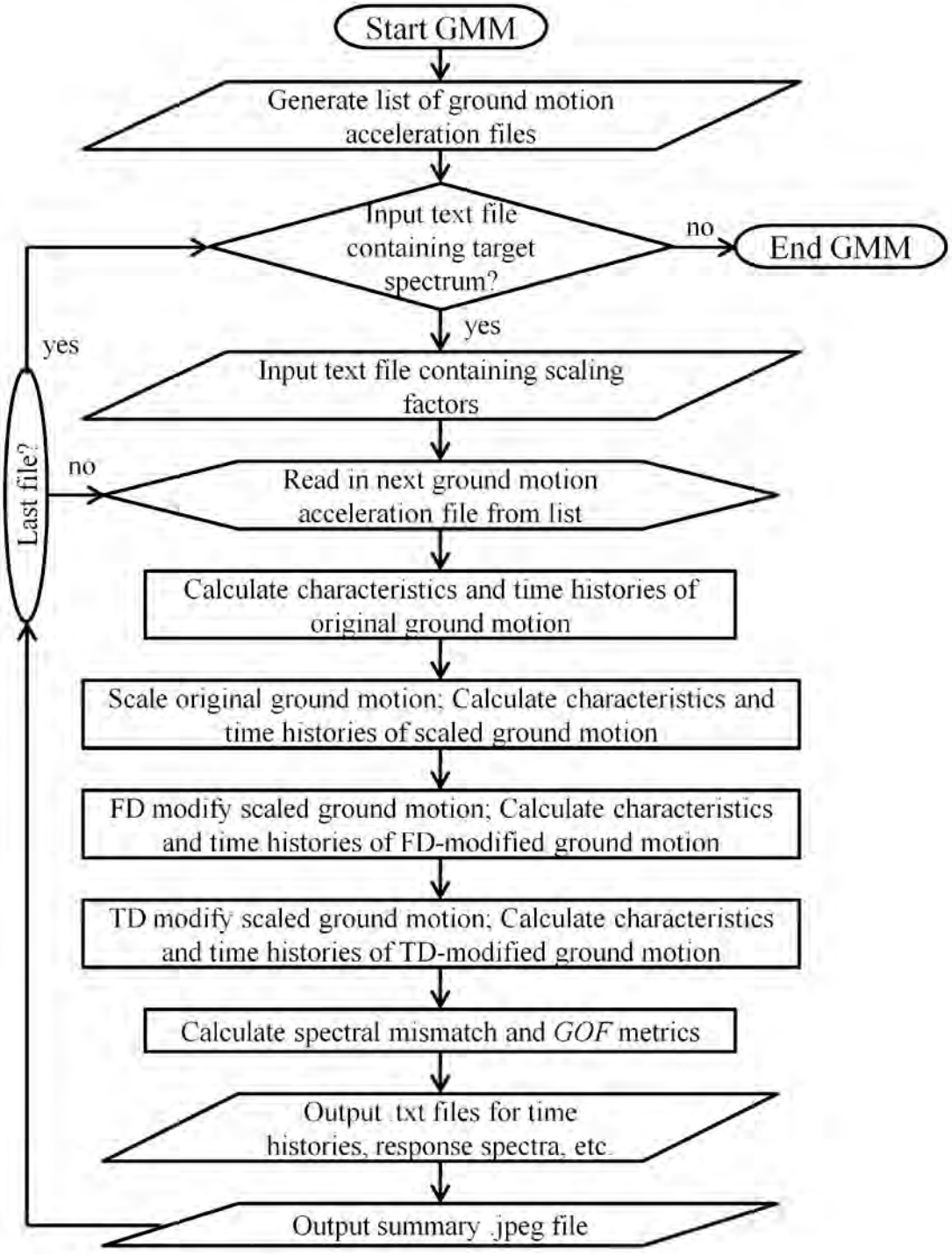

Figure 3.1. Flowchart for the algorithm used by GMM.

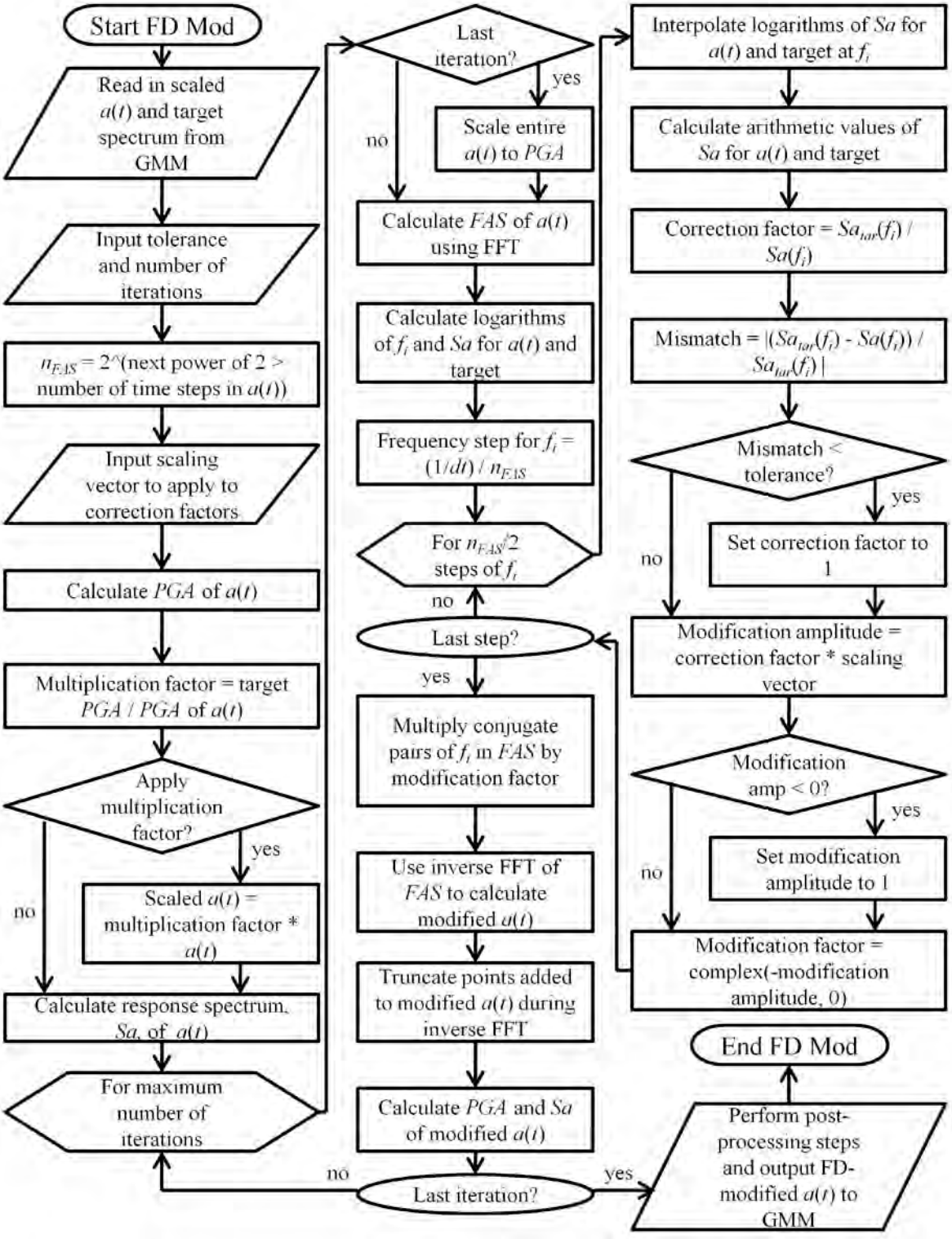

Figure 3.2. Flowchart for the algorithm used by the frequency domain (FD) modification subroutine in GMM.

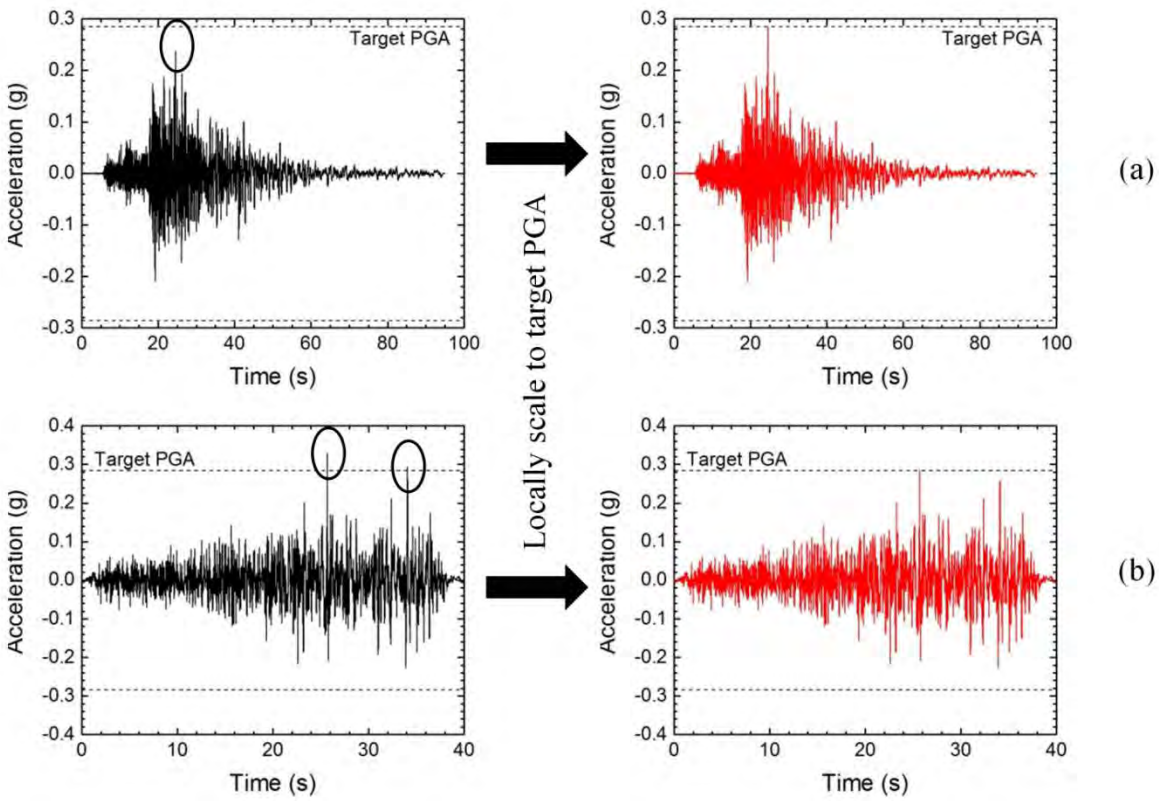

Figure 3.3. Illustration of the post-processing step of (a) scaling up and (b) scaling down the peak value(s) in the acceleration time histories to match the target peak ground acceleration (*PGA*) for two example FD-modified ground motions.

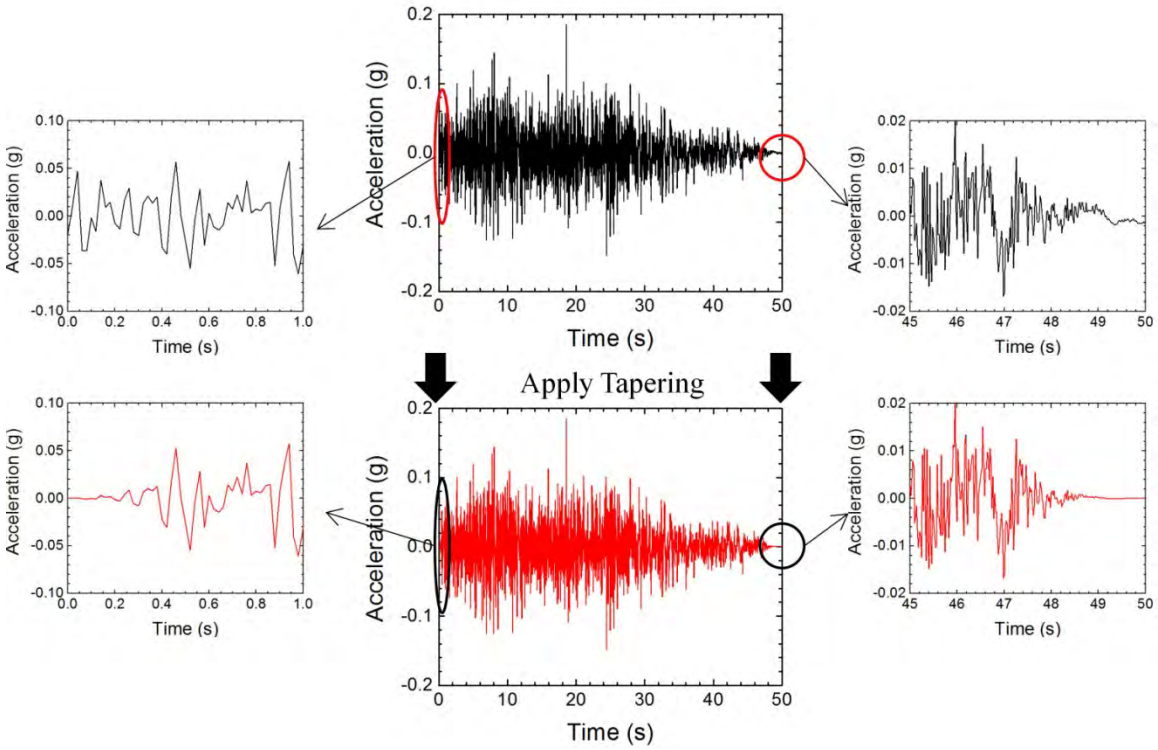

Figure 3.4. Illustration of the post-processing step of tapering the beginning and end of the acceleration time history of an example FD-modified ground motion.

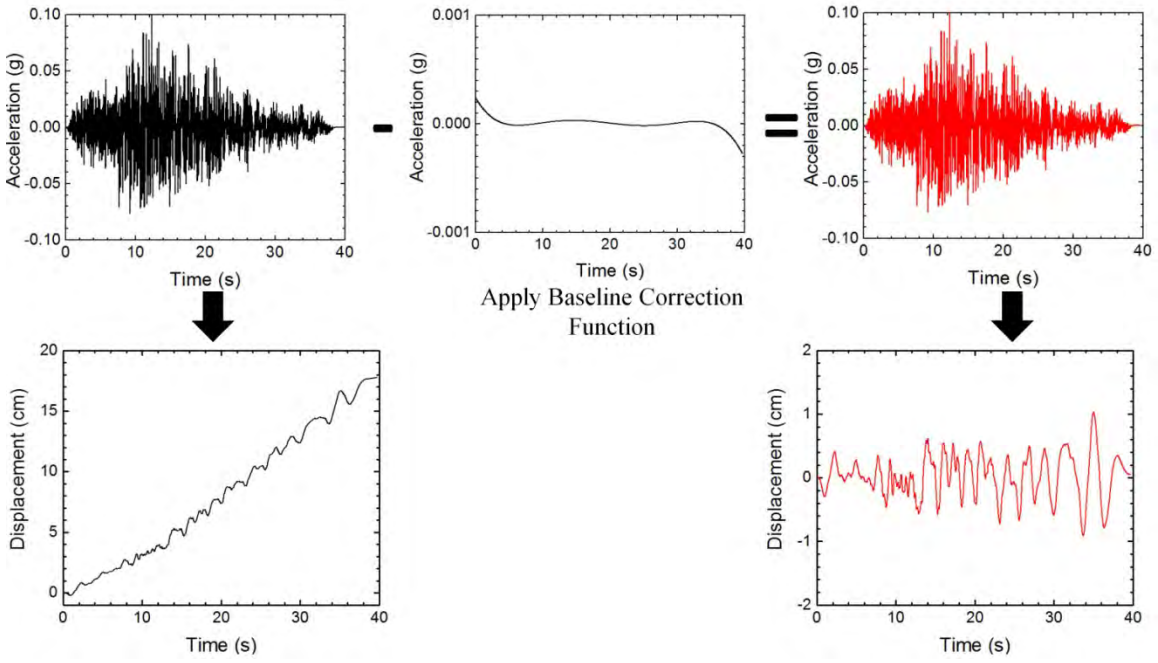

Figure 3.5. Illustration of the post-processing step of baseline correcting the acceleration time history and its effects on the displacement time history for an example FD-modified ground motion.

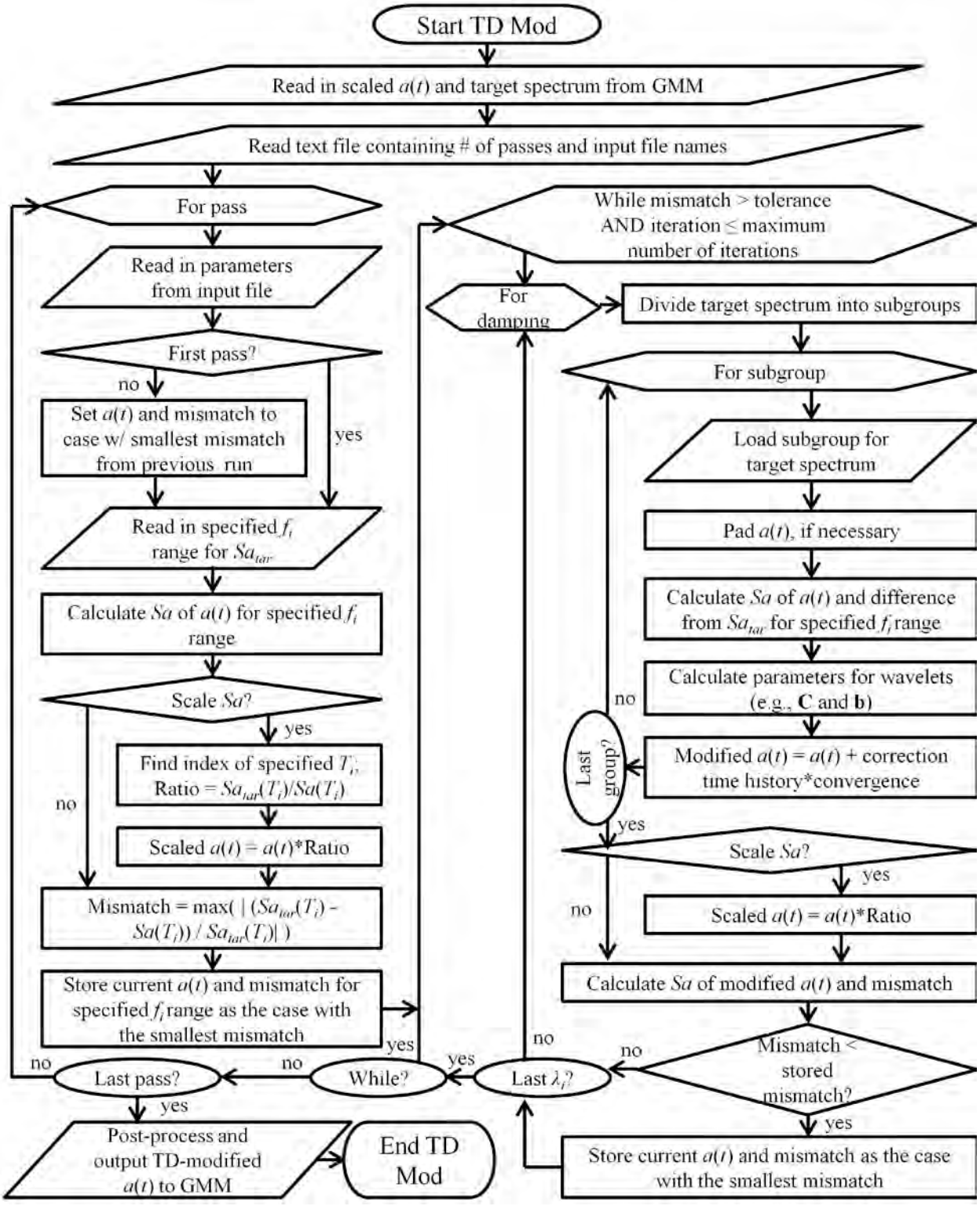

Figure 3.6. Flowchart for the algorithm used by the time domain (TD) modification subroutine in GMM.

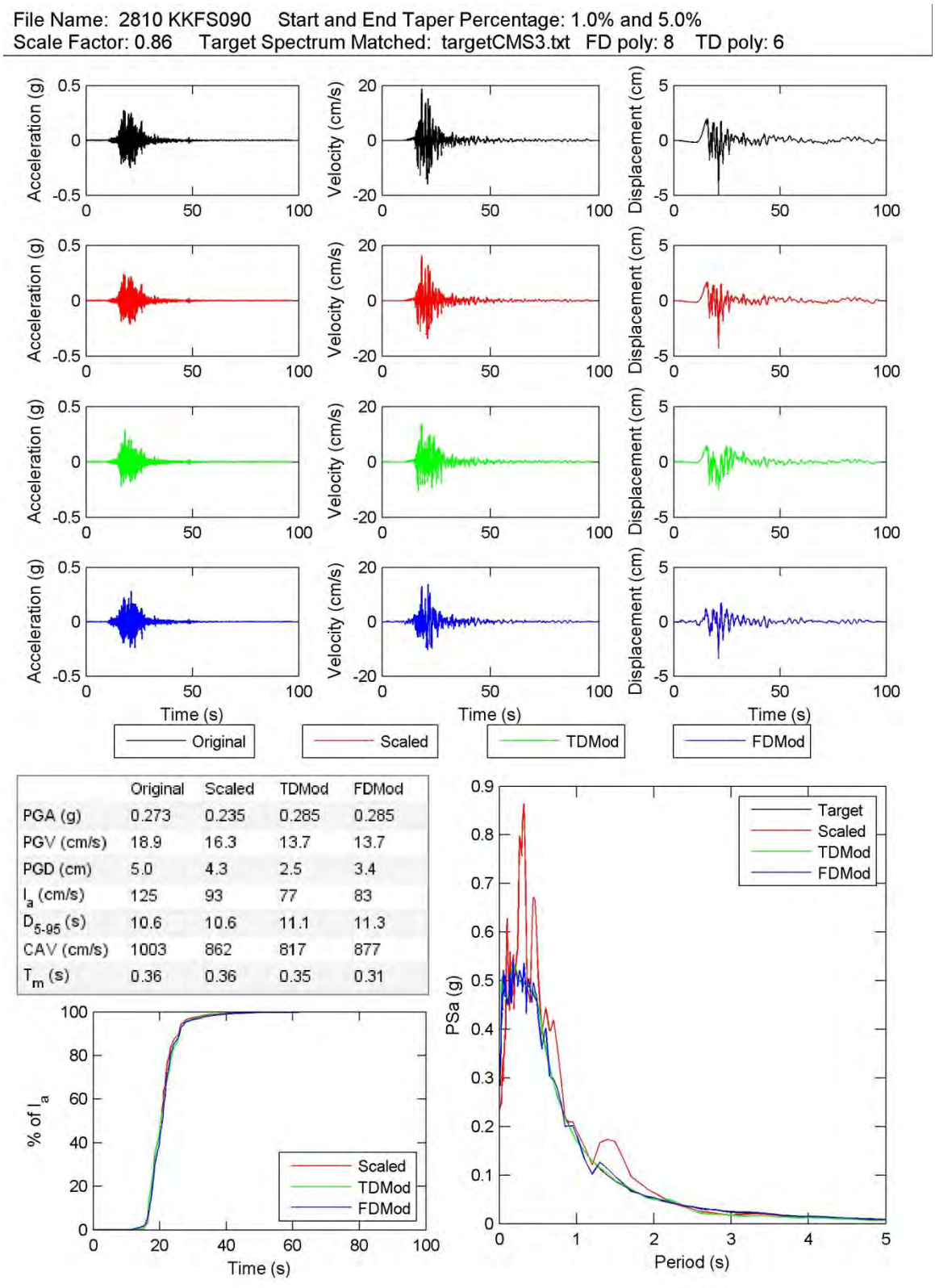

Figure 3.7. One-page output summary in .jpeg file generated by GMM for an example ground motion.

CHAPTER 4
Impact of Modification on Ground Motion Characteristics

This chapter examines the impact of modification on the ground motion characteristics of the seed motion. It is important to understand the impact of modification on the ground motion characteristics because the characteristics (e.g., *PGV*) are commonly used in empirical equations to predict the seismic responses of geotechnical systems (e.g., Saygili and Rathje 2008, Athanasopoulos-Zekkos and Saadi 2012). Based on previous research by Carlson et al. (2014a), spectral mismatch appears to have a significant impact on the effects of ground motion modification. The impact of modification and spectral mismatch on the ground motion characteristics of seed ground motions are examined for three earthquake scenarios, approximately one hundred ground motions for each scenario scaled using three different factors, and five target spectra with varying shapes. Regression equations are developed to describe the relationship between the ground motion characteristics of the modified motions and spectral mismatch.

4.1 Methodology

4.1.1 Earthquake Scenarios

Three earthquake scenarios were selected as a basis to investigate the impact of modification on the characteristics of ground motions. For each scenario, approximately 100 ground motions representative of that scenario were selected. Each ground motion was scaled using different scaling factors and then matched to five different target spectra using two modification techniques. The observed changes in critical ground motion characteristics caused by modification were studied.

The first scenario is a shallow crustal earthquake that is relatively common for a site in California (moment magnitude (M_w) of 7.1 and hypocentral source-to-site distance (R_{hyp}) of 12.5 km). The second scenario is a major earthquake in a subduction zone (8.7 M_w, 28.0 km R_{hyp}).

These two scenarios were used to investigate relationships between the spectral mismatch (i.e., the mismatch between the response spectra of the ground motions and the target spectra) and modified ground motion characteristics and develop equations to describe the relationships. A third scenario representative of an earthquake in a stable continental region in the Central and Eastern United States (CEUS) (7.1 M_w, 41.4 km R_{hyp}) was used to validate the general applicability of the proposed relationships. The CEUS scenario is very different than the other two scenarios and, as is the case with all typical CEUS earthquake scenarios, the availability of representative CEUS ground motions is limited. Thus, the criteria used for the ground motion selection process needed to be greatly relaxed to identify ground motions that could potentially be used for such a scenario. The changes in the ground motion characteristics (i.e., the modified-to-scaled ground motion characteristic ratios) with respect to spectral mismatch observed for this scenario were compared to the equations developed using the other two scenarios.

4.1.1.1 Scenario I: Shallow Crustal Earthquake

A site in Los Angeles, California (33.9°N, 118.4°W), shown in **Figure 4.1**, was used in the development of the first earthquake scenario. The site represents a location in an active tectonic region with many ground motions from shallow crustal earthquake events previously recorded. A deaggregation for a 2% probability of exceedance in 50 years earthquake was performed (USGS 2014a) for a soil profile assumed to be comprised of rock (i.e., NEHRP site class BC (FEMA 2004)) and for a period of 1 second. The results of the deaggregation are shown in **Figure 4.2**. For this site and a target period of 1 second, the mean earthquake event was computed to have an M_w of 7.1 and R_{hyp} of 12.5 km. Earthquake events along the Santa Monica Basin Section of the Palos Verdes fault (Treiman and Lundberg 1998), also shown in **Figure 4.1**, had the largest contribution to the mean event. A similar mean earthquake event (7.0 M_w, 10.9 km R_{hyp}) was calculated for a period of 0.5 seconds. The mean earthquake event for a target period of 1 second was used in the development of the target spectra and selection of motions.

Five alternative target spectra were developed for this scenario to produce a variety of spectral shapes and large range of spectral mismatch. The five elastic, 5% damped target spectra developed for scenario I are shown in **Figure 4.3**. The following target spectra are used because they are commonly used in practice:

- Uniform hazard spectra (UHS) with 2% and 10% probabilities of exceedance in 50 years: The UHS were calculated using the United States Geological Survey (USGS) website (USGS 2014b).
- A mean response spectrum calculated using attenuation relationships (MA): The 7.1 M_w, 12.5 km R_{hyp} mean earthquake event and equal contributions from four Next Generation Attenuation (NGA) relationships (Abrahamson and Silva 2008, Boore and Atkinson 2008, Campbell and Bozorgnia 2008, Chiou and Youngs 2008) were used to calculate the MA target spectrum. Based on information for the Palos Verdes fault, a strike-slip fault (i.e., dip angle of 85°) assumed to propagate to the surface and have a width of 15 km was used as input to the NGA relationships. The shear wave velocity in the top 30 m (V_{S30}) was set to 760 m/s in these relationships (i.e., NEHRP site class BC (FEMA 2004)).
- A conditional mean spectrum (CMS; Baker 2011): The MA response spectrum was conditioned on the 2% UHS at a target period of 1 second to calculate the CMS. The mean ($\mu_{\ln Sa,MA}$) and standard deviation ($\sigma_{\ln Sa,MA}$) of the MA spectrum were used to calculate the number of standard deviations (ε) between the spectral accelerations of the MA and 2% UHS ($\ln(Sa_{2\%UHS})$) at the target period (T^*) using **Equation 4.1** (Baker 2011).

$$\varepsilon(T^*) = \frac{\ln\left(Sa_{2\%UHS}(T^*)\right) - \mu_{\ln Sa,MA}(T^*)}{\sigma_{\ln Sa,MA}(T^*)} \quad (\mathbf{4.1})$$

  The CMS was calculated by taking the exponential of the $\mu_{\ln Sa,CMS}$ values calculated in **Equation 4.2** (Baker 2011).

$$\mu_{\ln Sa,CMS}(T_i) = \mu_{\ln Sa,MA}(T_i) + \rho(T_i, T^*)\varepsilon(T^*)\sigma_{\ln Sa,MA}(T_i) \quad (\mathbf{4.2})$$

  $\rho(T_i,T^*)$ represents the correlation between T^* and other periods (T_i). For this study, the more refined model for $\rho(T_i,T^*)$ (Baker and Jayaram 2008) was used. A CMS was also calculated using a target period of 0.5 seconds (and the corresponding mean earthquake event) and had some differences from the CMS for a target period of 1 second (see **Figure 4.4**).
- A mean plus one standard deviation response spectrum calculated using the Seed et al. (1997) procedure (Seed + σ): The Seed + σ spectrum was calculated for a stiff soil profile (i.e., site class B in Seed et al. (1997)) using the *PGA* for a rock site from the NGA relationships. The spectral accelerations were multiplied by 1.2 to obtain the mean plus one standard deviation response spectrum and have larger spectral accelerations than the other target spectra for longer periods.

Ground motions recorded for events with M_w between 6.6 and 7.7, R_{hyp} between 15 and 35 km, and soil profiles with NEHRP site class D (FEMA 2004) or higher were downloaded from the PEER NGA database (Chiou et al. 2008). Motions recorded at sites with R_{hyp} less than 15 km were not selected to remove any near-fault effects from the results (Somerville et al. 1997, Bray and Rodriguez-Marek 2004). R_{hyp} was used instead of epicentral source-to-site distance to account for depth to the origin of the earthquake (Bommer and Akkar 2012). Recordings for stations with Joyner-Boore distances (R_{JB}; Joyner and Boore 1981) less than 7 km were also removed from the selection. The R_{JB} criterion was included to avoid using motions from events where faulting extended below the station. **Table 4.1** provides a summary (i.e., M_w, R_{hyp}, type of faulting) of the 54 pairs of earthquake recordings in the PEER database that match the specified criteria. Eleven different earthquakes are represented in this selection and a majority of the stations (about 75%) are from regions dominated by shallow crustal events. Both horizontal components of ground motions recorded at each of these stations were downloaded to produce a suite of 108 motions. Information for all 108 ground motions used in this scenario, including the original ground motion characteristics (e.g., *PGA*, I_a, etc.), is shown in **Table 4.2**. The acceleration response spectra of the selected, unscaled ground motions are plotted with the target spectra in **Figure 4.5**.

Each motion was scaled using three different factors. First, motions were scaled to minimize the error between their acceleration response spectra and each target spectrum. Root mean squared error (*RMSE*), shown in **Equation 4.3**, was used to quantify the difference between the spectra of the scaled ground motions and the target.

$$RMSE = \sqrt{\frac{\sum_{i}^{n_s}\left[\ln\left(Sa_{tar}\left(T_i\right)\right) - \ln\left(Sa_{rec}\left(T_i\right)\right)\right]^2}{n_s}} \quad \textbf{(4.3)}$$

$Sa_{tar}(T_i)$ and $Sa_{rec}(T_i)$ represent the spectral acceleration at the ith period, T_i, for the target spectrum and scaled ground motion response spectrum, respectively, and n_s represents the number of spectral points. As mentioned in **Section 3.2**, 108 equally spaced (logarithmically) spectral points from 0.01 to 5 seconds were used for this study. The motions were multiplied by scaling factors ranging from 0.2 to 15 in increments of 0.01 to find the optimum scaling factor (i.e., the scaling factor that minimized *RMSE*) for each target spectrum. The scaled response spectra and their medians are plotted with the target spectra in **Figure 4.6**. The optimum scaling

factors for the motions for each target spectrum are provided in **Table 4.3**. The selected motions were also scaled by a factor of 0.5 and a factor of 2 to produce a larger range of spectral mismatch for each target spectrum. **Figure 4.7** shows the three different scaled spectra for an example ground motion with *RMSE* values included. For each target spectrum, the three scaled ground motions for each motion in the suite were modified using both the TD and FD techniques to match the target. The combination of 108 ground motions, five target spectra, and three scaling factors resulted in a suite of 1620 TD-modified ground motions and a suite of 1620 FD-modified ground motions.

4.1.1.2 Scenario II: Subduction Zone

A site in Tillamook, Oregon (45.5°N, 123.9°W) was used for the second scenario. A deaggregation for an earthquake with 2% probability of exceedance within 50 years was performed (USGS 2014a) for a soil profile assumed to be comprised of soft rock (i.e., NEHRP site class C (FEMA 2004)) and for a period of 0.5 seconds. The results of the deaggregation are shown in **Figure 4.8**. The mean earthquake event for this site and target period was computed to be an 8.7 M_w, 28.0 km R_{hyp} event.

Like scenario I, five target spectra were developed for scenario II. The five target spectra used for scenario II are the following (shown in **Figure 4.9**):

- 2% and 10% UHS: The UHS were calculated using the USGS website (USGS 2014b).
- A MA response spectrum plus one standard deviation (MA + σ): Four equally weighted attenuation relationships for subduction zones (Youngs et al. 1997, Atkinson and Boore 2003, 2008, Atkinson and Macias 2009, Ghofrani and Atkinson 2014) were used to calculate the MA for the mean earthquake event. For these attenuation relationships, an 8.7 M_w interface earthquake event with a focal depth of 10 km in a forearc region (i.e., near-site event) was assumed to occur 28.0 km away from a site with a V_{S30} equal to 700 m/sec (i.e., NEHRP site class C (FEMA 2004)). The *PGA* for a rock site calculated using the Youngs et al. (1997) attenuation relationship was used in the Atkinson and Boore model (2003, 2008). Because the MA spectrum had very similar spectral accelerations to the 10% UHS and alternative spectra with different frequency and intensity were needed for the purpose of this study, the MA + σ spectrum was used.

- A CMS (Baker 2011): The MA response spectrum developed using the attenuation relationships was conditioned on the 2% UHS at a target period of 0.5 seconds to calculate the CMS. The same procedure used for scenario I was used to calculate the CMS for this scenario.
- A mean response spectrum calculated using the Seed et al. (1997) procedure (Seed): The Seed et al. (1997) target spectrum was developed for a stiff soil (i.e., site class B in Seed et al. (1997)) in this scenario using the *PGA* for a rock site from the Youngs et al. (1997) attenuation. The mean spectrum from the Seed et al. (1997) procedure was used in order to have different spectral intensities from the 2% UHS for longer periods.

Ground motions recorded in subduction zones for earthquake events with M_w greater than 7.5, R_{hyp} between 30 and 125 km, and soil profiles with NEHRP site class D (FEMA 2004) and above were downloaded from the PEER NGA database (Chiou et al. 2008). Motions were also downloaded from the Consortium of Organization for Strong Motion Observation Systems (COSMOS) database (COSMOS 2014) to increase the total number of earthquake recording pairs to 55. Any motions from stations known to have R_{JB} less than 14 km were not included in the selection. Information for the 55 pairs of earthquake recordings matching the criteria for this scenario is shown in **Table 4.4**. Both horizontal components of ground motions recorded at each of these stations were downloaded to produce a suite of 108 motions (only one component of motion could be downloaded for two of the stations from the Denali, AK event). Some of the motions downloaded from COSMOS were filtered prior to being modified by first shifting the mean acceleration to zero then applying a 4^{th} order Butterworth filter with low- and high-pass filters of 40 and 0.1 Hz, respectively, using SeismoSignal (SeismoSoft 2013). The type and frequencies of the filter were selected based on the filters used for the corrected motions in the PEER and COSMOS databases. The filtered acceleration time histories were then baseline corrected using polynomial functions to remove any permanent displacement in the raw data or possibly introduced by the filtering process. Four motions from each of the Peru Coast and Valparaiso, Chile events could not be satisfactorily corrected, so they were removed from the suite of motions. Information for the suite of 100 ground motions used in scenario II, including the original ground motion characteristics, is shown in **Table 4.5**. The acceleration response spectra of the selected, unscaled motions are plotted with the target spectra in **Figure 4.10**.

The motions for the second scenario were scaled using the same procedure described in **Section 4.1.1.1** (i.e., three scaling factors applied to each motion for each target spectrum). The optimally scaled response spectra for the suite of ground motions and their medians are plotted with the different target spectra in **Figure 4.11**. The optimum scaling factors range from 0.4 to 20 for the motions in scenario II. The optimum scaling factors and the minimum *RMSE* values for the motions used in scenario II are shown in **Table 4.6**.

4.1.1.3 Scenario III: Stable Continental Region

Scenario III is representative of an earthquake event in a stable continental region outside Charleston, South Carolina (33.3°N, 80.6°W). A deaggregation for a 2% probability of exceedance in 50 years earthquake was performed (USGS 2014a) for a profile assumed to be comprised of rock (i.e., NEHRP site class BC (FEMA 2004)) and a period of 0.5 seconds. The results of the deaggregation are shown in **Figure 4.12**. The mean earthquake event for this site has an M_w of 7.1 and R_{hyp} of 41.4 km.

Five new target spectra were developed for scenario III. The five target spectra are the following and are shown in **Figure 4.13**:

- 2% and 10% UHS: The UHS were calculated using the USGS website (USGS 2014b).
- A MA + σ response spectrum: Four attenuation relationships for eastern North America (Campbell 2003, 2004, Atkinson and Boore 2006, 2007, Campbell 2007, Pezeshk et al. 2011) were used to calculate a MA target spectrum for the mean earthquake event. For these attenuation relationships, R_{hyp} was assumed to be the closest distance to the rupture plane/fault and V_{S30} was set to 760 m/s (i.e., NEHRP site class BC (FEMA 2004)). For the 2007 Campbell model, the following assumptions were also made:
  - The sediment depth ($Z_{2.5}$) was estimated using the relationships developed by Campbell and Bozorgnia (2007).
  - The fault type was unknown, so indicator variables for reverse or reverse-oblique and strike-slip fault mechanisms (F_{RV} and F_{SS}, respectively) were set to 0.5.
  - R_{JB} was assumed to be roughly half of R_{hyp} (i.e., 20.2 km).
  - The depth to the top of the rupture plane (Z_{TOR}) was assumed to be 1 km.
  - The average dip of the rupture plane (δ) was assumed to be 80°.

Site amplification factors were applied to the spectra developed for the 2003 Campbell and 2011 Pezeshk et al. models to convert them from NEHRP site class A to NEHRP site class BC (FEMA 2004). The calculated spectral accelerations were multiplied by factors developed by Hashash and Moon (2011) for an upland profile with a depth of 500 m. Short-period site amplification factors were used for periods less than or equal to 0.4 s, while long-period site amplification factors were used for periods greater than or equal to 0.5 s. Due to uncertainty in the application of the site amplification factors, the Campbell (2003) and Pezeshk et al. (2011) models were each given a weight of 0.2 in the calculation of the MA target spectrum while the other two models were each given a weight of 0.3. Since the MA had very similar spectral accelerations to the 10% UHS, the MA + σ target spectrum was used for scenario III.

- A CMS (Baker 2011): The MA response spectrum was conditioned on the 2% UHS at a target period of 0.5 seconds to calculate the CMS for scenario III. The CMS developed for scenario III is not smooth like it is for the other scenarios as a result of the response spectra for the Campbell (2003) and Pezeshk et al. (2011) models and the Atkinson and Boore (2006) and Campbell (2007) models having peaks at 0.05 and 0.2 seconds, respectively, as shown in **Figure 4.14**. Conditioning the MA response spectrum on the much larger 2% UHS amplifies the peaks at these periods.
- A Seed response spectrum (Seed et al. 1997): The mean response spectrum using the Seed et al. (1997) procedure was developed for this scenario using the *PGA* for a rock site from the Campbell (2003) and Pezeshk et al. (2011) attenuations and a stiff soil profile (i.e., site class B in Seed et al. (1997)). The mean spectrum from the Seed et al. (1997) procedure was used in order to have spectral intensities closer to (but still larger than) the other target spectra for longer periods.

Ground motions from earthquake events in stable continental regions with M_w between 5.0 and 8.0, R_{hyp} between 15 and 200 km, and NEHRP site class D (FEMA 2004) or higher were downloaded from the PEER NGA database (Chiou et al. 2008). Recordings with very small R_{JB} (i.e., less than about 5 km) were not included in the initial selection. Recordings matching the above criteria were also downloaded from the COSMOS (COSMOS 2014) and European Strong Motion (ESD; Ambraseys et al. 2001) databases. Additionally, some recordings from shallow active crustal and subduction regions were included in the initial selection. To increase the

number of recordings from the CEUS region in the initial selection, recordings from other regions that were modified to be representative of expected CEUS recordings as part of a study by McGuire et al. (2001) were included. The recordings selected from the McGuire et al. (2001) study were from earthquake events different from those of the recordings already included and recorded at rock sites with M_w and R_{hyp} matching the previously established criteria. A summary of the 119 recording pairs that match the criteria for this scenario is given in **Table 4.7**. Both horizontal components of ground motions recorded at each of these stations were downloaded and baseline corrected, if necessary (all the motions were previously filtered). Motions that could not be satisfactorily corrected (i.e., exhibited permanent acceleration, permanent displacement, etc.) were removed from the initial selection. As a result, only 213 motions from the 119 recordings were considered acceptable for use. The numbers of acceptable ground motions for each earthquake event are shown in **Table 4.7**.

The optimal scaling factors were calculated for all 213 ground motions for the CMS then ranked from smallest to largest calculated *RMSE*. No more than 12 motions were selected from each earthquake event. Also, motions with optimal scaling factors greater than 30 were dismissed. As a result, 72 ground motions from earthquake events in stable continental regions were selected. Additionally, four motions with the smallest *RMSE* from each of the Landers, Loma Prieta, and Hector Mine events and two motions with the smallest *RMSE* from the Chi-Chi, Taiwan event were included to increase the number of ground motions for the final suite of motions. Eight synthetic motions from the CEUS study (McGuire et al. 2001) with the smallest *RMSE* were also selected, bringing the total number of ground motions in the suite to 94. Information for the final suite of 94 ground motions used in scenario III is provided in **Table 4.8**. The acceleration response spectra of the selected, unscaled motions are plotted with the target spectra in **Figure 4.15**.

The motions for scenario III were scaled using the calculated optimal scaling factors then modified to match the five target spectra. The scaled response spectra and their medians are plotted with the different target spectra in **Figure 4.16**. The optimal scaling factors for the motions for each target spectrum range from 0.3 (for the 10% UHS spectrum) to 47 (for the 2% UHS and Seed spectra) and are provided in **Table 4.9**. A scaling factor of 0.5 and a scaling factor of 2 were also applied to the motions prior to matching to the target spectra to increase the range of spectral mismatch.

4.1.1.4 Observations in Response Spectra and Time Histories of Modified Motions

Overall, 4530 TD-modified and 4530 FD-modified ground motions matched to spectra with different shapes and amplitudes were generated for this study (1620, 1500, and 1410 ground motions for scenarios I, II, and III, respectively). The response spectra for some of these modified ground motions could not be matched to certain target spectra. In total, 495 out of 4530 (i.e., 11%) TD-modified ground motions (125, 222, and 148 motions for scenarios I, II, and III, respectively) and 117 out of 4530 (i.e., 3%) FD-modified ground motions (41, 22, and 54 motions for scenarios I, II, and III, respectively) were rejected from the study.

It was observed that there were two common problems with the rejected TD-modified motions:

- Spike in the response spectrum of the TD-modified motion at very short periods: Since a maximum frequency of 35 Hz (i.e., approximately 0.03 seconds) was used for TD modification in this study, the response spectra for 321 TD-modified motions were noticeably larger than the target at very short periods (i.e., 0.1 seconds). This mainly occurred when the scaled response spectrum prior to matching was much larger than the target in the short period range (e.g., motions in scenario II scaled by 2 then matched to the 10% UHS). The unmatched response spectrum for an example TD-modified ground motion with a spike at shorter periods is shown in **Figure 4.17** along with the response spectrum of the scaled ground motion. Only 193 of these 321 motions were judged to have large enough differences to be removed (3, 120, and 70 motions from scenarios I, II, and III, respectively).
- Response spectra of the scaled and TD-modified motions similar for longer periods: For scenarios I, II, and III, 174, 200, and 213 TD-modified ground motions, respectively, had response spectra that were similar to the scaled response spectrum in the long period range. For the third pass of TD modification in this study (i.e., matching the target spectrum between 0.03 and 5 seconds), the adjustments to the long period range of the spectra for some motions caused larger mismatches to develop in the short period range. Since the overall mismatch was not improved in the third pass of TD modification for these motions, their response spectra for periods greater than 2 seconds were not modified. For many of these motions, this resulted in much larger or smaller spectral values than the target spectrum as shown in **Figure 4.18**. A total of 243 TD-modified motions (80, 90, and 73 from scenarios I,

II, and III, respectively) had significant differences between the spectra and were rejected. This behavior also led to the $d(t)$ of the TD-modified motion being almost identical to that of the scaled motion (see **Figures 4.18b** and **4.18c**) as a result of the correlation between displacements and the long period range (Chopra 2007). Since FD modification was performed over the entire range of periods for multiple iterations, this behavior was observed for only a few FD-modified motions.

Other modified motions had systematic errors in their $a(t)$ and $d(t)$ despite generally matching the target spectrum. These motions were still included in this study (provided their response spectra matched the target) to include extreme cases and highlight the effects of modification for large mismatches. The $a(t)$ and $d(t)$ of the TD- and FD-modified motions were observed to have the following errors:

- $a(t)$ of TD-modified motion has short pulses with large amplitudes: This behavior was observed for 1564 TD-modified motions, particularly for the motions scaled by a factor of 0.5 prior to modification (1103 motions). When the scaled response spectrum is significantly smaller than the target, the amplitudes of the wavelets added during the TD modification process must be significantly larger than the $a(t)$ of the scaled motion in order to match the much larger target. The $a(t)$ of the TD-modified motions for these cases are essentially the correction wavelets added during the modification process. An example TD-modified ground motion with this observed behavior is shown in **Figure 4.19**. One hundred sixty-two of these motions were rejected because they did not match the target spectrum.
- $a(t)$ of TD-modified motion is constrained by target *PGA*: Several scaled ground motions had significantly larger *PGA* than the target spectra, particularly the motions scaled by 2 relative to the MA or 10% UHS. For $a(t)$ of scaled motions with several values larger than the target *PGA*, the post-processing step of scaling the peak value along with other values larger than the target *PGA* to the target *PGA* constrains the $a(t)$ of the TD-modified motions. This results in the $a(t)$ of the TD-modified motions having several peaks equal to the target *PGA* (218 TD-modified motions in total, with 142 being removed). This behavior is illustrated in **Figure 4.20**.
- Significantly smaller values for the $d(t)$ of the FD-modified motions: The *PGD* of 880 FD-modified motions were observed to be significantly less than those of the scaled motions (only 3 of these motions were removed). As discussed in Carlson et al. (2014a), motions with

response spectra larger than the target in the long period range led to a large decrease in the *PGD* for the FD-modified motions due to the addition of continuous sinusoidal wavelets. **Figure 4.21** shows the $d(t)$ and response spectra of scaled and FD-modified ground motions for an example motion where this behavior is observed.

- Baseline corrected $d(t)$ of the modified motion not satisfactory: For 482 TD-modified (1, 307, and 174 motions from scenarios I, II, and III, respectively) and 453 FD-modified motions (0, 286, and 167 motions from scenarios I, II, and III, respectively), using up to a 9^{th} order polynomial function for baseline correction did not lead to a satisfactory $d(t)$. An extreme example of this behavior is shown in **Figure 4.22**. Over half of the motions (approximately 54% and 51% for TD and FD modification, respectively) for which this behavior is observed are from the Tohoku, Japan or Tokachi-oki, Japan events. Motions from these events generally have a very long duration (over 200 seconds) and the motions from the Tohoku, Japan event have two distinct pulses of acceleration. Example $a(t)$ of motions from each of these events are shown in **Figure 4.23**. One hundred fifty-seven TD-modified motions (1, 131, and 25 motions from scenarios I, II, and III, respectively) and 46 FD-modified motions (15 and 31 motions from scenarios II and III, respectively) with this behavior were rejected.

The overall conclusion from these observations is that significant differences in the amplitude and shape between the response spectra of the scaled ground motions and target are more likely to result in numerical instabilities, incomplete matching, or unrealistic modified ground motions.

4.1.2 Data Analysis

Ground motion characteristics were calculated for the scaled, TD-modified, and FD-modified motions. The ground motion characteristics investigated in this study include *PGV*, *PGD*, I_a, $D_{5\text{-}95}$, *CAV*, and T_m which are described in more detail in **Section 3.2**. These characteristics were selected because they describe the amplitude (e.g., *PGV* or *PGD*), duration (e.g., $D_{5\text{-}95}$), frequency content (e.g., T_m), and energy (e.g., I_a or *CAV*) of the ground motions. *PGA* was not studied for this portion of the research because the *PGA* of the modified motions were locally scaled to the target *PGA* at the end of modification, as detailed in **Section 3.3.2**. Ratios of the modified-to-scaled ground motion characteristics were calculated for each ground

motion to assess the impact of modification. The modified motions are compared to the scaled motions to investigate any systematic bias between the modified and scaled ground motions since current practice commonly uses selected suites of scaled ground motions. The modified-to-scaled ground motion characteristic ratios were also plotted versus spectral mismatch to evaluate the impact of spectral mismatch on the ground motion characteristics resulting from modification.

4.1.2.1 Regression Equation Development

OriginPro 9.1.0 (OriginLab 2013) was used in the development of regression equations relating the modified-to-scaled ground motion characteristic ratios to the spectral mismatch. Equations with linear (**Equation 4.4**), parabolic (**Equation 4.5**), exponential (**Equation 4.6**), exponential decay (**Equation 4.7**), logarithmic (**Equation 4.8**), linear-exponential (**Equation 4.9**), and shifted power (**Equation 4.10**) forms were investigated to describe the relationship between the modified-to-scaled ground motion characteristic ratios and spectral mismatch.

$$y = a + bx \tag{4.4}$$

$$y = a + bx + cx^2 \tag{4.5}$$

$$y = a + b\exp(cx) \tag{4.6}$$

$$y = a_1 \exp\left(-\frac{x}{b_1}\right) + a_2 \exp\left(-\frac{x}{b_2}\right) + c \tag{4.7}$$

$$y = b\ln(x - a) \tag{4.8}$$

$$y = ae\left(-\frac{x}{b}\right) + c + dx \tag{4.9}$$

$$y = a(1 + x)^b \tag{4.10}$$

y represents the modified-to-scaled ground motion characteristic ratio and x represents the spectral mismatch. The terms a, b, c, d, a_1, a_2, b_1, and b_2 are coefficients calculated during the regression process. Chi-square minimization was employed to calculate the regression equations. In this process, the coefficients are iteratively estimated until the residual sum of squares (*RSS*), given in **Equation 4.11**, divided by the degrees of freedom (*DOF*; *DOF* = number of ground motions - number of coefficients in the regression equation) reaches a minimum value.

$$RSS = \sum_{i=1}^{DOF_T} \left(y_i - \hat{y}_i \right)^2 \quad \textbf{(4.11)}$$

$\hat{y}$ represents the ground motion characteristic ratio estimated by the regression equation. DOF_T represents the total number of ground motions used in the development of the regression equation.

The adjusted coefficient of determination (R^2) was calculated for the regression equations for the different functional forms using **Equations 4.12** and **4.13**.

$$R^2 = 1 - \frac{RSS / DOF}{TSS / DOF_T} \quad \textbf{(4.12)}$$

$$TSS = \sum_{i=1}^{DOF_T} y_i^2 \quad \textbf{(4.13)}$$

For each ground motion characteristic, R^2 values of the regression equations resulting from the different functional forms were compared to assess which form led to the least amount of dispersion in the modified-to-scaled ground motion characteristic ratios (i.e., larger R^2). Regression equations with coefficients that have significance levels above 0.05 were not selected because the coefficients were not statistically significant. Finally, residuals (i.e., y - $\hat{y}$) were calculated to ensure that they were uniformly distributed about zero (i.e., they did not exhibit any bias).

4.1.2.2 Residual Analyses

The residuals were also used to calculate standard deviations for the regression equations. Residuals were grouped into spectral mismatch bins with intervals such that at least 75 data points populated each bin. The standard deviations of the residuals were calculated for each bin then plotted against spectral mismatch. Best-fit curves were calculated for the standard deviations of the residuals and used to define the standard deviations of the regression equations.

The dependency of the modified-to-scaled ground motion characteristic ratios on M_w, R_{hyp}, fault type, and scale factor were also examined using the residuals. Residuals for the selected regression equations were plotted against M_w, R_{hyp}, and scale factor and fit with lines. The slopes of the best-fit lines for the residuals were examined to assess whether or not the regression equations should include terms for the M_w, R_{hyp}, and scale factor. Best-fit lines with small slopes signify that the parameter has no considerable impact on the estimated modified-to-

scaled ground motion characteristic ratios relative to spectral mismatch and thus, its inclusion in the regression equation is not necessary. Likewise, median residuals for motions from the different fault types were calculated to assess if the fault type should be included in the regression equations.

4.2 Impact of Spectral Mismatch on Ground Motion Characteristics

4.2.1 Results for Scenario I

The modified-to-scaled ratios for *PGV*, *PGD*, I_a, *CAV*, $D_{5\text{-}95}$, and T_m, for the motions in scenario I are first plotted versus the ground motion characteristics of the corresponding scaled motions in **Figures 4.24** to **4.29**, respectively, for the different target spectra and scaling factors. Well-defined trends, which are similar for each target spectrum, are observed in the relationships between the modified-to-scaled ground motion characteristic ratios and the characteristics of the scaled ground motions for both modification techniques. The slopes of these trends vary with the ground motion characteristic and modification technique, but appear to be independent of the scaling factor applied to the ground motion. Generally, as the ground motion characteristic of the scaled ground motion increases, the modified ground motion has a smaller characteristic value relative to that of the scaled ground motion. This is expected since many of these characteristics are indicators of the intensity of the motion. A motion with a larger intensity should be decreased during modification to match the target spectrum, leading to a modified ground motion with smaller characteristic values. Since the observed trends are very similar for each of the target spectra, relating the effects of modification on the ground motion characteristics to a metric describing the target spectrum may remove this dependency. Therefore, the modified-to-scaled ground motion characteristics were also plotted against spectral mismatch.

4.2.1.1 Regression Equation Development

Figures 4.30 to **4.35** show the plots of the modified-to-scaled ratios for *PGV*, *PGD*, I_a, *CAV*, $D_{5\text{-}95}$, and T_m, respectively, versus spectral mismatch, quantified using normalized error, *NE*. The *NE* for spectral mismatch is calculated using **Equation 4.14**.

$$NE_s = \frac{\sum_{i=1}^{n_s}\left(\frac{Sa_{scaled}(T_i) - Sa_{tar}(T_i)}{Sa_{tar}(T_{avg})}\right)}{n_s} \quad \textbf{(4.14)}$$

$Sa_{tar}(T_{avg})$ represents the spectral acceleration at the average period (T_{avg}) of the target spectrum, which is given in **Equation 4.15**.

$$T_{avg} = \frac{\sum_{i=1}^{n}\left(Sa_{tar}(T_i)^2 * T_i\right)}{\sum_{i=1}^{n} Sa_{tar}(T_i)^2} \quad \textbf{(4.15)}$$

The subscript *s* indicates the *NE* was calculated for spectral mismatch. In addition to calculating the NE_s for the entire range of spectral periods, NE_s was also calculated using only short periods ($T_i \leq 0.5$ s), only intermediate periods (0.5 s $\leq T_i \leq$ 3.0 s) and only long periods (3.0 s $\leq T_i$). Negative NE_s values for any period range indicate that the scaled response spectrum is smaller than the target spectrum in that period range and must be increased during modification while positive NE_s values indicate that the scaled response spectrum is larger than the target spectrum and must be decreased during modification. **Figure 4.7** shows example response spectra with negative and positive values of NE_s.

Additional spectral mismatch metrics discussed in **Section 3.4** were also investigated for the different period ranges. **S**pecifically, *TVM* (Oberkampf and Trucano 2002; Green et al. 2011), *imRMSE*, and *ERFCM* (Olsen and Mayhew 2010) were considered. TVM_s, $imRMSE_s$, and $ERFCM_s$ for spectral mismatch are calculated using **Equations 4.16**, **4.17**, and **4.18**, respectively.

$$TVM_s = \frac{\sum_{i=1}^{n_s}\left[1 - \tanh\left(\frac{\left|Sa_{scaled}(T_i) - Sa_{tar}(T_i)\right|}{Sa_{tar}(T_i)}\right)\right]}{n} \quad \textbf{(4.16)}$$

$$imRMSE_s = \frac{1}{\exp\sqrt{\frac{\sum_{i=1}^{n_s}\left(Sa_{scaled}(T_i) - Sa_{tar}(T_i)\right)^2}{\sum_{i=1}^{n_s} Sa_{tar}(T_i)^2}}} \quad \textbf{(4.17)}$$

$$ERFCM_s = \frac{\sum_{i=1}^{n_s}\left[erfc\left(\frac{2*\left|Sa_{scaled}(T_i) - Sa_{tar}(T_i)\right|}{\left|Sa_{scaled}(T_i)\right| + \left|Sa_{tar}(T_i)\right|} \right)\right]}{n_s} \quad \textbf{(4.18)}$$

TVM_s, $imRMSE_s$, and $ERFCM_s$ values approach 0 when the scaled response spectrum is larger than the target spectrum and values of 0.24, 0.37, and 0, respectively, when the scaled response spectrum is smaller than the target spectrum. NE_s was used for the spectral mismatch metric in the development of the regression equations below as opposed to these three metrics because its relationship with the modified-to-scaled ground motion characteristic ratios can be described with one equation while two equations are necessary to describe the relationships when TVM_s, $imRMSE_s$, and $ERFCM_s$ are used. NE_s also produces slightly less dispersion in the modified-to-scaled ground motion characteristic ratios than the other metrics. Plots for all modified-to-scaled ground motion characteristic ratios versus all spectral mismatch metrics calculated using the different ranges of periods can be found in **Appendix A**.

As illustrated in **Figures 4.30** to **4.35**, for scenario I, the effects of spectral mismatch on the modified-to-scaled ratios for a given ground motion characteristic are well-defined for each modification technique and are largely independent of the target spectrum and scaling factor used. This is an important finding because it indicates that the effects of modification on the ground motion characteristics can be predicted using the spectral mismatch calculated for the ground motion. For many of the ground motion characteristics, when spectral mismatch equals 0, the modified-to-scaled ratios are nearly 1, indicating no change in the ground motion characteristic during modification. This is expected because a response spectrum that is similar to the target spectrum prior to modification (i.e., NE_s approximately equal to 0), will not be significantly modified, resulting in a modified ground motion with similar characteristics to the scaled motion. This observation is true for both TD and FD modification signifying that either modification technique may be appropriate to use provided the NE_s is close to 0 since both techniques have similar effects on the ground motion characteristics in this range. The modified-to-scaled ground motion characteristic ratios are generally less than 1 for positive NE_s and greater than 1 for negative NE_s. Motions with response spectra less than the target (i.e., negative NE_s) should have an increase (i.e., modified-to-scaled ratios greater than 1) in their characteristics as the spectra are increased to match the target. Likewise, the ground motion characteristics of the motions should be decreased (i.e., modified-to-scaled ratios less than 1)

when their response spectra are decreased. Also, the effects of modification on the ground motion characteristics are more sensitive to changes in NE_s for motions with negative values of NE_s. This finding may support the use of ground motions with positive NE_s since the effects of modification on the ground motion characteristics are less sensitive to changes in the NE_s in this range. For many ground motion characteristics, an exponential relationship was observed between the modified-to-scaled ratios and spectral mismatch, so the natural logarithms of the modified-to-scaled ground motion characteristic ratios were also calculated and used in the development of the regression equations. The combinations of spectral mismatch metric and period range that produced the smallest amount of dispersion in the modified-to-scaled ground motion characteristic ratios were used in the calculation of the regression equations. These combinations were NE_s over the intermediate period range ($NE_{s,IP}$) for *PGV* and T_m (shown in **Figures 4.30** and **4.35**, respectively), NE_s over the long period range ($NE_{s,LP}$) for *PGD* and $D_{5\text{-}95}$ (shown in **Figures 4.31** and **4.34**, respectively), and NE_s over the entire range of spectral periods for I_a, *CAV*, and $D_{5\text{-}95}$ (shown in **Figures 4.32**, **4.33**, and **4.34**, respectively).

The regression equations developed for the natural logarithms of the modified-to-scaled *PGV* ratios have an exponential decay functional form as shown in **Figure 4.36**. TD and FD modification have similar effects on *PGV* when the response spectrum of the ground motion in the intermediate period range is increased to match the target spectrum (i.e., negative $NE_{s,IP}$). However, when the response spectrum of the recorded motion must be decreased to match the target spectrum, FD modification generally results in a smaller *PGV* than TD modification. The regression equations for the natural logarithms of the TD- and FD-modified-to-scaled *PGV* ratios are provided in **Equations 4.19** and **4.20**, respectively.

$$\ln\left(\frac{PGV_{TD}}{PGV_{scaled}}\right) = -2.009 + 0.112\exp\left(-\frac{NE_{s,IP}}{0.247}\right) + 1.811\exp\left(-\frac{NE_{s,IP}}{2.795}\right) \pm \sigma_{PGV,TD} \qquad \textbf{(4.19)}$$

$$\ln\left(\frac{PGV_{FD}}{PGV_{scaled}}\right) = -3.028 + 0.107\exp\left(-\frac{NE_{s,IP}}{0.240}\right) + 2.799\exp\left(-\frac{NE_{s,IP}}{3.822}\right) \pm \sigma_{PGV,FD} \qquad \textbf{(4.20)}$$

$\sigma_{PGV,TD}$ and $\sigma_{PGV,FD}$ represent the standard deviations of the natural logarithms of the modified-to-scaled *PGV* ratios for TD and FD modification, respectively. The R^2 values of the regression equations developed for TD and FD modification are 0.900 and 0.919, respectively. **Table 4.10** compares the R^2 values of the regression equations developed for the modified-to-scaled *PGV*, *PGD*, I_a, and *CAV* ratios using the different functional forms (i.e., **Equations 4.4** to **4.10**).

The regression equations developed for the natural logarithms of the modified-to-scaled *PGD* ratios, shown in **Figure 4.37**, have a parabolic functional form. Unlike the other ground motion characteristics, the modified-to-scaled *PGD* ratios appeared to be related to the spectral mismatch by a power relationship (i.e., log-log relationship), so the natural logarithms of the spectral mismatch metric were also calculated. Because NE_s approaches -1, the NE_s values were shifted by +1 before calculating their natural logarithms (i.e., $\ln(NE_{s,LP} + 1)$). For ground motions with response spectra that must be decreased in the long period range to match the target (i.e., $\ln(NE_{s,LP} + 1)$ greater than 0), *PGD* is significantly reduced (over 300%) during FD modification, but only somewhat reduced (approximately 50%) during TD modification. **Equations 4.21** and **4.22** provide the regression equations for the natural logarithms of the modified-to-scaled *PGD* ratios for the TD and FD modification techniques, respectively.

$$\ln\left(\frac{PGD_{TD}}{PGD_{scaled}}\right) = \begin{cases} 0.091 - 0.645\left(\ln\left(NE_{s,LP}+1\right)\right) + \\ \quad 0.143\left(\ln\left(NE_{s,LP}+1\right)\right)^2 \pm \sigma_{PGD,TD}, & for\ \ln\left(NE_{s,LP}+1\right) \le 2.26 \\ -0.636 \pm \sigma_{PGD,TD}, & otherwise \end{cases} \quad (\mathbf{4.21})$$

$$\ln\left(\frac{PGD_{FD}}{PGD_{scaled}}\right) = -0.318 - 1.058\left(\ln\left(NE_{s,LP}+1\right)\right) + 0.023\left(\ln\left(NE_{s,LP}+1\right)\right)^2 \pm \sigma_{PGD,FD} \quad (\mathbf{4.22})$$

$\sigma_{PGD,TD}$ and $\sigma_{PGD,FD}$ represent the standard deviations of the logarithmic modified-to-scaled *PGD* ratios for TD and FD modification, respectively. The R^2 values of the selected regression equations for TD and FD modification are 0.820 and 0.912, respectively. A piecewise linear function was also investigated, and although the R^2 values of the regression equations are approximately equal to those of **Equations 4.21** and **4.22**, biases were observed in the residuals when the piecewise linear form was used.

The regression equations developed for the logarithmic modified-to-scaled I_a ratios, shown in **Figure 4.38**, have an exponential decay form. **Figure 4.38** shows that small changes in NE_s result in larger changes in the I_a when FD modification is implemented as opposed to TD modification, indicating that I_a for FD-modified motions is more sensitive to spectral mismatch. **Equations 4.23** and **4.24** present the regression equations developed for the natural logarithms of the modified-to-scaled I_a ratios for the TD and FD modification techniques, respectively.

$$\ln\left(\frac{I_{a,TD}}{I_{a,scaled}}\right) = -3.473 + 0.112\exp\left(-\frac{NE_s}{0.148}\right) + 3.335\exp\left(-\frac{NE_s}{1.926}\right) \pm \sigma_{Ia,TD} \quad (\mathbf{4.23})$$

$$\ln\left(\frac{I_{a,FD}}{I_{a,scaled}}\right) = -4.153 + 0.137\exp\left(-\frac{NE_s}{0.161}\right) + 4.028\exp\left(-\frac{NE_s}{1.454}\right) \pm \sigma_{Ia,FD} \qquad \textbf{(4.24)}$$

$\sigma_{Ia,TD}$ and $\sigma_{Ia,FD}$ represent the standard deviations of the logarithmic TD- and FD-modified-to-scaled I_a ratios, respectively. The regression equations for the natural logarithms of the modified-to-scaled I_a ratios for TD and FD modification have R^2 values of 0.965 and 0.984, respectively.

Figure 4.39 shows the regression curves developed for the natural logarithms of the modified-to-scaled *CAV* ratios, which have an exponential linear form. Like I_a, the logarithmic modified-to-scaled *CAV* ratios are more sensitive to changes in NE_s when using FD modification opposed to TD modification. The regression equations for the natural logarithms of the modified-to-scaled *CAV* ratios for the TD and FD modification techniques are given in **Equations 4.25** and **4.26**, respectively.

$$\ln\left(\frac{CAV_{TD}}{CAV_{scaled}}\right) = 0.089\exp\left(-\frac{NE_s}{0.168}\right) - 0.050 - 0.434NE_s \pm \sigma_{CAV,TD} \qquad \textbf{(4.25)}$$

$$\ln\left(\frac{CAV_{FD}}{CAV_{scaled}}\right) = 0.226\exp\left(-\frac{NE_s}{0.224}\right) - 0.158 - 0.731NE_s \pm \sigma_{CAV,FD} \qquad \textbf{(4.26)}$$

$\sigma_{CAV,TD}$ and $\sigma_{CAV,FD}$ represent the standard deviations of the logarithmic modified-to-scaled *CAV* ratios for TD and FD modification, respectively. **Equations 4.25** and **4.26** show that the natural logarithms of the modified-to-scaled *CAV* ratios are exponentially related to NE_s in the negative range, but linearly related as NE_s increases. The R^2 values of the regression equations are 0.903 and 0.976 for the TD and FD modification techniques, respectively. Although there appears to be some bias in the residuals for the FD modification technique at larger NE_s values as seen in **Figure 4.40**, there is limited data in this range to support using a different functional form.

Unlike the other ground motion characteristics, no strong trends are observed in the modified-to-scaled $D_{5\text{-}95}$ and T_m ratios with respect to spectral mismatch. **Table 4.11** lists the R^2 values of the regression equations developed for the natural logarithms of the modified-to-scaled $D_{5\text{-}95}$ ratios using NE_s and $NE_{s,LP}$ for the spectral mismatch metric and for different functional forms. The modified-to-scaled T_m ratios also differ from the other ground motion characteristics in that they do not have an exponential relationship with spectral mismatch. Therefore, the arithmetic modified-to-scaled T_m ratios were used in the development of the regression equations. The R^2 values of the regression equations calculated for the arithmetic modified-to-scaled T_m ratios using the different functional forms are shown in **Table 4.12**. The R^2 values of

the regression equations for both of these ground motion characteristics are significantly smaller than those for the other characteristics (0.3 compared to 0.9). The regression equations with the largest R^2 and limited bias in the residuals for the modified-to-scaled $D_{5\text{-}95}$ and T_m ratios are presented below for completeness. However, the use of these equations in practice to predict the $D_{5\text{-}95}$ and T_m for the modified motions is not encouraged by the author due to the much larger uncertainty (i.e., relatively small R^2 values).

The selected regression equations for the natural logarithms of the modified-to-scaled $D_{5\text{-}95}$ ratios have an exponential form and are shown in **Figure 4.41**. The exponential form is selected over the other functional forms because it leads to the least amount of bias in the residuals. The calculated modified-to-scaled $D_{5\text{-}95}$ ratios have the least amount of dispersion when using NE_s as the spectral mismatch metric for TD modification, but $NE_{s,LP}$ for FD modification. The regression curves suggest that TD modification decreases the $D_{5\text{-}95}$ of the scaled motions when their response spectra must be increased to match the target spectrum, but increases the $D_{5\text{-}95}$ when their response spectra must be decreased. This is consistent with the expected impact on ground motion duration when wavelets are added during the modification process. FD modification does not appear to cause significant changes to the $D_{5\text{-}95}$ of the scaled motions, particularly when the scaled response spectra are larger than the target in the long period range. Equations of the regression curves for the logarithmic TD- and FD-modified-to-scaled $D_{5\text{-}95}$ ratios are given in **Equations 4.27** and **4.28**, respectively.

$$\ln\left(D_{5-95,TD} / D_{5-95,scaled}\right) = 0.938 - 0.781\exp\left(-0.784 NE_s\right) \pm \sigma_{D5-95,TD} \quad (\mathbf{4.27})$$

$$\ln\left(D_{5-95,FD} / D_{5-95,scaled}\right) = 0.057 + 0.109\exp\left(-0.899 NE_{s,LP}\right) \pm \sigma_{D5-95,FD} \quad (\mathbf{4.28})$$

$\sigma_{D5\text{-}95,TD}$ and $\sigma_{D5\text{-}95,FD}$ represent the standard deviations of the natural logarithms of the modified-to-scaled $D_{5\text{-}95}$ ratios for the TD and FD modification techniques, respectively.

Figure 4.42 shows the regression curves developed for the modified-to-scaled T_m ratios, which have a shifted power form. Modification appears to increase T_m when the scaled response spectrum is smaller than the target in the intermediate period range, but decrease T_m when the spectrum is larger than the target in this range. The regression equations for the modified-to-scaled T_m ratios for TD and FD modification are provided in **Equations 4.29** and **4.30**, respectively.

$$T_{m,TD} / T_{m,scaled} = 1.059\left(1 + NE_{s,IP}\right)^{-0.517} \pm \sigma_{Tm,TD} \quad (\mathbf{4.29})$$

$$T_{m,FD} / T_{m,scaled} = 1.078\left(1 + NE_{s,IP}\right)^{-0.432} \pm \sigma_{Tm,FD} \quad \textbf{(4.30)}$$

$\sigma_{Tm,TD}$ and $\sigma_{Tm,FD}$ represent the standard deviations of the TD- and FD-modified-to-scaled T_m ratios, respectively.

The modified-to-scaled ratios for many ground motion characteristics are strongly correlated to spectral mismatch for the motions in scenario I. Furthermore, these relationships appear to be independent of the scaling factor and target spectrum considered. This is an important finding as it indicates that the spectral mismatch can be used to accurately predict the effects of modification on the ground motion characteristics. Also, ground motions with positive NE_s may be more appropriate to use since the effects of modification on the ground motion characteristics in this range are less sensitive to changes in NE_s. Both TD and FD modification techniques have similar effects on the ground motion characteristics for values of NE_s close to 0. These relationships must be studied for scenario II to support these findings for a different scenario and a completely different set of motions.

4.2.1.2 Residual Analyses

Table 4.13 shows the intervals of the spectral mismatch bins for the different metrics (e.g., NE_s, $NE_{s,IP}$, etc.) used in the calculation of the standard deviations of the residuals. Standard deviations of the residuals within each bin were calculated for TD and FD modification and plotted against $NE_{s,IP}$ for *PGV* as shown in **Figure 4.43**. The standard deviations of the residuals for both modification techniques appear to decrease exponentially before approaching a constant value (i.e., asymptotic). This asymptotic behavior was observed in the standard deviations of residuals for all the other ground motion characteristics except *PGD*. The larger standard deviations for negative spectral mismatch illustrate the larger variability in the effects of modification on the characteristics of ground motions with response spectra that are increased to match the target spectrum. Best-fit curves (**Equations 4.31** and **4.32**) were derived for the standard deviations of the residuals for the logarithmic modified-to-scaled *PGV* ratios and used to represent $\sigma_{PGV,TD}$ and $\sigma_{PGV,FD}$.

$$\sigma_{PGV,TD} = 0.223 + 0.021\exp\left(-NE_{s,IP} / 0.351\right) \quad \textbf{(4.31)}$$

$$\sigma_{PGV,FD} = 0.234 + 0.009\exp\left(-NE_{s,IP} / 0.312\right) \quad \textbf{(4.32)}$$

In deriving the best-fit curves for the standard deviations of the residuals, the significance levels of the coefficients were not considered. The regression curves developed for the natural logarithms of the modified-to-scaled *PGV* ratios with the plus and minus standard deviations included are plotted in **Figure 4.36**.

The standard deviations of the residuals for *PGD*, shown in **Figure 4.44**, for both modification techniques appear to be decreasing linearly instead of exponentially. The equations for $\sigma_{PGD,TD}$ and $\sigma_{PGD,FD}$ are provided in **Equations 4.33** and **4.34**.

$$\sigma_{PGD,TD} = 0.369 - 0.062\ln\left(NE_{s,LP} + 1\right) \quad (\mathbf{4.33})$$

$$\sigma_{PGD,FD} = 0.347 - 0.016\ln\left(NE_{s,LP} + 1\right) \quad (\mathbf{4.34})$$

The standard deviations are included with the regression curves developed for the natural logarithms of the modified-to-scaled *PGD* ratios in **Figure 4.37**.

The standard deviations of the residuals for I_a are plotted versus NE_s in **Figure 4.45**. The equations for $\sigma_{Ia,TD}$ and $\sigma_{Ia,FD}$ are provided in **Equations 4.35** and **4.36**, respectively.

$$\sigma_{Ia,TD} = 0.157 + 0.026\exp\left(-NE_s / 0.184\right) \quad (\mathbf{4.35})$$

$$\sigma_{Ia,FD} = 0.130 + 0.004\exp\left(-NE_s / 0.109\right) \quad (\mathbf{4.36})$$

The regression curves developed for the logarithmic modified-to-scaled I_a ratios with the plus and minus standard deviations included are shown in **Figure 4.38**.

Figure 4.46 shows the standard deviations of the residuals for *CAV* plotted versus *NE*. **Equations 4.37** and **4.38** respectively provide the equations for $\sigma_{CAV,TD}$ and $\sigma_{CAV,FD}$.

$$\sigma_{CAV,TD} = 0.123 + 0.031\exp\left(-NE_s / 0.261\right) \quad (\mathbf{4.37})$$

$$\sigma_{CAV,FD} = 0.115 + 0.001\exp\left(-NE_s / 0.090\right) \quad (\mathbf{4.38})$$

The plus and minus standard deviations are plotted with the regression curves developed for the logarithmic modified-to-scaled *CAV* ratios in **Figure 4.39**.

The standard deviations of the residuals for $D_{5\text{-}95}$ for both modification techniques are plotted in **Figure 4.47**. The equations for $\sigma_{D5\text{-}95,TD}$ and $\sigma_{D5\text{-}95,FD}$ are given in **Equations 4.39** and **4.40**, respectively.

$$\sigma_{D5-95,TD} = 0.225 + 0.034\exp\left(-NE_s / 0.211\right) \quad (\mathbf{4.39})$$

$$\sigma_{D5-95,FD} = 0.098 + 0.060\exp\left(-NE_{LP} / 1.387\right) \quad (\mathbf{4.40})$$

The regression curves developed for the logarithmic modified-to-scaled $D_{5\text{-}95}$ ratios and the plus and minus standard deviations are shown in **Figure 4.41**.

The standard deviations of the residuals for T_m are plotted in **Figure 4.48**. The equations for $\sigma_{Tm,TD}$ and $\sigma_{Tm,FD}$, given by the best-fit curves for the standard deviations of the residuals, are provided in **Equations 4.41** and **4.42**, respectively.

$$\sigma_{Tm,TD} = 0.188 + 0.128\exp\left(-NE_{s,IP}/0.445\right) \quad (\mathbf{4.41})$$

$$\sigma_{Tm,FD} = 0.164 + 0.327\exp\left(-NE_{s,IP}/0.803\right) \quad (\mathbf{4.42})$$

Two things to note about the residuals for T_m shown in **Figure 4.49**: there appears to be a positive bias for negative $NE_{s,IP}$ and the values of the residuals are much larger than they are for the other ground motion characteristics. Both of these observations can be attributed to using the arithmetic instead of logarithmic modified-to-scaled T_m ratios as was done for the other ground motion characteristics. The regression curves for the modified-to-scaled T_m ratios with the standard deviations included are shown in **Figure 4.42**.

4.2.2 Results for Scenario II

4.2.2.1 Regression Equation Development

The regression curves calculated for the modified-to-scaled *PGV*, *PGD*, I_a, *CAV*, $D_{5\text{-}95}$, and T_m ratios for the motions in scenarios I and II are compared in **Figures 4.50** to **4.55**, respectively. The modified-to-scaled ground motion characteristic ratios calculated for the motions in scenario II generally plot along the same curves as those for the motions in scenario I with more noticeable differences observed for the regression curves of the logarithmic TD-modified-to-scaled $D_{5\text{-}95}$ ratios and the FD-modified-to-scaled T_m ratios for the two scenarios. However, as mentioned in **Section 4.2.1.1**, the relationships for $D_{5\text{-}95}$ and T_m are not particularly strong. R^2 values of the regression equations developed for the motions in the second scenario are, in most cases, smaller than those of the regression equations developed for the motions in the first scenario due to the larger dispersion observed in the modified-to-scaled ground motion characteristic ratios.

Since the modified-to-scaled ground motion characteristic ratios for both scenarios had very similar trends, regression equations were developed using the combined set of ratios from scenarios I and II. Using the modified-to-scaled ground motion characteristic ratios from both

scenarios in the regression development leads to more robust equations because of the use of larger ranges of M_w and R_{hyp} and more ground motions. As a result, the regression equations provide more generally applicable estimates of the impact of modification on the ground motion characteristics. For all ground motion characteristics (except $D_{5\text{-}95}$ for the TD-modified motions), the R^2 values of the regression equations developed using the combined set of ratios are slightly smaller than the R^2 values of the regression equations developed for scenario I due to the inclusion of the larger dispersions in the ratios observed for scenario II.

The regression curves developed for the natural logarithms of the combined set of modified-to-scaled *PGV* ratios are plotted in **Figure 4.56**. The corresponding equations for these regression curves are provided in **Equations 4.43** and **4.44** for the TD- and FD-modified motions, respectively.

$$\ln\left(\frac{PGV_{TD}}{PGV_{scaled}}\right) = 0.254\exp\left(-\frac{NE_{s,IP}}{0.329}\right) - 0.360 - 0.366NE_{s,IP} \pm \sigma_{PGV,TD} \quad (\mathbf{4.43})$$

$$\ln\left(\frac{PGV_{FD}}{PGV_{scaled}}\right) = 0.229\exp\left(-\frac{NE_{s,IP}}{0.314}\right) - 0.437 - 0.451NE_{s,IP} \pm \sigma_{PGV,FD} \quad (\mathbf{4.44})$$

An exponential linear form is used for the regression equations developed using the combined set of ratios since the coefficients of regression equations developed with an exponential decay form have significance levels above 0.2. The R^2 values of **Equations 4.43** and **4.44** are 0.881 and 0.878, respectively.

Figure 4.57 shows the regression curves developed using the combined set of logarithmic modified-to-scaled *PGD* ratios. The equations for these regression curves are given in **Equations 4.45** and **4.46** for the TD- and FD-modified motions, respectively.

$$\ln\left(\frac{PGD_{TD}}{PGD_{scaled}}\right) = 0.158 - 0.717\left(\ln\left(NE_{s,LP}+1\right)\right) + 0.125\left(\ln\left(NE_{s,LP}+1\right)\right)^2 \pm \sigma_{PGD,TD} \quad (\mathbf{4.45})$$

$$\ln\left(\frac{PGD_{FD}}{PGD_{scaled}}\right) = -0.393 - 1.130\left(\ln\left(NE_{s,LP}+1\right)\right) + 0.016\left(\ln\left(NE_{s,LP}+1\right)\right)^2 \pm \sigma_{PGD,FD} \quad (\mathbf{4.46})$$

The regression equations have a parabolic form as they did for the regression equations in the first scenario, but the regression equation developed for the combined set of logarithmic TD-modified-to-scaled *PGD* ratios is not piecewise. **Equations 4.45** and **4.46** have R^2 values of 0.760 and 0.858, respectively.

The regression curves developed for the logarithmic modified-to-scaled I_a ratios of scenarios I and II are shown in **Figure 4.58**. The regression equations developed for the combined set of logarithmic modified-to-scaled I_a ratios for the TD- and FD-modified motions have an exponential decay form as shown in **Equations 4.47** and **4.48**, respectively.

$$\ln\left(\frac{I_{a,TD}}{I_{a,scaled}}\right) = -3.985 + 0.131\exp\left(-\frac{NE_s}{0.153}\right) + 3.809\exp\left(-\frac{NE_s}{2.546}\right) \pm \sigma_{Ia,TD} \qquad (\mathbf{4.47})$$

$$\ln\left(\frac{I_{a,FD}}{I_{a,scaled}}\right) = -4.096 + 0.119\exp\left(-\frac{NE_s}{0.155}\right) + 3.983\exp\left(-\frac{NE_s}{1.306}\right) \pm \sigma_{Ia,FD} \qquad (\mathbf{4.48})$$

The regression equations developed for the combined set of logarithmic modified-to-scaled I_a ratios for the TD- and FD-modified motions have R^2 values of 0.934 and 0.960, respectively.

The regression curves for the natural logarithms of the modified-to-scaled *CAV* ratios developed using the combined set of ratios for scenarios I and II are shown in **Figure 4.59**. **Equations 4.49** and **4.50** provide the regression equations for these curves for the TD- and FD-modified motions, respectively.

$$\ln\left(\frac{CAV_{TD}}{CAV_{scaled}}\right) = 0.060\exp\left(-\frac{NE_s}{0.151}\right) - 0.044 - 0.411NE_s \pm \sigma_{CAV,TD} \qquad (\mathbf{4.49})$$

$$\ln\left(\frac{CAV_{FD}}{CAV_{scaled}}\right) = 0.264\exp\left(-\frac{NE_s}{0.232}\right) - 0.222 - 0.709NE_s \pm \sigma_{CAV,FD} \qquad (\mathbf{4.50})$$

The regression equations developed using the natural logarithms of the combined set of TD- and FD-modified-to-scaled *CAV* ratios from scenarios I and II have an exponential linear form and R^2 values of 0.878 and 0.952, respectively.

Figure 4.60 shows the regression curves developed using the natural logarithms of the combined set of modified-to-scaled $D_{5\text{-}95}$ ratios from scenarios I and II. The regression equations for the combined set of logarithmic TD- and FD-modified-to-scaled $D_{5\text{-}95}$ ratios are provided in **Equations 4.51** and **4.52**, respectively.

$$\ln\left(D_{5-95,TD} / D_{5-95,scaled}\right) = 0.692 - 0.584\exp\left(-1.427NE_s\right) \pm \sigma_{D5-95,TD} \qquad (\mathbf{4.51})$$

$$\ln\left(D_{5-95,FD} / D_{5-95,scaled}\right) = 0.068 + 0.067\exp\left(-1.054NE_{s,LP}\right) \pm \sigma_{D5-95,FD} \qquad (\mathbf{4.52})$$

The R^2 values of the regression equations developed for the combined set of logarithmic TD- and FD-modified-to-scaled $D_{5\text{-}95}$ ratios from scenarios I and II are 0.382 and 0.084, respectively.

The regression curves developed using the combined set of modified-to-scaled T_m ratios from scenarios I and II are shown in **Figure 4.61**. The regression equations developed for the modified-to-scaled T_m ratios for the TD- and FD-modified motions have a shifted power form and are provided in **Equations 4.53** and **4.54**, respectively.

$$T_{m,TD} / T_{m,scaled} = 1.043\left(1 + NE_{s,IP}\right)^{-0.486} \pm \sigma_{Tm,TD} \quad (\mathbf{4.53})$$

$$T_{m,FD} / T_{m,scaled} = 1.202\left(1 + NE_{s,IP}\right)^{-0.397} \pm \sigma_{Tm,FD} \quad (\mathbf{4.54})$$

Equations 4.53 and **4.54** have R^2 values of 0.324 and 0.116, respectively.

Strong relationships between the modified-to-scaled ground motion characteristic ratios and spectral mismatch are also observed for scenario II. The observed trends for scenarios I and II are nearly identical, which suggests the impact of the scenario on the effects of modification is minor compared to the impact of spectral mismatch. The similarities in the trends for scenarios I and II also allow for the development of more robust regression equations using the motions from both scenarios. The developed regression equations should be validated using scenario III, which contains motions from earthquake events with a wide range of M_w and R_{hyp} located in different tectonic regimes.

4.2.2.2 Residual Analyses

Following the procedure in **Section 4.1.1.2**, the residuals for the combined set of modified-to-scaled ground motion characteristic ratios from scenarios I and II are used to calculate the standard deviations for the calculated regression equations. Since the combined set of modified-to-scaled ground motion characteristic ratios includes more ground motions, the intervals of the bins in **Table 4.13** are slightly reduced to provide a better resolution of the standard deviation of the residuals with respect to spectral mismatch. Due to the larger dispersion in the modified-to-scaled ground motion characteristic ratios in scenario II, the standard deviations of the regression equations for the combined set of ratios are generally larger. However, the standard deviations calculated for the combined set of modified-to-scaled ground motion characteristic ratios generally have the same form for the standard deviations for scenario I. The residuals were also plotted against M_w, R_{hyp}, and scale factor to assess the dependency of the regression equations developed using the combined set of modified-to-scaled ground motion characteristic ratios from scenarios I and II on these parameters. The medians of the residuals for

the different fault types were also studied to assess if a term for fault type should be included in the regression equations developed using the combination of modified-to-scaled ground motion characteristic ratios from scenarios I and II.

The standard deviations of the residuals for the combined set of logarithmic modified-to-scaled *PGV* ratios are plotted in **Figure 4.62**. Equations for $\sigma_{PGV,TD}$ and $\sigma_{PGV,FD}$ (i.e., best-fit curves shown in **Figure 4.62**) using the combined set of residuals are given in **Equations 4.55** and **4.56**, respectively.

$$\sigma_{PGV,TD} = 0.211 + 0.025\exp\left(-NE_{s,IP}/0.299\right) \quad (\mathbf{4.55})$$

$$\sigma_{PGV,FD} = 0.255 + 0.024\exp\left(-NE_{s,IP}/0.336\right) \quad (\mathbf{4.56})$$

Equations 4.55 and **4.56** have R^2 values of 0.80 and 0.68, respectively. The regression curves developed for the natural logarithms of the modified-to-scaled *PGV* ratios using data from both scenarios with the plus and minus standard deviations included are plotted in **Figure 4.56**.

Figure 4.63 shows the standard deviations of the residuals for the natural logarithms of the combined set of modified-to-scaled *PGD* ratios from scenarios I and II. The equations for $\sigma_{PGD,TD}$ and $\sigma_{PGD,FD}$ are provided in **Equations 4.57** and **4.58**, respectively.

$$\sigma_{PGD,TD} = 0.400 - 0.113\ln\left(NE_{s,LP} + 1\right) \quad (\mathbf{4.57})$$

$$\sigma_{PGD,FD} = 0.466 \quad (\mathbf{4.58})$$

Unlike the first scenario, $\sigma_{PGD,FD}$ for the combined set of residuals appears to be constant with spectral mismatch. The R^2 value for **Equation 4.57** is 0.70. Since **Equation 4.58** is constant, it has an R^2 value of 0. The standard deviations calculated using the combined set of residuals are included with the regression curves developed for the natural logarithms of the combined set of modified-to-scaled *PGD* ratios in **Figure 4.57**.

The standard deviations of the combined set of residuals for the logarithmic modified-to-scaled I_a ratios from both scenarios are plotted versus NE_s in **Figure 4.64**. **Equations 4.59** and **4.60**, provide the equations for $\sigma_{Ia,TD}$ and $\sigma_{Ia,FD}$, respectively.

$$\sigma_{Ia,TD} = 0.148 + 0.061\exp\left(-NE_s/0.224\right) \quad (\mathbf{4.59})$$

$$\sigma_{Ia,FD} = 0.178 + 0.027\exp\left(-NE_s/0.165\right) \quad (\mathbf{4.60})$$

Equations 4.59 and **4.60** have R^2 values of 0.80 and 0.74, respectively. The regression curves developed for the combined set of logarithmic modified-to-scaled I_a ratios with the plus and minus standard deviations included are shown in **Figure 4.58**.

Figure 4.65 shows the standard deviations of the residuals for the combined set of logarithmic modified-to-scaled *CAV* ratios from the first and second scenarios. **Equations 4.61** and **4.62** respectively provide the equations for $\sigma_{CAV,TD}$ and $\sigma_{CAV,FD}$.

$$\sigma_{CAV,TD} = 0.104 + 0.041\exp\left(-NE_s / 0.258\right) \quad (\mathbf{4.61})$$

$$\sigma_{CAV,FD} = 0.140 + 0.006\exp\left(-NE_s / 0.135\right) \quad (\mathbf{4.62})$$

Equations 4.61 and **4.62** have R^2 values of 0.83 and 0.59, respectively. The regression curves developed using the natural logarithms of the modified-to-scaled *CAV* ratios from scenarios I and II and the standard deviations are shown in **Figure 4.59**.

The standard deviations of the residuals calculated for the combined set of logarithmic modified-to-scaled $D_{5\text{-}95}$ ratios from scenarios I and II are plotted in **Figure 4.66**. The equations for $\sigma_{D5\text{-}95,TD}$ and $\sigma_{D5\text{-}95,FD}$ are given in **Equations 4.63** and **4.64**, respectively.

$$\sigma_{D5-95,TD} = 0.188 + 0.055\exp\left(-NE_s / 0.237\right) \quad (\mathbf{4.63})$$

$$\sigma_{D5-95,FD} = 0.107 + 0.031\exp\left(-NE_{s,LP} / 0.803\right) \quad (\mathbf{4.64})$$

The R^2 values for **Equations 4.63** and **4.64** are 0.78 and 0.82, respectively. The regression curves developed using the combined set of logarithmic modified-to-scaled $D_{5\text{-}95}$ ratios from scenarios I and II with the plus and minus standard deviations included are shown in **Figure 4.60**.

The standard deviations of the residuals for the combined set of modified-to-scaled T_m ratios from scenarios I and II are plotted in **Figure 4.67**. The equations for $\sigma_{Tm,TD}$ and $\sigma_{Tm,FD}$ (i.e., the best-fit curves for the standard deviations of the residuals) are provided in **Equations 4.65** and **4.66**, respectively.

$$\sigma_{Tm,TD} = 0.188 + 0.093\exp\left(-NE_{s,IP} / 0.348\right) \quad (\mathbf{4.65})$$

$$\sigma_{Tm,FD} = 0.224 + 0.415\exp\left(-NE_{s,IP} / 0.732\right) \quad (\mathbf{4.66})$$

The R^2 values for **Equations 4.65** and **4.66** are respectively 0.98 and 0.75. The regression curves calculated using the modified-to-scaled T_m ratios from both scenarios and the corresponding standard deviations are shown in **Figure 4.61**.

The slopes of the lines fit to the combined set of residuals for the different ground motion characteristics when plotted versus M_w, R_{hyp}, and scale factors are shown in **Table 4.14**. **Table 4.15** shows the medians of the combined set of residuals for the different fault types and all ground motion characteristics. M_w may have some impact on the modified-to-scaled *PGV*, *PGD*,

$D_{5\text{-}95}$, and T_m ratios for certain modification techniques since the slopes of the best-fit lines for the combined set of residuals are greater than 0.05; however, its impact is far less significant than that of spectral mismatch and more research is needed to justify the inclusion of M_w in the development of the regression equations. There also appears to be some bias in the medians of the combined set of residuals for the modified-to-scaled *PGD* and T_m ratios for the different fault types. However, no bias is observed in the residuals (i.e., medians generally less than 0.05) for the different fault types for the other ground motion characteristics. The slopes of the best-fit lines and medians for these parameters for the modified-to-scaled T_m ratios are likely larger than those for the other characteristics because the regression curves are based on the arithmetic ratios instead of the logarithmic ratios for T_m. The best-fit lines for the combined set of residuals plotted versus R_{hyp} and scale factors have slopes less than 0.005 and 0.05, respectively, so these parameters do not need to be included in the regression equations. **Appendix B** shows the plots of the residuals with respect to M_w, R_{hyp}, and scale factors for all ground motion characteristics. Although this investigation provides an initial understanding of whether these parameters have an impact on the modified-to-scaled ground motion characteristic ratios, some notable limitations must be mentioned:

- The effects of earthquakes with M_w smaller than 6.5 are not examined.
- The effects of source-to-site distance for small R_{hyp} (less than 15 km) are not examined.
- A majority of the motions (over 60%) are from earthquake events with reverse faulting.

4.2.3 Results for Scenario III

The modified-to-scaled ground motion characteristic ratios of the motions in scenario III were plotted with the regression curves and the plus and minus one standard deviation lines calculated for the relationships between the modified-to-scaled ground motion characteristic ratios and spectral mismatch. Residuals were calculated for the motions by subtracting the modified-to-scaled ground motion characteristic ratio predicted by the regression equation from the calculated ratio. Best-fit lines were fit to the residuals and the R^2 values and slopes of the best-fit lines were studied. The slopes and R^2 values of the best-fit lines respectively identify any trends in the residuals and the strength of any trends.

The logarithmic modified-to-scaled *PGV* ratios of the motions in scenario III are plotted in **Figure 4.68** with the corresponding regression curves developed for the motions in scenarios I and II. Residuals for the logarithmic modified-to-scaled *PGV* ratios of the motions in scenario III are plotted in **Figure 4.69**. **Figure 4.70** shows the logarithmic modified-to-scaled *PGD* ratios of the motions in scenario III and **Figure 4.71** shows the corresponding residuals for the logarithmic modified-to-scaled *PGD* ratios. The logarithmic modified-to-scaled *PGV* and *PGD* ratios of the motions in scenario III are generally similar to the ratios predicted by the regression curves for $NE_{s,IP}$ and $NE_{s,LP}$ greater than -0.4 (i.e., $\ln(NE_{s,LP} + 1)$ greater than -0.5). However, there is a noticeable positive bias for the motions in scenario III for both characteristics and both techniques for smaller spectral mismatch values. These observed biases are likely the result of the response spectra for the motions in the third scenario having relatively small spectral values for intermediate and long periods which could potentially lead to smaller spectral mismatch and cause this shift towards an $NE_{s,IP}$ and $NE_{s,LP}$ of 0.

Figure 4.72 shows the logarithmic modified-to-scaled I_a ratios for the motions in scenario III and the corresponding regression curves developed for the motions in scenarios I and II. **Figure 4.73** shows the residuals for the logarithmic modified-to-scaled I_a ratios of the motions in scenario III. The logarithmic modified-to-scaled *CAV* ratios of the motions in scenario III and the corresponding residuals are shown in **Figures 4.74** and **4.75**, respectively. The logarithmic modified-to-scaled I_a and *CAV* ratios for the motions in scenario III have identical trends to the regression curves developed for the logarithmic modified-to-scaled ground motion characteristic ratio – spectral mismatch relationships using the motions from scenarios I and II. Although lines fit to the residuals for the I_a and *CAV* ratios have slopes of about 0.15 and 0.075, respectively, indicating some possible biases, the R^2 values of these best-fit lines are too low (less than 0.04) to support the presence of any strong biases. These findings support the general applicability of the regression curves developed for the logarithmic modified-to-scaled I_a and *CAV* ratios in predicting these ground motion characteristics for the modified motions.

The logarithmic modified-to-scaled $D_{5\text{-}95}$ ratios for the motions in scenario III are shown in **Figure 4.76** with the corresponding curves developed for the motions in scenarios I and III. **Figure 4.77** shows the residuals for the logarithmic modified-to-scaled $D_{5\text{-}95}$ ratios for the motions in scenario III. **Figure 4.78** compares the modified-to-scaled T_m ratios for the motions in scenario III and the modified-to-scaled T_m regression curves developed for the motions in

scenarios I and II and **Figure 4.79** shows the corresponding residuals for the motions in scenario III. Although the regression curves developed for $D_{5\text{-}95}$ and T_m have relatively small R^2 values, the modified-to-scaled ratios for the motions in scenario III for these two characteristics exhibit very similar trends to the developed regression curves. Furthermore, the lines fit to the residuals for the modified-to-scaled $D_{5\text{-}95}$ and T_m ratios have R^2 values less than 0.025. Based on these observations, the trends for the modified-to-scaled $D_{5\text{-}95}$ and T_m ratios may be general for all earthquake scenarios, but cannot be accurately described with regression equations due to the large amount of dispersion.

The modified-to-scaled ground motion characteristics of the motions in the third scenario, including $D_{5\text{-}95}$ and T_m, generally have the same trends as the regression curves developed for the motions in scenarios I and II. However, for large, negative $NE_{s,IP}$ and $NE_{s,LP}$ (less than -0.4), the logarithmic modified-to-scaled *PGV* and *PGD* ratios of the motions in scenario III are larger than the values predicted by the regression curves possibly due to the smaller spectral values leading to $NE_{s,IP}$ and $NE_{s,LP}$ closer to 0. This finding supports the use of the regression curves for the modified-to-scaled ground motion characteristic ratio – spectral mismatch relationships developed in this study for any general earthquake scenario within a NE_s range of about -0.4 to 1.

4.3 Conclusions

Major findings related to the investigation of the effects of ground motion modification on the ground motion characteristics include:

- Well-defined relationship between the effects of modification on certain ground motion characteristics and spectral mismatch: Overall, spectral mismatch appears to be the dominating factor behind the changes in *PGV*, *PGD*, I_a, and *CAV* of scaled motions during TD and FD modification. Generally, the same trends in the modified-to-scaled ground motion characteristic ratios are observed for two very different earthquake scenarios and two different suites of 100 or more ground motions each matched to five alternative target spectra. This observation is further supported for I_a and *CAV* by the modified-to-scaled ratios of the motions in the third scenario which generally plot within the plus and minus one standard deviation lines of the regression curves developed for the combined set of motions from scenarios I and II. The modified-to-scaled *PGV* and *PGD* ratios of the motions from the

third scenario are also similar to the regression curves for values of $NE_{s,IP}$ and $NE_{s,LP}$, respectively, greater than -0.4. The significance of this finding is that, using the proposed regression equations, earthquake engineers can predict the effects of modification on the ground motion characteristics prior to modification by calculating the spectral mismatch. Equations for the impact of modification on the ground motion characteristics (i.e., modified-to-scaled ground motion characteristic ratios) as a function of NE_s (over different period ranges) are provided separately for each technique (i.e., TD and FD).

- TD and FD modification have similar effects on the ground motion characteristics for values of NE_s within ± 0.1 of 0: This finding suggests that TD or FD modification may be appropriate provided the motions are scaled to minimize NE_s. The effects of modification on the ground motion characteristics in general are also reduced if the ground motion is scaled to minimize NE_s. Therefore, it is recommended that engineers scale ground motions to minimize the spectral mismatch, as quantified by NE_s for different period ranges, and then perform modification. Recommended ranges of NE_s for which the different modification techniques result in changes of less than 25% relative to the scaled ground motion characteristics (i.e., logarithmic modified-to-scaled ratios between approximately -0.25 and 0.25 or arithmetic modified-to-scaled ratios between 0.8 and 1.25) are provided in **Table 4.16**.
- Ground motion characteristics of ground motions with negative NE_s are more sensitive to changes in NE_s: The modified-to-scaled ground motion characteristic ratios, for the most part, are more sensitive for negative spectral mismatch values (i.e., response spectrum must be increased to match the target spectrum) than positive spectral mismatch values (i.e., response spectrum must be decreased to match the target spectrum). This finding signifies that decreasing response spectra to match the target is less likely to have a significant impact on the ground motion characteristics than increasing the response spectra. Therefore, it is recommended to select and modify ground motions with positive values of NE_s (or $NE_{s,IP}$ or $NE_{s,LP}$) in order to further reduce the impact of modification on the ground motion characteristics.

Other findings include:

- The dependency of the modified-to-scaled ground motion characteristic ratios on parameters including M_w, R_{hyp}, fault type, and the scaling factor used does not appear to be as significant

as their dependency on spectral mismatch. M_w may have a small impact on the modified-to-scaled *PGV*, *PGD*, $D_{5\text{-}95}$, and T_m ratios, but more research on this relationship is necessary before including an M_w term(s) in the regression equations. More ground motions from normal and strike-slip faulting events should also be studied to ensure the regression equations are not systematically biased for these fault types. R_{hyp} and scale factor terms are not necessary for the regression equations.

- *PGV*, *PGD*, and I_a (or *CAV*) of a scaled ground motion are increased during modification when its response spectrum must be increased to match the target spectrum in the intermediate, long, and overall period ranges, respectively. Conversely, these characteristics are decreased during modification when the response spectrum must be decreased to match the target spectrum in these period ranges.
- When the response spectrum is decreased to match the target in the intermediate or long period range, FD modification leads to larger decreases in *PGV* or *PGD* than TD modification (about 0.5 and 4 times larger decreases for *PGV* and *PGD*, respectively).
- Small changes in spectral mismatch lead to larger changes in I_a and *CAV* when using FD modification as opposed to using TD modification. For example, a decrease in spectral mismatch of 0.2 from 0 is expected to result in a 35% larger I_a and 30% larger *CAV* for the FD-modified motions.
- The effects of spectral mismatch on $D_{5\text{-}95}$ and T_m during the modification process are not as strong as they are for the other ground motion characteristics (i.e., the regression equations developed for these characteristics have much smaller R^2 values). Due to the lack of a strong relationship, the regression equations developed for the modified-to-scaled $D_{5\text{-}95}$ and T_m ratios are not recommended for use in practice. However, the impact of spectral mismatch on these characteristics for each modification technique is similar for all three earthquake scenarios.
- TD modification decreases $D_{5\text{-}95}$ when the response spectrum is increased to match the target spectrum, but increases it when the response spectrum is decreased to match the target spectrum. FD modification has a limited effect on $_{D5\text{-}95}$, but does slightly increase it (about 25%) when the response spectrum is increased to match the target spectrum in the long period range.

Table 4.1. Summary of the earthquake recordings matching the criteria for scenario I. The ranges of source-to-site hypocentral distance (R_{hyp}) of the stations for each earthquake event with moment magnitude (M_w) are shown.

Earthquake Name	Date	M_w	Fault Type	No. of Stations	R_{hyp} (km)
Northridge-01	1/17/1994	6.69	Reverse	19	21.9 – 35.0
Loma Prieta	10/18/1989	6.93	Reverse	10	21.5 – 33.8
San Fernando	2/9/1971	6.61	Reverse	8	23.9 – 34.2
Chi-Chi, Taiwan	9/20/1999	7.62	Reverse	5	23.2 – 26.8
Irpinia, Italy-01	11/23/1980	6.90	Normal	5	17.8 – 34.4
Duzce, Turkey	11/12/1999	7.14	Strike-Slip	2	31.1 – 34.5
Hector Mine	10/16/1999	7.13	Strike-Slip	1	30.4
Kobe, Japan	1/16/1995	6.90	Strike-Slip	1	19.9
Landers	6/28/1992	7.28	Strike-Slip	1	15.4
Cape Mendocino	4/25/1992	7.01	Reverse	1	31.0
New Zealand-02	3/2/1987	6.60	Normal	1	25.1

Table 4.2. Information for the 108 ground motions selected for scenario I.

No.	Earthquake	Station	M_w	R_{hyp} (km)	R_{rup} (km)	V_{S30} (m/s)	Fault Type	Component	PGA (g)	PGV (cm/s)	PGD (cm)	I_a (cm/s)	CAV (cm/s)	$D_{5\text{-}95}$ (s)	T_m (s)
1	Northridge-01	LA – UCLA Grounds	6.69	25.55	13.80	398	Reverse	90	0.28	21.9	4.1	87	820	11.3	0.34
2								360	0.47	22.0	7.3	165	1083	10.2	0.36
3	Northridge-01	LA – W 15th St	6.69	34.38	25.60	405	Reverse	90	0.10	11.6	5.7	23	482	20.8	0.71
4								180	0.16	13.4	3.3	28	530	18.3	0.58
5	Northridge-01	LA – Wadsworth VA Hospital North	6.69	26.24	14.55	392	Reverse	235	0.25	32.8	11.3	82	892	15.0	0.61
6								325	0.25	18.7	7.8	69	796	13.3	0.43
7	Northridge-01	LA – Wadsworth VA Hospital South	6.69	26.24	14.55	414	Reverse	235	0.30	33.0	10.1	86	824	13.5	0.58
8								325	0.38	21.2	4.7	108	863	10.5	0.44
9	Northridge-01	LA – Wonderland Ave	6.69	25.82	15.11	1223	Reverse	095	0.11	8.7	1.8	14	284	8.8	0.32
10								185	0.17	11.8	2.8	20	307	6.7	0.45
11	Northridge-01	LA 00	6.69	22.67	9.87	706	Reverse	0	0.26	27.4	4.8	98	798	8.1	0.43
12								90	0.39	38.0	4.6	107	782	8.0	0.38
13	Northridge-01	La Crescenta – New York	6.69	32.87	17.81	446	Reverse	90	0.18	12.5	1.1	45	504	9.7	0.37
14								180	0.16	11.3	3.0	29	418	11.0	0.35
15	Northridge-01	N Hollywood – Coldwater Can	6.69	21.87	7.89	446	Reverse	180	0.30	25.0	6.3	120	884	15.0	0.53
16								270	0.27	22.2	11.5	118	897	16.4	0.55
17	Northridge-01	Pacific Palisades – Sunset	6.69	25.26	13.34	446	Reverse	190	0.47	30.9	5.2	184	984	8.0	0.32
18								280	0.20	14.9	5.6	65	641	10.5	0.34
19	Northridge-01	Playa Del Rey – Saran	6.69	34.35	24.42	405	Reverse	0	0.14	18.6	4.5	32	548	17.1	0.66
20								270	0.08	13.8	6.9	19	462	22.5	0.95
21	Northridge-01	Sunland – Mt Gleason Ave	6.69	29.81	12.38	446	Reverse	170	0.13	13.8	5.5	35	534	15.9	0.59
22								260	0.16	14.4	4.4	46	565	11.8	0.67
23	Northridge-01	Topanga – Fire Station	6.69	22.53	10.31	376	Reverse	270	0.19	12.0	4.1	51	551	10.1	0.27
24								360	0.33	15.6	9.5	104	776	8.8	0.30
25	Kobe, Japan	Nishi-Akashi	6.90	19.90	7.08	609	Strike-Slip	0	0.51	37.3	11.3	335	1432	9.7	0.49
26								90	0.50	36.6	43.6	227	1196	11.2	0.52
27	Chi-Chi, Taiwan	CHY024	7.62	25.39	9.64	428	Reverse	E/W	0.28	52.9	31.1	183	1643	24.1	0.87
28								N/S	0.18	49.0	49.2	119	1384	26.9	0.84
29	Chi-Chi, Taiwan	TCU116	7.62	25.68	12.40	493	Reverse	E/W	0.18	48.7	30.1	157	1679	29.0	0.97
30								N/S	0.15	45.4	54.1	113	1473	33.3	1.04

E/W – East/West component; N/S – North/South Component

Table 4.2. continued.

No.	Earthquake	Station	M_w	R_{bjp} (km)	R_{jb} (km)	V_{s30} (m/s)	Fault Type	Component	PGA (g)	PGV (cm/s)	PGD (cm)	I_a (cm/s)	CAV (cm/s)	D_{5-95} (s)	T_m (s)
31	Chi-Chi, Taiwan	TCU120	7.62	26.79	7.41	459	Reverse	E/W	0.23	63.2	54.1	200	1897	32.6	1.06
32								N/S	0.19	36.9	33.3	133	1582	32.4	0.68
33	Chi-Chi, Taiwan	TCU122	7.62	23.22	9.35	476	Reverse	E/W	0.22	42.5	43.0	144	1577	30.8	0.71
34								N/S	0.26	34.1	36.1	154	1562	30.3	0.68
35	Chi-Chi, Taiwan	TCU138	7.62	25.50	9.79	653	Reverse	N/S	0.22	40.9	26.1	167	1883	32.1	0.96
36								E/W	0.19	41.0	36.4	160	1852	34.1	0.71
37	Duzce, Turkey	Lamont 1061	7.14	34.52	11.46	481	Strike-Slip	E/W	0.13	13.7	8.2	25	433	15.6	0.41
38								N/S	0.11	11.5	8.2	23	443	15.6	0.41
39	Duzce, Turkey	Lamont 531	7.14	31.07	8.03	660	Strike-Slip	E/W	0.12	14.0	9.5	41	613	15.1	0.47
40								N/S	0.16	13.0	7.9	45	618	14.5	0.35
41	Hector Mine	Hector	7.13	30.38	10.35	685	Strike-Slip	0	0.27	28.6	22.5	83	794	11.7	0.61
42								90	0.34	41.7	14.0	187	1179	9.7	0.63
43	Irpinia, Italy-01	Auletta	6.90	34.44	9.52	1000	Normal	0	0.06	5.2	3.2	6	234	19.0	0.45
44								270	0.06	6.1	3.7	7	259	19.2	0.49
45	Irpinia, Italy-01	Bagnoli Irpinio	6.90	24.56	8.14	1000	Normal	0	0.14	22.1	9.3	34	539	19.5	0.66
46								270	0.20	31.9	9.6	43	568	16.1	0.95
47	Irpinia, Italy-01	Bisaccia	6.90	25.13	17.51	1000	Normal	0	0.10	23.5	14.8	19	473	24.2	1.19
48								270	0.08	12.5	2.9	14	410	26.1	1.01
49	Irpinia, Italy-01	Calitri	6.90	17.79	13.34	600	Normal	0	0.13	16.4	4.7	58	819	23.3	0.75
50								270	0.18	18.4	4.9	81	979	24.2	0.74
51	Irpinia, Italy-01	Rionero In Vulture	6.90	32.52	27.49	530	Normal	0	0.11	6.3	0.6	35	663	24.5	0.34
52								270	0.10	6.1	1.2	32	639	25.0	0.33
53	San Fernando	Castaic – Old Ridge Route	6.61	28.50	19.33	450	Reverse	21	0.32	15.6	2.4	68	661	14.5	0.35
54								291	0.27	25.8	4.9	95	873	15.4	0.48
55	New Zealand-02	Matahina Dam	6.60	25.06	16.09	425	Normal	83	0.26	21.7	6.4	65	546	6.2	0.47
56								353	0.34	21.6	2.7	69	532	6.3	0.45
57	San Fernando	Fairmont Dam	6.61	32.16	25.58	685	Reverse	56	0.07	4.7	0.7	4	159	12.8	0.31
58								326	0.11	6.4	1.1	6	176	12.4	0.36
59	San Fernando	Lake Hughes #1	6.61	29.16	22.22	425	Reverse	21	0.14	17.3	2.9	24	402	14.2	0.70
60								111	0.11	14.0	1.9	19	400	17.1	0.55

E/W – East/West component; N/S – North/South Component

Table 4.2. continued.

No.	Earthquake	Station	M_w	R_{typ} (km)	R_{JB} (km)	V_{S30} (m/s)	Fault Type	Component	PGA (g)	PGV (cm/s)	PGD (cm)	I_a (cm/s)	CAV (cm/s)	$D_{5\text{-}95}$ (s)	T_m (s)
61	San Fernando	Lake Hughes #12	6.61	23.89	13.99	602	Reverse	21	0.37	16.9	1.7	93	696	10.7	0.22
62								291	0.28	12.6	3.0	78	642	11.9	0.22
63	San Fernando	Lake Hughes #4	6.61	27.46	19.45	822	Reverse	111	0.19	5.6	0.9	25	395	12.7	0.20
64								201	0.15	8.4	1.9	21	363	12.9	0.26
65	Loma Prieta	Anderson Dam (Downstream)	6.93	31.81	19.90	489	Reverse	250	0.24	20.3	7.7	80	715	10.5	0.46
66								340	0.24	18.4	6.7	80	721	10.9	0.47
67	San Fernando	Lake Hughes #9	6.61	26.51	17.22	671	Reverse	21	0.16	4.5	1.2	15	269	9.4	0.22
68								291	0.13	3.8	1.1	11	232	11.8	0.20
69	Loma Prieta	Anderson Dam (Left Abutment)	6.93	31.81	19.90	489	Reverse	250	0.06	12.2	11.8	9	295	15.6	1.20
70								340	0.08	10.0	5.5	9	266	12.7	0.81
71	Loma Prieta	Gilroy – Gavilan College	6.93	33.84	9.19	730	Reverse	67	0.36	28.6	6.4	90	587	5.0	0.36
72								337	0.33	22.2	4.6	70	512	4.8	0.32
73	Loma Prieta	Gilroy Array #1	6.93	33.55	8.84	1428	Reverse	0	0.41	31.6	6.3	106	660	6.5	0.29
74								90	0.47	33.9	8.0	168	731	3.7	0.39
75	San Fernando	Palmdale Fire Station	6.61	34.18	24.16	453	Reverse	120	0.12	12.3	2.6	31	522	17.5	0.59
76								210	0.15	8.1	1.9	24	443	17.3	0.47
77	Loma Prieta	San Jose – Santa Teresa Hills	6.93	26.66	14.18	672	Reverse	225	0.27	26.2	13.4	131	975	10.1	0.31
78								315	0.23	20.9	6.2	100	880	10.1	0.36
79	Loma Prieta	Saratoga – Aloha Avenue	6.93	32.35	7.58	371	Reverse	0	0.51	41.2	16.2	145	911	9.4	0.62
80								90	0.32	42.6	27.6	109	809	8.3	0.54
81	Loma Prieta	Saratoga – W Valley College	6.93	32.20	8.48	371	Reverse	0	0.26	42.4	19.5	108	890	11.1	0.84
82								270	0.33	61.5	36.3	124	888	10.7	0.97
83	Loma Prieta	UCSC	6.93	24.05	12.15	714	Reverse	0	0.31	12.5	5.9	86	679	9.0	0.20
84								90	0.39	15.4	5.1	158	932	8.6	0.22
85	Loma Prieta	UCSC Lick Observatory	6.93	23.93	12.04	714	Reverse	0	0.45	18.7	3.8	266	1310	9.5	0.27
86								90	0.39	17.5	5.0	204	1169	9.7	0.22
87	Loma Prieta	WAHO	6.93	21.52	11.03	376	Reverse	0	0.40	30.8	6.6	371	1551	10.5	0.28
88								90	0.67	35.0	8.4	627	2025	11.0	0.27
89	Cape Mendocino	Fortuna – Fortuna Blvd	7.01	31.04	15.97	457	Reverse	0	0.12	29.9	27.5	26	517	18.7	1.02
90								90	0.11	21.7	12.7	24	492	18.2	1.10

Table 4.2. continued.

No.	Earthquake	Station	M_w	R_{byp} (km)	R_{JB} (km)	V_{S30} (m/s)	Fault Type	Component	PGA (g)	PGV (cm/s)	PGD (cm)	I_a (cm/s)	CAV (cm/s)	$D_{5\text{-}95}$ (s)	T_m (s)
91	Landers	Joshua Tree	7.28	15.36	11.03	379	Strike-Slip	0	0.27	27.5	9.5	165	1533	27.2	0.72
92								90	0.28	43.1	14.3	235	1747	26.1	0.77
93	San Fernando	Santa Felita Dam (Outlet)	6.61	34.13	24.69	389	Reverse	172	0.15	9.4	6.9	20	418	23.5	0.46
94								262	0.15	6.5	3.5	20	388	16.3	0.30
95	Northridge-01	Beverly Hills – 12520 Mulhol	6.69	23.89	12.39	546	Reverse	35	0.62	40.7	8.6	299	1195	7.6	0.32
96								125	0.44	30.1	4.8	234	1090	7.8	0.33
97	Northridge-01	Burbank – Howard Rd.	6.69	29.05	15.87	822	Reverse	60	0.12	9.5	2.3	22	378	11.7	0.43
98								330	0.16	8.5	1.8	33	425	8.0	0.32
99	Northridge-01	Glendale – Las Palmas	6.69	34.49	21.64	446	Reverse	177	0.36	12.2	1.9	117	812	9.5	0.27
100								267	0.21	7.4	1.7	61	645	11.5	0.25
101	Northridge-01	LA – Brentwood VA Hospital	6.69	25.07	12.92	417	Reverse	195	0.19	23.7	5.9	45	606	11.4	0.63
102								285	0.16	18.0	7.7	48	635	12.7	0.65
103	Northridge-01	LA – Chalon Rd	6.69	22.99	9.87	740	Reverse	70	0.23	16.6	3.4	61	621	9.1	0.49
104								160	0.19	27.1	5.8	65	582	6.9	0.63
105	Northridge-01	LA – Fletcher Dr	6.69	34.96	25.66	446	Reverse	144	0.16	10.7	2.9	51	607	11.7	0.42
106								234	0.24	26.2	3.6	65	620	11.8	0.52
107	Northridge-01	LA – Griffith Park Observatory	6.69	30.86	21.20	1016	Reverse	270	0.29	26.5	3.9	152	1006	8.9	0.43
108								360	0.16	13.5	2.4	41	585	11.9	0.50

Table 4.3. Optimal scale factors and the corresponding minimum root mean squared error (*RMSE*) of the ground motions in scenario I for the different target spectra.

No.	CMS		MA		2% UHS		10% UHS		Seed + σ	
	Scaling Factor	*RMSE*	Scaling Factor	*RMSE*	Scaling Factor	*RMSE*	Scaling Factor	*RMSE*	Scaling Factor	*RMSE*
1	1.58	0.398	0.88	0.320	2.72	0.340	1.40	0.319	2.54	0.730
2	1.03	0.447	0.57	0.347	1.77	0.359	0.91	0.343	1.65	0.754
3	2.57	0.309	1.43	0.418	4.41	0.417	2.27	0.433	4.11	0.253
4	2.41	0.152	1.35	0.235	4.15	0.256	2.13	0.248	3.87	0.477
5	1.27	0.257	0.71	0.322	2.19	0.316	1.12	0.329	2.04	0.352
6	1.66	0.316	0.93	0.297	2.85	0.318	1.47	0.299	2.66	0.650
7	1.12	0.274	0.62	0.239	1.92	0.247	0.99	0.245	1.79	0.513
8	1.13	0.400	0.63	0.324	1.95	0.351	1.00	0.332	1.82	0.735
9	3.49	0.396	1.95	0.300	6.01	0.322	3.09	0.303	5.60	0.700
10	2.91	0.490	1.62	0.458	5.00	0.484	2.57	0.459	4.66	0.848
11	1.64	0.558	0.91	0.563	2.81	0.593	1.45	0.571	2.62	0.902
12	1.42	0.592	0.79	0.551	2.43	0.581	1.25	0.556	2.27	0.953
13	3.13	0.849	1.74	0.796	5.38	0.828	2.77	0.804	5.01	1.200
14	3.21	0.574	1.79	0.486	5.51	0.511	2.84	0.487	5.14	0.910
15	1.25	0.321	0.70	0.314	2.15	0.331	1.10	0.325	2.00	0.577
16	1.13	0.252	0.63	0.308	1.94	0.315	1.00	0.331	1.80	0.326
17	1.28	0.628	0.71	0.552	2.19	0.583	1.13	0.562	2.04	0.973
18	1.87	0.304	1.04	0.222	3.21	0.245	1.65	0.240	2.99	0.574
19	2.39	0.236	1.33	0.395	4.11	0.394	2.11	0.401	3.83	0.318
20	2.81	0.522	1.56	0.633	4.82	0.618	2.48	0.637	4.49	0.243
21	2.30	0.170	1.28	0.294	3.95	0.305	2.03	0.312	3.68	0.330
22	2.16	0.245	1.20	0.394	3.71	0.413	1.91	0.407	3.45	0.483
23	2.80	0.628	1.56	0.496	4.82	0.524	2.48	0.507	4.49	0.941
24	1.77	0.660	0.99	0.561	3.04	0.589	1.56	0.570	2.83	0.993
25	0.85	0.448	0.47	0.464	1.46	0.493	0.75	0.480	1.36	0.750
26	0.85	0.298	0.47	0.302	1.46	0.321	0.75	0.312	1.36	0.588
27	0.85	0.575	0.48	0.655	1.47	0.639	0.75	0.662	1.37	0.264
28	1.11	0.676	0.62	0.745	1.91	0.728	0.98	0.752	1.78	0.357
29	1.14	0.633	0.63	0.742	1.95	0.727	1.01	0.747	1.82	0.297
30	1.26	0.715	0.70	0.817	2.16	0.800	1.11	0.822	2.02	0.366
31	0.98	0.597	0.55	0.696	1.68	0.677	0.87	0.698	1.57	0.285
32	1.14	0.537	0.63	0.576	1.95	0.555	1.00	0.580	1.82	0.266
33	1.07	0.534	0.60	0.564	1.84	0.544	0.94	0.568	1.71	0.272
34	1.06	0.355	0.59	0.452	1.82	0.440	0.94	0.459	1.69	0.213
35	1.03	0.570	0.57	0.698	1.77	0.682	0.91	0.699	1.65	0.273
36	1.15	0.548	0.64	0.629	1.97	0.614	1.01	0.636	1.83	0.239
37	2.93	0.383	1.63	0.339	5.04	0.353	2.59	0.351	4.69	0.588
38	3.39	0.267	1.89	0.271	5.38	0.307	3.00	0.289	5.00	0.534
39	2.72	0.302	1.52	0.343	4.67	0.366	2.40	0.360	4.36	0.544
40	2.81	0.453	1.57	0.352	4.82	0.375	2.48	0.367	4.50	0.705
41	1.37	0.176	0.76	0.262	2.35	0.264	1.21	0.266	2.19	0.384
42	0.97	0.398	0.54	0.351	1.66	0.361	0.85	0.360	1.55	0.449

Table 4.3. continued.

No.	CMS		MA		2% UHS		10% UHS		Seed + σ	
	Scaling Factor	*RMSE*	Scaling Factor	*RMSE*	Scaling Factor	*RMSE*	Scaling Factor	*RMSE*	Scaling Factor	*RMSE*
43	5.58	0.238	3.11	0.247	9.59	0.239	4.93	0.258	8.94	0.347
44	4.93	0.256	2.75	0.256	8.47	0.251	4.36	0.261	7.89	0.405
45	2.02	0.264	1.13	0.376	3.48	0.365	1.79	0.371	3.24	0.380
46	1.48	0.292	0.83	0.485	2.55	0.467	1.31	0.480	2.38	0.303
47	2.46	0.384	1.37	0.755	4.22	0.736	2.17	0.758	3.94	0.370
48	3.74	0.666	2.09	0.562	6.43	0.568	3.31	0.571	5.99	0.467
49	2.00	0.391	1.11	0.463	3.43	0.468	1.77	0.473	3.20	0.361
50	1.75	0.287	0.98	0.465	3.01	0.466	1.55	0.471	2.81	0.350
51	5.75	0.297	3.21	0.965	9.89	0.995	5.08	0.968	9.21	1.362
52	3.99	1.002	2.22	0.403	6.85	0.426	3.53	0.408	6.39	0.782
53	2.18	0.454	1.21	0.779	3.74	0.809	1.93	0.784	3.49	1.205
54	1.89	0.843	1.05	0.588	3.25	0.617	1.67	0.592	3.03	0.943
55	1.36	0.584	0.76	0.240	2.34	0.263	1.20	0.267	2.18	0.462
56	1.61	0.238	0.90	0.643	2.76	0.674	1.42	0.650	2.57	1.039
57	7.47	0.682	4.17	0.569	12.85	0.592	6.61	0.568	11.97	1.004
58	5.83	0.658	3.25	0.592	10.02	0.609	5.15	0.584	9.34	0.986
59	3.02	0.634	1.68	0.527	5.19	0.542	2.67	0.526	4.84	0.677
60	3.57	0.394	1.99	0.471	6.13	0.494	3.15	0.473	5.71	0.738
61	2.53	0.414	1.41	0.960	4.35	0.985	2.24	0.961	4.05	1.423
62	2.41	1.067	1.34	0.819	4.14	0.839	2.13	0.820	3.86	1.290
63	4.25	0.965	2.37	0.844	7.30	0.865	3.75	0.841	6.80	1.308
64	3.70	0.956	2.06	0.630	6.36	0.652	3.27	0.626	5.93	1.075
65	1.54	0.722	0.86	0.313	2.64	0.338	1.36	0.326	2.46	0.611
66	1.69	0.296	0.94	0.360	2.90	0.384	1.49	0.366	2.70	0.688
67	4.83	0.371	2.69	0.810	8.30	0.823	4.27	0.800	7.73	1.280
68	5.04	0.942	2.81	0.678	8.67	0.687	4.46	0.667	8.08	1.144
69	3.70	0.829	2.06	0.689	6.36	0.668	3.27	0.687	5.93	0.327
70	3.44	0.583	1.92	0.431	5.91	0.416	3.04	0.436	5.51	0.181
71	1.16	0.332	0.65	0.376	1.99	0.403	1.03	0.381	1.86	0.811
72	1.48	0.470	0.82	0.421	2.54	0.448	1.31	0.432	2.37	0.866
73	1.18	0.558	0.66	0.462	2.02	0.479	1.04	0.465	1.89	0.913
74	0.94	0.623	0.53	0.538	1.62	0.567	0.83	0.545	1.51	0.951
75	2.83	0.607	1.58	0.440	4.87	0.457	2.51	0.442	4.54	0.700
76	3.34	0.401	1.87	0.470	5.75	0.491	2.96	0.468	5.36	0.850
77	1.45	0.512	0.81	0.357	2.49	0.372	1.28	0.354	2.32	0.751
78	1.65	0.466	0.92	0.369	2.84	0.397	1.46	0.374	2.65	0.741
79	0.82	0.395	0.46	0.273	1.41	0.273	0.73	0.268	1.32	0.497
80	0.89	0.236	0.49	0.407	1.52	0.391	0.78	0.415	1.42	0.319
81	1.04	0.416	0.58	0.484	1.79	0.481	0.92	0.493	1.67	0.279
82	0.81	0.327	0.45	0.588	1.39	0.571	0.72	0.589	1.30	0.196
83	1.85	0.481	1.03	0.596	3.18	0.599	1.63	0.587	2.96	1.024
84	1.56	0.775	0.87	0.709	2.68	0.725	1.38	0.702	2.50	1.176

Table 4.3. continued.

No.	CMS		MA		2% UHS		10% UHS		Seed + σ	
	Scaling Factor	*RMSE*	Scaling Factor	*RMSE*	Scaling Factor	*RMSE*	Scaling Factor	*RMSE*	Scaling Factor	*RMSE*
85	1.38	0.827	0.77	0.729	2.38	0.759	1.22	0.735	2.22	1.177
86	1.57	0.813	0.88	0.651	2.71	0.670	1.39	0.655	2.52	1.089
87	1.01	0.717	0.56	0.646	1.74	0.667	0.90	0.641	1.62	1.067
88	0.72	0.594	0.40	0.470	1.24	0.485	0.64	0.461	1.16	0.911
89	2.06	0.517	1.15	0.624	3.55	0.610	1.82	0.632	3.31	0.228
90	2.00	0.609	1.11	0.699	3.43	0.684	1.77	0.707	3.20	0.297
91	1.32	0.274	0.73	0.449	2.26	0.457	1.16	0.453	2.11	0.444
92	1.06	0.349	0.59	0.518	1.81	0.512	0.93	0.520	1.69	0.299
93	2.40	0.529	1.34	0.429	4.12	0.408	2.12	0.422	3.84	0.564
94	3.22	0.541	1.80	0.400	5.54	0.392	2.85	0.391	5.16	0.723
95	0.90	0.524	0.50	0.442	1.55	0.471	0.80	0.447	1.45	0.878
96	1.21	0.626	0.68	0.553	2.09	0.586	1.07	0.564	1.95	0.973
97	3.40	0.337	1.90	0.312	5.84	0.339	3.00	0.328	5.44	0.622
98	3.01	0.517	1.68	0.407	5.17	0.439	2.66	0.421	4.82	0.837
99	2.14	0.970	1.19	0.832	3.67	0.855	1.89	0.835	3.42	1.297
100	3.17	0.972	1.76	0.837	5.44	0.859	2.80	0.838	5.07	1.303
101	1.86	0.249	1.04	0.381	3.19	0.396	1.64	0.392	2.98	0.501
102	1.91	0.253	1.06	0.423	3.28	0.432	1.69	0.435	3.06	0.391
103	1.92	0.461	1.07	0.495	3.30	0.524	1.70	0.504	3.08	0.801
104	1.83	0.383	1.02	0.520	3.15	0.538	1.62	0.526	2.93	0.640
105	2.33	0.300	1.30	0.294	4.00	0.332	2.06	0.320	3.72	0.617
106	1.85	0.399	1.03	0.424	3.18	0.451	1.64	0.432	2.97	0.714
107	1.55	0.688	0.86	0.655	2.66	0.684	1.37	0.660	2.48	1.016
108	2.51	0.498	1.40	0.521	4.31	0.544	2.22	0.521	4.02	0.841

Table 4.4. Summary of the earthquake recordings matching the criteria for scenario II. The ranges of source-to-site hypocentral distance (R_{hyp}) of the stations for each earthquake event with moment magnitude (M_w) are shown.

Earthquake Name	Date	M_w	Fault Type	No. of Stations	R_{hyp} (km)
Tohoku, Japan	3/11/2011	9.00	Reverse	12	81.3 – 122.0
Chi-Chi, Taiwan	11/12/1999	7.62	Reverse	10	40.5 – 116.0
Kocaeli, Turkey	8/17/1999	7.51	Strike-Slip	10	42.9 – 103.1
El Salvador	1/13/2001	7.60	Normal	7	78.9 – 96.0
Tokachi-oki, Japan	9/25/2003	8.00	Reverse	4	58.6 – 112.0
Denali, Alaska	11/3/2002	7.90	Strike-Slip	4	62.6 – 116.4
Michoacan, Mexico	9/19/1985	8.00	Unknown	3	38.3 – 83.9
Valparaiso, Chile	3/3/1985	7.80	Unknown	3	101.0 – 122.2
Peru Coast	10/3/1974	8.10	Unknown	2	84.0 – 89.0

Table 4.5. Information for the 100 ground motions selected for scenario II.

No.	Earthquake	Station	M_w	R_{hyp} (km)	R_{JB} (km)	V_{S30} (m/s)	Fault Type	Component	PGA (g)	PGV (cm/s)	PGD (cm)	I_a (cm/s)	CAV (cm/s)	$D_{5\text{-}95}$ (s)	T_m (s)
1	Tohoku, Japan	MYGH04	9.00	110.00	NL	NL	Reverse	E/W	0.45	13.0	4.3	906	6587	89.8	0.16
2								N/S	0.55	20.4	9.0	1423	7891	82.0	0.14
3	Kocaeli, Turkey	Atakoy	7.51	100.97	56.49	275	Strike-Slip	0	0.11	22.4	23.5	24	683	35.9	0.84
4								90	0.16	16.2	11.6	28	701	31.8	0.66
5	Kocaeli, Turkey	Bursa Sivil	7.51	97.46	65.53	670	Strike-Slip	90	0.05	8.1	4.4	7	381	34.0	0.90
6								180	0.06	9.0	5.9	8	394	33.7	0.99
7	Kocaeli, Turkey	Bursa Tofas	7.51	96.36	60.43	275	Strike-Slip	0	0.10	19.8	18.0	35	970	41.0	0.96
8								90	0.11	22.3	10.7	49	1090	37.9	0.93
9	Kocaeli, Turkey	Fatih	7.51	95.21	53.34	339	Strike-Slip	0	0.19	18.5	17.1	96	1351	32.2	0.48
10								90	0.16	14.9	17.1	68	1207	34.3	0.42
11	Kocaeli, Turkey	Goynuk	7.51	79.27	31.74	425	Strike-Slip	0	0.13	8.8	3.0	25	409	11.4	0.34
12								90	0.12	10.5	3.9	19	349	10.4	0.46
13	Kocaeli, Turkey	Hava Alani	7.51	103.11	58.33	425	Strike-Slip	0	0.09	24.8	29.4	20	623	35.1	0.98
14								90	0.08	17.7	16.6	15	540	36.7	0.87
15	Kocaeli, Turkey	Iznik	7.51	42.92	30.74	275	Strike-Slip	90	0.14	28.9	17.5	42	619	16.9	1.04
16								180	0.10	16.0	7.7	25	491	19.3	0.99
17	Kocaeli, Turkey	Maslak	7.51	92.14	52.96	660	Strike-Slip	0	0.04	6.6	6.5	3	237	35.8	0.40
18								90	0.04	6.5	9.2	3	245	37.4	0.59
19	Kocaeli, Turkey	Mecidiyekoy	7.51	92.06	51.17	425	Strike-Slip	0	0.05	6.2	4.8	4	186	16.3	0.37
20								90	0.07	8.8	10.1	4	170	14.6	0.52
21	Kocaeli, Turkey	Zeytinburnu	7.51	96.17	51.98	275	Strike-Slip	0	0.11	18.5	13.0	26	751	39.3	0.79
22								90	0.11	15.2	18.2	34	854	38.9	0.62
23	Tohoku, Japan	MYGH06	9.00	121.00	NL	NL	Reverse	E/W	0.29	32.7	16.4	300	3518	85.6	0.62
24								N/S	0.26	24.7	11.5	230	3181	84.5	0.47
25	Chi-Chi, Taiwan	CHY034	7.62	46.82	14.82	379	Reverse	N/S	0.31	48.5	16.5	182	1682	24.4	0.93
26								E/W	0.25	38.8	11.5	146	1579	29.9	0.83
27	Chi-Chi, Taiwan	CHY036	7.62	44.74	16.06	233	Reverse	E/W	0.29	38.9	21.2	186	1704	26.4	0.92
28								N/S	0.21	41.5	34.2	156	1667	32.8	0.84
29	Chi-Chi, Taiwan	CHY041	7.62	51.77	19.37	492	Reverse	E/W	0.30	20.4	8.6	154	1556	30.2	0.46
30								N/S	0.64	39.6	11.3	364	2011	22.1	0.45

E/W – East/West component; N/S – North/South Component

NL – Information not listed on the database's website

Table 4.5. continued.

No.	Earthquake	Station	M_w	R_{typ} (km)	R_{JB} (km)	V_{S30} (m/s)	Fault Type	Component	PGA (g)	PGV (cm/s)	PGD (cm)	I_a (cm/s)	CAV (cm/s)	$D_{5\text{-}95}$ (s)	T_m (s)
31	Chi-Chi, Taiwan	CHY065	7.62	115.98	82.78	273	Reverse	E/W	0.12	15.8	8.4	50	988	37.9	0.79
32								N/S	0.10	12.5	8.3	34	833	37.9	0.91
33	Chi-Chi, Taiwan	HWA014	7.62	80.85	51.49	273	Reverse	E/W	0.10	17.5	24.4	37	793	32.4	1.11
34								N/S	0.09	26.0	13.7	31	708	25.2	1.41
35	Tohoku, Japan	MYGH12	9.00	93.90	NL	NL	Reverse	E/W	0.45	24.0	9.9	827	6207	87.4	0.16
36								N/S	0.54	24.2	7.2	1112	6637	82.2	0.15
37	Chi-Chi, Taiwan	KAU054	7.62	65.11	27.37	474	Reverse	E/W	0.09	8.5	6.0	15	508	32.5	0.49
38								N/S	0.08	5.2	3.6	15	505	31.9	0.45
39	Chi-Chi, Taiwan	TCU015	7.62	101.93	49.81	426	Reverse	E/W	0.12	49.8	49.8	43	849	26.5	0.96
40								N/S	0.11	29.5	24.2	35	749	23.3	0.96
41	Chi-Chi, Taiwan	TCU038	7.62	73.55	25.44	273	Reverse	E/W	0.14	48.9	64.2	76	1121	28.2	0.93
42								N/S	0.17	44.9	43.6	103	1274	25.7	0.69
43	Chi-Chi, Taiwan	TCU056	7.62	40.53	10.50	273	Reverse	E/W	0.13	42.5	50.8	89	1234	26.0	0.84
44								N/S	0.13	42.9	54.6	83	1245	31.8	0.87
45	Chi-Chi, Taiwan	TCU070	7.62	48.52	19.02	401	Reverse	E/W	0.26	52.2	48.1	230	1975	26.8	0.76
46								N/S	0.17	62.3	56.7	171	1774	28.9	1.02
47	El Salvador	UCA Station LI	7.60	96.00	NL	NL	Normal	0	1.12	52.0	23.7	970	2809	12.8	0.26
48								90	0.59	32.1	8.9	447	1946	12.1	0.25
49	Tohoku, Japan	IWT007	9.00	121.00	NL	NL	Reverse	E/W	0.69	32.8	6.2	2222	10414	81.5	0.21
50								N/S	0.67	27.2	4.4	1807	9682	84.3	0.20
51	Michoacan, Mexico	UNR Station CALE	8.00	38.30	NL	NL	Unknown	90	0.13	14.8	8.7	47	858	27.7	0.44
52								180	0.15	18.5	8.4	66	961	24.3	0.59
53	Tokachi-oki, Japan	HKD096	8.00	112.00	NL	NL	Reverse	E/W	0.22	28.1	16.5	105	1609	36.5	1.02
54								N/S	0.18	24.7	12.8	87	1515	41.5	0.77
55	Denali, AK	Carlo (temp)	7.90	68.39	49.94	964	Strike-Slip	90	0.10	7.6	3.9	15	482	24.6	0.33
56	Denali, AK	R109 (temp)	7.90	62.61	42.99	964	Strike-Slip	90	0.06	6.2	3.9	8	331	23.7	0.51
57	Denali, AK	TAPS Pump Station #08	7.90	116.37	104.16	425	Strike-Slip	49	0.05	5.3	3.6	5	284	33.7	0.56
58								319	0.04	4.4	3.3	4	286	40.9	0.45

E/W – East/West component; N/S – North/South Component

NL – Information not listed on the database's website

Table 4.5. continued.

No.	Earthquake	Station	M_w	R_{typ} (km)	R_{JB} (km)	V_{S30} (m/s)	Fault Type	Component	PGA (g)	PGV (cm/s)	PGD (cm)	I_a (cm/s)	CAV (cm/s)	$D_{5\text{-}95}$ (s)	T_m (s)
59	Denali, AK	TAPS Pump Station #09	7.90	93.93	53.01	383	Strike-Slip	13	0.06	11.4	9.0	21	954	98.7	0.57
60								103	0.08	12.1	11.0	20	933	97.5	0.54
61	El Salvador	UCA Station NO	7.60	86.10	NL	NL	Normal	0	0.54	41.7	7.2	589	2709	16.5	0.42
62								90	0.52	26.1	4.7	698	1978	16.4	0.31
63	Tohoku, Japan	IWT009	9.00	120.00	NL	NL	Reverse	E/W	0.54	22.0	5.2	2066	9974	87.3	0.15
64								N/S	0.57	17.1	3.5	2122	10493	89.1	0.15
65	Michoacan, Mexico	UNR Station UNIO	8.00	83.90	NL	NL	Unknown	90	0.15	12.7	5.6	90	1170	26.4	0.36
66								180	0.17	20.3	7.1	102	1228	24.3	0.53
67	Tokachi-oki, Japan	HKD098	8.00	88.80	NL	NL	Reverse	E/W	0.34	81.8	28.6	409	3078	33.4	1.12
68								N/S	0.38	74.6	43.7	436	3225	32.8	1.21
69	Valparaiso, Chile	DGG Station 4408	7.80	108.20	NL	NL	Unknown	0	0.22	10.5	3.0	32	693	23.0	0.39
70								90	0.09	5.8	2.3	17	561	29.9	0.33
71	El Salvador	UCA Station PA	7.60	95.70	NL	NL	Normal	0	0.19	10.8	5.2	56	816	19.0	0.22
72								90	0.16	8.9	5.0	26	568	19.7	0.29
73	Tohoku, Japan	IWTH05	9.00	113.00	NL	NL	Reverse	E/W	0.68	30.6	4.8	1388	7936	84.9	0.20
74								N/S	0.59	29.2	8.3	1447	8087	88.1	0.18
75	Michoacan, Mexico	UNR Station VILE	8.00	47.80	NL	NL	Unknown	90	0.12	10.8	6.6	28	733	41.9	0.52
76								180	0.11	20.1	13.8	42	882	44.1	0.66
77	Tokachi-oki, Japan	HKD109	8.00	95.60	NL	NL	Reverse	E/W	0.24	33.0	13.5	185	2112	36.3	0.59
78								N/S	0.20	34.6	19.1	163	1972	39.1	0.70
79	El Salvador	CIG Station QC	7.60	87.70	NL	NL	Normal	90	0.19	16.0	3.6	70	811	12.6	0.33
80								360	0.15	23.5	10.2	49	721	15.0	0.60
81	Tohoku, Japan	IWTH23	9.00	122.00	NL	NL	Reverse	E/W	0.52	14.4	4.3	1037	6761	73.6	0.14
82								N/S	0.35	12.7	5.2	799	6104	77.0	0.14
83	Tokachi-oki, Japan	HKD113	8.00	58.60	NL	NL	Reverse	E/W	0.21	15.0	7.0	149	1998	42.0	0.27
84								N/S	0.17	15.5	10.0	70	1377	41.9	0.45
85	El Salvador	CIG Station SM	7.60	79.70	NL	NL	Normal	90	0.72	40.4	8.4	1175	3529	15.5	0.30
86								360	0.88	27.8	6.0	963	3299	15.1	0.26
87	Tohoku, Japan	IWTH27	9.00	113.00	NL	NL	Reverse	E/W	0.66	17.9	4.6	1357	7975	85.4	0.17
88								N/S	0.76	16.6	3.6	2062	9483	79.8	0.14

E/W – East/West component; N/S – North/South Component

NL – Information not listed on the database's website

Table 4.5. continued.

No.	Earthquake	Station	M_w	R_{hyp} (km)	R_{JB} (km)	V_{S30} (m/s)	Fault Type	Component	PGA (g)	PGV (cm/s)	PGD (cm)	I_a (cm/s)	CAV (cm/s)	$D_{5\text{-}95}$ (s)	T_m (s)
89	El Salvador	CIG Station MG	7.60	92.2	NL	NL	Normal	270	0.14	12.8	4.4	55	1040	35.7	0.60
90								360	0.12	12.1	4.2	53	1001	37.3	0.60
91	Tohoku, Japan	MYG003	9.00	109.00	NL	NL	Reverse	E/W	0.81	35.2	7.5	2065	9874	87.8	0.16
92								N/S	0.54	24.7	9.0	1569	8714	94.9	0.16
93	El Salvador	UCA Station ZA	7.60	78.90	NL	NL	Normal	0	0.26	13.0	4.5	167	1488	19.0	0.24
94								90	0.32	18.1	8.4	148	1411	20.0	0.29
95	Tohoku, Japan	MYG008	9.00	91.00	NL	NL	Reverse	E/W	0.31	42.6	9.5	486	5227	110	0.44
96								N/S	0.40	23.6	8.3	617	5373	80.7	0.29
97	Tohoku, Japan	MYG011	9.00	81.30	NL	NL	Reverse	E/W	0.76	37.0	11.0	2016	8758	77.2	0.19
98								N/S	0.90	18.6	5.4	3327	10767	75.2	0.11
99	Tohoku, Japan	MYGH03	9.00	98.30	NL	NL	Reverse	E/W	0.47	14.3	7.0	908	6453	83.8	0.14
100								N/S	0.45	13.3	5.0	1101	6793	77.2	0.12

E/W – East/West component; N/S – North/South Component
NL – Information not listed on the database's website

Table 4.6. Optimal scale factors and the corresponding minimum root mean squared error (*RMSE*) of the ground motions in scenario II for the different target spectra.

No.	CMS		MA + σ		2% UHS		10% UHS		Seed	
	Scaling Factor	*RMSE*	Scaling Factor	*RMSE*	Scaling Factor	*RMSE*	Scaling Factor	*RMSE*	Scaling Factor	*RMSE*
1	2.24	0.776	1.80	0.817	3.66	0.844	1.01	0.705	2.46	1.078
2	2.07	0.978	1.67	0.954	3.39	0.968	0.93	0.857	2.28	1.192
3	4.43	0.425	3.57	0.292	7.25	0.276	2.00	0.362	4.88	0.233
4	4.10	0.316	3.31	0.351	6.72	0.389	1.85	0.284	4.52	0.559
5	8.99	0.432	7.25	0.367	14.72	0.372	4.05	0.467	9.91	0.301
6	7.82	0.545	6.30	0.442	12.80	0.413	3.53	0.532	8.61	0.255
7	4.03	0.582	3.25	0.449	6.60	0.412	1.82	0.545	4.44	0.214
8	3.61	0.585	2.91	0.473	5.91	0.448	1.63	0.571	3.98	0.250
9	3.24	0.468	2.61	0.521	5.30	0.539	1.46	0.426	3.57	0.680
10	4.14	0.545	3.33	0.626	6.77	0.656	1.87	0.538	4.56	0.859
11	4.58	0.384	3.69	0.373	7.49	0.403	2.06	0.309	5.04	0.631
12	4.12	0.365	3.32	0.294	6.74	0.299	1.86	0.269	4.54	0.405
13	4.25	0.599	3.43	0.478	6.96	0.439	1.92	0.571	4.69	0.231
14	5.05	0.515	4.07	0.402	8.27	0.377	2.28	0.489	5.57	0.213
15	3.11	0.500	2.51	0.411	5.10	0.404	1.40	0.518	3.43	0.314
16	4.24	0.477	3.42	0.387	6.95	0.381	1.91	0.500	4.68	0.371
17	12.01	0.671	9.68	0.502	19.66	0.458	5.42	0.499	13.23	0.456
18	10.28	0.701	8.28	0.525	16.82	0.466	4.64	0.568	11.33	0.372
19	9.70	0.565	7.82	0.419	15.87	0.385	4.37	0.407	10.69	0.533
20	8.08	0.667	6.51	0.495	13.23	0.437	3.65	0.494	8.91	0.422
21	4.45	0.411	3.59	0.291	7.28	0.275	2.01	0.375	4.90	0.200
22	4.46	0.271	3.59	0.257	7.30	0.274	2.01	0.303	4.91	0.316
23	1.52	0.364	1.23	0.250	2.49	0.262	0.69	0.341	1.68	0.339
24	2.17	0.194	1.75	0.238	3.55	0.296	0.98	0.209	2.39	0.514
25	1.75	0.396	1.41	0.376	2.86	0.393	0.79	0.429	1.93	0.408
26	1.92	0.344	1.55	0.340	3.14	0.359	0.86	0.404	2.11	0.358
27	1.50	0.550	1.21	0.443	2.45	0.412	0.67	0.517	1.65	0.265
28	1.75	0.617	1.41	0.489	2.86	0.452	0.79	0.570	1.92	0.235
29	2.26	0.333	1.82	0.414	3.70	0.445	1.02	0.342	2.49	0.607
30	1.61	0.617	1.29	0.741	2.63	0.778	0.72	0.641	1.77	0.966
31	4.22	0.424	3.40	0.376	6.90	0.368	1.90	0.446	4.65	0.291
32	4.72	0.484	3.81	0.413	7.73	0.403	2.13	0.507	5.20	0.291
33	3.80	0.590	3.06	0.512	6.22	0.494	1.71	0.619	4.19	0.346
34	3.47	0.859	2.80	0.746	5.68	0.709	1.57	0.855	3.82	0.501
35	1.55	0.588	1.25	0.568	2.53	0.577	0.70	0.461	1.71	0.812
36	1.77	0.896	1.43	0.895	2.90	0.916	0.80	0.795	1.95	1.153
37	6.59	0.368	5.31	0.300	10.79	0.299	2.97	0.277	7.26	0.369
38	6.94	0.389	5.59	0.344	11.35	0.337	3.13	0.331	7.64	0.426
39	2.89	0.725	2.33	0.567	4.73	0.517	1.30	0.651	3.18	0.302
40	3.27	0.650	2.63	0.491	5.35	0.442	1.47	0.590	3.60	0.254
41	2.37	0.833	1.91	0.694	3.88	0.646	1.07	0.778	2.62	0.418
42	2.28	0.630	1.84	0.523	3.73	0.490	1.03	0.597	2.51	0.294

Table 4.6. continued.

No.	CMS		MA + σ		2% UHS		10% UHS		Seed	
	Scaling Factor	*RMSE*	Scaling Factor	*RMSE*	Scaling Factor	*RMSE*	Scaling Factor	*RMSE*	Scaling Factor	*RMSE*
43	2.45	0.620	1.98	0.478	4.02	0.440	1.11	0.585	2.70	0.225
44	2.46	0.733	1.98	0.586	4.02	0.540	1.11	0.676	2.71	0.302
45	1.70	0.733	1.37	0.617	2.78	0.576	0.77	0.687	1.87	0.361
46	1.89	0.924	1.52	0.794	3.09	0.750	0.85	0.889	2.08	0.518
47	0.89	0.691	0.72	0.667	1.46	0.677	0.40	0.564	0.98	0.893
48	1.36	0.604	1.10	0.611	2.23	0.639	0.61	0.525	1.50	0.878
49	1.41	0.855	1.14	0.926	2.32	0.956	0.64	0.812	1.56	1.172
50	1.74	0.968	1.40	1.043	2.85	1.070	0.79	0.927	1.92	1.296
51	3.94	0.320	3.18	0.215	6.46	0.225	1.78	0.245	4.35	0.430
52	2.67	0.343	2.15	0.217	4.38	0.221	1.21	0.294	2.95	0.344
53	2.20	0.586	1.77	0.422	3.60	0.393	0.99	0.504	2.42	0.406
54	2.44	0.505	1.97	0.324	3.99	0.282	1.10	0.403	2.69	0.305
55	6.27	0.527	5.06	0.443	10.27	0.425	2.83	0.356	6.91	0.576
56	8.07	0.434	6.51	0.268	13.21	0.244	3.64	0.321	8.90	0.318
57	10.12	0.361	8.16	0.242	16.57	0.241	4.57	0.319	11.15	0.287
58	11.80	0.382	9.51	0.246	19.32	0.224	5.32	0.295	13.01	0.308
59	5.93	0.837	4.78	0.653	9.70	0.587	2.67	0.695	6.53	0.492
60	5.45	0.791	4.39	0.612	8.92	0.549	2.46	0.634	6.00	0.479
61	1.28	0.453	1.03	0.564	2.09	0.608	0.58	0.456	1.41	0.811
62	1.92	0.841	1.55	0.974	3.14	1.026	0.87	0.879	2.12	1.255
63	2.15	0.932	1.73	0.967	3.52	1.000	0.97	0.864	2.37	1.222
64	2.59	1.112	2.09	1.150	4.24	1.182	1.17	1.046	2.85	1.417
65	3.37	0.272	2.72	0.290	5.52	0.334	1.52	0.252	3.71	0.520
66	2.47	0.260	1.99	0.136	4.05	0.148	1.12	0.205	2.73	0.292
67	1.04	0.724	0.84	0.575	1.71	0.534	0.47	0.681	1.15	0.342
68	0.92	0.771	0.74	0.613	1.50	0.563	0.41	0.713	1.01	0.363
69	3.87	0.424	3.12	0.385	6.34	0.395	1.75	0.282	4.27	0.622
70	7.00	0.444	5.64	0.405	11.46	0.419	3.16	0.321	5.00	0.776
71	3.77	0.633	3.04	0.566	6.18	0.557	1.70	0.471	4.16	0.739
72	4.80	0.580	3.87	0.538	7.86	0.535	2.17	0.441	5.29	0.742
73	1.70	0.852	1.37	0.950	2.78	0.988	0.76	0.838	1.87	1.207
74	1.75	0.853	1.41	0.923	2.87	0.954	0.79	0.815	1.93	1.188
75	5.00	0.301	4.03	0.271	8.19	0.275	2.26	0.262	5.51	0.391
76	3.93	0.520	3.17	0.413	6.44	0.375	1.77	0.488	4.34	0.209
77	1.82	0.466	1.47	0.356	2.98	0.321	0.82	0.443	2.01	0.266
78	1.85	0.557	1.49	0.449	3.03	0.424	0.84	0.557	2.04	0.239
79	3.04	0.339	2.45	0.340	4.98	0.365	1.37	0.297	3.35	0.559
80	2.62	0.394	2.11	0.260	4.29	0.230	1.18	0.367	2.89	0.207
81	2.39	0.944	1.93	0.964	3.92	0.981	1.08	0.846	2.64	1.208
82	2.54	0.841	2.04	0.849	4.15	0.863	1.14	0.736	2.80	1.074
83	2.97	0.380	2.39	0.374	4.86	0.408	1.34	0.292	3.27	0.592
84	3.48	0.270	2.80	0.254	5.69	0.300	1.57	0.261	3.83	0.460

Table 4.6. continued.

No.	CMS		MA + σ		2% UHS		10% UHS		Seed	
	Scaling Factor	*RMSE*	Scaling Factor	*RMSE*	Scaling Factor	*RMSE*	Scaling Factor	*RMSE*	Scaling Factor	*RMSE*
85	1.06	0.610	0.86	0.706	1.74	0.749	0.48	0.607	1.17	0.964
86	1.31	0.839	1.06	0.916	2.15	0.951	0.59	0.801	1.45	1.178
87	2.10	1.043	1.69	1.082	3.44	1.106	0.95	0.965	2.32	1.341
88	2.25	1.163	1.81	1.150	3.68	1.161	1.01	1.043	2.48	1.378
89	4.06	0.299	3.27	0.291	6.64	0.336	1.83	0.265	4.47	0.507
90	3.89	0.282	3.13	0.188	6.36	0.216	1.75	0.243	4.28	0.330
91	1.39	0.780	1.12	0.816	2.27	0.842	0.63	0.707	1.53	1.086
92	1.71	0.861	1.38	0.872	2.80	0.889	0.77	0.766	1.89	1.132
93	2.87	0.624	2.32	0.655	4.71	0.678	1.30	0.554	3.17	0.881
94	2.29	0.475	1.84	0.397	3.74	0.392	1.03	0.300	2.52	0.580
95	1.76	0.360	1.42	0.360	2.88	0.406	0.79	0.326	1.94	0.576
96	1.57	0.505	1.26	0.511	2.56	0.538	0.71	0.415	1.73	0.762
97	1.03	0.657	0.83	0.695	1.69	0.722	0.47	0.588	1.14	0.966
98	1.60	1.216	1.29	1.218	2.62	1.227	0.72	1.100	1.77	1.452
99	2.04	0.840	1.65	0.838	3.34	0.844	0.92	0.721	2.25	1.067
100	2.37	1.008	1.91	1.024	3.87	1.037	1.07	0.906	2.61	1.263

Table 4.7. Summary of the earthquake recordings selected for scenario III including the number of usable motions from each event. The ranges of source-to-site hypocentral distance (R_{hyp}) of the stations for each earthquake event with moment magnitude (M_w) are shown.

Earthquake Name	Date	M_w	Fault Type	No. of Stations	No. of Usable Motions	R_{hyp} (km)
Kiholo Bay, HI	10/15/2006	6.70	Unknown	20	38	42.5 – 187.4
Bovec, Slovenia	4/12/1998	5.60	Strike-Slip	12	20	25.0 – 104.0*
Hector Mine	10/16/1999	7.13	Strike-Slip	10	20	30.4 – 145.6
Chi-Chi, Taiwan	9/20/1999	7.62	Reverse	10	20	40.5 – 142.2
Landers	6/28/1992	7.28	Strike-Slip	10	20	28.2 – 148.7
Loma Prieta	10/18/1989	6.93	Reverse	10	20	24.1 – 101.7
Dillon, MT	7/26/2005	5.60	Unknown	7	14	22.8 – 198.2
Vrancea 1986, Romania	8/30/1986	7.20	Reverse	7	4	123.0 – 148.0*
Borah Peak, ID	10/28/1983	6.88	Normal	6	12	87.6 – 96.3
Vrancea 1990, Romania	5/30/1990	6.90	Reverse	6	5	46.0 – 137.0*
Little Skull Mtn, NV	6/29/1992	5.65	Normal	5	10	18.5 – 100.4
Mineral, VA	8/23/2011	5.80	Unknown	2	4	53.8 – 57.8
Roermond, Netherlands	4/13/1992	5.30	Normal	2	4	59.5 – 104.5
Chalfant Valley-01	7/20/1986	5.77	Strike-Slip	2	4	25.4 – 26.9
Dinara Mt., Croatia	11/27/1990	5.50	Reverse	1	0	-
Nahanni, Canada	12/23/1985	6.76	Reverse	1	2	23.8
Mammoth Lakes-01	5/25/1980	6.06	Normal	1	2	15.5
Kocaeli, Turkey[+]	8/17/1999	7.51	Strike-Slip	1	2	56.0
Northridge-01[+]	1/17/1994	6.69	Reverse	1	2	82.1
Cape Mendocino[+]	4/25/1992	7.01	Reverse	1	2	37.5
Morgan Hill[+]	4/24/1984	6.19	Strike-Slip	1	2	39.7
Coalinga-01[+]	5/2/1983	6.36	Reverse	1	2	49.7
Tabas, Iran[+]	9/16/1978	7.35	Reverse	1	2	117.8
San Fernando[+]	2/9/1971	6.61	Reverse	1	2	75.8

[*] - R for these earthquake recordings are provided in terms of epicentral distance
[+] - Synthetic motions from McGuire et al. (2001) study

Table 4.8. Information for the 94 ground motions selected for scenario III.

No.	Earthquake	Station	M_w	R_{hyp} (km)	R_{JB} (km)	V_{S30} (m/s)	Fault Type	Component	PGA (g)	PGV (cm/s)	PGD (cm)	I_a (cm/s)	CAV (cm/s)	$D_{5\text{-}95}$ (s)	T_m (s)
1	Northridge-01[+]	Villa Park – Serrano Ave	6.69	82.14	76.38	309	Reverse	0	0.10	3.4	1.1	13	359	21.9	0.24
2								270	0.10	4.3	1.3	17	408	22.2	0.32
3	Kocaeli, Turkey[+]	Arcelik	7.51	56.02	10.56	523	Strike-Slip	0	0.30	23.7	4.2	140	1088	15.5	0.45
4								90	0.21	14.8	3.8	58	693	14.2	0.51
5	Chi-Chi, Taiwan	HWA022	7.62	104.02	58.76	474	Reverse	E/W	0.12	12.0	11.0	34	668	21.2	0.48
6								N/S	0.08	11.0	17.2	23	569	22.3	0.51
7	Tabas, Iran[+]	Ferdows	7.35	117.80	89.76	275	Reverse	LONG	0.28	6.7	3.1	57	787	25.1	0.20
8								TRAN	0.36	9.7	6.3	83	958	27.9	0.19
9	Little Skull Mountain, NV	Station #1-Lathrop Wells	5.65	18.53	14.12	275	Normal	0	0.13	4.1	0.5	14	255	5.1	0.23
10								270	0.21	11.5	1.0	24	292	3.5	0.25
11	Little Skull Mountain, NV	Station #2-NTS Control Pt. 1	5.65	32.47	23.83	660	Normal	0	0.12	5.0	0.5	5	146	5.5	0.28
12								270	0.09	4.7	0.7	3	127	7.5	0.32
13	Little Skull Mountain, NV	Station #3-Beaty	5.65	48.34	45.15	339	Normal	0	0.04	1.1	0.1	2	179	18.3	0.17
14								270	0.06	2.1	0.2	3	181	16.7	0.17
15	Little Skull Mountain, NV	Station #4-Pahrump 2	5.65	62.21	61.04	275	Normal	0	0.02	1.1	0.2	1	115	29.7	0.38
16								270	0.02	1.3	0.2	1	107	33.1	0.36
17	Hector Mine	Big Bear Lake – Fire Station	7.13	70.06	61.85	339	Strike-Slip	16	0.16	14.0	8.4	53	689	13.3	0.40
18	Hector Mine	Fort Irwin	7.13	85.09	65.04	345	Strike-Slip	360	0.11	6.5	3.1	18	446	15.6	0.31
19	Hector Mine	Wrightwood – Nielson Ranch	7.13	122.57	113.45	345	Strike-Slip	90	0.05	4.4	1.7	6	274	15.6	0.42
20								360	0.05	5.8	6.8	5	255	24.2	0.37
21	Mineral, VA	USGS Station CVVA	5.80	53.80	NL	NL	Unknown	90	0.10	1.1	0.1	17	558	32.9	0.08
22								360	0.12	1.7	0.2	18	549	30.5	0.07
23	Dillon, MT	USGS Station 2245	5.60	140.00	NL	NL	Unknown	90	0.03	1.0	0.1	1	69	6.7	0.24
24								360	0.02	0.6	0.1	< 1	63	21.9	0.21
25	Dillon, MT	USGS Station 2255	5.60	68.20	NL	NL	Unknown	90	0.02	1.4	0.2	< 1	54	9.1	0.33
26								360	0.02	0.7	0.1	< 1	65	16.4	0.20

E/W – East/West component; N/S – North/South Component; LONG – Longitudinal Component; TRAN – Transverse Component

NL – Information not listed on the database's website

[+] - Synthetic motions from McGuire et al. (2001) study

Table 4.8. continued.

No.	Earthquake	Station	M_w	R_{hyp} (km)	R_{jb} (km)	V_{s30} (m/s)	Fault Type	Component	PGA (g)	PGV (cm/s)	PGD (cm)	I_a (cm/s)	CAV (cm/s)	D_{5-95} (s)	T_m (s)
27	Mammoth Lakes-01	Long Valley Dam (Upr L Abut)	6.06	15.52	12.56	345	Normal	0	0.43	23.6	7.5	132	909	10.9	0.37
28								90	0.27	13.9	3.1	72	679	10.9	0.41
29	Vrancea 1990, Romania	Birlad	6.90	88.00*	NL	425	Reverse	LONG	0.03	2.9	1.0	1	70	8.5	0.57
30	Vrancea 1990, Romania	Istrita	6.90	80.00*	NL	425	Reverse	LONG	0.01	1.4	0.7	< 1	56	18.6	0.87
31								TRAN	0.02	3.8	1.2	1	79	16.6	1.02
32	Kiholo Bay, HI	USGS Station 2810	6.70	46.90	NL	NL	Unknown	90	0.27	18.9	5.0	125	1003	10.6	0.36
33								360	0.26	13.6	4.4	103	884	9.7	0.24
34	Kiholo Bay, HI	USGS Station 2816	6.70	118.60	NL	NL	Unknown	90	0.07	3.2	0.9	7	340	28.1	0.34
35								360	0.09	3.1	0.8	9	382	27.3	0.36
36	Kiholo Bay, HI	USGS Station 2822	6.70	103.50	NL	NL	Unknown	360	0.08	4.4	0.6	12	321	13.4	0.30
37	Kiholo Bay, HI	USGS Station 2839	6.70	95.80	NL	NL	Unknown	90	0.08	3.8	1.0	9	366	19.7	0.33
38								360	0.06	3.6	0.8	8	357	21.0	0.34
39	Kiholo Bay, HI	USGS Station 2845	6.70	64.40	NL	NL	Unknown	90	0.20	8.4	1.4	67	817	13.0	0.23
40								360	0.19	9.5	2.0	39	665	14.9	0.28
41	Kiholo Bay, HI	USGS Station 2846	6.70	101.60	NL	NL	Unknown	90	0.06	3.1	0.7	8	374	32.0	0.27
42								360	0.07	2.4	0.8	9	386	28.8	0.24
43	Kiholo Bay, HI	USGS Station 2847	6.70	42.50	NL	NL	Unknown	268	0.19	17.0	2.1	40	525	13.0	0.45
44	Mineral, VA	USGS Station CBN	5.80	57.80	NL	NL	Unknown	90	0.08	5.1	1.0	9	396	22.5	0.36
45								360	0.14	7.1	1.6	14	473	20.1	0.48
46	Coalinga-01+	Parkfield – Gold Hill 3W	6.36	49.68	38.10	438	Reverse	0	0.25	11.9	2.9	91	1047	29.8	0.40
47								90	0.22	9.4	1.7	64	852	28.8	0.41
48	Borah Peak, ID	CPP-601	6.88	90.58	82.60	425	Normal	89	0.04	2.4	1.6	3	168	16.3	0.34
49								179	0.04	1.6	0.7	2	135	16.7	0.32
50	Borah Peak, ID	CPP-610	6.88	90.90	83.00	425	Normal	E/W	0.07	2.6	1.8	5	203	16.4	0.25
51								N/S	0.09	2.4	0.7	5	190	14.1	0.20

E/W – East/West component; N/S – North/South Component; LONG – Longitudinal Component; TRAN – Transverse Component

NL – Information not listed on the database's website

+ - Synthetic motions from McGuire et al. (2001) study

* - R for these earthquake recordings are provided in terms of epicentral distance

Table 4.8. continued.

No.	Earthquake	Station	M_w	R_{typ} (km)	R_{JB} (km)	V_{S30} (m/s)	Fault Type	Component	PGA (g)	PGV (cm/s)	PGD (cm)	I_a (cm/s)	CAV (cm/s)	$D_{5\text{-}95}$ (s)	T_m (s)
52	Borah Peak, ID	PBF (second bsmt)	6.88	95.68	87.69	660	Normal	E/W	0.05	2.9	1.1	4	158	13.9	0.35
53								N/S	0.05	2.4	0.4	3	127	13.6	0.31
54	Borah Peak, ID	TAN-719	6.88	96.33	84.80	425	Normal	260	0.05	2.8	1.1	4	198	17.6	0.26
55								350	0.04	2.8	2.2	3	185	19.4	0.27
56	Borah Peak, ID	TRA-642 ETR Reactor Bldg(Bsmt)	6.88	87.62	79.59	660	Normal	89	0.03	1.8	0.4	2	134	17.2	0.39
57								179	0.03	2.1	0.5	2	140	17.0	0.36
58	Borah Peak, ID	TRA-670 ATR Reactor Bldg(Bsmt)	6.88	88.00	80.00	660	Normal	179	0.02	1.6	0.4	1	117	17.3	0.36
59								269	0.02	1.1	0.4	1	106	18.4	0.31
60	Bovec, Slovenia	Moggio	5.60	36.00*	NL	NL	Strike-Slip	E/W	0.02	0.7	0.1	< 1	50	12.4	0.26
61								N/S	0.01	0.8	0.2	< 1	40	13.1	0.32
62	Bovec, Slovenia	Valle	5.60	25.00*	NL	NL	Strike-Slip	E/W	0.03	1.9	0.6	1	71	10.3	0.36
63								N/S	0.03	1.5	0.4	1	70	13.8	0.41
64	Bovec, Slovenia	Gemona – Li Furmie	5.60	40.00*	NL	NL	Strike-Slip	E/W	0.02	1.4	0.3	1	103	21.1	0.48
65								N/S	0.03	1.3	0.2	1	87	17.9	0.39
66	Bovec, Slovenia	Gemona – Piazza del Ferro	5.60	38.00*	NL	NL	Strike-Slip	E/W	0.01	0.6	0.2	< 1	38	15.9	0.43
67								N/S	0.01	0.6	0.2	< 1	30	17.8	0.54
68	Bovec, Slovenia	Casacco – Piazza Noacco	5.60	37.00*	NL	NL	Strike-Slip	E/W	0.01	0.7	0.3	< 1	34	19.2	0.49
69								N/S	0.01	0.8	0.4	< 1	37	19.9	0.46
70	Nahanni, Canada	Site 3	6.76	23.75	4.93	660	Reverse	270	0.15	6.1	3.1	28	412	11.0	0.15
71								360	0.14	3.3	1.0	31	434	11.6	0.12
72	Chalfant Valley-01	Bishop – LADWP South St	5.77	25.37	23.38	271	Strike-Slip	180	0.13	8.5	2.4	12	341	20.2	0.82
73								270	0.09	8.6	3.1	9	315	21.7	0.75
74	Chalfant Valley-01	Lake Crowley – Shehorn Res.	5.77	26.92	24.37	339	Strike-Slip	9	0.05	2.2	0.5	2	115	16.1	0.31
75								99	0.03	1.8	0.5	1	90	17.3	0.37
76	Bovec, Slovenia	Faculty of Civil and Geodetic Eng - Lubljana	5.60	73.00*	NL	NL	Strike-Slip	N/S	0.03	1.3	0.2	1	81	10.2	0.30
77	Bovec, Slovenia	Golovec - Lubljana	5.60	75.00*	NL	NL	Strike-Slip	N/S	0.01	0.8	0.1	< 1	47	10.4	0.33

E/W – East/West component; N/S – North/South Component

NL – Information not listed on the database's website

* - R for these earthquake recordings are provided in terms of epicentral distance

Table 4.8. continued.

No.	Earthquake	Station	M_w	R_{hyp} (km)	R_{JB} (km)	V_{S30} (m/s)	Fault Type	Component	PGA (g)	PGV (cm/s)	PGD (cm)	I_a (cm/s)	CAV (cm/s)	D_{5-95} (s)	T_m (s)
78	Vrancea 1986, Romania	Bacau	7.20	123.00	NL	425	Reverse	E/W	0.07	8.1	3.4	15	407	20.3	0.47
79	Vrancea 1986, Romania	Bucharest	7.20	134.00	NL	270	Reverse	N/S	0.14	22.3	3.7	26	546	27.4	0.81
80	Vrancea 1986, Romania	Carcaliu	7.20	148.00	NL	425	Reverse	E/W	0.07	4.8	0.6	10	391	31.8	0.24
81								N/S	0.07	4.0	1.2	11	447	35.2	0.20
82	Vrancea 1990, Romania	Carcaliu	6.90	137.00	NL	425	Reverse	N/S	0.17	11.5	5.3	28	549	17.7	0.22
83	Vrancea 1990, Romania	Surduc	6.90	46.00	NL	690	Reverse	N40 W	0.09	18.8	11.2	13	273	13.9	0.71
84	Dillon, MT	USGS Station 7210	5.60	198.20	NL	NL	Unknown	360	0.01	0.7	0.1	< 1	33	12.7	0.44
85	Dillon, MT	USGS Station 7216	5.60	22.80	NL	NL	Unknown	90	0.13	13.1	2.5	15	289	7.7	0.53
86								360	0.09	6.1	1.3	7	245	11.6	0.52
87	Loma Prieta	Bear Valley #1, Fire Station	6.93	83.02	61.15	339	Reverse	310	0.08	4.9	1.5	11	310	16.2	0.36
88	Loma Prieta	San Jose – Santa Teresa Hills	6.93	26.66	14.18	672	Reverse	225	0.28	26.2	13.4	131	975	10.1	0.31
89								315	0.23	20.9	6.2	100	880	10.1	0.36
90	Loma Prieta	UCSC	6.93	24.05	12.15	714	Reverse	90	0.39	15.4	5.1	158	932	8.6	0.22
91	Landers	Baker Fire Station	7.28	124.08	87.94	271	Strike-Slip	50	0.11	9.3	6.3	24	574	26.3	0.49
92	Landers	Desert Hot Springs	7.28	28.21	21.78	345	Strike-Slip	0	0.17	20.0	13.0	71	1072	31.8	0.52
93	Landers	Indio – Coachella Canal	7.28	60.09	54.25	345	Strike-Slip	0	0.10	9.6	5.1	28	731	35.9	0.64
94	Landers	Twentynine Palms	7.28	44.65	41.43	685	Strike-Slip	0	0.08	3.6	2.3	12	427	30.7	0.23

E/W – East/West component; N/S – North/South Component
NL – Information not listed on the database's website

Table 4.9. Optimal scale factors and the corresponding minimum root mean squared error (*RMSE*) of the ground motions in scenario III for the different target spectra.

No.	CMS		MA + σ		2% UHS		10% UHS		Seed	
	Scaling Factor	*RMSE*	Scaling Factor	*RMSE*	Scaling Factor	*RMSE*	Scaling Factor	*RMSE*	Scaling Factor	*RMSE*
1	3.29	0.404	2.29	0.281	5.84	0.361	1.38	0.387	5.81	0.913
2	2.52	0.347	1.75	0.232	4.47	0.266	1.05	0.314	4.45	0.807
3	0.72	0.391	0.50	0.376	1.28	0.372	0.30	0.372	1.28	0.857
4	1.05	0.407	0.73	0.414	1.87	0.397	0.44	0.420	1.86	0.789
5	1.70	0.619	1.19	0.619	3.03	0.588	0.71	0.694	3.01	0.501
6	2.04	0.683	1.42	0.672	3.63	0.630	0.86	0.745	3.61	0.394
7	1.75	0.461	1.22	0.422	3.10	0.523	0.73	0.483	3.08	1.139
8	1.31	0.613	0.91	0.457	2.32	0.555	0.55	0.595	2.31	1.026
9	3.84	0.685	2.68	0.815	6.83	0.870	1.61	0.759	6.79	1.497
10	2.08	0.579	1.45	0.747	3.69	0.792	0.87	0.680	3.67	1.397
11	4.24	0.560	2.95	0.637	7.53	0.686	1.78	0.586	7.49	1.312
12	4.43	0.394	3.09	0.532	7.87	0.550	1.86	0.421	7.83	1.193
13	14.52	0.892	10.11	0.979	25.78	1.047	6.08	0.925	25.65	1.730
14	10.05	0.880	6.99	0.939	17.84	1.017	4.21	0.922	17.75	1.659
15	12.70	0.296	8.84	0.378	22.55	0.368	5.32	0.339	22.44	0.879
16	12.65	0.290	8.81	0.387	22.46	0.360	5.30	0.287	22.35	0.936
17	1.40	0.520	0.98	0.561	2.49	0.549	0.59	0.624	2.48	0.656
18	2.26	0.421	1.58	0.372	4.02	0.386	0.95	0.469	4.00	0.701
19	3.56	0.528	2.48	0.484	6.31	0.445	1.49	0.552	6.28	0.536
20	3.78	0.538	2.63	0.472	6.71	0.438	1.58	0.553	6.68	0.544
21	10.08	1.090	7.02	1.086	17.90	1.186	4.22	1.096	17.81	1.853
22	9.09	1.039	6.33	1.026	16.15	1.107	3.81	1.009	16.07	1.788
23	16.93	0.561	11.79	0.683	30.06	0.714	7.09	0.598	29.91	1.341
24	26.36	0.677	18.35	0.810	46.81	0.857	11.04	0.734	46.57	1.499
25	16.50	0.373	11.49	0.579	29.29	0.607	6.91	0.541	29.15	1.106
26	21.63	0.503	15.06	0.633	38.41	0.675	9.06	0.555	38.22	1.323
27	0.68	0.248	0.47	0.230	1.21	0.284	0.29	0.317	1.20	0.811
28	0.99	0.311	0.69	0.358	1.76	0.381	0.42	0.386	1.75	0.868
29	6.52	0.683	4.54	0.591	11.59	0.501	2.73	0.622	11.53	0.368
30	11.59	0.946	8.07	0.856	20.58	0.784	4.86	0.920	20.48	0.204
31	7.27	0.953	5.07	0.876	12.92	0.792	3.05	0.913	12.85	0.331
32	0.86	0.282	0.60	0.445	1.53	0.434	0.36	0.412	1.52	0.868
33	1.12	0.275	0.78	0.336	1.99	0.350	0.47	0.273	1.98	0.976
34	4.52	0.293	3.15	0.374	8.02	0.373	1.89	0.296	7.98	0.970
35	3.92	0.282	2.73	0.452	6.96	0.466	1.64	0.379	6.92	1.041
36	3.66	0.349	2.55	0.518	6.50	0.508	1.53	0.398	6.47	1.092
37	3.69	0.295	2.57	0.395	6.55	0.386	1.54	0.346	6.52	0.917
38	4.27	0.327	2.97	0.436	7.58	0.401	1.79	0.364	7.54	0.874
39	1.57	0.342	1.10	0.464	2.80	0.485	0.66	0.366	2.78	1.139
40	1.69	0.272	1.18	0.412	3.00	0.427	0.71	0.337	2.99	1.037
41	4.89	0.262	3.40	0.371	8.68	0.404	2.05	0.324	8.64	1.016
42	4.48	0.347	3.12	0.342	7.95	0.360	1.88	0.300	7.91	0.981

Table 4.9. continued.

No.	CMS		MA + σ		2% UHS		10% UHS		Seed	
	Scaling Factor	*RMSE*	Scaling Factor	*RMSE*	Scaling Factor	*RMSE*	Scaling Factor	*RMSE*	Scaling Factor	*RMSE*
43	1.39	0.325	0.97	0.492	2.47	0.469	0.58	0.450	2.45	0.862
44	3.21	0.274	2.24	0.344	5.71	0.369	1.35	0.318	5.68	0.941
45	2.18	0.289	1.52	0.367	3.87	0.376	0.91	0.346	3.85	0.892
46	1.09	0.368	0.76	0.338	1.93	0.368	0.46	0.368	1.92	0.885
47	1.38	0.274	0.96	0.369	2.45	0.412	0.58	0.348	2.44	0.994
48	5.47	0.565	3.81	0.471	9.71	0.435	2.29	0.541	9.66	0.598
49	6.28	0.517	4.37	0.416	11.15	0.416	2.63	0.499	11.09	0.738
50	4.17	0.490	2.90	0.368	7.40	0.363	1.75	0.388	7.37	0.884
51	4.83	0.558	3.36	0.471	8.57	0.524	2.02	0.510	8.53	1.084
52	4.91	0.322	3.42	0.369	8.71	0.341	2.06	0.322	8.67	0.847
53	6.04	0.352	4.20	0.447	10.72	0.465	2.53	0.418	10.66	0.995
54	5.09	0.435	3.54	0.378	9.03	0.406	2.13	0.460	8.99	0.808
55	5.11	0.671	3.56	0.519	9.07	0.516	2.14	0.645	9.03	0.598
56	8.66	0.399	6.03	0.461	15.38	0.398	3.63	0.417	15.30	0.748
57	9.56	0.353	6.66	0.530	16.98	0.540	4.01	0.498	16.89	0.997
58	9.66	0.448	6.73	0.457	17.16	0.375	4.05	0.422	17.07	0.674
59	12.37	0.340	8.62	0.487	21.97	0.472	5.18	0.392	21.86	1.021
60	19.16	0.346	13.34	0.427	34.03	0.446	8.03	0.369	33.86	1.054
61	18.94	0.382	13.18	0.308	33.63	0.259	7.93	0.294	33.46	0.788
62	8.15	0.696	5.68	0.510	14.48	0.432	3.42	0.547	14.41	0.605
63	8.44	0.655	5.87	0.472	14.98	0.389	3.53	0.496	14.90	0.620
64	10.03	0.365	6.99	0.447	17.82	0.393	4.20	0.368	17.73	0.842
65	11.33	0.342	7.89	0.446	20.13	0.455	4.75	0.367	20.03	1.047
66	18.88	0.381	13.15	0.396	33.53	0.323	7.91	0.361	33.36	0.707
67	22.86	0.515	15.92	0.479	40.59	0.402	9.58	0.496	40.39	0.519
68	16.95	0.767	11.80	0.583	30.10	0.512	7.10	0.655	29.95	0.432
69	14.85	0.640	10.34	0.455	26.38	0.369	6.22	0.495	26.25	0.568
70	1.87	0.715	1.30	0.485	3.32	0.531	0.78	0.581	3.30	0.991
71	3.41	0.757	2.37	0.743	6.05	0.818	1.43	0.707	6.02	1.519
72	1.70	0.582	1.19	0.515	3.02	0.421	0.71	0.519	3.01	0.492
73	1.83	0.667	1.28	0.566	3.25	0.488	0.77	0.618	3.24	0.363
74	5.81	0.363	4.05	0.327	10.32	0.323	2.43	0.316	10.26	0.880
75	7.40	0.416	5.15	0.342	13.13	0.300	3.10	0.371	13.07	0.708
76	14.87	0.512	10.36	0.709	26.41	0.727	6.23	0.623	26.28	1.263
77	23.78	0.523	16.56	0.738	42.23	0.750	9.96	0.656	42.01	1.244
78	2.35	0.529	1.63	0.515	4.17	0.449	0.98	0.550	4.15	0.470
79	1.37	0.678	0.96	0.661	2.44	0.596	0.58	0.692	2.43	0.462
80	4.16	0.396	2.89	0.508	7.38	0.531	1.74	0.497	7.35	1.016
81	3.58	0.425	2.49	0.291	6.35	0.261	1.50	0.306	6.32	0.811
82	1.45	0.534	1.01	0.360	2.57	0.319	0.61	0.416	2.56	0.711
83	1.44	1.084	1.00	0.957	2.56	0.895	0.60	1.043	2.54	0.304
84	26.88	0.390	18.72	0.614	47.74	0.631	11.26	0.563	47.50	1.100

Table 4.9. continued.

No.	CMS		MA + σ		2% UHS		10% UHS		Seed	
	Scaling Factor	*RMSE*	Scaling Factor	*RMSE*	Scaling Factor	*RMSE*	Scaling Factor	*RMSE*	Scaling Factor	*RMSE*
85	1.76	0.384	1.23	0.515	3.13	0.469	0.74	0.484	3.12	0.756
86	2.68	0.338	1.86	0.388	4.76	0.344	1.12	0.368	4.73	0.736
87	2.90	0.437	2.02	0.369	5.15	0.322	1.21	0.409	5.12	0.652
88	0.79	0.399	0.55	0.362	1.40	0.375	0.33	0.436	1.39	0.750
89	0.90	0.329	0.63	0.383	1.60	0.337	0.38	0.360	1.59	0.740
90	0.85	0.430	0.59	0.451	1.51	0.516	0.36	0.422	1.50	1.176
91	1.72	0.696	1.20	0.557	3.05	0.484	0.72	0.618	3.04	0.415
92	1.17	0.474	0.81	0.480	2.07	0.406	0.49	0.483	2.06	0.563
93	1.59	0.714	1.11	0.661	2.83	0.604	0.67	0.730	2.82	0.320
94	3.20	0.683	2.22	0.473	5.67	0.452	1.34	0.568	5.65	0.699

Table 4.10. R^2 values of the regression equations developed for the relationships between the logarithmic modified-to-scaled ground motion characteristic ratios and spectral mismatch for the motions in scenario I for the different functional forms examined.

Functional Form	*PGV*		*PGD*		I_a		*CAV*	
	TD	FD	TD	FD	TD	FD	TD	FD
Linear	0.613	0.656	0.775	0.912	0.696	0.771	0.619	0.758
Piecewise Linear	0.884	0.905	0.820	0.913	0.948	0.966	0.889	0.962
Parabolic	0.795	0.818	0.820	0.912	0.855	0.915	0.775	0.901
Exponential	0.884	0.897	0.816	0.913	0.945	0.971	0.885	0.963
Exponential Decay	0.900	0.919	0.816*	0.913*	0.965	0.984	0.903*	0.977
Logarithmic	0.862	0.885	0+	0+	0.880	0.936	0+	0+
Linear-Exponential	0.900	0.918	0.820*	0.913	0.964	0.983	0.903	0.976
Shifted Power	0.025	0.071	0.225	0.655	0+	0+	0.807	0.808

* - The coefficients in the regression equation had significance levels greater than 0.05.
+ - The solution for the regression equation did not converge or led to negative R^2 values.

Table 4.11. R^2 values of the regression equations developed for the relationships between the logarithmic modified-to-scaled significant duration ratios and spectral mismatch, quantified by NE_s or $NE_{s,LP}$, for the motions in scenario I for the different functional forms examined.

Functional Form	NE_s		$NE_{s,LP}$	
	TD	FD	TD	FD
Linear	0.267	0.030	0.003	0.078
Piecewise Linear	0.287	0.035*	0.004*	0.135*
Parabolic	0.286	0.033	0.003*	0.123
Exponential	0.285	0.030*	0.007*	0.130
Exponential Decay	0.286*	0+	0.010*	0+
Logarithmic	0.286	0.031	0.002	0+
Linear-Exponential	0.286*	0.030*	0.003*	0.132*
Shifted Power	0.197	0.031	0.004	0.106

* - The coefficients in the regression equation had significance levels greater than 0.05.
+ - The solution for the regression equation did not converge or led to negative R^2 values.

Table 4.12. R^2 values of the regression equations developed for the relationships between the modified-to-scaled mean period ratios and spectral mismatch for the motions in scenario I for the different functional forms examined.

Functional Form	T_m	
	TD	FD
Linear	0.244	0.135
Piecewise Linear	0.342	0.181*
Parabolic	0.326	0.172
Exponential	0.357	0.175
Exponential Decay	0+	0.175*
Logarithmic	0+	0+
Linear-Exponential	0.361	0.175*
Shifted Power	0.364	0.174

* - The coefficients in the regression equation had significance levels greater than 0.05
+ - The solution for the regression equation did not converge or led to negative R^2 values

Table 4.13. Intervals of the bins used for the different mismatch metrics in calculating the standard deviations of the residuals.

Spectral Mismatch Metric	Bin Spacing	Range
NE	0.1	-0.5 to 0.5
	0.25	0.5 to 1
	2	1 to 3
NE_{IP}	0.1	-0.8 to 0.4
	0.2	0.4 to 0.6
	0.3	0.6 to 0.9
	0.4	0.9 to 1.3
	0.7	1.3 to 2
	2	2 to 4
NE_{LP}	0.1	-1 to 0
	0.2	0 to 0.4
	0.3	0.4 to 1
	1	1 to 2
	3	2 to 5
	5	5 to 10
$\ln(NE_{LP} + 1)$	0.5	-3.5 to -2
	0.25	-2 to 1
	1	1 to 3

Table 4.14. Slopes of lines fit to the residuals for the combined set of different modified-to-scaled ground motion characteristic ratios when plotted against moment magnitude (M_w), source-to-site hypocentral distance (R_{hyp}), and scale factor.

Ground Motion Characteristic		M_w	R_{hyp}	Scale Factor
PGV	TD	-0.020	< -0.001	-0.002
	FD	-0.077	-0.001	-0.007
PGD	TD	0.072	0.001	-0.002
	FD	0.022	< -0.001	-0.026
I_a	TD	0.007	< 0.001	0.001
	FD	-0.011	< 0.001	0.004
CAV	TD	-0.033	< -0.001	-0.001
	FD	-0.041	< -0.001	0.006
$D_{5\text{-}95}$	TD	-0.030	-0.001	-0.006
	FD	-0.060	-0.001	0.002
T_m	TD	-0.010	< -0.001	0.025
	FD	0.324	0.005	0.048

Table 4.15. Medians of the residuals for the combined set of different modified-to-scaled ground motion characteristic ratios for different fault types.

Ground Motion Characteristic		Normal	Reverse	Strike-Slip	Unknown
PGV	TD	0.023	-0.004	0.003	0.017
	FD	0.071	0.021	-0.002	0.016
PGD	TD	-0.039	-0.065	-0.067	-0.018
	FD	0.179	0.055	-0.069	0.053
I_a	TD	-0.004	-0.013	-0.030	0.016
	FD	-0.005	-0.015	-0.020	0.009
CAV	TD	-0.012	-0.010	-0.032	-0.038
	FD	-0.005	-0.012	0.004	0.001
$D_{5\text{-}95}$	TD	-0.035	-0.034	-0.057	-0.036
	FD	-0.011	-0.018	-0.052	-0.097
T_m	TD	-0.004	0.007	-0.122	-0.027
	FD	-0.181	-0.191	-0.428	-0.278

Table 4.16. Recommended ranges of spectral mismatch, as quantified by NE_s, $NE_{s,IP}$, or $NE_{s,LP}$, where modification changes the ground motion characteristic of the scaled ground by less than 25% (i.e., modified-to-scaled ratios between 0.8 and 1.25).

Characteristic	Technique	Spectral Mismatch Range
PGV	TD	$-0.24 < NE_{s,IP} < 0.14$
	FD	$-0.28 < NE_{s,IP} < 0.04$
PGD	TD	$-0.12 < NE_{s,LP} < 0.90$
	FD	$-0.56 < NE_{s,LP} < -0.12$
I_a	TD	$-0.11 < NE_s < 0.10$
	FD	$-0.06 < NE_s < 0.07$
CAV	TD	$-0.19 < NE_s < 0.51$
	FD	$-0.10 < NE_s < 0.20$

Figure 4.1. Locations of the site used (labeled LAX) and the fault that contributes most significantly to the mean earthquake event for scenario I.

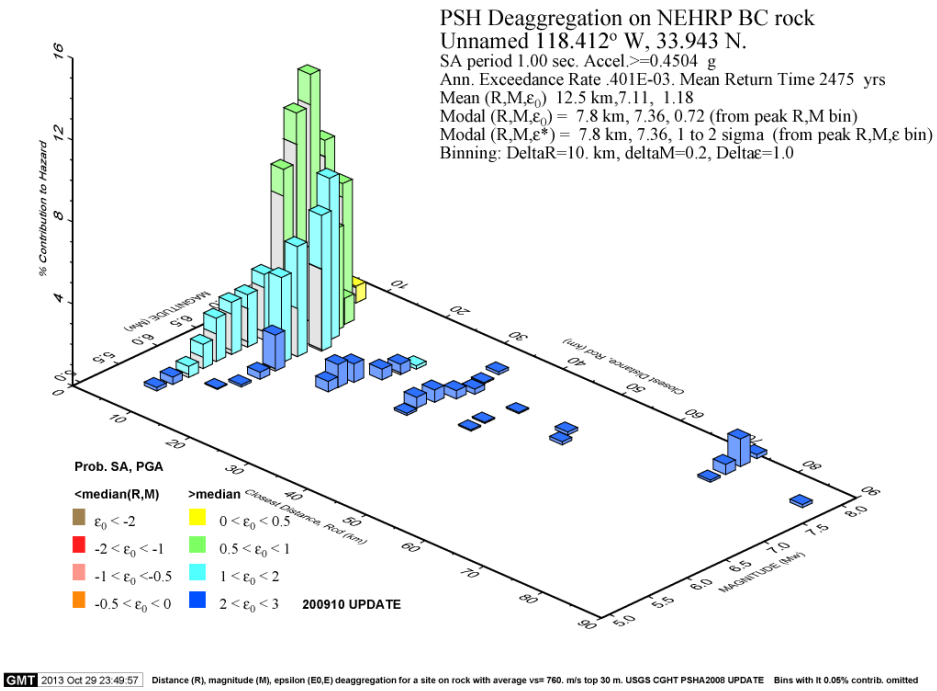

Figure 4.2. Deaggregation plot for scenario I assuming 2% probability of exceedance within 50 years for a site class BC soil profile (FEMA 2004) with a period of 1 second.

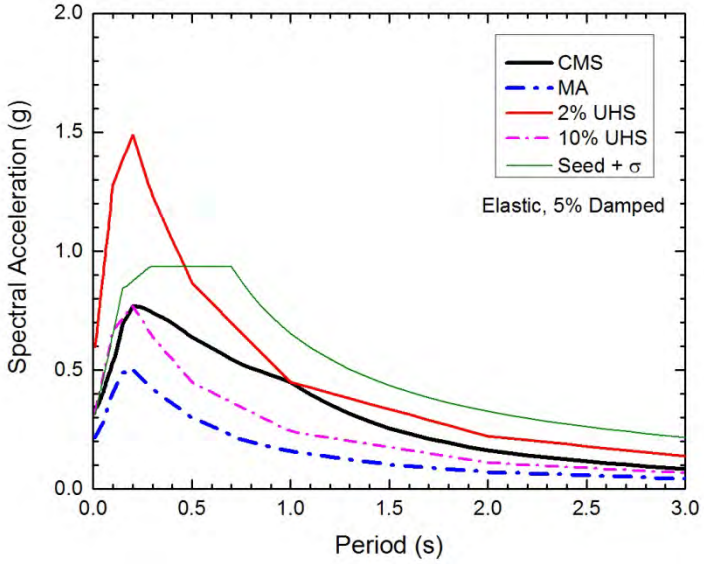

Figure 4.3. Target conditional mean spectrum (CMS; Baker 2011), mean spectrum from attenuation relationships (MA), 2% and 10% uniform hazard spectra (2% UHS and 10% UHS, respectively), and mean plus one standard deviation spectrum from Seed et al. (1997) (Seed + σ) developed for scenario I.

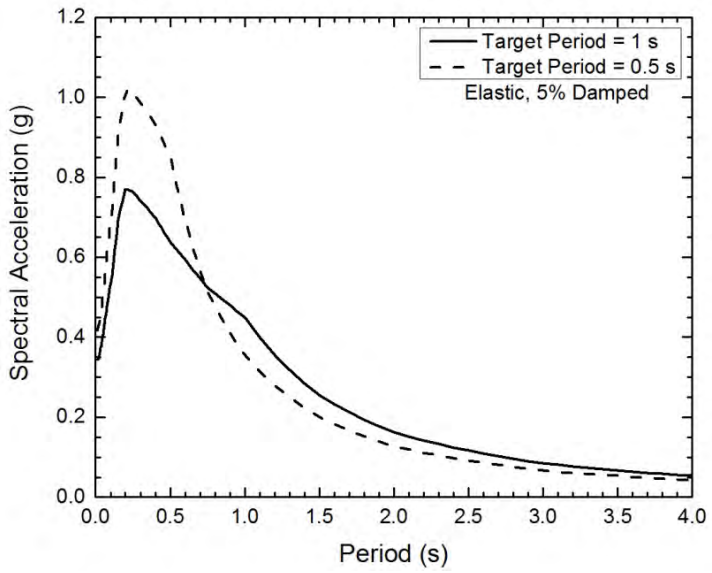

Figure 4.4. Conditional mean spectra calculated for scenario I using target periods of 1 and 0.5 seconds.

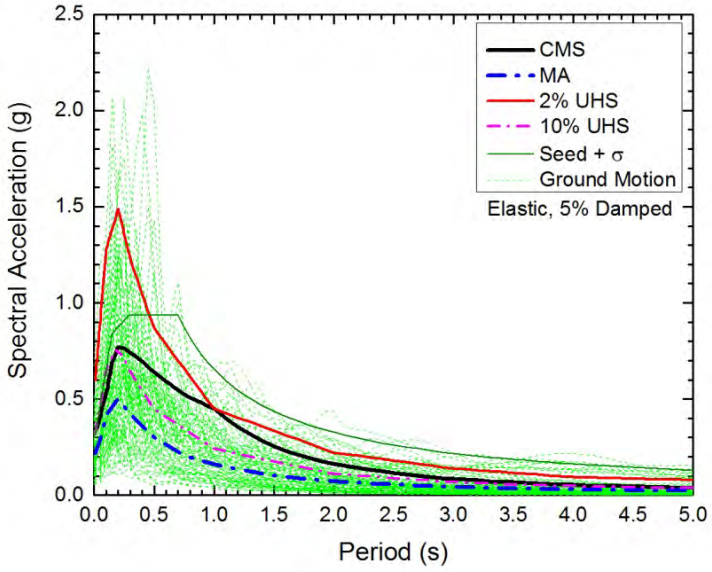

Figure 4.5. Response spectra of the selected, unscaled ground motions for scenario I compared to the five target spectra developed for this scenario.

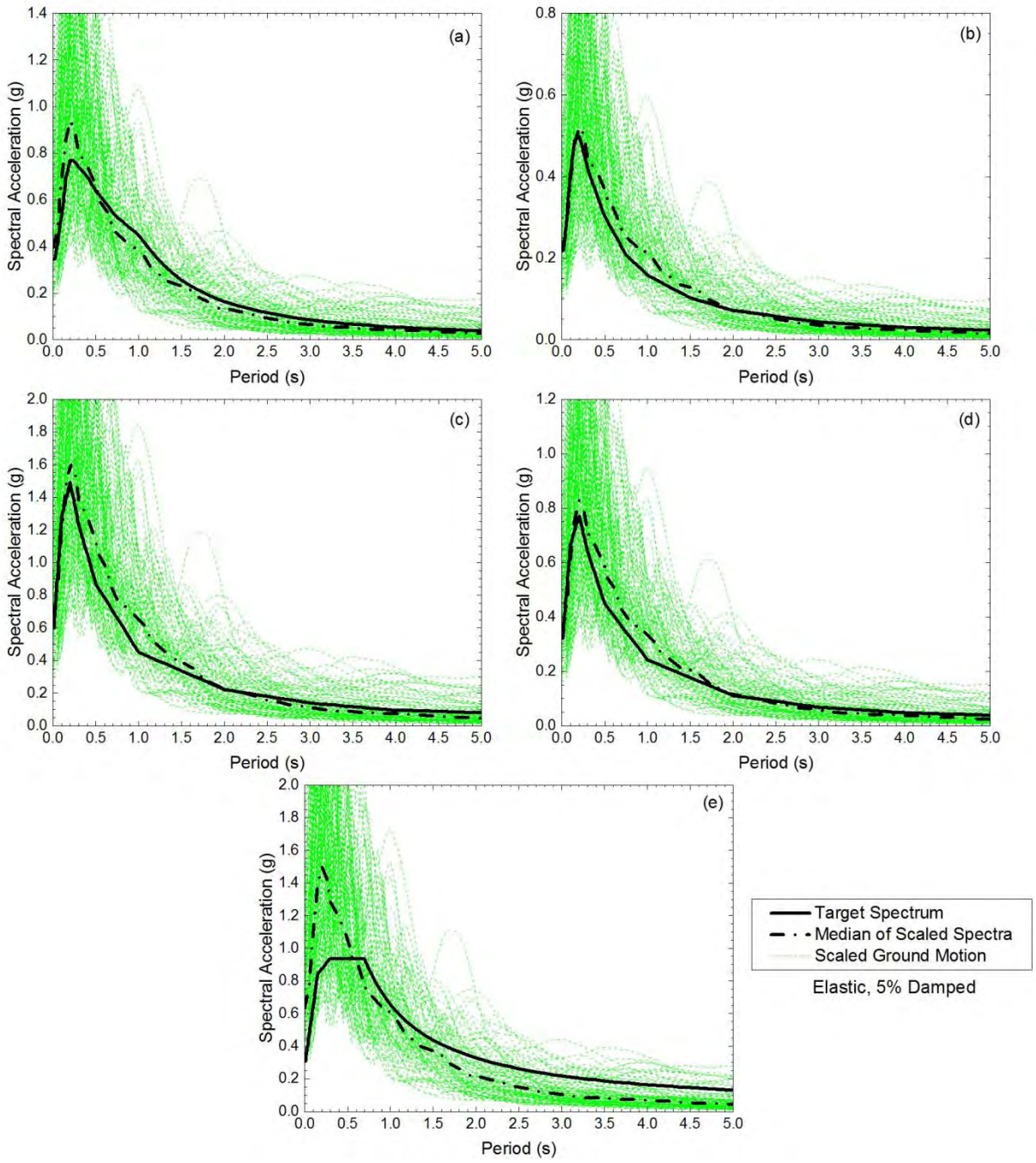

Figure 4.6. Response spectra of the optimally scaled ground motions and their medians from scenario I compared to the (a) conditional mean spectrum, (b) mean spectrum from the NGA relationships, (c) 2% uniform hazard spectrum, (d) 10% uniform hazard spectrum, and (e) mean plus one standard deviation spectrum from Seed et al. (1997).

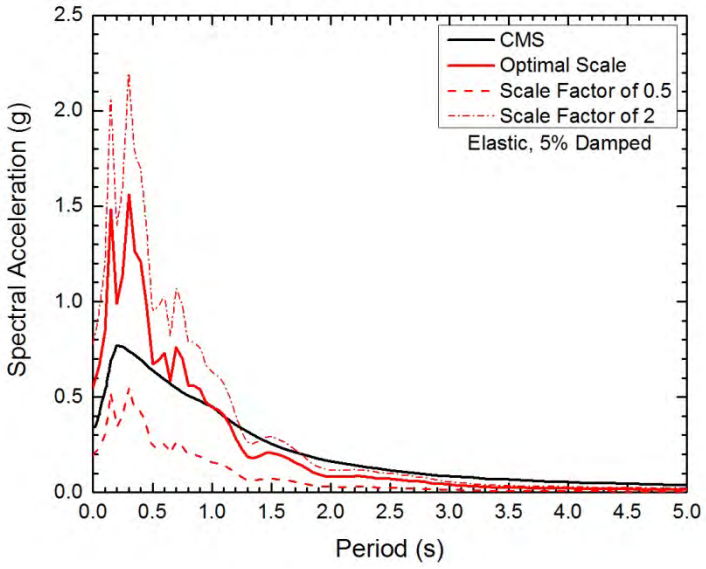

Figure 4.7. Response spectra for an example ground motion scaled using an optimal factor and factors of 0.5 and 2 compared to the target conditional mean spectrum (CMS) for scenario I.

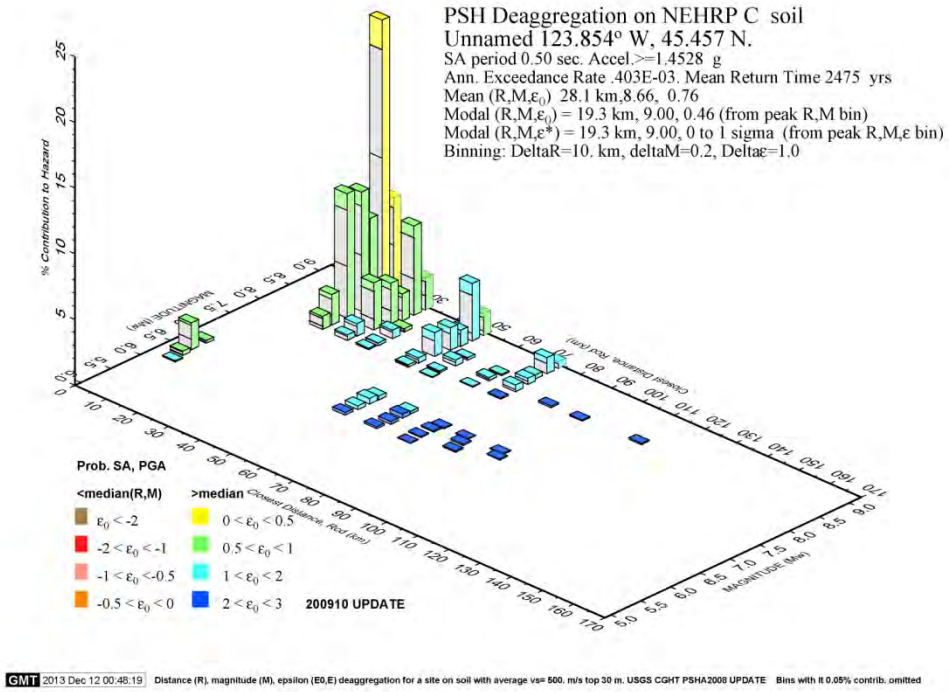

Figure 4.8. Deaggregation plot for scenario II assuming 2% probability of exceedance within 50 years for a site class C soil profile with a period of 0.5 seconds.

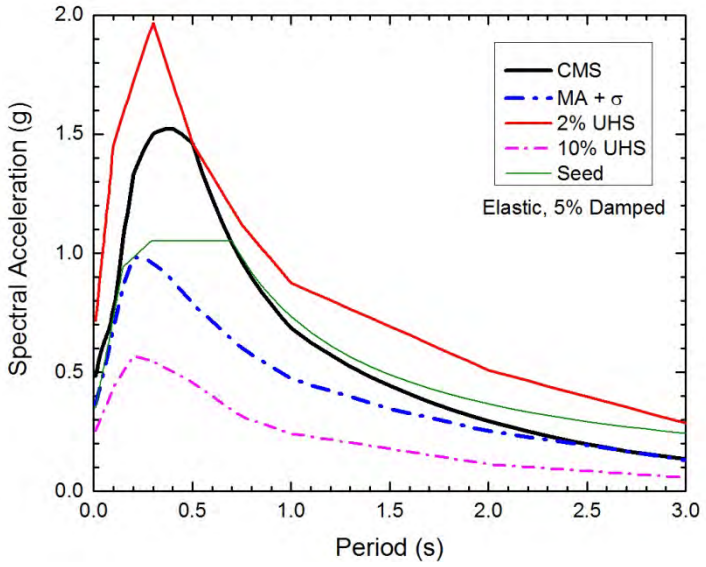

Figure 4.9. Target conditional mean spectrum (CMS; Baker 2011), mean plus one standard deviation spectrum from attenuation relationships (MA + σ), 2% and 10% uniform hazard spectra (2% UHS and 10% UHS, respectively), and mean spectrum from Seed et al. (1997) (Seed) developed for scenario II.

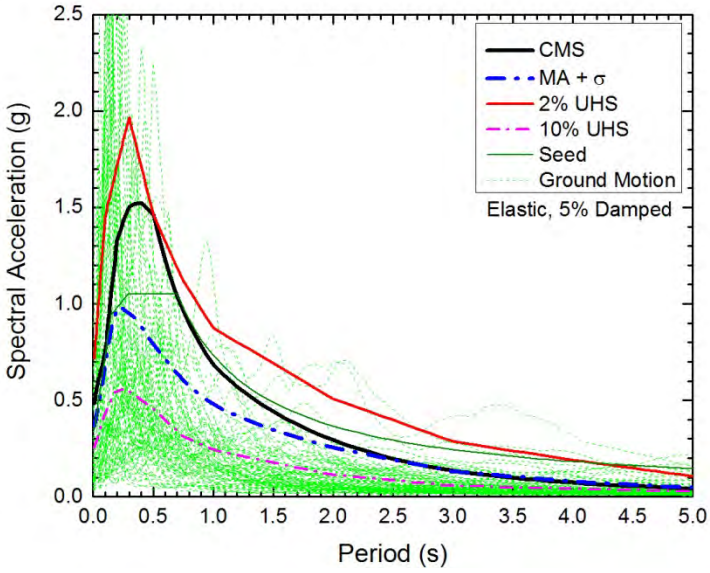

Figure 4.10. Response spectra of the selected, unscaled ground motions for scenario II compared to the five target spectra developed for this scenario.

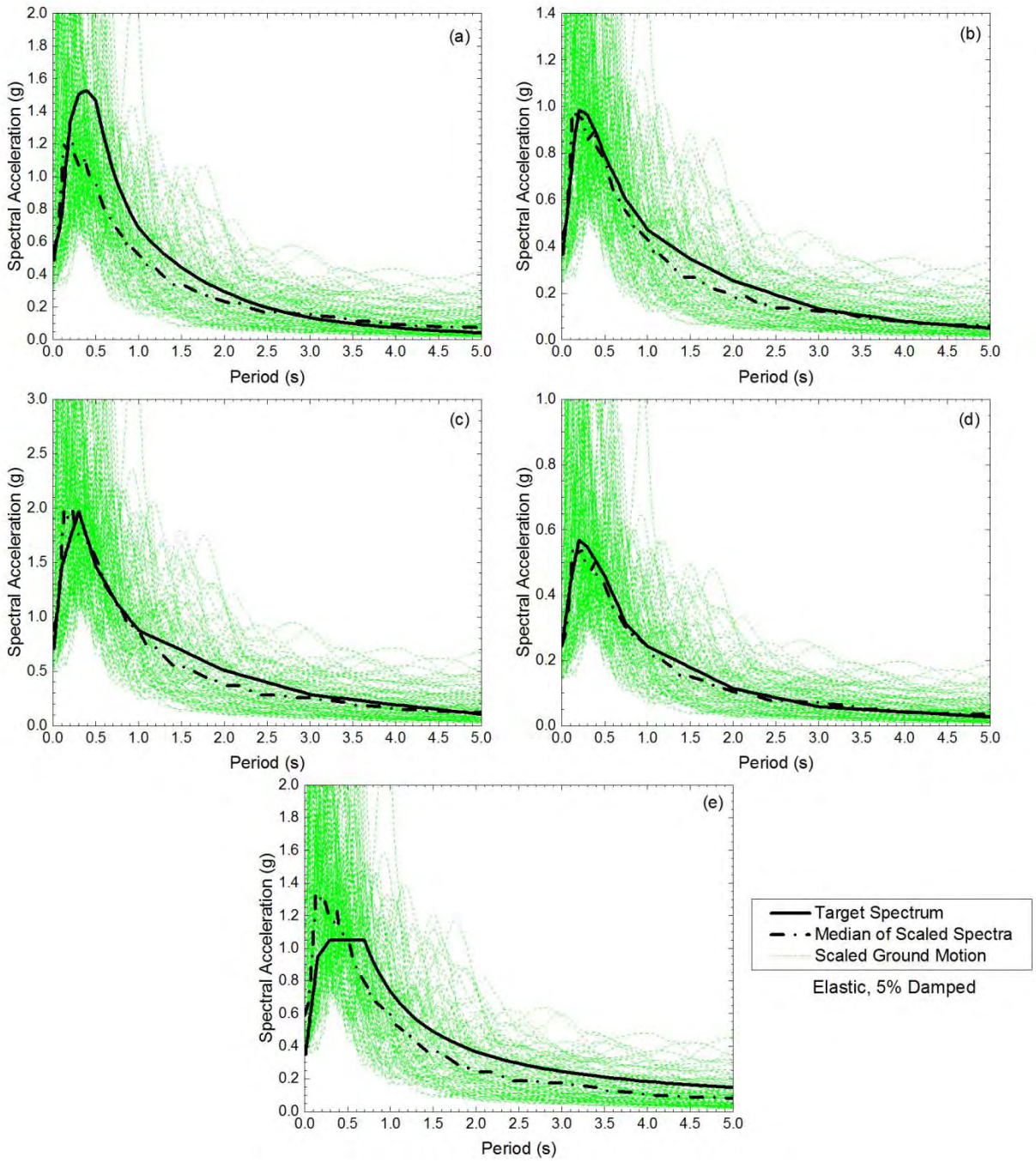

Figure 4.11. Response spectra of the optimally scaled ground motions and their medians from scenario II compared to the (a) conditional mean spectrum, (b) mean plus one standard deviation spectrum from the attenuation relationships, (c) 2% uniform hazard spectrum, (d) 10% uniform hazard spectrum, and (e) mean spectrum from Seed et al. (1997).

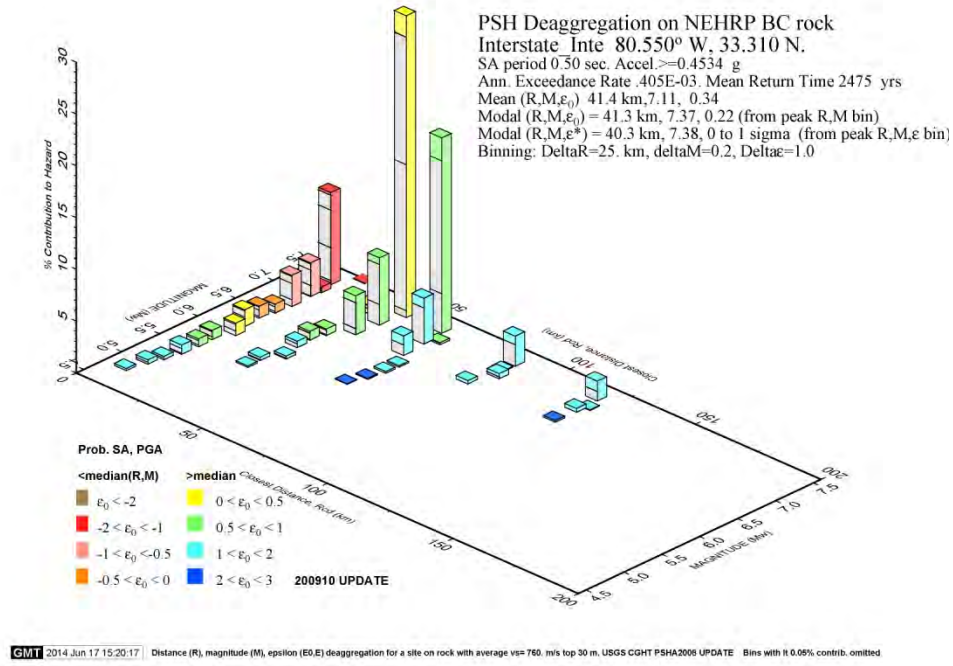

Figure 4.12. Deaggregation plot for scenario III assuming 2% probability of exceedance within 50 years for a site class BC soil profile with a period of 0.5 seconds.

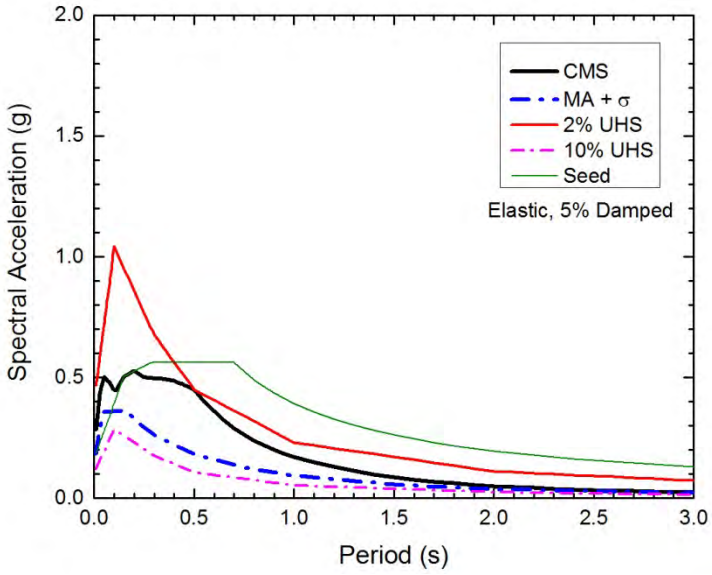

Figure 4.13. Target conditional mean spectrum (CMS; Baker 2011), mean plus one standard deviation spectrum from attenuation relationships (MA + σ), 2% and 10% uniform hazard spectra (2% UHS and 10% UHS, respectively), and mean spectrum from Seed et al. (1997) (Seed) developed for scenario III.

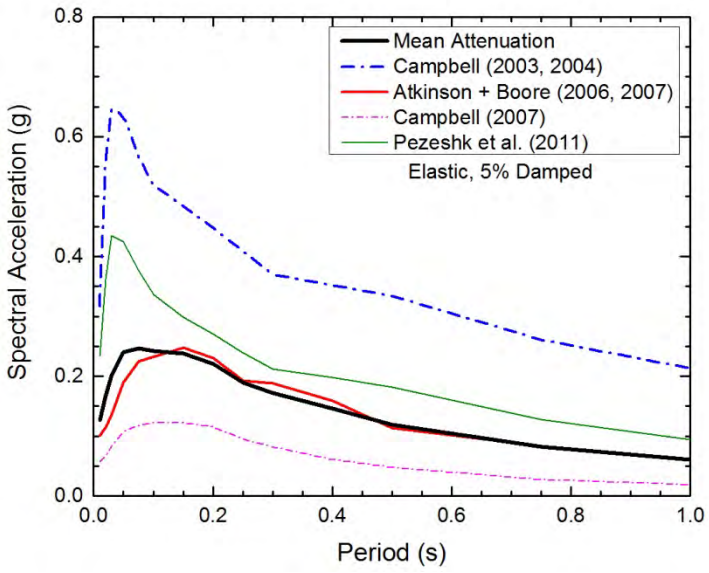

Figure 4.14. Overall mean attenuation response spectrum compared to the mean response spectra of the different attenuation relationships for scenario III.

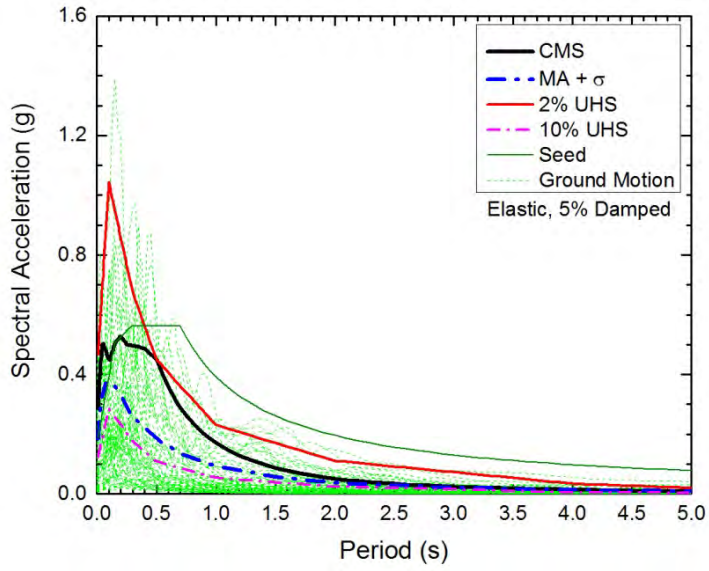

Figure 4.15. Response spectra of the selected, unscaled ground motions for scenario III compared to the five target spectra developed for this scenario.

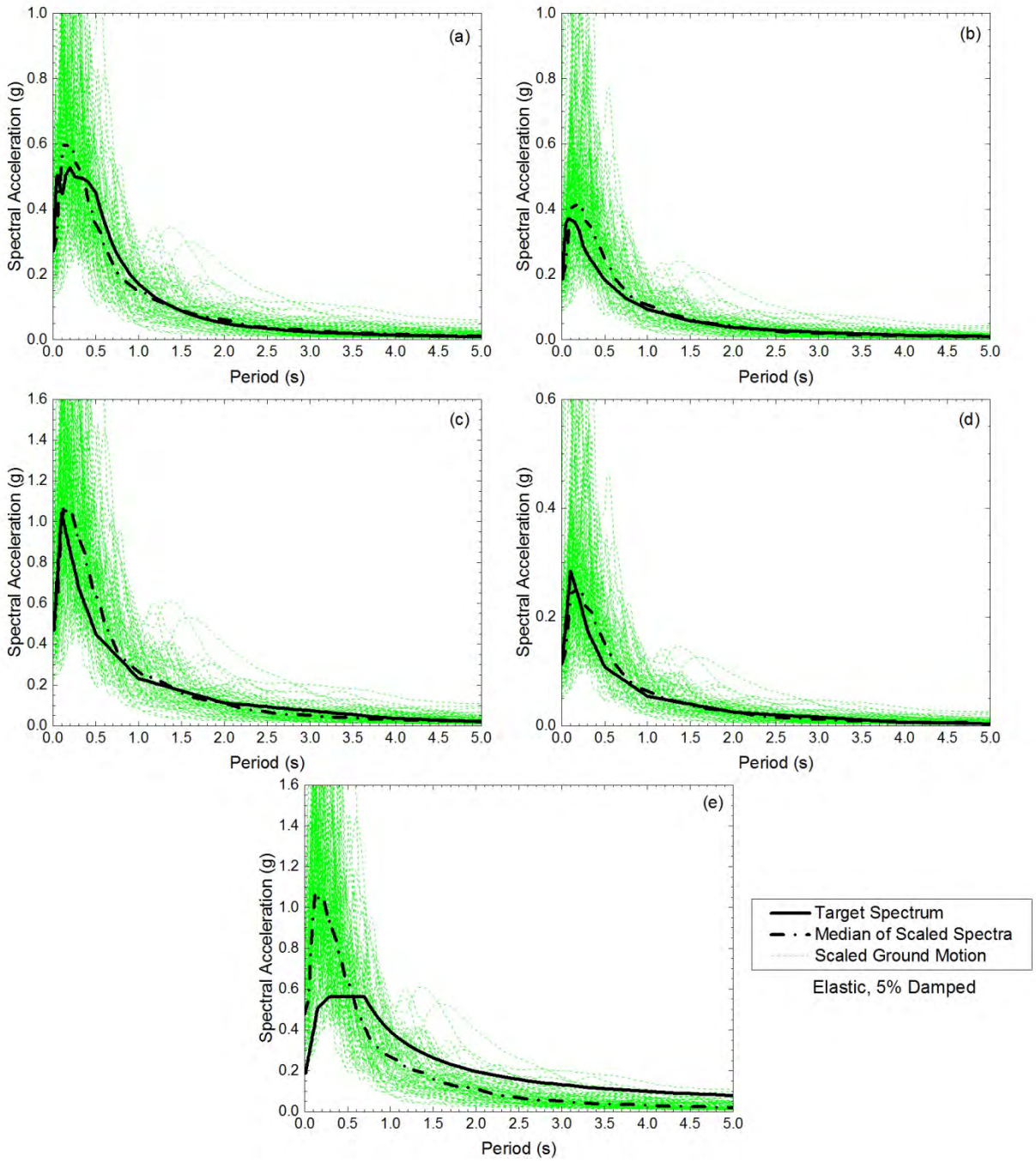

Figure 4.16. Response spectra of the optimally scaled ground motions and their medians from scenario III compared to the (a) conditional mean spectrum, (b) mean plus one standard deviation spectrum from the attenuation relationships, (c) 2% uniform hazard spectrum, (d) 10% uniform hazard spectrum, and (e) mean spectrum from Seed et al. (1997).

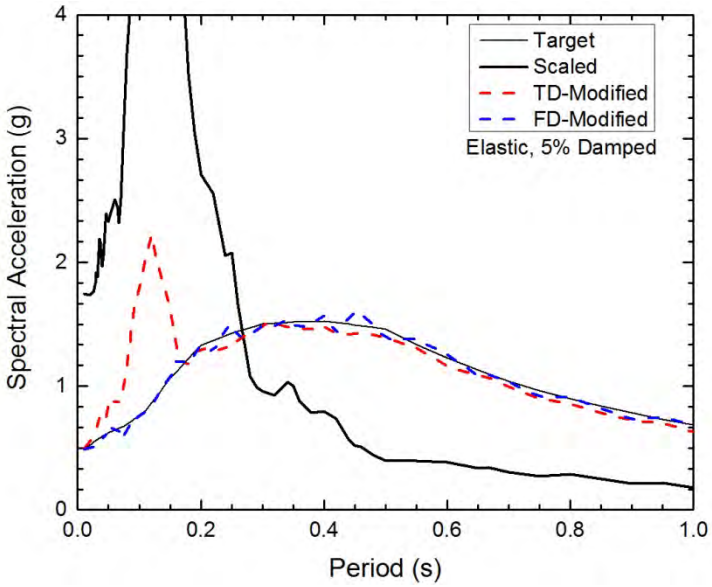

Figure 4.17. Target spectrum compared to the response spectra for an example TD-modified motion with a large spike at short periods and the corresponding scaled and FD-modified motions.

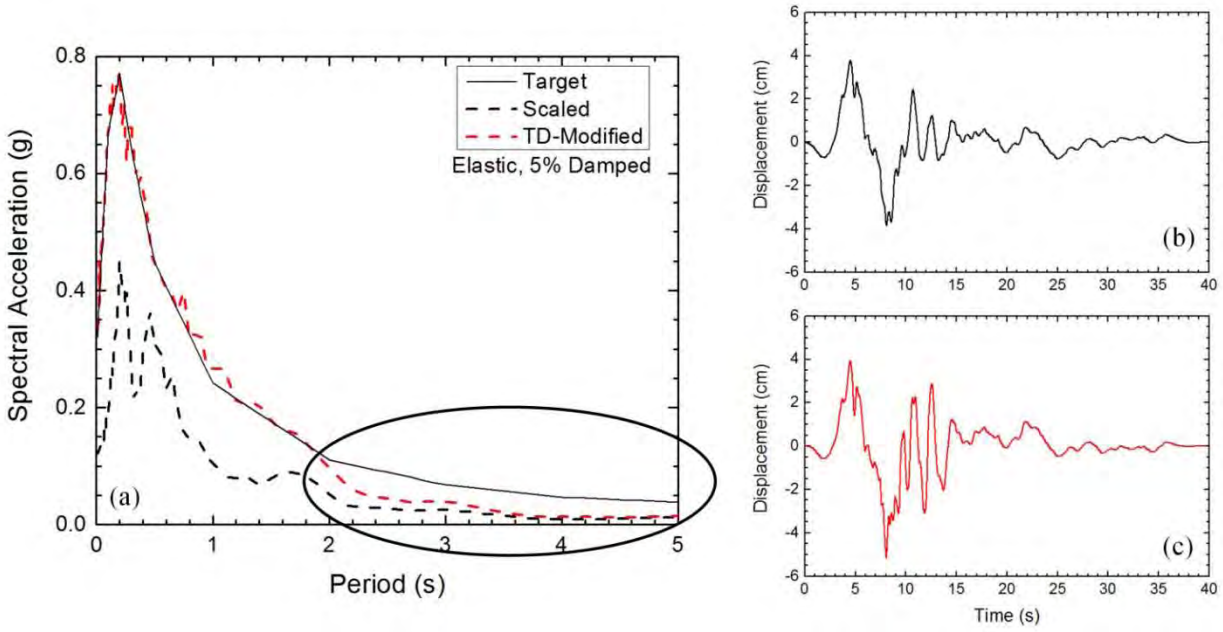

Figure 4.18. (a) Response spectra of scaled and TD-modified ground motions that match in the long period range and the corresponding displacement time histories of the (b) scaled and (c) TD-modified ground motions for one example motion.

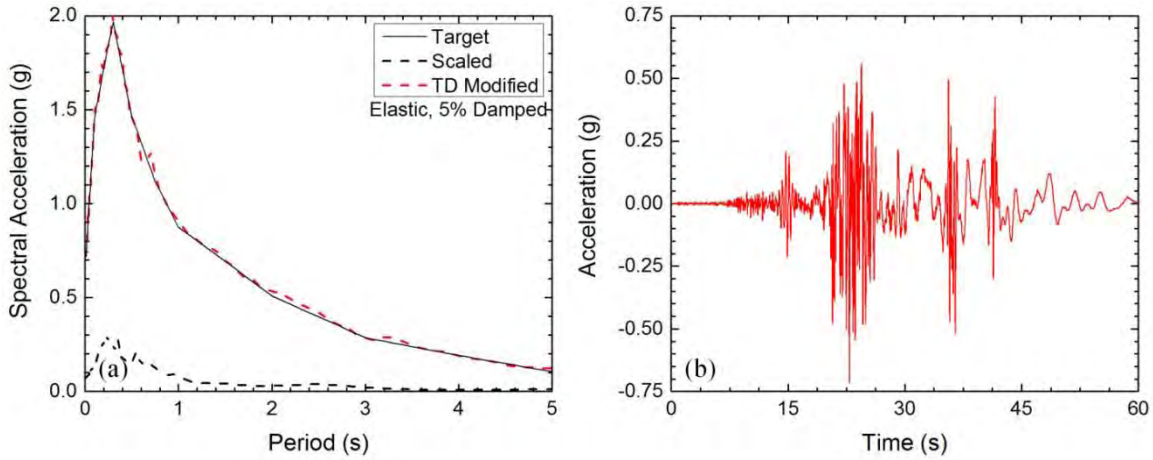

Figure 4.19. (a) Response spectra of scaled and TD-modified ground motions for an example motion with large amplitude pulses in the (b) acceleration time history of the TD-modified motion.

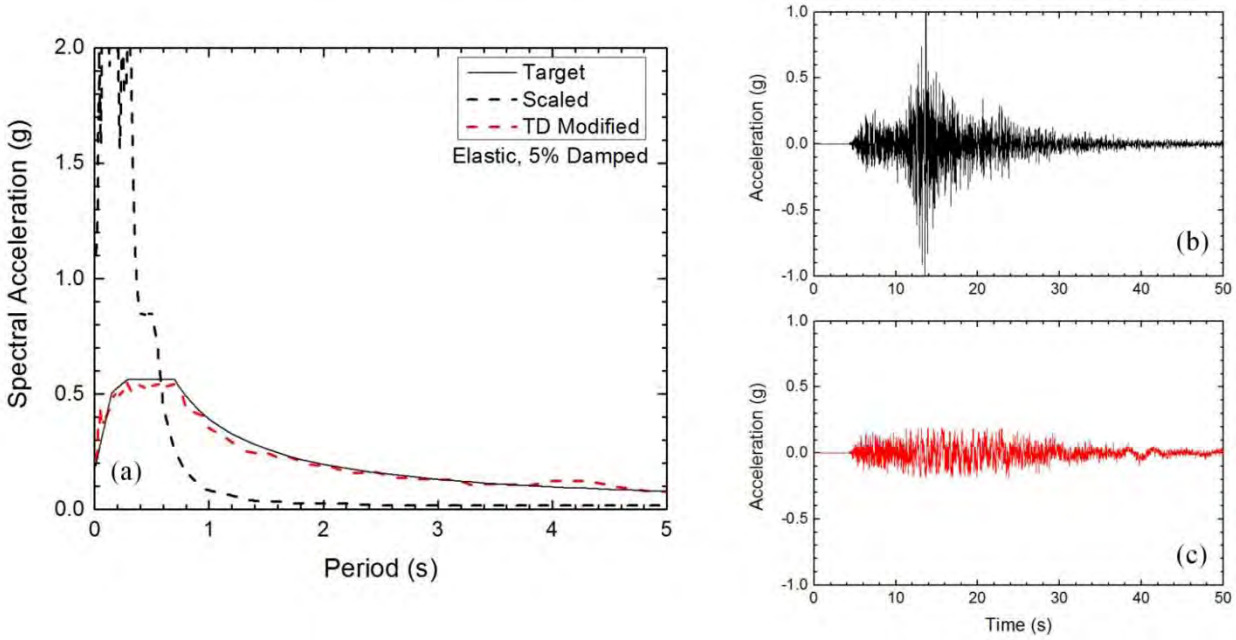

Figure 4.20. (a) Response spectra of scaled and TD-modified ground motions for an example motion where (b) peaks in the acceleration time history of the scaled ground motion (c) were constrained to the target peak ground acceleration for the acceleration time history of the TD-modified ground motion.

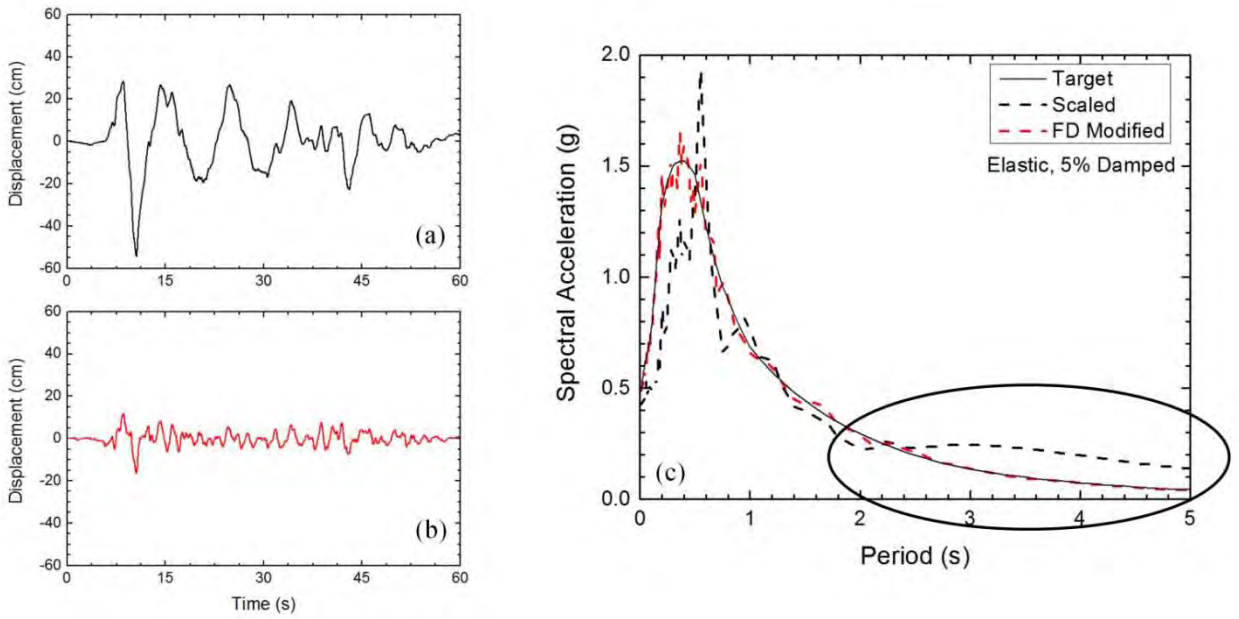

Figure 4.21. Displacement time histories of (a) scaled and (b) FD-modified ground motions for an example motion where the displacements of the FD-modified motion are significantly decreased. (c) The response spectra of the scaled motions were generally larger than the target spectrum in the long period range for motions where this behavior was observed.

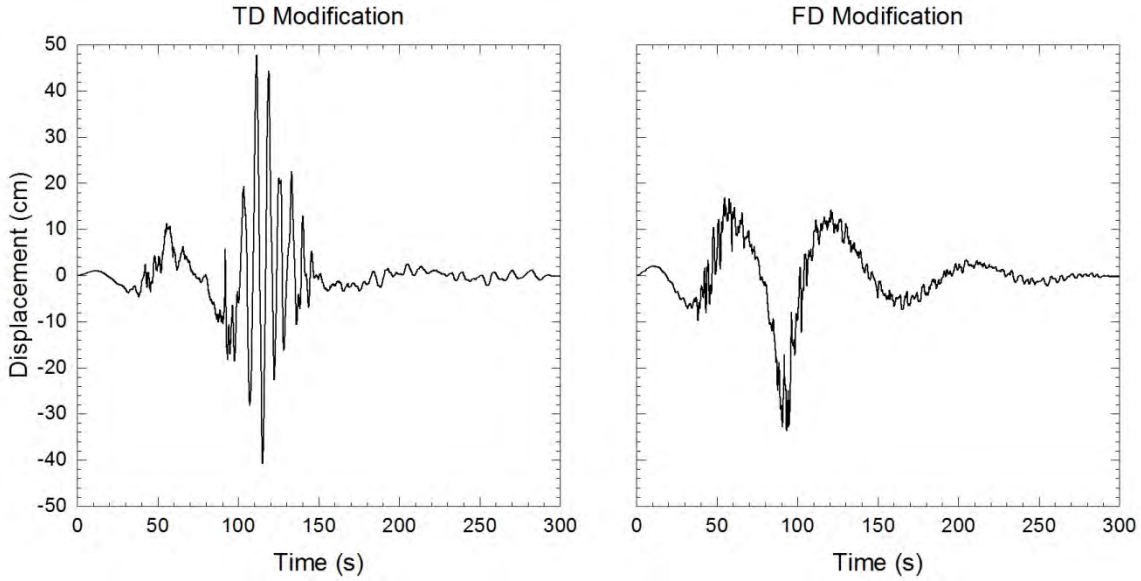

Figure 4.22. Displacement time histories for an example motion where using up to a 9th order polynomial correction function did not lead to satisfactory corrected displacement time histories for TD- and FD-modified motions.

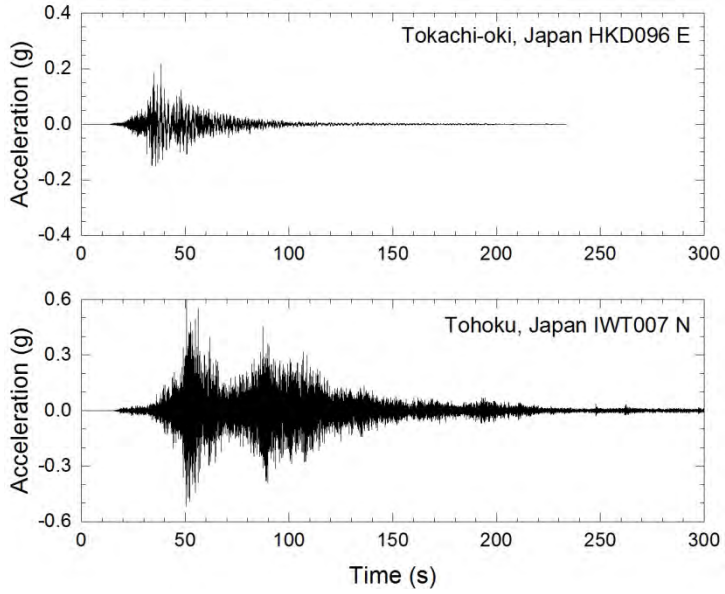

Figure 4.23. Example acceleration time histories from the Tokachi-oki, Japan and Tohoku, Japan events selected for the second scenario.

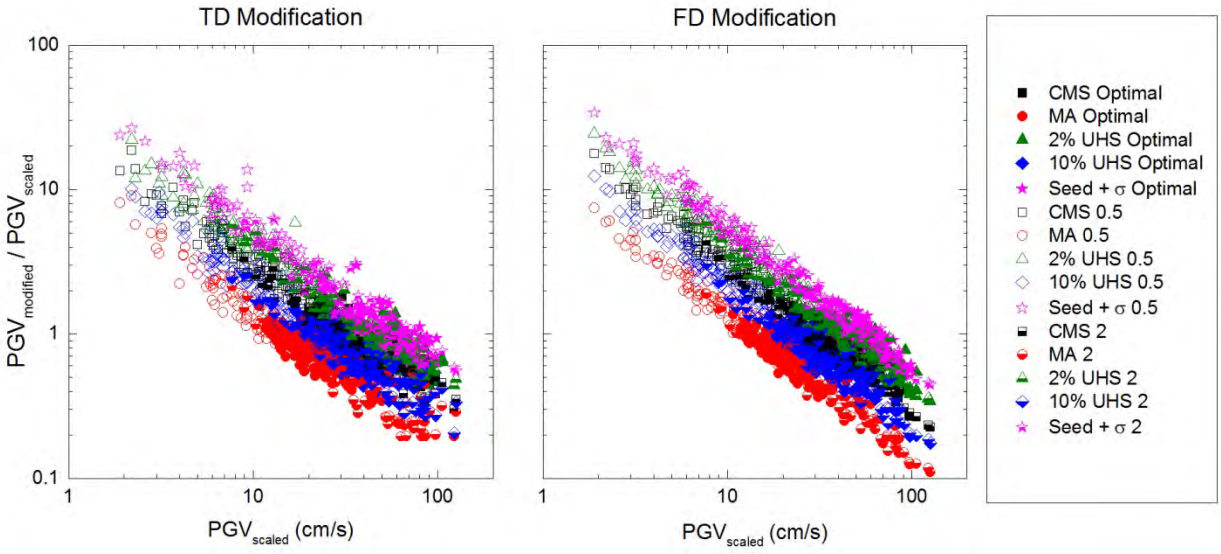

Figure 4.24. Modified-to-scaled peak ground velocity (*PGV*) ratios for TD and FD modification plotted versus the *PGV* of the scaled motions for all target spectra and scaling factors. In the legend, "Optimal," "0.5," and "2" refer to the scaling factors applied to the motions.

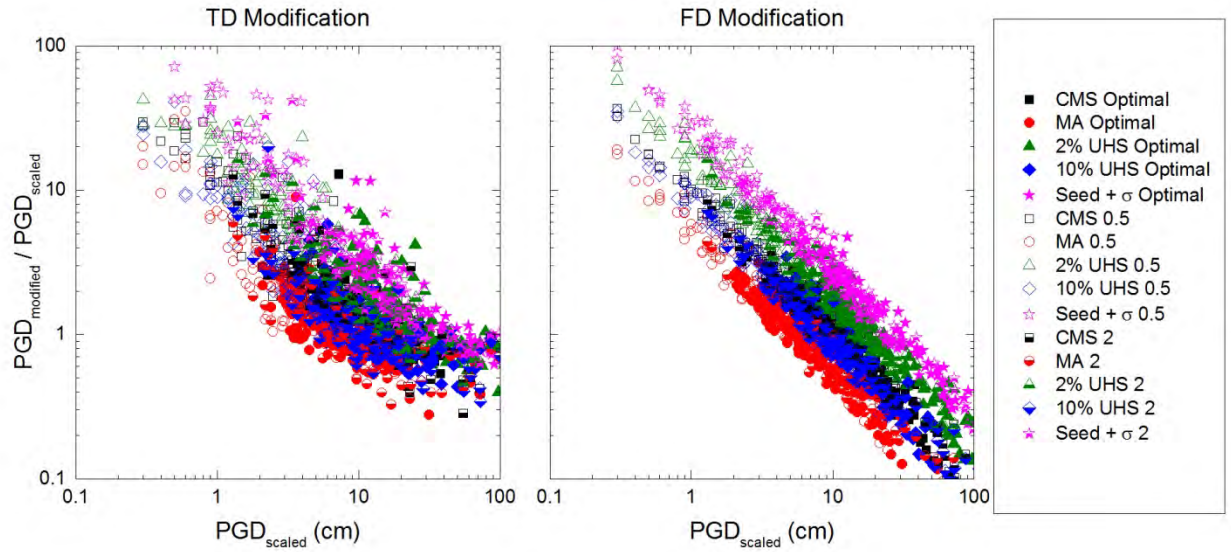

Figure 4.25. Modified-to-scaled peak ground displacement (*PGD*) ratios for TD and FD modification plotted versus the *PGD* of the scaled motions for all target spectra and scaling factors. In the legend, "Optimal," "0.5," and "2" refer to the scaling factors applied to the motions.

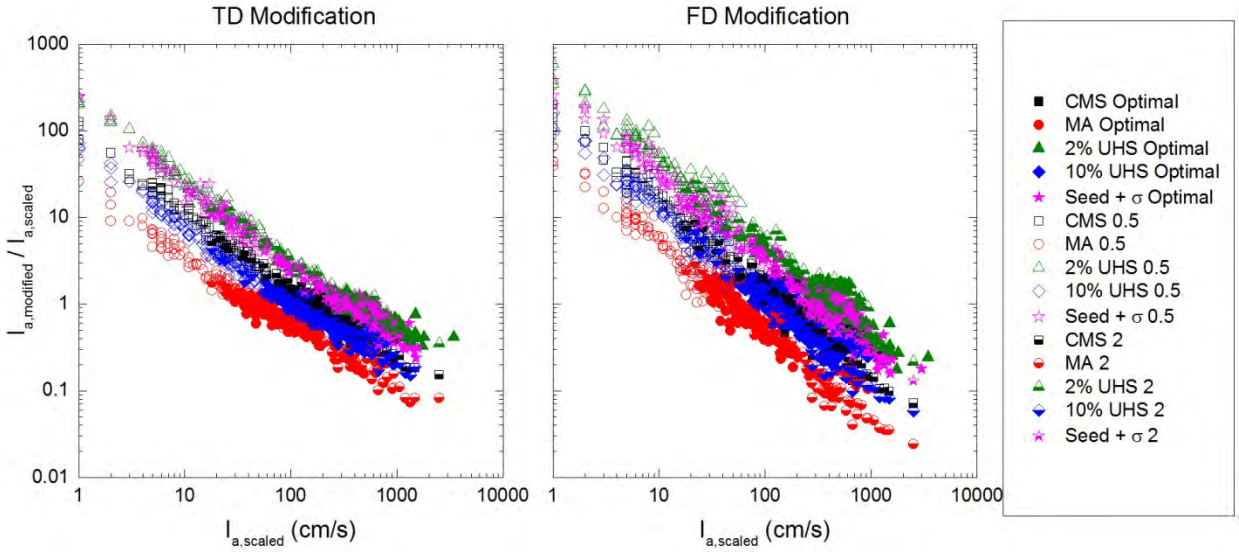

Figure 4.26. Modified-to-scaled Arias intensity (I_a) ratios for TD and FD modification plotted versus the I_a of the scaled motions for all target spectra and scaling factors. In the legend, "Optimal," "0.5," and "2" refer to the scaling factors applied to the motions.

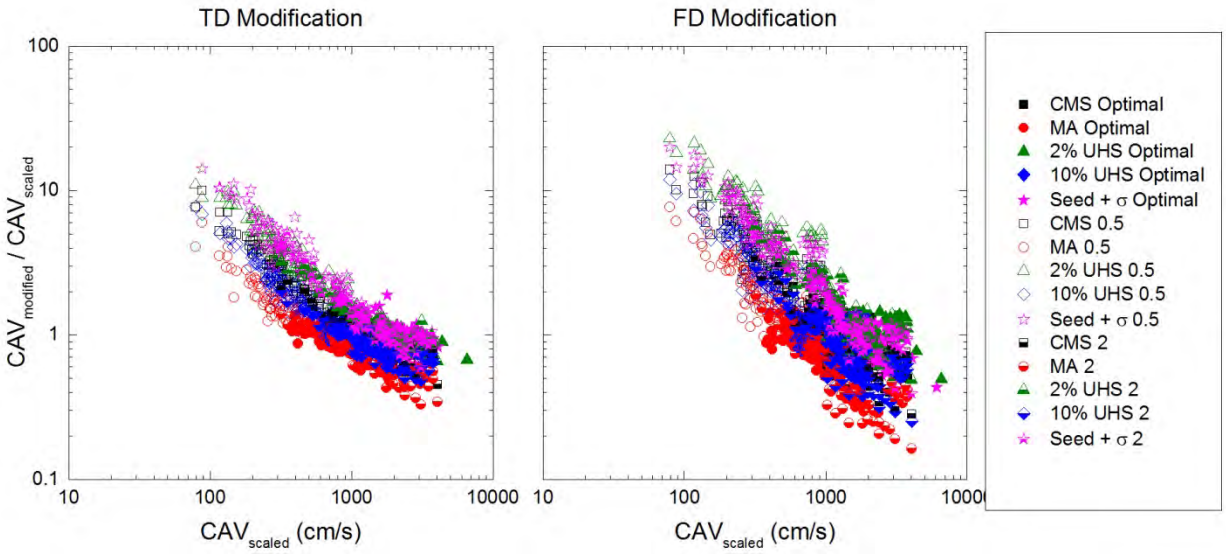

Figure 4.27. Modified-to-scaled cumulative absolute velocity (*CAV*) ratios for TD and FD modification plotted versus the *CAV* of the scaled motions for all target spectra and scaling factors. In the legend, "Optimal," "0.5," and "2" refer to the scaling factors applied to the motions.

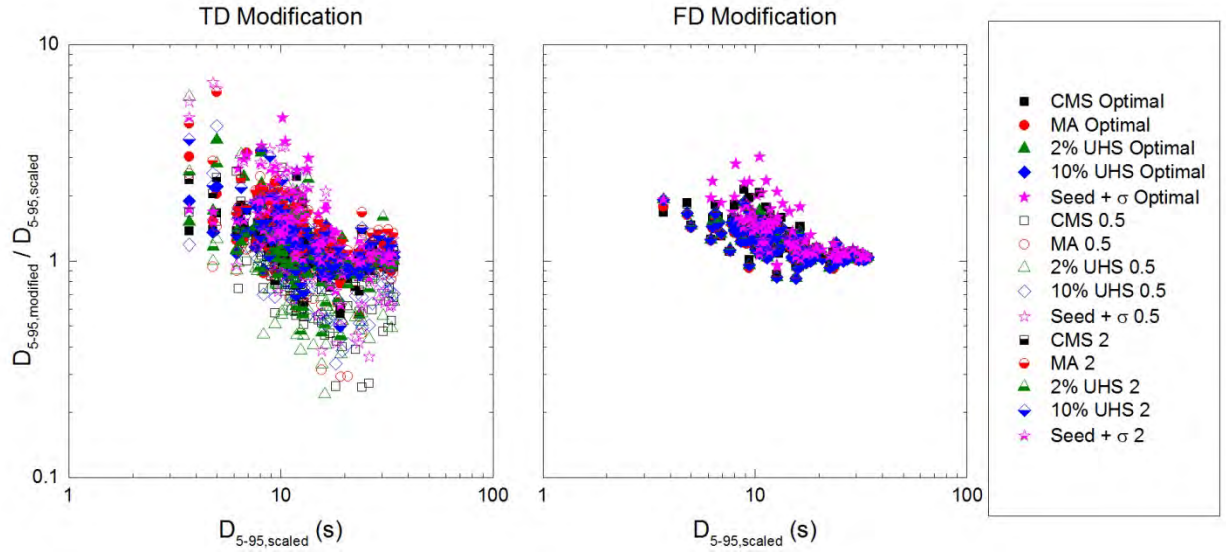

Figure 4.28. Modified-to-scaled significant duration ($D_{5\text{-}95}$) ratios for TD and FD modification plotted versus the $D_{5\text{-}95}$ of the scaled motions for all target spectra and scaling factors. In the legend, "Optimal," "0.5," and "2" refer to the scaling factors applied to the motions.

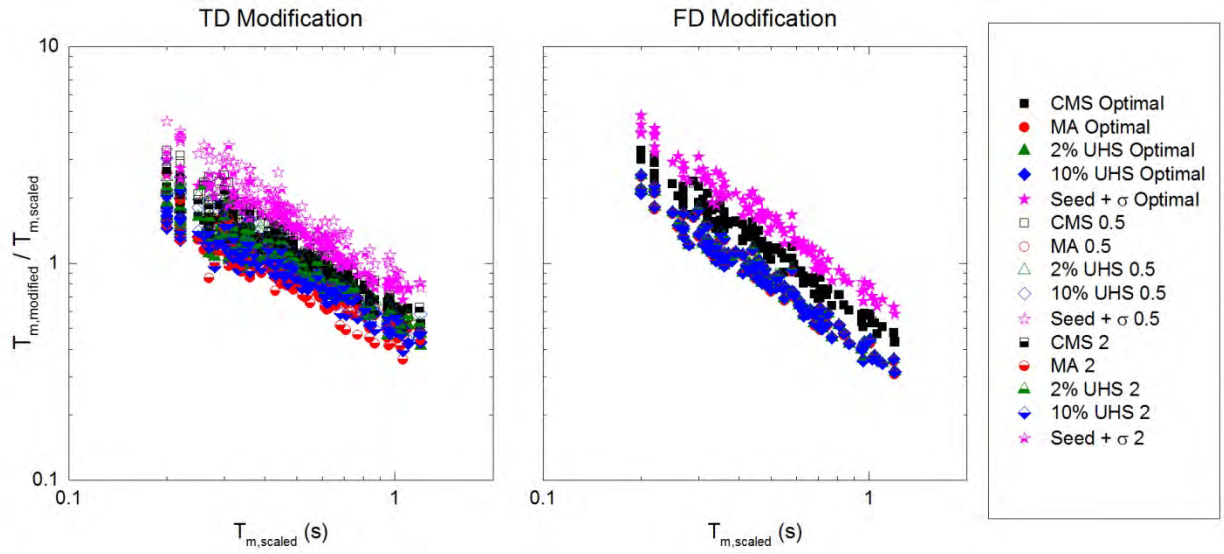

Figure 4.29. Modified-to-scaled mean period (T_m) ratios for TD and FD modification plotted versus the T_m of the scaled motions for all target spectra and scaling factors. In the legend, "Optimal," "0.5," and "2" refer to the scaling factors applied to the motions.

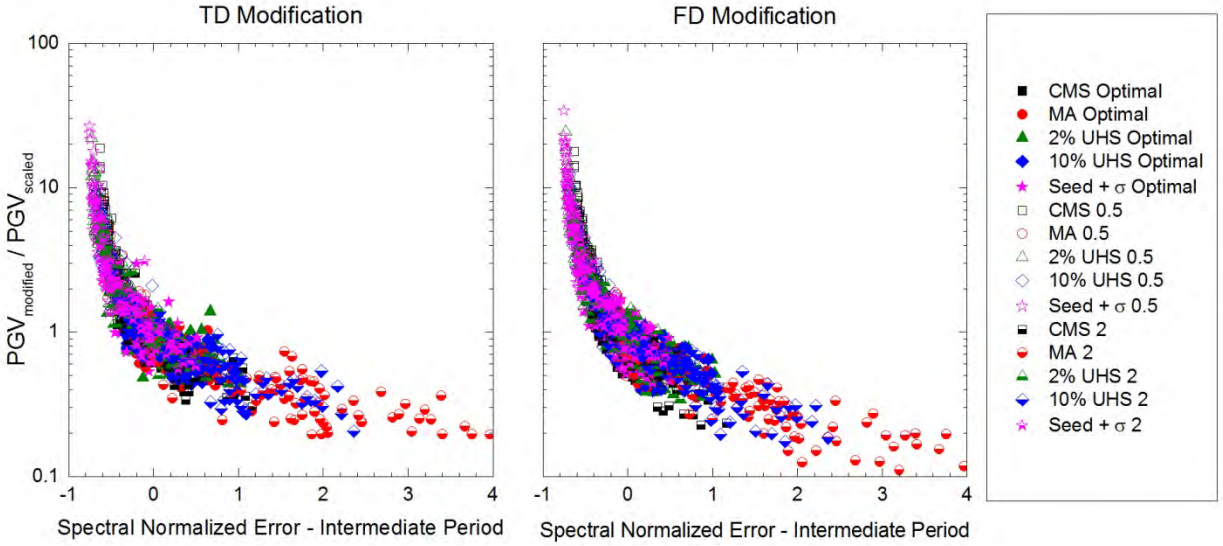

Figure 4.30. Modified-to-scaled peak ground velocity (*PGV*) ratios for TD and FD modification plotted versus spectral mismatch in the intermediate period range, quantified by $NE_{s,IP}$, for all target spectra and scaling factors. In the legend, "Optimal," "0.5," and "2" refer to the scaling factors applied to the motions.

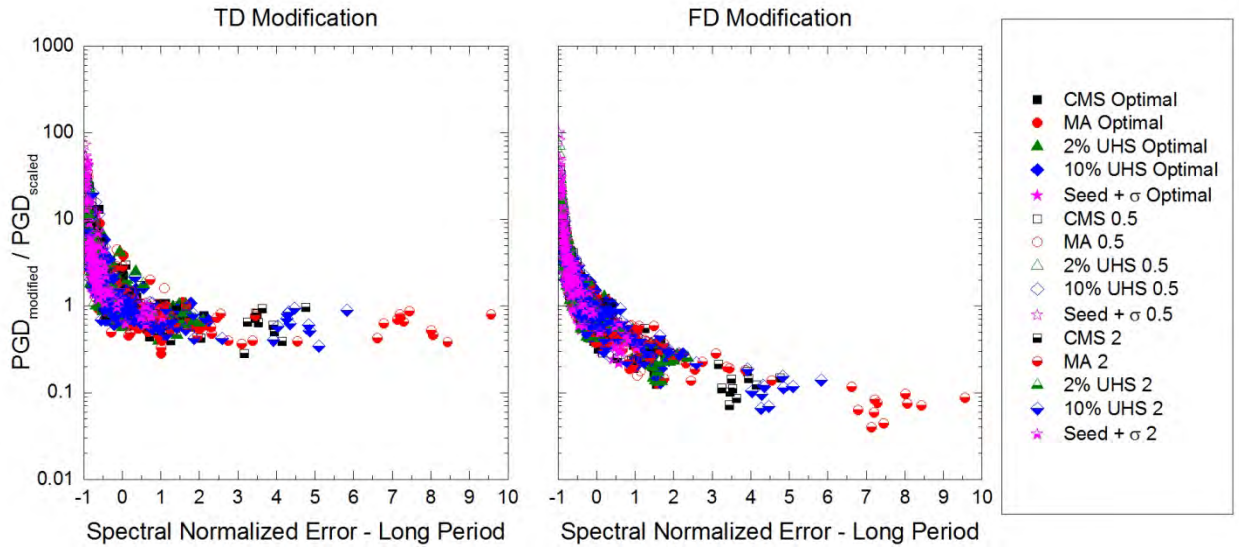

Figure 4.31. Modified-to-scaled peak ground displacement (*PGD*) ratios for TD and FD modification plotted versus spectral mismatch in the long period range, quantified by $NE_{s,LP}$, for all target spectra and scaling factors. In the legend, "Optimal," "0.5," and "2" refer to the scaling factors applied to the motions.

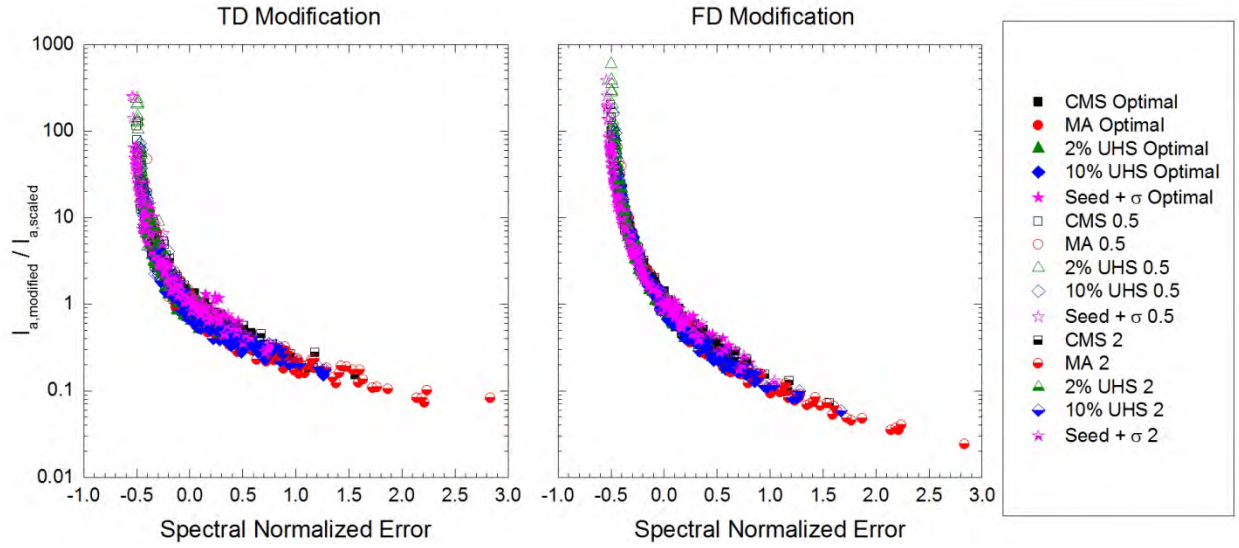

Figure 4.32. Modified-to-scaled Arias intensity (I_a) ratios for TD and FD modification plotted versus spectral mismatch, quantified by NE_s, for all target spectra and scaling factors. In the legend, "Optimal," "0.5," and "2" refer to the scaling factors applied to the motions.

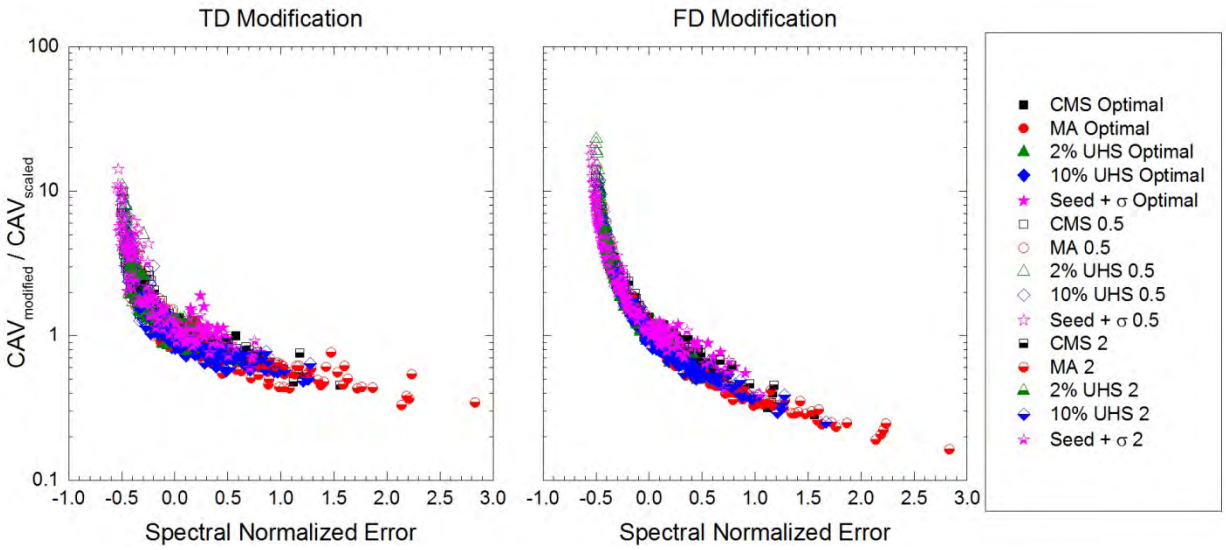

Figure 4.33. Modified-to-scaled cumulative absolute velocity (*CAV*) ratios for TD and FD modification plotted versus spectral mismatch, quantified by NE_s, for all target spectra and scaling factors. In the legend, "Optimal," "0.5," and "2" refer to the scaling factors applied to the motions.

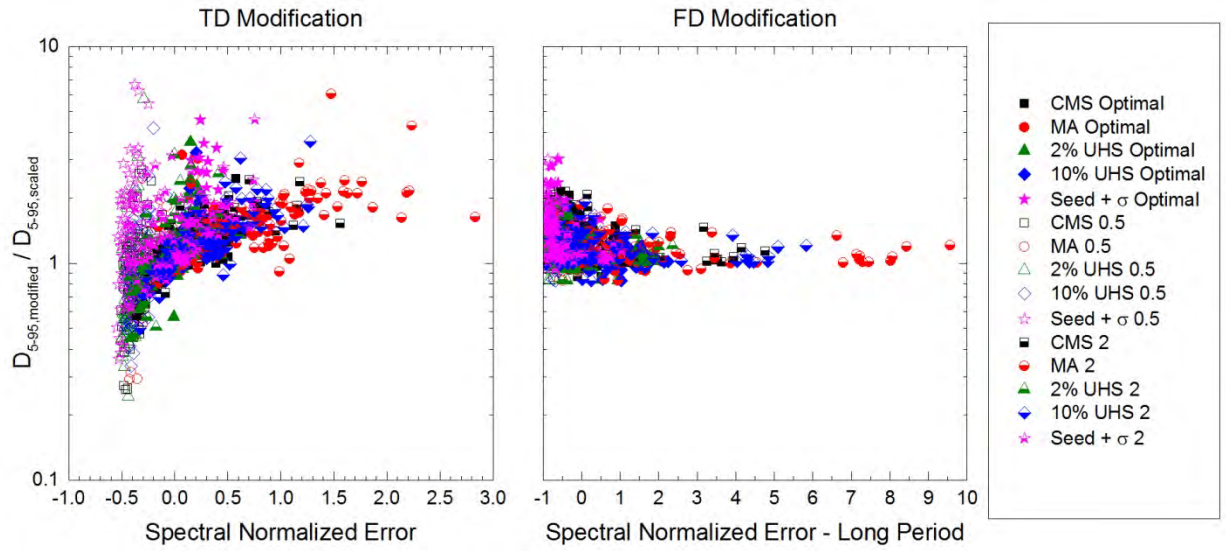

Figure 4.34. Modified-to-scaled significant duration ($D_{5\text{-}95}$) ratios for TD and FD modification plotted versus spectral mismatch, quantified by NE_s and $NE_{s,LP}$, for all target spectra and scaling factors. In the legend, "Optimal," "0.5," and "2" refer to the scaling factors applied to the motions.

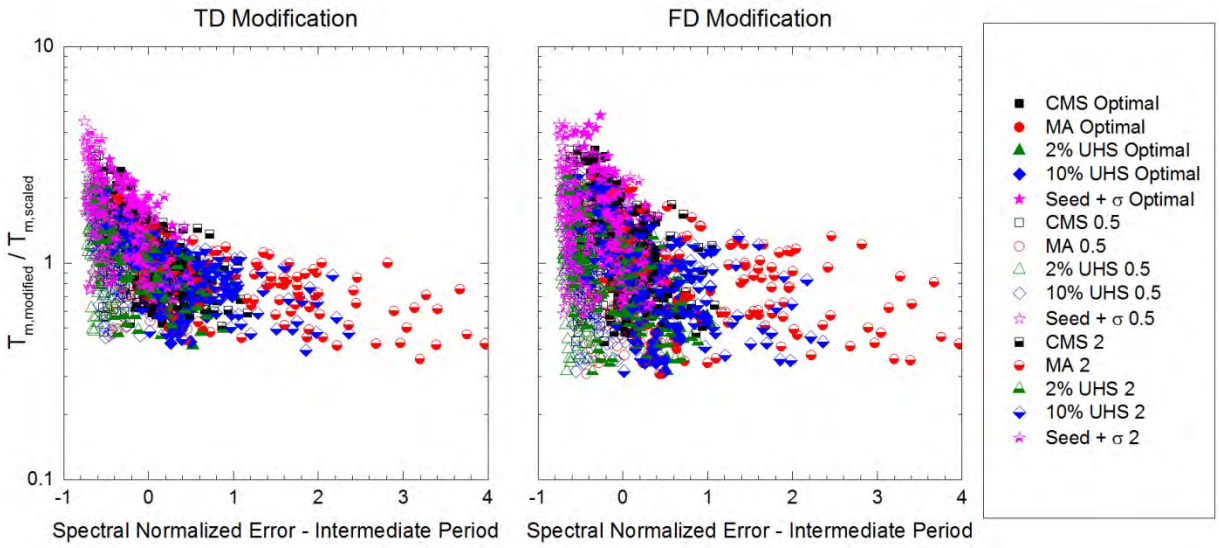

Figure 4.35. Modified-to-scaled mean period (T_m) ratios for TD and FD modification plotted versus spectral mismatch in the intermediate period range, quantified by $NE_{s,IP}$, for all target spectra and scaling factors. In the legend, "Optimal," "0.5," and "2" refer to the scaling factors applied to the motions.

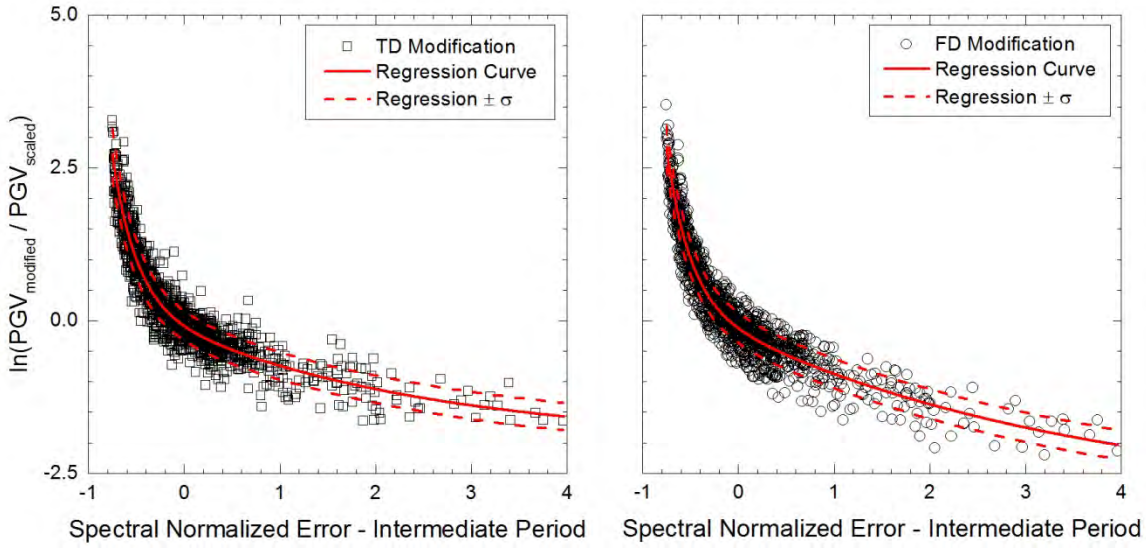

Figure 4.36. Regression curves, with plus and minus one standard deviation lines, developed for the relationship between the logarithmic modified-to-scaled peak ground velocity (*PGV*) ratios and spectral mismatch in the intermediate period range for the motions in scenario I.

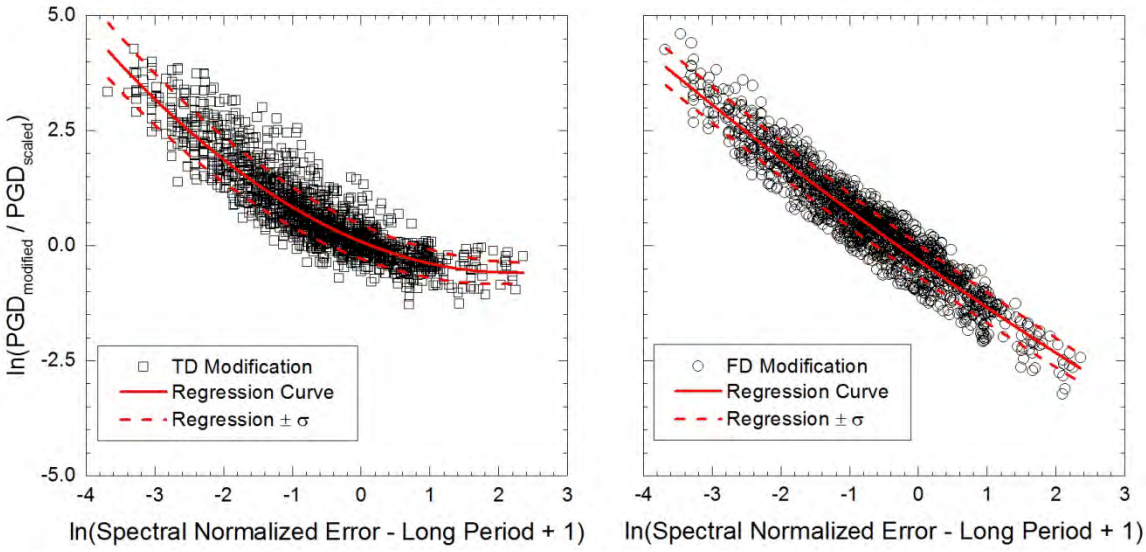

Figure 4.37. Regression curves, with plus and minus one standard deviation lines, developed for the relationship between the logarithmic modified-to-scaled peak ground displacement (*PGD*) ratios and spectral mismatch in the long period range for the motions in scenario I.

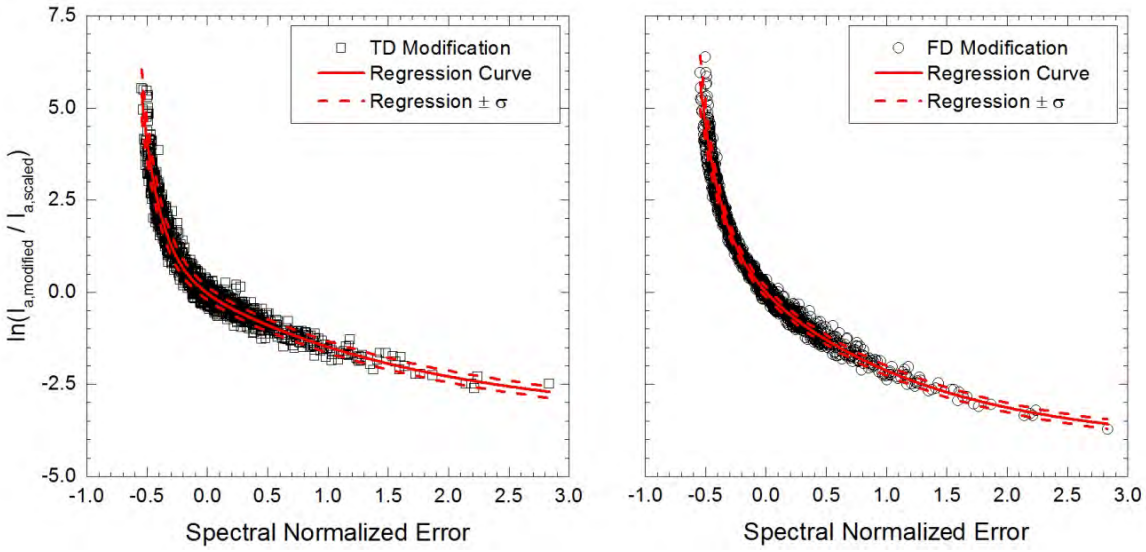

Figure 4.38. Regression curves, with plus and minus one standard deviation lines, developed for the relationship between the logarithmic modified-to-scaled Arias intensity (I_a) ratios and spectral mismatch for the motions in scenario I.

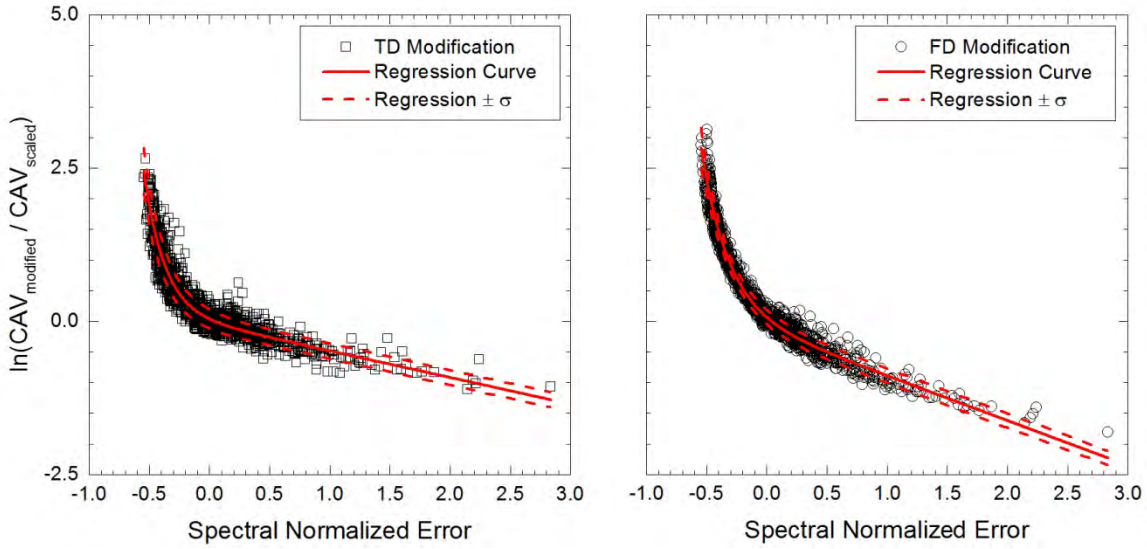

Figure 4.39. Regression curves, with plus and minus one standard deviation lines, developed for the relationship between the logarithmic modified-to-scaled cumulative absolute velocity (*CAV*) ratios and spectral mismatch for the motions in scenario I.

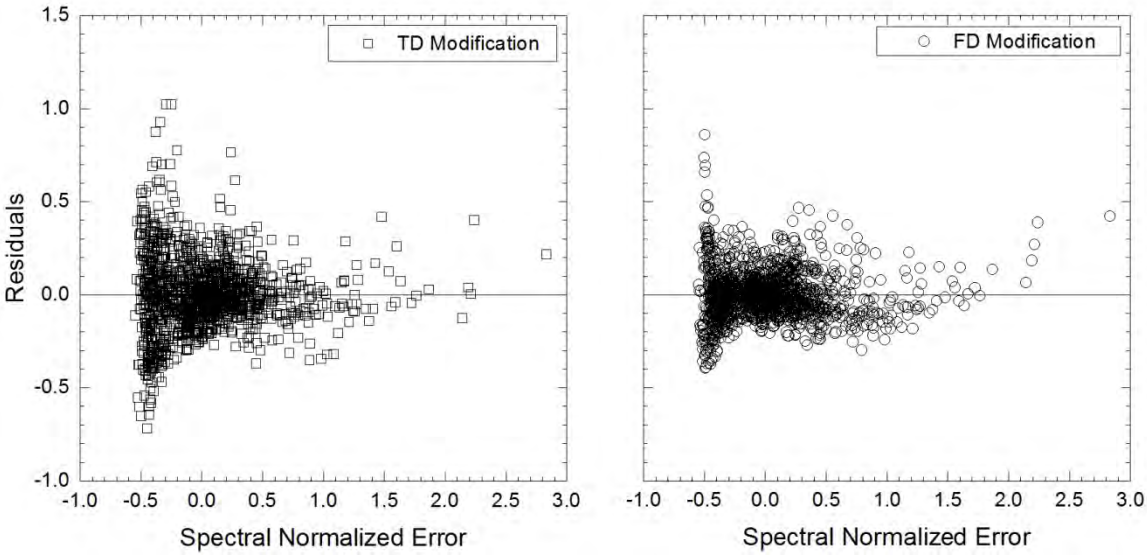

Figure 4.40. Residuals for the regression equations developed for the relationship between the logarithmic modified-to-scaled cumulative absolute velocity ratios and spectral mismatch for the motions in scenario I.

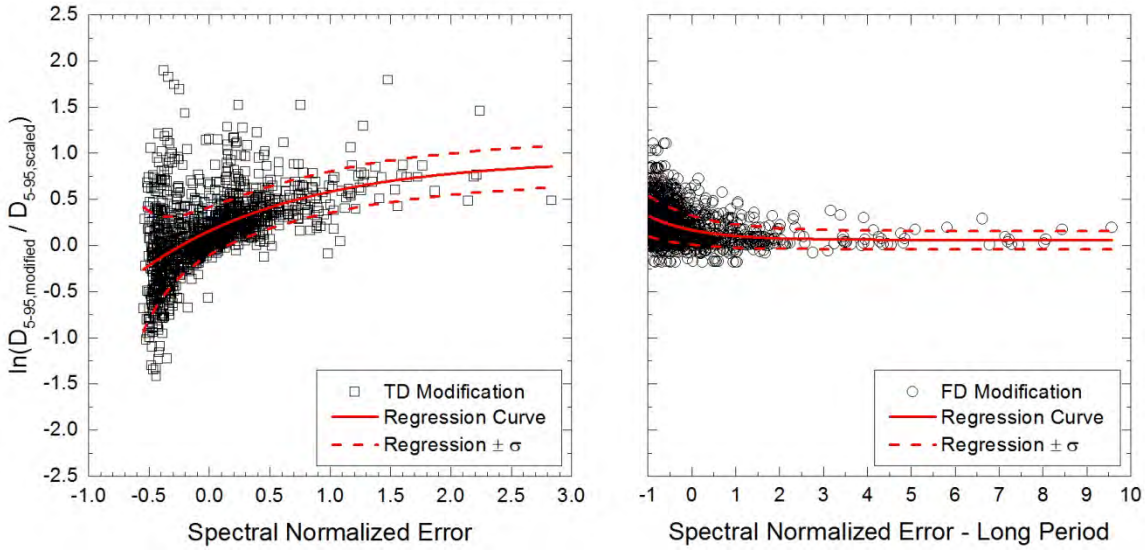

Figure 4.41. Regression curves, with plus and minus one standard deviation lines, developed for the relationship between the logarithmic modified-to-scaled significant duration ($D_{5\text{-}95}$) ratios and spectral mismatch for the entire period range and in the long period range for the TD- and FD-modified motions in scenario I, respectively.

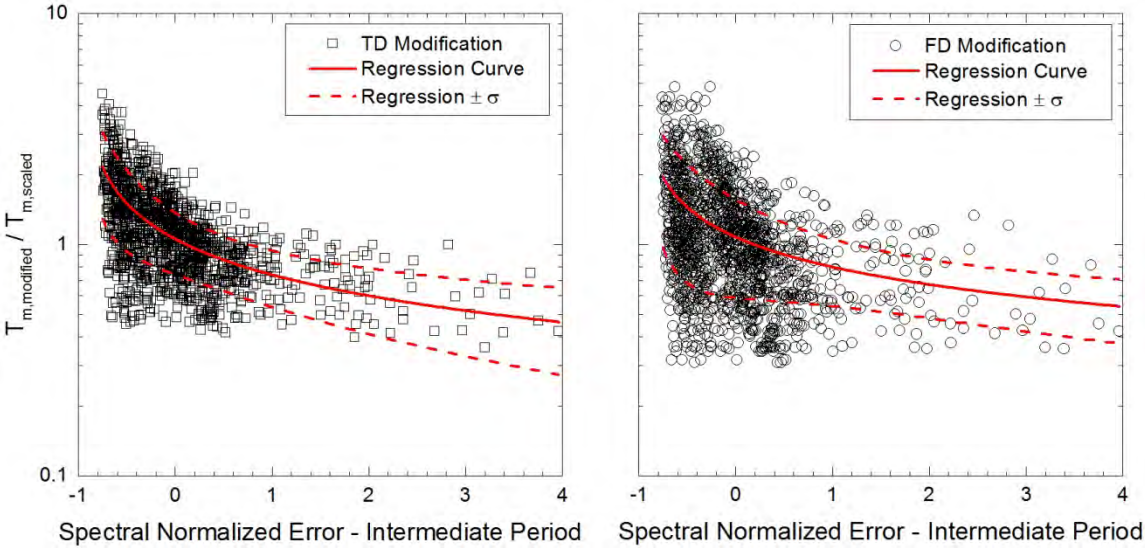

Figure 4.42. Regression curves, with plus and minus one standard deviation lines, developed for the relationship between the modified-to-scaled mean period (T_m) ratios and spectral mismatch in the intermediate period range for the motions in scenario I.

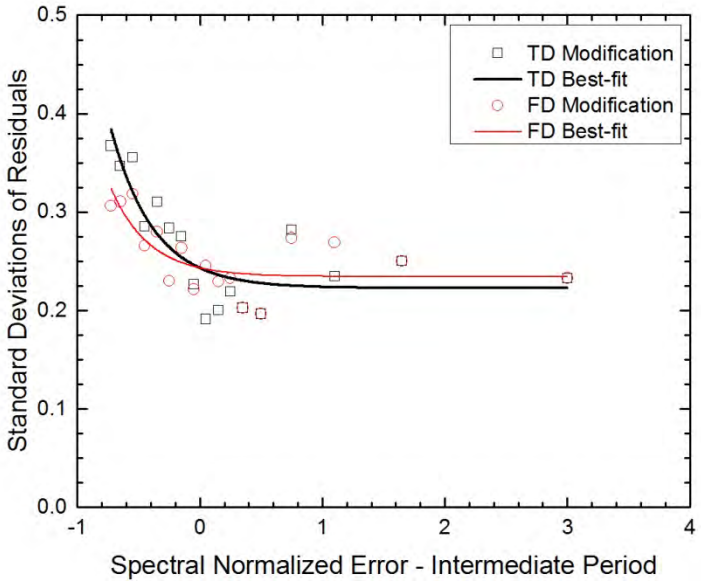

Figure 4.43. Standard deviations of the residuals, and corresponding best-fit curves, for the regression equations developed for the relationship between the logarithmic modified-to-scaled peak ground velocity ratios and spectral mismatch in the intermediate period range for the motions in scenario I.

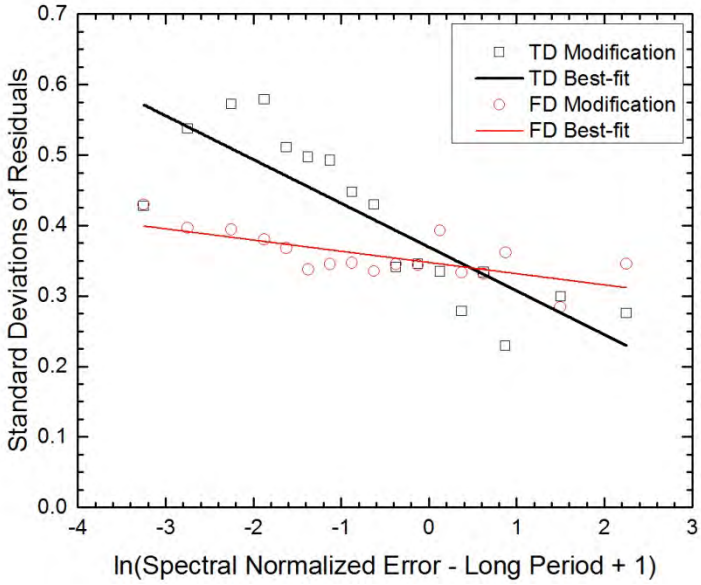

Figure 4.44. Standard deviations of the residuals, and corresponding best-fit curves, for the regression equations developed for the relationship between the logarithmic modified-to-scaled peak ground displacement ratios and spectral mismatch in the long period range for the motions in scenario I.

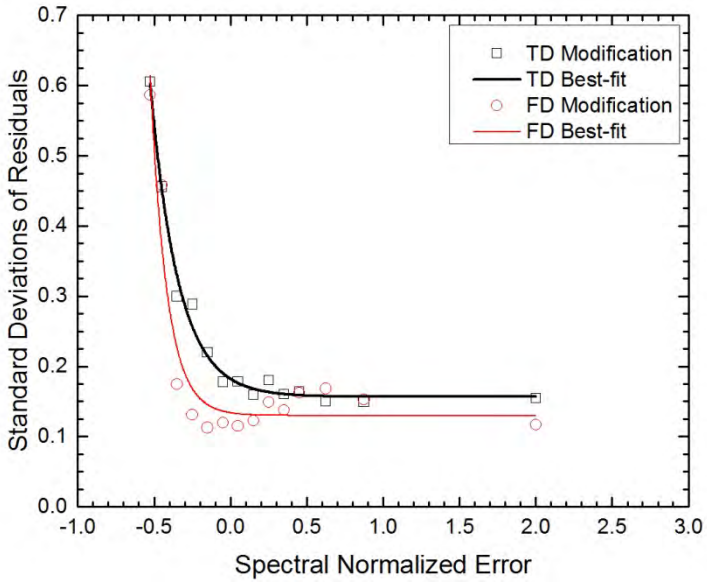

Figure 4.45. Standard deviations of the residuals, and corresponding best-fit curves, for the regression equations developed for the relationship between the logarithmic modified-to-scaled Arias intensity ratios and spectral mismatch for the motions in scenario I.

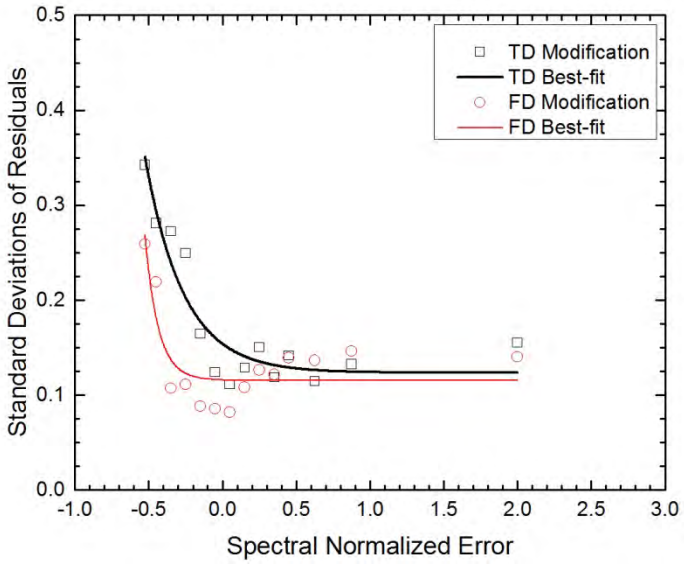

Figure 4.46. Standard deviations of the residuals, and corresponding best-fit curves, for the regression equations developed for the relationship between the logarithmic modified-to-scaled cumulative absolute velocity ratios and spectral mismatch for the motions in scenario I.

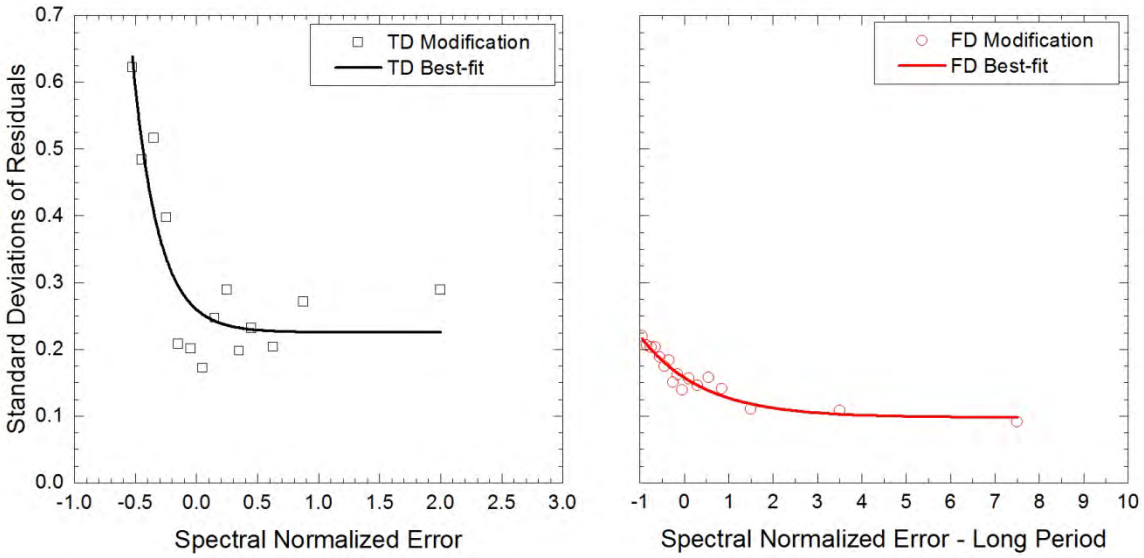

Figure 4.47. Standard deviations of the residuals, and corresponding best-fit curves, for the regression equations developed for the relationship between the logarithmic modified-to-scaled significant duration ratios and spectral mismatch for the entire period range and in the long period range for the TD- and FD-modified motions in scenario I, respectively.

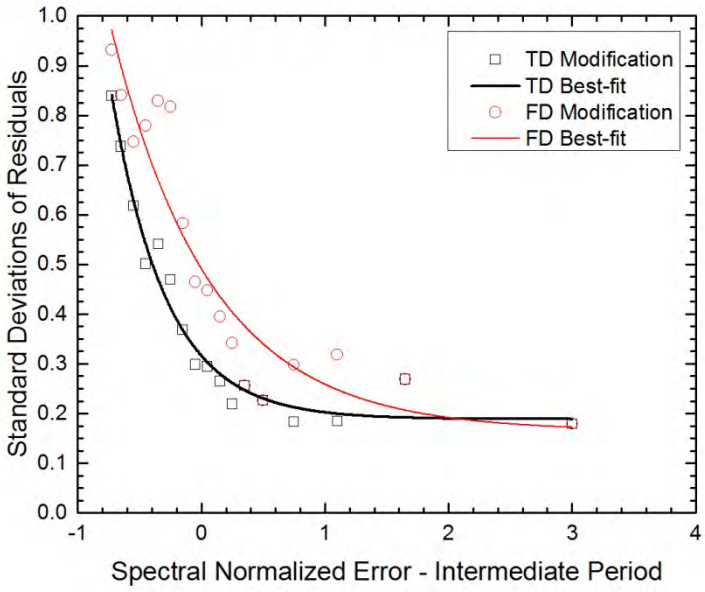

Figure 4.48. Standard deviations of the residuals, and corresponding best-fit curves, for the regression equations developed for the relationship between the modified-to-scaled mean period ratios and spectral mismatch in the intermediate period range for the motions in scenario I.

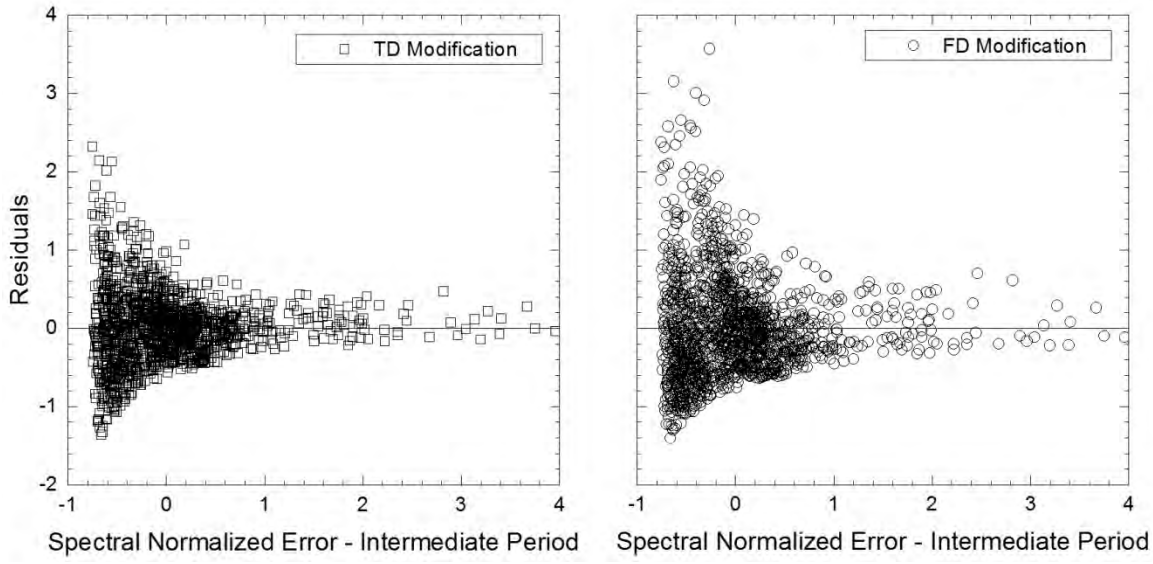

Figure 4.49. Residuals for the regression equations developed for the relationship between the modified-to-scaled mean period ratios and spectral mismatch in the intermediate period range for the motions in scenario I.

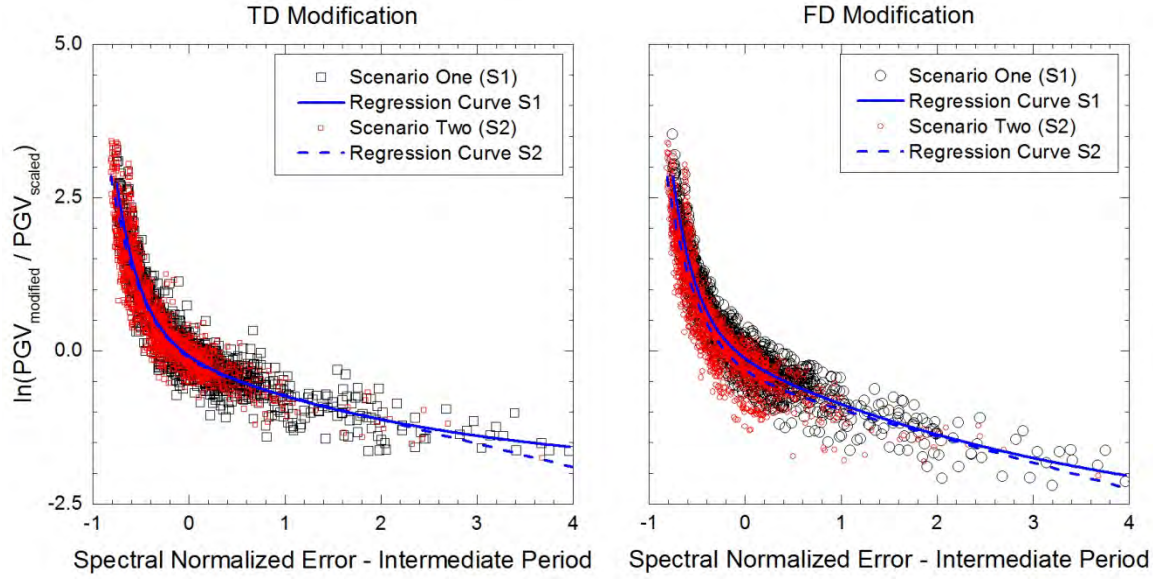

Figure 4.50. Comparison of the regression curves developed for the relationship between logarithmic modified-to-scaled peak ground velocity (*PGV*) ratios and spectral mismatch in the intermediate period range for the motions in scenarios I and II.

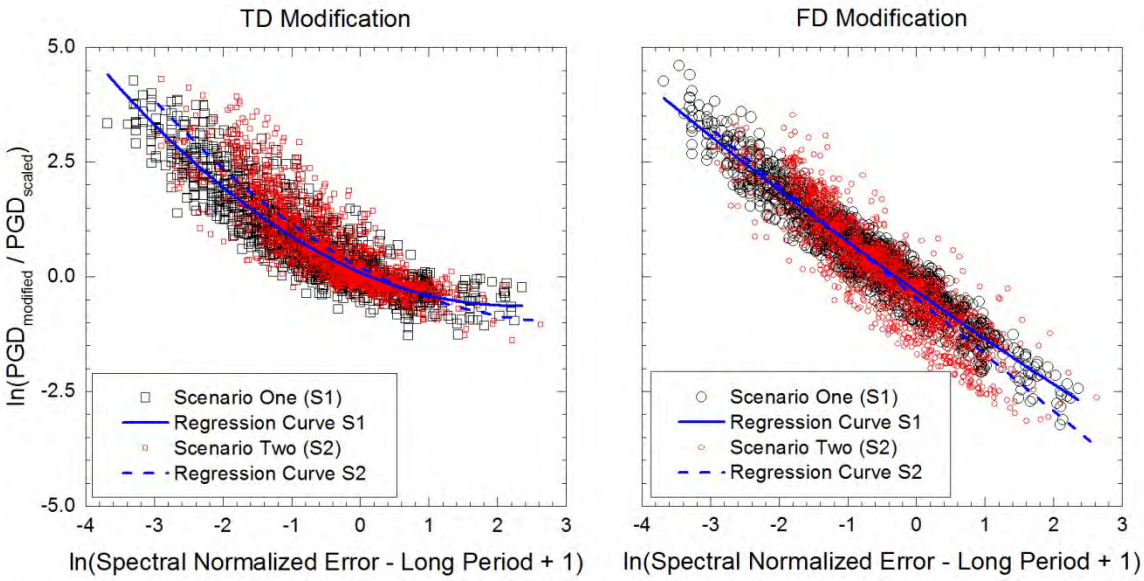

Figure 4.51. Comparison of the regression curves developed for the relationship between logarithmic modified-to-scaled peak ground displacement (*PGD*) ratios and spectral mismatch in the long period range for the motions in scenarios I and II.

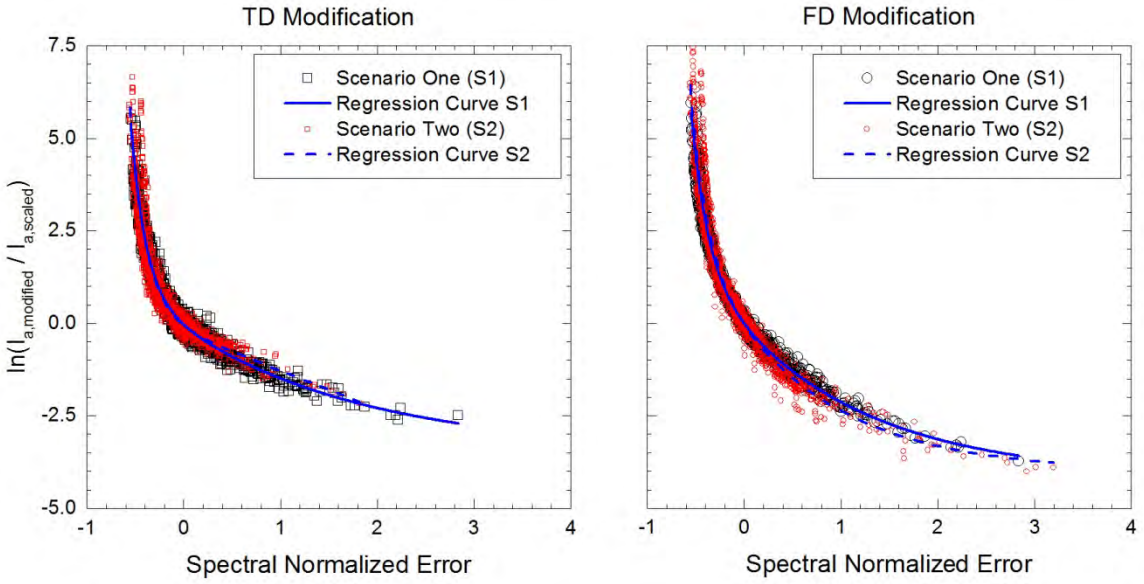

Figure 4.52. Comparison of the regression curves developed for the relationship between logarithmic modified-to-scaled Arias intensity (I_a) ratios and spectral mismatch for the motions in scenarios I and II.

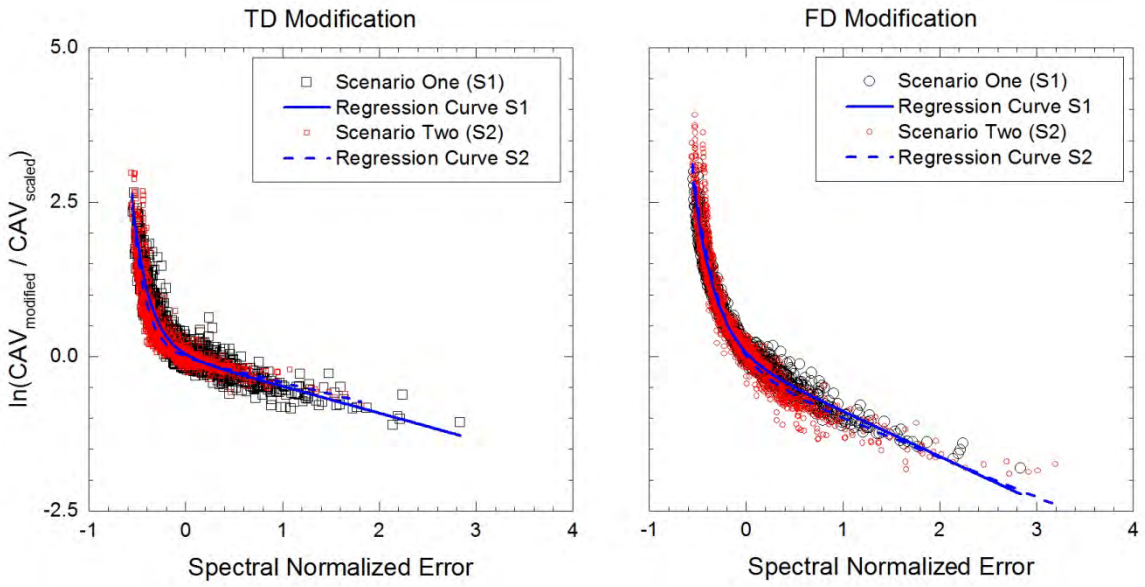

Figure 4.53. Comparison of the regression curves developed for the relationship between logarithmic modified-to-scaled cumulative absolute velocity (*CAV*) ratios and spectral mismatch for the motions in scenarios I and II.

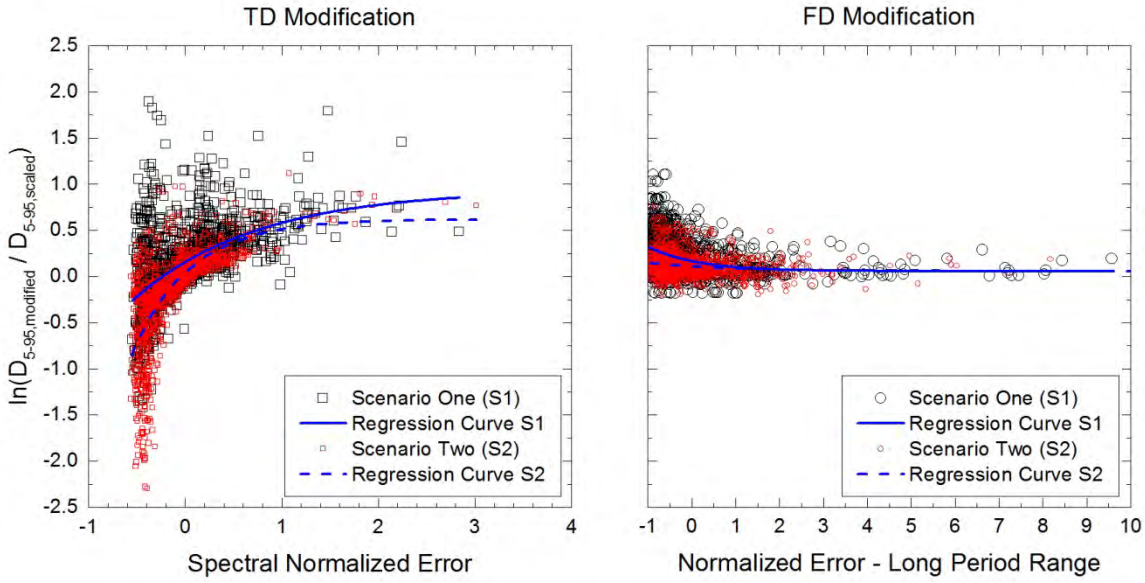

Figure 4.54. Comparison of the regression curves developed for the relationship between logarithmic modified-to-scaled significant duration ($D_{5\text{-}95}$) ratios and spectral mismatch for the entire period range and in the long period range for the TD- and FD-modified motions, respectively, in scenarios I and II.

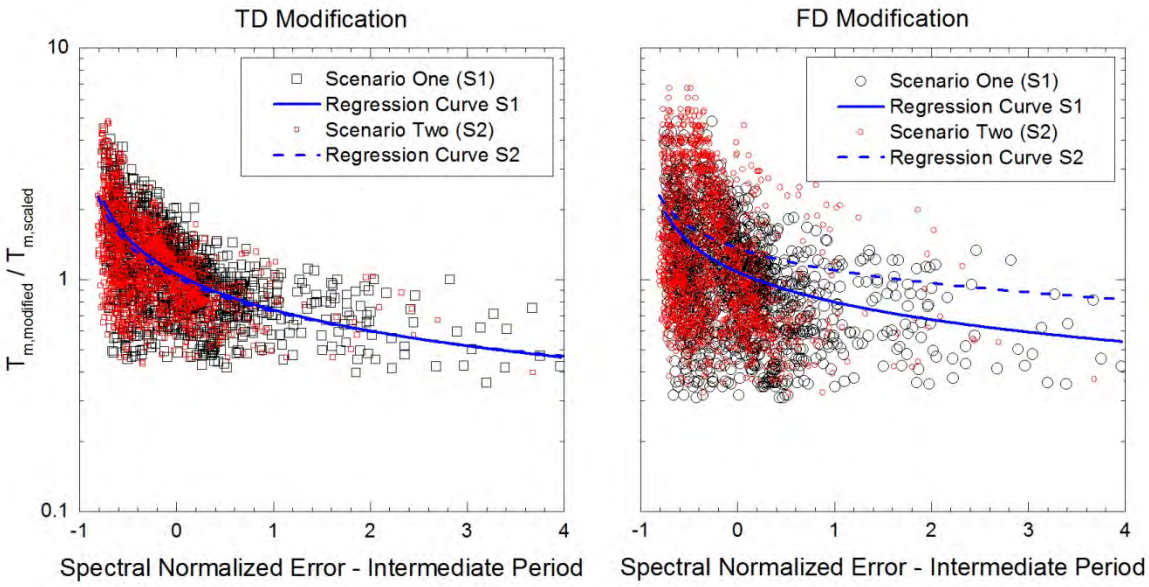

Figure 4.55. Comparison of the regression curves developed for the relationship between modified-to-scaled mean period (T_m) ratios and spectral mismatch in the intermediate period range for the motions in scenarios I and II.

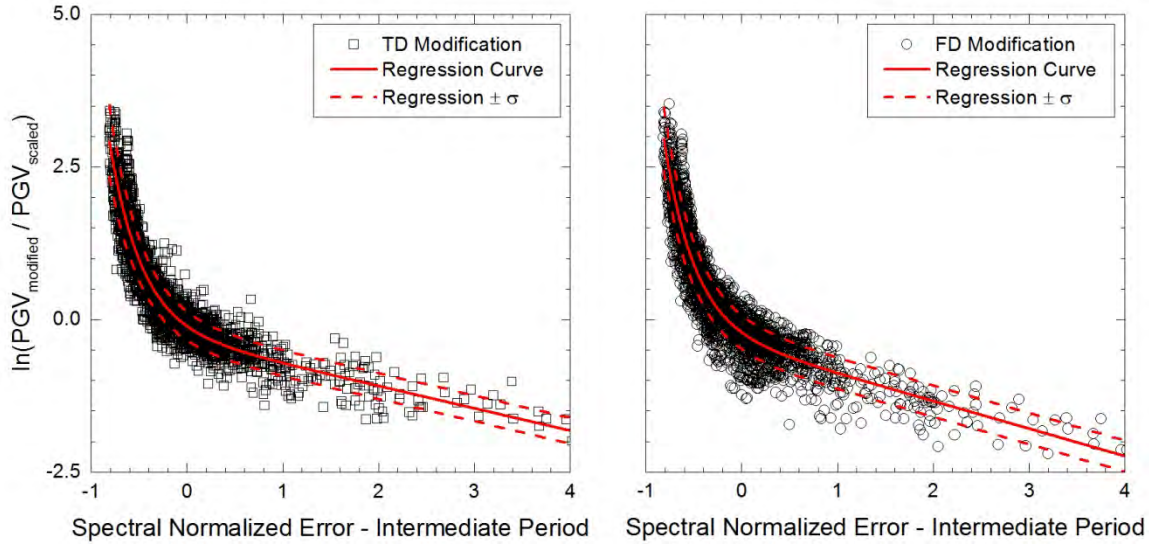

Figure 4.56. Regression curves, with plus and minus one standard deviation lines, developed for the relationship between the logarithmic modified-to-scaled peak ground velocity (*PGV*) ratios and spectral mismatch in the intermediate period range for the combined set of motions from scenarios I and II.

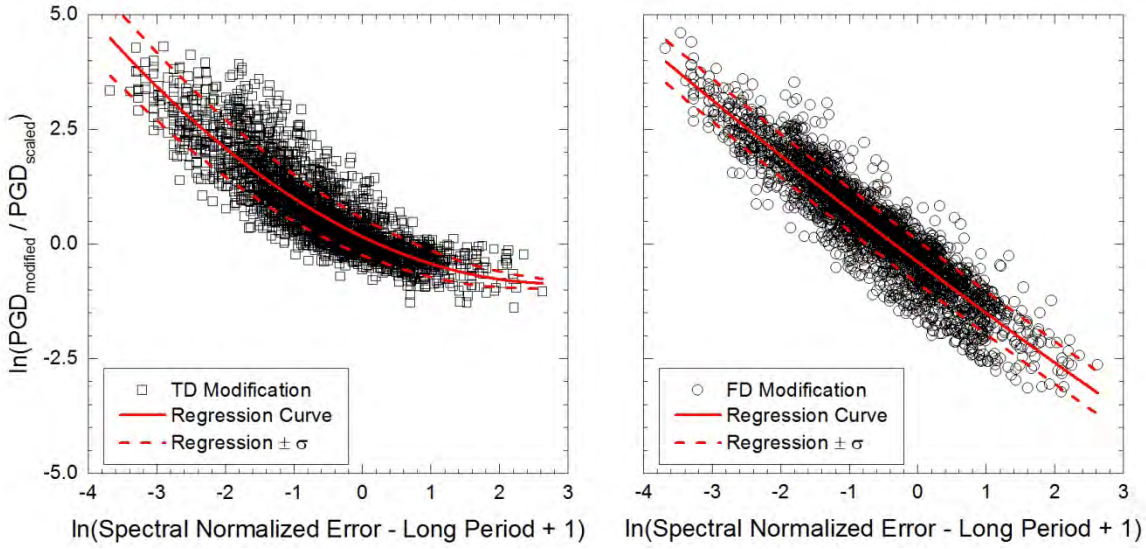

Figure 4.57. Regression curves, with plus and minus one standard deviation lines, developed for the relationship between the logarithmic modified-to-scaled peak ground displacement (*PGD*) ratios and spectral mismatch in the long period range for the combined set of motions from scenarios I and II.

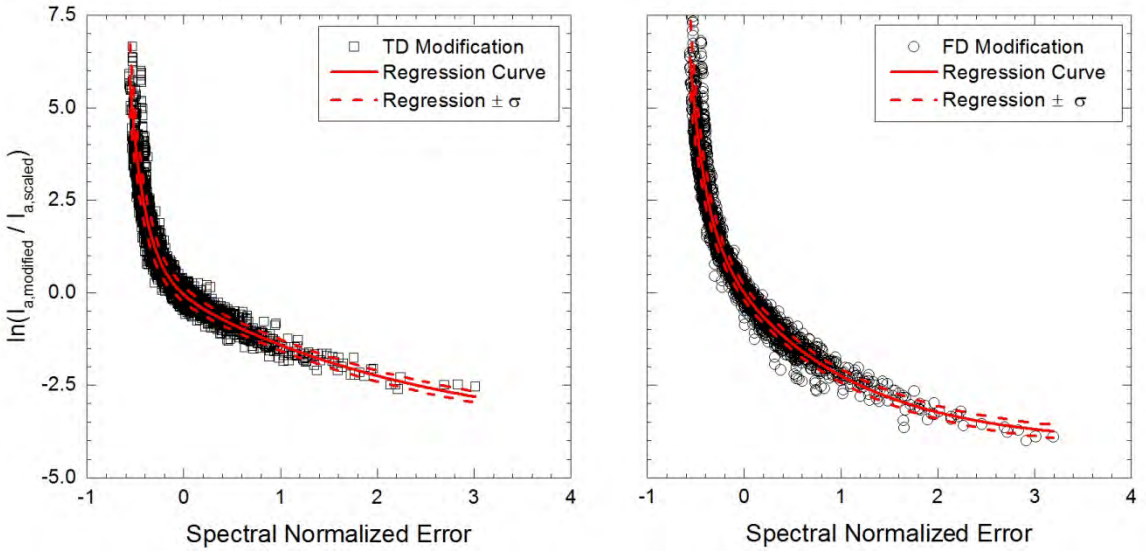

Figure 4.58. Regression curves, with plus and minus one standard deviation lines, developed for the relationship between the logarithmic modified-to-scaled Arias intensity (I_a) ratios and spectral mismatch for the combined set of motions from scenarios I and II.

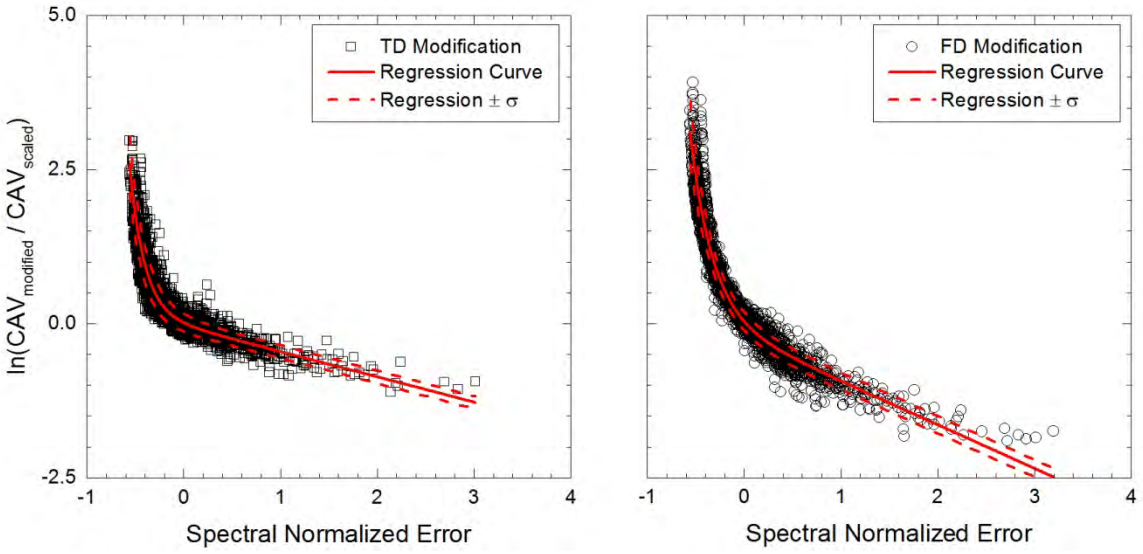

Figure 4.59. Regression curves, with plus and minus one standard deviation lines, developed for the relationship between the logarithmic modified-to-scaled cumulative absolute velocity (*CAV*) ratios and spectral mismatch for the combined set of motions from scenarios I and II.

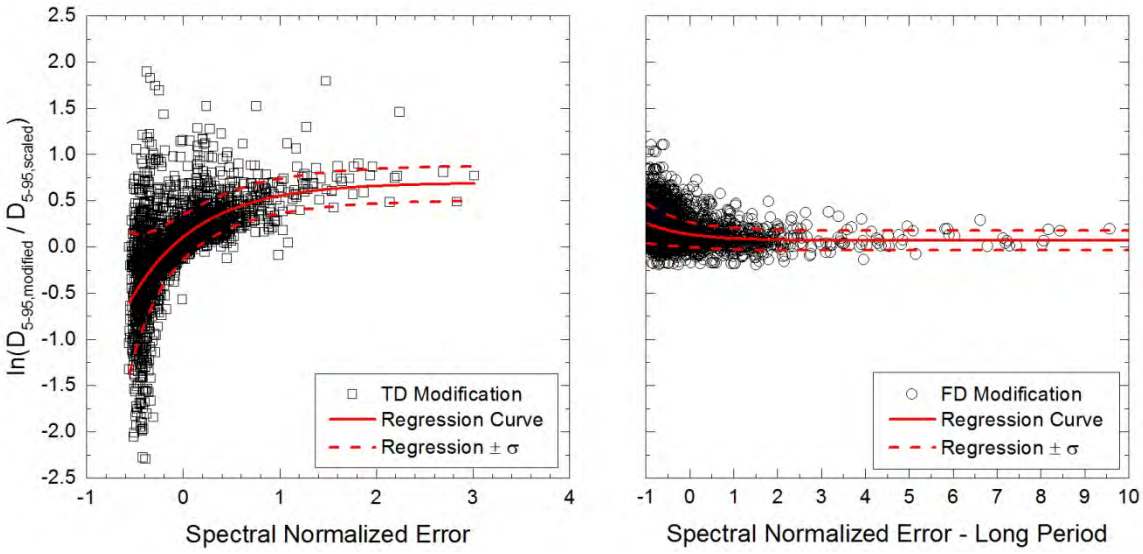

Figure 4.60. Regression curves, with plus and minus one standard deviation lines, developed for the relationship between the logarithmic modified-to-scaled significant duration ($D_{5\text{-}95}$) ratios and spectral mismatch for the combined set of motions from scenarios I and II.

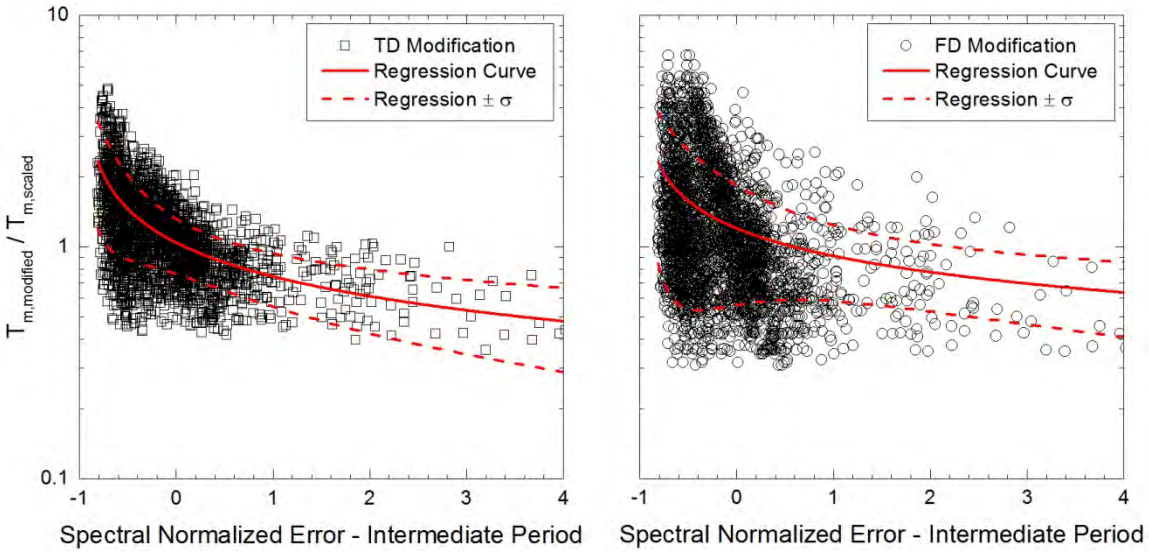

Figure 4.61. Regression curves, with plus and minus one standard deviation lines, developed for the relationship between the modified-to-scaled mean period (T_m) ratios and spectral mismatch in the intermediate period range for the combined set of motions from scenarios I and II.

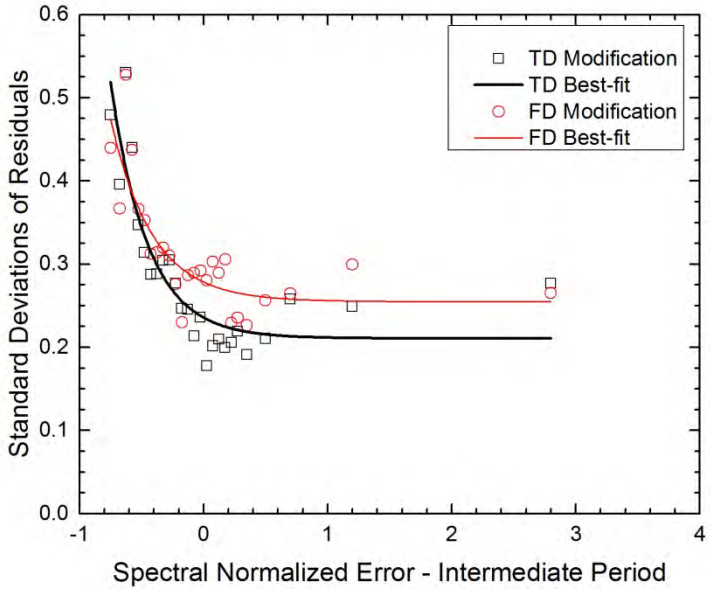

Figure 4.62. Standard deviations of the residuals, and corresponding best-fit curves, for the regression equations developed for the relationship between the logarithmic modified-to-scaled peak ground velocity ratios and spectral mismatch in the intermediate period range for the combined set of motions from scenarios I and II.

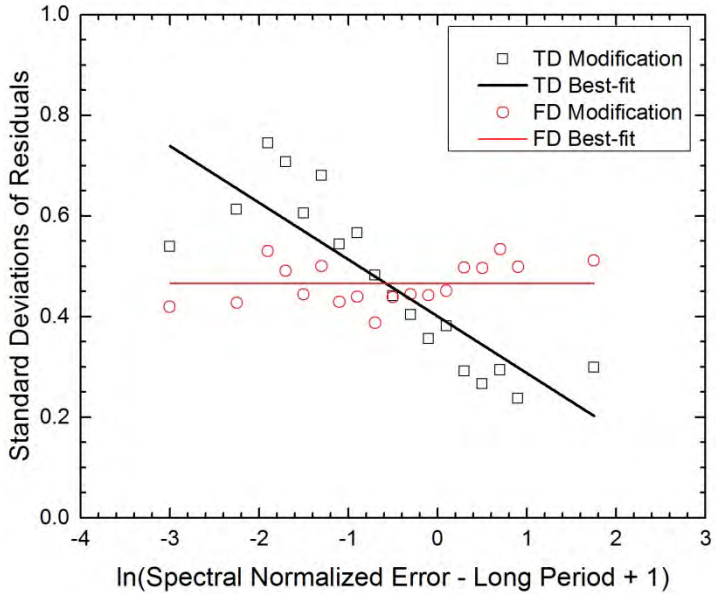

Figure 4.63. Standard deviations of the residuals, and corresponding best-fit curves, for the regression equations developed for the relationship between the logarithmic modified-to-scaled peak ground displacement ratios and spectral mismatch in the long period range for the combined set of motions from scenarios I and II.

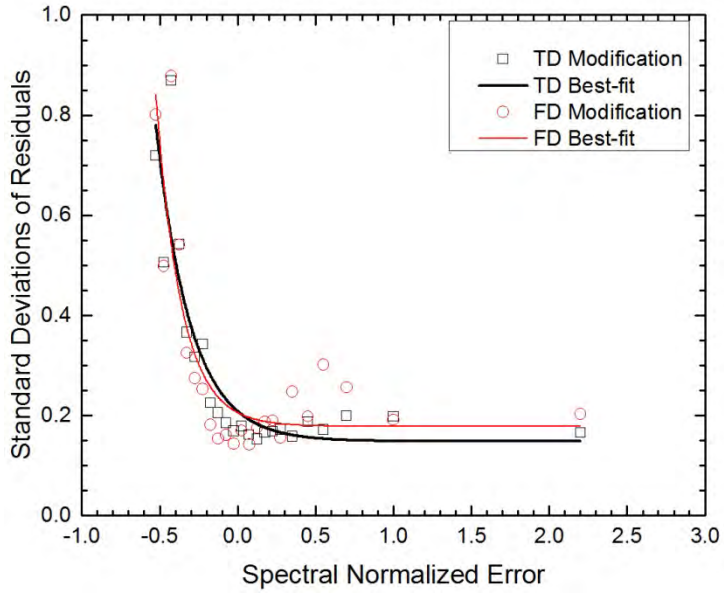

Figure 4.64. Standard deviations of the residuals, and corresponding best-fit curves, for the regression equations developed for the relationship between the logarithmic modified-to-scaled Arias intensity ratios and spectral mismatch for the combined set of motions from scenarios I and II.

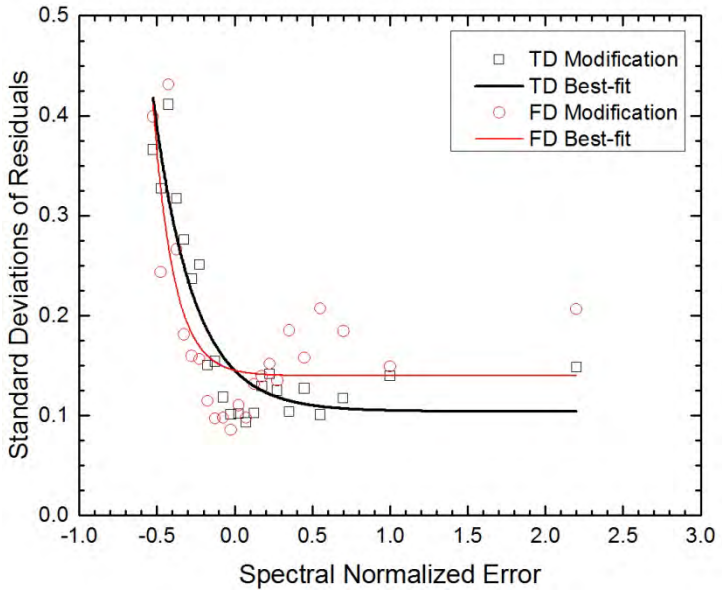

Figure 4.65. Standard deviations of the residuals, and corresponding best-fit curves, for the regression equations developed for the relationship between the logarithmic modified-to-scaled cumulative absolute velocity ratios and spectral mismatch for the combined set of motions from scenarios I and II.

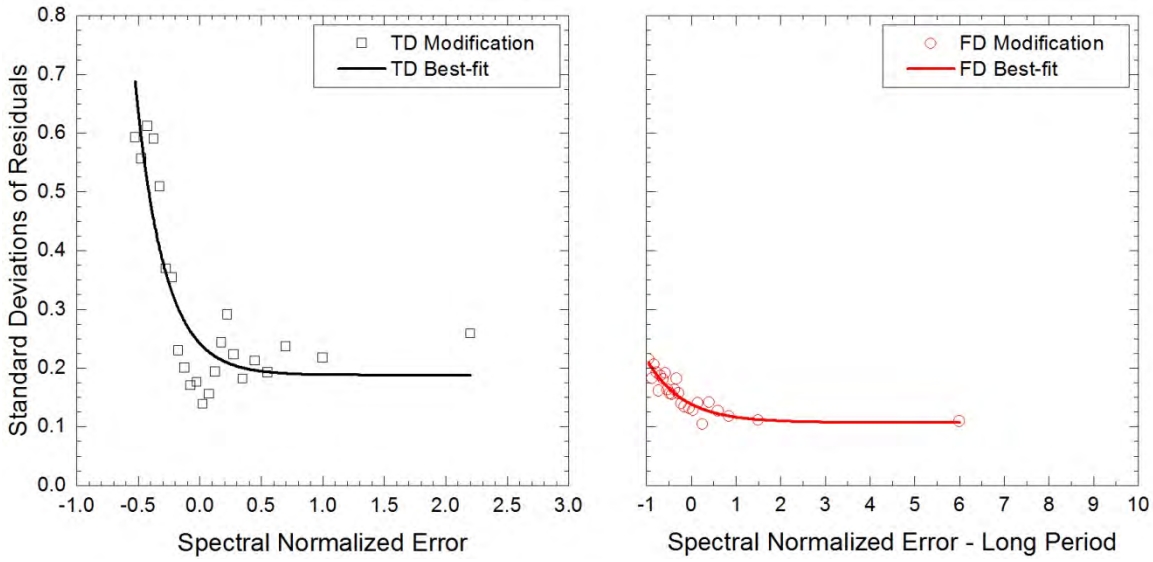

Figure 4.66. Standard deviations of the residuals, and corresponding best-fit curves, for the regression equations developed for the relationship between the logarithmic modified-to-scaled significant duration ratios and spectral mismatch for the combined set of motions from scenarios I and II.

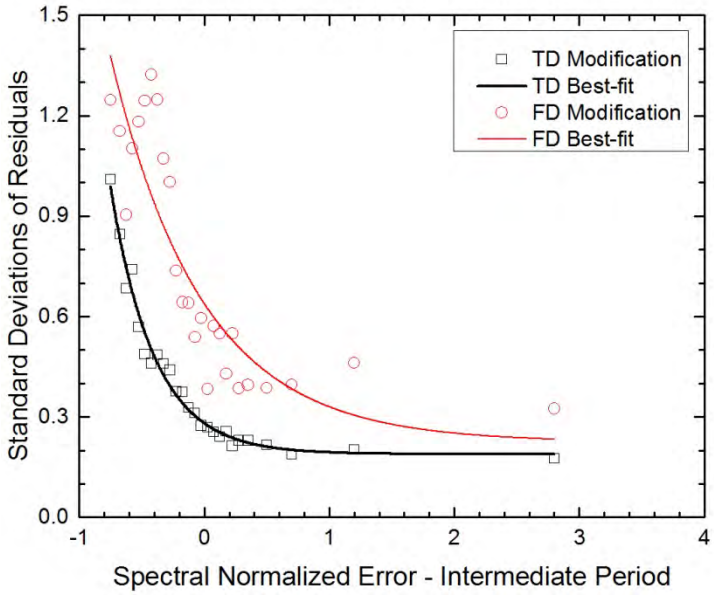

Figure 4.67. Standard deviations of the residuals, and corresponding best-fit curves, for the regression equations developed for the relationship between the modified-to-scaled mean period ratios and spectral mismatch in the intermediate period range for the combined set of motions from scenarios I and II.

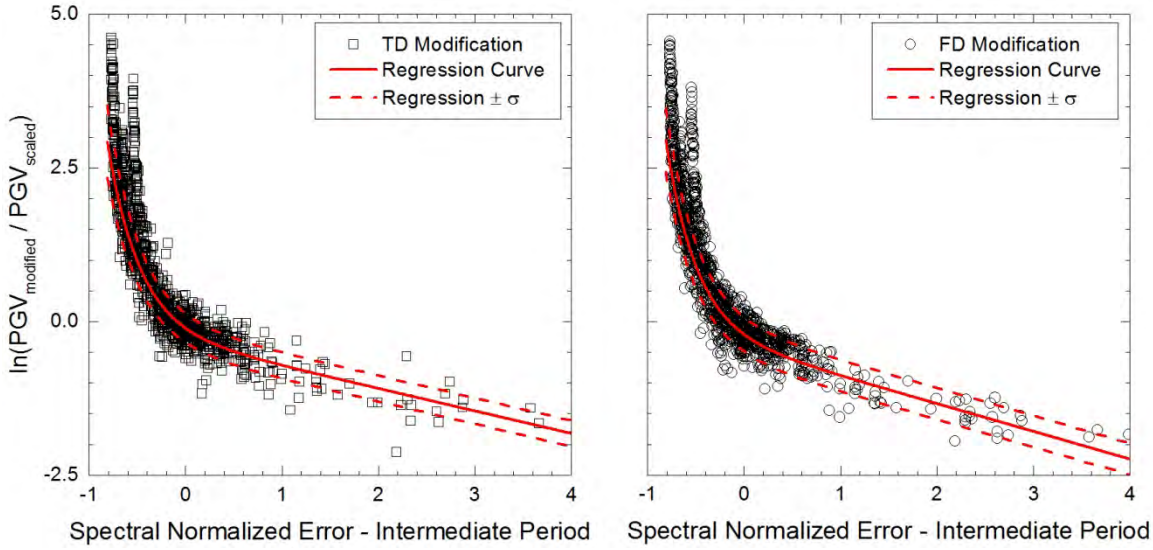

Figure 4.68. Comparison of the logarithmic modified-to-scaled peak ground velocity (*PGV*) ratios of the motions in scenario III to the regression curves developed for the relationship between the logarithmic modified-to-scaled *PGV* ratio and spectral mismatch in the intermediate period range for the combined set of motions from scenarios I and II.

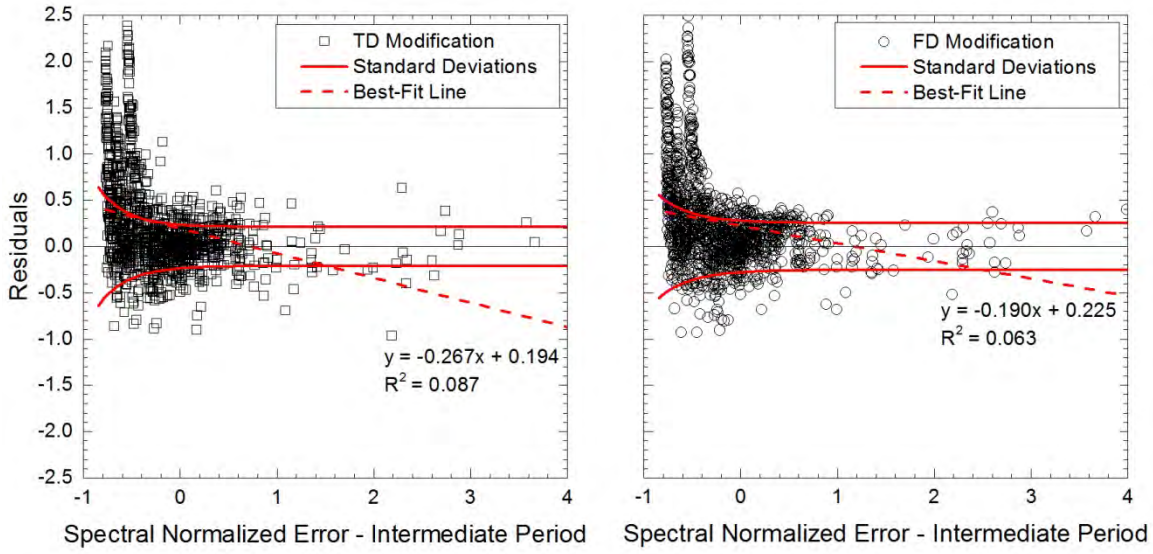

Figure 4.69. Comparison of the residuals for the logarithmic modified-to-scaled peak ground velocity (*PGV*) ratios of the motions in scenario III to the standard deviations developed for the relationship between the logarithmic modified-to-scaled *PGV* ratios and spectral mismatch in the intermediate period range for the combined set of motions from scenarios I and II. Lines fit to the residuals are also shown.

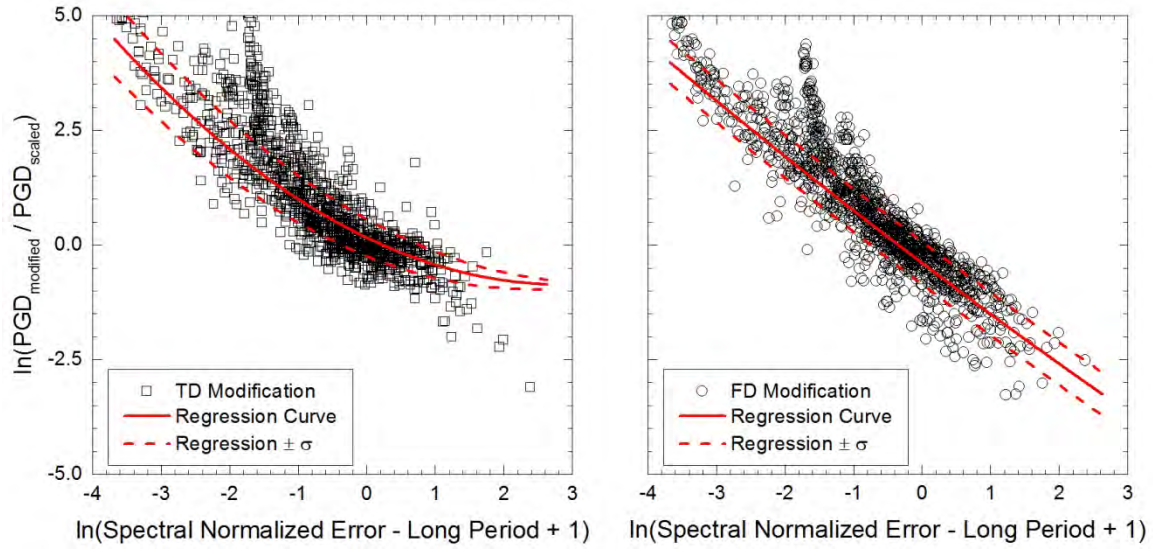

Figure 4.70. Comparison of the logarithmic modified-to-scaled peak ground displacement (*PGD*) ratios of the motions in scenario III to the regression curves developed for the relationship between the logarithmic modified-to-scaled *PGD* ratio and spectral mismatch in the long period range for the combined set of motions from scenarios I and II.

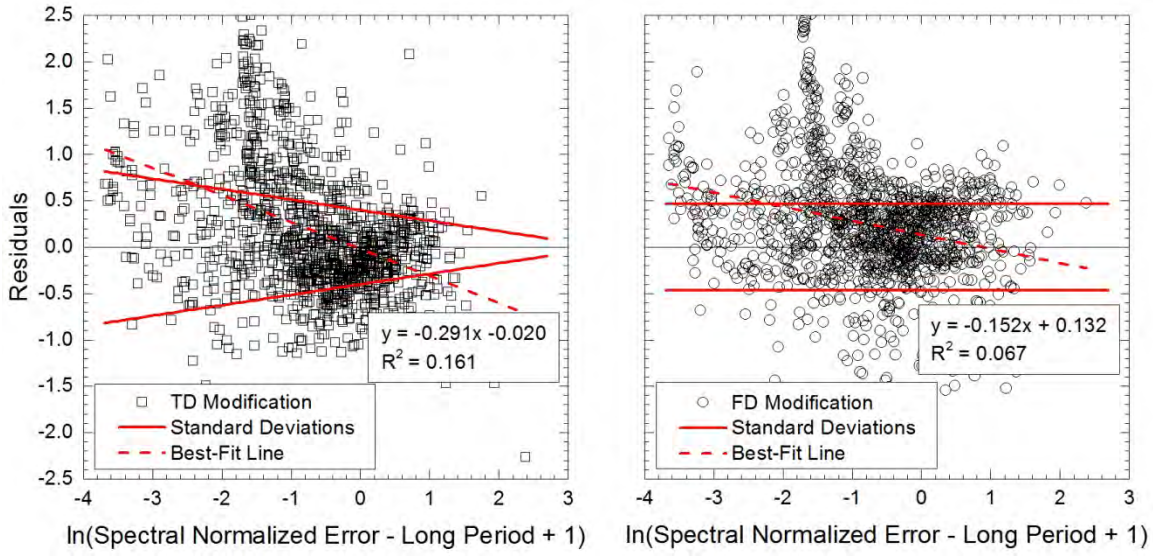

Figure 4.71. Comparison of the residuals for the logarithmic modified-to-scaled peak ground displacement (*PGD*) ratios of the motions in scenario III to the standard deviations developed for the relationship between the logarithmic modified-to-scaled *PGD* ratios and spectral mismatch in the long period range for the combined set of motions from scenarios I and II. Lines fit to the residuals are also shown.

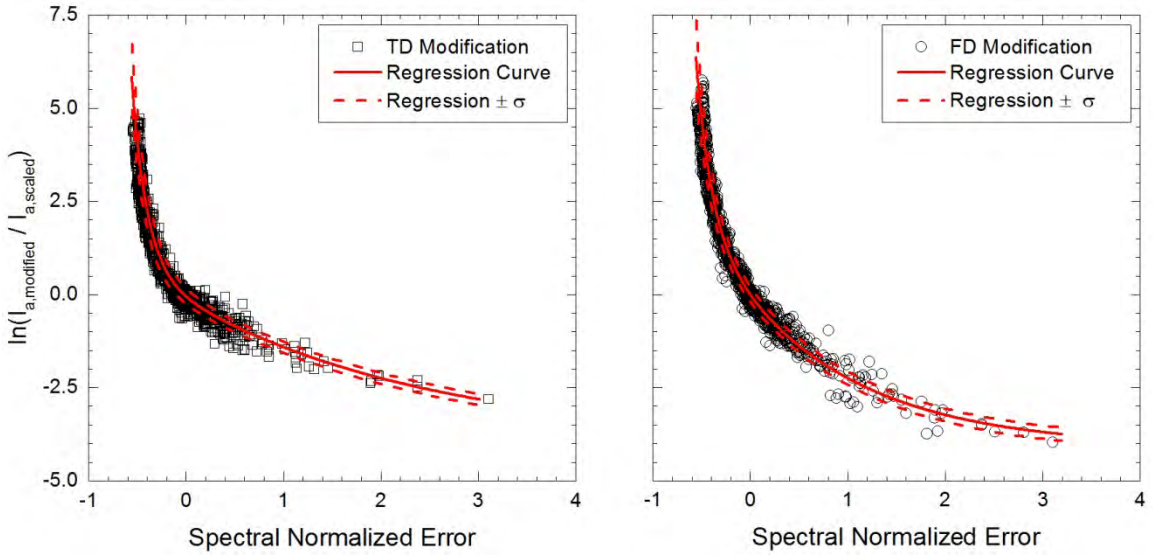

Figure 4.72. Comparison of the logarithmic modified-to-scaled Arias intensity (I_a) ratios of the motions in scenario III to the regression curves developed for the relationship between the logarithmic modified-to-scaled I_a ratio and spectral mismatch for the combined set of motions from scenarios I and II.

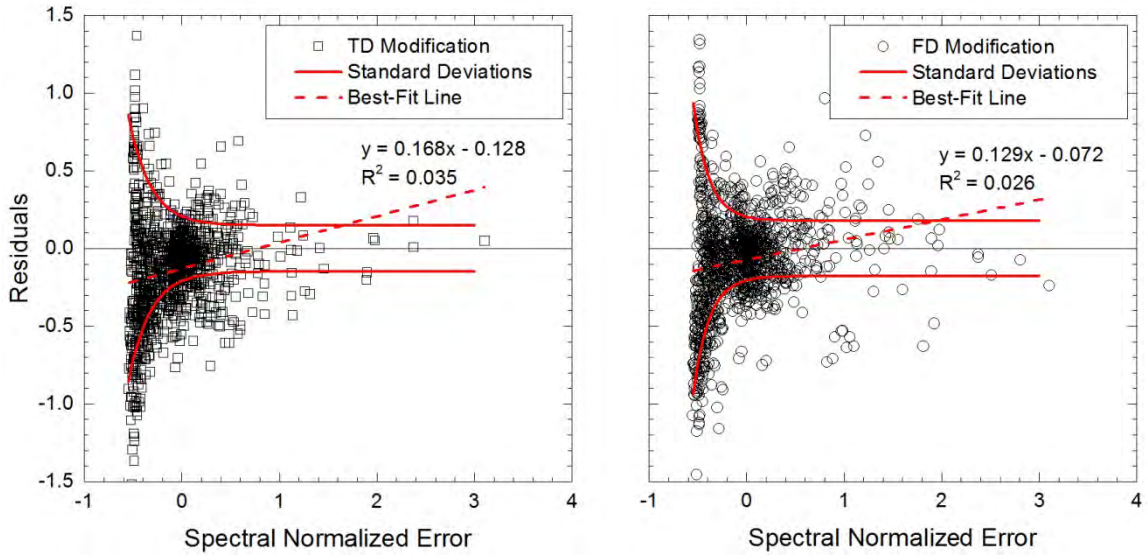

Figure 4.73. Comparison of the residuals for the logarithmic modified-to-scaled Arias intensity (I_a) ratios of the motions in scenario III to the standard deviations developed for the relationship between the logarithmic modified-to-scaled I_a ratios and spectral mismatch for the combined set of motions from scenarios I and II. Lines fit to the residuals are also shown.

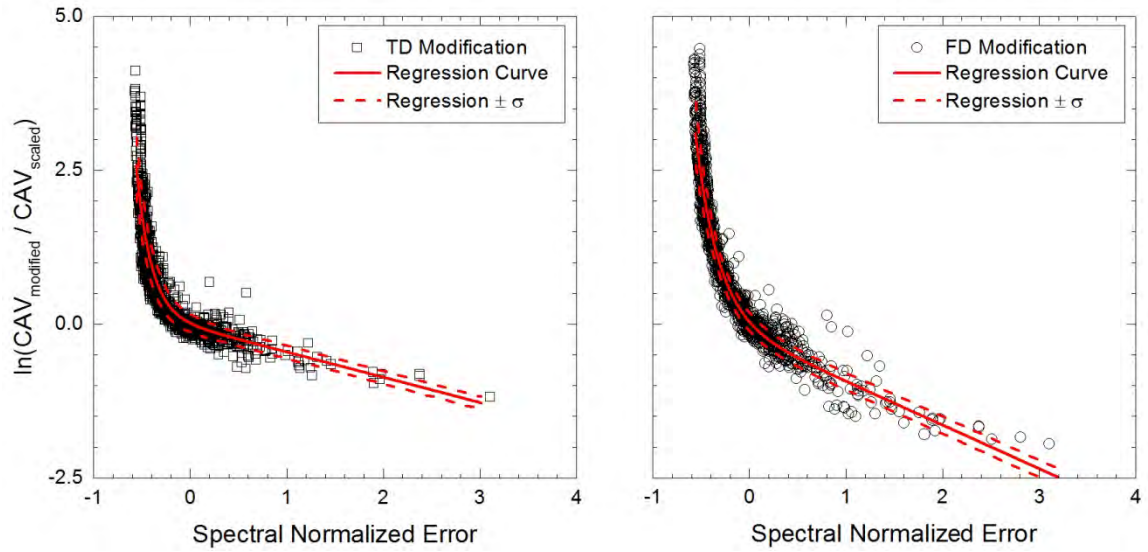

Figure 4.74. Comparison of the logarithmic modified-to-scaled cumulative absolute velocity (*CAV*) ratios of the motions in scenario III to the regression curves developed for the relationship between the logarithmic modified-to-scaled *CAV* ratio and spectral mismatch for the combined set of motions from scenarios I and II.

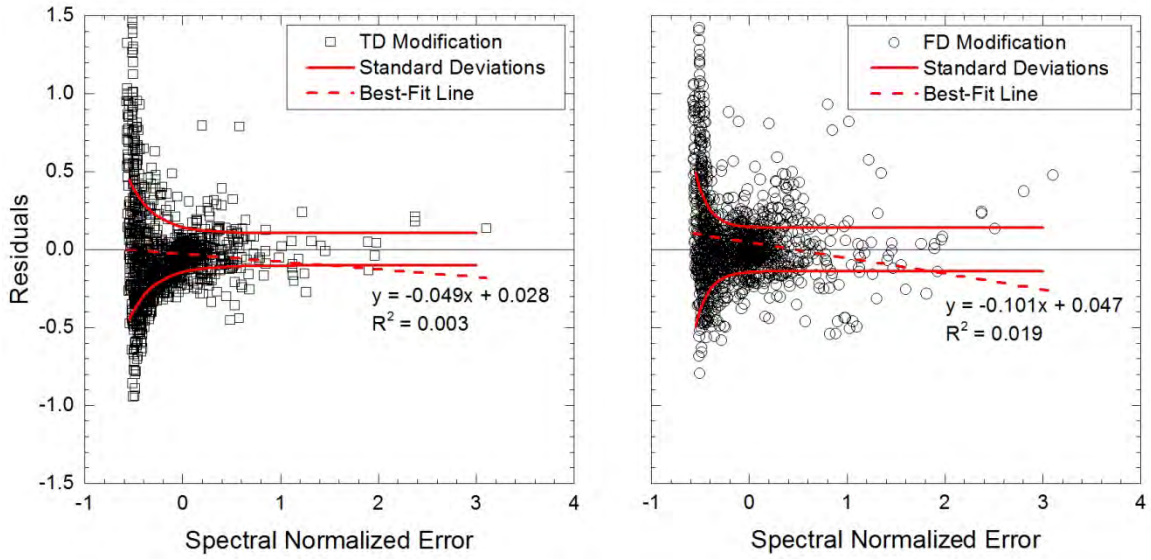

Figure 4.75. Comparison of the residuals for the logarithmic modified-to-scaled cumulative absolute velocity (*CAV*) ratios of the motions in scenario III to the standard deviations developed for the relationship between the logarithmic modified-to-scaled *CAV* ratios and spectral mismatch for the combined set of motions from scenarios I and II. Lines fit to the residuals are also shown.

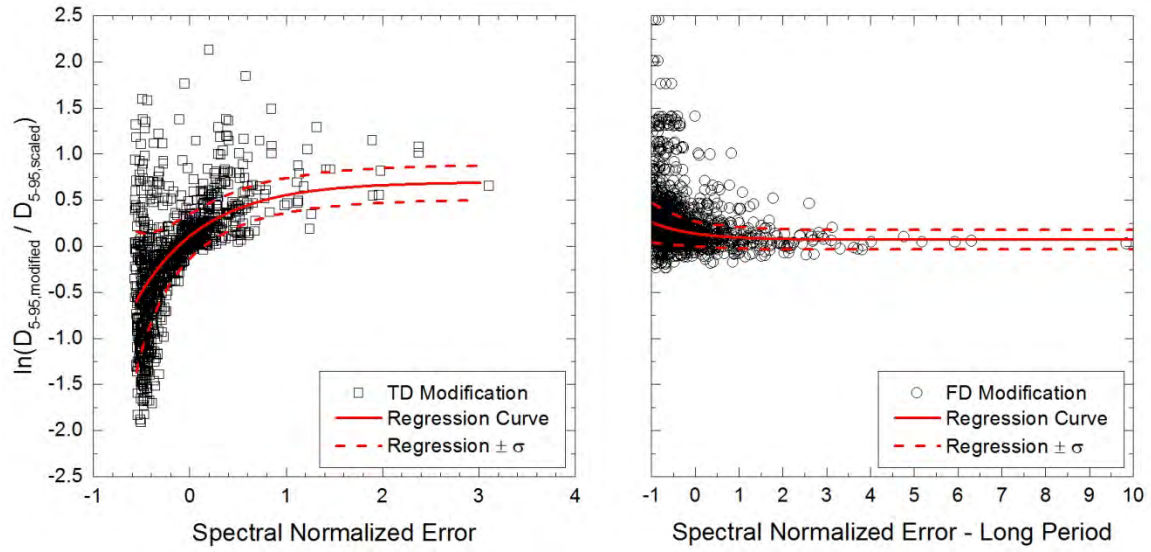

Figure 4.76. Comparison of the logarithmic modified-to-scaled significant duration ($D_{5\text{-}95}$) ratios of the motions in scenario III to the regression curves developed for the relationship between the logarithmic modified-to-scaled $D_{5\text{-}95}$ ratio and spectral mismatch for the combined set of motions from scenarios I and II.

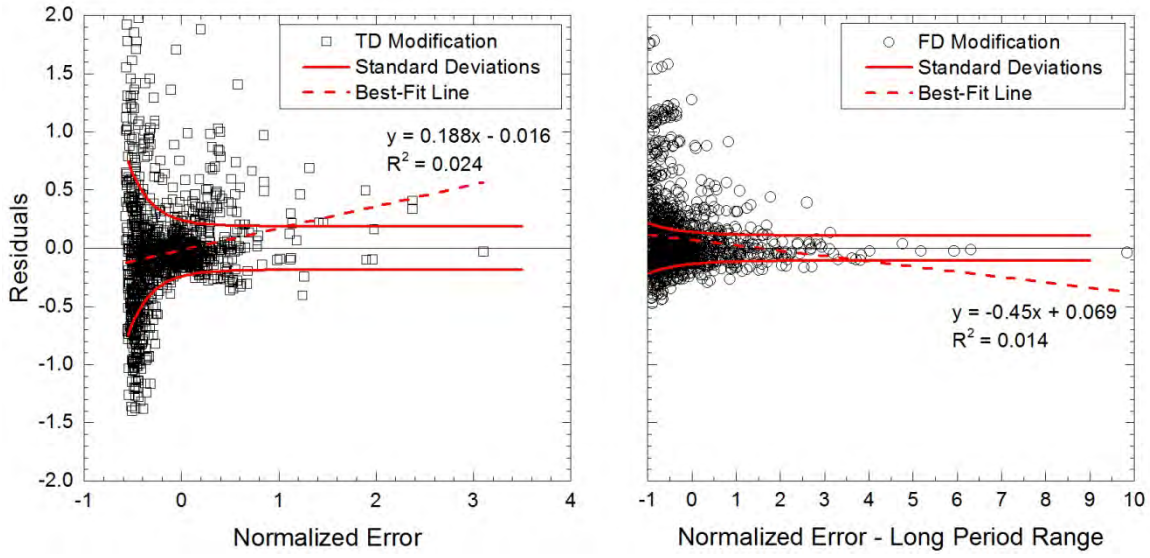

Figure 4.77. Comparison of the residuals for the logarithmic modified-to-scaled significant duration ($D_{5\text{-}95}$) ratios of the motions in scenario III to the standard deviations developed for the relationship between the logarithmic modified-to-scaled $D_{5\text{-}95}$ ratios and spectral mismatch for the combined set of motions from scenarios I and II. Lines fit to the residuals are also shown.

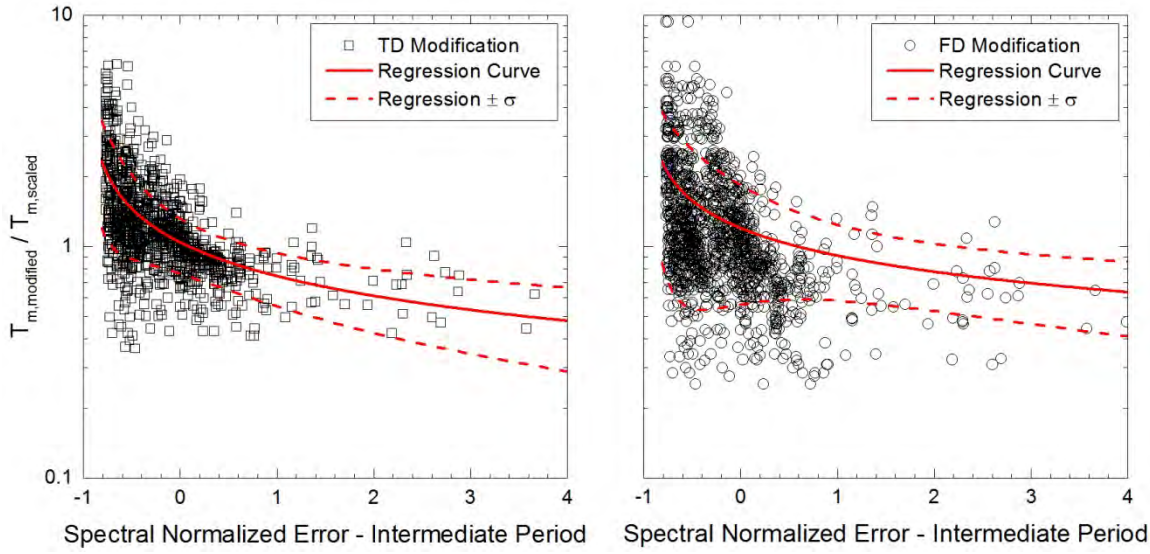

Figure 4.78. Comparison of the modified-to-scaled mean period (T_m) ratios of the motions in scenario III to the regression curves developed for the relationship between the modified-to-scaled T_m ratio and spectral mismatch in the intermediate period range for the combined set of motions from scenarios I and II.

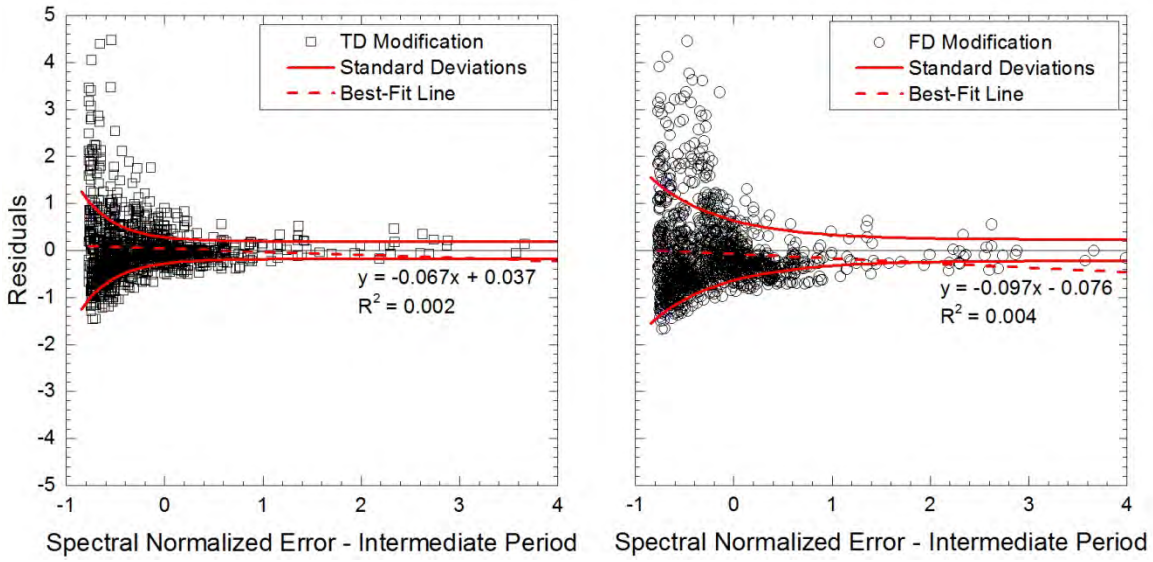

Figure 4.79. Comparison of the residuals for the modified-to-scaled mean period (T_m) ratios of the motions in scenario III to the standard deviations developed for the relationship between the modified-to-scaled T_m ratios and spectral mismatch in the intermediate period range for the combined set of motions from scenarios I and II. Lines fit to the residuals are also shown.

CHAPTER 5
Impact of Modification on Ground Motion Time Histories

The effects of modification on the time histories of the ground motions, as quantified by the goodness-of-fit (*GOF*) between the scaled and modified time histories, are examined in this chapter. The time histories of the ground motions are used as input for the response history analyses for the geotechnical and structural systems, so it is important to understand how they are impacted by modification. Since well-defined trends were observed between the effects of modification on the ground motion characteristics and spectral mismatch, this portion of the research studies the impact of spectral mismatch on the effects of modification on the *GOF* values. Currently, in practice, modified ground motions are accepted or rejected based on a subjective visual comparison between the time histories of the modified motion and the original or scaled ground motion. The relationships between *GOF* and the modified-to-scaled ground motion characteristic ratios are examined to possibly quantify *GOF* values required to achieve a desired value(s) for the ground motion characteristics of the modified motion. Also, quantitative threshold values for *GOF* between the modified and scaled time histories are established in this chapter using a visual examination of the scaled and modified time histories to identify likely acceptable and likely unacceptable modified ground motions.

5.1 Methodology

In this research, $a(t)$, $v(t)$, $d(t)$, $I_a(t)$, and *FAS* of the scaled and modified motions are studied to examine how they are impacted by ground motion modification. Metrics in **Section 3.4** were used to calculate the goodness-of-fit (*GOF*) between the scaled and modified time histories and *FAS*. In addition to the *GOF* for the $a(t)$, $v(t)$, and $d(t)$, an overall *GOF* was calculated for the ground motions by combining the *GOF* calculated for these three time histories. The overall *GOF* was calculated using the mean (**Equation 5.1**) and geometric mean (**Equation 5.2**) of the *GOF* values for the $a(t)$, $v(t)$, and $d(t)$.

$$OGOF = \frac{GOF_{a(t)} + GOF_{v(t)} + GOF_{d(t)}}{3} \quad \textbf{(5.1)}$$

$$OGOF_{geo} = \sqrt[3]{GOF_{a(t)} * GOF_{v(t)} * GOF_{d(t)}} \quad \textbf{(5.2)}$$

OGOF and $OGOF_{geo}$ represent the overall *GOF* calculated using the mean and geometric mean of the time histories, respectively. $GOF_{a(t)}$, $GOF_{v(t)}$, and $GOF_{d(t)}$, represent the *GOF* calculated for the $a(t)$, $v(t)$, and $d(t)$, respectively.

The *GOF* values for the time histories and *FAS* were plotted versus spectral mismatch to assess the impact of spectral mismatch on the resulting *GOF* between the modified and scaled time histories. The *GOF* values for the time histories and the corresponding spectral mismatches of the motions in scenarios I and II were studied and used to develop regression equations for the relationship between *GOF* and spectral mismatch. The regression equations were developed using the same procedure detailed in **Section 4.1.2.1**. The R^2 values of regression equations calculated for these relationships using different functional forms were compared. The significance levels of the coefficients in these regression equations were checked to ensure the coefficients were statistically significant and the residuals were checked to ensure there was no bias in the *GOF* values with respect to the calculated regression curves. For each time history, the regression equation with the largest R^2 value, statistically significant coefficients, and no bias in the residuals was used to define the relationship between the *GOF* and spectral mismatch. Standard deviations were calculated for the regression equations developed using the combined set of motions from scenarios I and II.

In an effort to establish acceptable values for the *GOF* between the modified and scaled time histories, the *GOF* values were plotted against the modified-to-scaled ground motion characteristic ratios discussed in **Chapter 4** (e.g., *PGV*, *PGD*, etc.). Limits can be placed on the modified-to-scaled ground motion characteristic ratios then used to set threshold values for *GOF* for the time histories to identify likely acceptable and likely unacceptable modified ground motions. Similar to the *GOF* – spectral mismatch relationships, regression equations were developed for the relationship between *GOF* and the modified-to-scaled ground motion characteristic ratios for the motions in scenarios I and II using the procedure in **Section 4.1.2.1**. The *GOF* values for the time histories of the motions in scenario III and the corresponding modified-to-scaled ground motion characteristic ratios were then compared to these regression equations to assess their general applicability.

A qualitative assessment of the *GOF* between the modified and scaled time histories was also performed to establish threshold *GOF* values for the time histories. This investigation was performed to provide quantitative values of *GOF* for likely acceptable and likely unacceptable modified ground motions, making the decision to accept or reject modified ground motions based on the time histories a more objective process. For the qualitative assessment, only $a(t)$, $v(t)$, $d(t)$, and the resulting *OGOF*, were investigated. The $a(t)$, $v(t)$, and $d(t)$ of the modified motions were visually compared to their scaled counterparts and assigned rankings from 1 (i.e., very large differences) to 5 (i.e., nearly identical). The descriptions for each qualitative ranking are provided in **Table 5.1** and are consistent with observations in the time histories used in practice to accept or reject modified motions. A ranking for the *OGOF* was then calculated using the rankings assigned to $a(t)$, $v(t)$, and $d(t)$ for a given TD- or FD-modified ground motion. Only the motions scaled using the optimal scale factors and their resulting modified counterparts were studied as part of the visual assessment. The visual assessment was performed by the author for the time histories of three sets of motions for both scenarios I and II:

- A set of motions matched to the target spectrum with the smallest overall intensity: The time histories of the motions matched to the MA and 10% UHS target spectra were examined for scenarios I and II, respectively, for this case.
- A set of motions matched to a target spectrum with intermediate intensity: The time histories of the sets of motions for scenarios I and II that were matched to the CMS target spectrum were studied for this case.
- A set of motions matched to the target spectrum with the largest overall intensity: For both scenarios, the time histories of the motions matched to the 2% UHS target spectrum were examined for this case.

The author's rankings for the $d(t)$ of the motions matched to the CMS in scenario I were compared to the rankings assigned to the same motions by the author's advisor. This comparison was made to ensure that the visual assessment made by the author was objective. For each motion examined in the visual assessment, the *GOF* values for the $a(t)$, $v(t)$, and $d(t)$ were plotted against their corresponding assigned rankings and the *OGOF* value was plotted against its corresponding calculated ranking. The medians and standard deviations of the *GOF* and *OGOF* values within each ranking were then calculated for scenarios I and II and used to establish

threshold values for *GOF* for the different time histories and the *OGOF* to identify likely acceptable, possibly acceptable, and likely unacceptable modified motions.

5.2 Impact of Modification on Time Histories

5.2.1 Results for Scenario I

5.2.1.1 Goodness-of-Fit versus Spectral Mismatch

The *GOF* metrics studied for the time histories included *NE*, *TVM* (Oberkampf and Trucano 2002, Green et al. 2011), *imRMSE*, *ERFCM* (Olsen and Mayhew 2010), *AC*1 (Anderson 2004), and *AC*10 (Anderson 2004), which were calculated using **Equations 5.3** to **5.8**, respectively. The subscript *t* indicates these metrics are calculated for the time histories.

$$NE_t = \frac{\sum_{i=1}^{n_t}\left(\frac{a_{\mathrm{mod}}(t_i) - a_{scaled}(t_i)}{PGA_{scaled}}\right)}{\sqrt{n_t}} \quad \textbf{(5.3)}$$

$$TVM_t = \frac{\sum_{i=1}^{n_t}\left[1 - \tanh\left(\frac{\left|a_{\mathrm{mod}}(t_i) - a_{scaled}(t_i)\right|}{a_{scaled}(t_i)}\right)\right]}{n_t} \quad \textbf{(5.4)}$$

$$imRMSE_t = \frac{1}{\exp\sqrt{\frac{\sum_{i=1}^{n_t}\left(a_{\mathrm{mod}}(t_i) - a_{scaled}(t_i)\right)^2}{\sum_{i=1}^{n_t} a_{scaled}(t_i)^2}}} \quad \textbf{(5.5)}$$

$$ERFCM_t = \frac{\sum_{i=1}^{n_t}\left[erfc\left(\frac{2*\left|a_{\mathrm{mod}}(t_i) - a_{scaled}(t_i)\right|}{\left|a_{\mathrm{mod}}(t_i)\right| + \left|a_{scaled}(t_i)\right|}\right)\right]}{n_t} \quad \textbf{(5.6)}$$

$$AC1_t = \min_{i=1}^{n_t}\left(1 - \left|\frac{\left|a_{\mathrm{mod}}(t_i)\right| - \left|a_{scaled}(t_i)\right|}{PGA_{scaled}}\right|\right) \quad \textbf{(5.7)}$$

$$AC10_t = \frac{\int_0^{t_D} a_{\mathrm{mod}}(t) * a_{scaled}(t) dt}{\sqrt{\int_0^{t_D} a_{\mathrm{mod}}(t)^2 dt} * \sqrt{\int_0^{t_D} a_{scaled}(t)^2 dt}} \quad (\mathbf{5.8})$$

$a_{\mathrm{mod}}(t)$ and $a_{scaled}(t)$ represent the acceleration time histories of the modified and scaled ground motions, respectively, while PGA_{scaled} represents the *PGA* of the scaled ground motion. As described in **Section 3.1**, n_t represents the number of acceleration values recorded for the time history. The built-in function in MATLAB for coherence, shown in the numerator of **Equation 5.9** (The Mathworks, Inc. 2013), was used to calculate the average coherence.

$$Average \quad Coherence = \frac{\sum_{i=1}^{n_{FAS}} \frac{\left|P_{\mathrm{mod},scaled}(f_i)\right|^2}{P_{\mathrm{mod}}(f_i) * P_{scaled}(f_i)}}{n_{FAS}} \quad (\mathbf{5.9})$$

$P_{\mathrm{mod}}(f_i)$ and $P_{scaled}(f_i)$ represent the power spectral density of the modified and scaled time histories, respectively, at frequency, f_i. $P_{\mathrm{mod},scaled}(f_i)$ represents the cross-spectral density between the modified and scaled time histories. As described in **Section 3.2**, n_{FAS} represents the number of frequencies for which the *FAS* (and also coherence) is calculated. These metrics were used to calculate the *GOF* for the other time histories by replacing $a(t)$ with $v(t)$, $d(t)$, $I_a(t)$, and *FAS* and *PGA* with *PGV*, *PGD*, 100% (i.e., the maximum value in the $I_a(t)$), and the peak amplitude of the *FAS* for the scaled ground motion, respectively. The same spectral mismatch metrics examined in **Chapter 4** (i.e., NE_s, TVM_s, $imRMSE_s$, $ERFCM_s$) were studied for the relationship between *GOF* and spectral mismatch.

The relationship between some of the *GOF* metrics and spectral mismatch, as quantified by NE_s or $NE_{s,LP}$, have notable trends. NE_s and $NE_{s,LP}$ are used for the spectral mismatch metrics because they produce slightly less dispersion in the *GOF* values than TVM_s, $imRMSE_s$, and $ERFCM_s$. Many of the *GOF* metrics reach peak values around NE_s or $NE_{s,LP}$ equal to 0. This is expected since motions with small amounts of spectral mismatch (i.e., NE_s or $NE_{s,LP}$ equal to 0) undergo limited changes during modification and should have similar scaled and modified time histories. *GOF* values calculated using the TVM_t, $imRMSE_t$, and $ERFCM_t$ metrics have the least amount of dispersion when plotted against spectral mismatch as observed in **Figures 5.1**, **5.2**, and **5.3**, respectively, for the $d(t)$ of the motions in scenario I. The $imRMSE_t$ metric results in the least amount of dispersion in the *GOF* values. Also, *GOF* values calculated using the TVM_t and

$ERFCM_t$ metrics for the TD-modified motions are larger than those for the FD-modified motions. Although the *GOF* values calculated with the $AC1_t$ metric also have a small amount of dispersion, motions for which the modified time history has much larger values than the scaled time history approach *GOF* values of negative infinity. As shown in **Figure 5.4** for the $d(t)$ of the motions in scenario I, this causes the *GOF* values for the $AC1_t$ metric to be sensitive to changes in spectral mismatch for motions with negative NE_s or $NE_{s,LP}$. There is more dispersion in the *GOF* values calculated with the $AC10_t$ metric. Also, the FD-modified motions generally have larger *GOF* values than the TD-modified motions for $a(t)$, $v(t)$, $d(t)$, and $I_a(t)$ when calculated using the $AC10_t$ metric, as observed in **Figure 5.5**. The larger *GOF* values for the $AC10_t$ metric (which is similar to cross-correlation (Anderson 2004)) are observed for the FD-modified motions because, during FD modification, sinusoidal wavelets are added to the time history which cause a smaller shift in the time history and lead to a larger overall cross-correlation, or $AC10_t$ metric. The wavelets added during TD modification occasionally cause a shift in the time history and a smaller value for the *GOF* when using the $AC10_t$ metric. **Figure 5.6** shows the *GOF* values calculated using NE_t for the $d(t)$ of the motions in scenario I plotted against $NE_{s,LP}$. One major issue with using NE_t for the *GOF* metric is that it approaches positive or negative infinity if the modified time history has much larger values than the scaled time history, resulting in a much larger dispersion in the *GOF* values. Also, the NE_t metric approaches values of 0 for time histories with a lot of recorded data points with values of approximately 0 (e.g., $d(t)$ for some motions from the Tohoku, Japan earthquake), which could erroneously lead one to believe that the scaled and modified time histories are a perfect match. For these reasons, NE_t is not used as the metric to calculate the *GOF* between the modified and scaled time histories. Average coherence is also not acceptable to use for the *GOF* metric as it leads to a significant amount of dispersion in the *GOF* values, as shown in **Figure 5.7**. The major issue with using coherence for the *GOF* metric is that it varies with frequency (as shown in **Figure 5.8**) and it is difficult to describe with a single parameter (i.e., average). The $imRMSE_t$ metric is used to calculate the *GOF* between the modified and scaled time histories in this study because it leads to the least amount of dispersion and produces similar values for both modification techniques. Plots of the *GOF* values versus spectral mismatch for all the *GOF* metrics, time histories, spectral mismatch metrics, and different period ranges can be found in **Appendix C**.

The *GOF* values for the $a(t)$ and *FAS* have the least amount of dispersion when plotted versus NE_s as shown in **Figures 5.9** and **5.10**, respectively. The *GOF* values, quantified by $imRMSE_t$, for the $a(t)$ of the FD-modified motions have slightly larger values and smaller dispersion than their TD-modified counterparts. However, the *GOF* values for the *FAS* of both sets of modified motions are very similar in magnitude and amount of dispersion. For the FD-modified motions, the *GOF* values calculated using the $imRMSE_t$ metric are very similar for $a(t)$ and *FAS*. Since the $a(t)$ is directly calculated from the *FAS*, scaling the *FAS* during FD modification (i.e., no shift in the *FAS*) leads to the similar *GOF* values between the $a(t)$ and *FAS* of the FD-modified motions. The $imRMSE_t$ metric calculates the summation of differences before applying exponential and square root terms while other metrics for *GOF* (e.g., TVM_t) calculate the hyperbolic tangent or complementary error of the difference for each point in the time history and then sum those values. This observation could explain why the similarity between the *GOF* values for the $a(t)$ and *FAS* of the FD-modified motions is only observed for the $imRMSE_t$ metric. For $v(t)$ and $d(t)$, the *GOF* values have the least amount of dispersion when $NE_{s,LP}$ is used to quantify spectral mismatch, as shown in **Figures 5.11** and **5.12**, respectively. For the $v(t)$, the *GOF* values of the TD- and FD-modified motions have similar magnitudes, but the FD-modified motions have *GOF* values with a much smaller dispersion. The *GOF* values for the $d(t)$ of the TD-modified motions reach greater values than those of the FD-modified motions, but also have a much larger dispersion. The *OGOF* values have the least amount of dispersion when plotted versus NE_s, as shown in **Figure 5.13**; however, the relationship of *OGOF* with spectral mismatch is much weaker than the relationships observed for the $a(t)$, $v(t)$, $d(t)$, and *FAS*. **Figure 5.14** shows that using *OGOF* (i.e., **Equation 5.1**) results in slightly less dispersion in the values than using $OGOF_{geo}$ (i.e., **Equation 5.2**). This is because the *OGOF* is not as heavily influenced by the *GOF* of one of the $a(t)$, $v(t)$, or $d(t)$ being low. In the extreme case, $OGOF_{geo}$ equals 0 if the *GOF* for the $a(t)$, $v(t)$, or $d(t)$ equals 0. For this reason, *OGOF* is used for the remainder of this study. The *GOF* values for the $I_a(t)$ have similar amounts of dispersion when plotted against the different spectral mismatch metrics in the short period range. However, for all the metrics, the *GOF* values for the $I_a(t)$ are much greater than those for the other time histories (see **Figure 5.15**), leading to a less pronounced relationship with spectral mismatch. Since there is not a strong relationship between the *GOF* for the $I_a(t)$ and spectral mismatch, particularly for the FD-modified motions, $I_a(t)$ is not investigated further in this study. The *GOF*

values of the motions are clearly affected differently by spectral mismatch for motions with negative NE_s and motions with positive NE_s. The *GOF* values for motions with negative NE_s are more sensitive to changes in spectral mismatch. For this reason, the development of regression equations and acceptable *GOF* values should consider motions with positive NE_s and motions with negative NE_s separately.

When $imRMSE_s$ is used to calculate spectral mismatch, motions with response spectra that are increased to match the target spectrum (data along "Increase Spectrum" line in **Figure 5.16**) approach a limiting spectral mismatch of 0.37 when the *GOF* is poor (i.e., 0 for the $imRMSE_t$ metric). This point is the result of the modified time history and target spectrum being much larger than the scaled time history and response spectrum. Since the scaled motion is used for normalizing differences in the $imRMSE_t$ metric for *GOF*, the *GOF* values approach 1/exp(infinity), or 0. The target spectrum is used to normalize differences for the $imRMSE_s$ metric for spectral mismatch, so spectral mismatch approaches 1/exp(1), or 0.37, in this case. Conversely, motions for which the scaled time history and response spectrum are much larger than the modified time history and target spectrum approach a spectral mismatch of 0 at *GOF* values of 0.37 (data along "Decrease Spectrum" line in **Figure 5.16**). For the same reasons, the *GOF* values approach 0 and 0.37 for negative and positive NE_s values, respectively. Both trendlines approach larger *GOF* values when spectral mismatch becomes smaller (i.e., spectral mismatch, as quantified by $imRMSE_s$, equal to 1). Given these observations, rearranging the equation for the $imRMSE_t$ metric provided in **Equation 5.5** to the form shown in **Equation 5.10** should result in one trendline in the *GOF* – spectral mismatch relationship with possibly less dispersion in the *GOF* values.

$$imRMSE_t^* = \frac{1}{\exp\sqrt{\dfrac{\sum_{i=1}^{n_t}\left(a_{\mathrm{mod}}(t_i) - a_{scaled}(t_i)\right)^2}{\sum_{i=1}^{n_t} a_{\mathrm{mod}}(t_i)^2}}} \qquad \textbf{(5.10)}$$

Indeed, normalizing the differences between the time histories by the modified time history for the $imRMSE_t^*$ metric for *GOF* in the same way that the spectral differences are normalized by the target spectra (i.e., the modified acceleration response spectra) for spectral mismatch leads to one trendline in the *GOF* values with respect to spectral mismatch, as shown in **Figure 5.17**. However, the smaller displacements of the FD-modified motions leads to smaller *GOF* values

than the TD-modified motions (**Figure 5.18**) when $imRMSE_t$* is used. Therefore, the $imRMSE_t$ metric for *GOF* (i.e., **Equation 5.5**), is used in the development of the regression equations relating spectral mismatch to *GOF*.

For the development of the regression equations describing the relationship between the *GOF* values and the spectral mismatch, the motions were split between those with positive spectral mismatch (i.e., positive NE_s or $NE_{s,LP}$) and those with negative spectral mismatch (i.e., negative NE_s or $NE_{s,LP}$). For positive spectral mismatches, a shifted power function shown in **Equation 5.11** was used in the development of the regression equations.

$$GOF = a_{ts}\left(1 + NE_s\right)^{b_{ts}} \quad (\mathbf{5.11})$$

a_{ts} and b_{ts} represent coefficients for the estimated regression equations for the *GOF* – spectral mismatch relationships. A sigmoidal logistic function, shown in **Equation 5.12**, was used to describe the *GOF* – spectral mismatch relationships for the negative spectral mismatch range.

$$GOF = \frac{a_{ts}}{1 + c_{ts} * \exp\left(-k_{ts} * NE_s\right)} \quad (\mathbf{5.12})$$

a_{ts}, c_{ts}, and k_{ts} represent coefficients estimated during the regression process to define the relationship between the *GOF* for the time histories and spectral mismatch. Regression curves were separately calculated for the negative and positive NE_s or $NE_{s,LP}$ range. However, to ensure that the regression equations developed for positive and negative NE_s or $NE_{s,LP}$ were approximately equal at 0 (i.e., a continuous equation), constraints were placed on the a_{ts} coefficients in **Equations 5.11** and **5.12** and the regression curves were recalculated. An example of this process is shown in **Figure 5.19**. The R^2 values of the regression equations developed for the positive and negative ranges of spectral mismatch were only slightly reduced by this adjustment. The regression equations developed for both the negative and positive spectral mismatch range and all time histories had coefficients with p-values less than 0.10. Values for the coefficients of the regression equations developed for all the time histories along with the corresponding R^2 values of the equations for both positive and negative NE_s or $NE_{s,LP}$ are shown in **Table 5.2**.

Overall, the developed regression equations for the motions in scenario I do not accurately describe the relationship between the *GOF* values for the time histories and spectral mismatch, particularly for positive values of spectral mismatch (R^2 values of 0 to 0.42; see **Table 5.2**). The regression curves developed for the *GOF* values for the $a(t)$ and *FAS* with respect to

NE_s are shown in **Figures 5.20** and **5.21**, respectively. The regression curves for $a(t)$ and *FAS* describe the behavior of the *GOF* values for negative NE_s well (R^2 values above 0.85) for both modification techniques. For *TD* modification, the regression curve developed for the *GOF* – spectral mismatch relationship for $a(t)$ in the positive spectral mismatch range is nearly constant and has an R^2 value less than 0.05. For both $a(t)$ and *FAS*, the regression curves developed for the FD-modified motions are slightly less than the calculated *GOF* values for NE_s greater than 1.2. As shown in **Figure 5.21** and **Table 5.2**, the regression curves developed for the relationship between the *GOF* values for the *FAS* and spectral mismatch are similar for TD and FD modification. The regression curves developed for the *GOF* – spectral mismatch relationships for $v(t)$ and $d(t)$ are shown in **Figures 5.22** and **5.23**, respectively. For both of these time histories, the regression curves developed for the TD-modified motions for positive spectral mismatch actually increase with increasing $NE_{s,LP}$. As previously discussed, the *GOF* values should approach 0.37 for very large $NE_{s,LP}$, indicating these regression curves are not acceptable. This observation is supported by the very small (and even negative) R^2 values for the regression curves developed for the $v(t)$ and $d(t)$ for positive spectral mismatch. The regression curves developed for the relationship between *OGOF* and NE_s increase for positive NE_s for both modification techniques, as shown in **Figure 5.24**. Also, the R^2 values of the regression equations developed for the relationship between *OGOF* and NE_s for negative values of NE_s are lower than those of the regression equations developed for the other time histories for negative spectral mismatch (less than 0.45). These observations further show the relationship between the *OGOF* and NE_s is weaker than the relationships between the *GOF* for the time histories (and *FAS*) and spectral mismatch.

Trends are present in the relationships between *GOF*, quantified by $imRMSE_t$, and spectral mismatch, quantified by NE_s, for $a(t)$, $v(t)$, $d(t)$, and *FAS*. However, the regression curves developed for these relationships do not accurately describe the behavior of the *GOF* values due to the large amount of dispersion in the *GOF* values, particularly for motions with positive NE_s. The results for the second scenario should be compared to these results to check whether the observed trends are similar for other scenarios and if the amount of dispersion in the *GOF* values is smaller for other scenarios when plotted against spectral mismatch.

5.2.1.2 Goodness-of-Fit versus Modified-to-Scaled Ground Motion Characteristic Ratios

The *GOF* values for certain time histories are related to certain modified-to-scaled ground motion characteristic ratios. Example plots of *GOF* values calculated using the TVM_t, $imRMSE_t$, $imRMSE_t$*, and $ERFCM_t$ metrics versus modified-to-scaled *PGA* ratios are shown in **Figure 5.25**. Plots for all the *GOF* metrics versus the modified-to-scaled ground motion characteristic ratios for all the time histories and ground motion characteristics are shown in **Appendix D**. For all of the ground motion characteristics and time histories, the $imRMSE_t$ metric results in the most apparent trends and least amount of dispersion in the relationships between the *GOF* values and the modified-to-scaled ground motion characteristic ratios. Using the TVM_t or $ERFCM_t$ metric to calculate *GOF* for the time histories leads to similar relationships between the *GOF* values and the modified-to-scaled ground motion characteristic ratios, but larger dispersions in the *GOF* values. Also, larger *GOF* values are calculated for the time histories of the TD-modified motions than for the FD-modified motions when the TVM_t or $ERFCM_t$ metrics are used. As previously discussed, $imRMSE_t$* leads to much smaller *GOF* values for the $d(t)$ of the FD-modified motions. Peaks in the *GOF* values are observed around modified-to-scaled ground motion characteristic ratios of 1 (i.e., no change in the characteristic). If the characteristics of a ground motion are not changed by modification, it is expected that the time histories of the motions are also relatively unchanged during modification. The *GOF* values tend towards 0 for very large modified-to-scaled ground motion characteristic ratios (i.e., the response spectrum is increased to match the target spectrum, so the characteristics of the ground motions are increased). Conversely, the *GOF* values approach 0.37 for small modified-to-scaled ground motion characteristic ratios.

The $imRMSE_t$ metric is used in the development of regression equations relating the modified-to-scaled ground motion characteristic ratios to the *GOF* for the $a(t)$, $v(t)$, $d(t)$, and *FAS* and the *OGOF*. The *GOF* values for the $a(t)$ and *FAS* have the least amount of dispersion when plotted against the modified-to-scaled *PGA* ratios, as shown in **Figures 5.26** and **5.27**, respectively. For the $v(t)$, the *GOF* values have the least amount of dispersion when plotted against the modified-to-scaled *PGV* ratios, as shown in **Figure 5.28**. **Figures 5.29** and **5.30** respectively show that using the modified-to-scaled *PGD* ratios leads to the least amount of dispersion in the *GOF* values for the $d(t)$ and *OGOF* values. The *GOF* values for $v(t)$ and $d(t)$

and the *OGOF* values have more dispersion than the *GOF* values for $a(t)$ and *FAS* when plotted against the modified-to-scaled ground motion characteristics.

The relationships between the *GOF* and modified-to-scaled ground motion characteristic ratios require only one equation to describe the behavior for all ratios. The *GOF* – modified-to-scaled ground motion characteristic ratio relationships are best described using a Lorentzian peak functional form, given in **Equation 5.15**.

$$GOF = y_{0tg} + \frac{2A_{tg}}{\pi} \frac{w_{tg}}{4\left(PGA_{\text{mod}} / PGA_{scaled} - x_{ctg}\right)^2 + w_{tg}^2} \quad \textbf{(5.15)}$$

In this equation, A_{tg}, w_{tg}, and x_{ctg} represent coefficients calculated during the regression process for the *GOF* – modified-to-scaled ground motion characteristic ratio relationships. For the development of the regression equations for the relationship between the *GOF* values and the modified-to-scaled ground motion characteristic ratios, the y_{0tg} term was set to 0 since the *GOF* values approach 0 for very large modified-to-scaled ground motion characteristic ratios. Also, the $x_{c,tg}$ term is constrained to values between 0.5 and 1.5 to ensure the regression equations peak around modified-to-scaled ground motion characteristic ratios equal to 1. For all the regression equations developed to describe the *GOF* relationship with the modified-to-scaled ground motion characteristic ratios, the coefficients have significance levels less than 0.05. Coefficients and R^2 values of the regression equations developed for the relationships between the *GOF* values for the different time histories and the modified-to-scaled ground motion characteristic ratios are shown in **Table 5.3**.

The regression curves developed for the relationship between the *GOF* values for the $a(t)$ and the modified-to-scaled *PGA* ratios are shown in **Figure 5.31**. The *GOF* values for the $a(t)$ of the FD-modified motions are generally larger than those of their TD-modified counterparts around modified-to-scaled *PGA* ratios of 1 (0.65 compared to 0.45). **Figure 5.32** shows the regression curves developed for the *GOF* values for the *FAS* with respect to the modified-to-scaled *PGA* ratios. The regression curves developed for the *GOF* values for the *FAS* of the TD- and FD-modified motions practically have the same shape and magnitude. The regression curves developed for the relationship between the *GOF* values for the $v(t)$ and modified-to-scaled *PGV* ratios are shown in **Figure 5.33**. Although the TD- and FD-modified motions have similar maximum *GOF* values for the $v(t)$ (0.75 to 0.8), the *GOF* values for the $v(t)$ of the FD-modified motions are generally larger than those of the TD-modified motions for modified-to-scaled *PGV*

ratios less than about 2. **Figure 5.34** shows the regression curves calculated for the relationship between the *GOF* values for the $d(t)$ and the modified-to-scaled *PGD* ratios. The TD-modified motions have the largest maximum *GOF* values for $d(t)$ (0.95), but the regression curves developed for TD and FD modification are approximately equal for modified-to-scaled *PGD* ratios greater than 0.6. The regression curves developed for the *OGOF* with respect to the modified-to-scaled *PGD* ratios are shown in **Figure 5.35**. The regression curves developed for the *OGOF* for the TD- and FD-modified motions shown in **Figure 5.35** have very similar shapes and magnitudes. The R^2 values of the regression equations for all of the *GOF* – modified-to-scaled ground motion characteristic ratio relationships are relatively large (between 0.65 and 0.9). However, the regression equations for $a(t)$ and *FAS* have slightly larger R^2 values (0.78 to 0.89) than those for $v(t)$, $d(t)$, and *OGOF* (0.67 to 0.87).

The *GOF* values for the $a(t)$, $v(t)$, $d(t)$, and *FAS* and the *OGOF* of the motions in scenario I are clearly related to certain modified-to-scaled ground motion characteristic ratios. This observation is further supported by the relatively large R^2 values (greater than 0.67) of the regression equations fit to the *GOF* – modified-to-scaled ground motion characteristic ratio relationships for both modification techniques (see **Table 5.3**). These relationships must be studied for scenario II to check if they are similar for a different scenario and a completely different set of motions.

5.2.1.3 Visual Assessment of Goodness-of-Fit

A comparison of the independently assigned rankings for the $d(t)$ of the TD- and FD-modified motions matched to the CMS in scenario I by the author and author's advisor are shown in **Figures 5.36** and **5.37**, respectively. Although the author and his advisor agree on the ranking for only 50% of the motions, the author and the author's advisor agree on whether the modified motions should be accepted (i.e., rankings of 5, 4, or 3) or rejected (i.e., rankings of 1 or 2) for 86% of the TD-modified motions and 90% of the FD-modified motions. Some systematic differences are observed in the two assigned rankings. Specifically, the author's assigned rankings are generally lower than or equal to the advisor's rankings. This comparison shows that the author's assessment is fairly objective overall.

The *GOF* values for the $a(t)$, $v(t)$, and $d(t)$ of the motions in scenario I are plotted versus their corresponding rankings assigned by the author in **Figures 5.38**, **5.39**, and **5.40**, respectively.

The *OGOF* values of the motions are plotted in **Figure 5.41** against their corresponding rankings calculated using the average of the rankings for the $a(t)$, $v(t)$, and $d(t)$. Median *GOF* values with plus and minus one standard deviation bars are also shown for each ranking in these plots. **Table E.1** in **Appendix E** shows the rankings assigned to the $a(t)$, $v(t)$, and $d(t)$ of the TD- and FD-modified motions for each individual motion and **Figures E.1** to **E.3** in **Appendix E** show the corresponding one-page output summaries for the motions examined in scenario I. In **Figures E.1** to **E.3**, time histories of modified motions rejected because their response spectra did not match the target spectra are crossed out. For all of the time histories and both modification techniques, the *GOF* values decrease as the qualitative ranking decreases, indicating that it is possible to quantify the selection process used in practice. The decrease in the median *GOF* values for the $a(t)$ is less apparent with the decrease in ranking due to difficulties in visually distinguishing differences between the modified and scaled $a(t)$. The *GOF* values decrease more significantly with a decrease in ranking for the $d(t)$ of the TD-modified motions than for the $d(t)$ of the FD-modified motions. As shown in **Figure 5.40**, the median *GOF* values for the $d(t)$ of the TD- and FD-modified motions decrease by about 0.6 and 0.4, respectively, going from a ranking of 5 to a ranking of 1. This observation is the result of the larger dispersion observed in the *GOF* values for the $d(t)$ of the TD-modified motions.

Recommended threshold *GOF* values that can be used for the modified time histories to identify modified motions that are likely acceptable, possibly acceptable, and likely unacceptable are shown in **Figures 5.38** to **5.41** with dashed lines. The recommended limit for possibly acceptable and likely unacceptable modified ground motions is set to the median *GOF* value for the ranking of 3 and the recommended limit for likely acceptable and possibly acceptable modified ground motions is set to the median *GOF* value for the ranking of 4. Modified time histories with *GOF* values less than the median *GOF* value for the ranking of 3 are considered likely unacceptable and modified time histories with *GOF* values greater than the median *GOF* value for the ranking of 4 are considered likely acceptable. These limits are shown in **Figures 5.38** to **5.41** as an example.

As shown in **Section 5.2.1.1**, significantly different trends are observed in the *GOF* values for ground motions with positive NE_s or $NE_{s,LP}$ and ground motions with negative NE_s or $NE_{s,LP}$ (i.e., response spectrum is decreased or increased, respectively). Therefore, *GOF* limits are established for motions with negative NE_s or $NE_{s,LP}$ and motions with positive NE_s or $NE_{s,LP}$

separately. Based on observations from **Chapter 4**, it is recommended to use motions with positive NE_s or $NE_{s,LP}$; however limits for *GOF* are provided for motions with positive spectral mismatch and motions with negative spectral mismatch. **Figures 5.42** to **5.45** show the median, with plus and minus one standard deviation bars, *GOF* values for the motions with positive spectral mismatch and the motions with negative spectral mismatch within each ranking for the $a(t)$, $v(t)$, $d(t)$, and *OGOF*, respectively. As expected, there is a noticeable difference between the median *GOF* values for the time histories corresponding to motions with positive NE_s or $NE_{s,LP}$ and those corresponding to motions with negative NE_s or $NE_{s,LP}$. For the $a(t)$, $v(t)$, and $d(t)$, the median *GOF* values of the motions with positive NE_s or $NE_{s,LP}$ are generally larger than those of the motions with negative NE_s or $NE_{s,LP}$. This is a result of the *GOF* values for the $a(t)$, $v(t)$, and $d(t)$ of motions with positive NE_s or $NE_{s,LP}$ generally ranging from about 0.4 to 0.9 while the *GOF* values of motions with negative NE_s or $NE_{s,LP}$ range from 0 to 0.9. For the *OGOF*, the motions with negative NE_s have larger median *GOF* values for each ranking than the motions with positive NE_s. This can likely be attributed to a larger number of motions with positive NE_s having *OGOF* values less than 0.4 due to the weak relationship observed between the *OGOF* and the spectral mismatch (see **Figure 5.24**). Based on the results of the visual assessment for scenario I, recommended threshold *GOF* values for the $a(t)$, $v(t)$, $d(t)$, and the *OGOF* for motions with positive and negative spectral mismatch to identify likely acceptable, possibly acceptable, and likely unacceptable ground motions are provided in **Table 5.4**.

Increasing values in the qualitative rankings based on the visual assessments for the $v(t)$ and $d(t)$ of the motions in scenario I coincide with increasing values of *GOF* for the same time histories. Only slight increases in the *GOF* values are observed for an increase in the qualitative rankings for the $a(t)$. Motions from the second scenario must be visually examined to ensure these trends are observed for multiple scenarios and also to increase the number of motions used in establishing the recommended limits for *GOF*.

5.2.2 Results for Scenario II

5.2.2.1 Goodness-of-Fit versus Spectral Mismatch

The *GOF* values for the $a(t)$, *FAS*, $v(t)$, and $d(t)$ of the motions in scenarios I and II are plotted against spectral mismatch (i.e., NE_s or $NE_{s,LP}$) in **Figures 5.46** to **5.49**, respectively. For

both scenarios, the *GOF* values have very similar trends when plotted against spectral mismatch. However, the *GOF* values for the time histories of the FD-modified motions in scenario II are generally smaller than those of the FD-modified motions in scenario I while the *GOF* values for the time histories of the TD-modified motions in scenario II are slightly larger than those of the TD-modified motions in scenario I for larger values of NE_s or $NE_{s,LP}$.

Since similar relationships between the *GOF* for the different time histories and spectral mismatch were observed for both scenarios, regression equations were developed using the combined sets of motions from scenarios I and II. Regression equations for the relationship between *GOF* for the time histories and spectral mismatch were developed using the same procedure presented in **Section 5.2.1.1**. The *OGOF* values of the motions in the second scenario follow a similar trend with respect to spectral mismatch to the trend observed for the motions in the first scenario as shown in **Figure 5.50**. However, regression equations are not presented for the relationship between the *OGOF* and spectral mismatch since this relationship is relatively weak compared to the other time histories. Coefficients and R^2 values of the regression equations developed for the relationship between *GOF* and spectral mismatch using the combined set of motions from scenarios I and II are provided in **Table 5.5**.

Standard deviations were also calculated for the regression curves by plotting the residuals for the regression equations against spectral mismatch and calculating the standard deviations of the residuals for different bins of spectral mismatch. The standard deviations of these residuals, σ_{ts}, are best described by an extreme function, provided in **Equation 5.16**.

$$\sigma_{ts} = y_{0ts,\sigma} + A_{ts,\sigma} * \exp\left(-\exp\left(-\frac{NE_s - x_{cts,\sigma}}{w_{ts,\sigma}}\right) - \frac{NE_s - x_{cts,\sigma}}{w_{ts,\sigma}} + 1\right) \quad \textbf{(5.16)}$$

$y_{0ts,\sigma}$, $A_{ts,\sigma}$, $x_{cts,\sigma}$, and $w_{ts,\sigma}$ represent coefficients for the standard deviations developed for the regression curves of the *GOF* – spectral mismatch relationships. The values for the coefficients and R^2 values of the standard deviation equations calculated for the *GOF* – spectral mismatch relationships are provided in **Table 5.6**.

Figure 5.51 shows the regression curves developed for the relationship between *GOF* for the $a(t)$ and spectral mismatch using the combined set of motions from scenarios I and II. The standard deviations of the residuals of the regression equations developed for the relationship between *GOF* for the $a(t)$ and spectral mismatch and the best-fit curves (i.e., σ_{ts}) are shown in **Figure 5.52**. The regression equations developed for the relationship between *GOF* for the *FAS*

and spectral mismatch using the combined set of motions from scenarios I and II and the corresponding standard deviations of the residuals are plotted in **Figures 5.53** and **5.54**, respectively. The regression curves developed for the relationship between *GOF* for the $v(t)$ and spectral mismatch using the combined set of motions from scenarios I and II and the corresponding standard deviations of residuals are respectively shown in **Figures 5.55** and **5.56**. **Figure 5.57** shows the regression curves developed for the relationship between *GOF* for the $d(t)$ and spectral mismatch and **Figure 5.58** shows the corresponding standard deviations of residuals for this relationship.

The observed trends in the relationships between the *GOF* values and spectral mismatch for the motions in scenario II are similar to the observed trends for the same relationships for the motions in scenario I. Although trends are observed between the *GOF* values for the time histories and spectral mismatch, the developed regression curves do not accurately describe the behavior of this relationship due to the large amount of dispersion in the *GOF* values when plotted against spectral mismatch. Therefore, the regression curves developed to describe the relationship between the *GOF* values and spectral mismatch are not recommended and are not compared to the results for scenario III.

5.2.2.2 Goodness-of-Fit versus Modified-to-Scaled Ground Motion Characteristic Ratios

Overall, the *GOF* values for the time histories of the motions in scenarios I and II have similar relationships with the modified-to-scaled ground motion characteristic ratios. **Figures 5.59** and **5.60** show the regression curves developed for the relationships between the *GOF* values for the $a(t)$ and *FAS*, respectively, and the modified-to-scaled *PGA* ratios for scenarios I and II. The regression curves developed for the *GOF* values for the $v(t)$ – modified-to-scaled *PGV* ratios relationship for both scenarios are shown in **Figure 5.61**. The regression curves developed for the relationships between the *GOF* values for the $d(t)$ and the modified-to-scaled *PGD* ratios and the *OGOF* values and the modified-to-scaled PGD ratios for scenarios I and II are respectively shown in **Figures 5.62** and **5.63**. As observed in the plots for the *GOF* – spectral mismatch relationships for scenarios I and II, the *GOF* values of the motions in scenario II are slightly larger than the *GOF* values of the motions in scenario I for TD modification, but slightly smaller for FD modification. For all the time histories, the regression curves developed for the *GOF* – modified-to-scaled ground motion characteristic ratio relationships using the motions

from scenario II generally predict *GOF* values within 0.05 units of the *GOF* values predicted by the corresponding regression curves developed for scenario I.

The sets of ground motions from scenarios I and II were combined to develop regression equations to describe the relationship between the *GOF* and modified-to-scaled ground motion characteristic ratios for the different time histories since the observed trends of both scenarios for these relationships were very similar. All of the calculated regression equations for these relationships have a Lorentzian peak functional form (**Equation 5.15**). The coefficients of the regression equations have significance levels less than 0.05 for all of the time histories. **Table 5.7** provides the coefficients and R^2 values of the regression equations developed for the GOF – modified-to-scaled ground motion characteristic ratio relationships for all the time histories using the combined set of motions from scenarios I and II.

Standard deviations were also calculated for the regression curves using the residuals. The standard deviations of the residuals for the regression equations developed for the relationships between *GOF* and the modified-to-scaled ground motion characteristics are also best described by a Lorentzian peak function; however, y_{0tg} is not constrained to 0 for the standard deviations. Values for the coefficients and R^2 of the equations calculated for the standard deviations of the *GOF* – spectral mismatch relationships are provided in **Table 5.8**.

Overall, the regression equations developed for the relationship between *GOF* and the modified-to-scaled ground motion characteristic ratios using the combined set of motions from scenarios I and II appear to accurately describe the behavior of the *GOF* values (R^2 values greater than 0.7). **Figure 5.64** shows the regression curves calculated for the *GOF* values for the $a(t)$ with respect to the modified-to-scaled *PGA* ratios using the combined set of motions from scenarios I and II and **Figure 5.65** shows the corresponding standard deviations of residuals. As observed for these regression curves in scenario I, the *GOF* values for $a(t)$ predicted by the regression curves are larger for the FD-modified motions (0.6) than the TD-modified motions (0.5) around modified-to-scaled *PGA* ratios equal to 1. As shown in **Figure 5.66**, the regression curves developed for the relationship between *GOF* for the *FAS* and the modified-to-scaled *PGA* ratios are similar for both modification techniques. The standard deviations of residuals for the regression curves for the *GOF* for the *FAS* – modified-to-scaled *PGA* ratio relationship are shown in **Figure 5.67**. Figures **5.68** and **5.69** respectively show the regression curves developed for the relationship between the *GOF* for the $v(t)$ and the modified-to-scaled *PGV* ratios and the

corresponding standard deviations of residuals. The R^2 value of the regression equation for the *GOF* for the $v(t)$ – modified-to-scaled *PGV* ratio relationship for TD modification is slightly improved using the combined set of motions (0.68 for scenario I and 0.72 for combined set). **Figure 5.70** shows the regression curves developed for the *GOF* values for the $d(t)$ with respect to the modified-to-scaled *PGD* ratios while the corresponding standard deviations of residuals are shown in **Figure 5.71**. The *GOF* values for the $d(t)$ of the combined set of TD-modified motions from scenarios I and II are somewhat larger than those for the $d(t)$ of their FD-modified counterparts for modified-to-scaled *PGD* ratios equal to 1 (0.55 compared to 0.5). The regression equations developed for the *OGOF* – modified-to-scaled *PGD* ratio relationship, shown in **Figure 5.72**, are the only equations that experience a decrease in the R^2 values when the combined set of motions is used as opposed to just the motions in the first scenario. This observation is the result of the *OGOF* values of the motions in the second scenario having a much weaker relationship with larger modified-to-scaled *PGD* ratios, as shown in **Figure 5.63**. The standard deviations of the residuals for the regression curves developed for the *OGOF* are shown in **Figure 5.73**.

Overall, the trends observed between the *GOF* values and the modified-to-scaled ground motion characteristic ratios for the motions in scenario II are similar to the trends observed for these relationships for the motions in scenario I. Furthermore, the regression equations developed for these relationships appear to describe the behavior of the *GOF* values with respect to the modified-to-scaled ground motion characteristic fairly well (i.e., R^2 values greater than 0.7). The *GOF* values for the time histories of the ground motions in scenario III must be compared to these results to examine the general applicability of these regression equations.

5.2.2.3 Visual Assessment of Goodness-of-Fit

The *GOF* values for the $a(t)$, $v(t)$, and $d(t)$ of the visually examined motions from scenarios I and II are plotted versus their assigned visual rankings in **Figures 5.74**, **5.75**, and **5.76**, respectively. **Figure 5.77** shows the *OGOF* values of the motions in scenarios I and II plotted against their corresponding calculated rankings. **Table E.2** in **Appendix E** shows the rankings assigned to the $a(t)$, $v(t)$, and $d(t)$ of each individual motion and **Figures E.4** to **E.6** in **Appendix E** show the corresponding one-page output summaries for the motions examined in scenario II. Overall, the *GOF* values for all the time histories have similar ranges for each

ranking for both scenarios. Since the time histories of the motions for both scenarios have similar trends and ranges of values for the different rankings, the *GOF* values for the time histories of the sets of motions examined for scenarios I and II are combined and used in the establishment of threshold *GOF* values. Since $v(t)$ and $d(t)$ are commonly used in practice to choose whether to accept or reject the modified motion, recommended threshold *GOF* values are only provided for these time histories.

The median *GOF* values within each ranking, with plus and minus one standard deviation bars, calculated for the $v(t)$ of the motions with negative and positive $NE_{s,LP}$ from scenarios I and II are plotted in **Figures 5.78** and **5.79**, respectively. **Figures 5.80** and **5.81** show the median *GOF* values within each ranking, with plus and minus one standard deviation bars, calculated for the $d(t)$ of the motions with negative and positive $NE_{s,LP}$ from both scenarios, respectively. Recommended threshold *GOF* values to identify likely acceptable, possibly acceptable, and likely unacceptable time histories of the modified motions are established using the same limits presented in **Section 5.2.1.3**. **Table 5.9** shows the threshold values of the *GOF* recommended for the $v(t)$ and $d(t)$ based on the visual assessments for motions with either positive or negative spectral mismatch (i.e., response spectrum must be decreased or increased, respectively). For motions with negative $NE_{s,LP}$, the *GOF* values between the $v(t)$ and $d(t)$ of the scaled and modified motions should be greater than 0.46 for TD modification and greater than 0.545 and 0.455, respectively, for FD modification in order for the ground motion to be likely acceptable. For motions with positive $NE_{s,LP}$, the threshold *GOF* values for likely acceptable TD-modified ground motions increase to 0.50 and 0.585 for the $v(t)$ and $d(t)$, respectively, and for likely acceptable FD-modified motions to 0.595 and 0.565 for the $v(t)$ and $d(t)$, respectively.

The threshold values of *GOF* for likely acceptable and likely unacceptable $v(t)$ and $d(t)$ are superimposed on **Figures 5.78** to **5.81**. The engineer can now perform modification, calculate the *GOF* values between the $v(t)$ and $d(t)$ of the modified and scaled motions, then compare the *GOF* values to the threshold values to objectively decide whether the modified motion should be accepted or rejected.

5.2.3 Results for Scenario III

5.2.3.1 Goodness-of-Fit versus Modified-to-Scaled Ground Motion Characteristic Ratios

The *GOF* values for the $a(t)$, *FAS*, $v(t)$, and $d(t)$ and the *OGOF* values of the motions in scenario III were plotted with the regression curves and the plus and minus one standard deviation lines calculated for the relationship between *GOF* and modified-to-scaled ground motion characteristic ratios. Residuals were calculated for all the motions by subtracting the *GOF* value predicted by the regression equation from the calculated *GOF* value. Power functions (i.e., $y = ax^b$) were fit to the residuals and the R^2 values and slopes of these best-fit curves were studied to identify any biases and the statistical significance of any biases.

Figures 5.82 and **5.83** respectively show the *GOF* values for the $a(t)$ of the motions in scenario III plotted with the regression curves and the residuals for the *GOF* values for the $a(t)$ of the motions in scenario III. The regression curves developed for the relationship between the *GOF* for the *FAS* and the modified-to-scaled *PGA* ratios are shown with the *GOF* values for the motions in scenario III in **Figure 5.84**. The corresponding residuals for the *GOF* values for the *FAS* of the motions in scenario III and the standard deviations developed for the regression curves are shown in **Figure 5.85**. For both the $a(t)$ and the *FAS*, the *GOF* values for the motions in scenario III are slightly greater than the regression curves for modified-to-scaled *PGA* ratios between 1 and 5. However, the residuals for the *GOF* values of these motions do not exhibit any bias and are generally enveloped by the standard deviations developed for the regression equations. **Figure 5.86** shows the *GOF* values for the $v(t)$ of the motions in scenario III plotted with the regression curves developed for the *GOF* for $v(t)$ – modified-to-scaled *PGV* ratio relationship and **Figure 5.87** shows the resulting residuals for this relationship. The *GOF* values for the $d(t)$ of the motions in scenario III are plotted with the regression curves for the *GOF* for $d(t)$ – modified-to-scaled *PGD* ratio relationship in **Figure 5.88** and the corresponding residuals are shown in **Figure 5.89**. **Figures 5.90** and **5.91** respectively show the *OGOF* values for the motions in scenario III plotted with regression curves developed for the relationship between *OGOF* and the modified-to-scaled *PGD* ratio and the resulting residuals. **Figures 5.86**, **5.88**, and **5.90** show that the regression curves developed using the motions in scenarios I and II describe the trends between the *GOF* values for the $v(t)$, $d(t)$, and *OGOF*, respectively, and the modified-

to-scaled *PGD* ratios of the motions in scenario III very well. The residuals for the $v(t)$, $d(t)$, and *OGOF* do not exhibit any apparent biases.

The regression equations developed for the relationship between *GOF* and the modified-to-scaled ground motion characteristic ratios using the motions from scenarios I and II also appear to describe the trends in the *GOF* values for the motions in scenario III with respect to the modified-to-scaled ground motion characteristic ratios. This observation is supported by the residuals plotting within the standard deviations developed for the regression curves and the lack of any trends in the residuals. Based on this finding, limits can be placed on *PGA*, *PGV*, or *PGD* given the design scenario then used to estimate a required *GOF* between the scaled and modified time histories.

5.3 Conclusions

Major findings related to the investigation of the effects of ground motion modification on the time histories include:

- Strong relationship between the *GOF* for the $v(t)$ and $d(t)$ and qualitative rankings assigned to these time histories based on a visual assessment: The *GOF* values for the $v(t)$ and $d(t)$ decrease as the qualitative rankings assigned to the time histories based on a visual assessment of ground motions in scenarios I and II decrease. This observed relationship allows for the establishment of threshold *GOF* values for the different time histories to identify modified motions that are likely acceptable, possibly acceptable, and likely unacceptable. Due to the different effects of modification on motions with response spectra that must be decreased to match the target spectrum (i.e., positive $NE_{s,LP}$) and motions with response spectra that must be increased to match the target spectrum (i.e., negative $NE_{s,LP}$), threshold *GOF* values were established for motions with positive and negative $NE_{s,LP}$ separately. However, the threshold *GOF* values for the motions with positive $NE_{s,LP}$ are recommended since ground motions with positive $NE_{s,LP}$ should be used based on observations in **Chapter 4**. For motions with positive $NE_{s,LP}$, modified motions should have $v(t)$ with *GOF* values, as quantified by $imRMSE_t$, greater than 0.50 and 0.595 for TD and FD modification, respectively, and $d(t)$ with *GOF* values greater than 0.585 and 0.565 for TD and FD modification, respectively, in order to be considered possibly acceptable.

- Well-defined relationship between the effects of modification on the time histories and the ground motion characteristics: Strong relationships are observed between the *GOF* between the modified and scaled $a(t)$, *FAS*, $v(t)$, and $d(t)$ and the modified-to-scaled ground motion characteristic ratios of the motions. This finding means the engineer can set acceptable values for the characteristics of the modified motion (e.g., modified motions with characteristics within 100% of those of the scaled motions) then use the regression equations developed for the *GOF* – modified-to-scaled ground motion characteristic ratio relationships to estimate limits for acceptable *GOF* values. The relatively strong relationships between the *GOF* and the modified-to-scaled ground motion characteristics were observed for scenarios I and II then validated by the results for scenario III. The regression curves developed for all of these relationships have R^2 values greater than 0.7.

Some comments must be made in terms of establishing *GOF* limits for the time histories. These observations show why it is recommended that both the ratios of the modified-to-scaled ground motion characteristics and the results of the visual inspection performed in this study should be used together to establish the *GOF* limits.

- Establishing acceptable limits for the modified-to-scaled ground motion characteristic ratios is a subjective process. Suggestions for the modified-to-scaled ratio limits largely depend on the project and the ground motion characteristic under consideration. Additionally, differences in the suggested limits for the modified-to-scaled ground motion characteristic ratios can have a large effect on the corresponding *GOF* limits. The effects of changes in the limits for the modified-to-scaled ground motion characteristic ratios on the resulting "acceptable" *GOF* values for the $v(t)$ and $d(t)$ for TD modification are shown in **Figures 5.92** and **5.93**, respectively. Setting *GOF* limits based on the visual assessment is also a subjective process as the engineer could choose to use median *GOF* values or plus one standard deviations for lower rankings to establish limits between time histories that are likely acceptable, possibly acceptable, and likely unacceptable.
- Depending on the limit used for the ratios of the modified-to-scaled ground motion characteristics, the acceptable *GOF* value could be very similar to the values approached when either the modified or scaled time history has much larger amplitudes than the other (i.e., values near 0 or 0.37). For instance, given a limit of 100% change in *PGD*, the acceptable *GOF* values for the $d(t)$ of the TD-modified motions are 0.455 and 0.13 (see

Figure 5.93) for motions with modified-to-scaled *PGD* ratios less than and greater than 1, respectively.

Other important findings include:

- The *GOF* between the modified and scaled $a(t)$, *FAS*, $v(t)$, and $d(t)$ and the *OGOF* are not strongly related to the spectral mismatch of the motions. The trends in these relationships for scenarios I and II appear to be very similar. However, there is too much dispersion in the *GOF* values when plotted against spectral mismatch to develop accurate regression equations for these relationships.
- The *GOF* values for ground motions with negative spectral mismatch (i.e., NE_s or $NE_{s,LP}$) are more sensitive to changes in spectral mismatch, modified-to-scaled ground motion characteristic ratios, and qualitative ranking than the *GOF* values for motions with positive spectral mismatch. However, the *GOF* values have different ranges for negative and positive NE_s, so a *GOF* value of 0.4 could be acceptable for a motion with negative NE_s, but unacceptable for a motion with positive NE_s.
- For motions with spectral mismatch in the long period range that is close to 0 (i.e., $NE_{s,LP}$ between -0.5 and 0.5), the TD-modified motions potentially have larger *GOF* values for $d(t)$ than the FD-modified motions. However, the *GOF* values for the $d(t)$ of the TD-modified motions have more dispersion in this range than those of the FD-modified motions.

Table 5.1. Descriptions for the qualitative rankings of the goodness-of-fit between the scaled and modified time histories based on the visual assessment.

Visual Ranking	Description
5	Time histories have very similar shapes and amplitudes except for one or two differences
4	Some differences in the shapes of the time histories and a couple of the maximums/minimums – OR – modified time history has a similar shape and amplitude with the unscaled time history
3	Only a portion of the time histories have the same shape and amplitude; still an acceptable time history
2	Time histories have different shapes and amplitudes – OR – modified time history has a significantly different amplitude than the scaled and unscaled time history; not an acceptable time history
1	Very different time histories; time histories of modified motions are not realistic and may be the result of numerical errors

Table 5.2. Values for the coefficients and R^2 of the regression equations developed for the goodness-of-fit – spectral mismatch relationships in the negative and positive spectral mismatch ranges for the motions in scenario I.

Time History		Negative NE_s or $NE_{s,LP}$				Positive NE_s or $NE_{s,LP}$		
		a_{ts}	c_{ts}	k_{ts}	R^2	a_{ts}	b_{ts}	R^2
$a(t)$	TD	0.489	0.030	13.192	0.878	0.475	-0.073	0.019
	FD	0.626	0.029	14.270	0.949	0.608	-0.367	0.422
FAS	TD	0.619	0.020	13.854	0.916	0.607	-0.248	0.283
	FD	0.626	0.029	14.272	0.948	0.609	-0.368	0.427
$v(t)$	TD	0.417	0.003	9.088	0.633	0.416	0.044	-0.030
	FD	0.566	0.001	10.218	0.800	0.565	-0.170	0.367
$d(t)$	TD	0.439	0.036	6.988	0.443	0.424	0.157	0.049
	FD	0.518	0.012	8.368	0.802	0.512	-0.166	0.225
OGOF	TD	0.541	0.393	6.013	0.379	0.389	0.143	-0.033
	FD	0.511	0.119	8.196	0.449	0.456	0.071	-0.015

Table 5.3. Values for the coefficients and R^2 of the regression equations developed for the goodness-of-fit – modified-to-scaled ground motion characteristic ratio relationships for the motions in scenario I.

Time History		A_{tg}	w_{tg}	x_{ctg}	R^2
$a(t)$	TD	2.131	2.803	0.740	0.787
	FD	2.135	2.213	0.873	0.890
FAS	TD	2.620	2.810	0.845	0.821
	FD	2.192	2.249	0.873	0.887
$v(t)$	TD	1.377	2.093	0.549	0.676
	FD	1.667	1.956	0.690	0.865
$d(t)$	TD	1.149	1.353	0.779	0.739
	FD	1.672	2.047	0.687	0.864
OGOF	TD	2.500	3.337	0.500	0.785
	FD	2.834	3.581	0.712	0.808

Table 5.4. Recommended goodness-of-fit limits, quantified by $imRMSE_t$, indicating likely acceptable, possibly acceptable, and likely unacceptable acceleration, velocity, and displacement time histories and the overall goodness-of-fit (*OGOF*) for the modified motions based on the visual assessment of motions from scenario I. The recommended limits are further split between motions with positive and negative spectral mismatch.

Time History		Likely Acceptable	Possibly Acceptable	Likely Unacceptable
Motions with negative *NE* or NE_{LP}				
$a(t)$	TD	$imRMSE_t > 0.525$	$0.525 > imRMSE_t > 0.46$	$0.525 > imRMSE_t$
	FD	$imRMSE_t > 0.56$	-	$0.56 > imRMSE_t$
$v(t)$	TD	$imRMSE_t > 0.465$	$0.465 > imRMSE_t > 0.42$	$0.42 > imRMSE_t$
	FD	$imRMSE_t > 0.555$	$0.555 > imRMSE_t > 0.505$	$0.505 > imRMSE_t$
$d(t)$	TD	$imRMSE_t > 0.46$	$0.46 > imRMSE_t > 0.35$	$0.35 > imRMSE_t$
	FD	$imRMSE_t > 0.425$	$0.425 > imRMSE_t > 0.375$	$0.375 > imRMSE_t$
OGOF	TD	$imRMSE_t > 0.595$	$0.595 > imRMSE_t > 0.47$	$0.47 > imRMSE_t$
	FD	$imRMSE_t > 0.59$	$0.59 > imRMSE_t > 0.50$	$0.50 > imRMSE_t$
Motions with positive *NE* or NE_{LP}				
$a(t)$	TD	$imRMSE_t > 0.52$	$0.52 > imRMSE_t > 0.505$	$0.505 > imRMSE_t$
	FD	$imRMSE_t > 0.61$	$0.61 > imRMSE_t > 0.585$	$0.585 > imRMSE_t$
$v(t)$	TD	$imRMSE_t > 0.53$	$0.53 > imRMSE_t > 0.49$	$0.49 > imRMSE_t$
	FD	$imRMSE_t > 0.60$	$0.60 > imRMSE_t > 0.555$	$0.555 > imRMSE_t$
$d(t)$	TD	$imRMSE_t > 0.60$	$0.60 > imRMSE_t > 0.495$	$0.495 > imRMSE_t$
	FD	$imRMSE_t > 0.565$	$0.565 > imRMSE_t > 0.48$	$0.48 > imRMSE_t$
OGOF	TD	$imRMSE_t > 0.545$	$0.545 > imRMSE_t > 0.45$	$0.45 > imRMSE_t$
	FD	$imRMSE_t > 0.555$	$0.555 > imRMSE_t > 0.47$	$0.47 > imRMSE_t$

Table 5.5. Values for the coefficients and R^2 of the regression equations developed for the goodness-of-fit – spectral mismatch relationships in the negative and positive spectral mismatch ranges for the combined set of motions from scenarios I and II.

Time History		Negative NE_s or $NE_{s,LP}$				Positive NE_s or $NE_{s,LP}$		
		a_{ts}	c_{ts}	k_{ts}	R^2	a_{ts}	b_{ts}	R^2
$a(t)$	TD	0.495	0.017	14.317	0.861	0.487	-0.117	-0.025
	FD	0.614	0.030	14.235	0.941	0.596	-0.352	0.420
FAS	TD	0.621	0.013	14.713	0.902	0.614	-0.247	0.193
	FD	0.614	0.030	14.229	0.941	0.596	-0.352	0.420
$v(t)$	TD	0.414	0.008	8.365	0.585	0.411	0.036	-0.047
	FD	0.538	0.004	9.169	0.703	0.536	-0.152	0.164
$d(t)$	TD	0.463	0.046	6.641	0.418	0.443	0.123	0.024
	FD	0.476	0.006	9.011	0.773	0.473	-0.135	0.087

Table 5.6. Values for the coefficients and R^2 of the standard deviations for the equations developed for the goodness-of-fit – spectral mismatch relationships for the combined set of motions from scenarios I and II.

Time History		$y_{0ts,\sigma}$	$A_{ts,\sigma}$	$w_{ts,\sigma}$	$x_{cts,\sigma}$	R^2
$a(t)$	TD	0.017	0.071	0.338	-0.053	0.694
	FD	0.014	0.057	0.303	-0.031	0.816
FAS	TD	0.036	0.059	0.149	-0.244	0.660
	FD	0.014	0.057	0.303	-0.031	0.817
$v(t)$	TD	0.047	0.094	0.475	-0.229	0.740
	FD	0.045	0.100	0.272	-0.504	0.868
$d(t)$	TD	0.061	0.200	0.483	-0.093	0.773
	FD	0.037	0.073	0.426	-0.292	0.597

Table 5.7. Values for the coefficients and R^2 of the regression equations developed for the goodness-of-fit – modified-to-scaled ground motion characteristic ratio relationships for the combined set of motions from scenarios I and II.

Time History		A_{tg}	w_{tg}	x_{ctg}	R^2
$a(t)$	TD	2.216	2.840	0.705	0.824
	FD	2.015	2.132	0.853	0.886
FAS	TD	2.810	2.945	0.812	0.858
	FD	2.016	2.131	0.853	0.886
$v(t)$	TD	1.444	2.127	0.588	0.716
	FD	1.684	1.997	0.692	0.874
$d(t)$	TD	1.233	1.441	0.806	0.742
	FD	1.668	2.188	0.680	0.865
OGOF	TD	2.463	3.290	0.500	0.734
	FD	2.791	3.684	0.574	0.720

Table 5.8. Values for the coefficients and R^2 of the standard deviations for the equations developed for the goodness-of-fit – modified-to-scaled ground motion characteristic ratio relationships for the combined set of motions from scenarios I and II.

Time History		$y_{0tg,\sigma}$	$A_{tg,\sigma}$	$w_{tg,\sigma}$	$x_{ctg,\sigma}$	R^2
$a(t)$	TD	0.005	0.585	3.333	1.969	0.954
	FD	0.004	0.408	2.100	1.721	0.941
FAS	TD	0.008	0.660	3.191	2.334	0.915
	FD	0.004	0.408	2.104	1.720	0.941
$v(t)$	TD	0.005	0.525	2.491	1.395	0.901
	FD	0.002	0.358	1.926	1.402	0.914
$d(t)$	TD	0.013	0.467	1.736	1.230	0.921
	FD	0.003	0.348	1.976	1.426	0.900
OGOF	TD	0.058	0.512	4.000	2.186	0.379
	FD	0.045	0.299	3.740	1.945	0.608

Table 5.9. Recommended goodness-of-fit limits, quantified by $imRMSE_t$, indicating likely acceptable, possibly acceptable, and likely unacceptable velocity and displacement time histories for the modified motions based on the visual assessment of motions from scenarios I and II. The recommended limits are further split between motions with positive and negative spectral mismatch.

Time History		Likely Acceptable	Possibly Acceptable	Likely Unacceptable
Motions with negative NE_{LP}				
$v(t)$	TD	$imRMSE_t > 0.46$	$0.46 > imRMSE_t > 0.395$	$0.395 > imRMSE_t$
	FD	$imRMSE_t > 0.545$	$0.545 > imRMSE_t > 0.48$	$0.48 > imRMSE_t$
$d(t)$	TD	$imRMSE_t > 0.46$	$0.46 > imRMSE_t > 0.365$	$0.365 > imRMSE_t$
	FD	$imRMSE_t > 0.455$	$0.455 > imRMSE_t > 0.40$	$0.40 > imRMSE_t$
Motions with positive NE_{LP}				
$v(t)$	TD	$imRMSE_t > 0.50$	$0.50 > imRMSE_t > 0.47$	$0.47 > imRMSE_t$
	FD	$imRMSE_t > 0.595$	$0.595 > imRMSE_t > 0.55$	$0.55 > imRMSE_t$
$d(t)$	TD	$imRMSE_t > 0.585$	$0.585 > imRMSE_t > 0.475$	$0.475 > imRMSE_t$
	FD	$imRMSE_t > 0.565$	$0.565 > imRMSE_t > 0.48$	$0.48 > imRMSE_t$

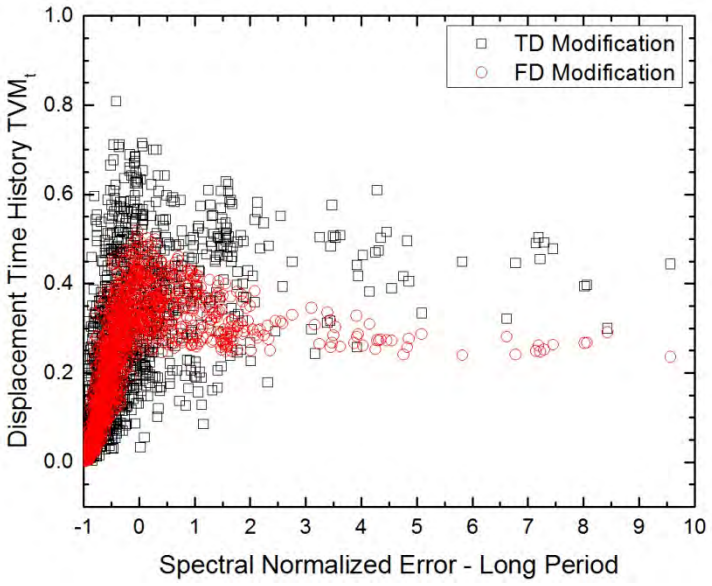

Figure 5.1. Values for goodness-of-fit between the displacement time histories of the scaled and modified motions in scenario I calculated using the TVM_t metric plotted against spectral mismatch in the long period range.

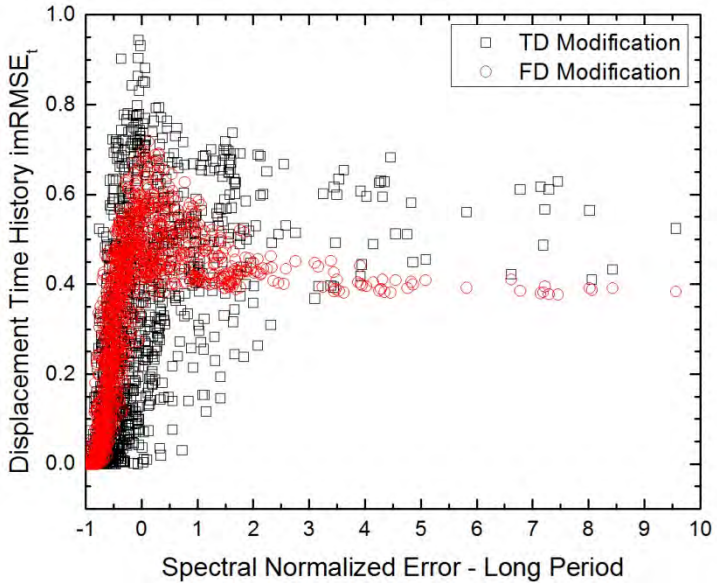

Figure 5.2. Values for goodness-of-fit between the displacement time histories of the scaled and modified motions in scenario I calculated using the $imRMSE_t$ metric plotted against spectral mismatch in the long period range.

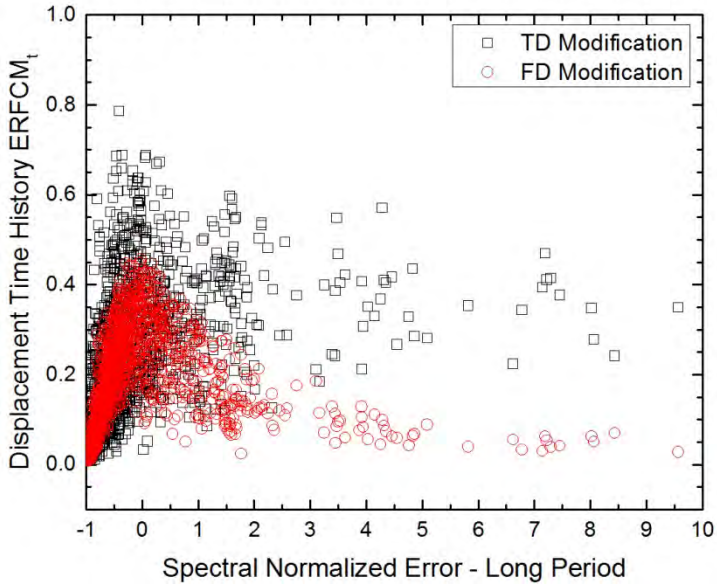

Figure 5.3. Values for goodness-of-fit between the displacement time histories of the scaled and modified motions in scenario I calculated using the $ERFCM_t$ metric plotted against spectral mismatch in the long period range.

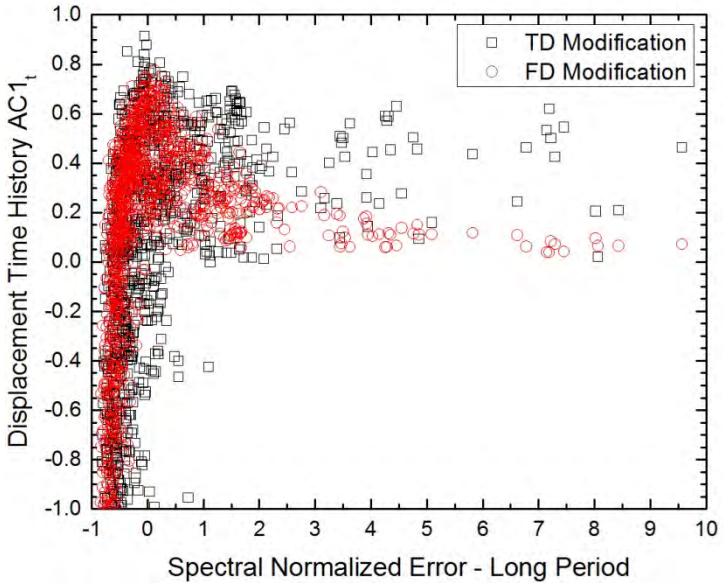

Figure 5.4. Values for goodness-of-fit between the displacement time histories of the scaled and modified motions in scenario I calculated using the $AC1_t$ metric plotted against spectral mismatch in the long period range.

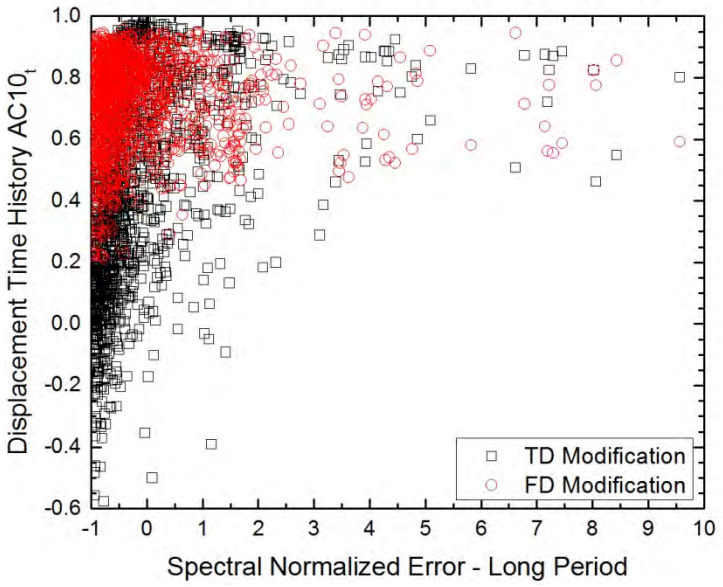

Figure 5.5. Values for goodness-of-fit between the displacement time histories of the scaled and modified motions in scenario I calculated using the $AC10_t$ metric plotted against spectral mismatch in the long period range.

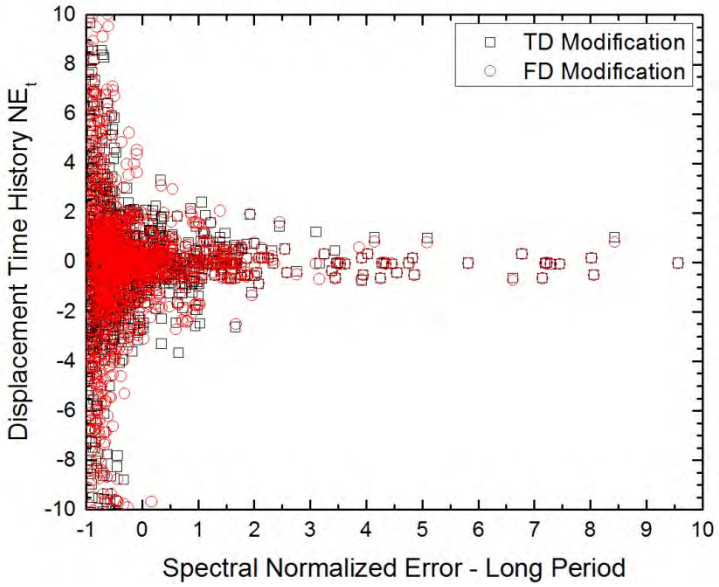

Figure 5.6. Values for goodness-of-fit between the displacement time histories of the scaled and modified motions in scenario I calculated using the NE_t metric plotted against spectral mismatch in the long period range.

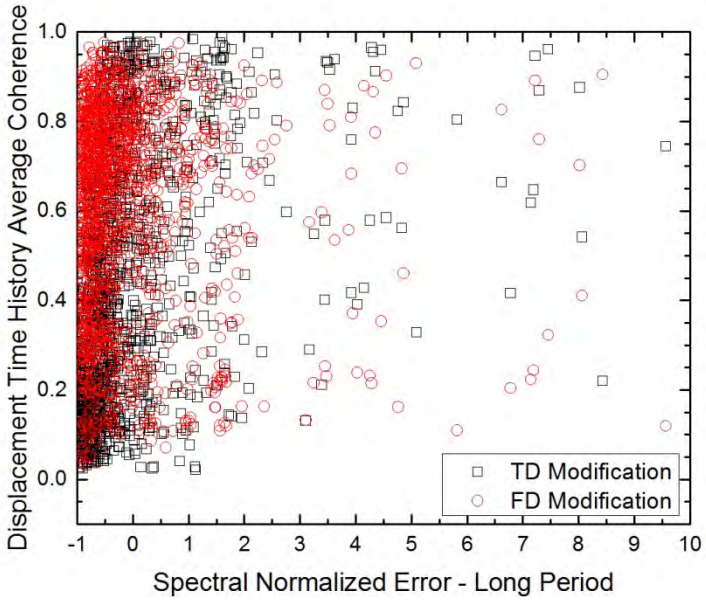

Figure 5.7. Values for goodness-of-fit between the displacement time histories of the scaled and modified motions in scenario I calculated using average coherence plotted against spectral mismatch in the long period range.

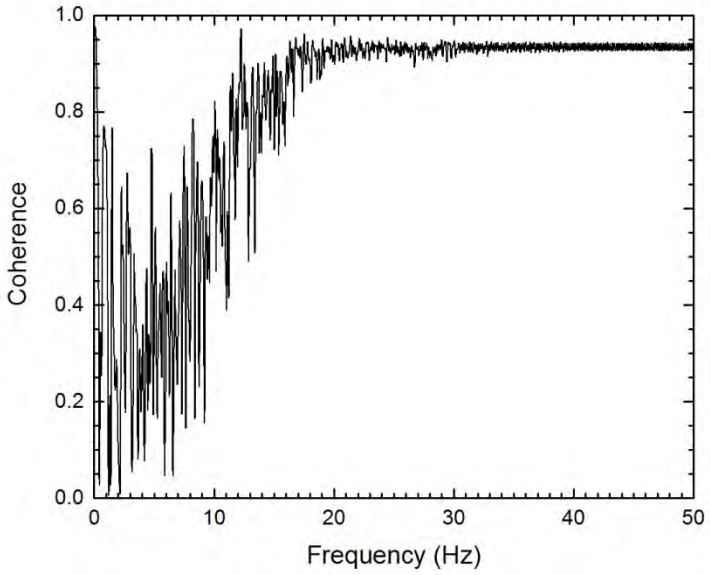

Figure 5.8. Variation of the coherence between the scaled and modified displacement time histories with respect to frequency for an example ground motion.

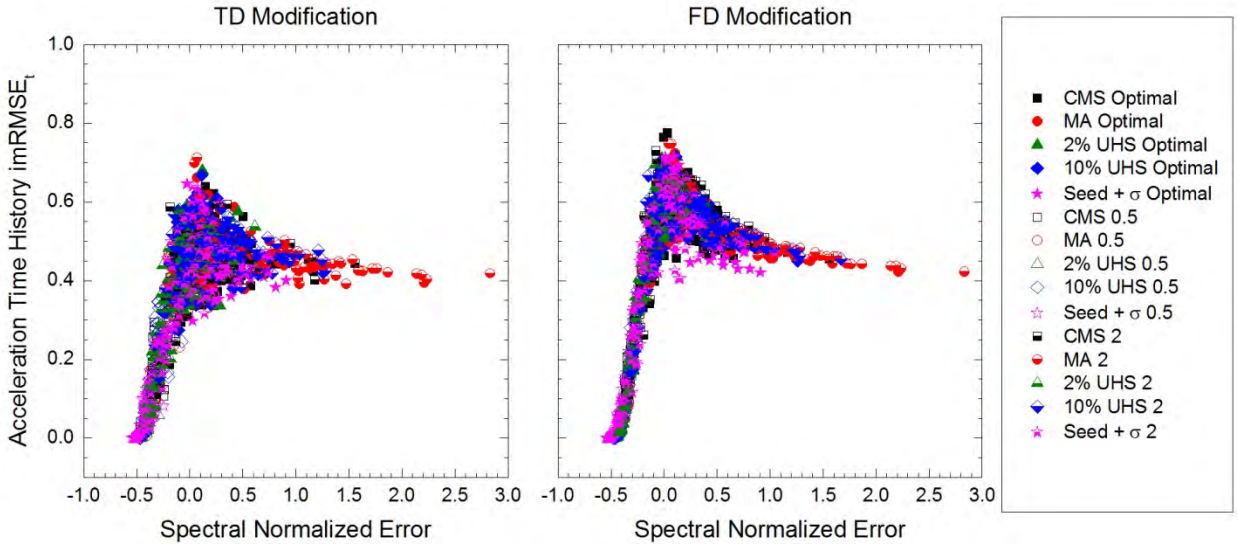

Figure 5.9. Values for goodness-of-fit between the acceleration time histories of the scaled and modified motions in scenario I plotted versus spectral mismatch for all target spectra and scaling factors. In the legend, "Optimal," "0.5," and "2" refer to the scaling factors applied to the motions.

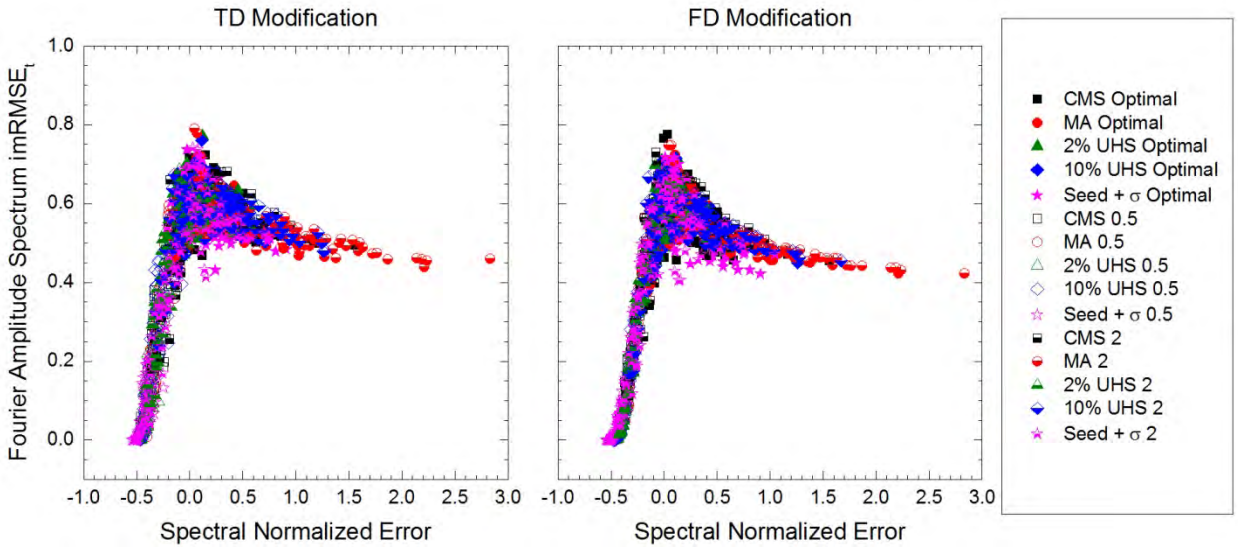

Figure 5.10. Values for goodness-of-fit between the Fourier amplitude spectra of the scaled and modified motions in scenario I plotted versus spectral mismatch for all target spectra and scaling factors. In the legend, "Optimal," "0.5," and "2" refer to the scaling factors applied to the motions.

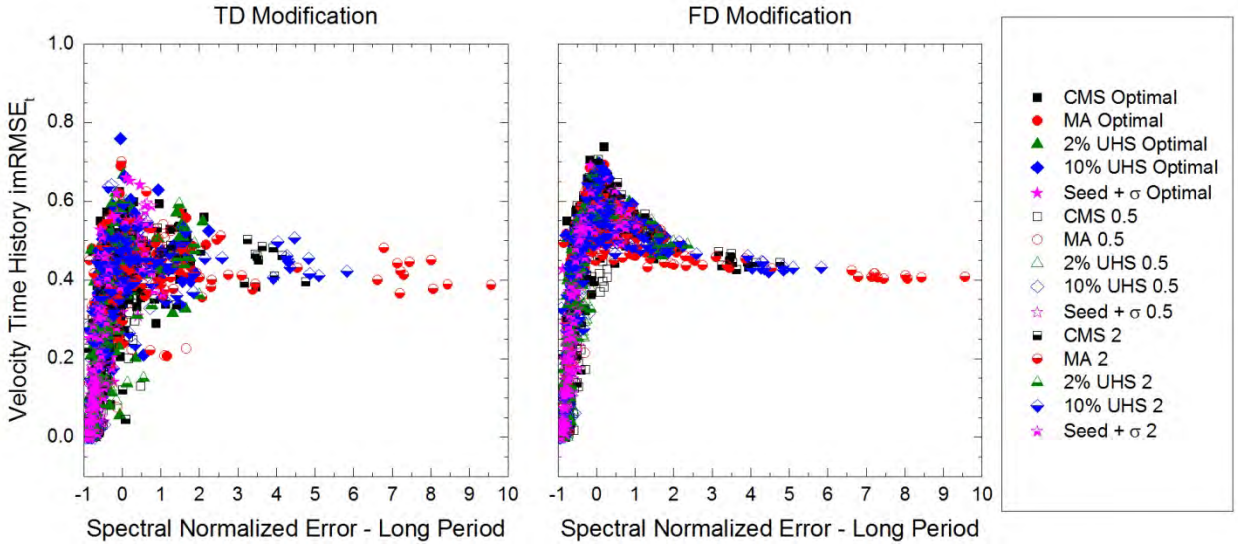

Figure 5.11. Values for goodness-of-fit between the velocity time histories of the scaled and modified motions in scenario I plotted versus spectral mismatch in the long period range for all target spectra and scaling factors. In the legend, "Optimal," "0.5," and "2" refer to the scaling factors applied to the motions.

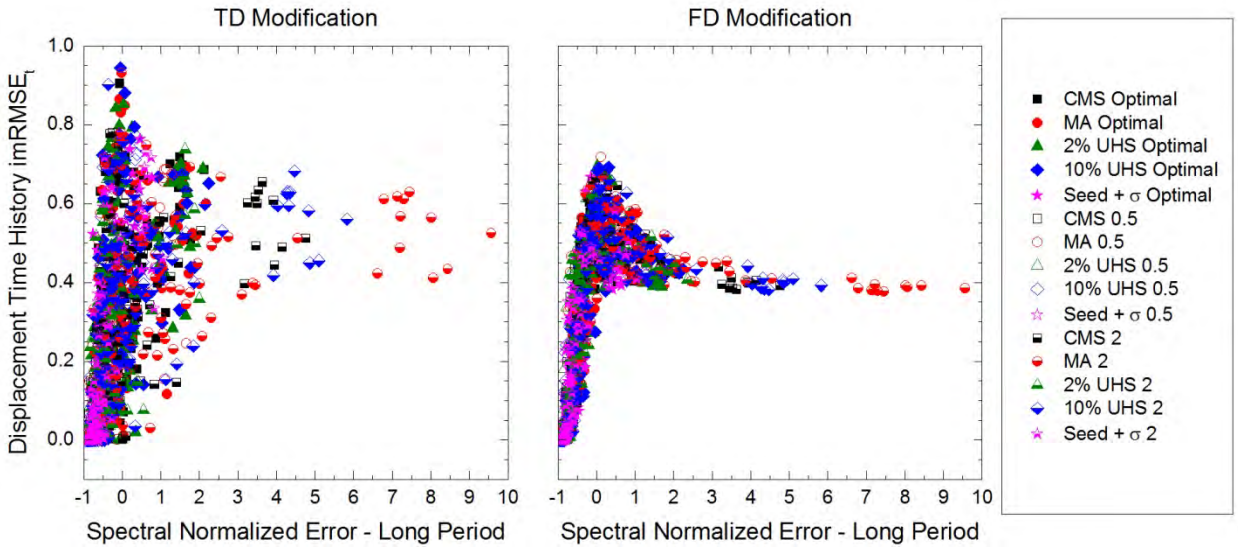

Figure 5.12. Values for goodness-of-fit between the displacement time histories of the scaled and modified motions in scenario I plotted versus spectral mismatch in the long period range for all target spectra and scaling factors. In the legend, "Optimal," "0.5," and "2" refer to the scaling factors applied to the motions.

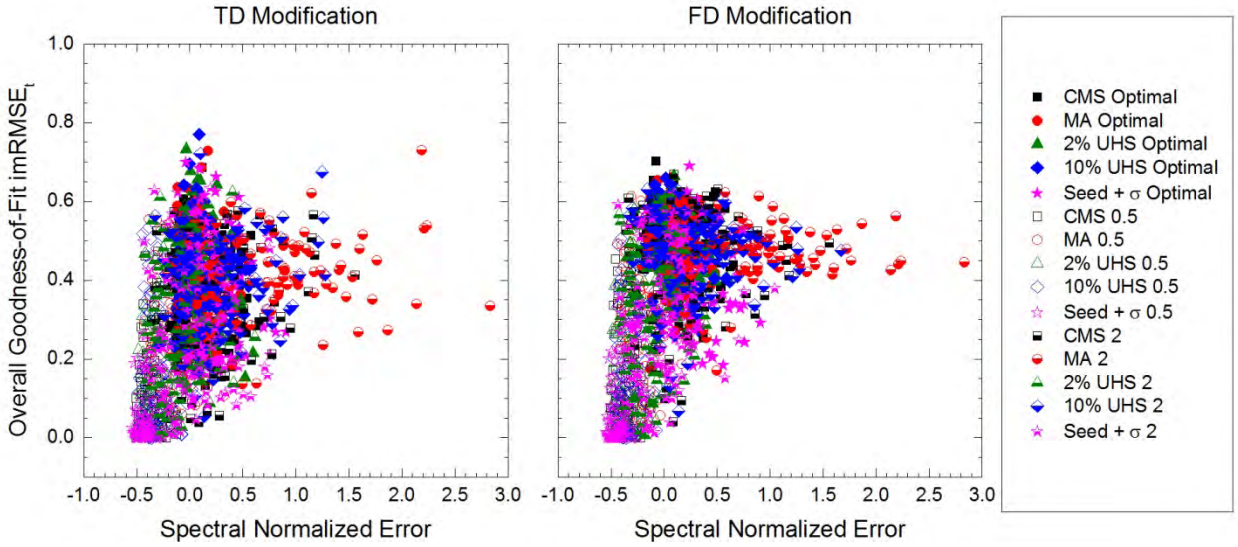

Figure 5.13. Overall goodness-of-fit between the scaled and modified motions in scenario I plotted versus spectral mismatch for all target spectra and scaling factors. In the legend, "Optimal," "0.5," and "2" refer to the scaling factors applied to the motions.

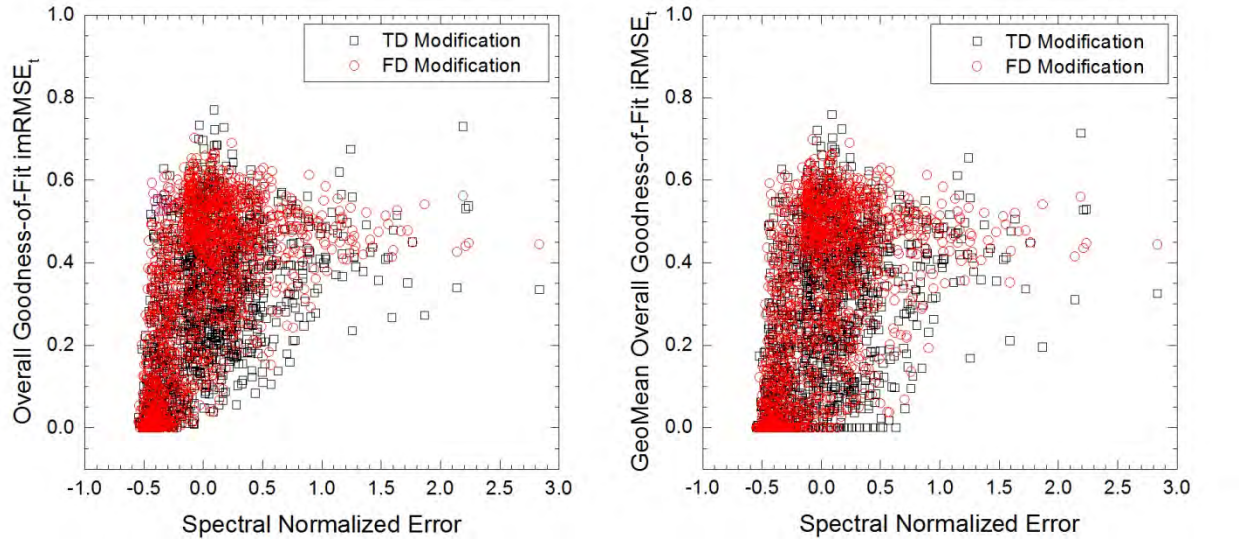

Figure 5.14. Comparison of the overall goodness-of-fit values calculated using the mean (**Equation 5.1**) and geometric mean (**Equation 5.2**) of the goodness-of-fit values for the acceleration, velocity, and displacement time histories of the motions in scenario I.

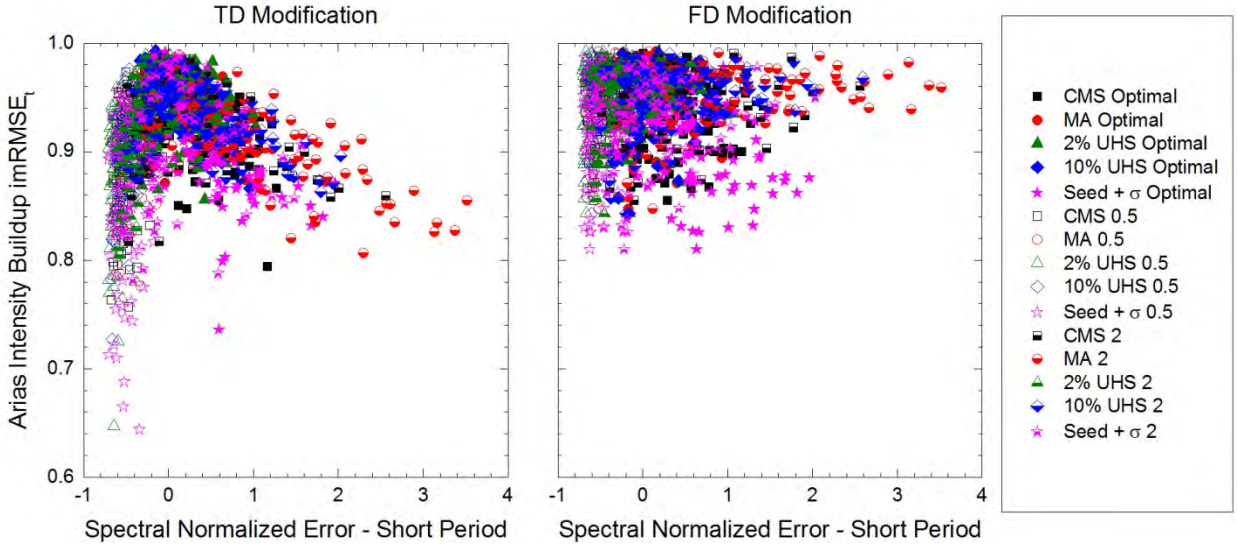

Figure 5.15. Values for goodness-of-fit between the Arias intensity buildups of the scaled and modified motions in scenario I plotted versus spectral mismatch in the short period range for all target spectra and scaling factors. In the legend, "Optimal," "0.5," and "2" refer to the scaling factors applied to the motions.

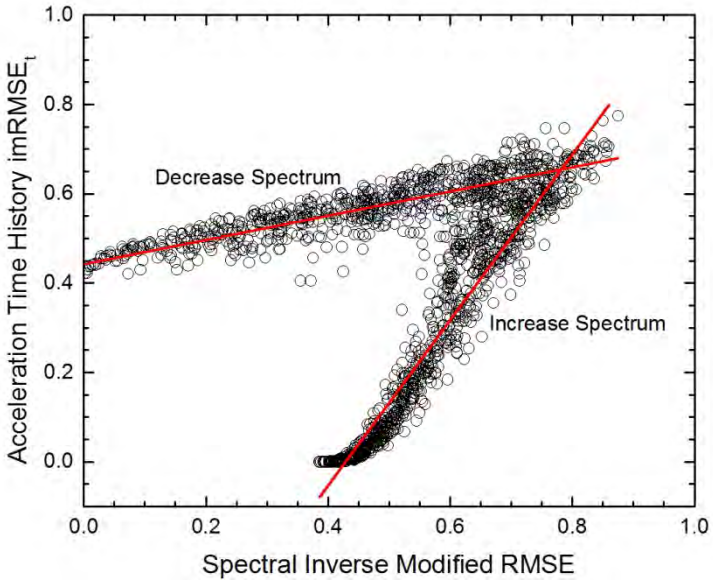

Figure 5.16. Example of the different trends observed between the goodness-of-fit values and spectral mismatch, quantified by *imRMSE*$_t$ and *imRMSE*$_s$, respectively, for motions with response spectra that are increased and decreased to match the target spectrum.

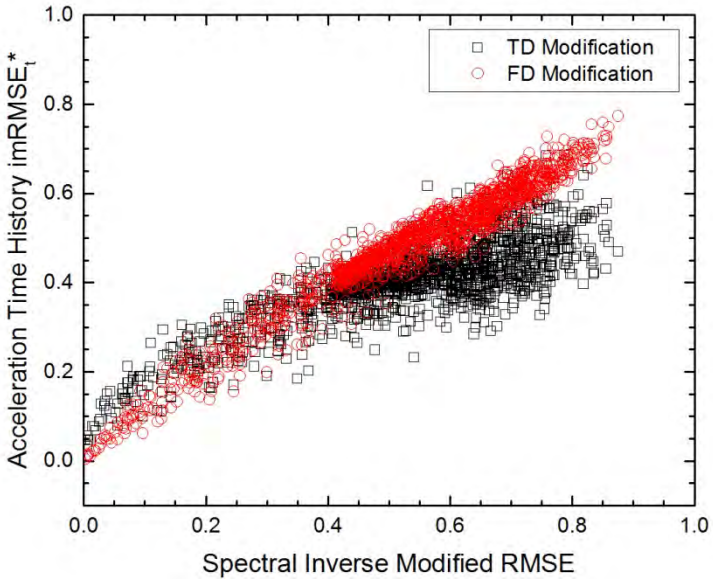

Figure 5.17. Values for goodness-of-fit, quantified by the *imRMSE*$_t$* metric, of the acceleration time histories plotted against spectral mismatch, quantified by *imRMSE*$_s$.

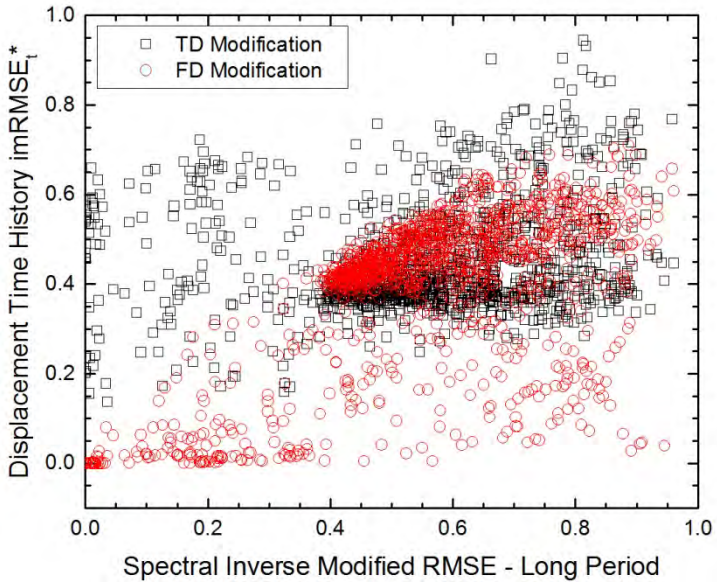

Figure 5.18. Values for goodness-of-fit, quantified by the *imRMSE$_t$** metric, of the displacement time histories plotted against spectral mismatch, quantified by *imRMSE$_{s,LP}$*.

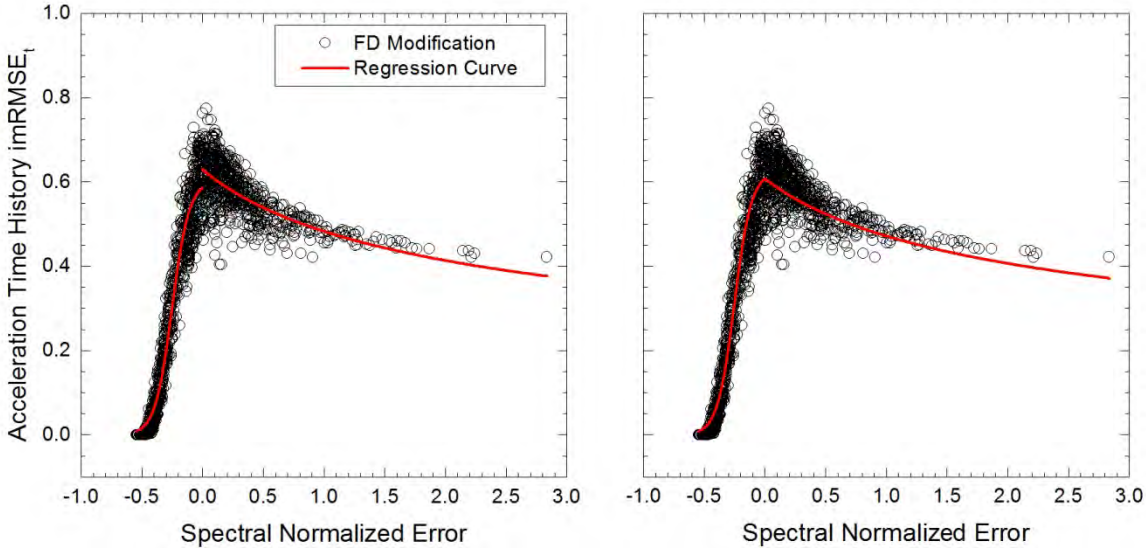

Figure 5.19. Example of the adjustment made to regression curves separately developed for the negative and positive spectral mismatch range in order to have a continuous equation for the goodness-of-fit – spectral mismatch relationship.

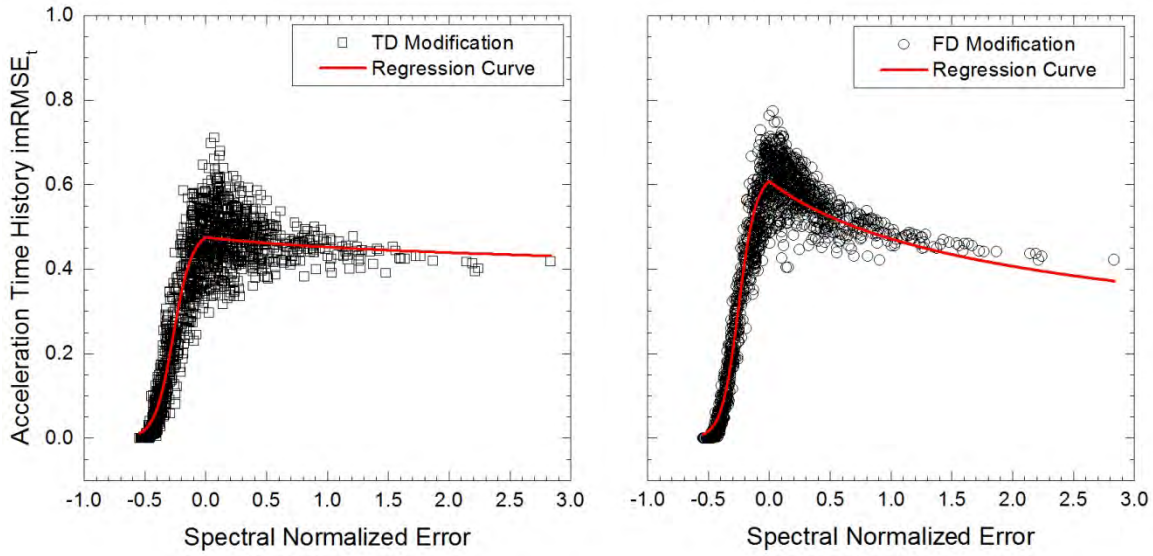

Figure 5.20. Regression curves developed for the relationship between goodness-of-fit for the acceleration time histories of the ground motions in scenario I and spectral mismatch.

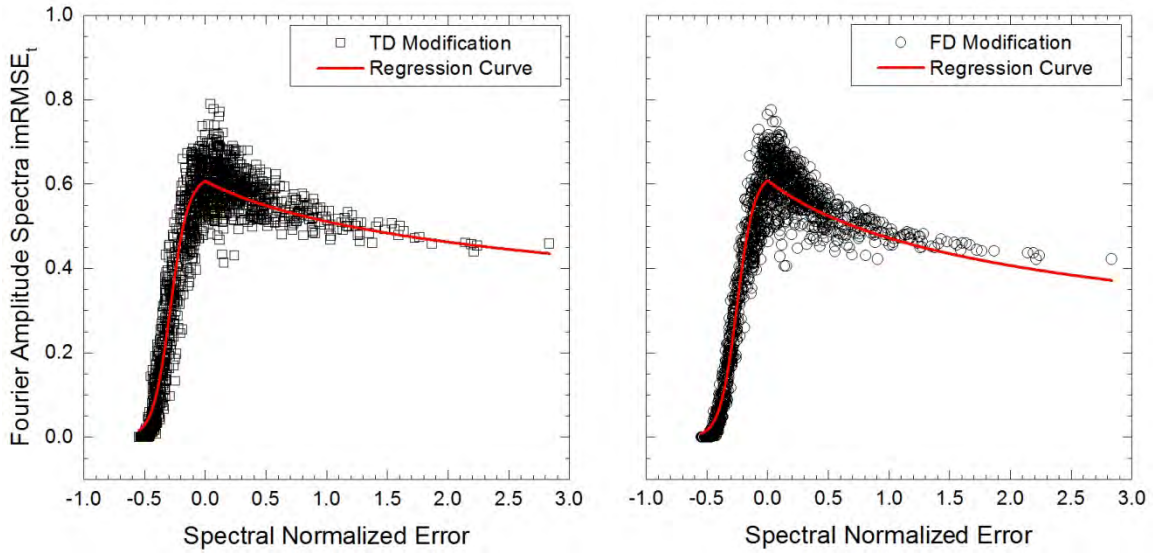

Figure 5.21. Regression curves developed for the relationship between goodness-of-fit for the Fourier amplitude spectra of the ground motions in scenario I and spectral mismatch.

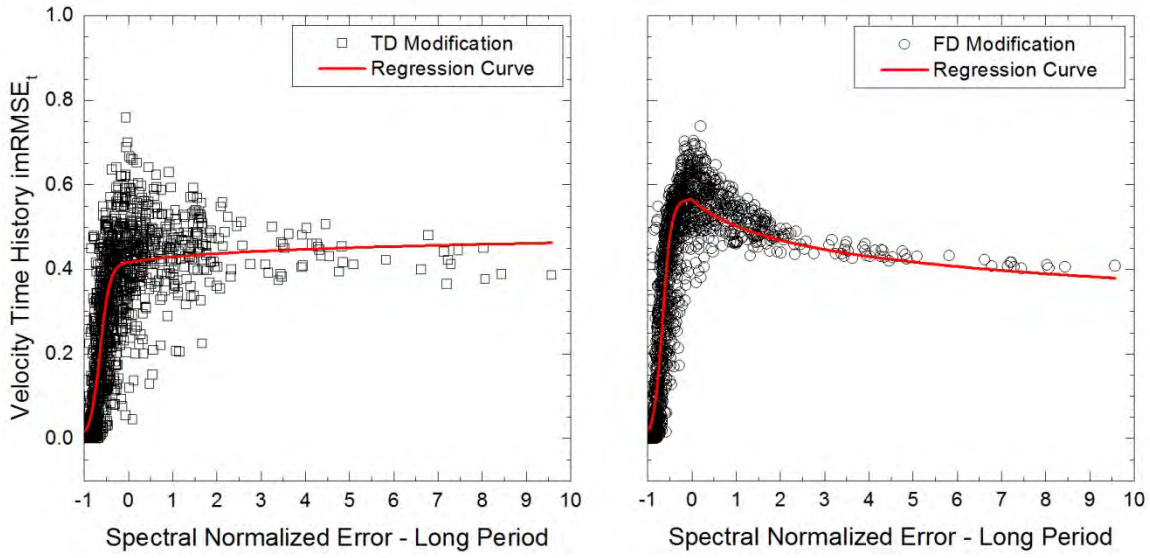

Figure 5.22. Regression curves developed for the relationship between goodness-of-fit for the velocity time histories of the ground motions in scenario I and spectral mismatch in the long period range.

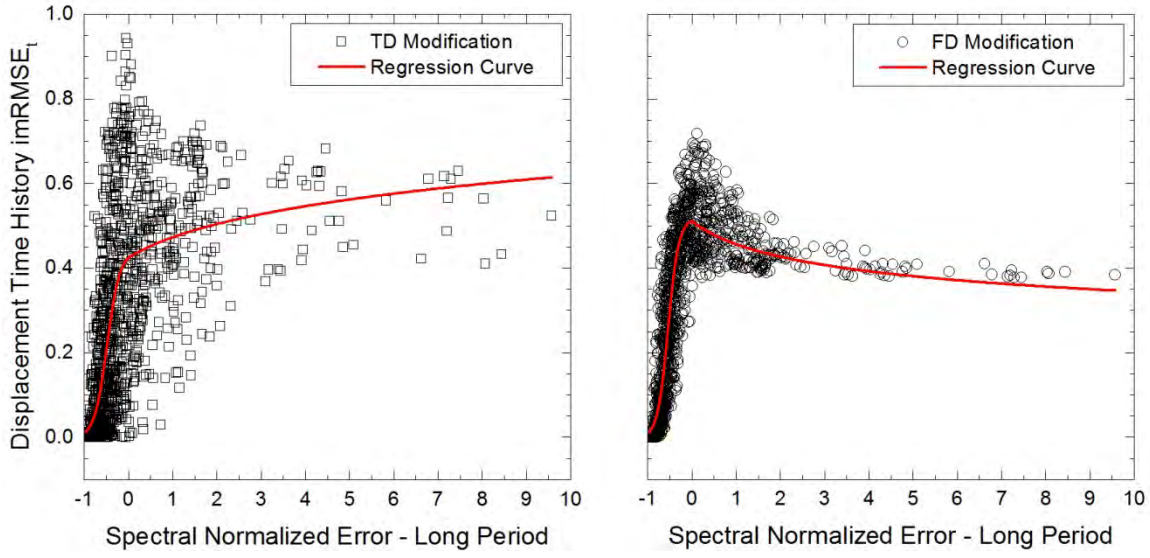

Figure 5.23. Regression curves developed for the relationship between goodness-of-fit for the displacement time histories of the ground motions in scenario I and spectral mismatch in the long period range.

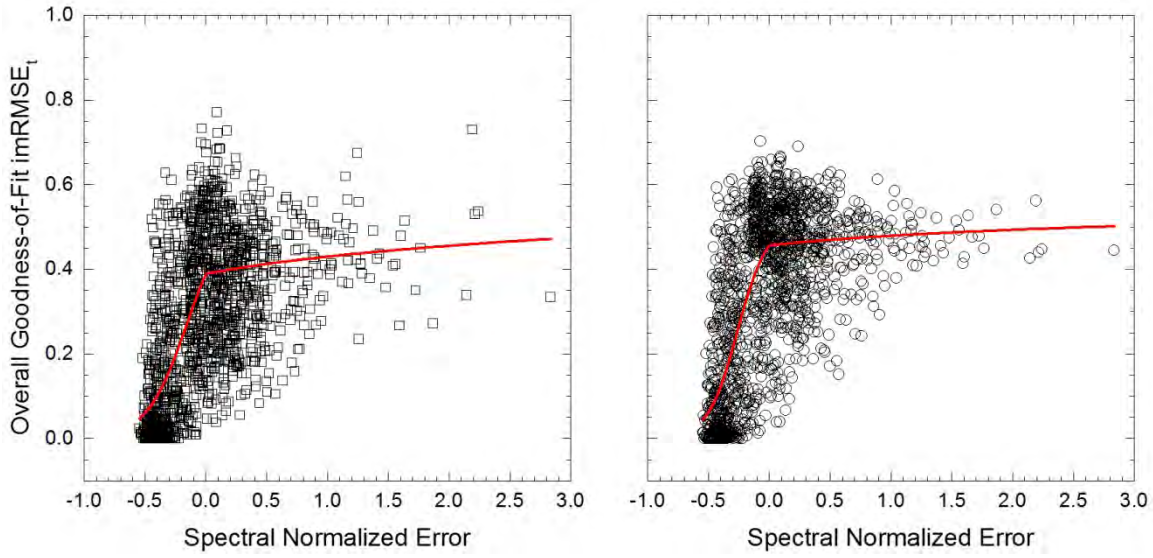

Figure 5.24. Regression curves developed for the relationship between overall goodness-of-fit for the ground motions in scenario I and spectral mismatch.

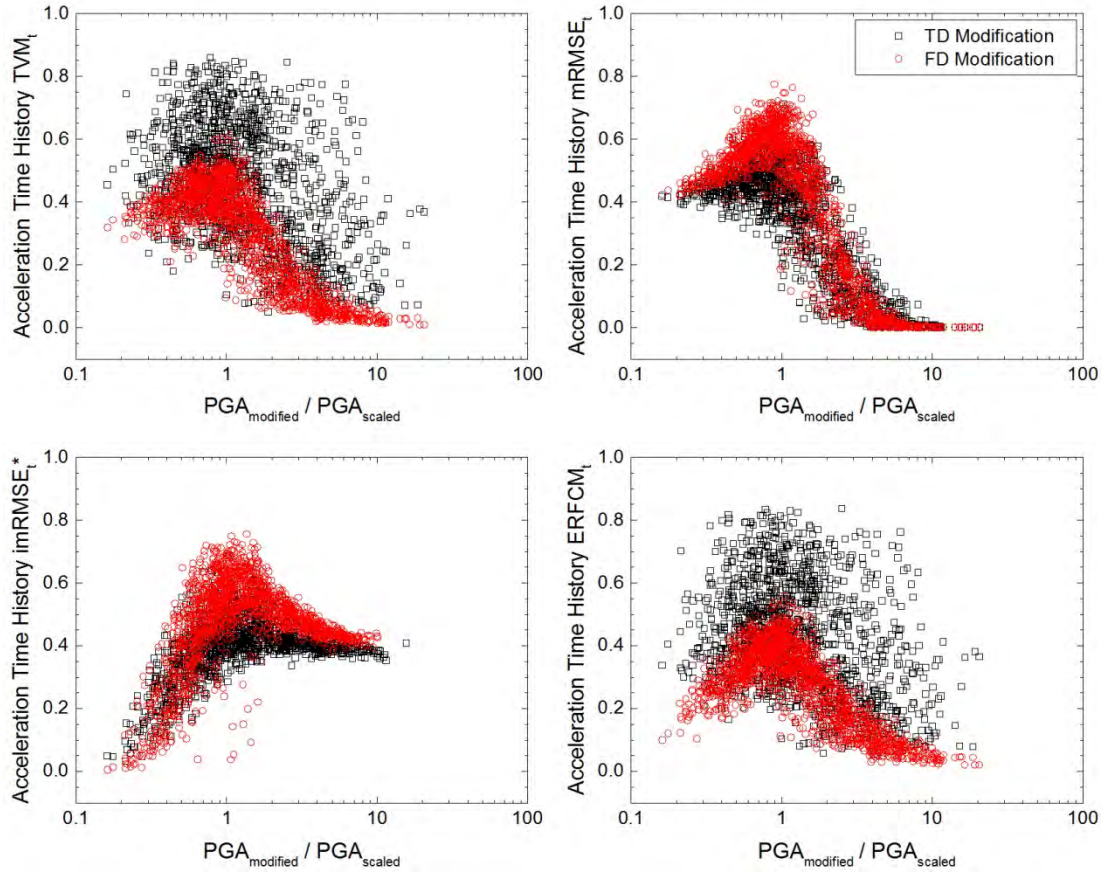

Figure 5.25. Values for goodness-of-fit for the acceleration time histories calculated using different metrics plotted versus the modified-to-scaled peak ground acceleration (*PGA*) ratios.

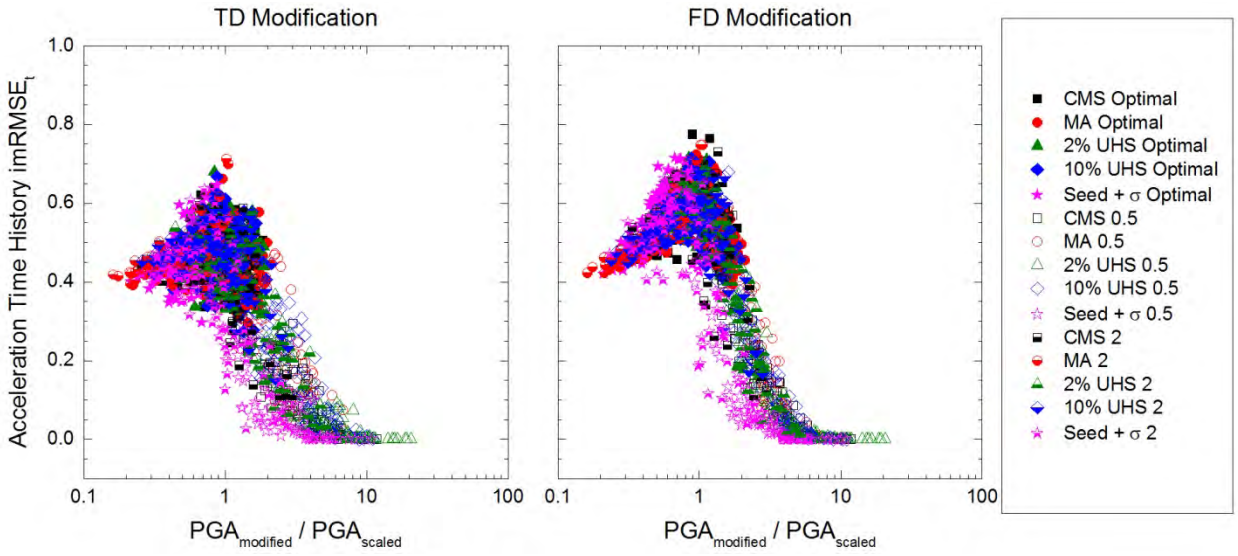

Figure 5.26. Values for goodness-of-fit between the acceleration time histories of the scaled and modified motions in scenario I plotted versus the modified-to-scaled peak ground acceleration (*PGA*) ratios for all target spectra and scaling factors. In the legend, "Optimal," "0.5," and "2" refer to the scaling factors applied to the motions.

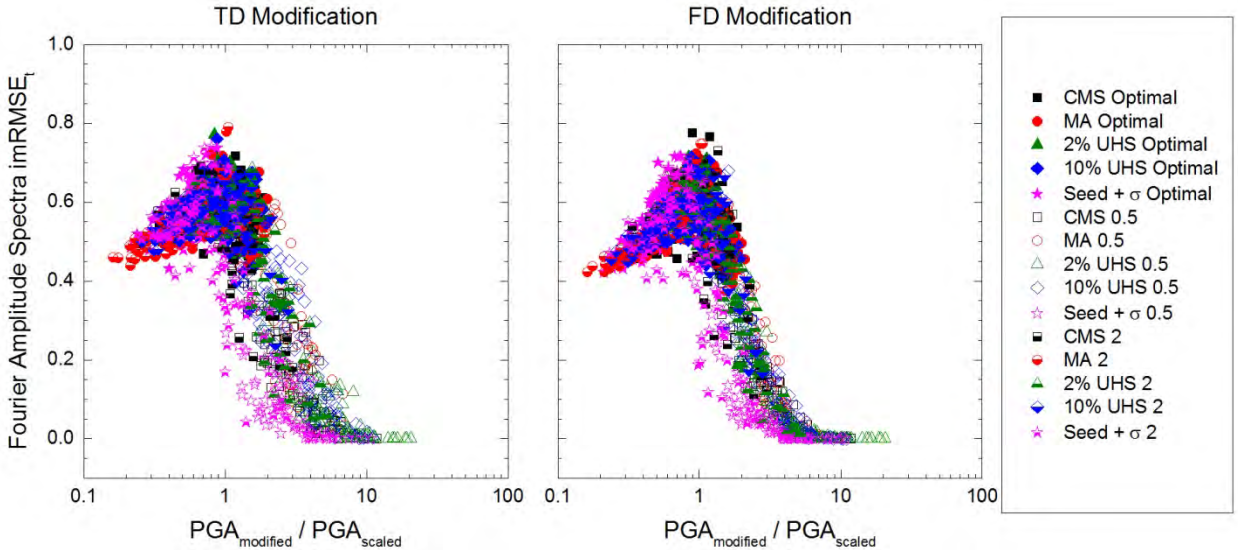

Figure 5.27. Values for goodness-of-fit between the Fourier amplitude spectra of the scaled and modified motions in scenario I plotted versus the modified-to-scaled peak ground acceleration (*PGA*) ratios for all target spectra and scaling factors. In the legend, "Optimal," "0.5," and "2" refer to the scaling factors applied to the motions.

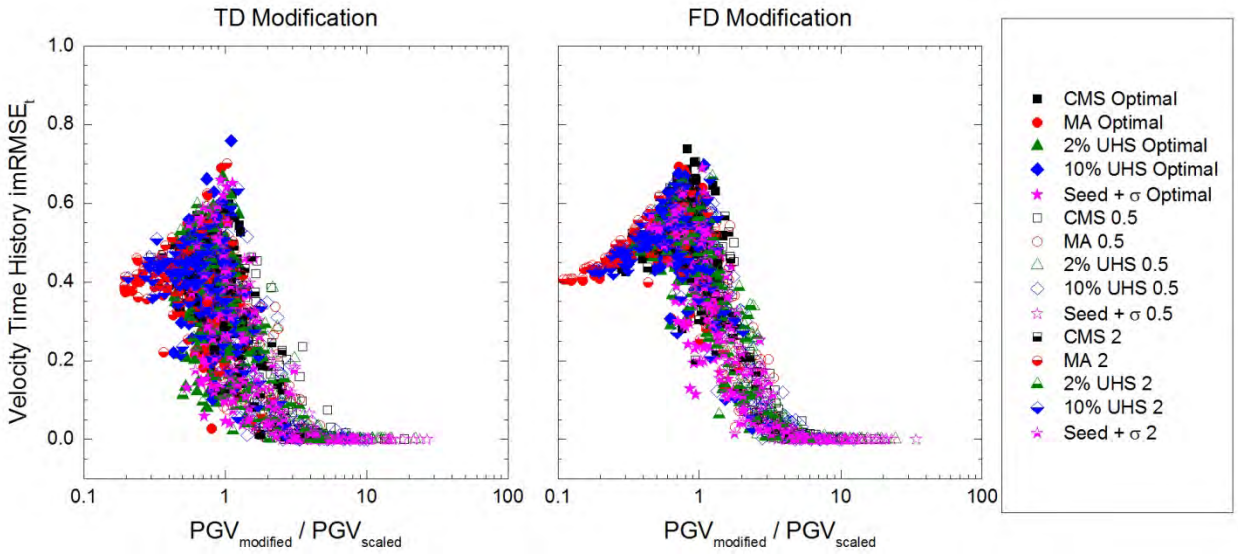

Figure 5.28. Values for goodness-of-fit between the velocity time histories of the scaled and modified ground motions in scenario I plotted versus the modified-to-scaled peak ground velocity (*PGV*) ratios for all target spectra and scaling factors. In the legend, "Optimal," "0.5," and "2" refer to the scaling factors applied to the motions.

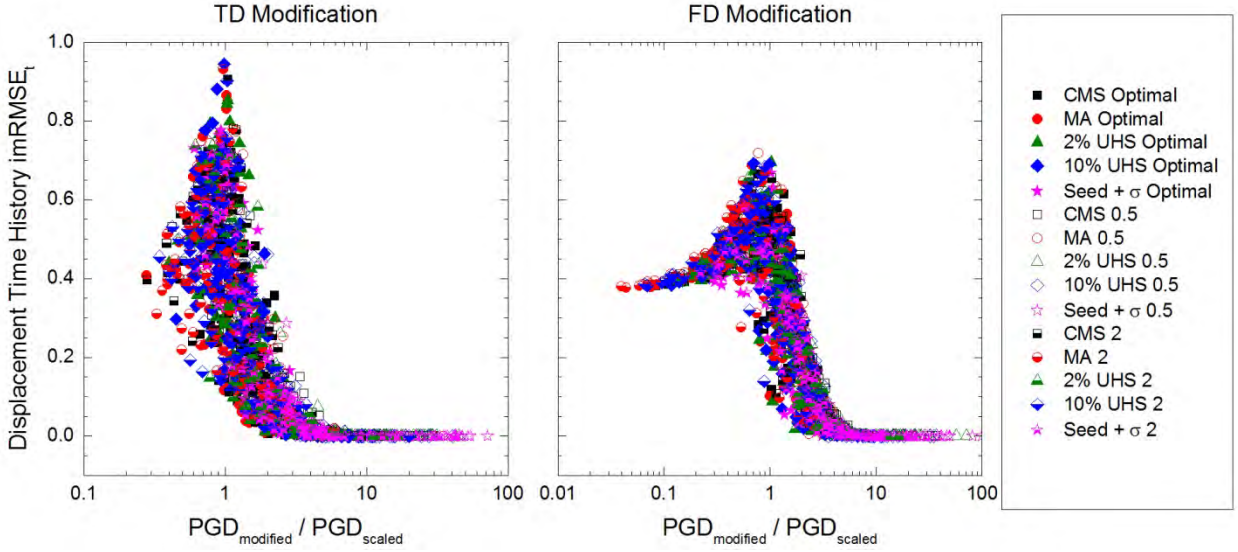

Figure 5.29. Values for goodness-of-fit between the displacement time histories of the scaled and modified motions in scenario I plotted versus the modified-to-scaled peak ground displacement (*PGD*) ratios for all target spectra and scaling factors. In the legend, "Optimal," "0.5," and "2" refer to the scaling factors applied to the motions.

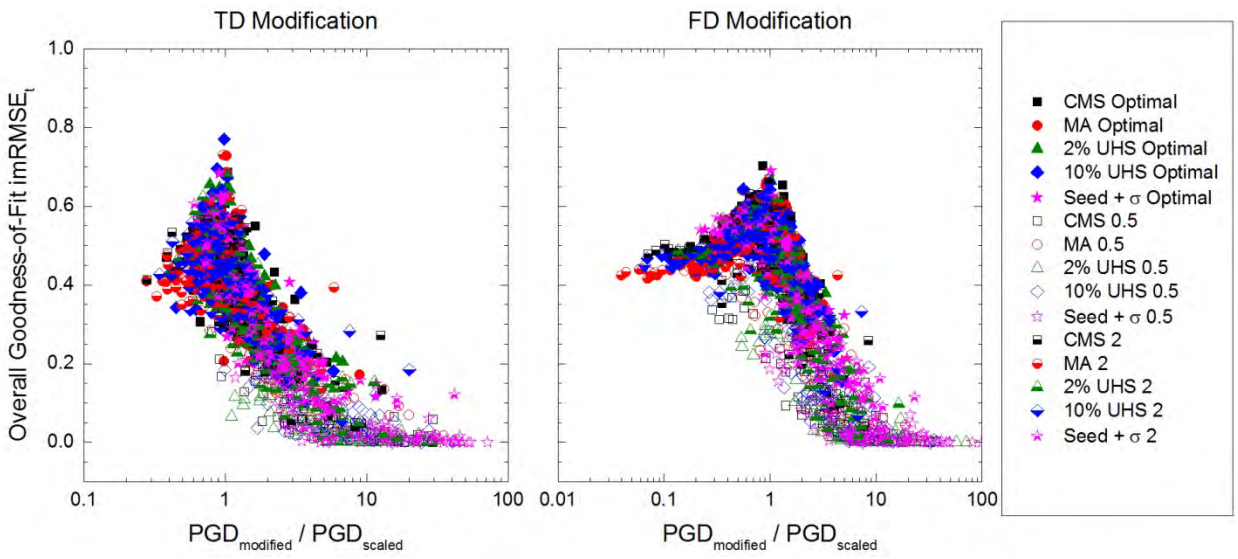

Figure 5.30. Overall goodness-of-fit between the scaled and modified motions in scenario I plotted versus the modified-to-scaled peak ground displacement (*PGD*) ratios for all target spectra and scaling factors. In the legend, "Optimal," "0.5," and "2" refer to the scaling factors applied to the motions.

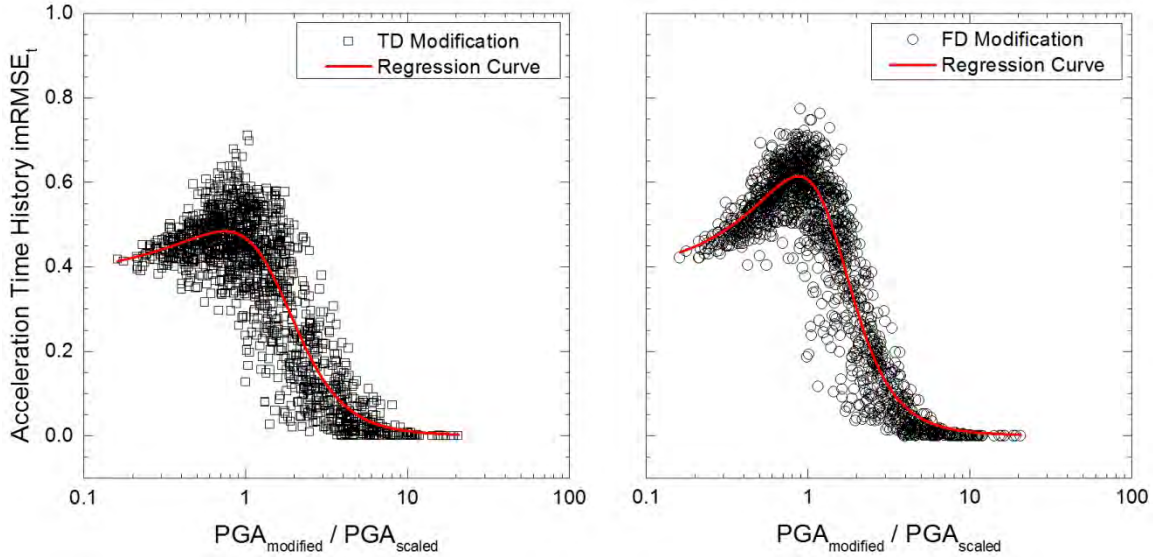

Figure 5.31. Regression curves developed for the relationship between goodness-of-fit for the acceleration time histories of the ground motions in scenario I and the modified-to-scaled peak ground acceleration (*PGA*) ratios.

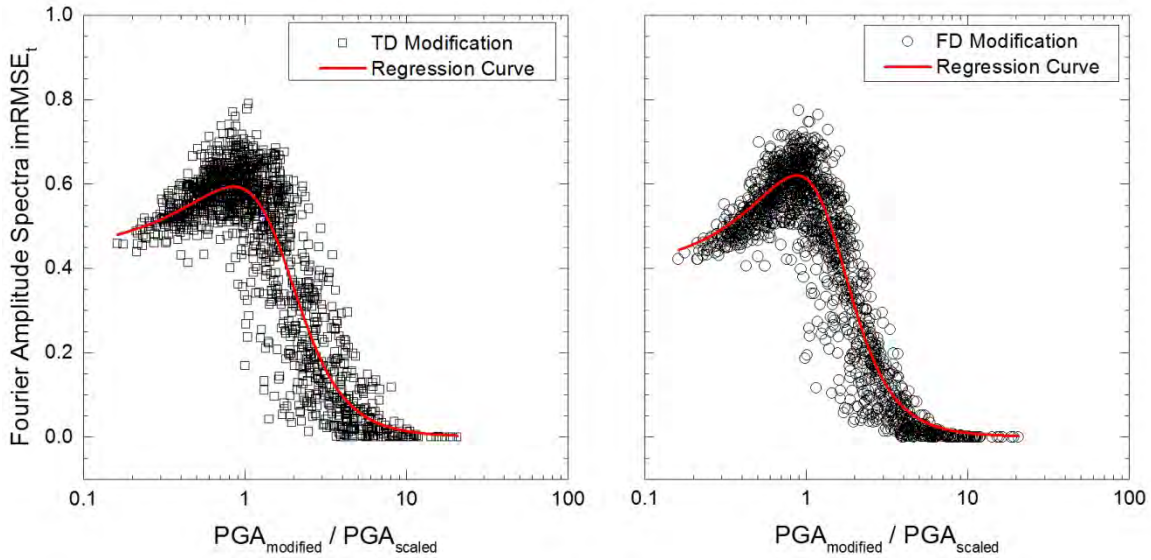

Figure 5.32. Regression curves developed for the relationship between goodness-of-fit for the Fourier amplitude spectra of the ground motions in scenario I and the modified-to-scaled peak ground acceleration (*PGA*) ratios.

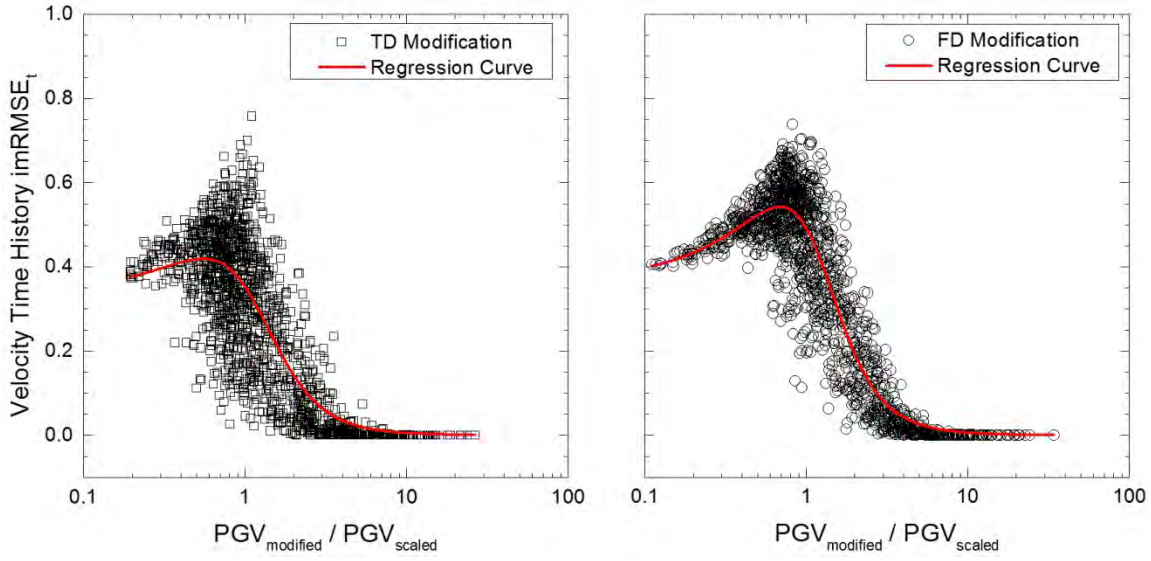

Figure 5.33. Regression curves developed for the relationship between goodness-of-fit for the velocity time histories of the ground motions in scenario I and the modified-to-scaled peak ground velocity (*PGV*) ratios.

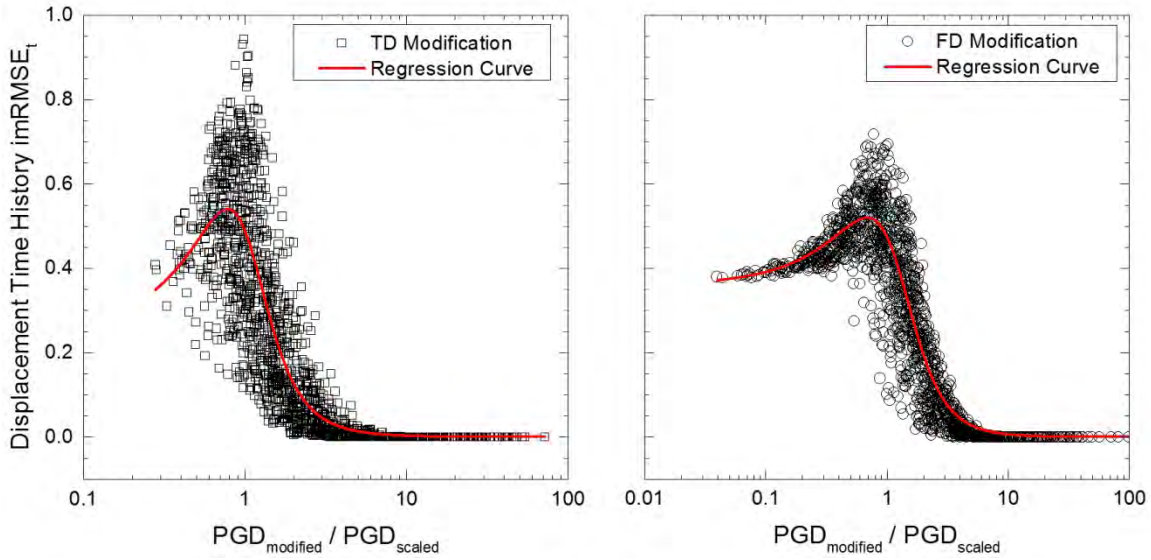

Figure 5.34. Regression curves developed for the relationship between goodness-of-fit for the displacement time histories of the ground motions in scenario I and the modified-to-scaled peak ground displacement (*PGD*) ratios.

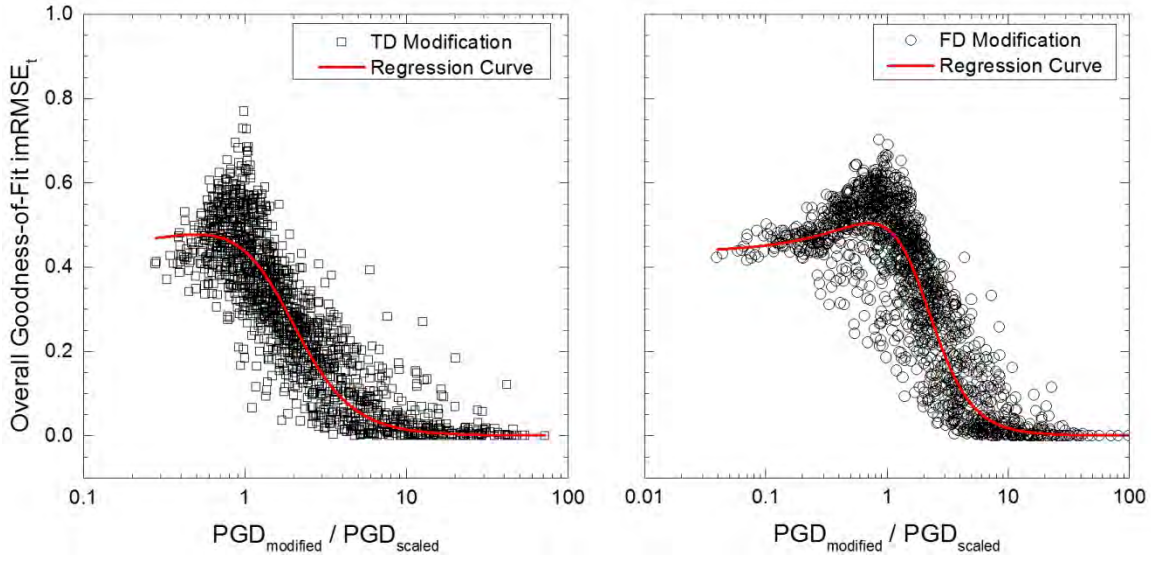

Figure 5.35. Regression curves developed for the relationship between overall goodness-of-fit for the motions in scenario I and the modified-to-scaled peak ground displacement (*PGD*) ratios.

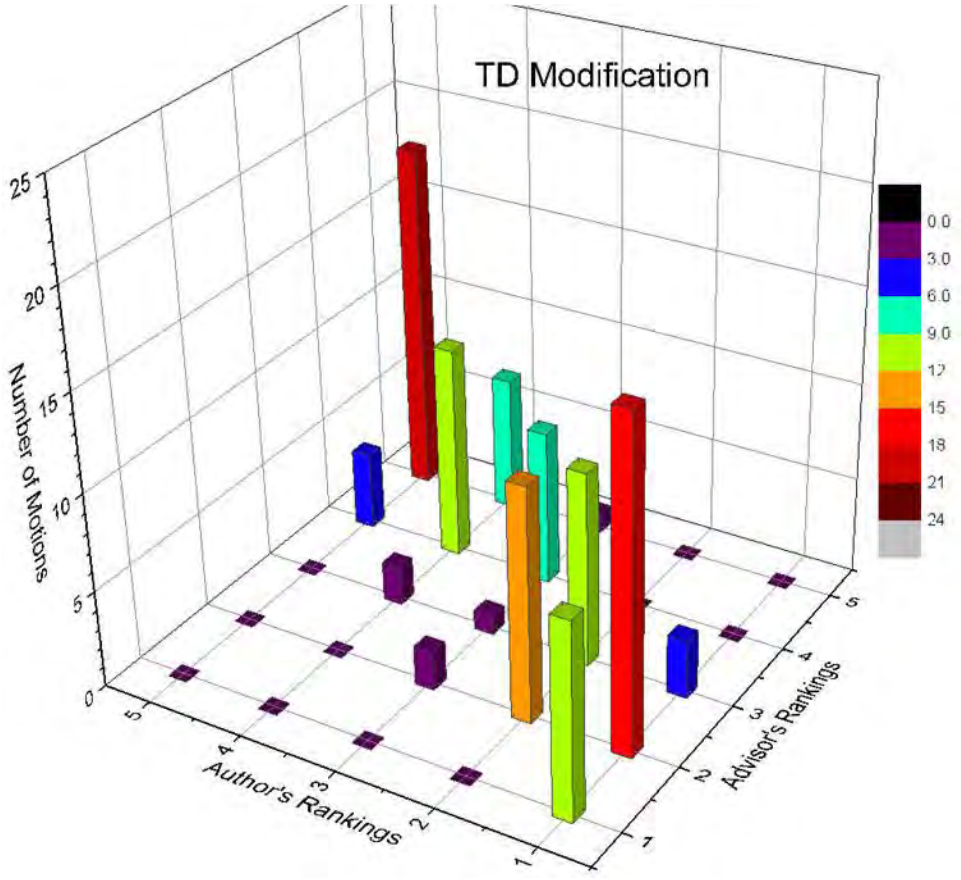

Figure 5.36. Comparison of rankings assigned to the displacement time histories of the TD-modified motions by the author and advisor based on the visual inspection of the optimally scaled motions matched to the CMS for scenario I.

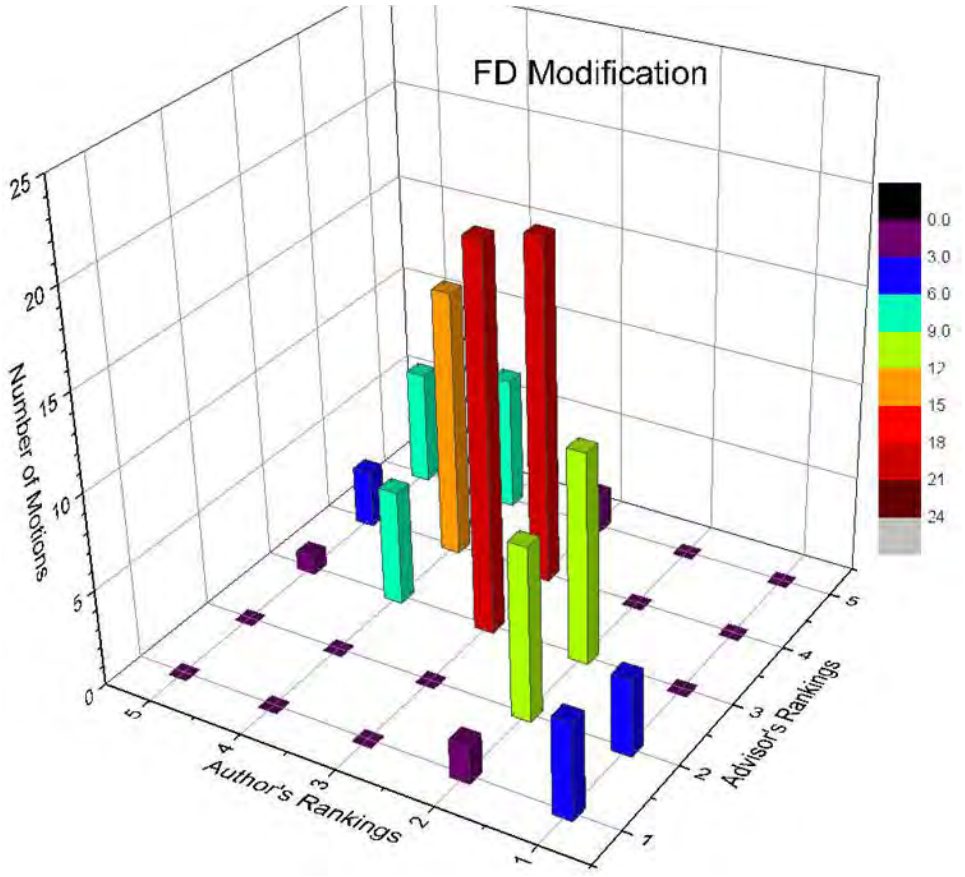

Figure 5.37. Comparison of rankings assigned to the displacement time histories of the FD-modified motions by the author and advisor based on the visual inspection of the optimally scaled motions matched to the CMS for scenario I.

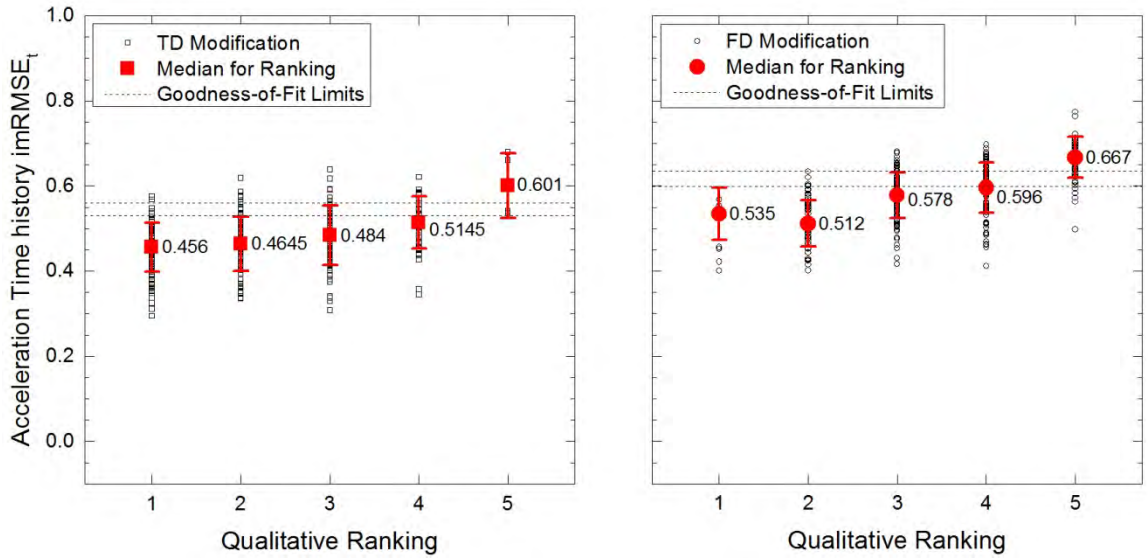

Figure 5.38. Values for goodness-of-fit between the acceleration time histories of the scaled and modified motions from scenario I with medians and plus and minus standard deviations for each ranking. Possible limits for goodness-of-fit to identify likely acceptable, possibly acceptable, and likely unacceptable acceleration time histories are shown with the dashed lines.

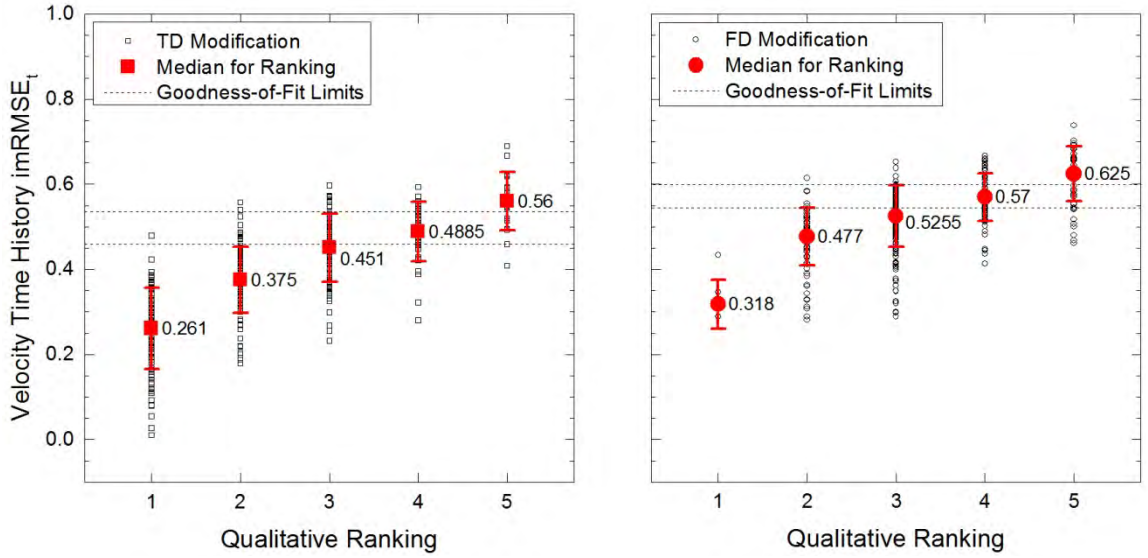

Figure 5.39. Values for goodness-of-fit between the velocity time histories of the scaled and modified motions from scenario I with medians and plus and minus standard deviations for each ranking. Possible limits for goodness-of-fit to identify likely acceptable, possibly acceptable, and likely unacceptable velocity time histories are shown with the dashed lines.

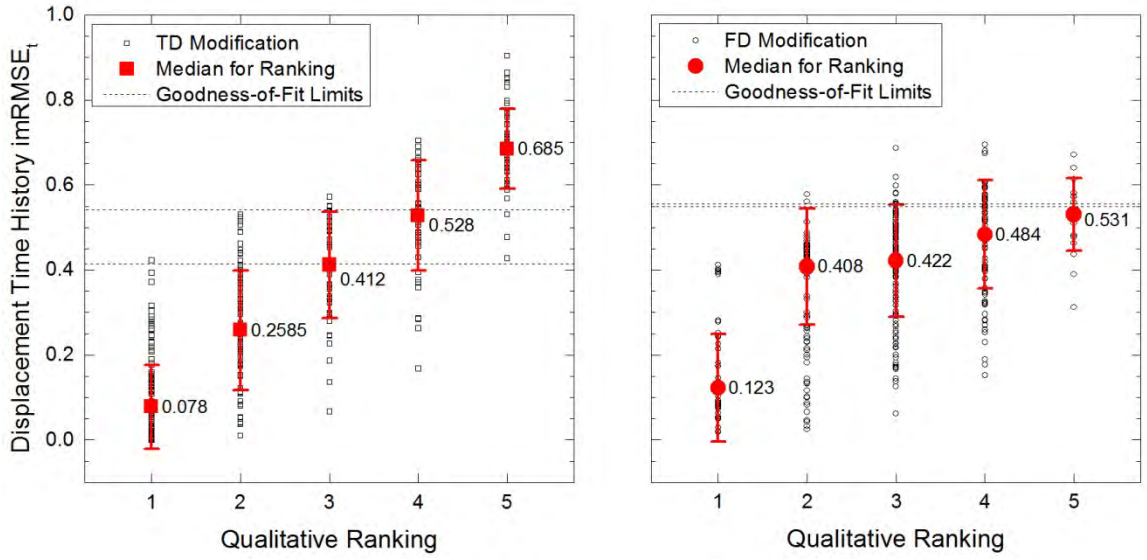

Figure 5.40. Values for goodness-of-fit between the displacement time histories of the scaled and modified motions from scenario I with medians and plus and minus standard deviations for each ranking. Possible limits for goodness-of-fit to identify likely acceptable, possibly acceptable, and likely unacceptable displacement time histories are shown with the dashed lines.

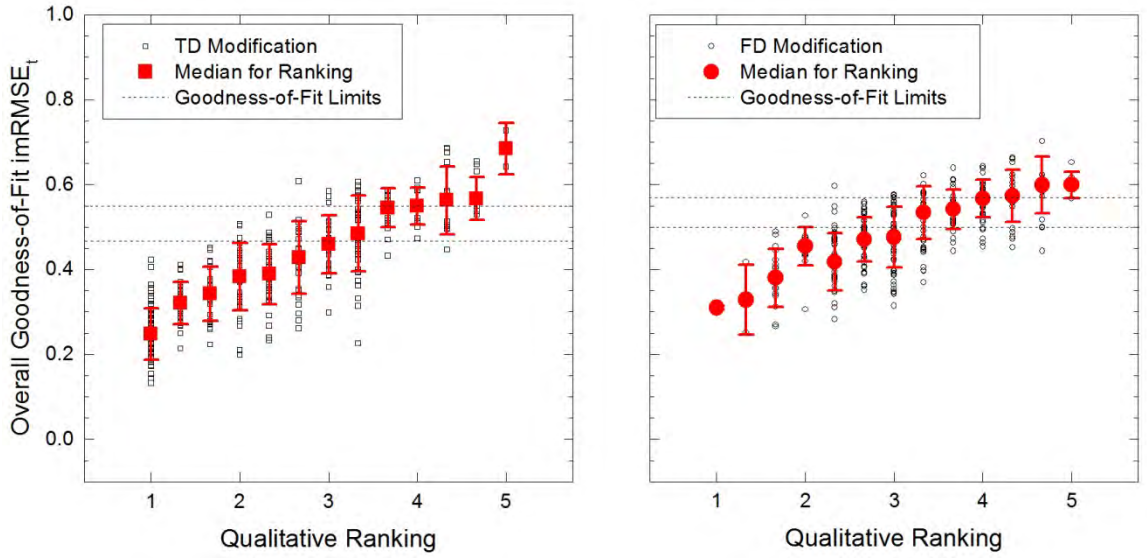

Figure 5.41. Overall goodness-of-fit values between the scaled and modified motions from scenario I with medians and plus and minus standard deviations for each ranking. Possible limits to identify likely acceptable, possibly acceptable, and likely unacceptable time histories for the overall ground motion are shown with the dashed lines.

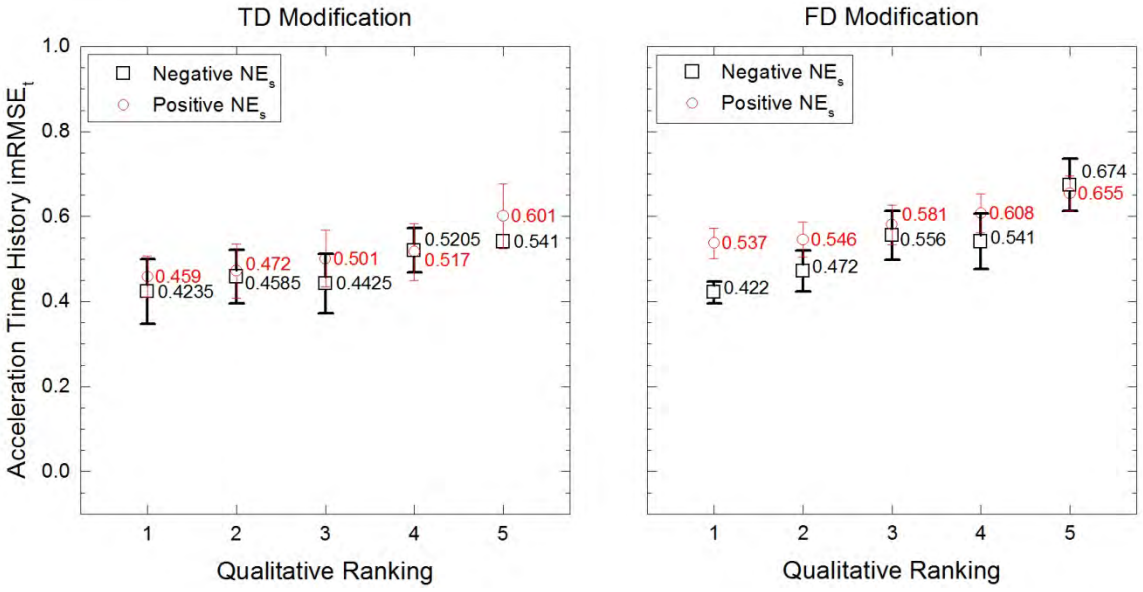

Figure 5.42. Median goodness-of-fit values, with plus and minus one standard deviation, between the acceleration time histories of the scaled and modified motions in scenario I with positive and negative spectral mismatch, quantified by NE_s, plotted against ranking.

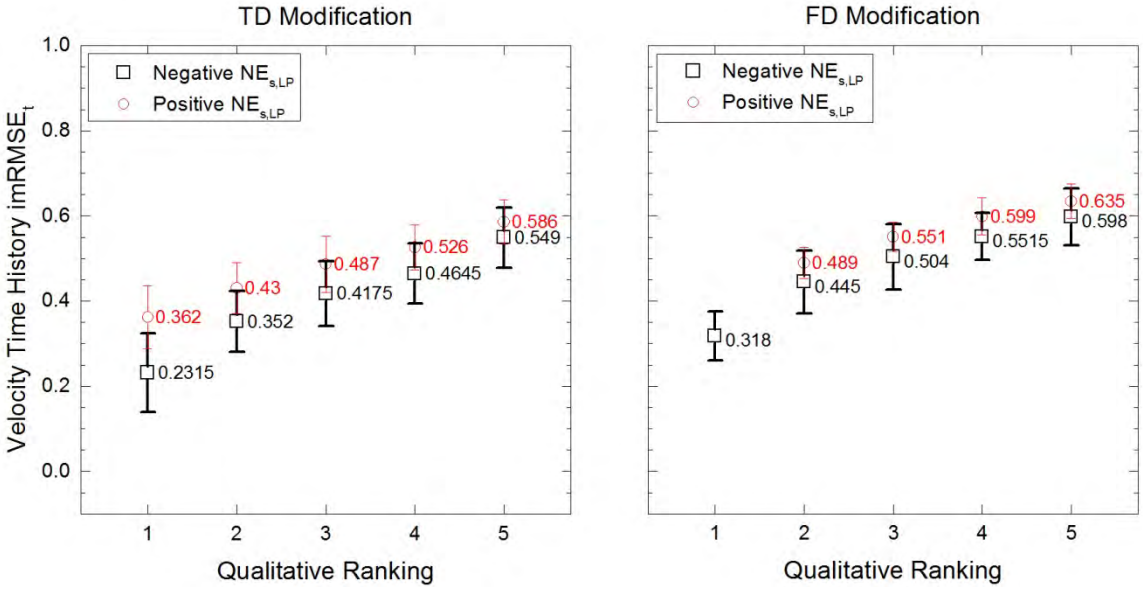

Figure 5.43. Median goodness-of-fit values, with plus and minus one standard deviation, between the velocity time histories of the scaled and modified motions in scenario I with positive and negative spectral mismatch, quantified by $NE_{s,LP}$, plotted against ranking.

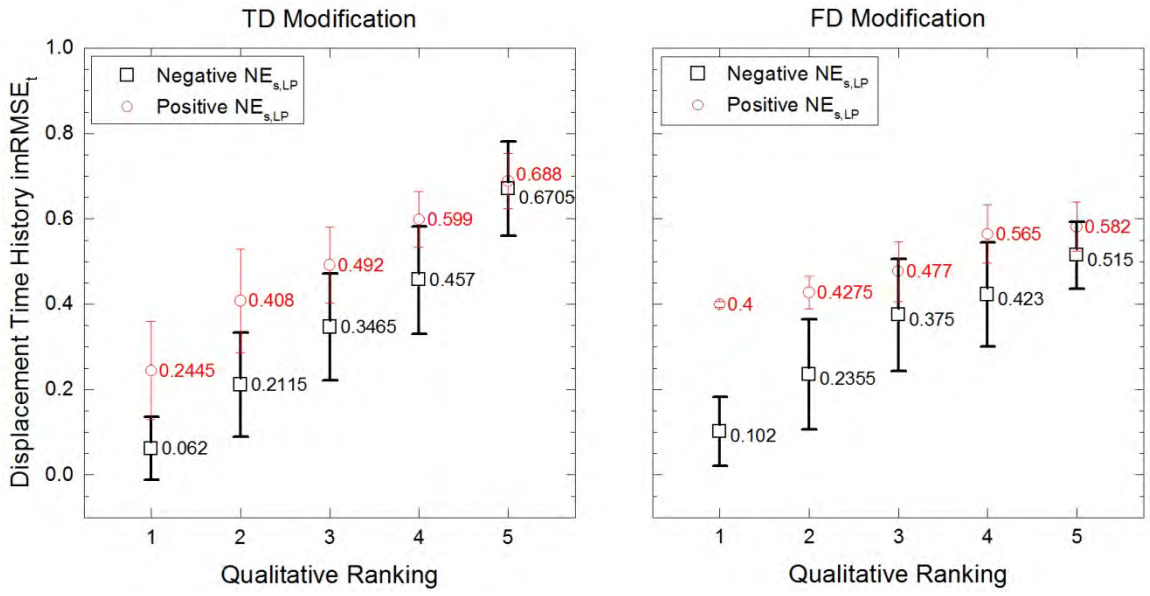

Figure 5.44. Median goodness-of-fit values, with plus and minus one standard deviation, between the displacement time histories of the scaled and modified motions in scenario I with positive and negative spectral mismatch, quantified by $NE_{s,LP}$, plotted against ranking.

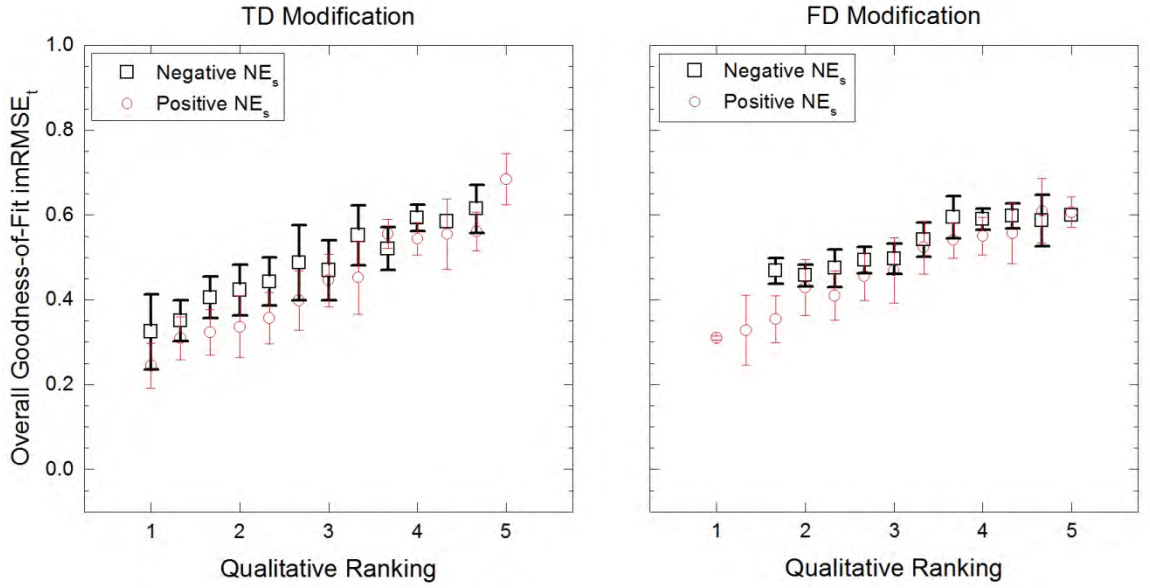

Figure 5.45. Median overall goodness-of-fit, with plus and minus one standard deviation, between the scaled and modified motions in scenario I with positive and negative spectral mismatch, quantified by NE_s, plotted against ranking.

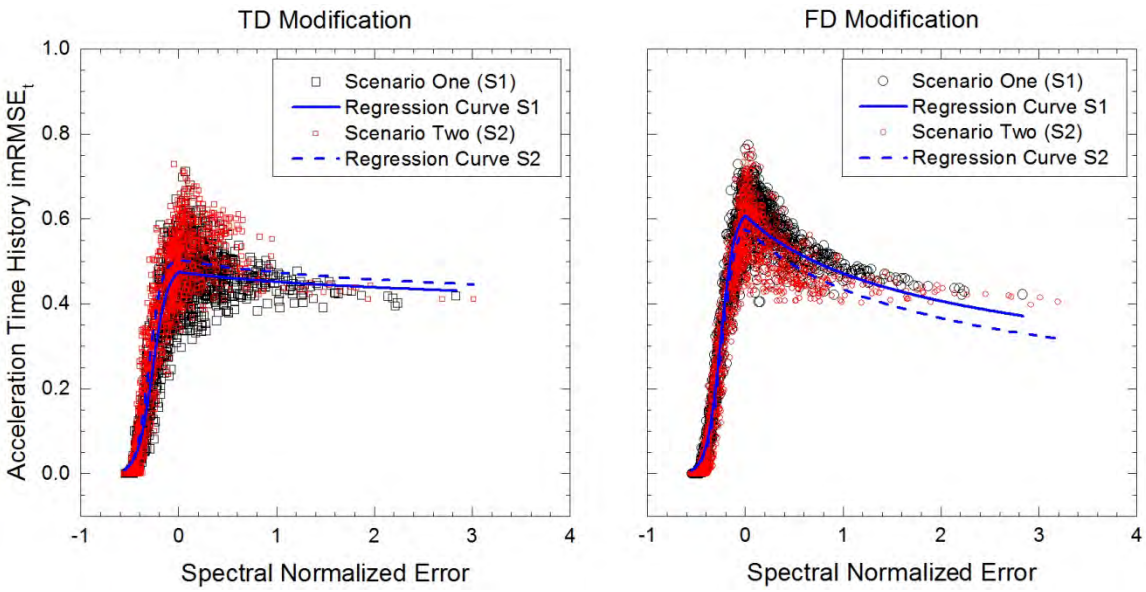

Figure 5.46. Comparison of the regression curves developed for the relationship between goodness-of-fit for the acceleration time histories and spectral mismatch for the ground motions in scenarios I and II.

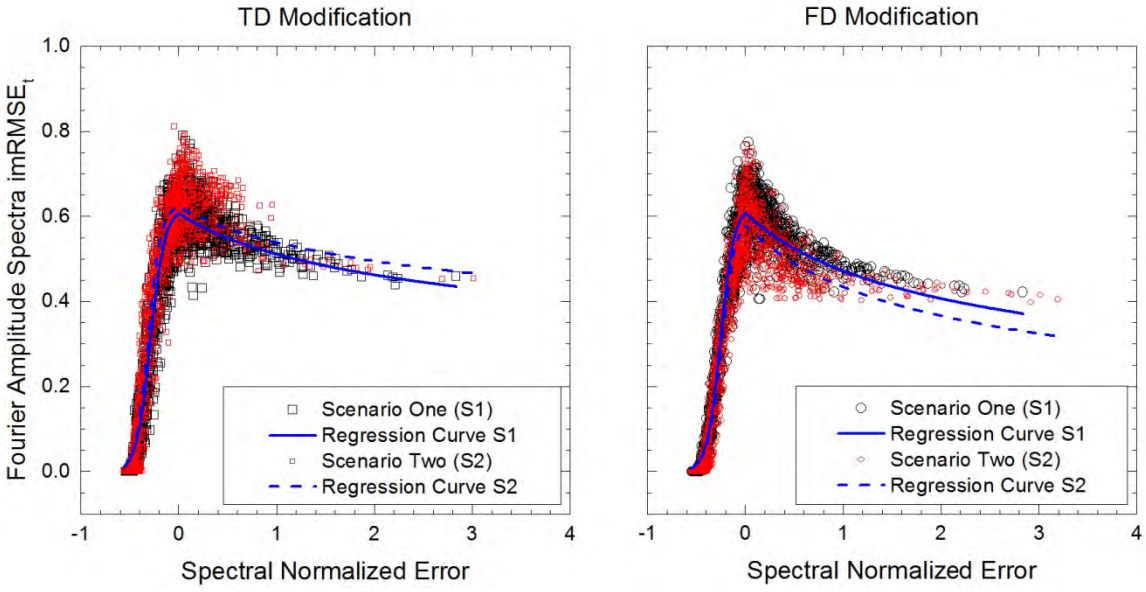

Figure 5.47. Comparison of the regression curves developed for the relationship between goodness-of-fit for the Fourier amplitude spectra and spectral mismatch for the ground motions in scenarios I and II.

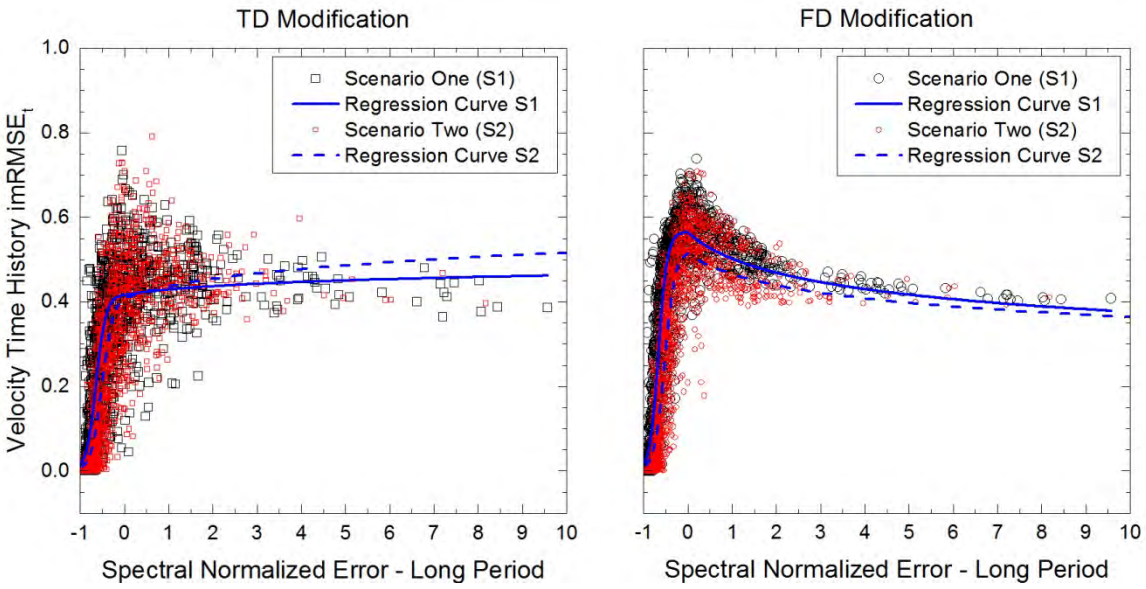

Figure 5.48. Comparison of the regression curves developed for the relationship between goodness-of-fit for the velocity time histories and spectral mismatch in the long period range for the ground motions in scenarios I and II.

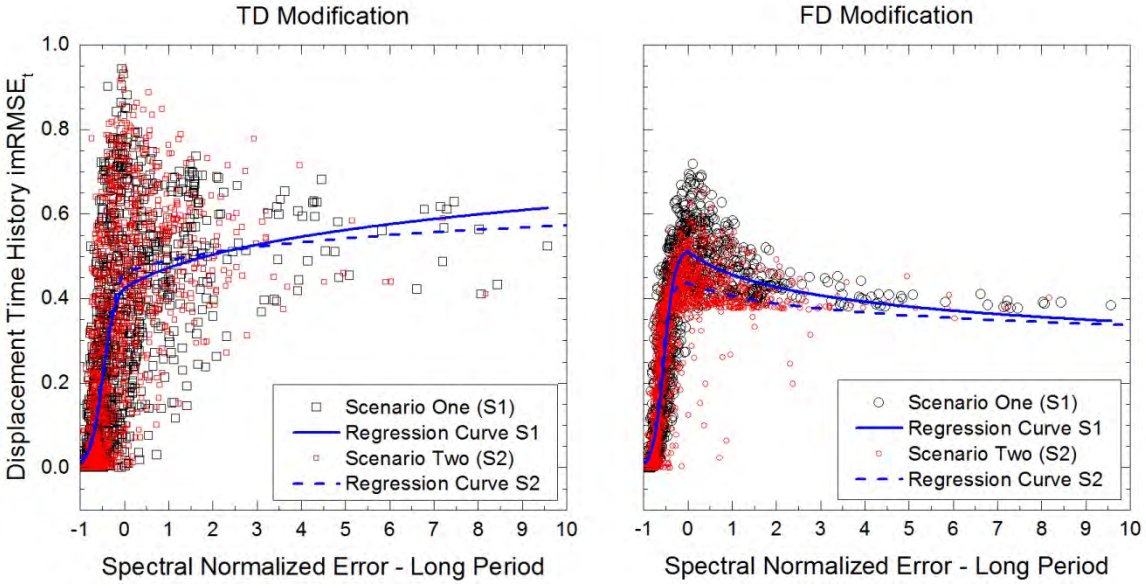

Figure 5.49. Comparison of the regression curves developed for the relationship between goodness-of-fit for the displacement time histories and spectral mismatch in the long period range for the ground motions in scenarios I and II.

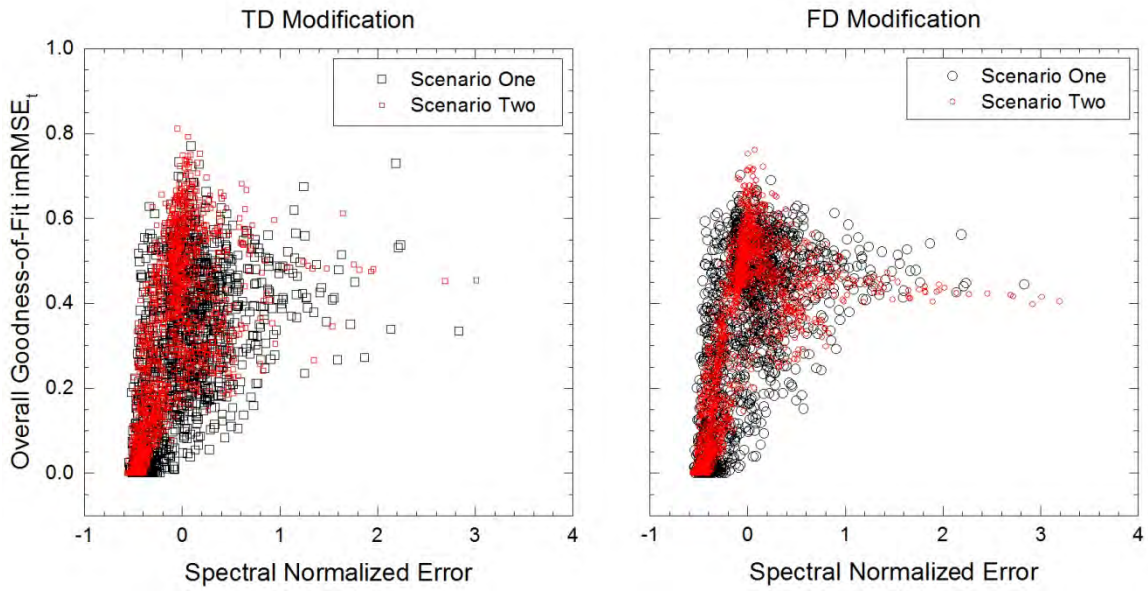

Figure 5.50. Comparison of overall goodness-of-fit between the scaled and modified motions from scenarios I and II plotted versus spectral mismatch.

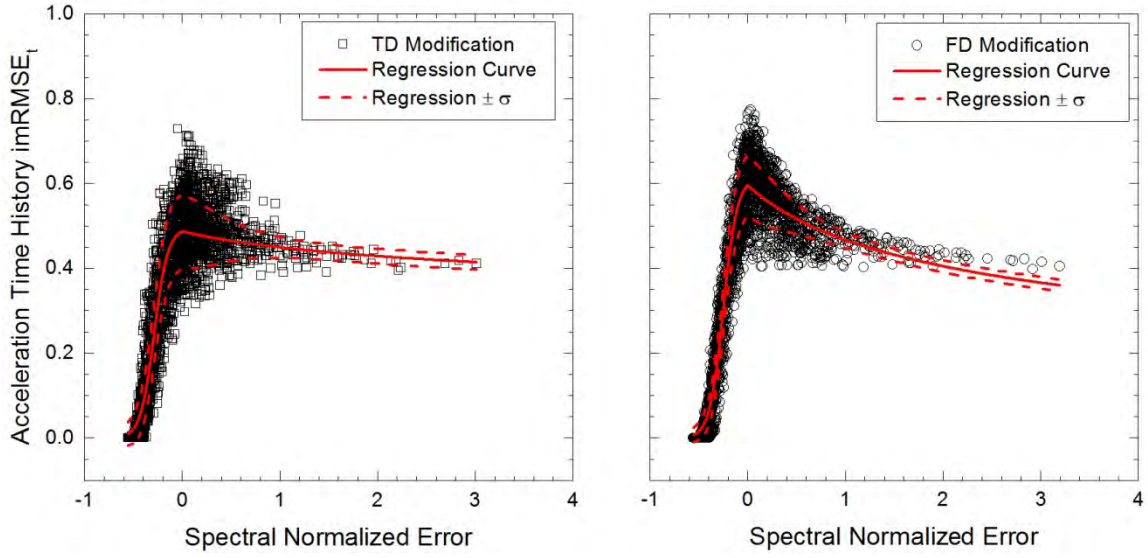

Figure 5.51. Regression curves, with plus and minus one standard deviation, developed for the relationship between goodness-of-fit for the acceleration time histories and spectral mismatch using the combined set of motions from scenarios I and II.

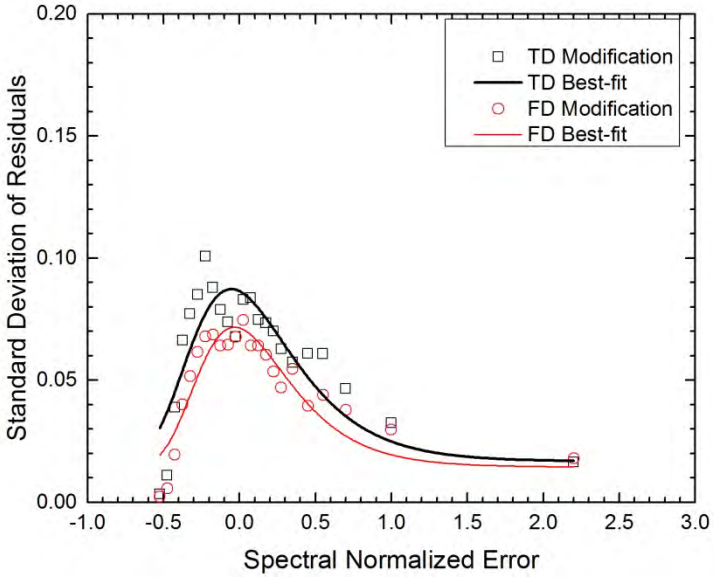

Figure 5.52. Standard deviations of the residuals and corresponding best-fit curves for the regression equations developed to describe the relationship between the goodness-of-fit values for the acceleration time histories of the combined set of motions from scenarios I and II and spectral mismatch.

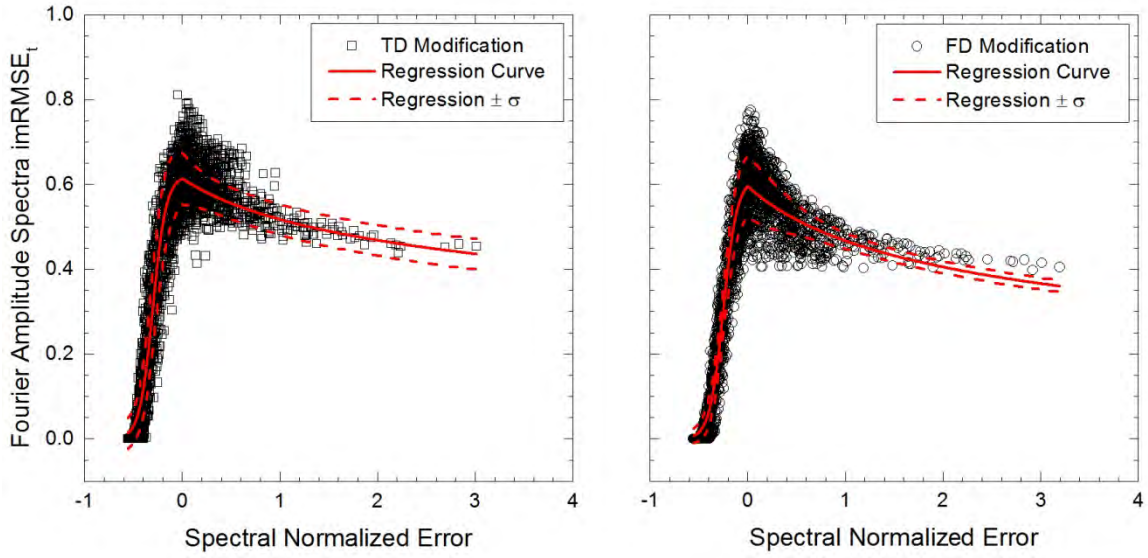

Figure 5.53. Regression curves, with plus and minus one standard deviation, developed for the relationship between goodness-of-fit for the Fourier amplitude spectra and spectral mismatch using the combined set of motions from scenarios I and II.

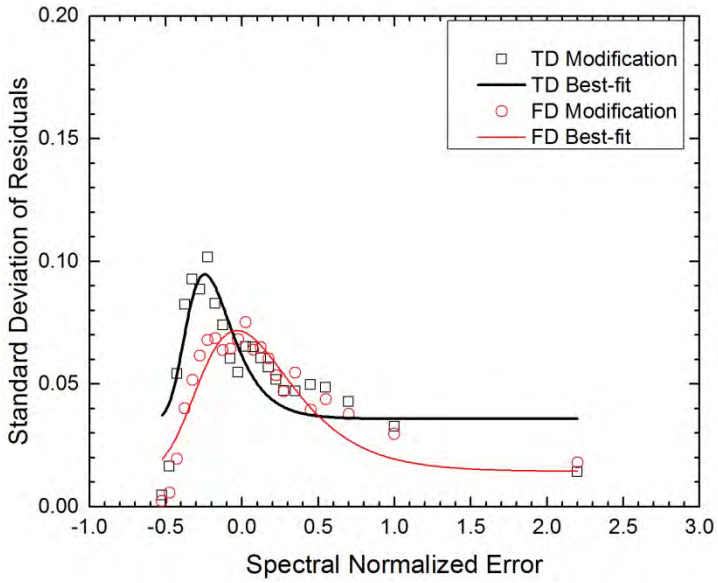

Figure 5.54. Standard deviations of the residuals and corresponding best-fit curves for the regression equations developed to describe the relationship between the goodness-of-fit values for the Fourier amplitude spectra of the combined set of motions from scenarios I and II and spectral mismatch.

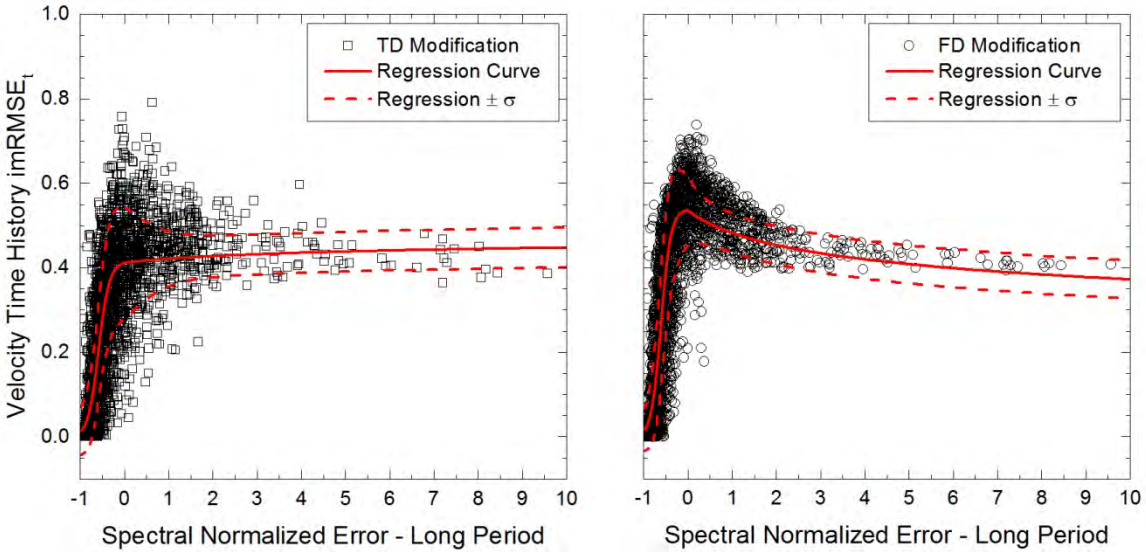

Figure 5.55. Regression curves, with plus and minus one standard deviation, developed for the relationship between goodness-of-fit for the velocity time histories and spectral mismatch in the long period range using the combined set of motions from scenarios I and II.

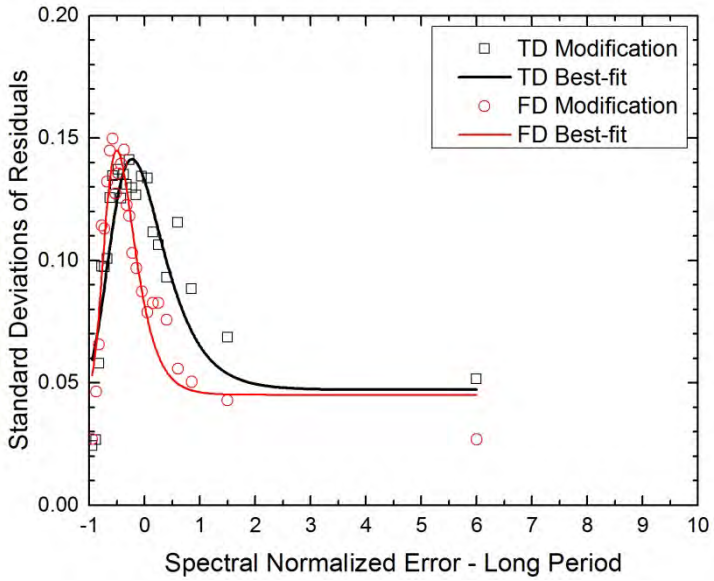

Figure 5.56. Standard deviations of the residuals and corresponding best-fit curves for the regression equations developed to describe the relationship between the goodness-of-fit values for the velocity time histories of the combined set of motions from scenarios I and II and spectral mismatch in the long period range.

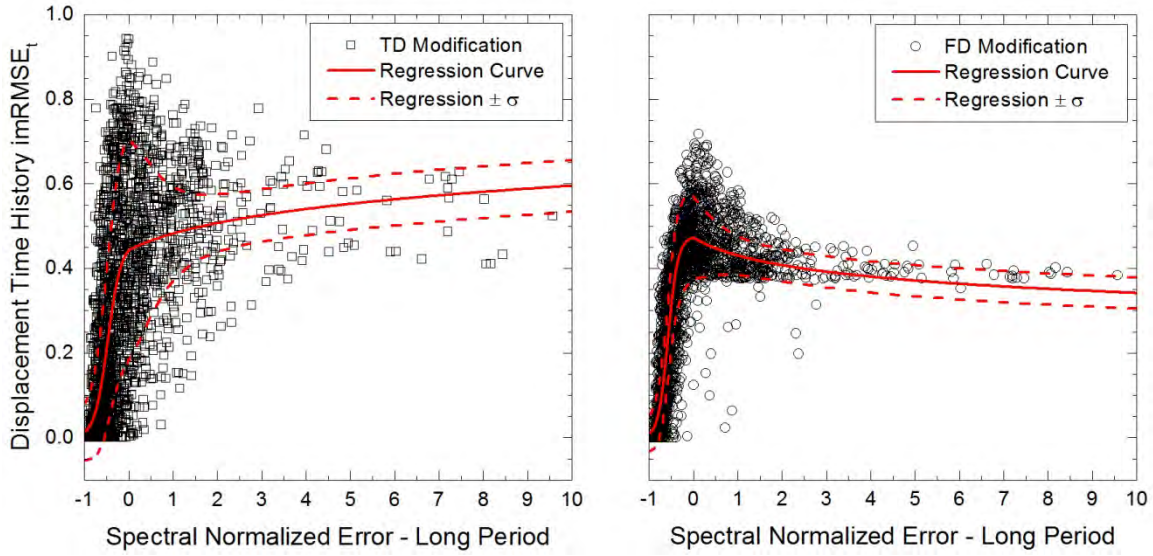

Figure 5.57. Regression curves, with plus and minus one standard deviation, developed for the relationship between goodness-of-fit for the displacement time histories and spectral mismatch in the long period range using the combined set of motions from scenarios I and II.

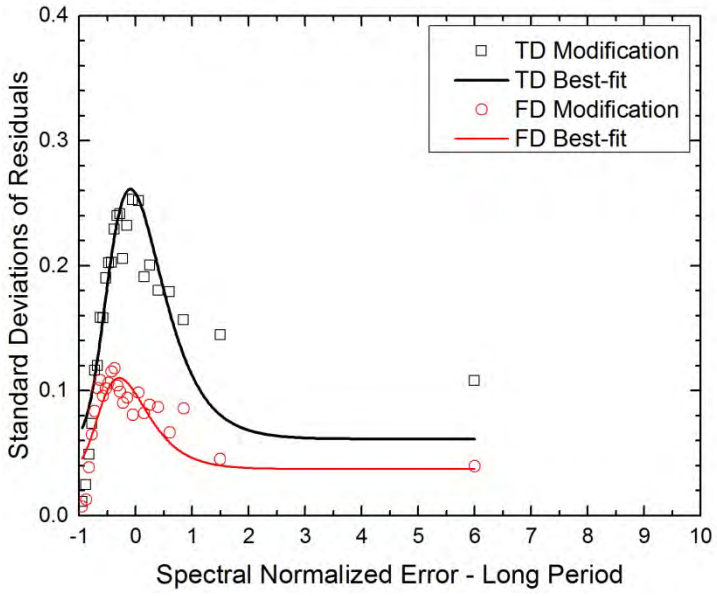

Figure 5.58. Standard deviations of the residuals and corresponding best-fit curves for the regression equations developed to describe the relationship between the goodness-of-fit values for the displacement time histories of the combined set of motions from scenarios I and II and spectral mismatch in the long period range.

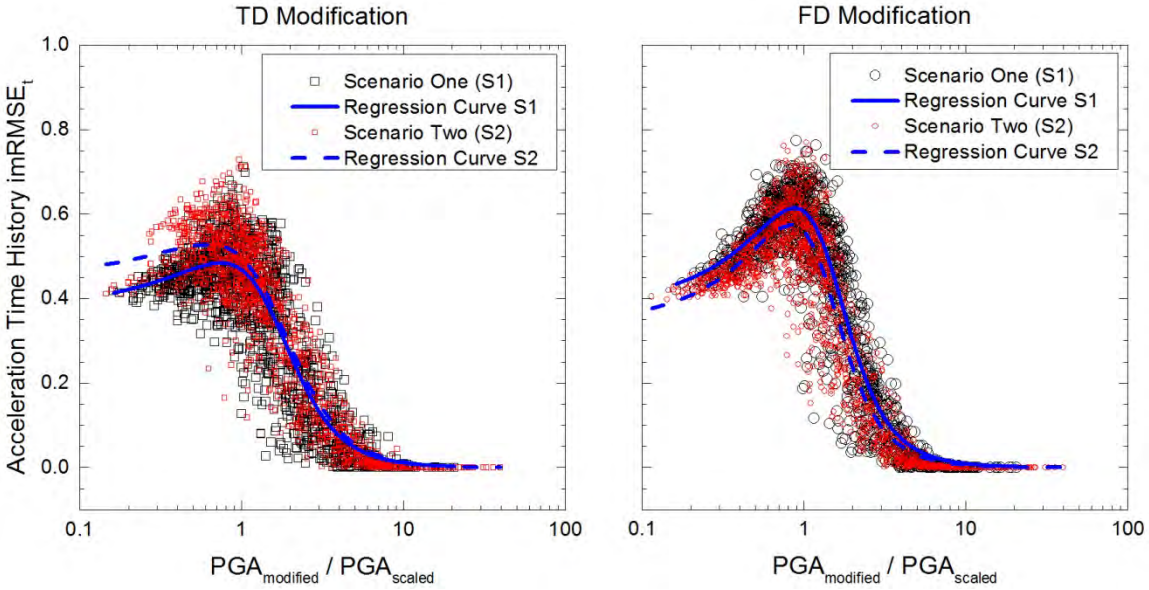

Figure 5.59. Comparison of the regression curves developed for the relationship between goodness-of-fit for the acceleration time histories and the modified-to-scaled peak ground acceleration (*PGA*) ratios for the ground motions in scenarios I and II.

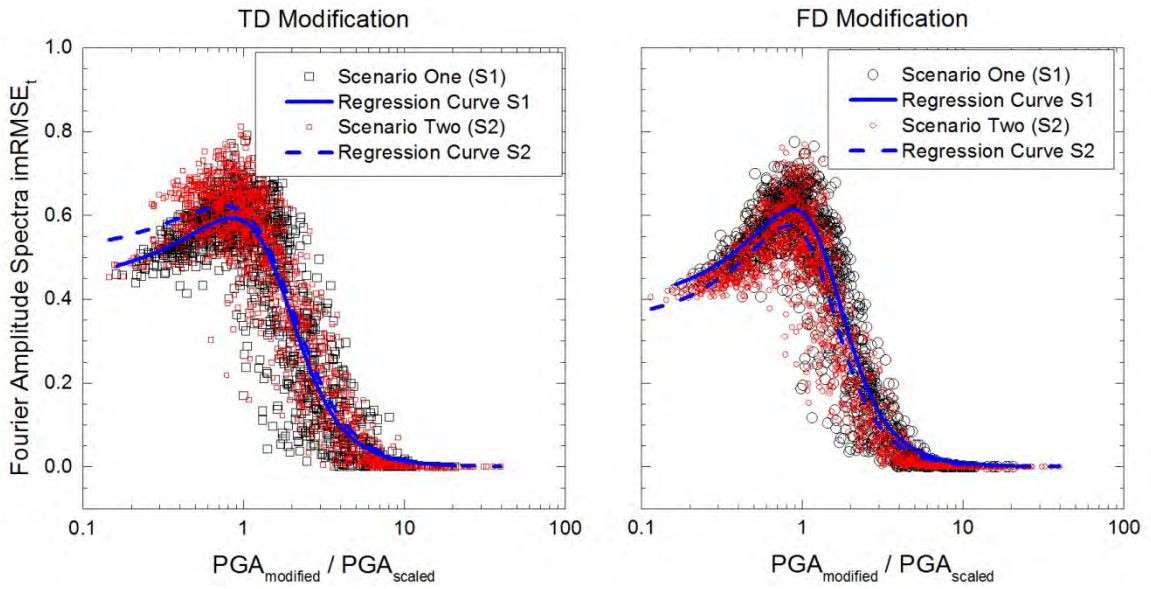

Figure 5.60. Comparison of the regression curves developed for the relationship between goodness-of-fit for the Fourier amplitude spectra and the modified-to-scaled peak ground acceleration (*PGA*) ratios for the ground motions in scenarios I and II.

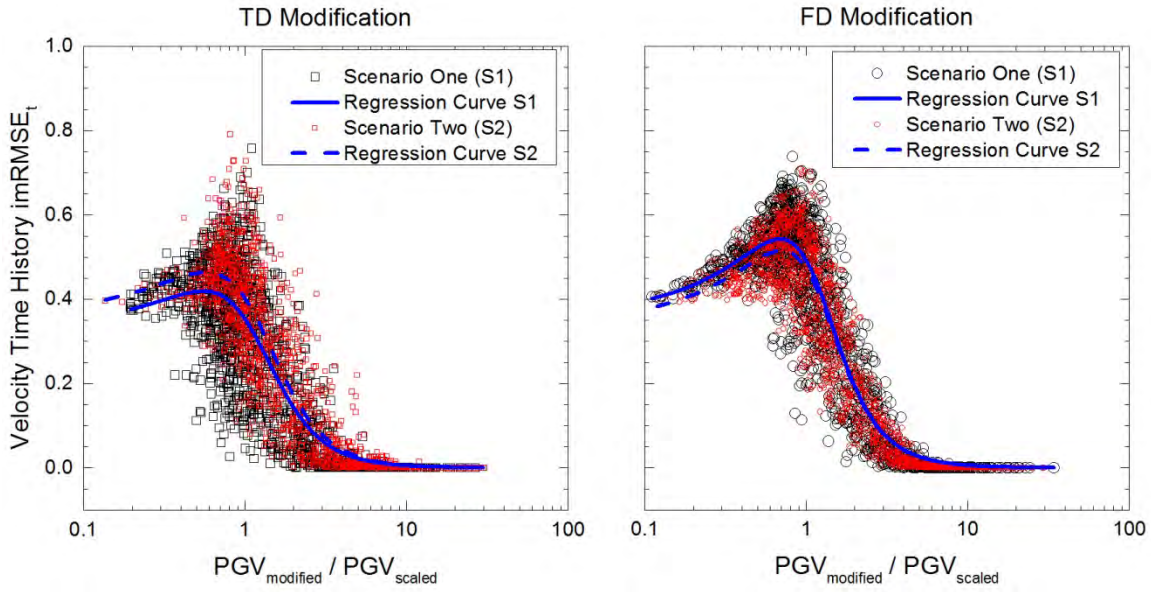

Figure 5.61. Comparison of the regression curves developed for the relationship between goodness-of-fit for the velocity time histories and the modified-to-scaled peak ground velocity (*PGV*) ratios for the ground motions in scenarios I and II.

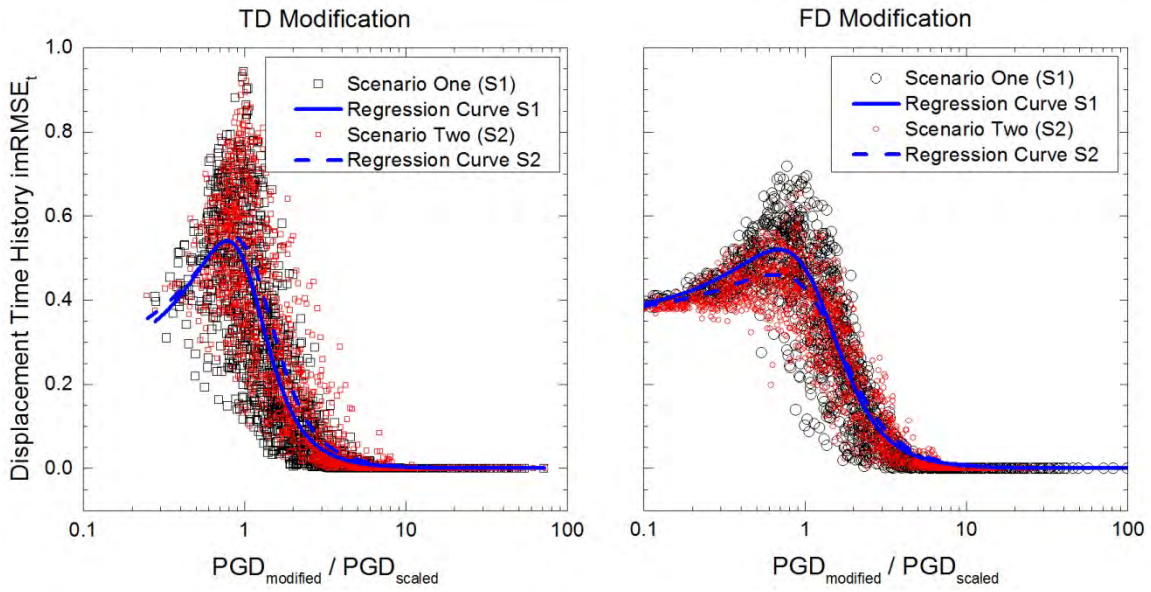

Figure 5.62. Comparison of the regression curves developed for the relationship between goodness-of-fit for the displacement time histories and the modified-to-scaled peak ground displacement (*PGD*) ratios for the ground motions in scenarios I and II.

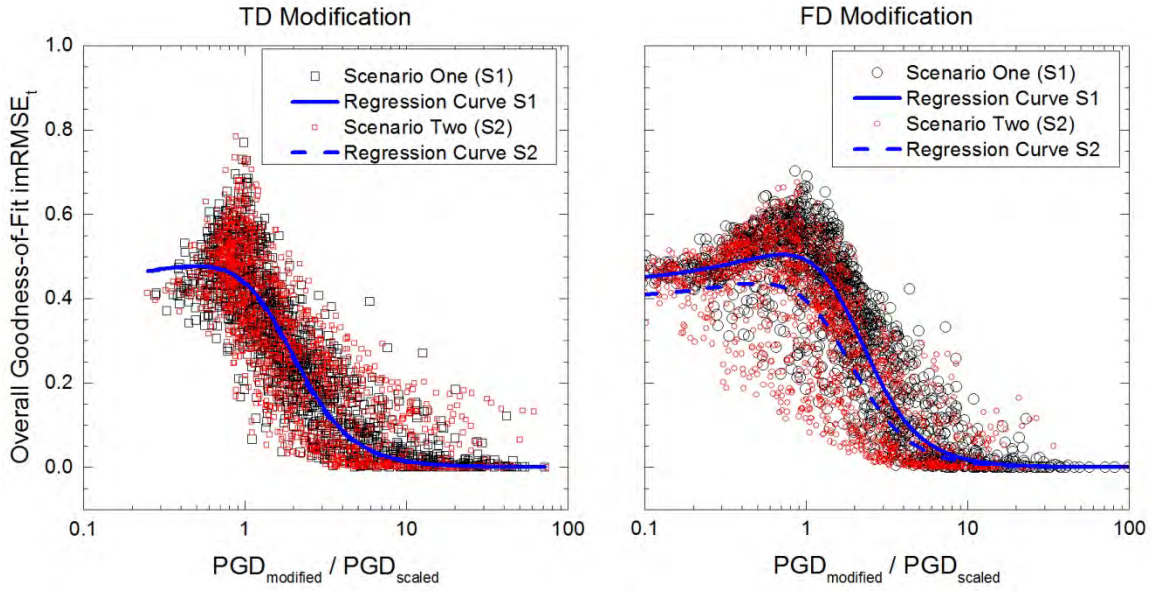

Figure 5.63. Comparison of the regression curves developed for the relationship between overall goodness-of-fit and the modified-to-scaled peak ground displacement (*PGD*) ratios for the ground motions in scenarios I and II.

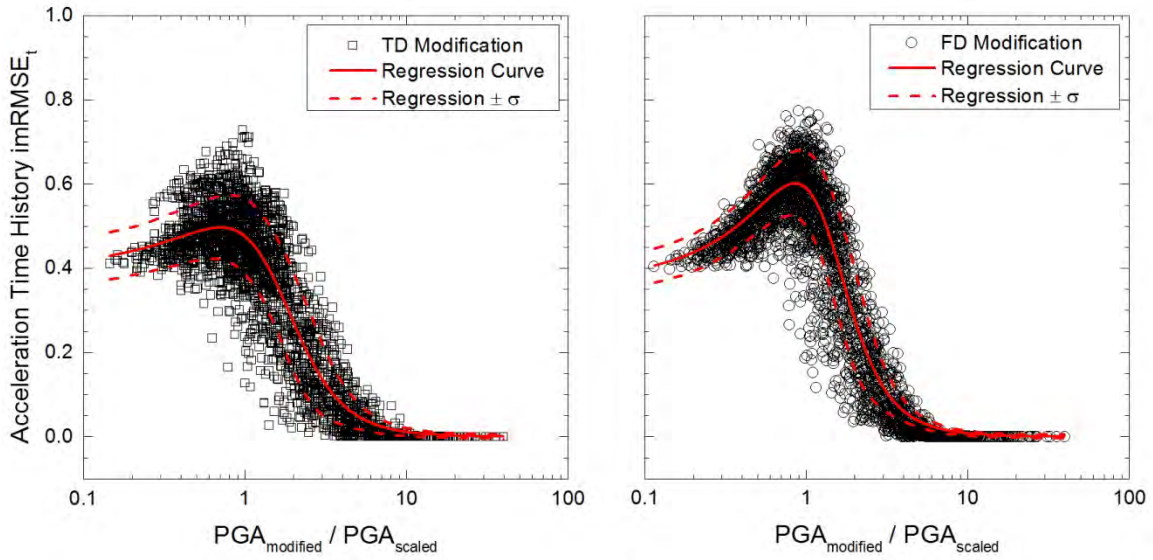

Figure 5.64. Regression curves, with plus and minus one standard deviation, developed for the relationship between goodness-of-fit for the acceleration time histories and the modified-to-scaled peak ground acceleration (*PGA*) ratios using the combined set of motions from scenarios I and II.

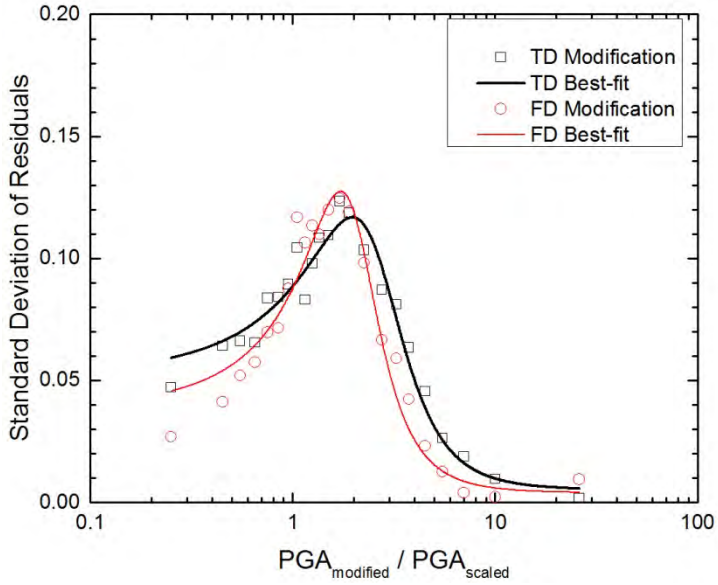

Figure 5.65. Standard deviations of the residuals and corresponding best-fit curves for the regression equations developed to describe the relationship between the goodness-of-fit values for the acceleration time histories of the combined set of motions from scenarios I and II and the modified-to-scaled peak ground acceleration (*PGA*) ratios.

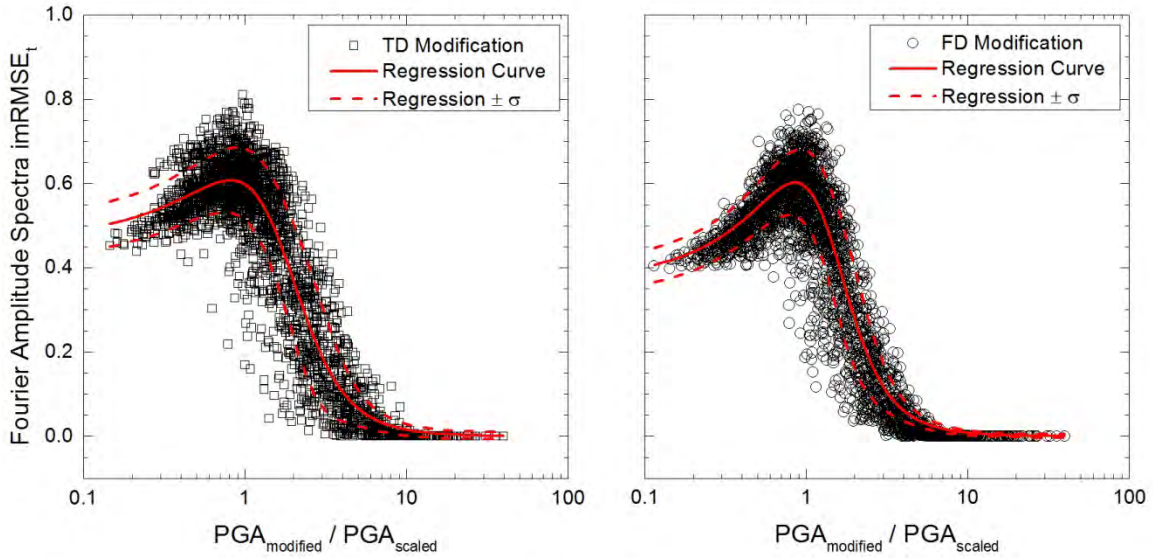

Figure 5.66. Regression curves, with plus and minus one standard deviation, developed for the relationship between goodness-of-fit for the Fourier amplitude spectra and the modified-to-scaled peak ground acceleration (*PGA*) ratios using the combined set of motions from scenarios I and II.

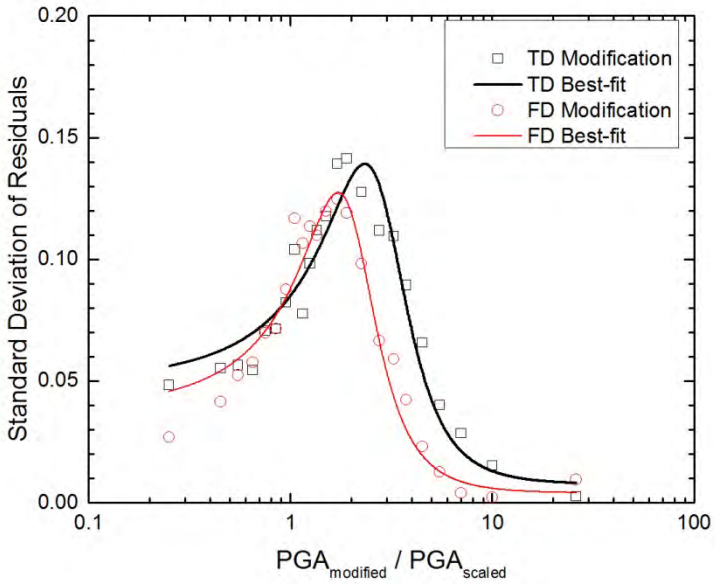

Figure 5.67. Standard deviations of the residuals and corresponding best-fit curves for the regression equations developed to describe the relationship between the goodness-of-fit values for the Fourier amplitude spectra of the combined set of motions from scenarios I and II and the modified-to-scaled peak ground acceleration (*PGA*) ratios.

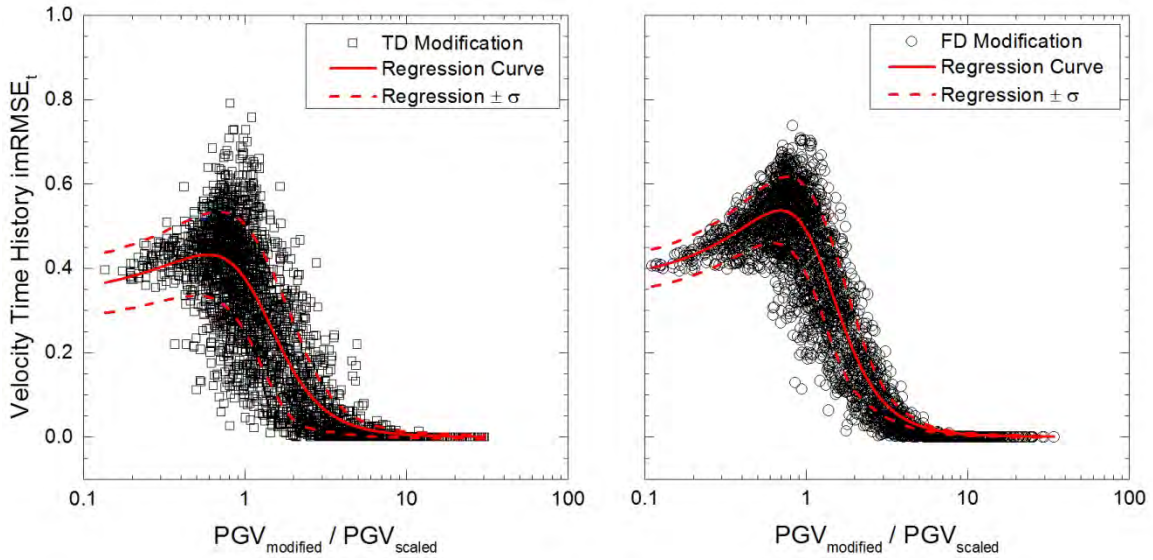

Figure 5.68. Regression curves, with plus and minus one standard deviation, developed for the relationship between goodness-of-fit for the velocity time histories and the modified-to-scaled peak ground velocity (*PGV*) ratios using the combined set of motions from scenarios I and II.

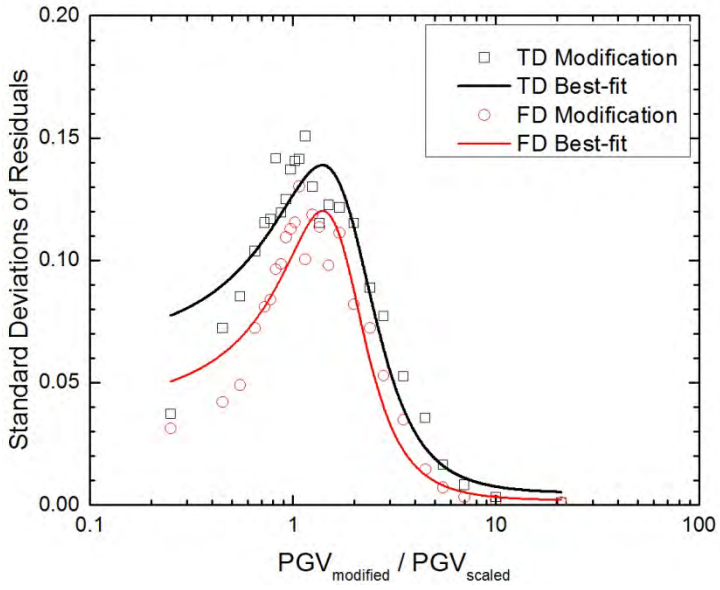

Figure 5.69. Standard deviations of the residuals and corresponding best-fit curves for the regression equations developed to describe the relationship between the goodness-of-fit values for the velocity time histories of the combined set of motions from scenarios I and II and the modified-to-scaled peak ground velocity (*PGV*) ratios.

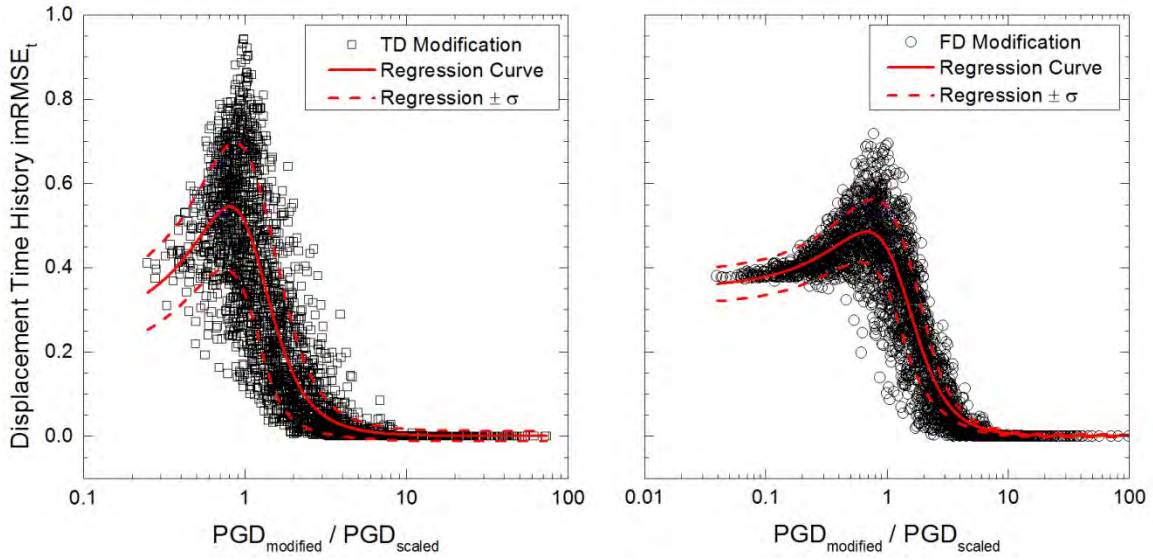

Figure 5.70. Regression curves, with plus and minus one standard deviation, developed for the relationship between goodness-of-fit for the displacement time histories and the modified-to-scaled peak ground displacement (*PGD*) ratios using the combined set of motions from scenarios I and II.

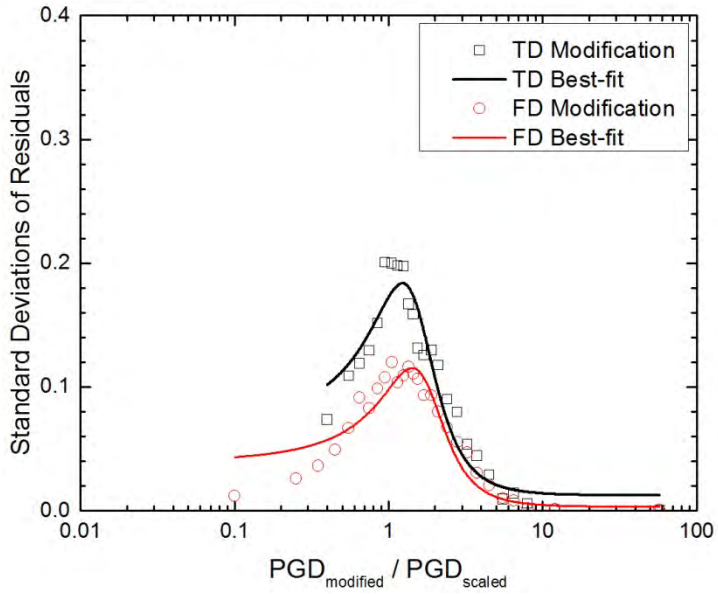

Figure 5.71. Standard deviations of the residuals and corresponding best-fit curves for the regression equations developed to describe the relationship between the goodness-of-fit values for the displacement time histories of the combined set of motions from scenarios I and II and the modified-to-scaled peak ground displacement (*PGD*) ratios.

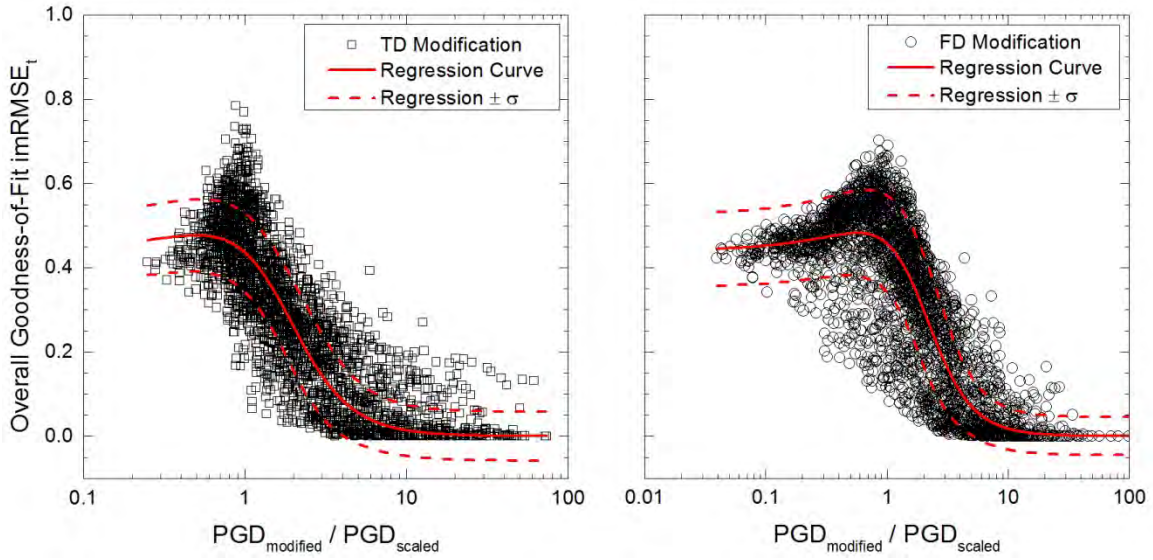

Figure 5.72. Regression curves, with plus and minus one standard deviation, developed for the relationship between overall goodness-of-fit and the modified-to-scaled peak ground displacement (*PGD*) ratios using the combined set of motions from scenarios I and II.

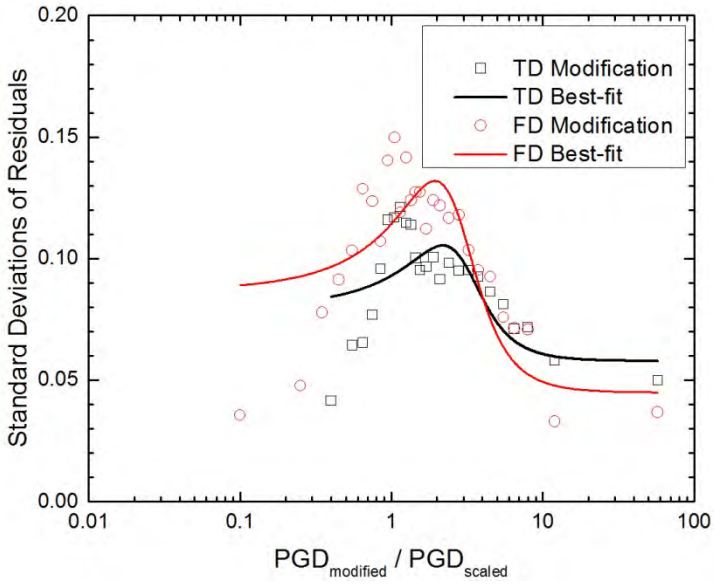

Figure 5.73. Standard deviations of the residuals and corresponding best-fit curves for the regression equations developed to describe the relationship between the overall goodness-of-fit of the combined set of motions from scenarios I and II and the modified-to-scaled peak ground displacement (*PGD*) ratios.

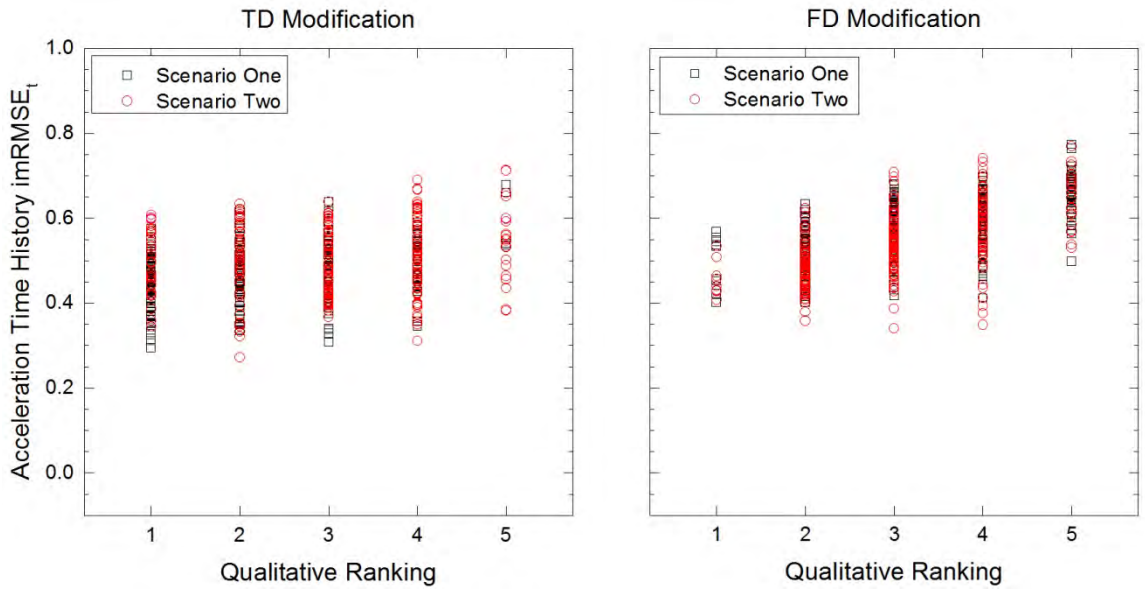

Figure 5.74. Comparison of the goodness-of-fit values for the acceleration time histories of the motions visually examined in scenarios I and II plotted against their assigned rankings.

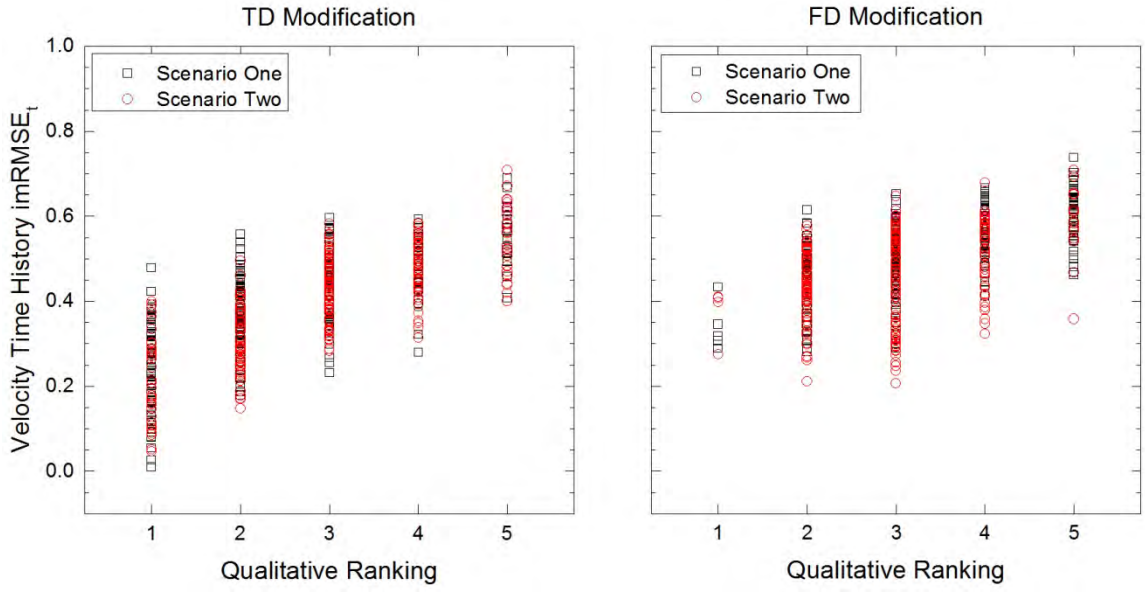

Figure 5.75. Comparison of the goodness-of-fit values for the velocity time histories of the motions visually examined in scenarios I and II plotted against their assigned rankings.

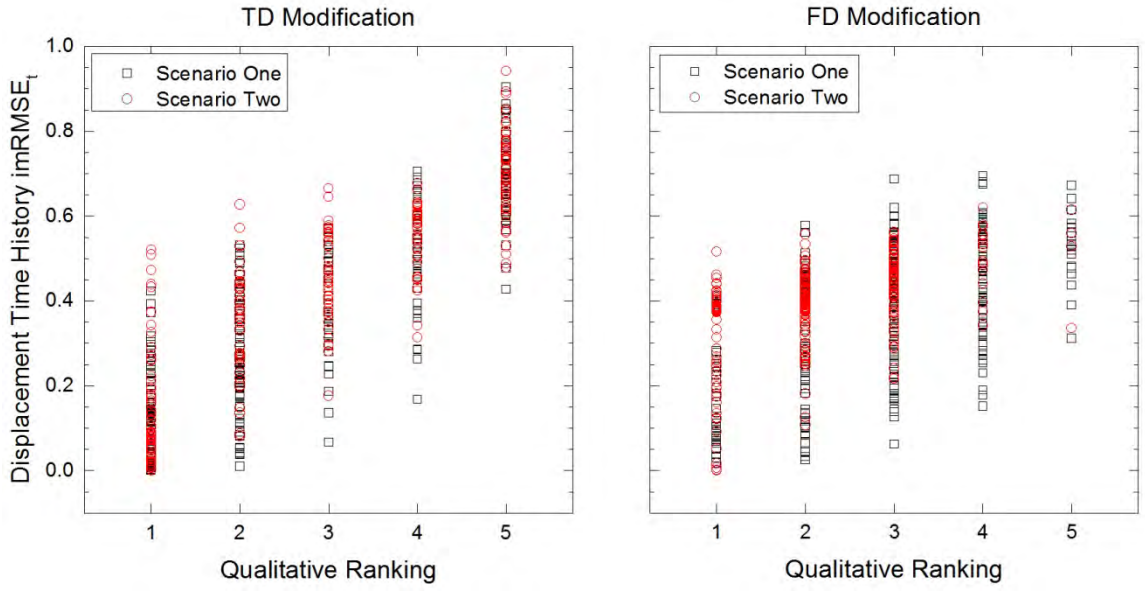

Figure 5.76. Comparison of the goodness-of-fit values for the displacement time histories of the motions visually examined in scenarios I and II plotted against their assigned rankings.

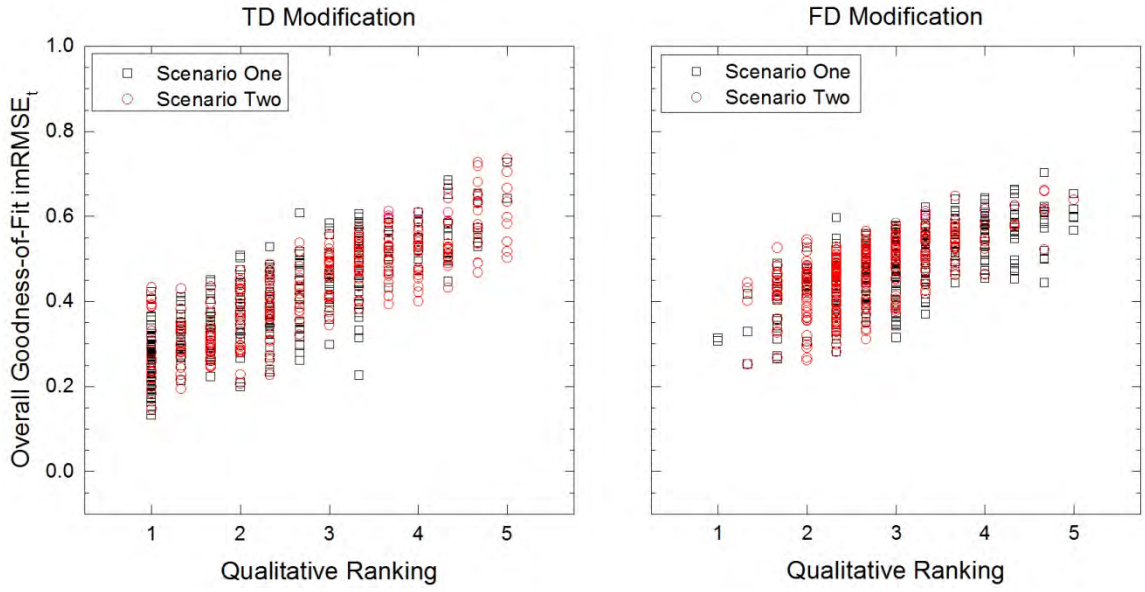

Figure 5.77. Comparison of the overall goodness-of-fit values of the motions visually examined in scenarios I and II plotted against their assigned rankings.

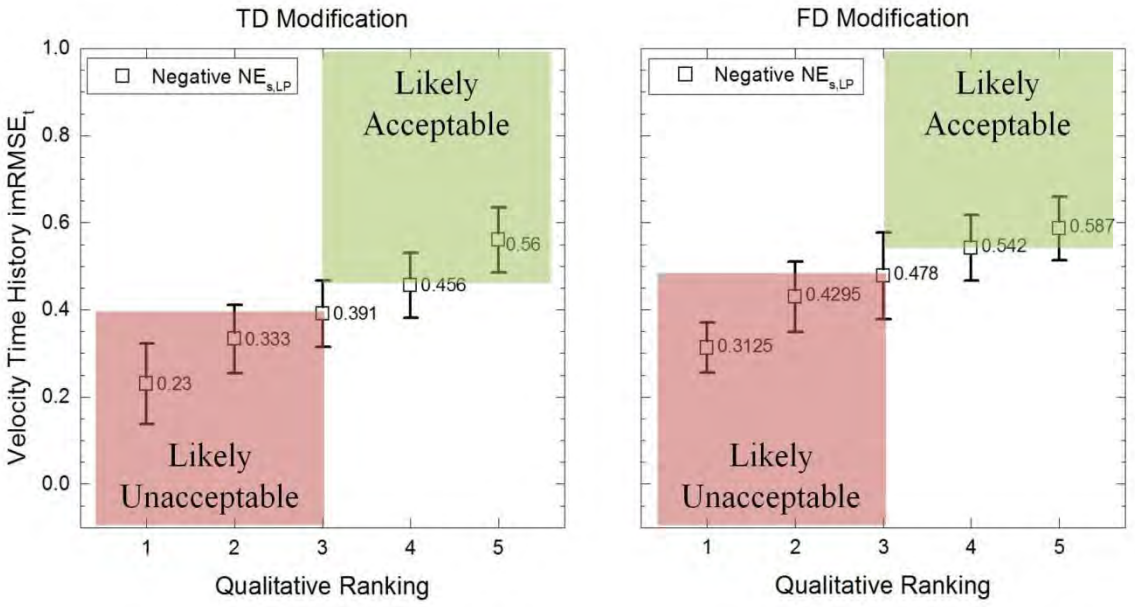

Figure 5.78. Medians and standard deviations of the goodness-of-fit values for each ranking for the velocity time histories of the combined set of motions visually examined in scenarios I and II with negative $NE_{s,LP}$. Recommended threshold values for *GOF* of likely acceptable and likely unacceptable time histories are also included.

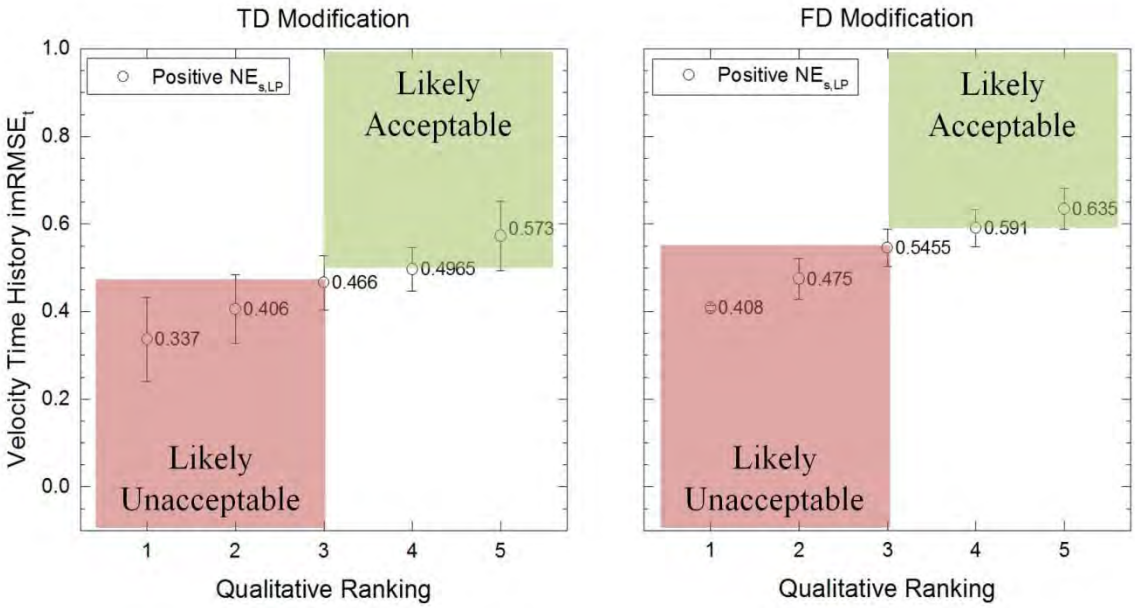

Figure 5.79. Medians and standard deviations of the goodness-of-fit values for each ranking for the velocity time histories of the combined set of motions visually examined in scenarios I and II with positive $NE_{s,LP}$. Recommended threshold values for *GOF* of likely acceptable and likely unacceptable time histories are also included.

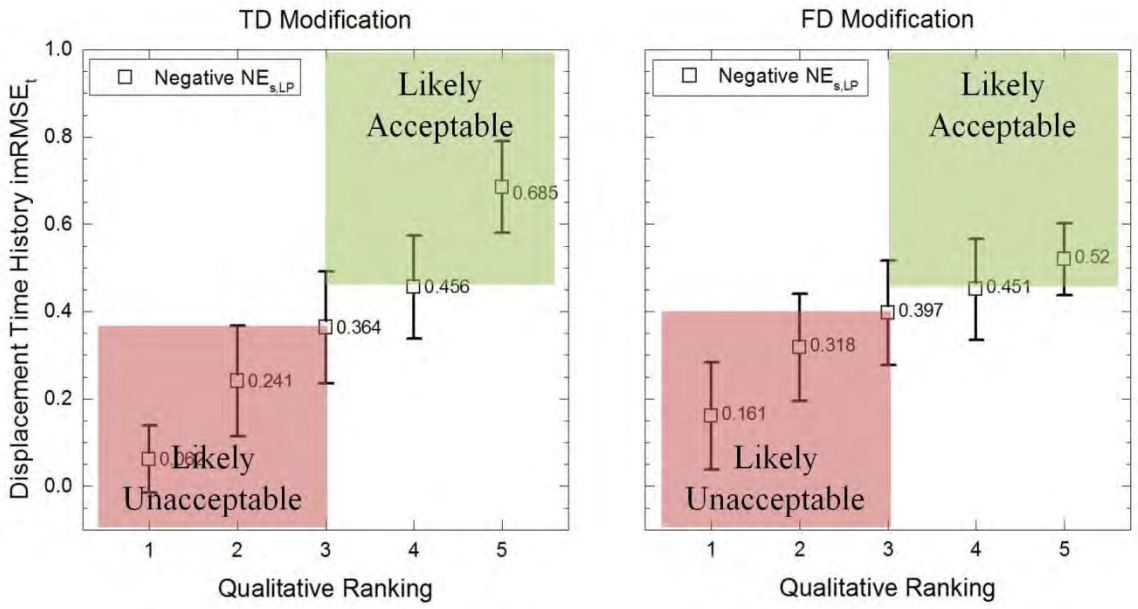

Figure 5.80. Medians and standard deviations of the goodness-of-fit values for each ranking for the displacement time histories of the combined set of motions visually examined in scenarios I and II with negative $NE_{s,LP}$. Recommended threshold values for *GOF* of likely acceptable and likely unacceptable time histories are also included.

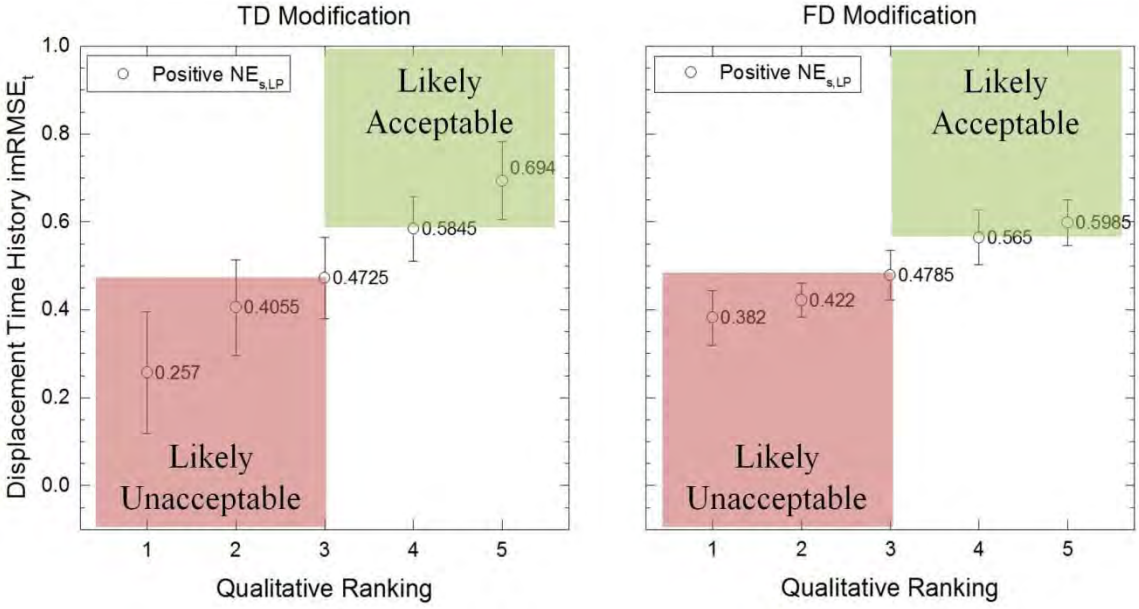

Figure 5.81. Medians and standard deviations of the goodness-of-fit values for each ranking for the displacement time histories of the combined set of motions visually examined in scenarios I and II with positive $NE_{s,LP}$. Recommended threshold values for *GOF* of likely acceptable and likely unacceptable time histories are also included.

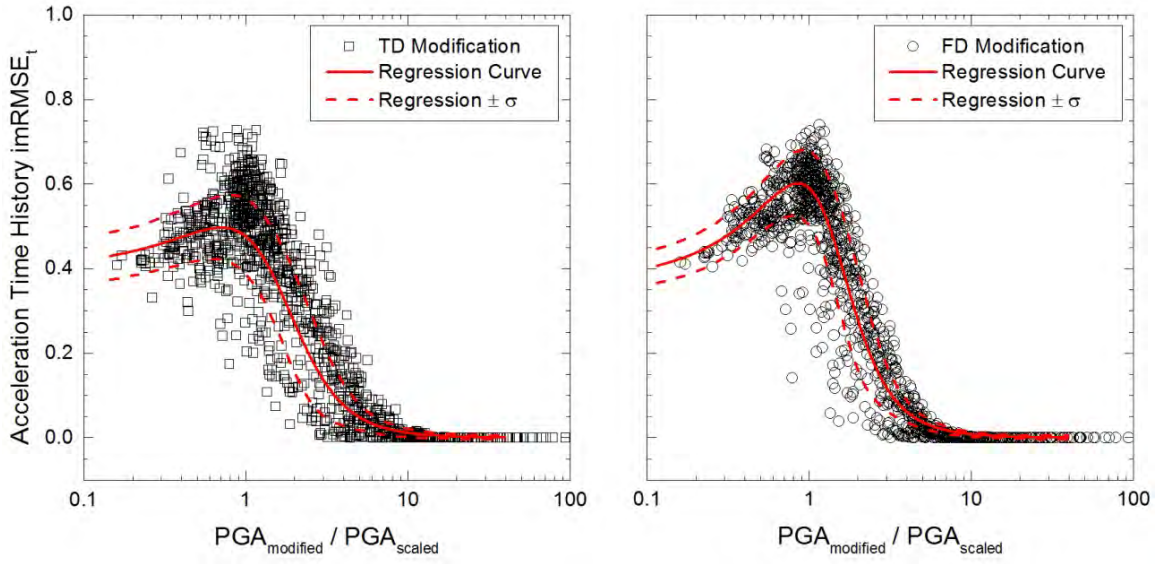

Figure 5.82. Comparison of the goodness-of-fit values for the acceleration time histories of the motions in scenario III to the regression curves developed for the relationship between the goodness-of-fit for the acceleration time histories and the modified-to-scaled peak ground acceleration (*PGA*) ratios using the combined set of motions from scenarios I and II.

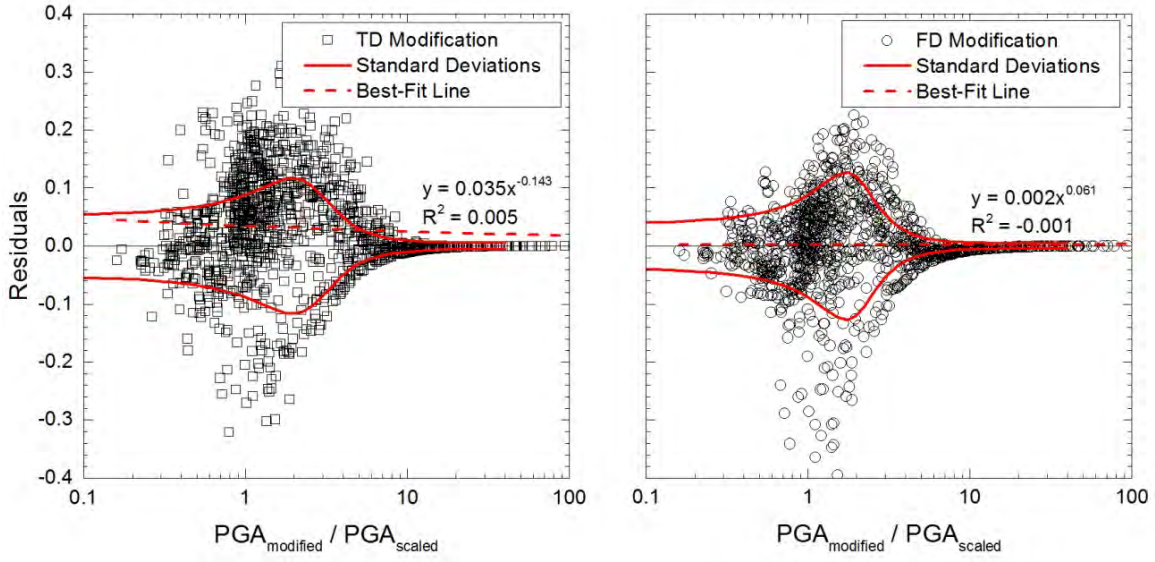

Figure 5.83. Comparison of the residuals for the acceleration time histories of the motions in scenario III to the standard deviations developed for the relationship between the goodness-of-fit for the acceleration time histories and the modified-to-scaled peak ground acceleration (*PGA*) ratios using the combined set of motions from scenarios I and II. Curves fit to the residuals are also shown.

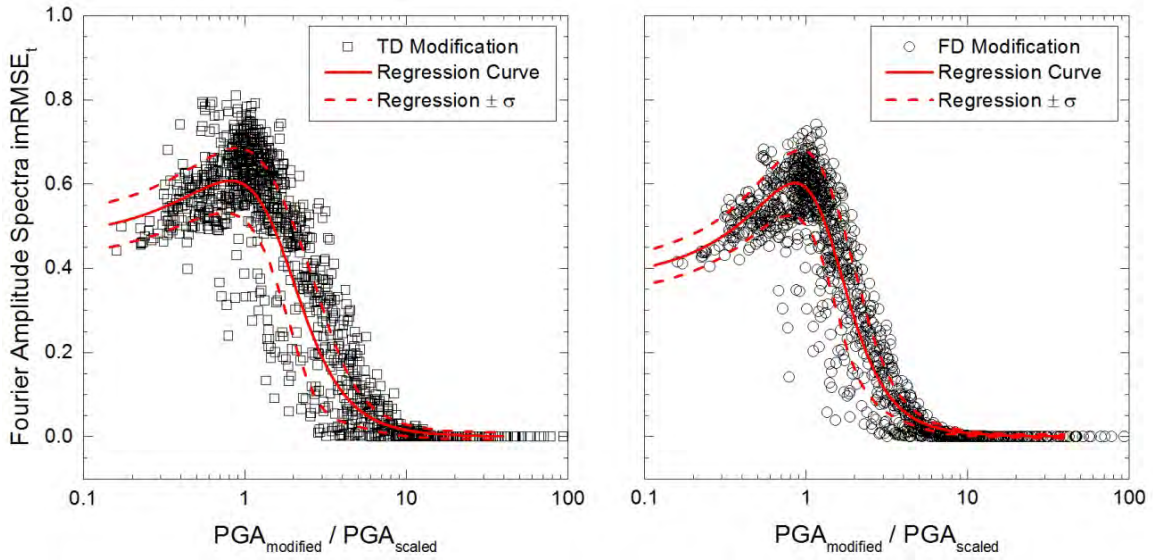

Figure 5.84. Comparison of the goodness-of-fit values for the Fourier amplitude spectra of the motions in scenario III to the regression curves developed for the relationship between the goodness-of-fit for the Fourier amplitude spectra and the modified-to-scaled peak ground acceleration (*PGA*) ratios using the combined set of motions from scenarios I and II.

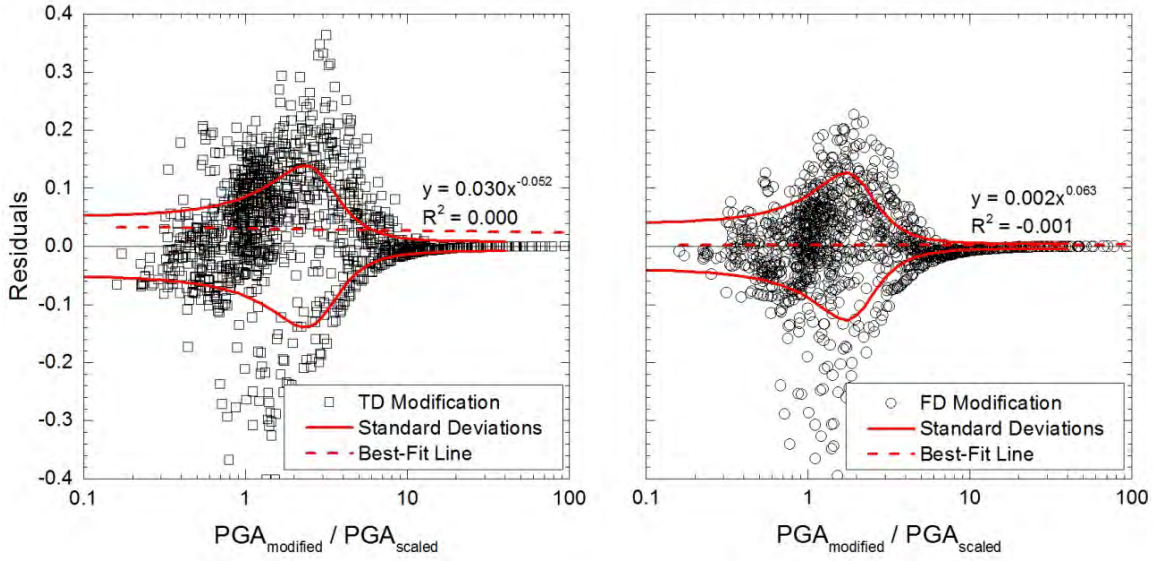

Figure 5.85. Comparison of the residuals for the Fourier amplitude spectra of the motions in scenario III to the standard deviations developed for the relationship between the goodness-of-fit for the Fourier amplitude spectra and the modified-to-scaled peak ground acceleration (*PGA*) ratios using the combined set of motions from scenarios I and II. Curves fit to the residuals are also shown.

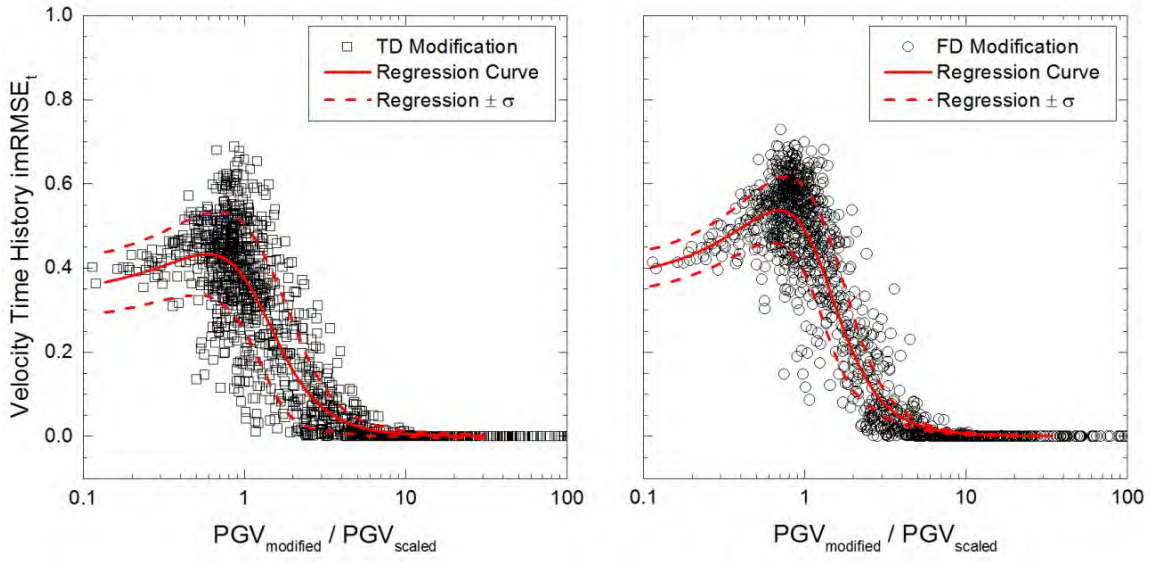

Figure 5.86. Comparison of the goodness-of-fit values for the velocity time histories of the motions in scenario III to the regression curves developed for the relationship between the goodness-of-fit for the velocity time histories and the modified-to-scaled peak ground velocity (*PGV*) ratios using the combined set of motions from scenarios I and II.

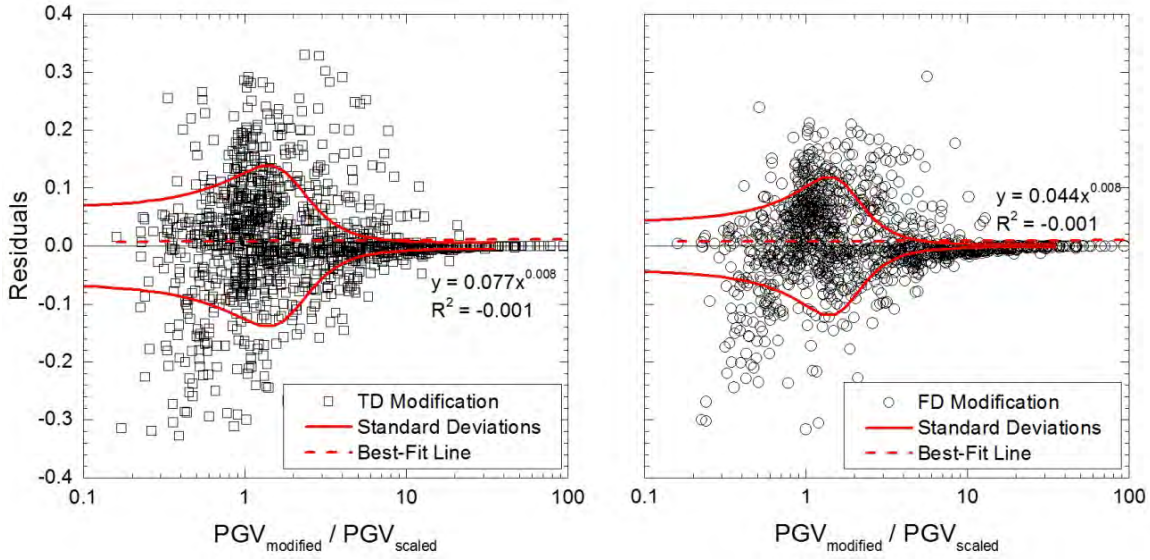

Figure 5.87. Comparison of the residuals for the velocity time histories of the motions in scenario III to the standard deviations developed for the relationship between the goodness-of-fit for the velocity time histories and the modified-to-scaled peak ground velocity (*PGV*) ratios using the combined set of motions from scenarios I and II. Curves fit to the residuals are also shown.

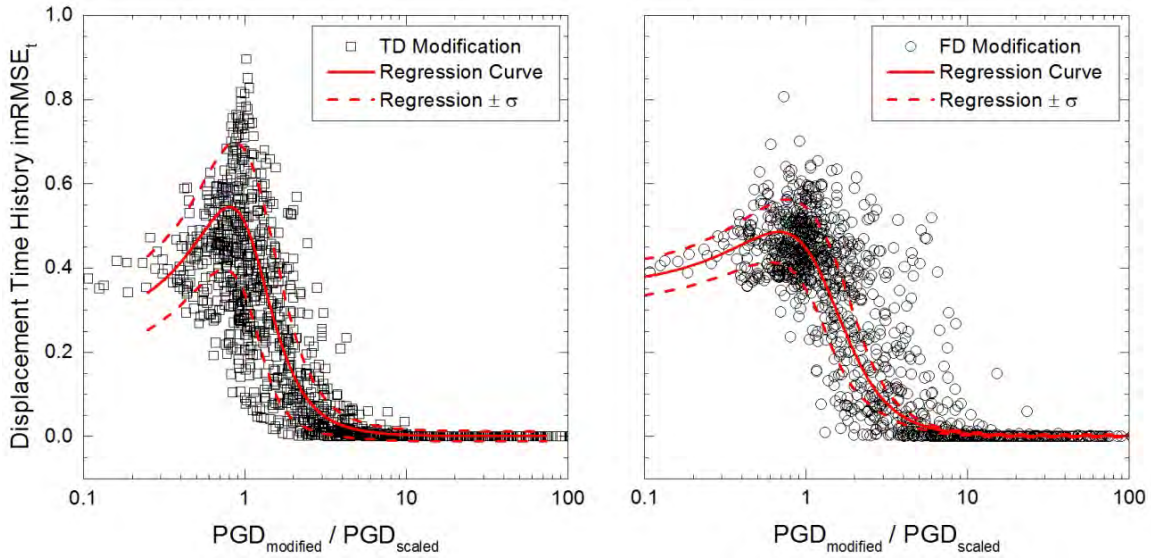

Figure 5.88. Comparison of the goodness-of-fit values for the displacement time histories of the motions in scenario III to the regression curves developed for the relationship between the goodness-of-fit for the displacement time histories and the modified-to-scaled peak ground displacement (*PGD*) ratios using the combined set of motions from scenarios I and II.

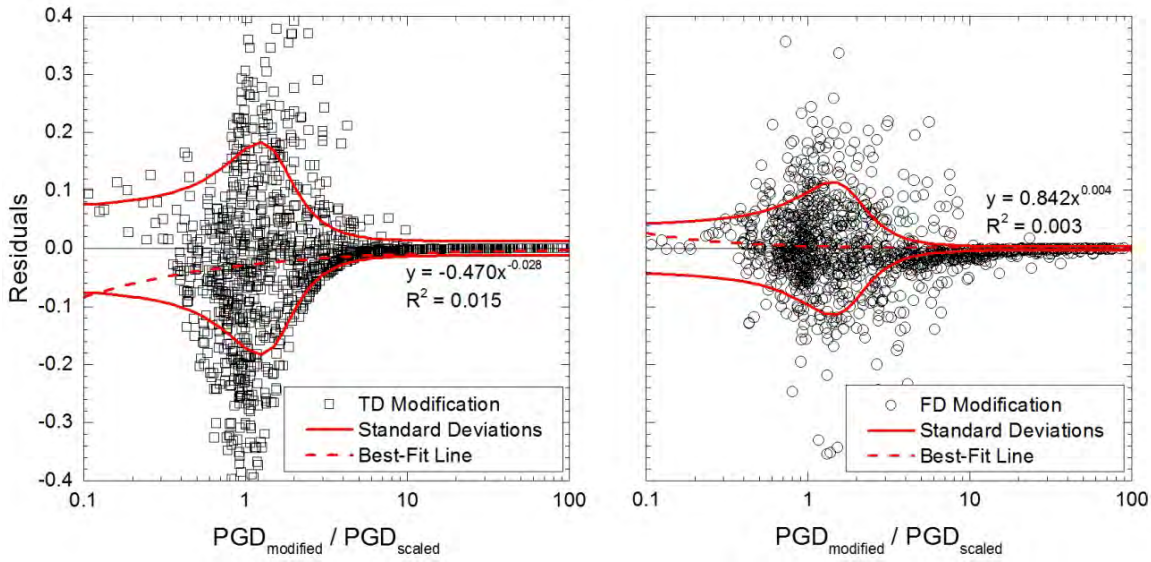

Figure 5.89. Comparison of the residuals for the displacement time histories of the motions in scenario III to the standard deviations developed for the relationship between the goodness-of-fit for the displacement time histories and the modified-to-scaled peak ground displacement (*PGD*) ratios using the combined set of motions from scenarios I and II. Curves fit to the residuals are also shown.

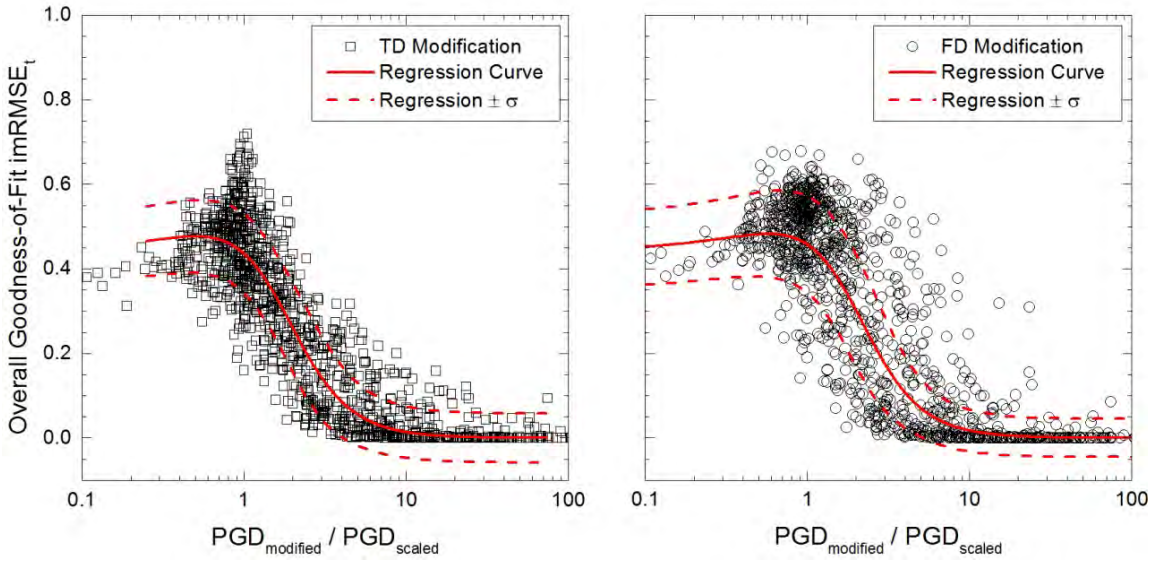

Figure 5.90. Comparison of the overall goodness-of-fit of the motions in scenario III to the regression curves developed for the relationship between the overall goodness-of-fit and the modified-to-scaled peak ground displacement (*PGD*) ratios using the combined set of motions from scenarios I and II.

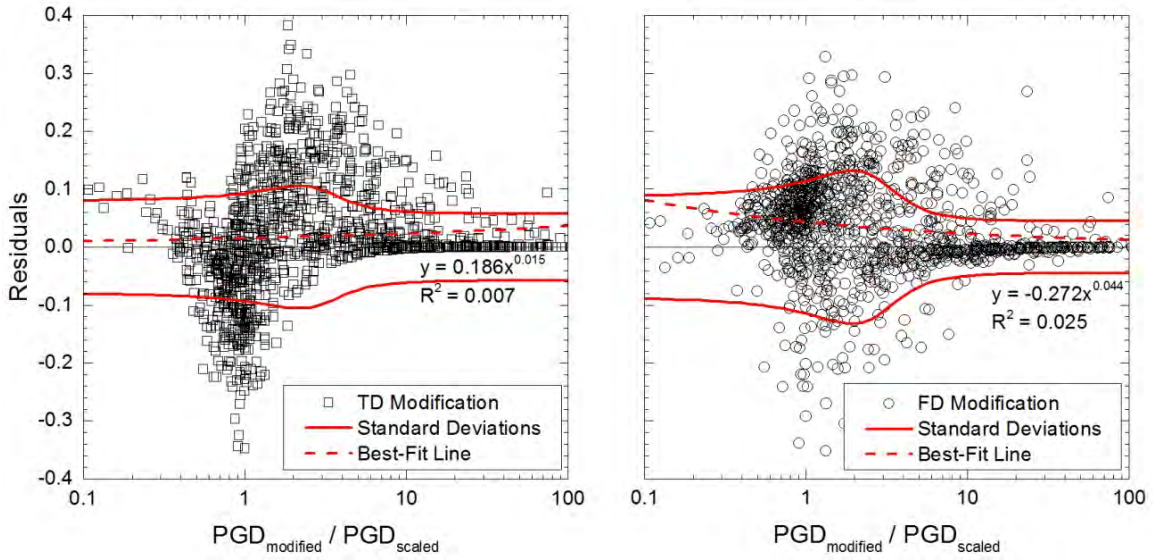

Figure 5.91. Comparison of the residuals for the overall goodness-of-fit of the motions in scenario III to the standard deviations developed for the relationship between the overall goodness-of-fit and the modified-to-scaled peak ground displacement (*PGD*) ratios using the combined set of motions from scenarios I and II. Curves fit to the residuals are also shown.

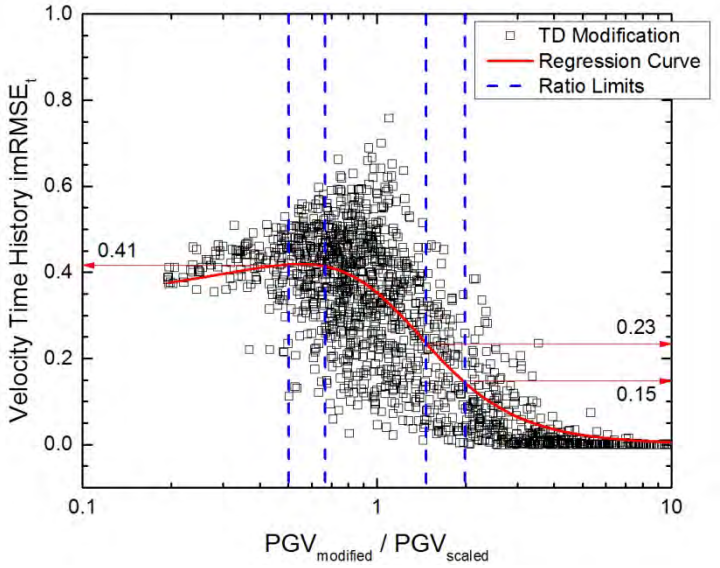

Figure 5.92. Effects of changing the limits of the modified-to-scaled peak ground velocity (*PGV*) ratios from 50 to 100% on the acceptable goodness-of-fit values for the velocity time histories.

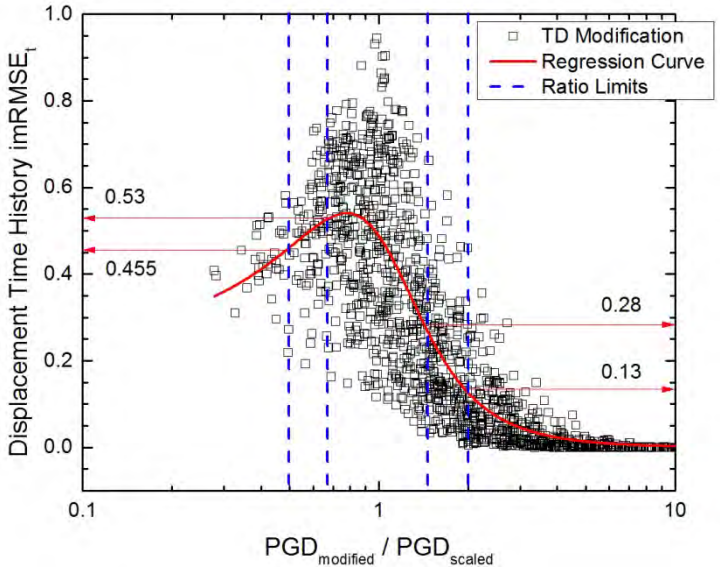

Figure 5.93. Effects of changing the limits of the modified-to-scaled peak ground displacement (*PGD*) ratios from 50 to 100% on the acceptable goodness-of-fit values for the displacement time histories.

CHAPTER 6

Impact of Modification on the Results of Site Response Analyses

The effects of modification on geotechnical seismic response analyses are examined for two different soil profiles to investigate the potential bias of modified ground motions on the results of seismic response analyses relative to the results for scaled ground motions. Relationships between the modified-to-scaled geotechnical seismic response ratios and spectral mismatch are examined to assess the impact of spectral mismatch on the geotechnical seismic responses caused by modified motions relative to those caused by scaled motions.

6.1 Methodology

6.1.1 Soil Profiles

Geotechnical seismic response analyses were performed for scenarios I and II by using the scaled and modified ground motions from each scenario as input to two soil profiles. Two different soil profiles are used for the geotechnical seismic response analyses to explore the impact of the site conditions on the geotechnical seismic responses and attempt to separate these effects from the effects of ground motion modification. Equivalent linear seismic response analyses were performed. For both soil profiles, the ground water table is assumed to be at a depth of 4.6 m and bedrock is assumed to be at a depth of roughly 41 m having a unit weight of 23.6 kN/m^3 and a shear wave velocity (V_S) of 550 m/s.

The first soil profile represents a typical levee site in the Sacramento area with 7.6 m of fill overlaying 18.3 m of Holocene medium-dense sand and 15.2 m of Pleistocene clay (Athanasopoulos-Zekkos 2010). This site has a V_{S30} of 200 m/s (NEHRP Site Class D (FEMA 2004)), which corresponds to a period of 0.48 seconds. The unit weight and V_S profiles for the levee site are shown in **Figure 6.1**. The assumed shear strength (τ_{all}) profile is also shown in **Figure 6.1**. The τ_{all} profile for this site was developed by assuming the fill and medium-dense sand had effective friction angles of 33° and 37°, respectively, while the cohesion of the clay was

assumed to increase linearly with depth from 200 to 250 kN/m^2. The Seed and Idriss (1970) normalized shear modulus (G/G_{max}) and damping (λ) curves were used to describe the dynamic behavior of the fill and sand for this profile while the Vucetic and Dobry (1991) curves for a plasticity index of 30 were used to describe the behavior of the clay. Values were extrapolated to a shear strain of 5% for these G/G_{max} and λ curves to ensure the motions did not exceed the maximum calculated shear strains. The G/G_{max} and λ curves of the models for the first soil profile are shown in **Figure 6.2**.

The second soil profile represents a stiffer site with 7.6 m of dense sand overlaying 12.2 m of very dense sand with gravel and 21.3 m of soft rock. Relative to the first soil profile, this profile has a higher V_{S30} of 385 m/s (NEHRP Site Class C (FEMA 2004)) and a shorter site period of 0.31 seconds. **Figure 6.3** shows the unit weight and V_S profiles for the stiff site. **Figure 6.3** also shows the assumed τ_{all} profile for the stiff site. Effective friction angles of 37°, 39°, and 42° were assumed for the dense sand, very dense sand, and soft rock, respectively. The Darendeli (2001) G/G_{max} and λ curves for a plasticity index of 0 and mean effective stresses of 0.4 and 1.2 atm were used to describe the dynamic behavior of the dense sand and very dense sand with gravel, respectively. Although the soft rock is non-plastic, the Vucetic and Dobry (1991) G/G_{max} and λ curves for a plasticity index of 50 were used to model the dynamic behavior of the soft rock. Much larger shear strains occurred in the stiff soil profile due to the larger intensity of ground motions for shorter periods, so values for the G/G_{max} and λ curves were extrapolated to shear strains of 20%. Although the shear strains in these models were extended to 20%, only about 4% of the scaled motions and less than 1% of the modified motions exceed shear strains of 5%. **Figure 6.4** shows the G/G_{max} and λ curves for the stiff site.

6.1.2 Geotechnical Seismic Responses

The geotechnical seismic responses examined in this study are maximum shear strain (γ_{max}), cyclic stress ratio (*CSR*) (Seed and Idriss 1971), maximum horizontal acceleration (*MHA*), spectral ratios, and Newmark-type slope displacements (Newmark 1965). γ_{max} and *MHA* are the maximum values of shear strain and horizontal acceleration at a given depth in the soil profile that occur over the duration of an input time history. *CSR* is calculated using **Equation 6.1**.

$$CSR = 0.65\frac{\tau_{max}}{\sigma'_{v0}} \quad (\mathbf{6.1})$$

τ_{max} represents the maximum shear stress at a given depth in the soil profile over the duration of a shear stress time history, $\tau(t)$, caused by an input time history. Profiles of σ'_{v0}, which represents the initial (i.e., prior to shaking) vertical effective stress, for the levee and stiff sites are shown in **Figure 6.5**. γ_{max}, *CSR*, and *MHA* were calculated for 100 equally-spaced points over the 41 m depth for both sites. Spectral ratio is, in general, the ratio between the response spectra at two different depths in the soil profile resulting from an input ground motion. For this study, spectral ratios refer to the ratio between the surface and base acceleration response spectra in the soil profiles (i.e., $Sa(T_i)$ at 0 m / $Sa(T_i)$ at 41 m). Spectral ratios were calculated for 100 periods, equally spaced (logarithmically) from 0.01 to 5 seconds. Newmark-type analyses were performed to calculate seismic slope displacements for three sliding depths within the soil profiles: 3.0 m (i.e., representing a potential shallow slope failure), 7.6 m (i.e., intermediate slope failure), and 13.7 m (i.e., deep slope failure). The displacements were calculated for yield coefficients (k_y) ranging from 0.025 to 0.175 in increments of 0.025. In order to provide a fair comparison between the scaled and modified motions, differences in the magnitudes of acceleration were removed by normalizing k_y by k_{max} (Chopra and Zhang 1991), which is calculated using **Equation 6.2**.

$$k_{max} = \frac{\tau_{max}}{\sigma_v} \quad (\mathbf{6.2})$$

Profiles of σ_v, which represents the total vertical stress, for the levee and stiff sites are shown in **Figure 6.5**. The τ_{max} used in **Equation 6.2** are taken at the depths of the considered sliding masses.

The software program Strata (Rathje and Kottke 2013) was used to perform 1-D equivalent linear site response analyses for both sites using the scaled and modified motions as input. Calculations were performed until the difference in G/G_{max} or λ between iterations was within 2%, or a maximum of ten iterations was reached. An effective strain ratio of 0.65 was used in Strata for the calculations of G/G_{max} and λ after each iteration. The γ_{max}, τ_{max}, *MHA* profiles and the spectral ratios produced by the input ground motions were calculated using Strata then used to calculate the *CSR* and k_{max} profiles. $\tau(t)$ were also calculated using Strata at the sliding depths used for the Newmark-type displacement analyses. The $\tau(t)$ were normalized by σ_v at the corresponding depths to produce horizontal equivalent acceleration time histories, $HEA(t)$ (**Equation 6.3**).

$$HEA(t) = \frac{\tau(t)}{\sigma_v} g \quad \textbf{(6.3)}$$

The $HEA(t)$ were input to the program SLAMMER (Jibson et al. 2013) and used to calculate the Newmark-type slope displacements induced by the ground motions at different depths for varying k_y. Rigid block analyses (i.e., Newmark-type analyses) were performed considering only the downslope action of the ground motions. For each ground motion in the suite, the maximum displacement induced by either the original or inverse of the ground motion was recorded as the Newmark-type displacement. The k_y values were normalized by the k_{max} values of the ground motions at the corresponding depth for the sliding mass. Interpolation was then used to calculate displacements at k_y / k_{max} values of 0.025, 0.05, 0.1, 0.15, 0.2, 0.3, 0.4, 0.5, and 0.75 to allow comparisons between scaled and modified motions for specific k_y / k_{max} ratios.

6.1.3 Data Analysis

The median geotechnical seismic responses caused by the sets of the scaled, TD-modified, and FD-modified motions for scenarios I and II were calculated and compared to investigate if using the modified motions in site response analyses introduced any biases compared to using scaled motions. Modified motions were first scaled using the optimal factors (i.e., the factor that minimizes mismatch with the target spectrum) for each of five target spectra. Comparisons were not made between the median responses produced by the modified and scaled motions for the sets scaled using factors of 0.5 and 2 because their median response spectra may significantly deviate from the target spectra. For example, the response spectra of the motions scaled by 0.5 are generally lower than the target spectra (see **Figure 6.6**), which leads to the modified motions producing larger geotechnical seismic responses than the scaled motions. Target spectra developed for scenarios I and II are compared to the median response spectra for the corresponding optimally scaled motions in **Figure 6.7** and **6.8**. **Tables 6.1** and **6.2** compare the median ground motion characteristics of the modified motions to the scaled motions, using the modified-to-scaled ratios, for the optimally scaled sets of motions in scenarios I and II, respectively. Ratios of the modified-to-scaled medians were calculated for γ_{max}, *CSR*, *MHA*, spectral ratio, and Newmark-type displacements. The median profiles for γ_{max}, *CSR*, and *MHA* were also normalized by the corresponding median response at the base of the soil profile (i.e., *CSR*(depth, *z*) / *CSR*(41 m)). This normalization removes any differences in the magnitudes of

the median responses produced by the scaled and modified motions, allowing for the impact of site effects on the responses caused by the scaled, TD-modified, and FD-modified motions to be more accurately investigated.

Ratios of the modified-to-scaled responses were also calculated for the individual motions in scenarios I and II and plotted against spectral mismatch, quantified by NE_s for different period ranges, to examine the impact of mismatch on the geotechnical seismic responses caused by the motions. The spectral mismatch – modified-to-scaled geotechnical seismic response ratio relationships were investigated because of the strong relationships observed between spectral mismatch and the modified-to-scaled ground motion characteristic ratios described in **Chapter 4** and the correlations noted between certain ground motion characteristics and geotechnical seismic responses (e.g., Athanasopoulos-Zekkos 2010; Rathje and Antonakos 2011; Athanasopoulos-Zekkos and Saadi 2012). For the *CSR* and *MHA* profiles, the ratios were calculated at depths corresponding to the mid-depths for the layers of different soils: 3.8, 16.8, and 33.5 m for the levee site and 3.8, 13.7, and 30.5 m for the stiff site. The ratios for γ_{max} were not investigated since γ_{max} is related to τ_{max}, and thus *CSR*. The ratios of the modified-to-scaled spectral ratios for the motions were examined for periods of 0.25, 0.49, and 1.95 seconds. Periods of 0.25 and 0.49 seconds were selected to investigate the impact of spectral mismatch at roughly the periods of the sites, while a period of 1.95 seconds was selected to study the impact of spectral mismatch for longer periods. Finally, the ratios of modified-to-scaled Newmark-type displacements caused by the ground motions for all three sliding depths for k_y / k_{max} values of 0.05 and 0.15 were examined.

6.2 Impact of Modification on Site Response Analyses

6.2.1 Results for Scenario I

For scenario I, only 30 out of 1620 scaled ground motions (and no modified ground motions) produce τ_{max} that exceed τ_{all} by more than 10%. Over 300 scaled motions and 60 TD- and FD-modified motions out of 1620 motions produce τ_{max} that exceed τ_{all} by more than 10% in the stiff soil profile for scenario I. Most of the scaled motions and all of the modified motions for which the τ_{max} values exceed τ_{all} for the stiff site in scenario I are those matched to the 2% UHS or Seed + σ target spectra. Therefore, the geotechnical seismic responses produced by the scaled

and modified motions for the 2% UHS and the Seed + σ target spectra may not represent the true response of the stiff site and a truly nonlinear analysis may be warranted; however, the results for these two spectra are included for completeness. τ_{all} for the stiff site is generally not exceeded by the scaled or modified motions in scenario I for the motions matched to the other target spectra.

6.2.1.1 Median Response Comparison

The scaled motions referred to in the study of the median responses are those that were optimally scaled to match the target spectra. The median profiles of γ_{max} for both sites produced by the TD- and FD-modified motions are compared to those produced by the scaled motions in **Figures 6.9** and **6.10**, respectively. As observed in the modified-to-scaled ratios of the medians in **Figure 6.11**, the medians of the γ_{max} induced by the sets of TD- and FD-modified motions appear to be very similar. This observation is the result of the modified motions for both techniques closely matching the target spectra with little variability. The modified-to-scaled ratios of the medians in **Figure 6.11** show that the γ_{max} caused by the scaled motions are larger than those caused by the modified motions (i.e., ratios less than 1) for both soil profiles. Typically, the medians of the γ_{max} caused by the sets of modified motions are 25 to 60% less than (i.e., ratios between 0.6 and 0.8) the medians caused by the sets of scaled motions. For the CMS and Seed + σ target spectra, the medians of the γ_{max} caused by the sets of scaled and modified motions are similar between depths of 10 and 20 m for the levee site. However, for the stiff site, the medians of the γ_{max} caused by the modified motions for these two target spectra are at least 10% and as much as 5 times smaller than the medians caused by their scaled counterparts. The generally smaller γ_{max} caused by the modified motions relative to those caused by the scaled motions may be the result of the scaled motions having larger median *PGA* than the modified motions for the different target spectra (see **Table 6.1**) and the median spectra of the scaled motions generally having larger values than the target spectra (see **Figure 6.7**). The normalized median profiles for γ_{max}, shown in **Figures 6.12** and **6.13** for TD and FD modification, respectively, show that the impact of the site effects on the γ_{max} produced by the scaled and modified motions is similar (i.e., the normalized medians of γ_{max} for the scaled and modified motions are generally within 20% of each other). There are exceptions to this observation, particularly for depths between 3 and 10 m for the stiff site, where site effects cause the normalized medians of the γ_{max} caused by the scaled motions to be up to 4.5 times larger than the

medians caused by their modified counterparts. There are also generally differences between the impact of site effects on the γ_{max} caused by the scaled and modified motions for the Seed + σ target spectrum.

The median *CSR* profiles that result from using the sets of TD- and FD-modified motions as input are compared to the median *CSR* profiles produced by the scaled motions in **Figures 6.14** and **6.15**, respectively. The ratios of modified-to-scaled *CSR* medians caused by the sets of motions are shown in **Figure 6.16**. There is practically no difference between the median *CSR* produced by the TD- and FD-modified motions. The scaled motions generally produce somewhat larger median *CSR* than the modified motions (about 15 to 35%). At depths between 10 and 30 m for the levee site, the sets of scaled and modified motions for the CMS and Seed + σ target spectra produce similar median *CSR* (within 10% of each other). Although the median *CSR* produced by the scaled and modified motions are similar for the levee site for the Seed + σ target spectrum, the scaled motions produce much larger median *CSR* (up to 60% larger for depths less than 5 m) for the stiff site. When comparing the impact of site effects on the median *CSR* produced by the scaled and modified motions in **Figures 6.17** and **6.18**, it is observed that the median *CSR* produced by the modified motions are more largely impacted by site effects than those produced by the scaled motions, leading to 10 to 20% larger normalized median *CSR* for the modified motions. For the stiff site, site effects have a larger impact on the median *CSR* produced by the scaled motions for the CMS and Seed + σ target spectra. This is more evident at shallow depths, where the normalized median *CSR* produced by the scaled motions are 15 and 35% larger than their modified counterparts for the CMS and Seed + σ target spectra, respectively. The observed trends for the medians of γ_{max} and *CSR* are very similar since shear strain is directly related to shear stress and thus, *CSR*.

Figures 6.19 and **6.20** show the median *MHA* profiles produced by the suites of TD- and FD-modified motions, respectively, compared to those produced by the suites of scaled motions. The ratios of the modified-to-scaled median *MHA* are shown in **Figure 6.21**. There is practically no difference between the median *MHA* produced by the TD-modified motions and those produced by the FD-modified motions (differences between the two are generally less than 10%). The scaled motions produce larger median *MHA* than the modified motions (15 to 35% larger) for both sites. Motions matched to the Seed + σ target spectrum produce even smaller median *MHA* than their scaled counterparts, with differences as large as a factor of 2 and 1.75 for

the levee and stiff sites, respectively. At the base of the soil profiles, the ratios of the modified-to-scaled median *MHA* are only slightly smaller than the modified-to-scaled median *PGA* ratios for many of the target spectra (see **Table 6.1**). The scaled and modified motions for the Seed + σ target spectrum are observed to have the largest differences between the median *PGA* and the median *MHA* they produce. Therefore, the differences observed in the median *MHA* produced by the modified and scaled motions may be caused by differences in their *PGA* and spectral shape. **Figures 6.22** and **6.23** compare the normalized medians of *MHA* caused by the scaled motions to those caused by the TD- and FD-modified motions, respectively. Overall, site effects cause the median *MHA* produced by the scaled motions to be 20 and 10% larger than the median *MHA* produced by their modified counterparts for the levee and stiff sites, respectively. The normalized median *MHA*s produced by the scaled and modified motions for the Seed + σ target spectrum are more significantly affected by site effects, leading to factors of difference of 1.5 and 1.25 for the levee and stiff sites, respectively. Normalized median *MHA* produced by the modified motions are larger at a depth of 5 m, but normalized median *MHA* produced by the scaled motions are larger at a depth of 25 m.

The median spectral ratios of the scaled motions are compared to those of the TD- and FD-modified motions in **Figures 6.24** and **6.25**, respectively. Ratios of the modified-to-scaled median spectral ratios are shown in **Figure 6.26**. The median spectral ratios of the FD-modified motions are slightly larger (10 to 25%) than the median spectral ratios of the TD-modified motions for periods less than 0.1 seconds, but this is not in the period range of engineering interest. For the MA, 2% UHS, and 10% UHS target spectra, the modified motions have median spectral ratios that are less than the median spectral ratios of the scaled motions (by a factor of 1.5) for periods less than 0.1 seconds, but median spectral ratios greater than (by a factor of 1.7) those resulting from the scaled motions for periods between 0.1 and 1 seconds. At periods less than 0.1 seconds, the median spectral ratios for the modified motions are less than those of the scaled motions due to their smaller *PGA*. For the MA, 2% UHS, and 10% UHS target spectra, there is a shift in the median spectral ratios of the modified motions towards shorter periods and larger amplitudes when compared to the medians of the scaled motions. This observation corresponds with these three target spectra having slightly shorter average periods than the medians of the scaled motions and the scaled response spectra shifting to match these targets (see **Figure 6.7**). These differences are observed for both sites, although the noted differences occur

at slightly shorter periods for the stiff site as a result of its shorter site period (i.e., larger stiffness).

For the shallow sliding mass, **Figures 6.27** and **6.28** respectively compare the median Newmark-type displacements caused by the TD- and FD-modified motions to those caused by the scaled motions. Ratios of the modified-to-scaled median displacements for this depth are shown in **Figure 6.29**. Using the TD-modified motions generally results in slightly larger median displacements than using the FD-modified motions (within 20% of each other) possibly due to the TD-modified motions having larger I_a than their FD-modified counterparts. Travasarou and Bray (2003) showed that slope displacements and I_a are correlated. Newmark-type displacements caused by the modified motions for a shallow sliding mass are slightly larger than the displacements caused by their scaled counterparts for the CMS and Seed + σ target spectra. The modified motions produce 25 to 75% larger median displacements than their scaled counterparts for the CMS and Seed + σ target spectra, respectively, for the levee site. For the stiff site, the median displacements caused by the motions matched to the CMS and Seed + σ target spectra are only up to 25% larger than the displacements caused by the scaled motions. The median displacements caused by the motions matched to the MA and 10% UHS target spectra are less than those caused by the scaled motions. For these two target spectra, the scaled motions caused median Newmark-type displacements that were up to 35% larger than those caused by their modified counterparts for the levee site and 25 to 65% larger for the stiff site. The CMS and Seed + σ target spectra for scenario I are larger than the median response spectra of the scaled motions in the intermediate and long period ranges (see **Figure 6.7**). Conversely, the median response spectra of the scaled ground motions are larger than the MA, 2% UHS, and 10% UHS target spectra in this range of periods. These observations are likely what cause the Newmark-type displacements produced by the modified motions to be larger than those produced by the scaled motions for the CMS and Seed + σ target spectra, but smaller for the other target spectra. With increasing depth, the same observations are made. Median Newmark-type displacements produced by the sets of scaled motions for an intermediate sliding mass are compared to the median displacements produced by the sets of the TD- and FD-modified motions at the same depth in **Figures 6.30** and **6.31**, respectively, and the modified-to-scaled ratios for the median displacements at the corresponding depth are shown in **Figure 6.32**. **Figures 6.33** and **6.34** compare the median displacements produced by the scaled motions to those produced by the TD-

and FD-modified motions, respectively, for a deep sliding mass and **Figure 6.35** shows the corresponding modified-to-scaled ratios for these median displacements.

For scenario I, the responses caused by the TD-modified motions are very similar to those caused by the FD-modified motions (differences of less than 10% for many of the responses). The modified motions do generally cause responses that are less than the responses the scaled motions cause by factors of 1.2 to 1.35; however, these biases may be attributed to changes in the characteristics of the ground motions caused by modification rather than an inherent property of the modification techniques. The results of the seismic site response analyses for scenario II must be investigated to support these findings.

6.2.1.2 Geotechnical Seismic Responses versus Spectral Mismatch

Overall, the modified-to-scaled geotechnical seismic response ratios have well-defined trends with respect to spectral mismatch, as quantified by NE_s, for different period ranges. This finding signifies that it may be possible to estimate the seismic response produced by the modified motion given the mismatch and the seismic response produced by the scaled motion. Only NE_s was investigated for the spectral mismatch metric in these relationships since it is the optimum metric for the modified-to-scaled ground motion characteristic ratios (see **Section 4.2.1.1**). These relationships are generally observed for both sites, modification techniques, and the different values investigated for depth and k_y / k_{max}. The relationships between the modified-to-scaled geotechnical seismic response ratios and NE_s for all combinations of the site, modification technique, and depth (or period, or k_y / k_{max} value) appear to have exponential trends, so the natural logarithms of the ratios are calculated and plotted versus spectral mismatch. The modified-to-scaled geotechnical seismic response ratios were plotted against NE_s for all period ranges, as shown in **Figure 6.36**, to identify which period range results in the least amount of dispersion in the ratios. The period ranges used to define NE_s in the short ($NE_{s,SP}$), intermediate ($NE_{s,IP}$), and long period ($NE_{s,LP}$) ranges are 0.01 to 0.5 seconds, 0.5 to 3 seconds, and 3 to 5 seconds, respectively. The modified-to-scaled ratios for *CSR*, *MHA*, and spectral ratio have the least amount of dispersion when plotted versus NE_s while the modified-to-scaled displacement ratios have the least amount of dispersion when plotted versus $NE_{s,IP}$. **Appendix F** shows all the modified-to-scaled geotechnical seismic response ratios for scenario I plotted

against NE_s for the different period ranges at both sites for the different depths (or periods or k_y / k_{max} values).

The modified-to-scaled *CSR* ratios are plotted against spectral mismatch for the different sites and depths in **Figure 6.37**. Given an initial spectral mismatch, the TD- and FD-modified motions produce practically the same *CSR* which is likely the result of the modified motions having the same *PGA* and spectral shapes. The *CSR* produced by the modified motions are larger than those produced by the scaled motions when NE_s is negative and smaller than those produced by the scaled motions when NE_s is positive. As the response spectrum of the ground motion is increased to match the target spectrum (i.e., negative NE_s), the intensity of the ground motion and the *CSR* it produces should also be increased. Conversely, when the response spectrum of the ground motion is decreased, the *CSR* caused by the ground motion should decrease. With increasing depth, the slopes in the trends of the modified-to-scaled *CSR* ratios for the levee site somewhat increase while those of the trends for the stiff site remain relatively unchanged. This observation may be a result of the levee site being softer than the stiff site. At larger depths (i.e., 30 to 33 m), the trends for the levee and stiff sites are similar, which is expected given these responses are calculated at the base of the soil profile and have not been significantly impacted by any site effects. This observation suggests that near the base of the soil profile (i.e., within the bottom 25% of the soil profile), the effects of modification on the geotechnical seismic responses are independent of the site. Similar observations are made for the relationship between the modified-to-scaled *MHA* ratios and spectral mismatch, as shown in **Figure 6.38**, since *MHA* and *CSR* are closely related.

Figure 6.39 shows the ratios of the modified-to-scaled spectral ratios for periods of 0.25, 0.49, and 1.95 seconds for the motions at both sites. For a given spectral mismatch, the TD- and FD-modified motions are observed to have similar spectral ratios for both sites and all three periods, as both sets of modified motions closely match the target spectra. For the levee site, relatively strong relationships are observed between ratios of the modified-to-scaled spectral ratios and spectral mismatch for periods of 0.25 and 0.49 seconds. For the levee site at these periods, the ratio of the *Sa* at the surface to the *Sa* at the base of the soil profile is larger for the modified motions when NE_s is positive, but smaller when NE_s is negative. This trend is not observed at larger periods for the levee site or at any of the periods for the stiff site.

The modified-to-scaled Newmark-type displacement ratios for both modification techniques and the different sliding masses at both sites are shown in **Figures 6.40** and **6.41** for k_y / k_{max} values of 0.05 and 0.15, respectively. For negative $NE_{s,IP}$, the response spectrum of the scaled ground motion is increased to match the target spectrum at periods slightly above those of the sites. As a result, the intensity of the motion is increased during modification, causing it to produce larger displacements than its scaled counterpart. Slope displacements caused by the modified motions are less than those caused by the scaled motions for positive $NE_{s,IP}$. For more positive $NE_{s,IP}$, the displacements produced by the TD-modified motions are slightly larger than those produced by the FD-modified motions. FD-modified motions with large positive NE_s or $NE_{s,IP}$ are observed to have smaller intensities, as quantified by I_a, than their TD-modified counterparts (see **Section 4.2.1.1**). Slope displacements have been found to be correlated to I_a (Travasarou and Bray 2003) which could explain why the TD-modified motions cause larger displacements than the FD-modified motions for a large $NE_{s,IP}$. There is a slight increase in the slopes of the trends for the levee site with increasing depth probably as a result of the levee soil profile being softer. For varying k_y / k_{max}, there does not appear to be any change in the relationship between the modified-to-scaled displacement ratios and spectral mismatch; however, only two k_y / k_{max} values have been examined.

The modified-to-scaled seismic response ratios are clearly related to spectral mismatch. Furthermore, the observed trends do not appear to be significantly affected by the site conditions or depth (or period or k_y / k_{max} value). The results for the second scenario must be examined to support these observations.

6.2.2 Results for Scenario II

Eighty out of 1500 scaled ground motions, including 30 of the optimally scaled motions for the 2% UHS, and 15 TD- and FD-modified ground motions from scenario II produce τ_{max} that exceed τ_{all} by more than 10% for the levee site. Approximately 300 scaled and 250 TD- and FD-modified motions from scenario II produce τ_{max} that exceed τ_{all} by at least 10% for the stiff site. For the MA + σ, 10% UHS, and Seed target spectra, none of the modified motions produce τ_{max} that exceed τ_{all}. Excluding the motions optimally scaled to match the 2% UHS target, only 25 or fewer scaled motions for each target spectrum exceed the τ_{all} by more than 10%. Many of the motions from scenario II that exceed τ_{all} for the stiff site (105 and 170 scaled and modified

motions, respectively) are matched to the 2% UHS. Truly nonlinear analyses may be required for the scaled and modified motions for the 2% UHS target spectrum in scenario II for the stiff site, but the results of the geotechnical seismic analyses for these two spectra are included for completeness.

6.2.2.1 Median Response Comparison

The median responses caused by the motions from the second scenario have similar shapes to those caused by the motions from scenario I, although the median responses for scenario II are generally larger in intensity as a result of the larger intensities for the ground motions in this scenario. Relative to the median responses caused by the optimally scaled motions, the modified motions in scenario II produce larger responses than the modified motions in scenario I. The target spectra for scenario II have larger values than the medians of the optimally scaled ground motions (see **Figure 6.8**), which leads to the modified motions producing larger responses than the scaled motions in this scenario. For scenario I, the optimally scaled ground motions generally have median response spectra that are approximately equal to or slightly greater than the target spectra (see **Figure 6.7**), causing the modified motions to produce smaller responses than their scaled counterparts.

Figures 6.42 and **6.43** respectively show the γ_{max} median profiles produced by the TD- and FD-modified motions from scenario II compared to those produced by the scaled motions. The modified-to-scaled ratios for these median profiles are shown in **Figure 6.44**. Generally, the TD- and FD-modified motions for scenario II produce very similar γ_{max} for both sites as a result of both sets of modified motions closely matching the target spectra. The γ_{max} caused by the scaled motions are only slightly larger than those caused by the modified motions for scenario II (within approximately 25%) for both soil profiles and most of the target spectra. For the CMS target spectrum, the medians of the γ_{max} produced by the modified motions are equal to or greater than those produced by the scaled motions at all depths for both sites. For depths between 15 and 20 m, the modified motions for the CMS cause significantly larger γ_{max} than their scaled counterparts (up to factors of 1.8 and 2.3 for the levee and stiff sites, respectively) because the CMS has significantly larger values than the median response spectrum of the optimally scaled motions between periods of 0.2 and 2.5 seconds. The motions matched to the Seed target spectrum using both techniques for the stiff site produce significantly smaller γ_{max} than the

optimally scaled motions for depths to 10 m (factors as large as 3). This observation may be the result of the scaled motions for the Seed target spectrum having a larger median *PGA* than the modified motions, as shown in **Table 6.2**. The normalized median profiles of γ_{max} for the TD- and FD-modified motions are shown in **Figures 6.45** and **6.46**, respectively. For the levee site, the γ_{max} produced by the modified motions are more impacted by the site effects, leading to about 50% larger normalized γ_{max} than those for the scaled motions. The normalized γ_{max} for the motions matched to the CMS are also about 50% larger than those of their scaled counterparts for the stiff site. However, for the motions matched to the Seed spectrum for the stiff site, the normalized γ_{max} for the scaled ground motions are more largely impacted by the site effects than their modified counterparts (normalized γ_{max} for the scaled ground motions are larger by a factor of 2).

The median *CSR* profiles produced by the TD- and FD-modified motions from scenario II for both sites are compared to the CSR profiles produced by the scaled motions in **Figures 6.47** and **6.48**, respectively. **Figure 6.49** shows the modified-to-scaled ratios for these *CSR* medians. The TD- and FD-modified motions from scenario II produce very similar *CSR* for both sites. The *CSR* produced by the scaled and modified motions from scenario II for both sites are within about 20% of each other, with the scaled ground motions producing slightly larger *CSR*. For the stiff site, the motions matched to the Seed target spectrum result in 30% smaller *CSR* than their scaled counterparts at depths less than 5 m. The motions matched to the CMS produce larger *CSR* than the scaled motions for all depths within the stiff soil profile. **Figures 6.50** and **6.51** show the normalized median *CSR* profiles for the TD- and FD-modified motions, respectively, compared to those for the scaled ground motions. Site effects for the levee site lead to the modified motions for scenario II producing 10 to 30% larger *CSR* than the scaled motions. In the top 5 to 10 m of the profile for the stiff site, the scaled motions cause about 25% larger *CSR* than the motions matched to the 2% UHS and Seed target spectra. The motions matched to the other spectra and their scaled counterparts for the stiff site are similarly affected by site effects.

Figures 6.52 and **6.53** compare the median *MHA* caused by the TD- and FD-modified motions, respectively, to those caused by the scaled motions. The modified-to-scaled ratios for the medians of *MHA* are shown in **Figure 6.54**. The TD- and FD-modified ground motions produced similar *MHA* for both sites. Since the TD- and FD-modified motions both closely

match the target spectra, they produce similar medians for γ_{max}, *CSR*, and *MHA*. Overall, the scaled ground motions result in 10 to 30% larger *MHA* than the modified motions for both sites. Since the modified-to-scaled median *PGA* ratios for scenario II, shown in **Table 6.2**, are approximately between 0.8 and 1.0 (ratios of 0.6 for the Seed target spectrum), the median *MHA* produced by the modified motions are slightly smaller than those produced by the optimally scaled motions. The *MHA* produced by the motions matched to the Seed target spectrum for scenario II are smaller than those produced by their scaled counterparts by factors as large as 1.65 since the modified-to-scaled *PGA* ratio for this target spectrum is significantly smaller than 1. The median *MHA* produced by the motions matched to the CMS for scenario II are equal to or slightly larger than those produced by their scaled counterparts, possibly due to this target spectrum being larger than the median response spectrum for the corresponding scaled ground motions. The normalized median *MHA* for the TD- and FD-modified motions are shown in **Figures 6.55** and **6.56**, respectively. For the levee site, the normalized *MHA* medians for the scaled and modified motions are impacted the same by site effects (within 15%). The normalized median *MHA* produced by the motions matched to the Seed target spectrum for the levee site are increased more (up to 30%) by site effects than those produced by the scaled motions. Site effects for the stiff site result in the motions matched to the CMS and 2% UHS target spectra producing 10% larger normalized *MHA* medians than the scaled motions for depths to 5 m.

The median spectral ratios for the TD- and FD-modified motions from scenario II are compared to those for the scaled motions in **Figures 6.57** and **6.58**, respectively. Ratios of the modified-to-scaled median spectral ratios for the motions in scenario II are shown in **Figure 6.59**. The median spectral ratios for the TD- and FD-modified motions are similar for both sites; however, the FD-modified motions result in slightly larger (up to 20%) spectral ratios than the TD-modified motions for periods less than 0.1 seconds. The modified motions have spectral ratios that are generally within 25% of those for the optimally scaled motions from scenario II for both sites.

Median Newmark-type displacements caused by the TD- and FD-modified motions in scenario II for a shallow sliding mass are compared to those caused by the scaled motions in **Figures 6.60** and **6.61**, respectively, and the modified-to-scaled median displacement ratios for this sliding mass are shown in **Figure 6.62**. For both sites, the displacements caused by the FD-modified motions are only slightly larger (about 10% larger) than those caused by the TD-

modified motions for this sliding mass. However, the motions matched to the CMS using the FD technique induce 25 to 40% larger slope displacements than their TD-modified counterparts for this sliding mass at both sites. This observation is likely the result of the motions matched to the CMS in scenario II using the FD technique having 25% larger I_a than the motions matched to the CMS using the TD technique (see **Table 6.2**). For both sites, the displacements caused by the modified motions in scenario II for all target spectra are generally equal to or larger than (factors up to 2) those caused by the scaled motions as a result of the target spectra for scenario II having larger values than the scaled motions in the intermediate and long period ranges. Similar observations are made for the median Newmark-type displacements induced by the scaled and modified motions for intermediate and deep sliding masses as well. **Figures 6.63** and **6.64** compare the median Newmark-type displacements caused by the TD- and FD-modified motions, respectively, to those caused by the scaled motions for an intermediate sliding mass. The ratios of modified-to-scaled median Newmark-type displacements caused by the motions in scenario II for the intermediate sliding mass are shown in **Figure 6.65**. For a deep sliding mass, **Figures 6.66** and **6.67** compare the median slope displacements induced by the TD- and FD-modified motions, respectively, to those induced by the scaled motions in scenario II. **Figure 6.68** shows the modified-to-scaled median Newmark-type displacement ratios for a deep sliding mass.

Based on the results of scenarios I and II, it appears that motions modified using the TD technique produce similar responses to the motions modified using the FD technique for geotechnical dynamic analyses. This finding suggests that both modification techniques may be appropriate for use in geotechnical dynamic analyses. Also, differences between the responses caused by the scaled motions and the modified motions appear to be the result of the effects of modification on the ground motion characteristics rather than a property of the modification technique.

6.2.2.2 Geotechnical Seismic Responses versus Spectral Mismatch

Overall, the trends observed in the relationships between the logarithmic modified-to-scaled geotechnical seismic response ratios and spectral mismatch are very similar for scenarios I and II. The dispersion in the logarithmic modified-to-scaled response ratios for scenarios I and II also appear to be very similar. These observations are made for both modification techniques for the different depths (or periods, or k_y / k_{max} values) and both sites investigated in this study.

Figures 6.69 and **6.70** show the plots of the logarithmic modified-to-scaled *CSR* ratios versus NE_s for the TD- and FD-modified motions, respectively, from scenarios I and II. The logarithmic modified-to-scaled *MHA* ratios are plotted against NE_s in **Figures 6.71** and **6.72** for the TD- and FD-modified motions, respectively, from scenarios I and II. The natural logarithms of the modified-to-scaled *CSR* and *MHA* ratios for the FD-modified motions from scenario II appear to be slightly larger than those of the FD-modified motions from scenario I for all three depths at both sites when NE_s is positive (see **Figures 6.70** and **6.72**, respectively). This observation for both response parameters can likely be attributed to the FD-modified motions from the second scenario having larger intensities than the FD-modified motions from the first scenario, as exhibited by the larger modified-to-scaled median I_a ratios in **Table 6.2**. **Figures 6.73** and **6.74** show the logarithmic ratios of the modified-to-scaled spectral ratios plotted versus NE_s for the TD- and FD-modified motions, respectively, from scenarios I and II. Ratios of the modified-to-scaled spectral ratios for the FD-modified motions from scenario II are slightly smaller than those of the FD-modified motions from scenario I for periods of 0.25 and 0.49 seconds, but slightly larger than those of the FD-modified motions from scenario I for 1.95 seconds for both sites. For a k_y / k_{max} value of 0.05, **Figures 6.75** and **6.76** show the natural logarithms of the modified-to-scaled Newmark-type slope displacement ratios plotted against $NE_{s,IP}$ for the TD- and FD-modified motions, respectively, from scenarios I and II. Similar plots for a k_y / k_{max} value of 0.15 are shown in **Figures 6.77** and **6.78** for the TD- and FD-modified motions, respectively, from scenarios I and II.

Since the relationships between the logarithmic modified-to-scaled displacement ratios and spectral mismatch are similar for scenarios I and II, the ratios for the motions in scenarios I and II are combined to develop preliminary regression equations for the Newmark-type slope displacements. Regression equations were developed for the different sites, modification techniques, and sliding depths investigated. The development of the regression equations was only performed for a k_y / k_{max} value of 0.05 since the two k_y / k_{max} values investigated had very similar trends.

Regression curves for the TD- and FD-modified motions for both sites and the three different sliding masses are shown in **Figure 6.79**. A logarithmic functional form, shown in **Equation 6.4**, is observed to best define the trends (i.e., largest R^2 values) while still having significant coefficients.

$$\ln\left(Displacement_{\text{mod}} / Displacement_{scaled}\right) = b_{gs} \ln\left(NE_{s,IP} - a_{gs}\right) \quad \textbf{(6.4)}$$

a_{gs} and b_{gs} represent coefficients of the regression equations for the modified-to-scaled geotechnical seismic response ratio – spectral mismatch relationships. The coefficients of the regression curves developed for the relationship between the modified-to-scaled Newmark-type displacement ratios and spectral mismatch are shown in **Table 6.3** for each combination of depth, site, and modification technique. R^2 values of the calculated regression equations are also shown in **Table 6.3**. The regression curves shown in **Figure 6.79** further illustrate the small differences between the modified-to-scaled Newmark-type slope displacement ratios estimated for the TD and FD modification techniques using spectral mismatch. Although the modified-to-scaled slope displacement ratios estimated for large, positive $NE_{s,IP}$ are larger for the TD-modified motions relative to those for the FD-modified motions (approximately one log unit larger), the predicted modified-to-scaled ratios for Newmark-type displacements are identical for both modification techniques for $NE_{s,IP}$ values less than 1. Therefore, either modification technique can be used to calculate Newmark-type slope displacement when the $NE_{s,IP}$ of the scaled ground motion is less than 1.

The relationships between the modified-to-scaled seismic response ratios and spectral mismatch for scenario II have similar trends to those observed for scenario I. This observation suggests that these relationships may generally apply to all earthquake scenarios. Regression equations were developed to describe the relationship between the modified-to-scaled Newmark-type displacement ratios and spectral mismatch for both sites and three sliding masses and a k_y / $k_{\max}$ value of 0.05; however, more sites, sliding masses, and k_y / $k_{\max}$ values must be investigated before these regression equations can be recommended for use in practice.

6.3 Conclusions

The following conclusions and recommendations are made from the study of the impact of ground motion modification on the results of site response analyses:

- No significant differences were observed between the median geotechnical seismic responses produced by the TD-modified motions and those produced by the FD-modified motions: This is a major finding as it potentially signifies that either technique (i.e., TD or FD) is appropriate for geotechnical seismic response analyses. The TD-modified motions generally

produce γ_{max}, *CSR*, *MHA*, and spectral ratios within 10% of those the FD-modified motions produce for both scenarios. One notable difference between the medians produced by the TD- and FD-modified motions is observed in the Newmark-type displacements. The TD-modified motions cause 10 to 20% larger Newmark-type displacements than the FD-modified motions for scenario I while the FD-modified motions cause about 10% larger displacements than the TD-modified motions for scenario II. The TD-modified motions generally have larger median I_a values than the FD-modified motions for scenario I (see **Table 6.1**), but the FD-modified motions have larger median values for I_a than the TD-modified motions for scenario II (see **Table 6.2**), which may explain the differences observed in the median Newmark-type displacements caused by the TD- and FD-modified motions. It should be noted that these observations are based on using the optimally scaled ground motions, with *RMSE* values generally less than 0.65, and thus, supports the recommendation of scaling the ground motions to reduce mismatch prior to modification.

- Impact of modification on the geotechnical seismic responses appears to be influenced by the ground motion characteristics and response spectra of the scaled and modified motions: Overall, the scaled motions produce about 25 to 35% larger γ_{max}, *CSR*, and *MHA* medians than their modified counterparts for scenario I. However, the scaled and modified motions for scenario II produce median values of γ_{max}, *CSR*, and *MHA* that are similar (differences generally less than 20%). The differences observed in the responses produced by the scaled and modified motions are likely caused by differences between the median *PGA* and I_a of the scaled and modified motions (see **Tables 6.1** and **6.2**). Median Newmark-type displacements caused by the motions matched to the CMS and Seed + σ target spectra in scenario I are larger than those caused by the scaled motions for both sites (factors of 1.25 to 1.75 for the levee site and up to 1.25 for the stiff site), but those caused by the motions matched to the other spectra in this scenario are less than the displacements caused by the corresponding scaled motions by factors up to 1.65. For scenario II, the displacements caused by the modified motions for all target spectra are approximately equal to or larger than (factors as large as 2) the displacements caused by their scaled counterparts for both sites. As observed in **Figures 6.7** and **6.8** (for scenarios I and II, respectively), the target spectra are generally smaller than the median response spectra of the scaled motions for scenario I for periods in the intermediate and long period ranges, but larger than the median response spectra of the

scaled motions in the same range of periods for scenario II. Additionally, the TD-modified motions have larger median values for I_a than the FD-modified motions for scenario I (see **Table 6.1**), but the FD-modified motions have larger median values for I_a than the TD-modified motions for scenario II. As a result, the TD-modified motions cause 10 to 20% larger Newmark-type displacements than the FD-modified motions for scenario I while the FD-modified motions cause about 10% larger displacements than their TD-modified counterparts for scenario II. These observations suggest that biases observed between the dynamic responses caused by scaled and modified motions may be an effect of differences in their characteristics rather than the modification technique.

- Well-defined relationships are observed between the effects of modification on the geotechnical seismic responses and spectral mismatch, as quantified by normalized error (NE_s): When the modified-to-scaled *CSR*, *MHA*, and Newmark-type slope displacement ratios for the individual motions are plotted against NE_s (or $NE_{s,IP}$), well-defined trends are observed for the different modification techniques, sites, and sliding masses (or k_y / k_{max} values) investigated. Additionally, the relationships between the modified-to-scaled geotechnical seismic response ratios and spectral mismatch may be general for any earthquake scenario since similar results are observed in the trends for two different earthquake scenarios. These trends appear to be only somewhat impacted by the different site conditions and sliding masses, but further research on the impact of site condition and sliding mass on these trends is necessary. Given these well-defined relationships, the effect of modification on these geotechnical seismic responses can potentially be predicted using NE_s (or $NE_{s,IP}$), but more sites, sliding masses, and k_y / k_{max} values must be studied before providing regression equations for these relationships.
- Similar impact of site conditions on site response for scaled or modified motions: The impact of the site conditions on the γ_{max}, *CSR*, and *MHA* produced by the scaled and modified motions is similar (differences generally within 10 to 20%). This observation suggests that a direct comparison was made between the effects of different modification techniques on the medians for these responses of geotechnical dynamic analyses.

Table 6.1. Modified-to-scaled median ground motion characteristic ratios of the motions in scenario I for the different target spectra.

Ground Motion Characteristic		Target Spectrum				
		CMS	MA	2% UHS	10% UHS	Seed + σ
PGA	TD	0.87	0.99	0.88	0.92	0.49
	FD	0.87	0.99	0.88	0.92	0.49
PGV	TD	0.93	0.79	0.78	0.78	1.03
	FD	0.90	0.75	0.74	0.75	0.97
PGD	TD	1.44	1.35	1.60	1.39	2.18
	FD	1.07	1.04	1.08	1.07	1.85
I_a	TD	0.83	0.82	0.76	0.78	0.69
	FD	0.74	0.77	0.72	0.74	0.56
CAV	TD	0.97	0.94	0.94	0.93	0.95
	FD	0.90	0.91	0.89	0.90	0.84
$D_{5\text{-}95}$	TD	1.25	1.25	1.36	1.24	1.58
	FD	1.38	1.29	1.31	1.30	1.56
T_m	TD	1.17	0.94	0.98	0.96	1.51
	FD	1.21	0.85	0.85	0.85	1.62

Table 6.2. Modified-to-scaled median ground motion characteristic ratios of the motions in scenario II for the different target spectra.

Ground Motion Characteristic		Target Spectrum				
		CMS	MA + σ	2% UHS	10% UHS	Seed
PGA	TD	0.90	0.84	0.81	1.05	0.60
	FD	0.90	0.84	0.81	1.05	0.60
PGV	TD	1.02	0.97	0.98	0.89	1.15
	FD	0.92	0.85	0.82	0.79	0.98
PGD	TD	1.24	1.35	1.34	1.15	1.83
	FD	0.57	0.60	0.64	0.58	1.10
I_a	TD	1.09	0.87	0.81	0.89	0.81
	FD	1.35	0.98	0.88	1.03	0.82
CAV	TD	1.03	0.96	0.93	0.98	0.93
	FD	1.22	1.04	0.99	1.05	0.98
$D_{5\text{-}95}$	TD	0.96	1.03	1.02	1.02	1.03
	FD	1.09	1.14	1.15	1.13	1.17
T_m	TD	1.12	1.16	1.20	1.06	1.43
	FD	1.14	1.18	1.20	1.01	1.52

Table 6.3. Coefficients of the regression curves developed for the relationship between the logarithmic modified-to-scaled Newmark-type displacement ratios and spectral mismatch for different sites, depths, and modification technique for the motions from scenarios I and II and R^2 values.

		TD Modification			FD Modification		
Site	Depth (m)	a_g	b_g	R^2	a_g	b_g	R^2
Levee	3.0	-0.808	-1.424	0.79	-0.818	-1.749	0.85
	7.6	-0.808	-1.572	0.80	-0.815	-1.871	0.85
	13.7	-0.807	-1.797	0.78	-0.810	-1.904	0.80
Stiff	3.0	-0.811	-1.521	0.73	-0.816	-1.848	0.77
	7.6	-0.809	-1.556	0.75	-0.817	-1.904	0.80
	13.7	-0.808	-1.690	0.77	-0.835	-1.935	0.79

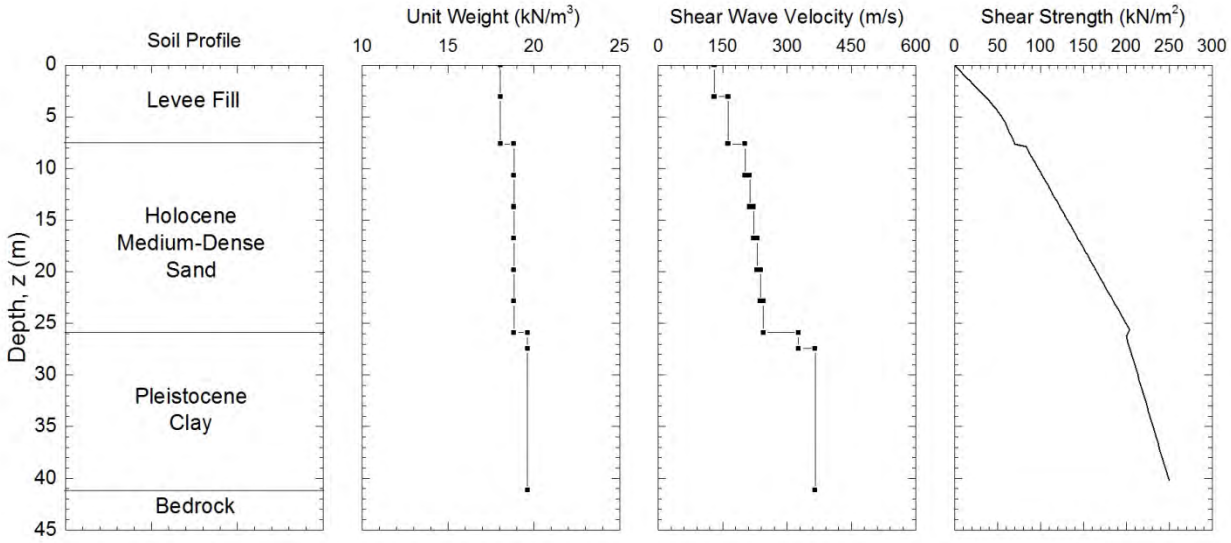

Figure 6.1. Soil profile, unit weight, shear wave velocity, and shear strength profiles for the levee site used in the study of the effects of modification on the geotechnical seismic responses.

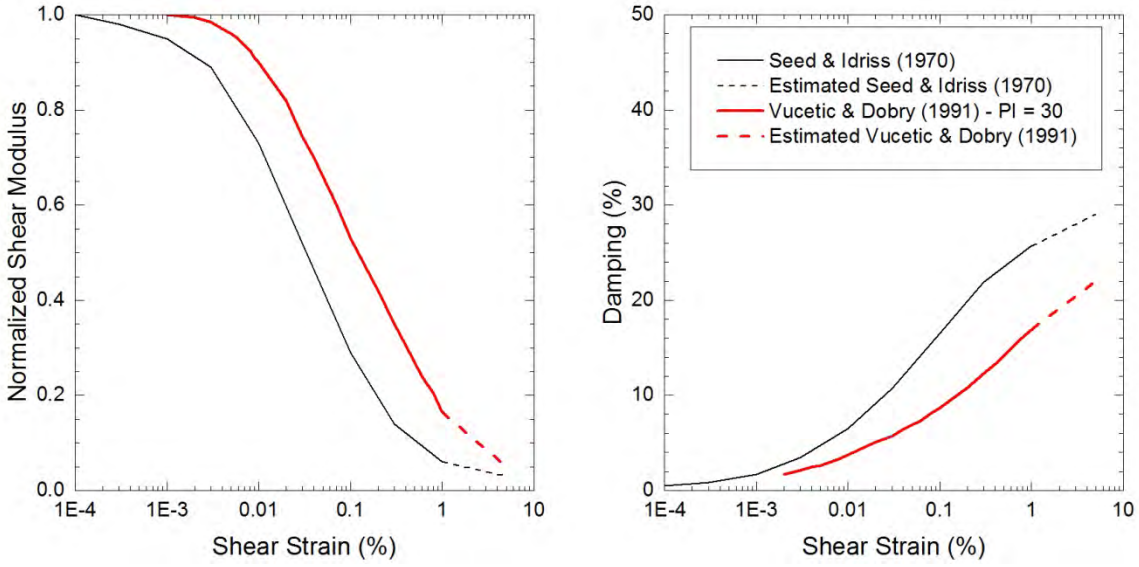

Figure 6.2. Normalized shear modulus and damping curves of the soil models for the levee site used in the study of the effects of modification on the geotechnical seismic responses. Extrapolated values are shown with a dashed line.

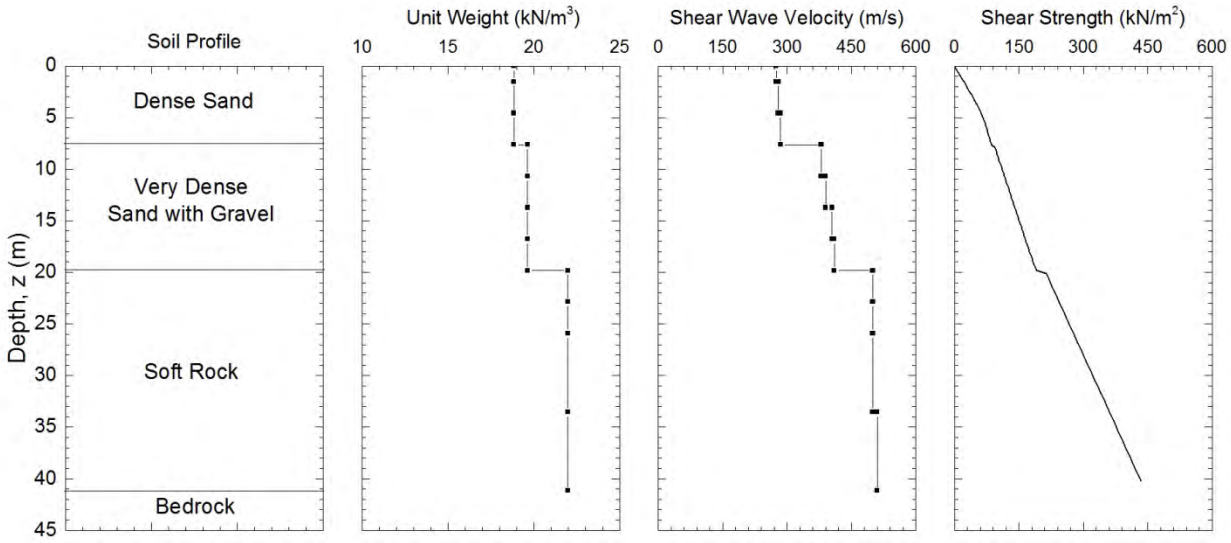

Figure 6.3. Soil profile, unit weight, shear wave velocity, and shear strength profiles for the stiff site used in the study of the effects of modification on the geotechnical seismic responses.

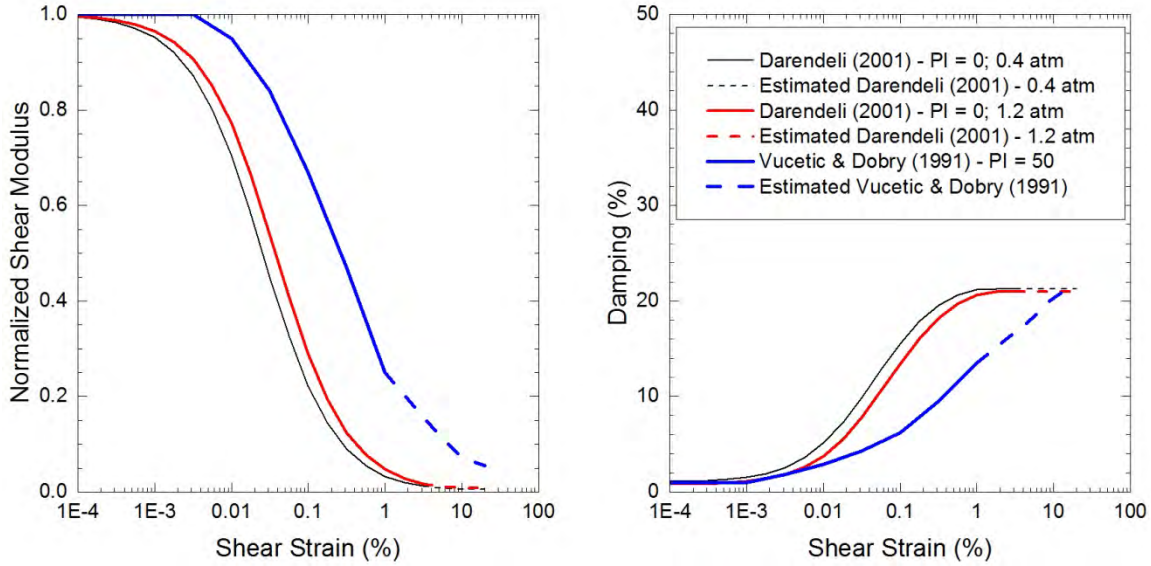

Figure 6.4. Normalized shear modulus and damping curves of the soil models for the stiff site used in the study of the effects of modification on the geotechnical seismic responses. Extrapolated values are shown with a dashed line.

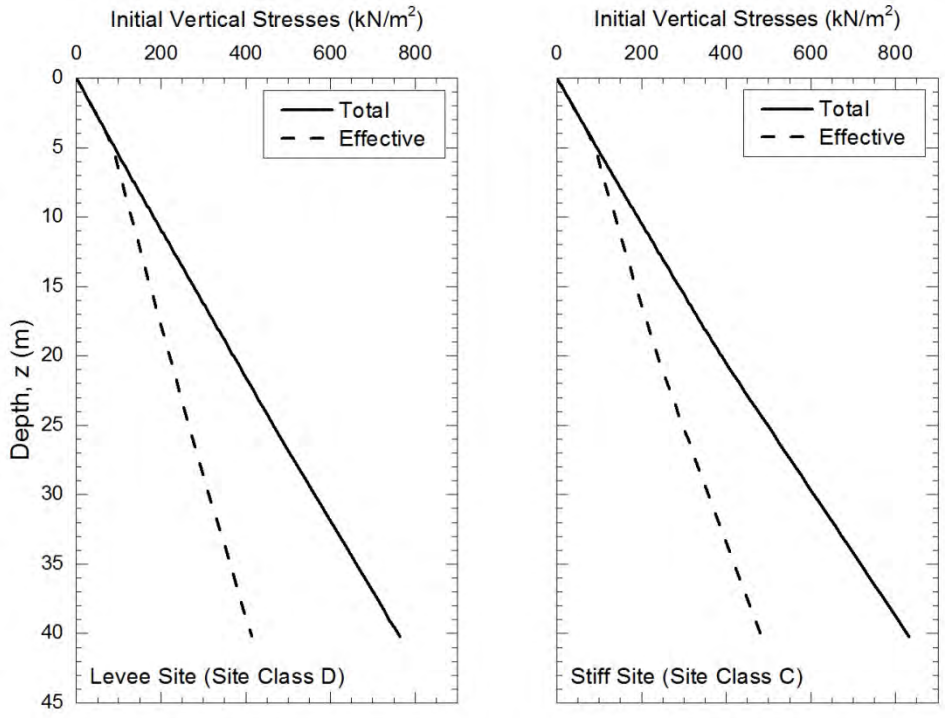

Figure 6.5. Initial total and effective vertical stress profiles for the levee and stiff sites.

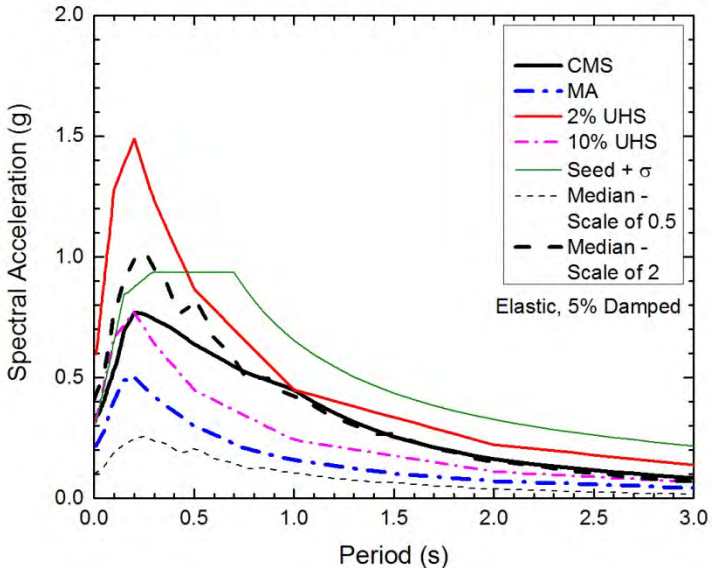

Figure 6.6. Median response spectra of the motions scaled by factors of 0.5 and 2 for scenario I compared to the target conditional mean spectrum (CMS; Baker 2011), mean spectrum from attenuation relationships (MA), 2% and 10% uniform hazard spectra (2% UHS and 10% UHS, respectively), and mean plus one standard deviation spectrum from Seed et al. (1997) (Seed + σ).

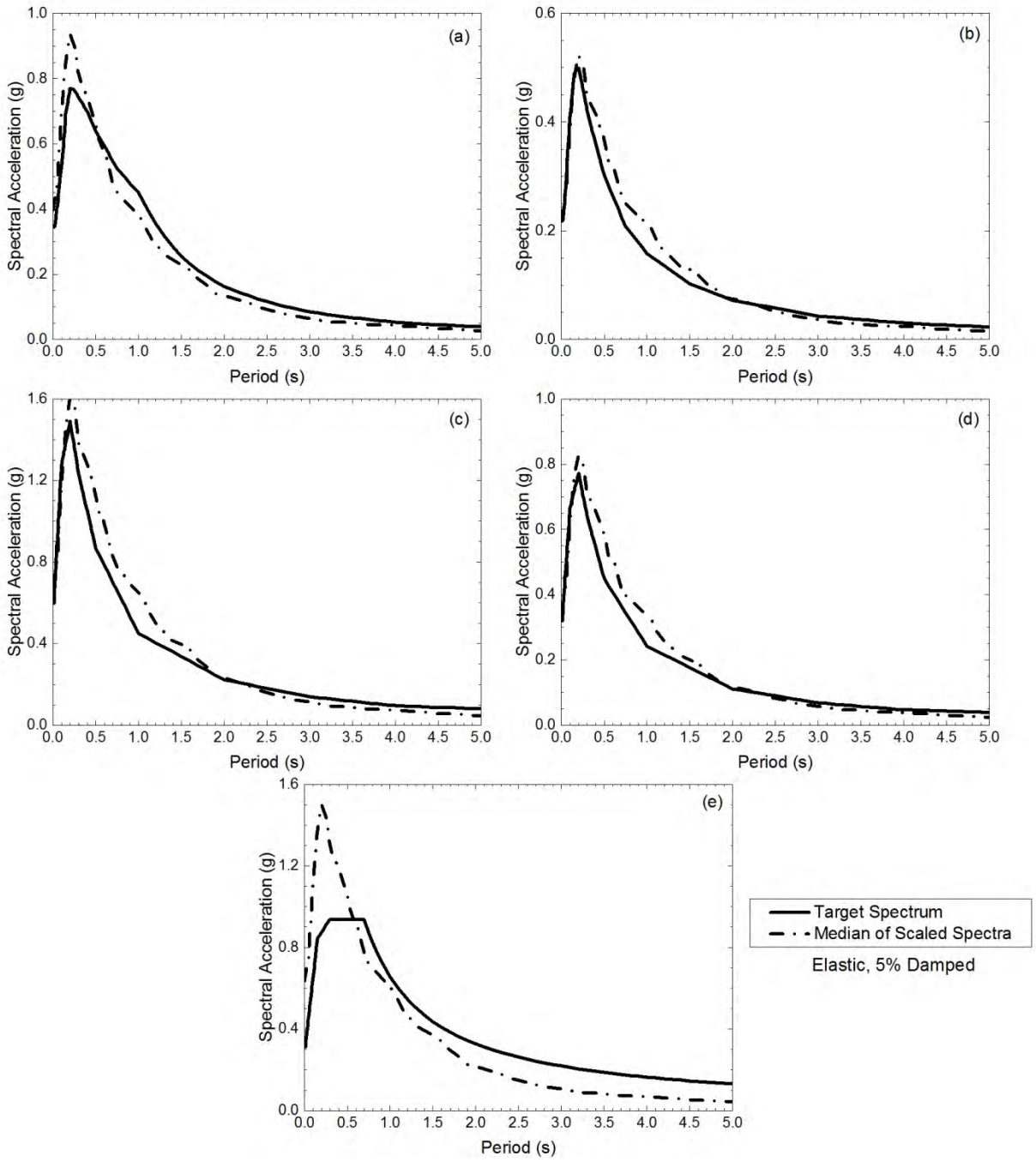

Figure 6.7. (a) Conditional mean spectrum (Baker 2011), (b) mean spectrum from attenuation relationships, (c) 2% uniform hazard spectrum, (d) 10% uniform hazard spectrum, (e) and mean plus one standard deviation spectrum from Seed et al. (1997) compared to the corresponding median response spectra of the optimally scaled ground motions for scenario I.

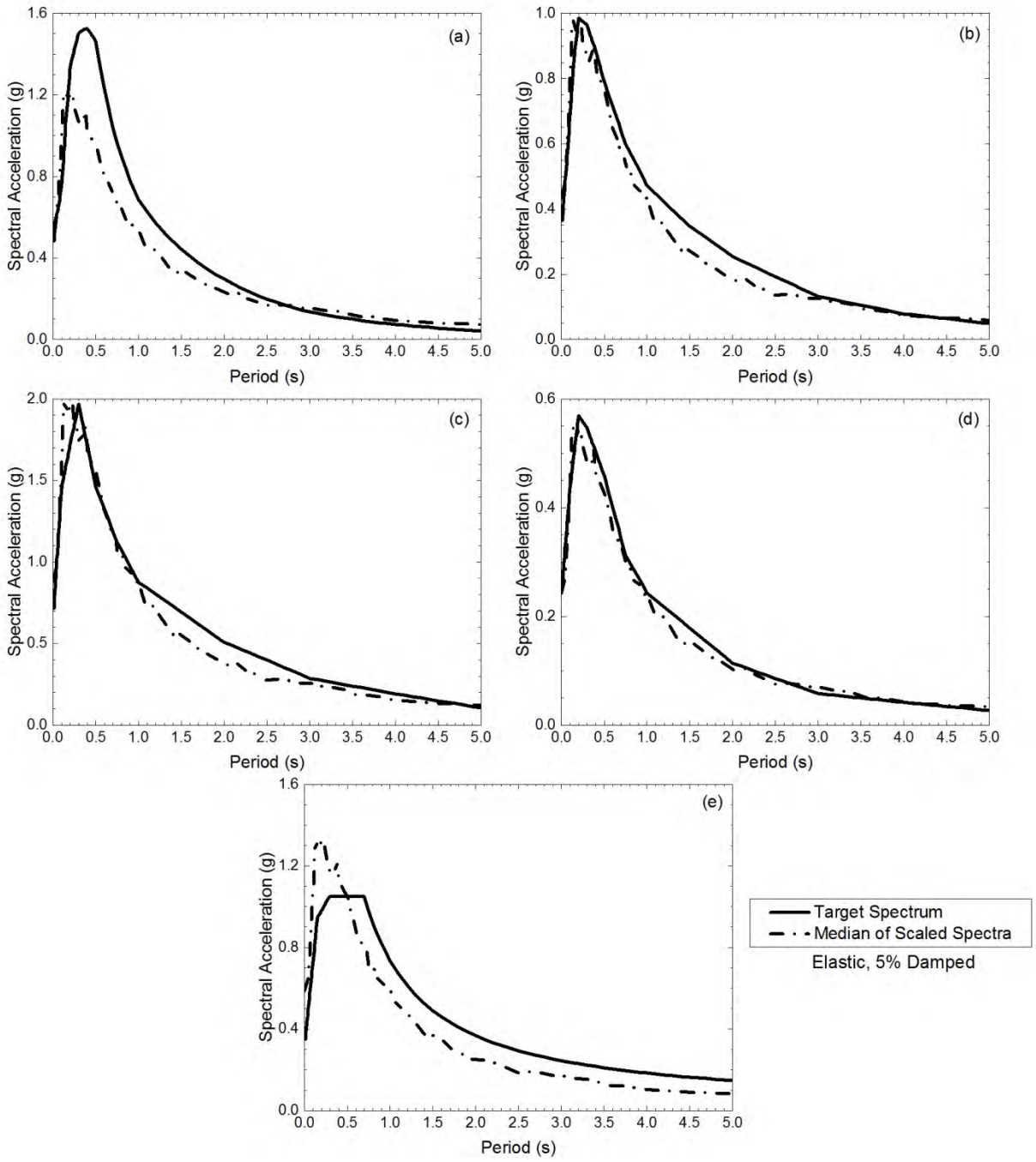

Figure 6.8. (a) Conditional mean spectrum (Baker 2011), (b) mean plus one standard deviation spectrum from attenuation relationships, (c) 2% uniform hazard spectrum, (d) 10% uniform hazard spectrum, (e) and mean spectrum from Seed et al. (1997) compared to the corresponding median response spectra of the optimally scaled ground motions for scenario II.

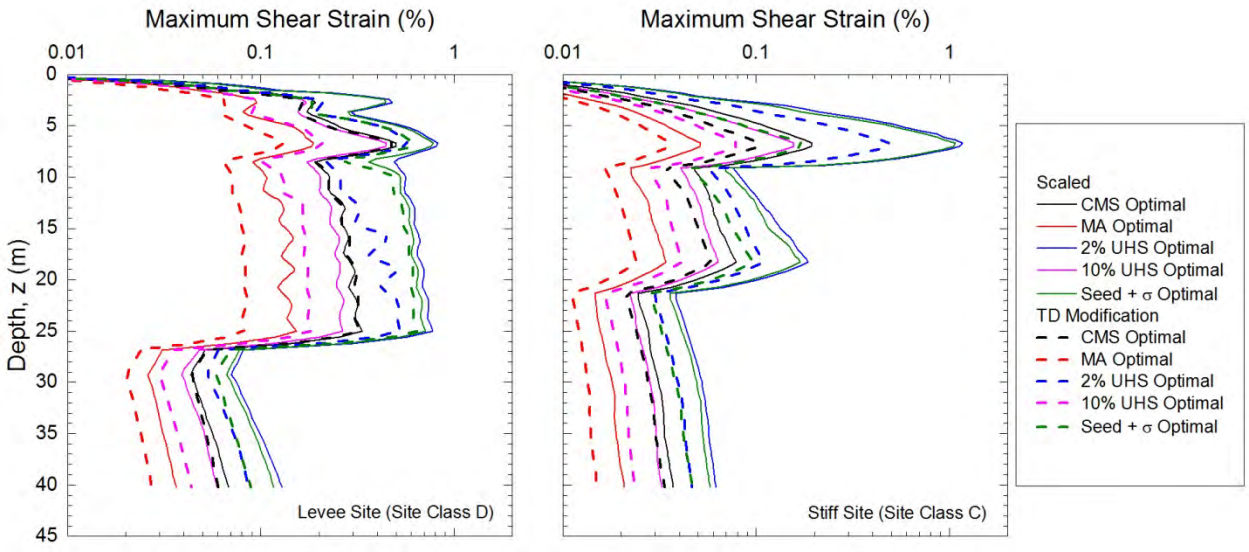

Figure 6.9. Median profiles of the maximum shear strains produced by the optimally scaled and TD-modified motions from scenario I at both sites for the different target spectra.

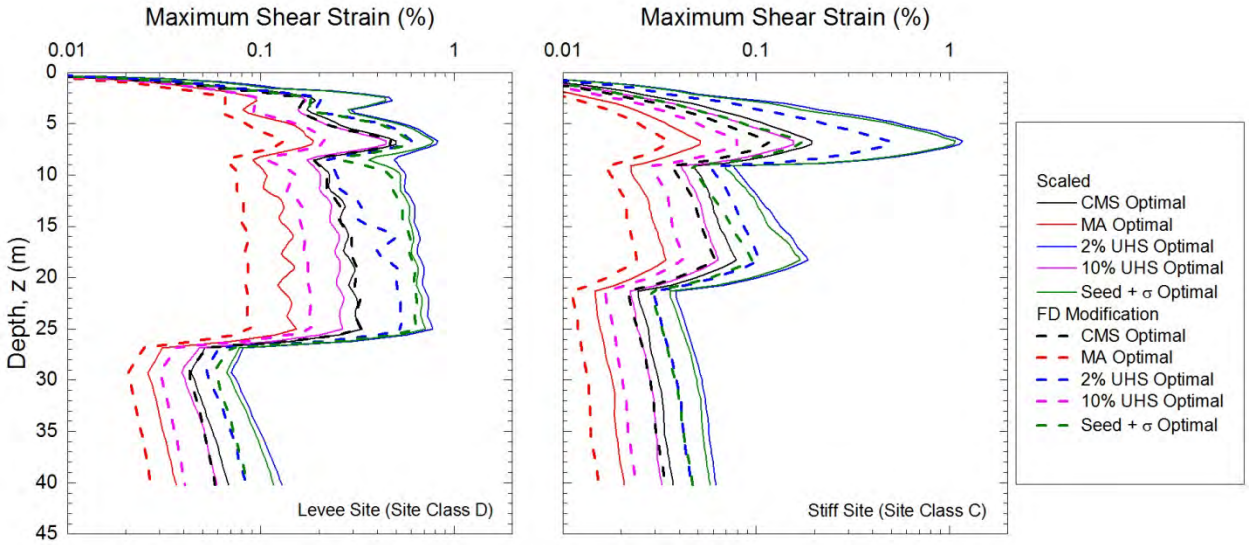

Figure 6.10. Median profiles of the maximum shear strains produced by the optimally scaled and FD-modified motions from scenario I at both sites for the different target spectra.

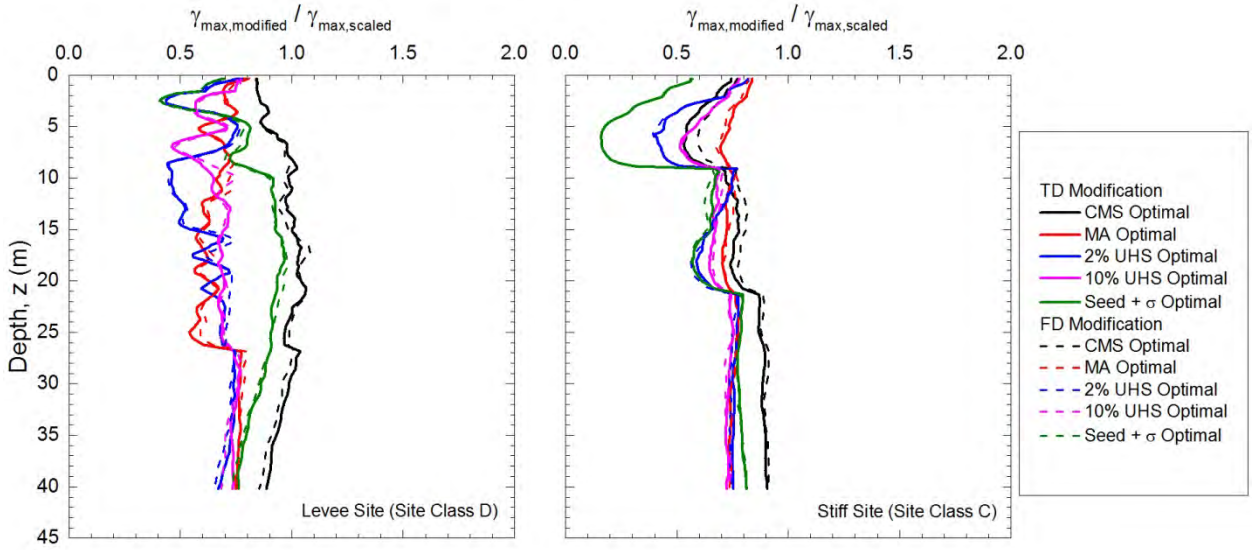

Figure 6.11. Profiles of the ratios of modified-to-scaled maximum shear strains (γ_{max}) for the medians produced by the optimally scaled and modified motions from scenario I at both sites for the different target spectra.

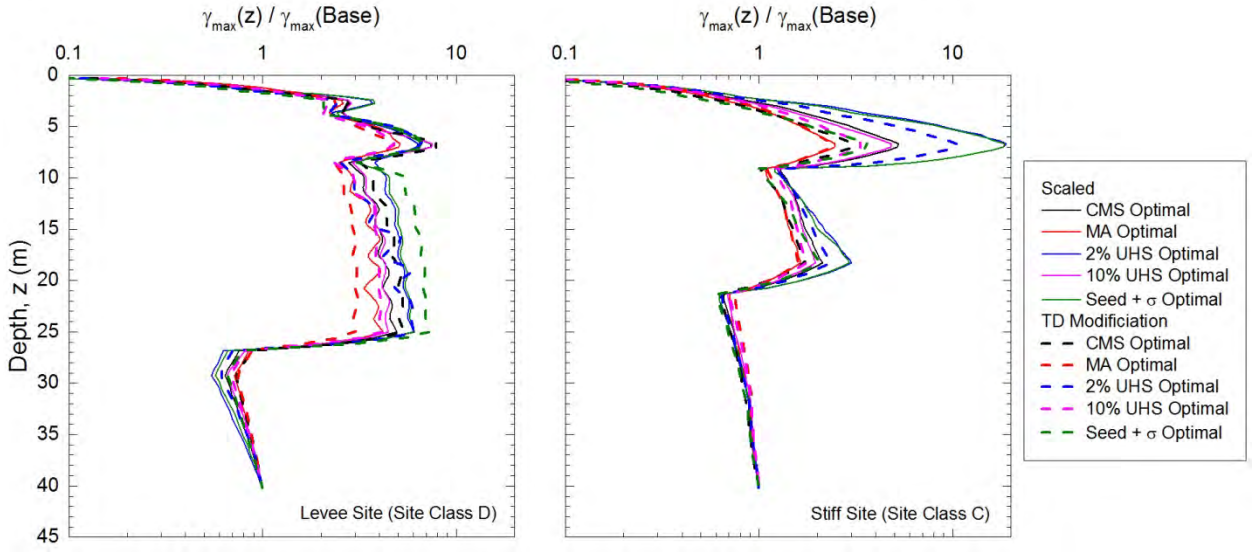

Figure 6.12. Profiles of the normalized maximum shear strain (γ_{max}) medians produced by the optimally scaled and TD-modified motions from scenario I at both sites for the different target spectra.

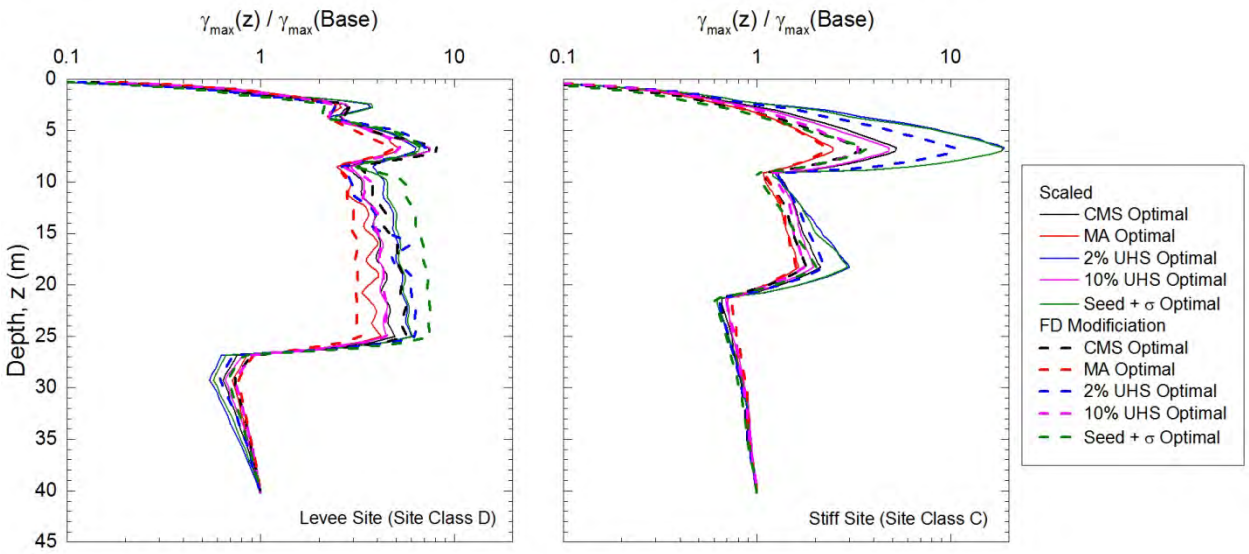

Figure 6.13. Profiles of the normalized maximum shear strain (γ_{max}) medians produced by the optimally scaled and FD-modified motions from scenario I at both sites for the different target spectra.

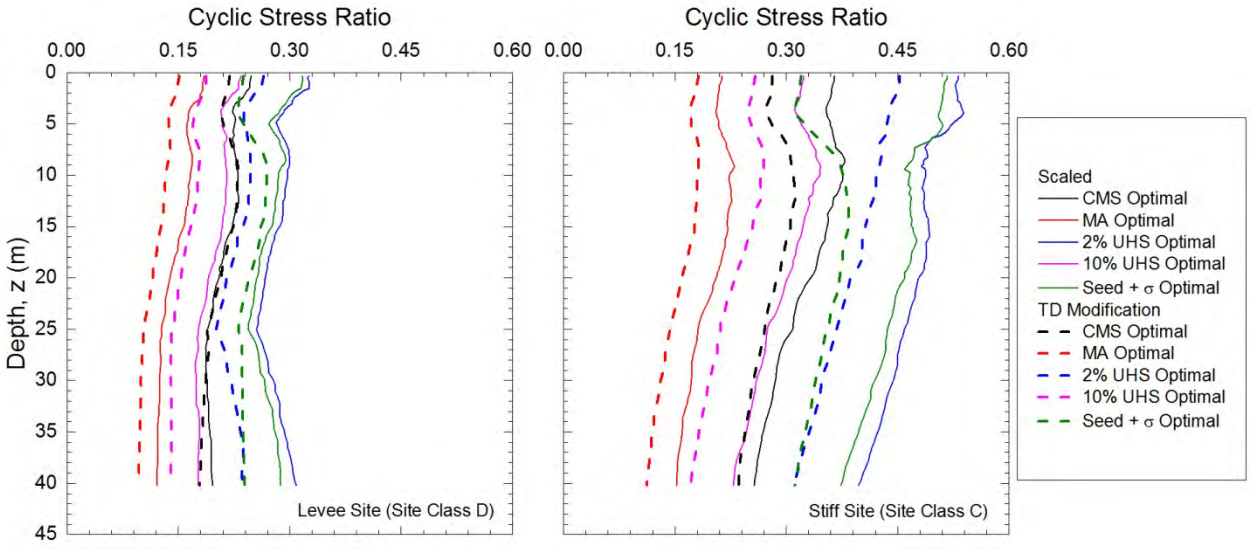

Figure 6.14. Median profiles for the cyclic stress ratios produced by the optimally scaled and TD-modified motions from scenario I at both sites for the different target spectra.

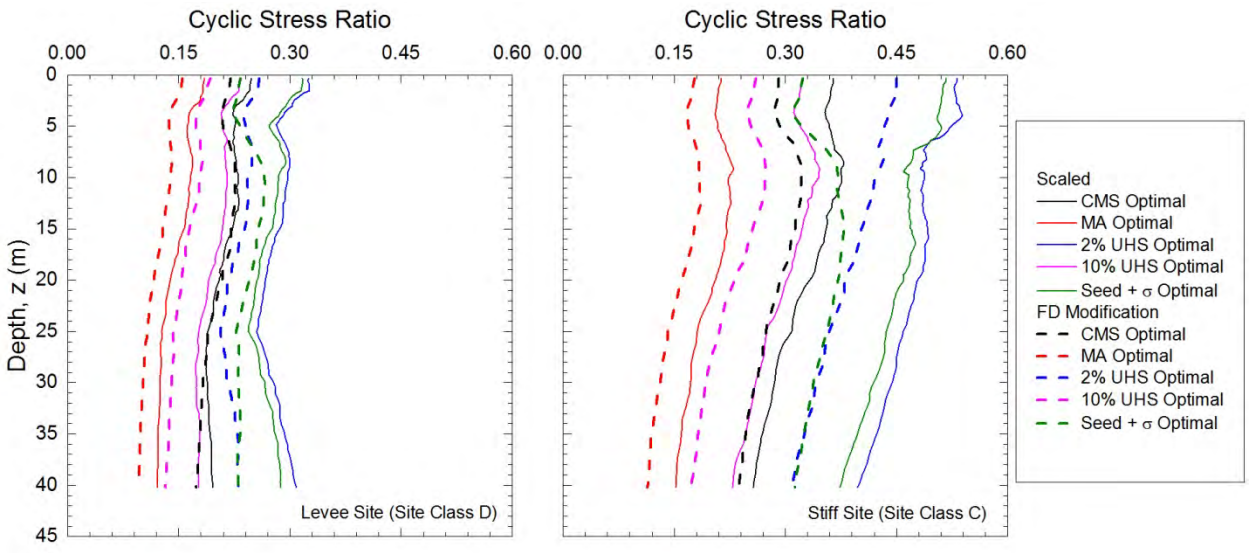

Figure 6.15. Median profiles for the cyclic stress ratios produced by the optimally scaled and FD-modified motions from scenario I at both sites for the different target spectra.

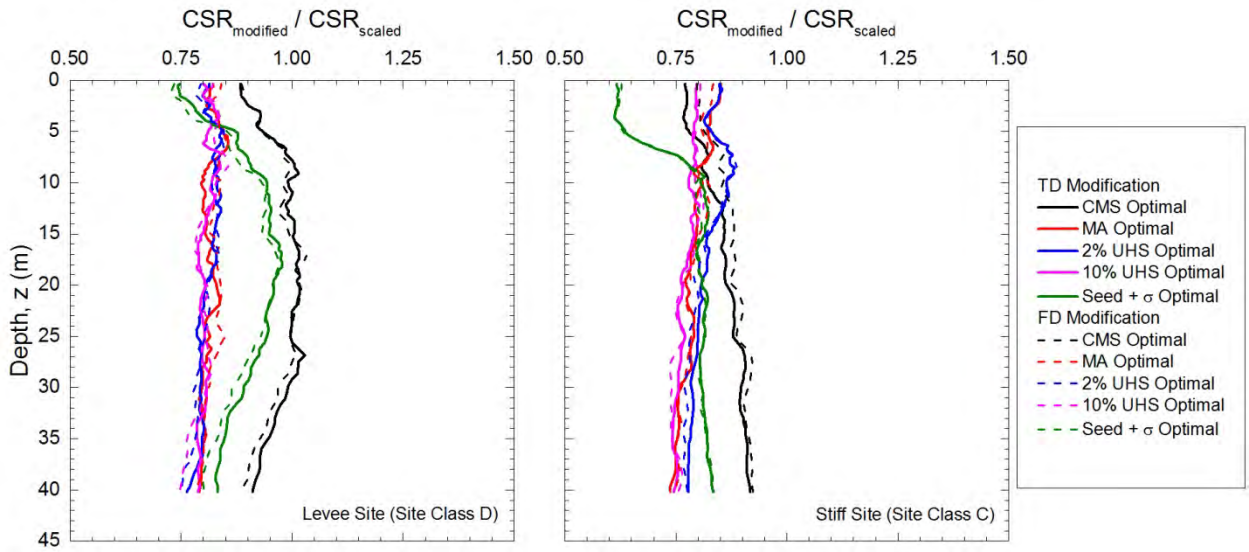

Figure 6.16. Profiles of the ratios of modified-to-scaled cyclic stress ratios (*CSR*) for the medians produced by the optimally scaled and modified motions from scenario I at both sites for the different target spectra.

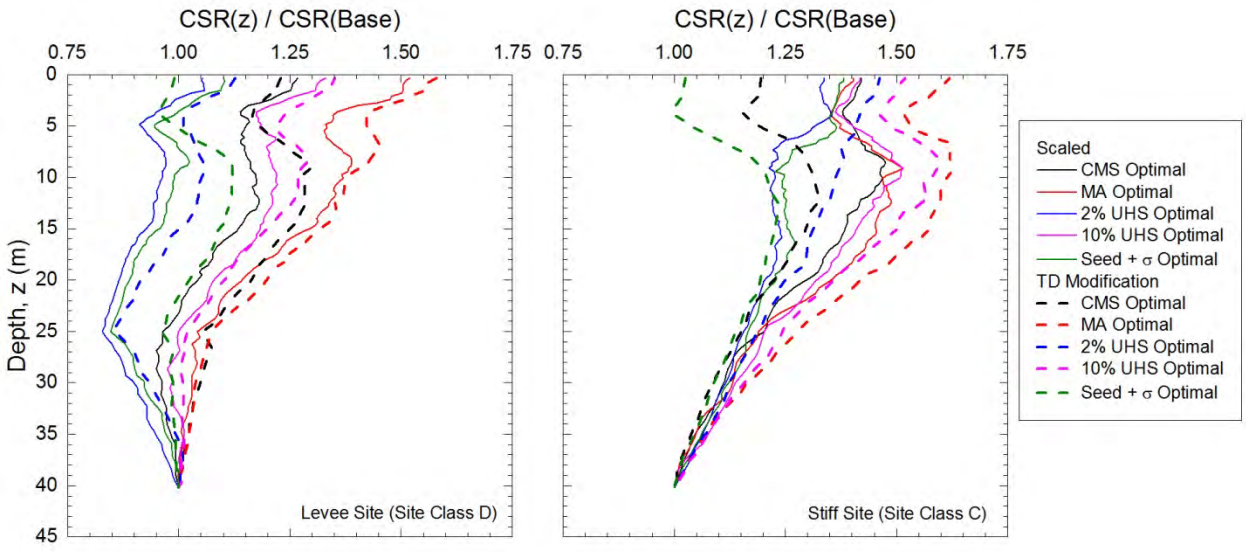

Figure 6.17. Profiles of the normalized median cyclic stress ratios (*CSR*) produced by the optimally scaled and TD-modified motions from scenario I at both sites for the different target spectra.

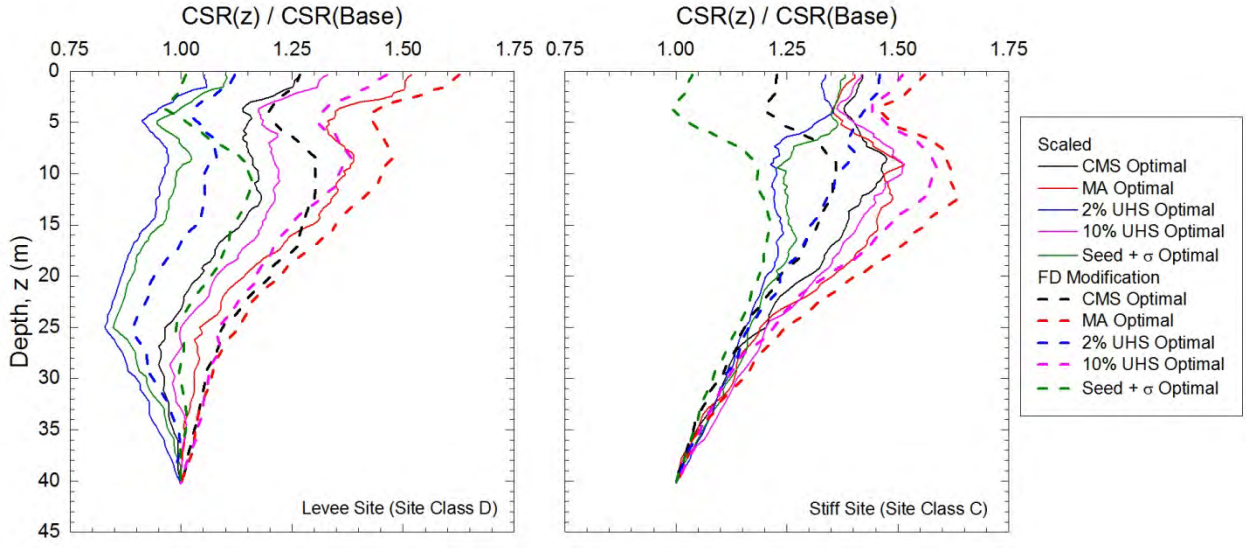

Figure 6.18. Profiles of the normalized median cyclic stress ratios (*CSR*) produced by the optimally scaled and FD-modified motions from scenario I at both sites for the different target spectra.

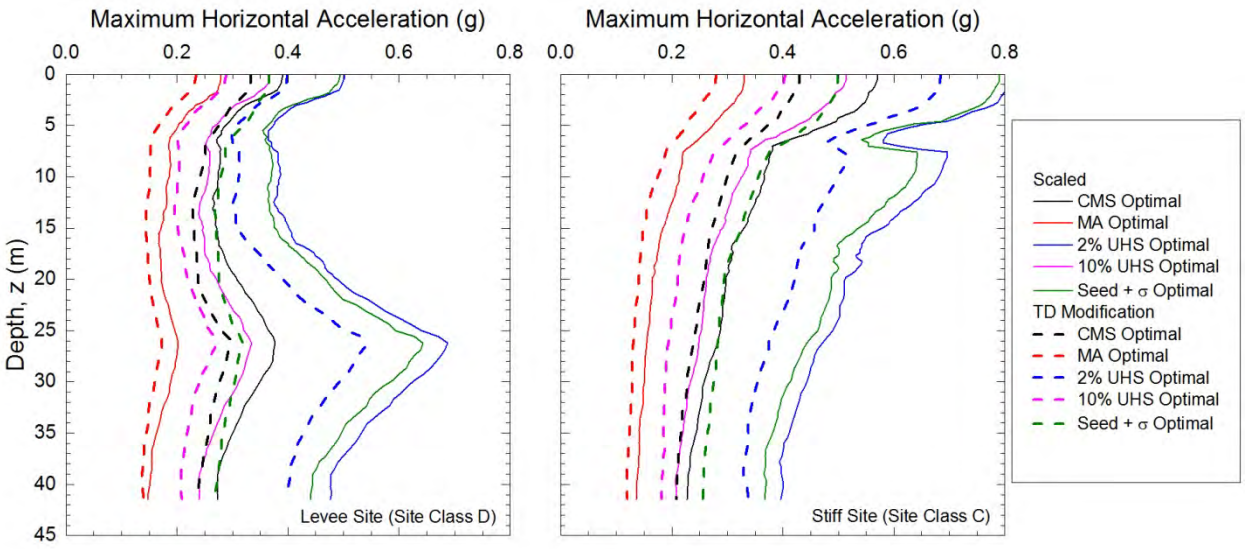

Figure 6.19. Median profiles of the maximum horizontal accelerations produced by the optimally scaled and TD-modified motions from scenario I at both sites for the different target spectra.

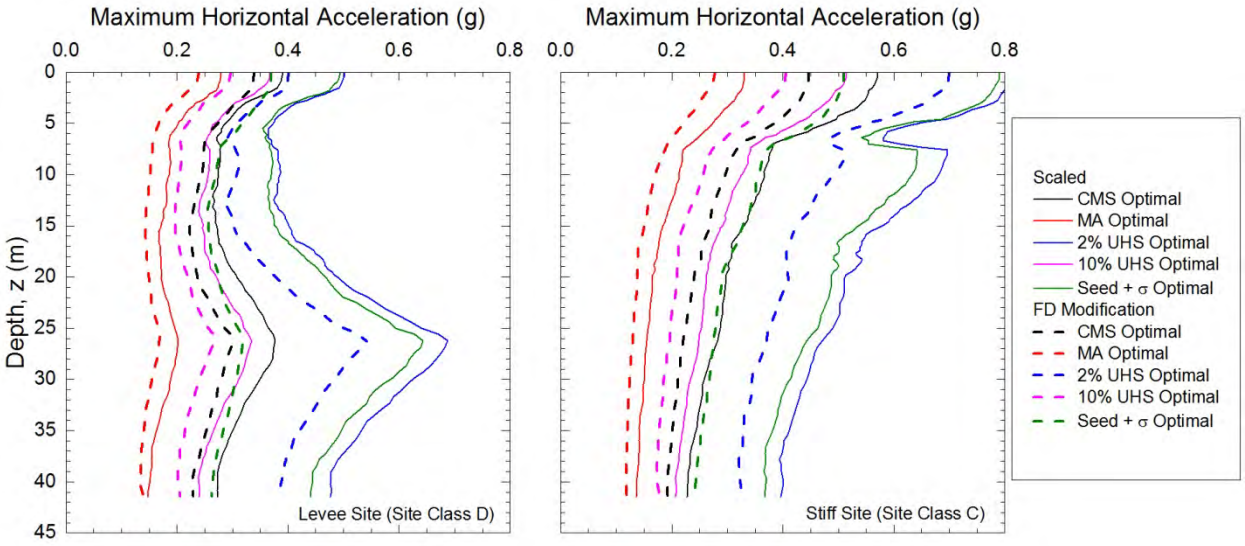

Figure 6.20. Median profiles of the maximum horizontal accelerations produced by the optimally scaled and FD-modified motions from scenario I at both sites for the different target spectra.

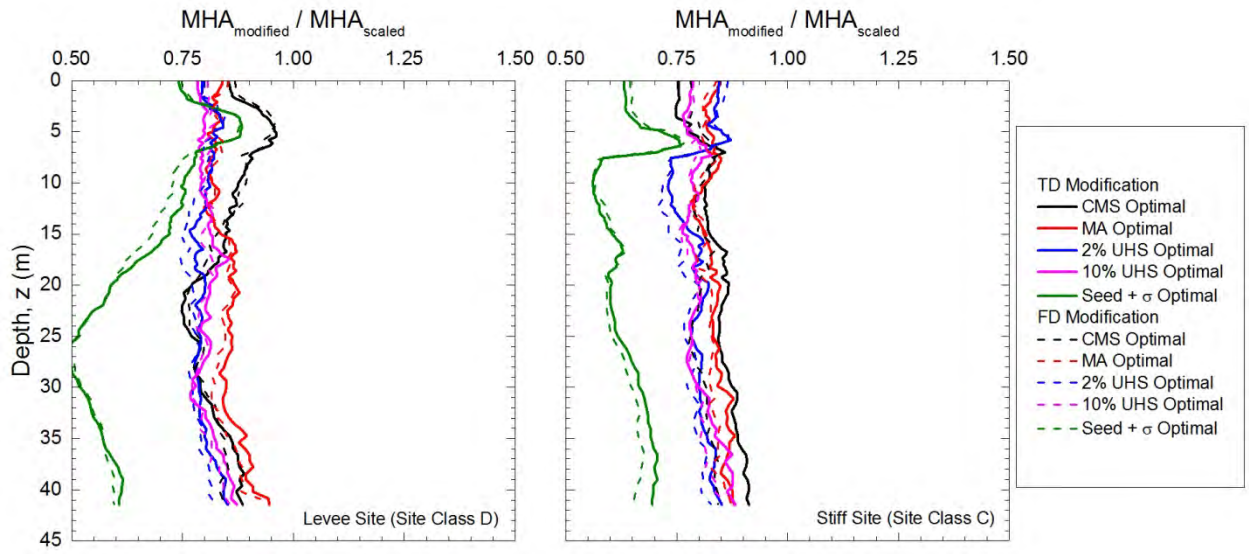

Figure 6.21. Profiles of the ratios of modified-to-scaled maximum horizontal accelerations (*MHA*) for the medians produced by the optimally scaled and modified motions from scenario I at both sites for the different target spectra.

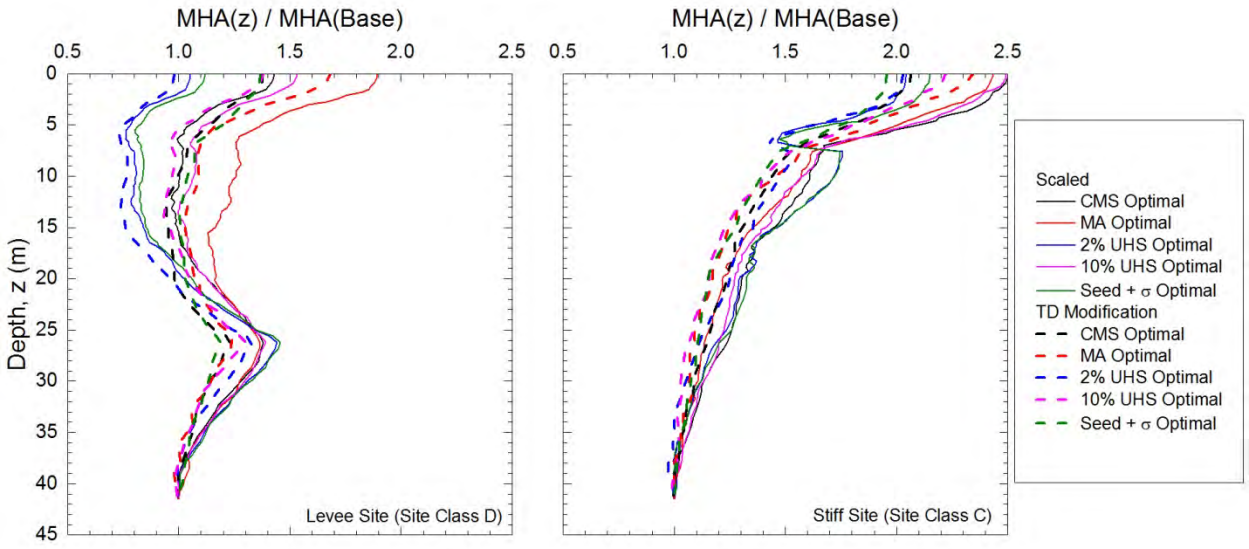

Figure 6.22. Profiles of the normalized maximum horizontal acceleration (*MHA*) medians produced by the optimally scaled and TD-modified motions from scenario I at both sites for the different target spectra.

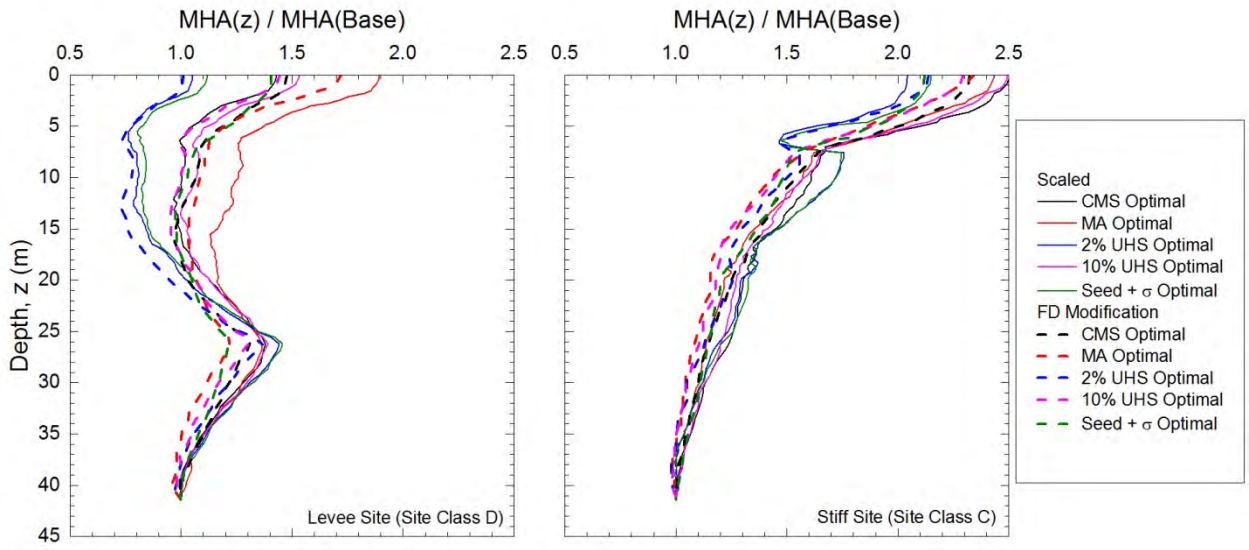

Figure 6.23. Profiles of the normalized maximum horizontal acceleration (*MHA*) medians produced by the optimally scaled and FD-modified motions from scenario I at both sites for the different target spectra.

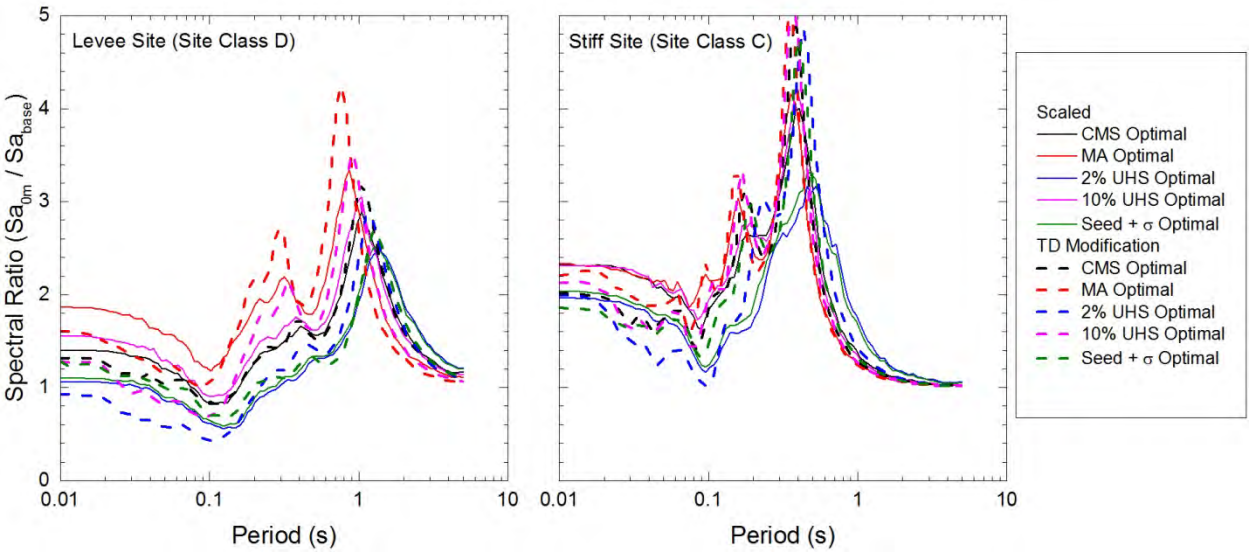

Figure 6.24. Median spectral ratios of the optimally scaled and TD-modified motions from scenario I at both sites for the different target spectra.

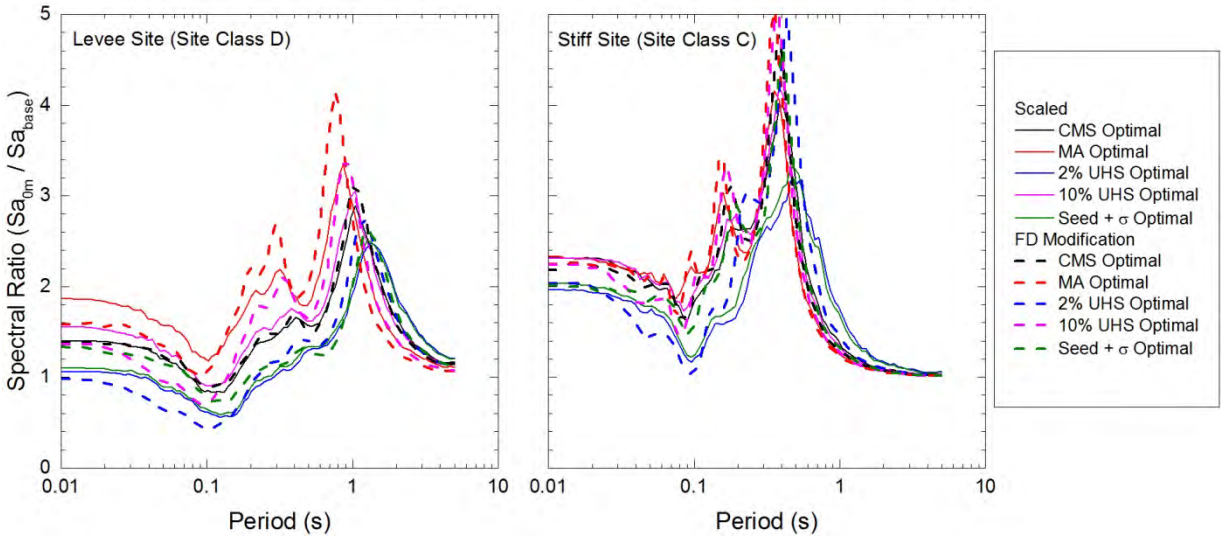

Figure 6.25. Median spectral ratios of the optimally scaled and FD-modified motions from scenario I at both sites for the different target spectra.

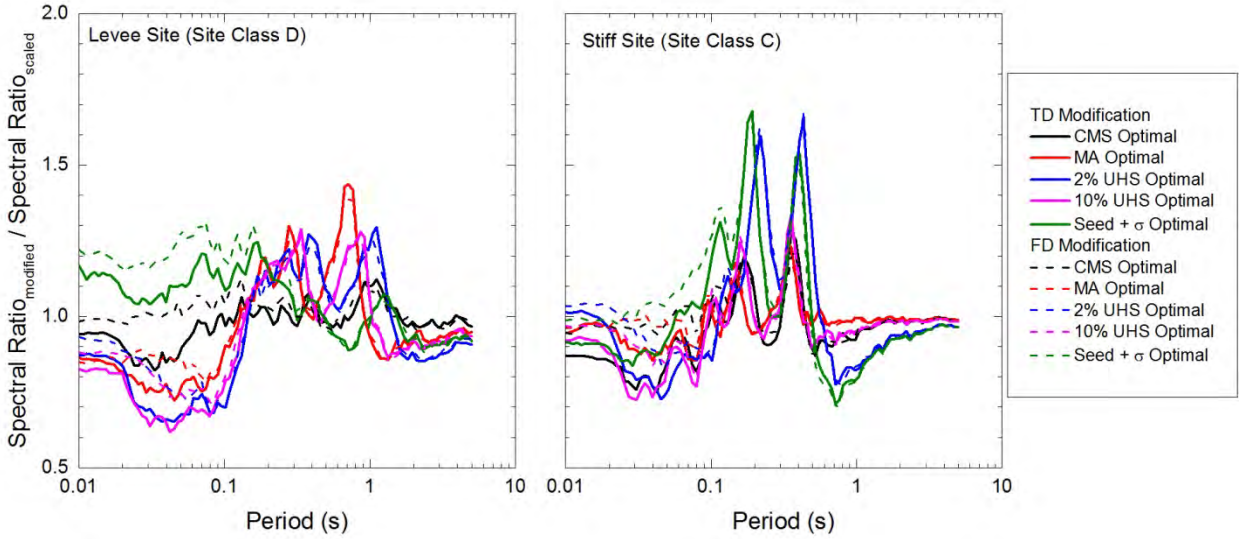

Figure 6.26. Ratios of the modified-to-scaled spectral ratio medians calculated for the optimally scaled and modified motions from scenario I at both sites for the different target spectra.

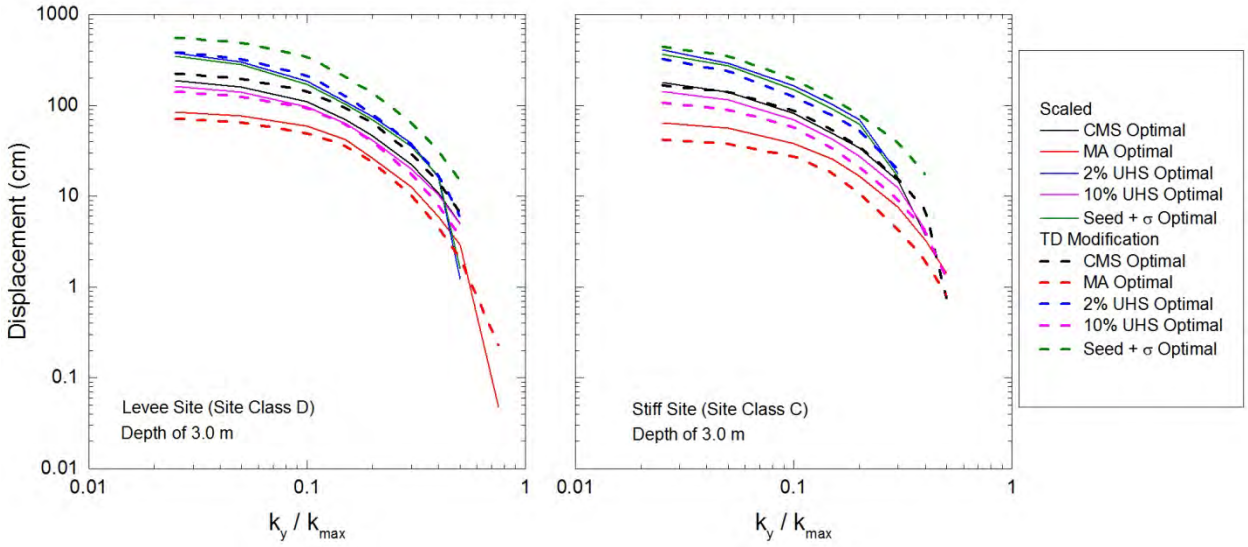

Figure 6.27. Median Newmark-type displacements caused by the optimally scaled and TD-modified motions from scenario I for a shallow sliding mass at both sites for varying k_y / k_{max} and the different target spectra.

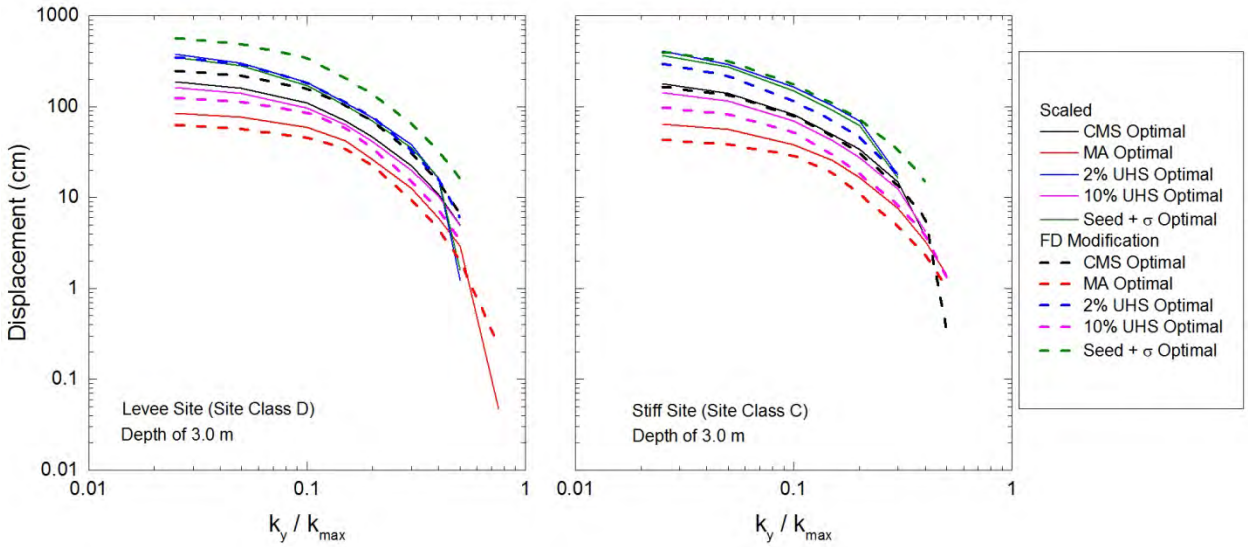

Figure 6.28. Median Newmark-type displacements caused by the optimally scaled and FD-modified motions from scenario I for a shallow sliding mass at both sites for varying k_y / k_{max} and the different target spectra.

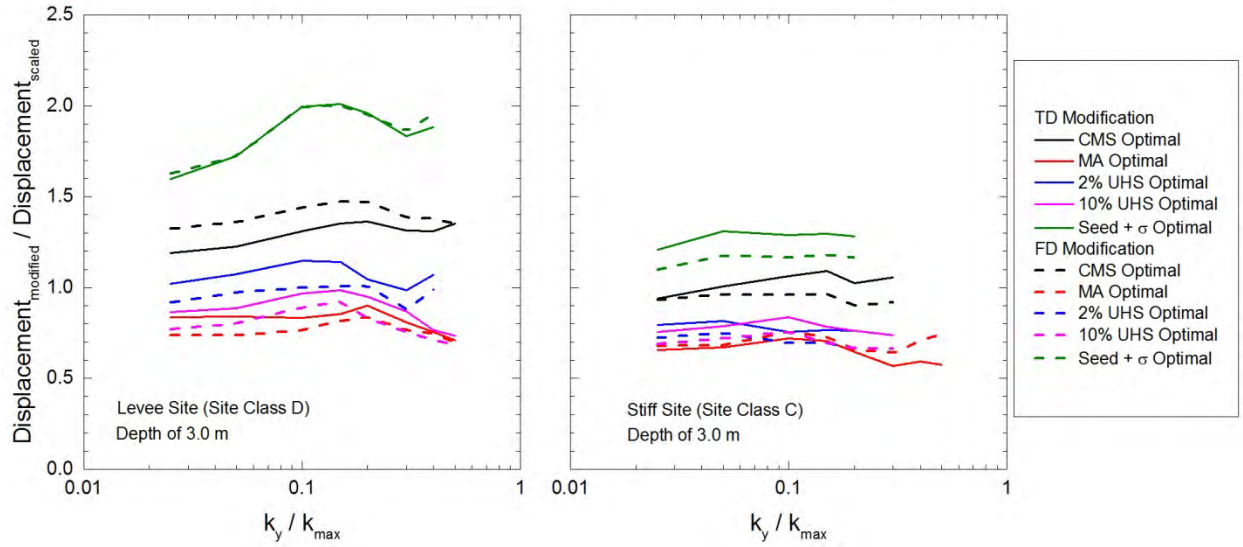

Figure 6.29. Ratios of the modified-to-scaled median Newmark-type displacements caused by the optimally scaled and modified motions from scenario I for a shallow sliding mass at both sites for varying k_y / k_{max} and the different target spectra.

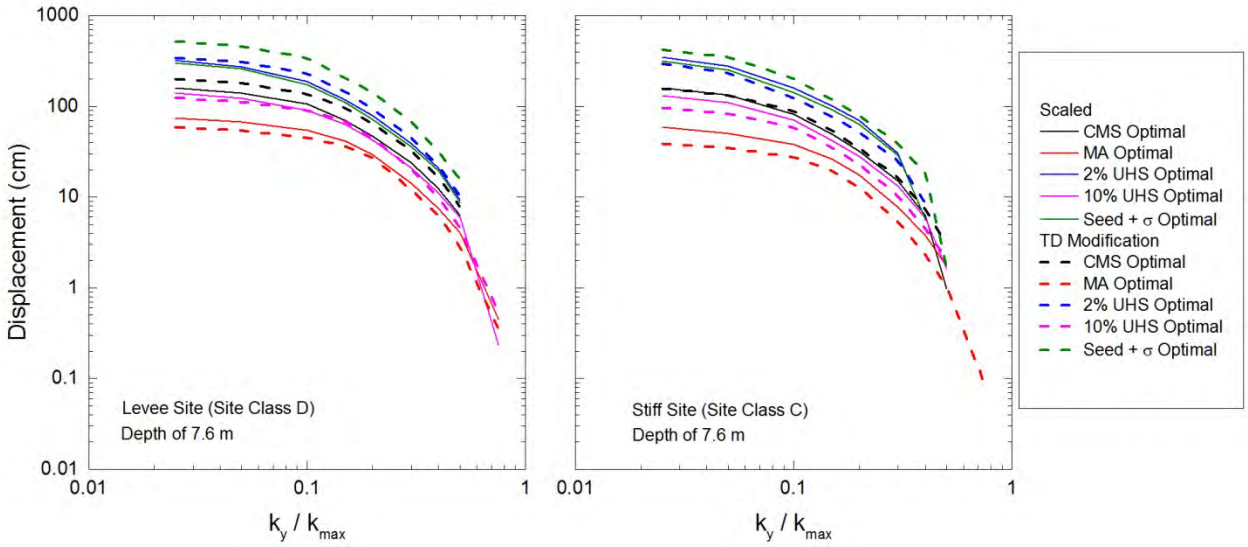

Figure 6.30. Median Newmark-type displacements caused by the optimally scaled and TD-modified motions from scenario I for an intermediate sliding mass at both sites for varying k_y / k_{max} and the different target spectra.

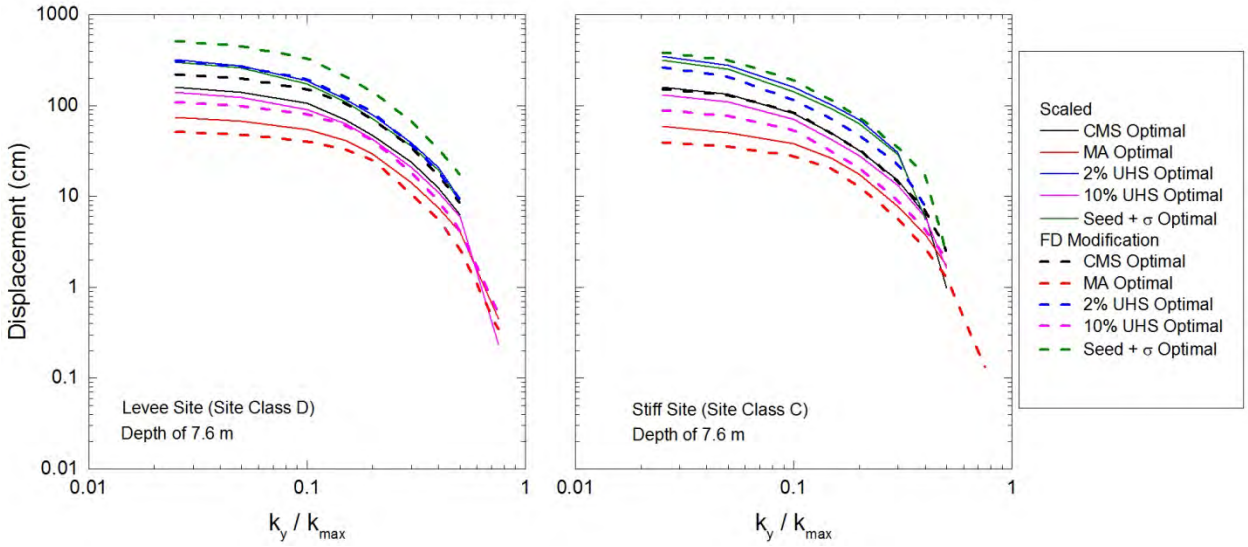

Figure 6.31. Median Newmark-type displacements caused by the optimally scaled and FD-modified motions from scenario I for an intermediate sliding mass at both sites for varying k_y / k_{max} and the different target spectra.

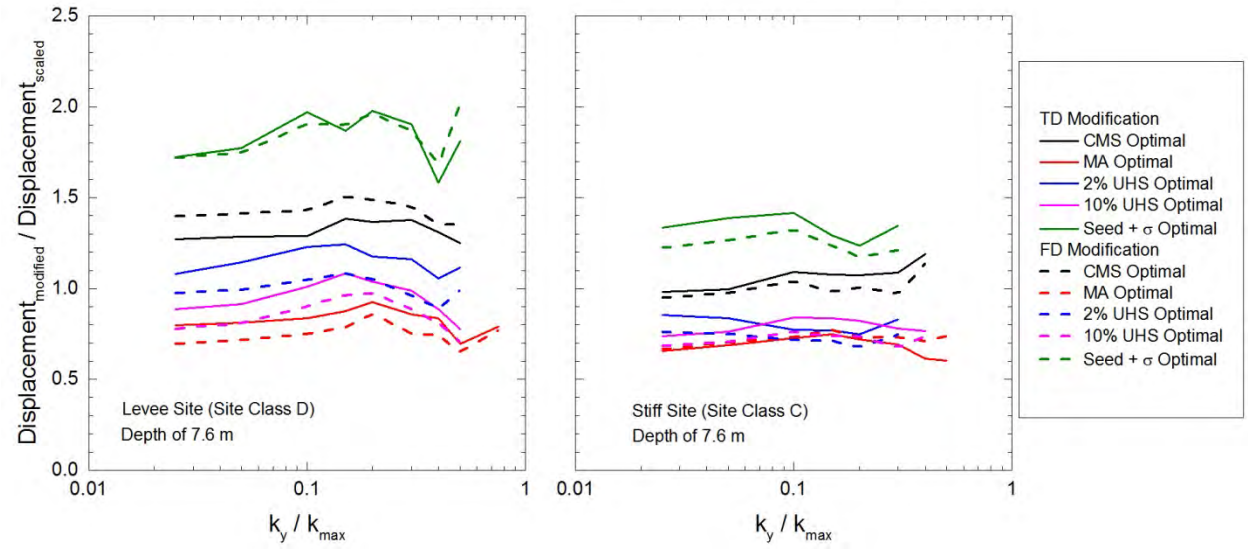

Figure 6.32. Ratios of the modified-to-scaled median Newmark-type displacements caused by the optimally scaled and modified motions from scenario I for an intermediate sliding mass at both sites for varying k_y / k_{max} and the different target spectra.

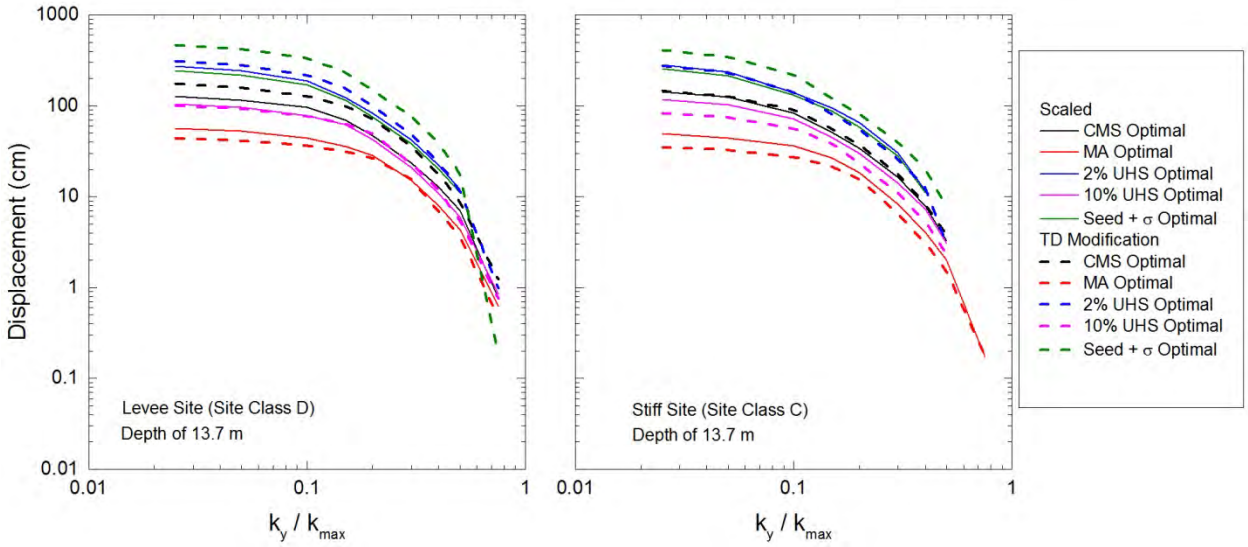

Figure 6.33. Median Newmark-type displacements caused by the optimally scaled and TD-modified motions from scenario I for a deep sliding mass at both sites for varying k_y / k_{max} and the different target spectra.

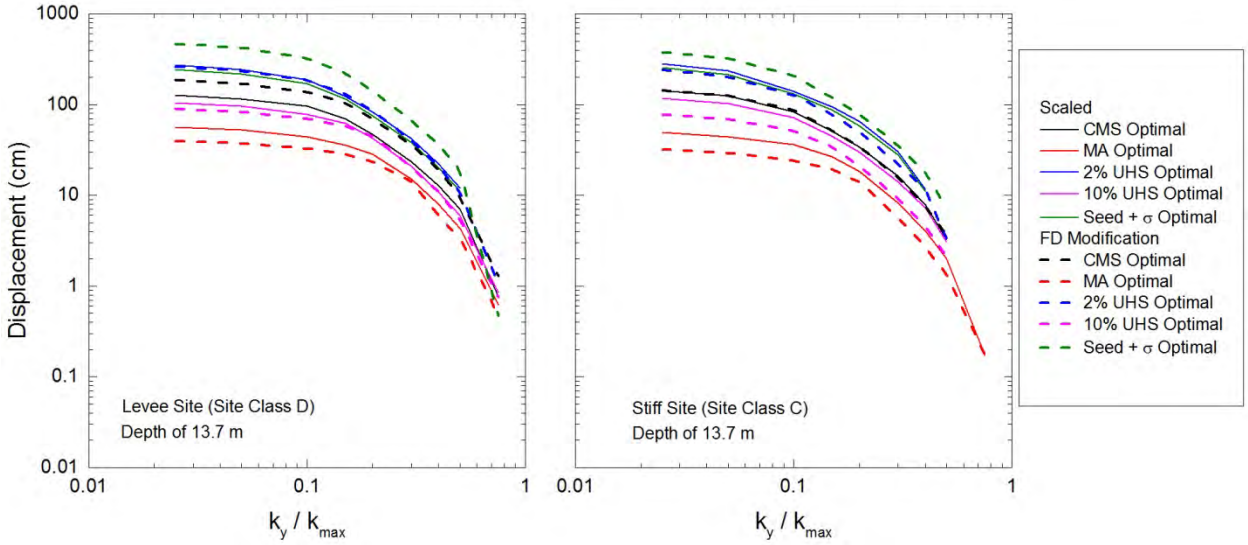

Figure 6.34. Median Newmark-type displacements caused by the optimally scaled and FD-modified motions from scenario I for a deep sliding mass at both sites for varying k_y / k_{max} and the different target spectra.

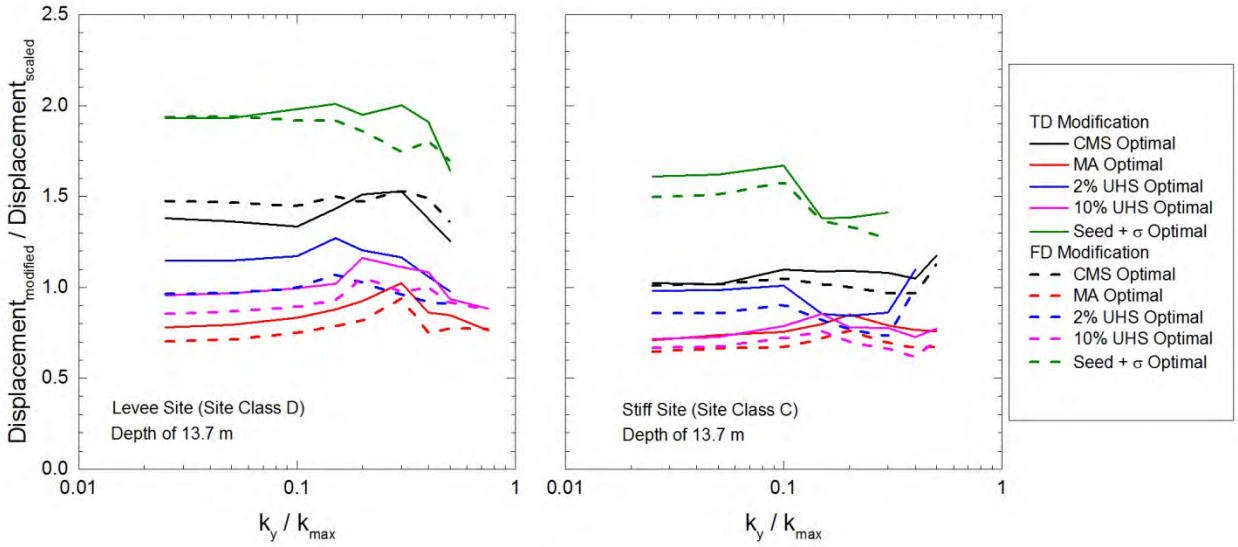

Figure 6.35. Ratios of the modified-to-scaled median Newmark-type displacements caused by the optimally scaled and modified motions from scenario I for a deep sliding mass at both sites for varying k_y / k_{max} and the different target spectra.

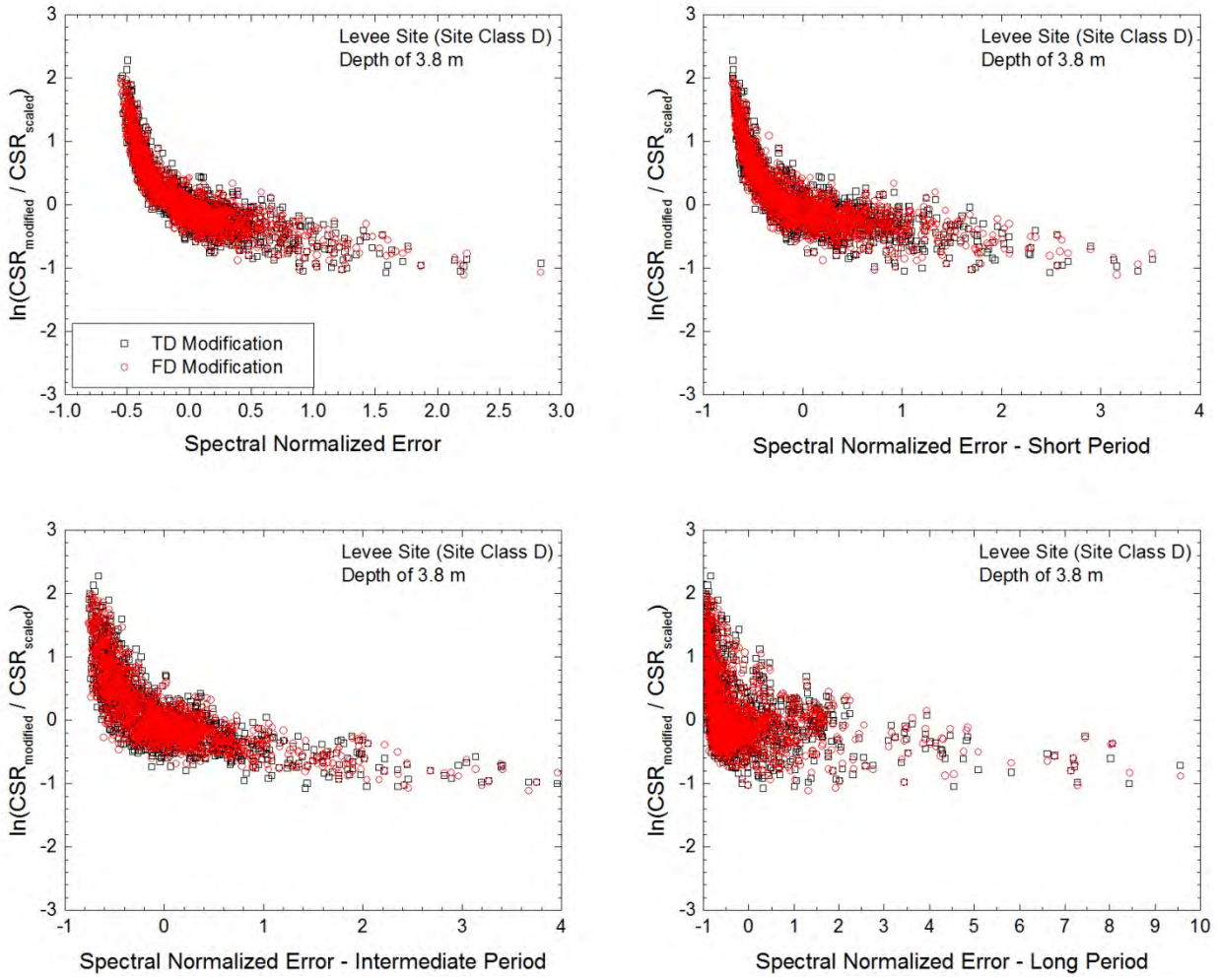

Figure 6.36. Logarithmic ratios of the modified-to-scaled cyclic stress ratios (*CSR*) for the motions in scenario I for the levee site at a depth of 3.8 m plotted against spectral mismatch, as quantified by NE_s, over different period ranges.

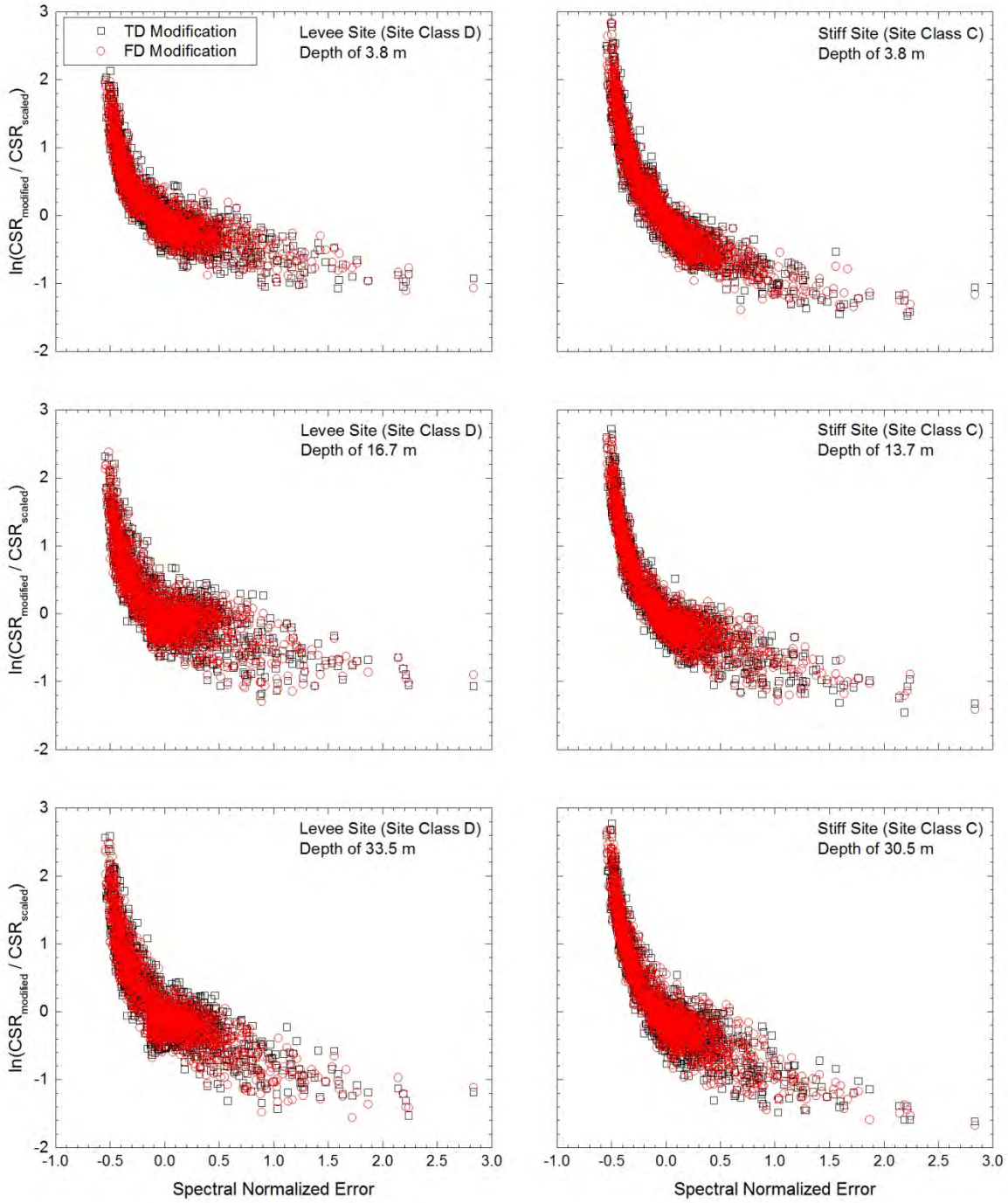

Figure 6.37. Logarithmic ratios of the modified-to-scaled cyclic stress ratios (*CSR*) for the TD- and FD-modified motions in scenario I for both sites at all three depths plotted versus spectral mismatch, quantified by NE_s.

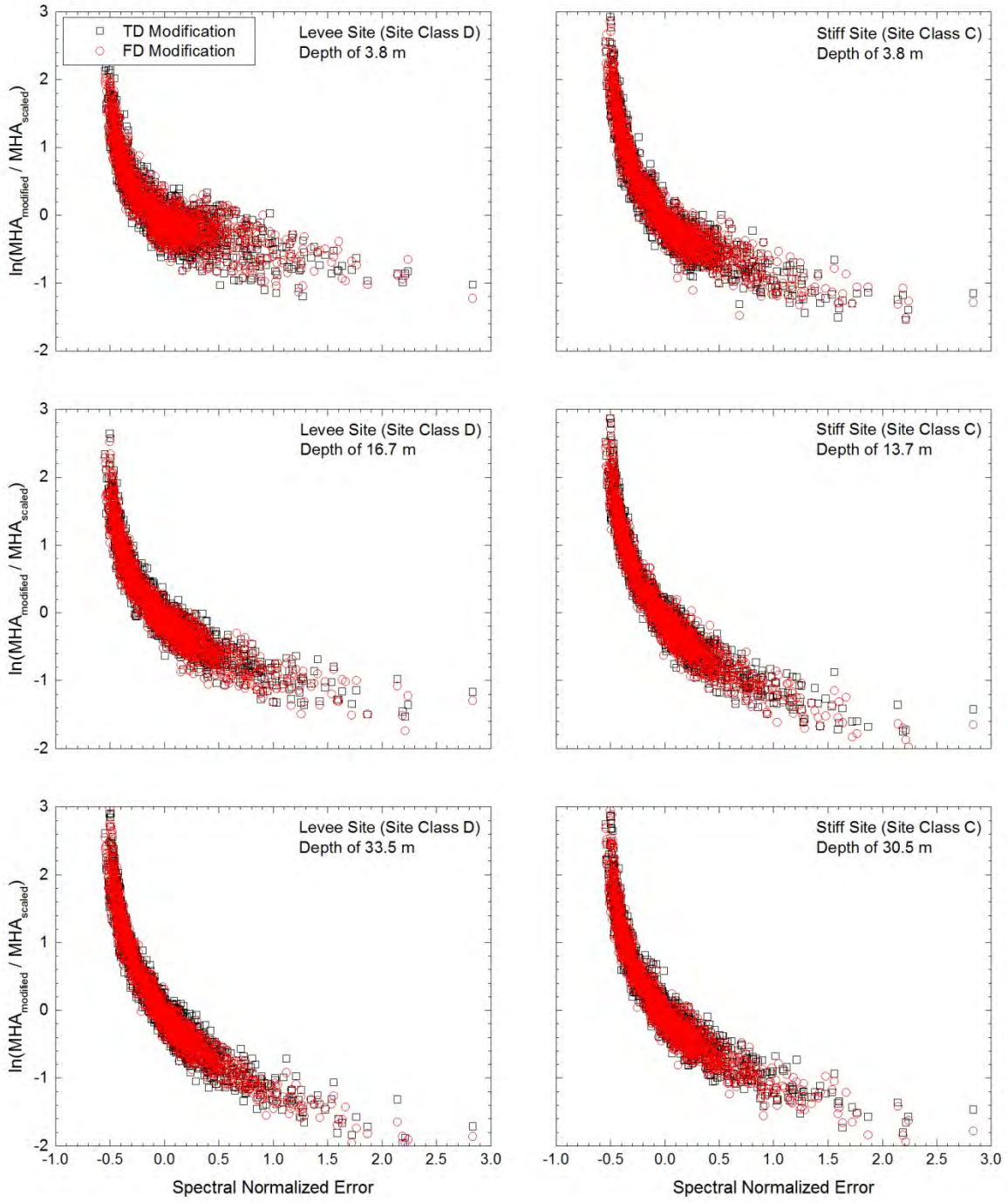

Figure 6.38. Logarithmic modified-to-scaled maximum horizontal acceleration (*MHA*) ratios for the TD- and FD-modified motions in scenario I for both sites at all three depths plotted versus spectral mismatch, quantified by NE_s.

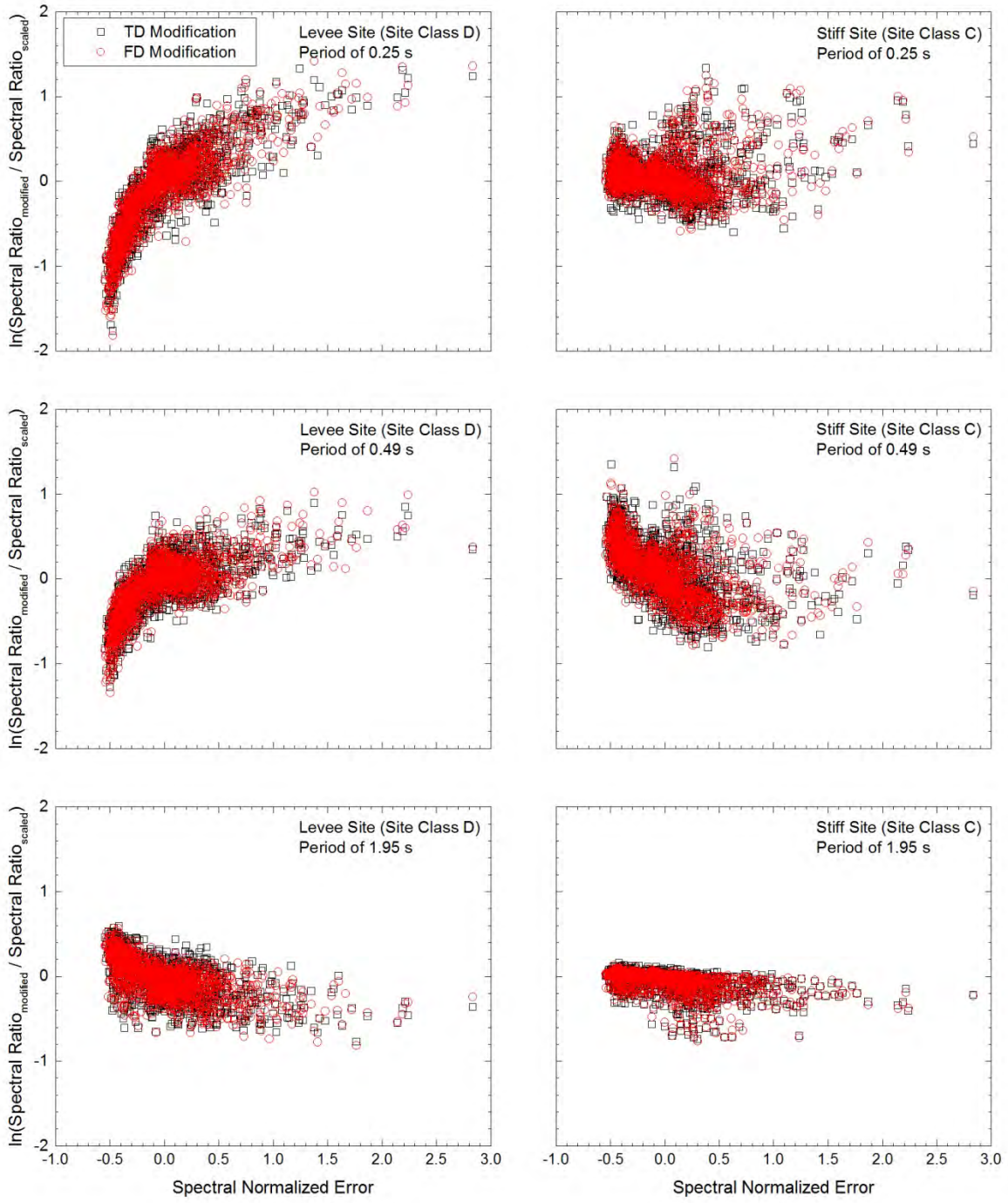

Figure 6.39. Logarithmic ratios of the modified-to-scaled spectral ratios for the TD- and FD-modified motions in scenario I for both sites at all three periods plotted versus spectral mismatch, quantified by NE_s.

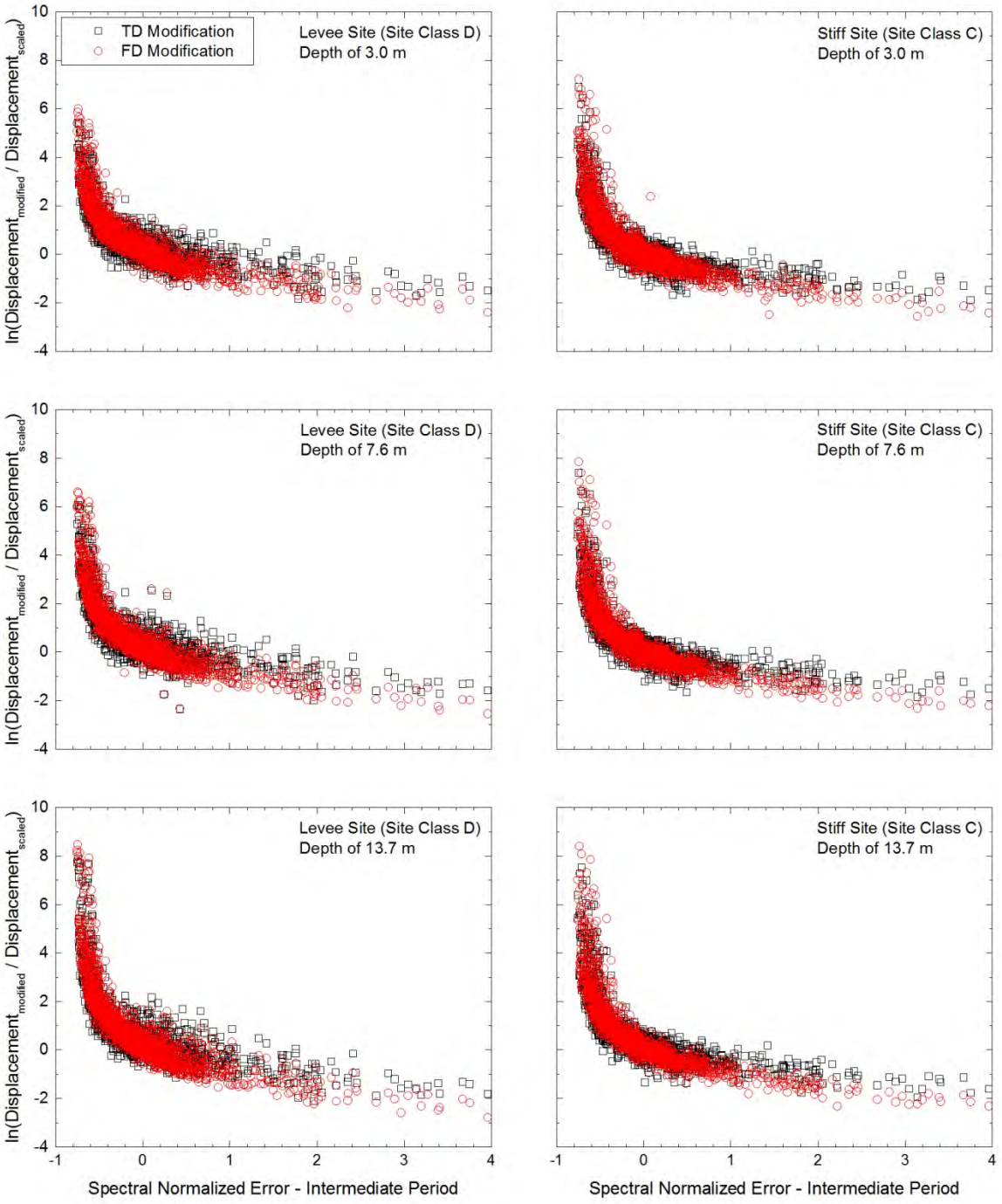

Figure 6.40. Logarithmic modified-to-scaled Newmark-type slope displacement ratios of the TD- and FD-modified motions in scenario I for both sites, all three depths, and a k_y / k_{max} value of 0.05 plotted versus spectral mismatch in the intermediate period range, quantified by $NE_{s,IP}$.

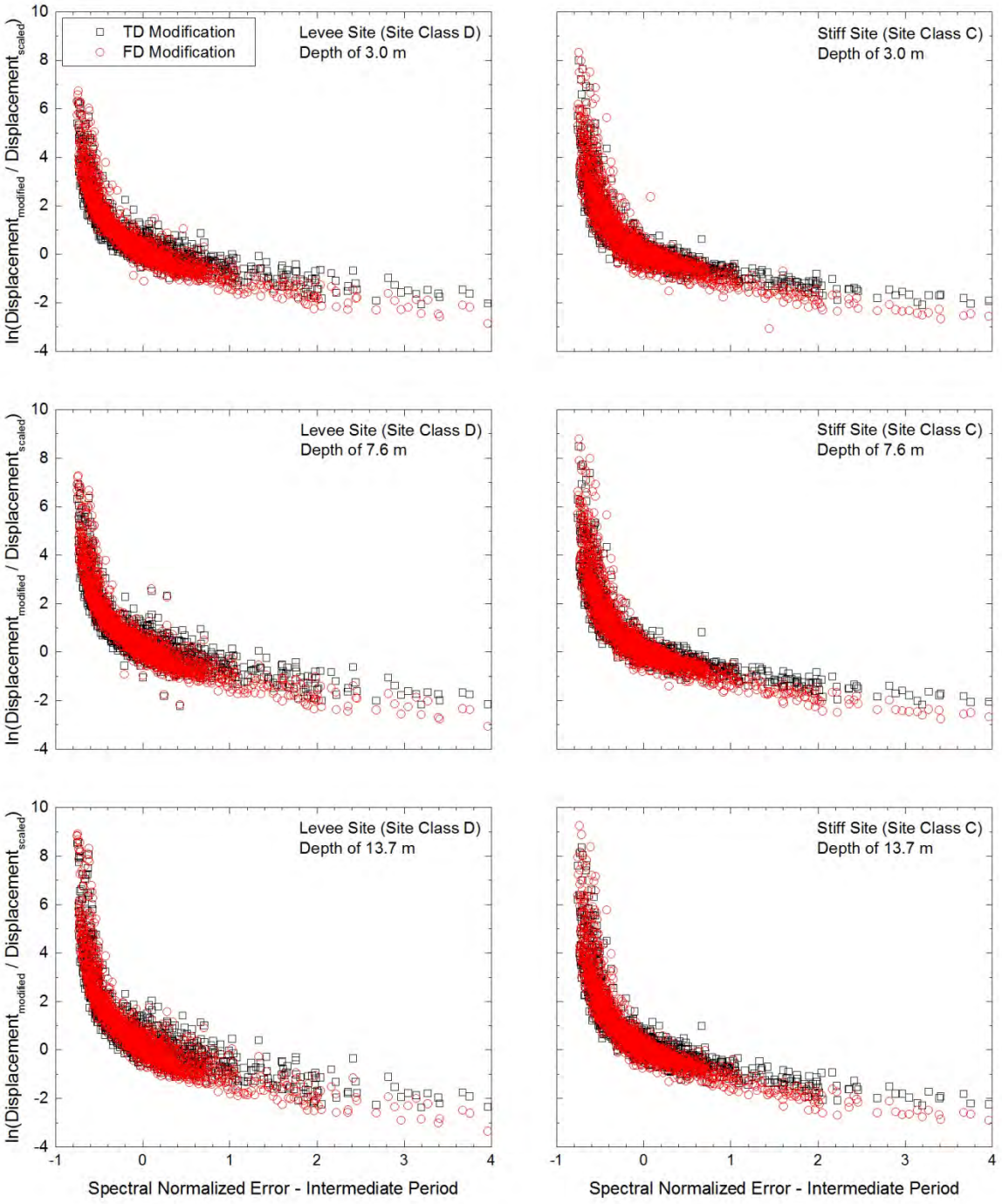

Figure 6.41. Logarithmic modified-to-scaled Newmark-type slope displacement ratios of the TD- and FD-modified motions in scenario I for both sites, all three depths, and a k_y / k_{max} value of 0.15 plotted versus spectral mismatch in the intermediate period range, quantified by $NE_{s,IP}$.

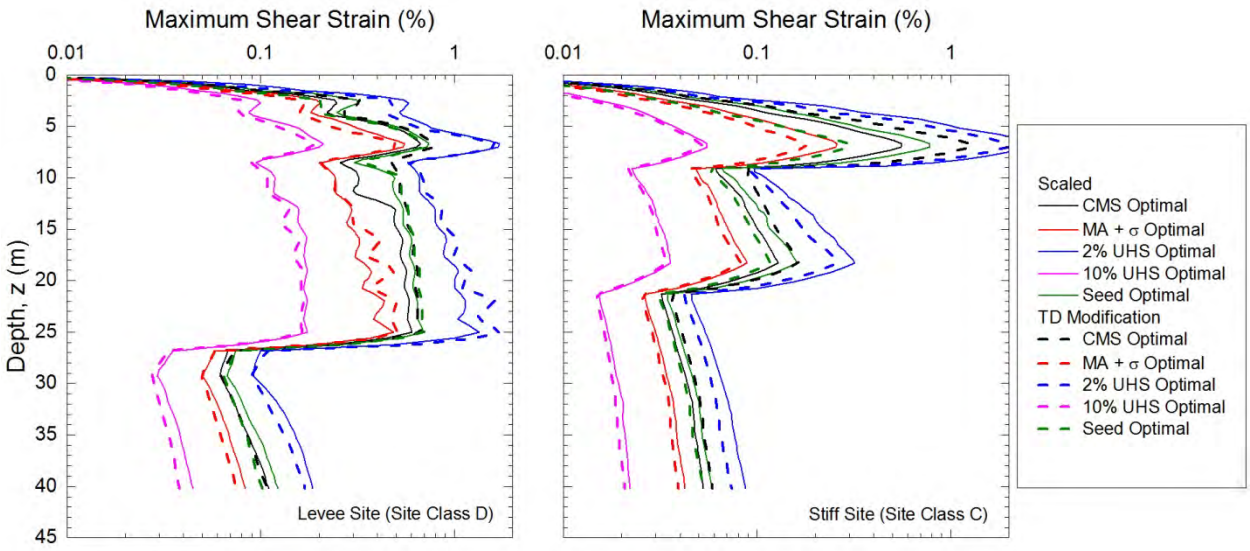

Figure 6.42. Median profiles for the maximum shear strains produced by the optimally scaled and TD-modified motions from scenario II at both sites for the different target spectra.

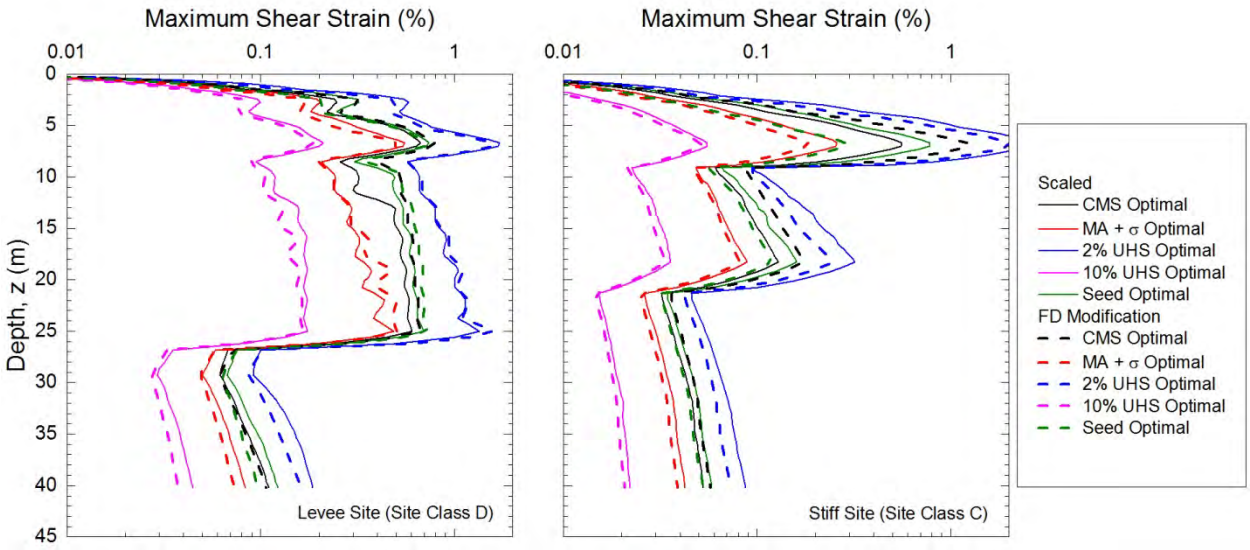

Figure 6.43. Median profiles for the maximum shear strains produced by the optimally scaled and FD-modified motions from scenario II at both sites for the different target spectra.

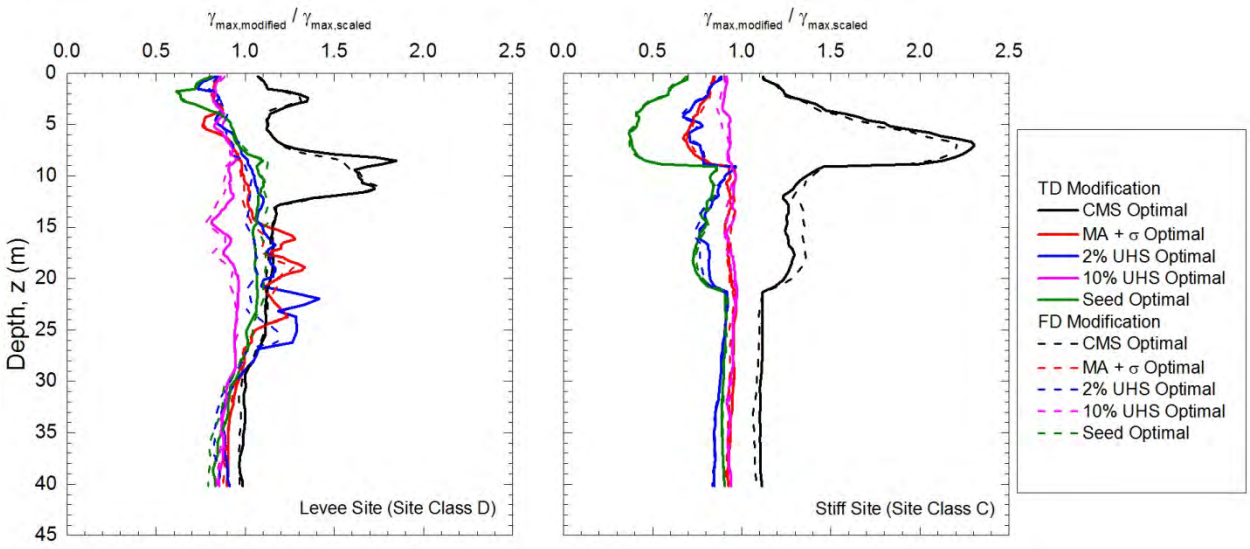

Figure 6.44. Profiles of the ratios of modified-to-scaled maximum shear strains (γ_{max}) for the medians produced by the optimally scaled and modified motions from scenario II at both sites for the different target spectra.

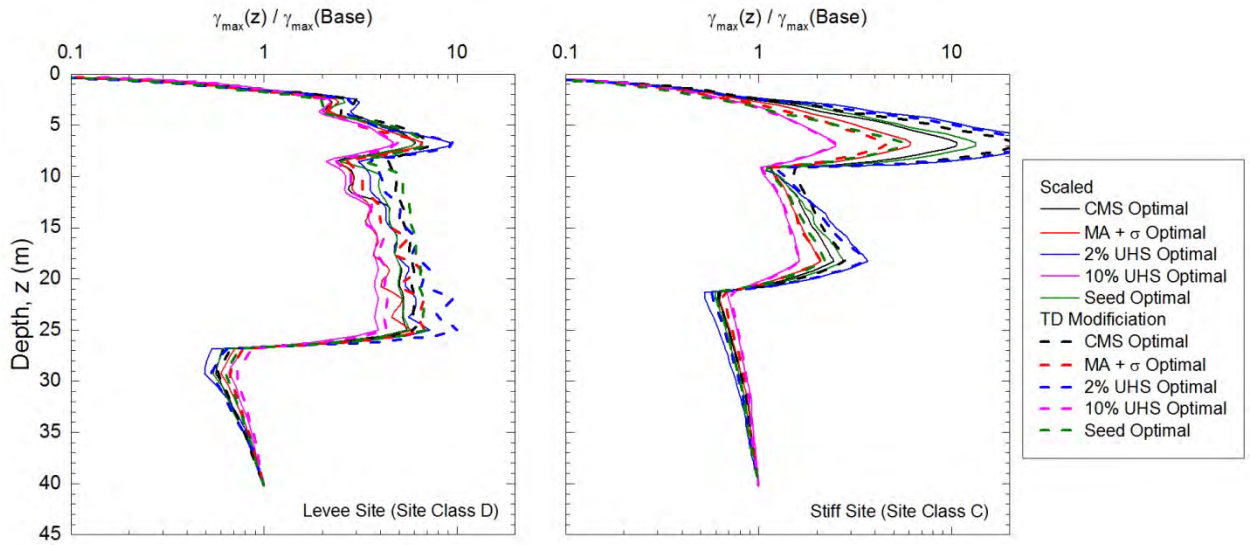

Figure 6.45. Profiles of the normalized maximum shear strain (γ_{max}) medians produced by the optimally scaled and TD-modified motions from scenario II at both sites for the different target spectra.

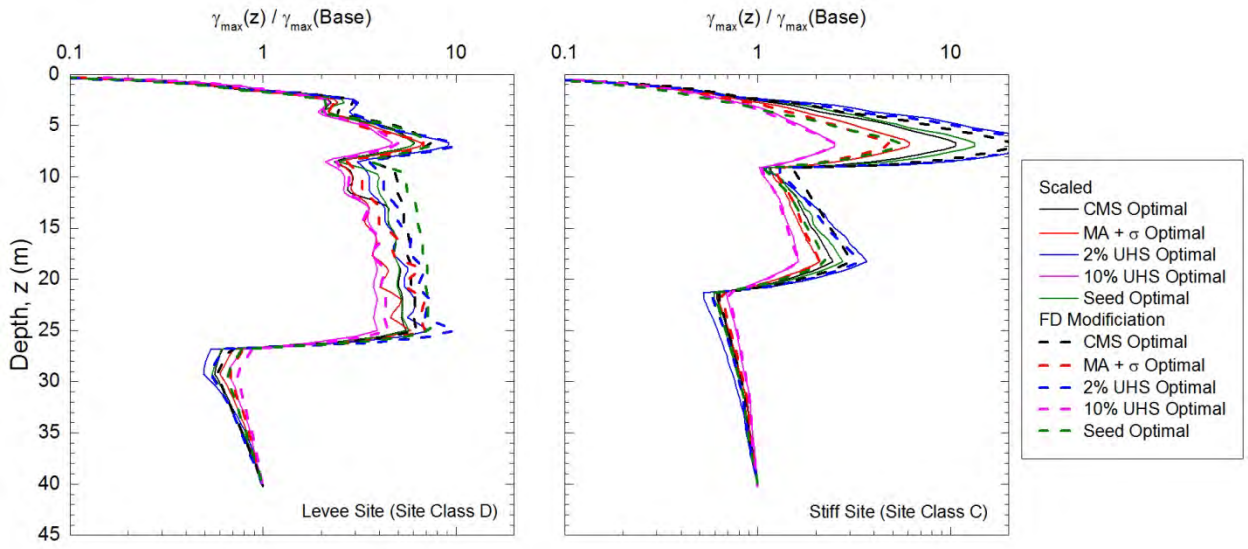

Figure 6.46. Profiles of the normalized maximum shear strain (γ_{max}) medians produced by the optimally scaled and FD-modified motions from scenario II at both sites for the different target spectra.

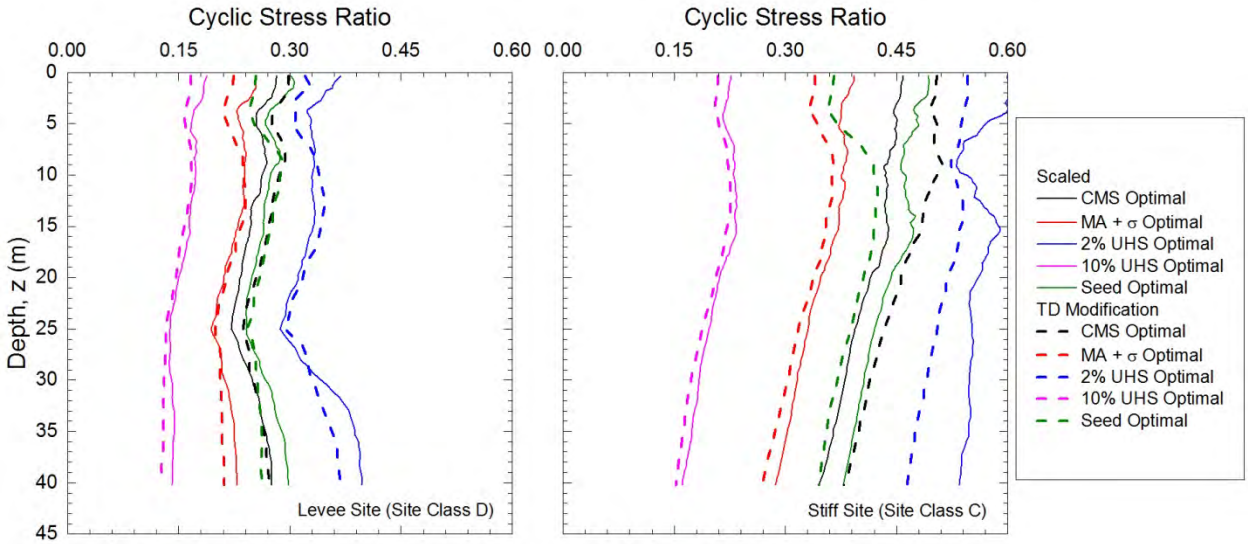

Figure 6.47. Median profiles of the cyclic stress ratios produced by the optimally scaled and TD-modified motions from scenario II at both sites for the different target spectra.

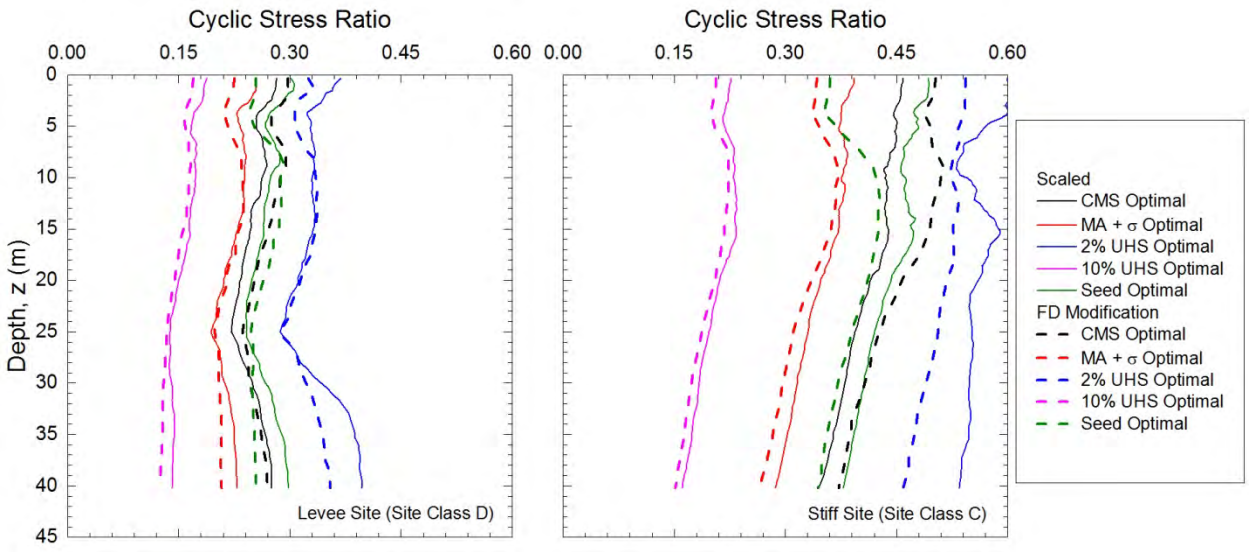

Figure 6.48. Median profiles of the cyclic stress ratios produced by the optimally scaled and FD-modified motions from scenario II at both sites for the different target spectra.

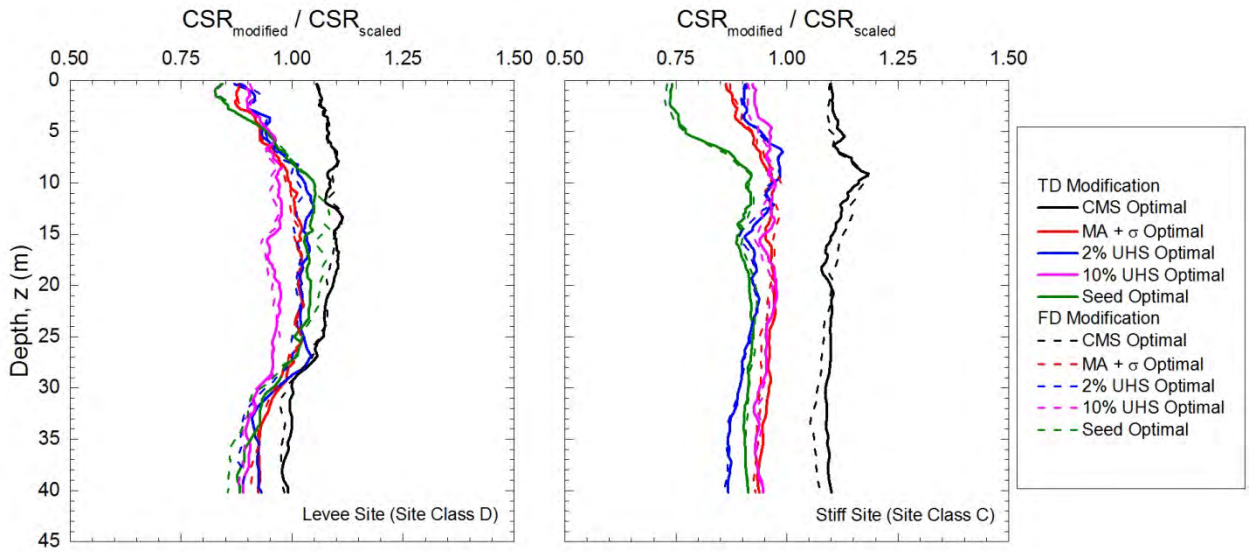

Figure 6.49. Profiles of the ratios of modified-to-scaled cyclic stress ratios (*CSR*) for the medians produced by the optimally scaled and modified motions from scenario II at both sites for the different target spectra.

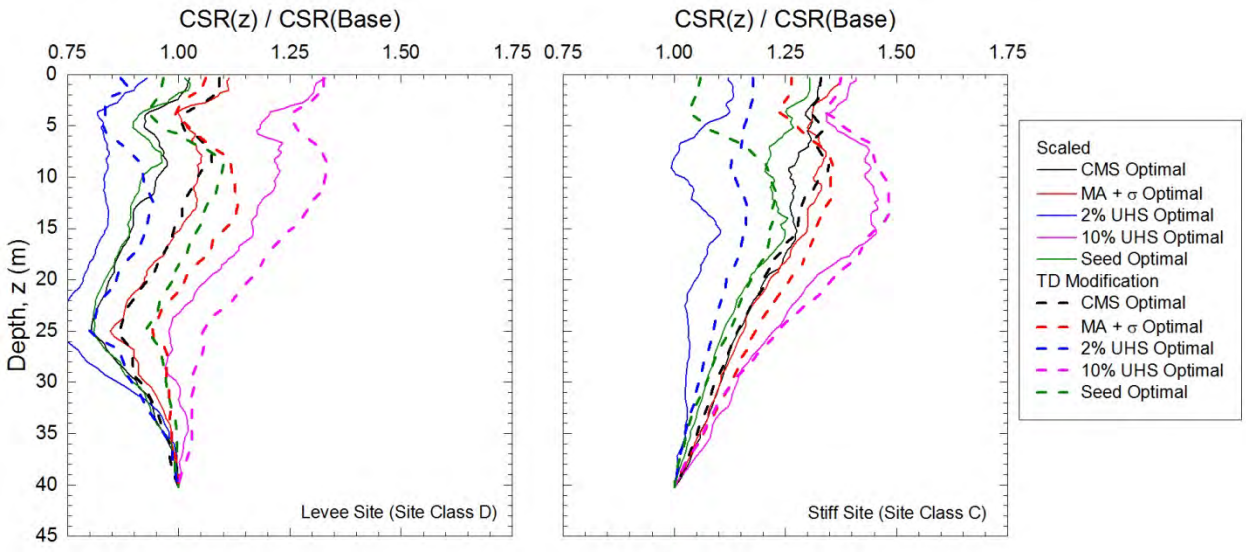

Figure 6.50. Profiles of the normalized median cyclic stress ratios (*CSR*) produced by the optimally scaled and TD-modified motions from scenario II at both sites for the different target spectra.

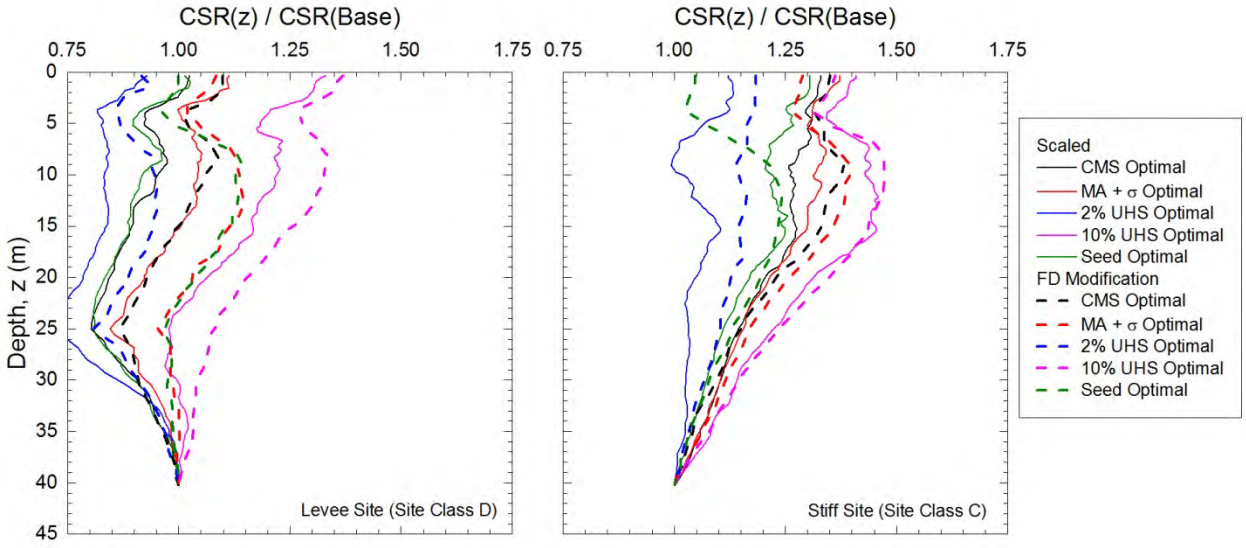

Figure 6.51. Profiles of the normalized median cyclic stress ratios (*CSR*) produced by the optimally scaled and FD-modified motions from scenario II at both sites for the different target spectra.

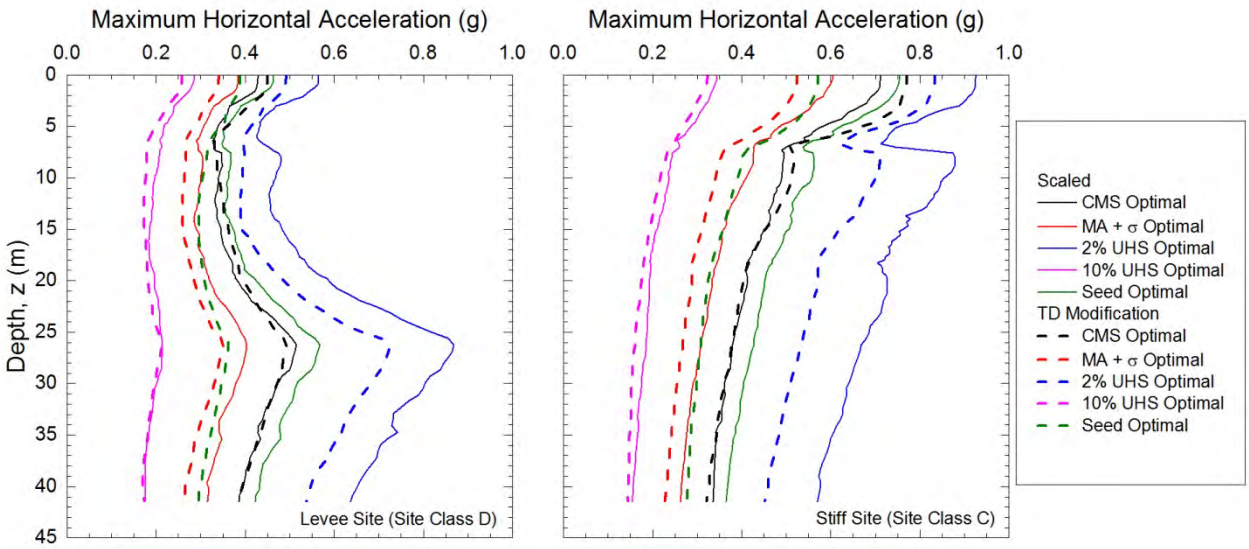

Figure 6.52. Median profiles of the maximum horizontal accelerations produced by the optimally scaled and TD-modified motions from scenario II at both sites for the different target spectra.

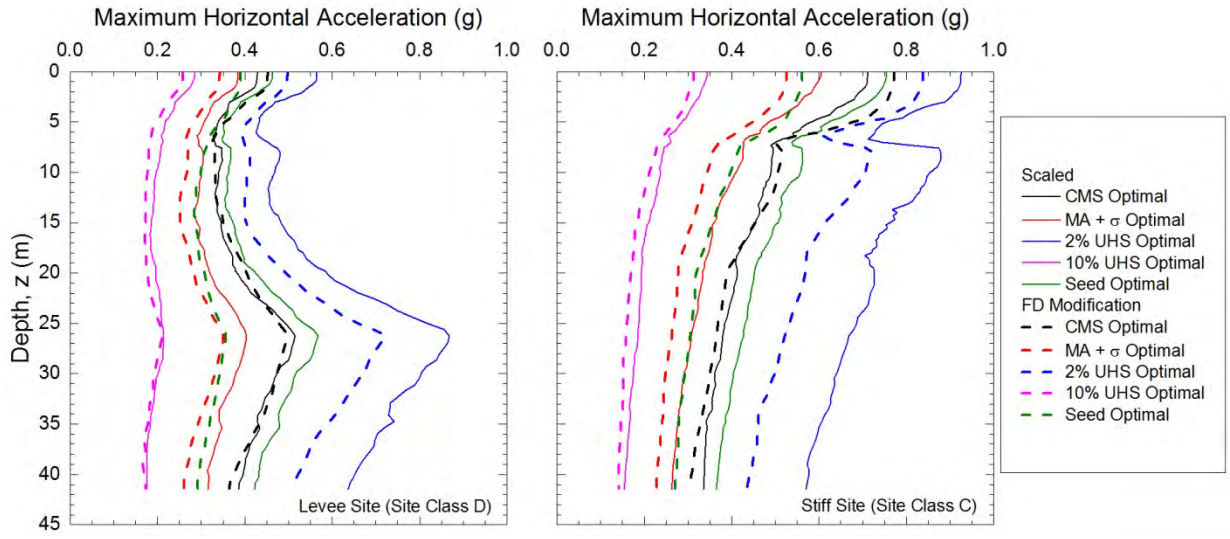

Figure 6.53. Median profiles of the maximum horizontal accelerations produced by the optimally scaled and FD-modified motions from scenario II at both sites for the different target spectra.

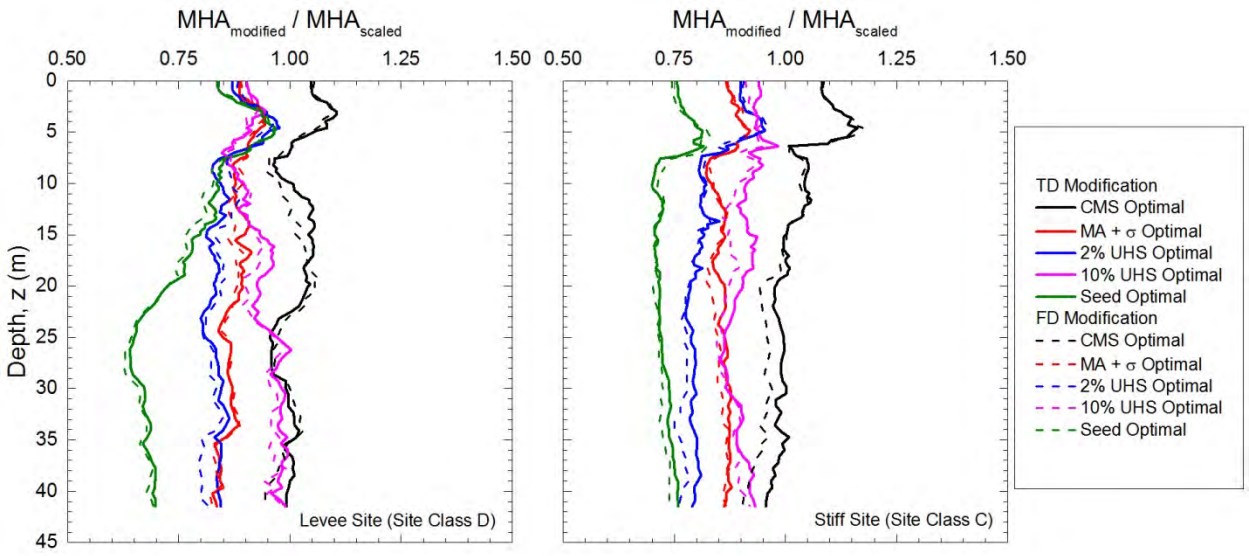

Figure 6.54. Profiles of the ratios of modified-to-scaled maximum horizontal accelerations (*MHA*) for the medians produced by the optimally scaled and modified motions from scenario II at both sites for the different target spectra.

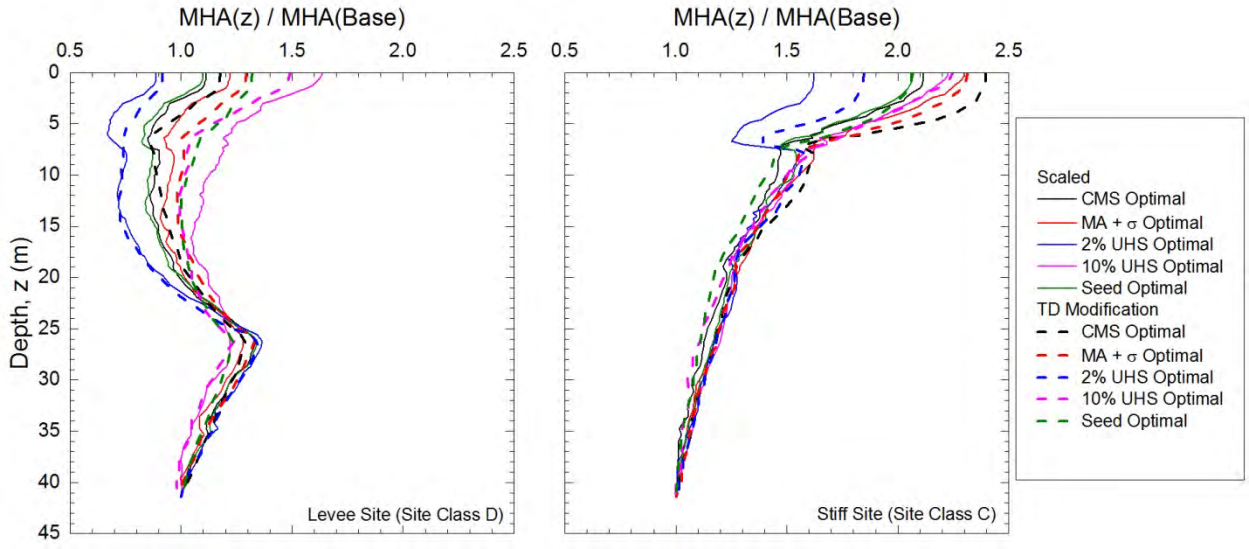

Figure 6.55. Profiles of the normalized maximum horizontal acceleration (*MHA*) medians produced by the optimally scaled and TD-modified motions from scenario II at both sites for the different target spectra.

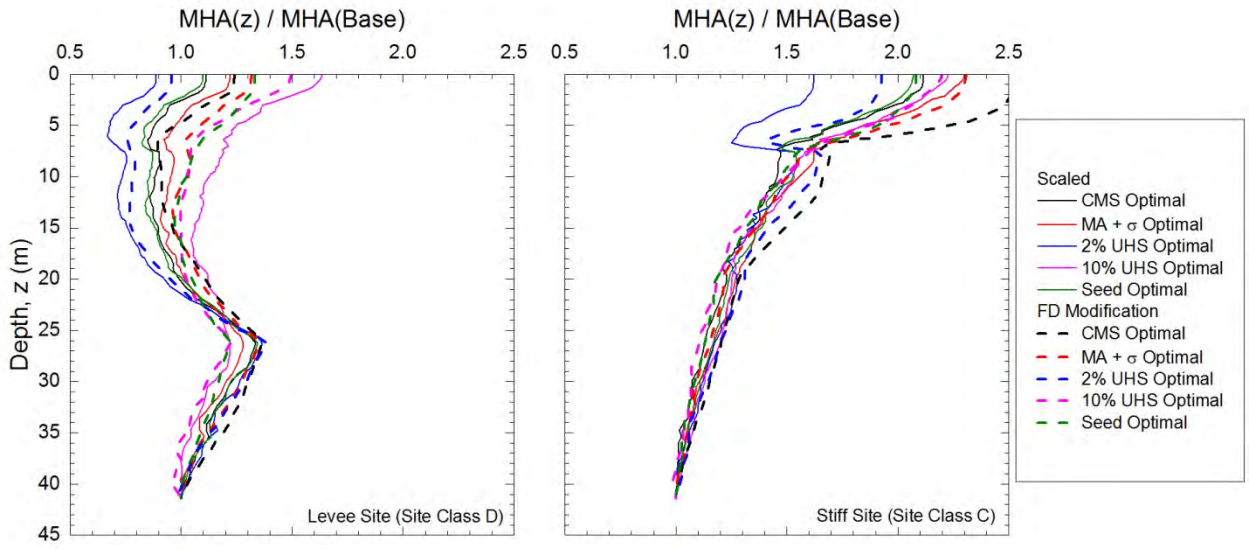

Figure 6.56. Profiles of the normalized maximum horizontal acceleration (*MHA*) medians produced by the optimally scaled and FD-modified motions from scenario II at both sites for the different target spectra.

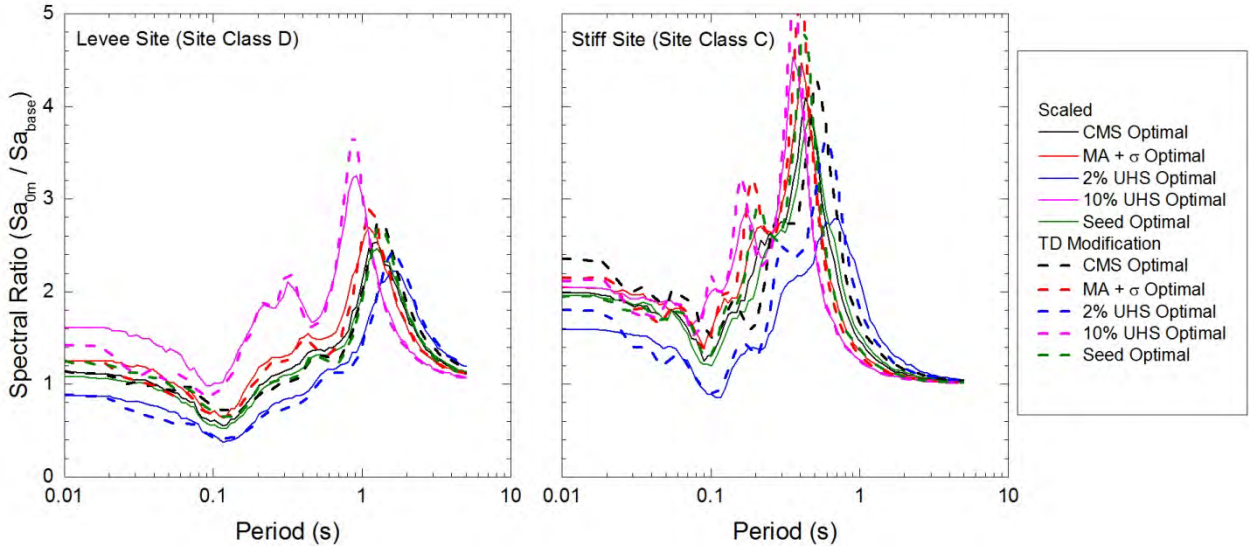

Figure 6.57. Median spectral ratios produced by the optimally scaled and TD-modified motions from scenario II at both sites for the different target spectra.

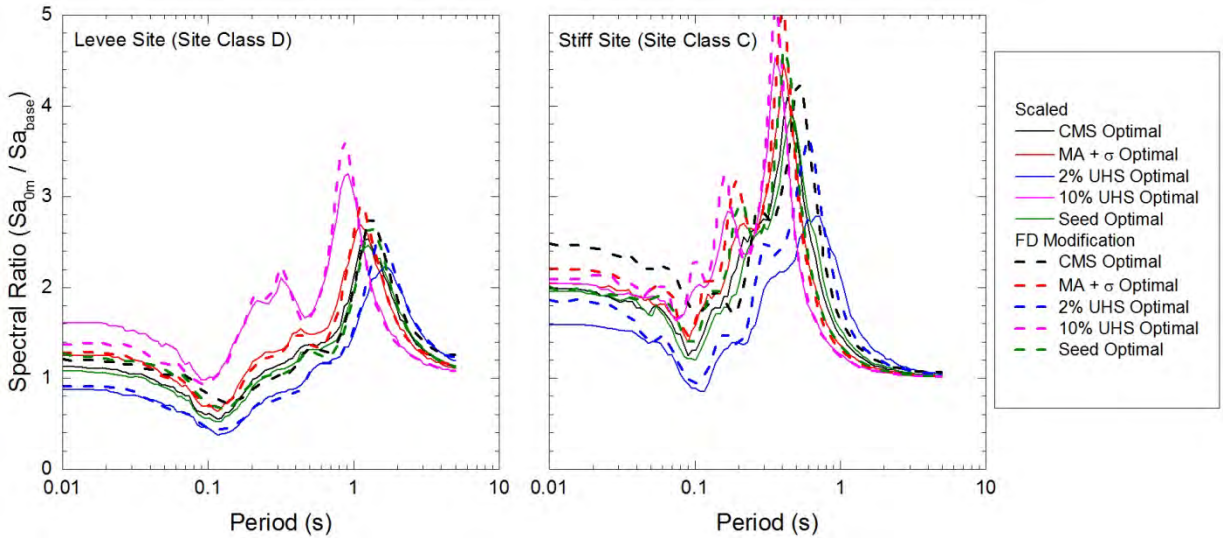

Figure 6.58. Median spectral ratios produced by the optimally scaled and FD-modified motions from scenario II at both sites for the different target spectra.

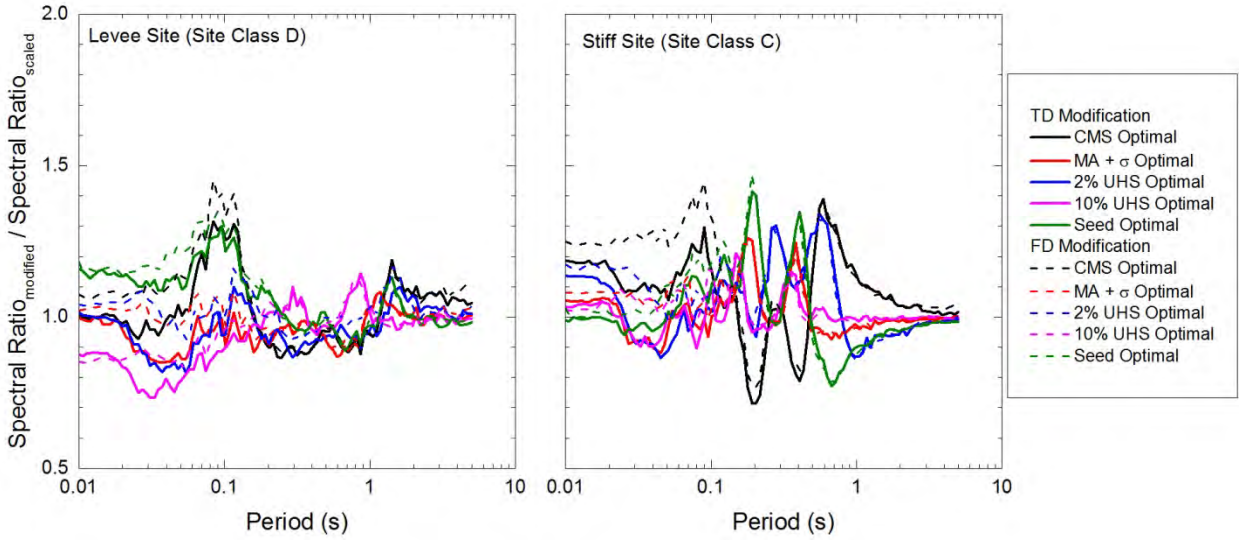

Figure 6.59. Ratios of the modified-to-scaled spectral ratio medians calculated for the optimally scaled and modified motions from scenario II at both sites for the different target spectra.

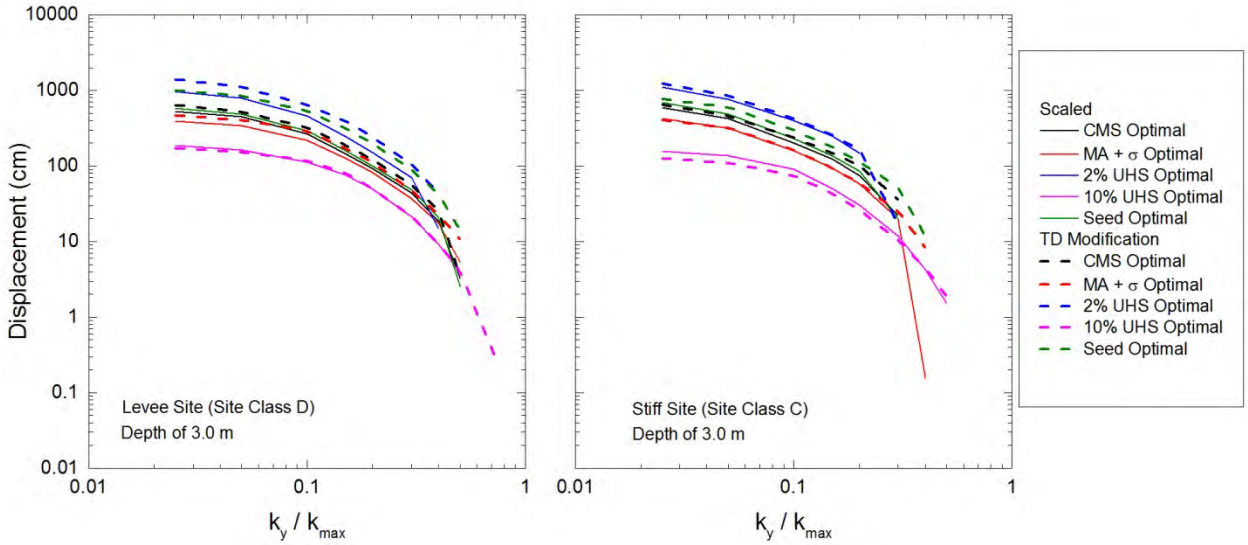

Figure 6.60. Median Newmark-type slope displacements caused by the optimally scaled and TD-modified motions from scenario II for a shallow sliding mass at both sites for varying k_y / k_{max} and the different target spectra.

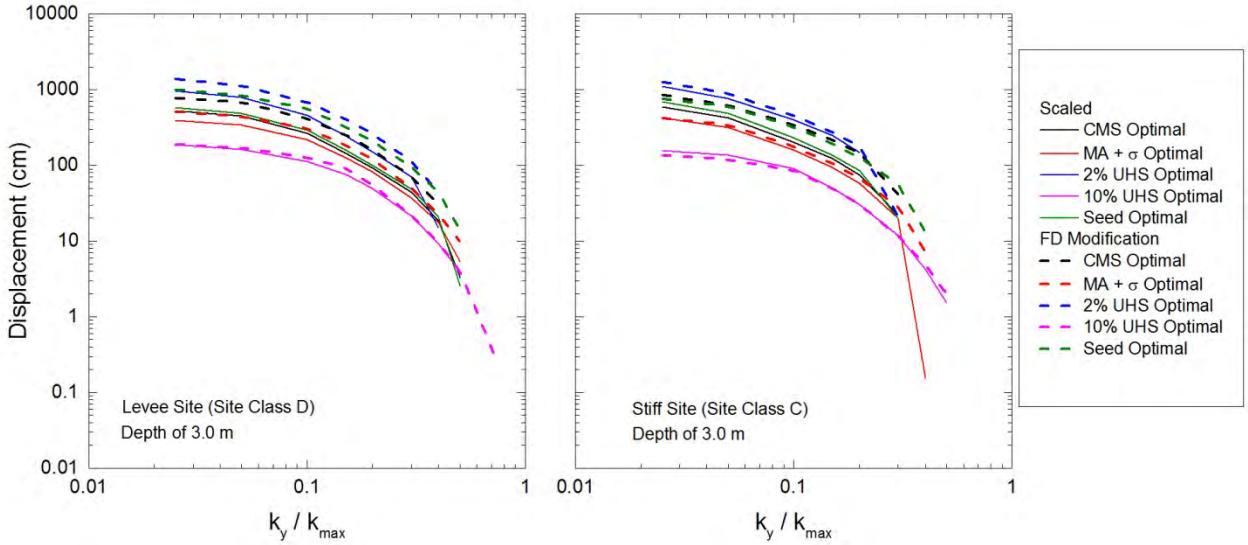

Figure 6.61. Median Newmark-type slope displacements caused by the optimally scaled and FD-modified motions from scenario II for a shallow sliding mass at both sites for varying k_y / k_{max} and the different target spectra.

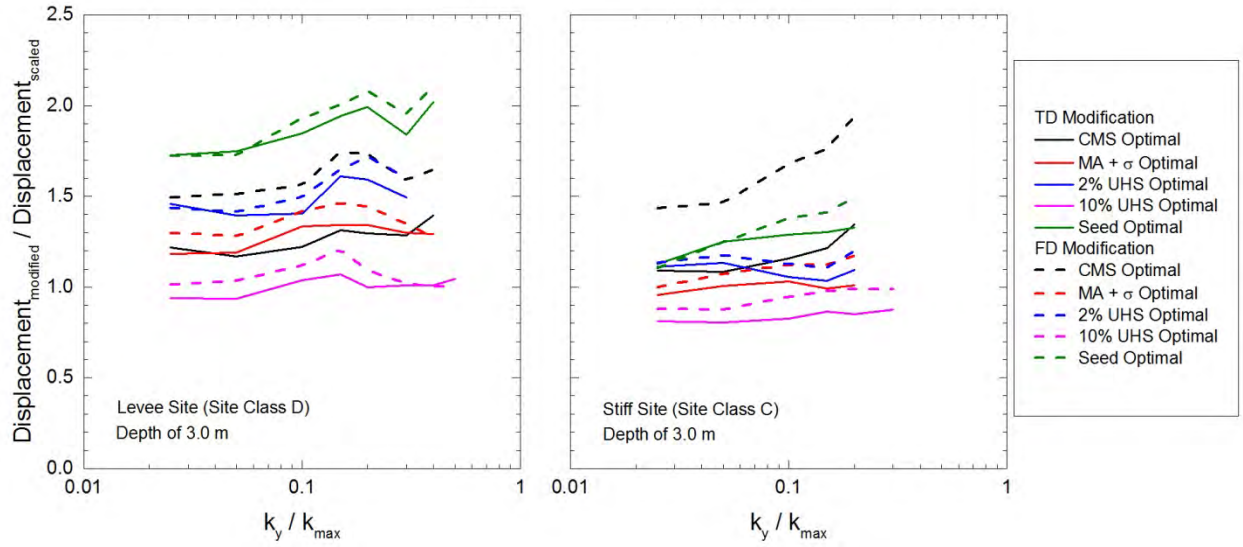

Figure 6.62. Ratios of the modified-to-scaled median Newmark-type displacements caused by the optimally scaled and modified motions from scenario II for a shallow sliding mass at both sites for varying k_y / k_{max} and the different target spectra.

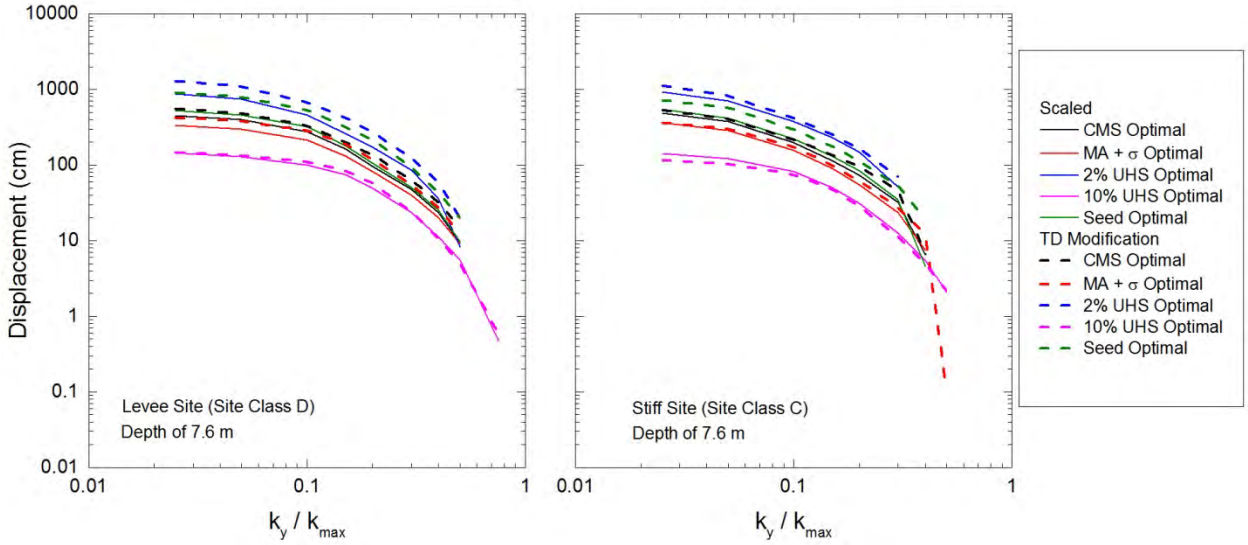

Figure 6.63. Median Newmark-type slope displacements caused by the optimally scaled and TD-modified motions from scenario II for an intermediate sliding mass at both sites for varying k_y / k_{max} and the different target spectra.

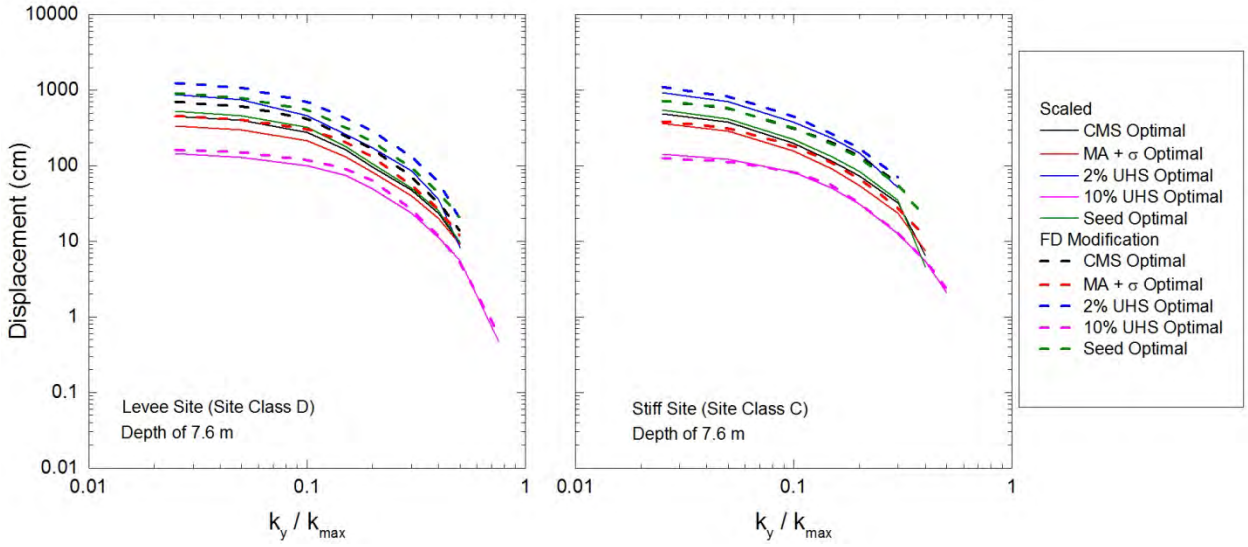

Figure 6.64. Median Newmark-type slope displacements caused by the optimally scaled and FD-modified motions from scenario II for an intermediate sliding mass at both sites for varying k_y / k_{max} and the different target spectra.

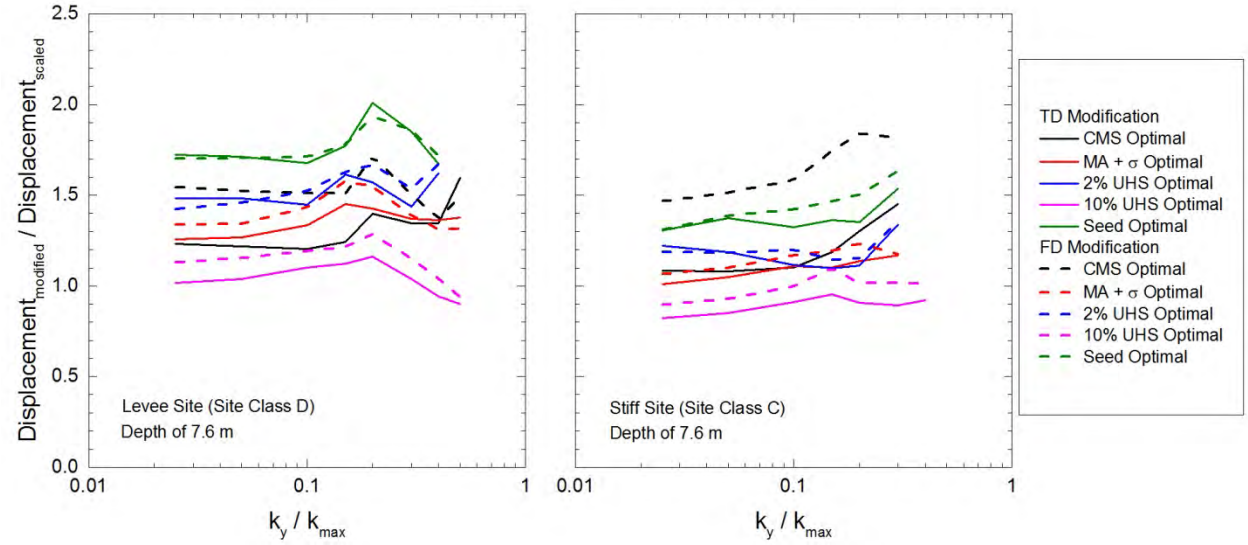

Figure 6.65. Ratios of the modified-to-scaled median Newmark-type displacements caused by the optimally scaled and modified motions from scenario II for an intermediate sliding mass at both sites for varying k_y / k_{max} and the different target spectra.

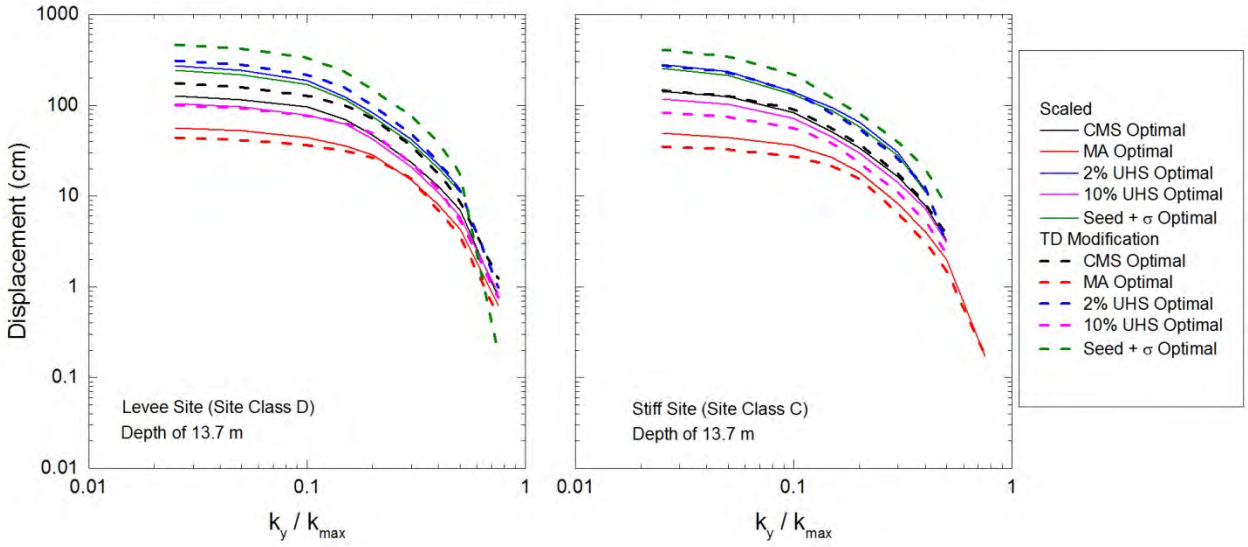

Figure 6.66. Median Newmark-type slope displacements caused by the optimally scaled and TD-modified motions from scenario II for a deep sliding mass at both sites for varying k_y / k_{max} and the different target spectra.

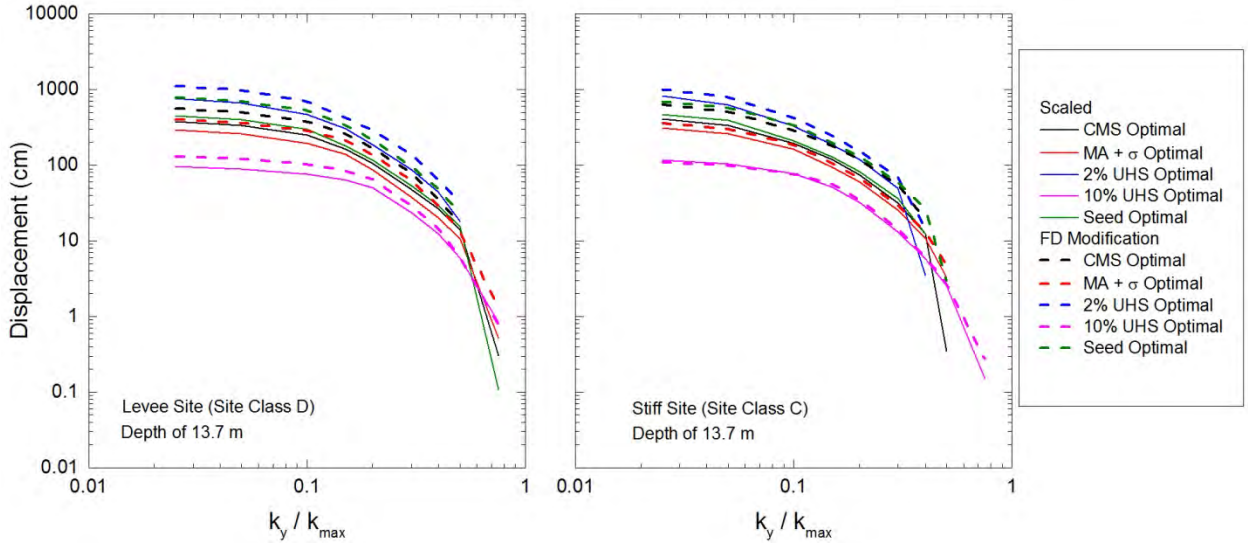

Figure 6.67. Median Newmark-type slope displacements caused by the optimally scaled and FD-modified motions from scenario II for a deep sliding mass at both sites for varying k_y / k_{max} and the different target spectra.

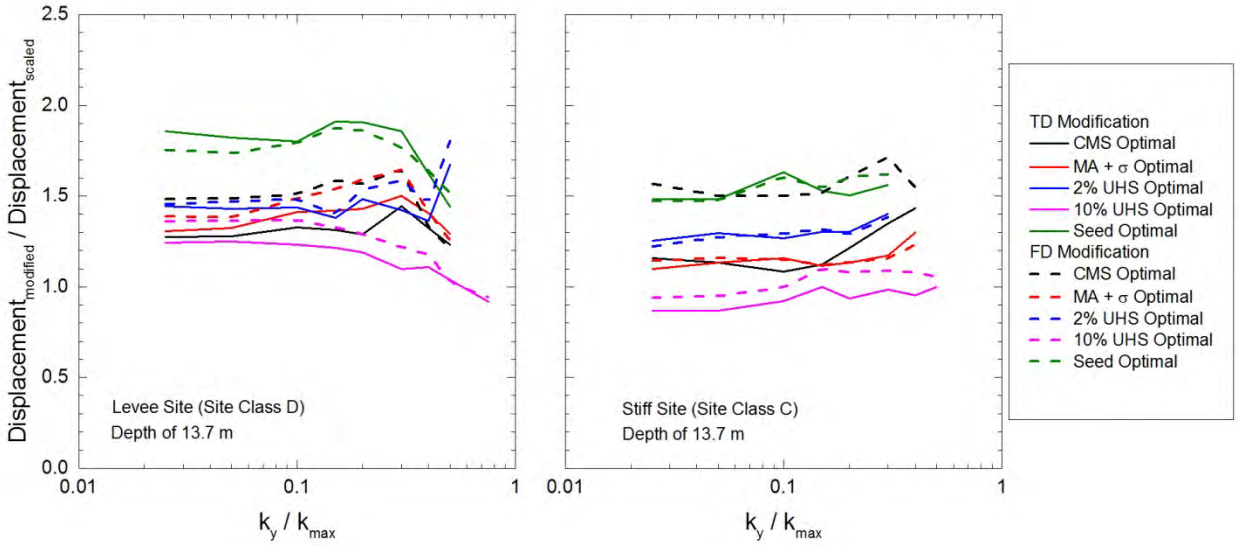

Figure 6.68. Ratios of the modified-to-scaled median Newmark-type displacements caused by the optimally scaled and modified motions from scenario II for a deep sliding mass at both sites for varying k_y / k_{max} and the different target spectra.

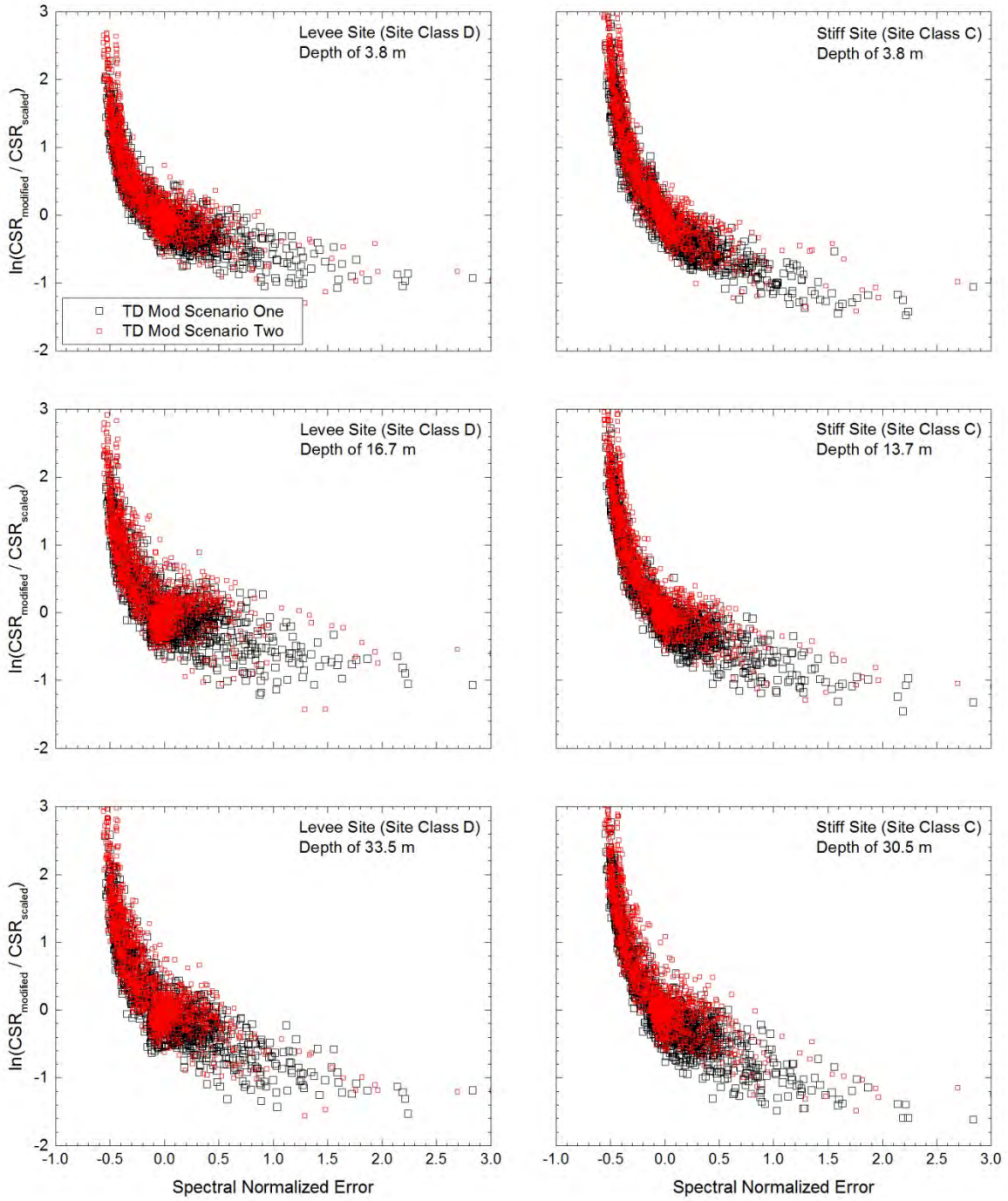

Figure 6.69. Logarithmic ratios of the modified-to-scaled cyclic stress ratios (*CSR*) of the TD-modified motions in scenarios I and II for both sites at all three depths plotted versus spectral mismatch, quantified by NE_s.

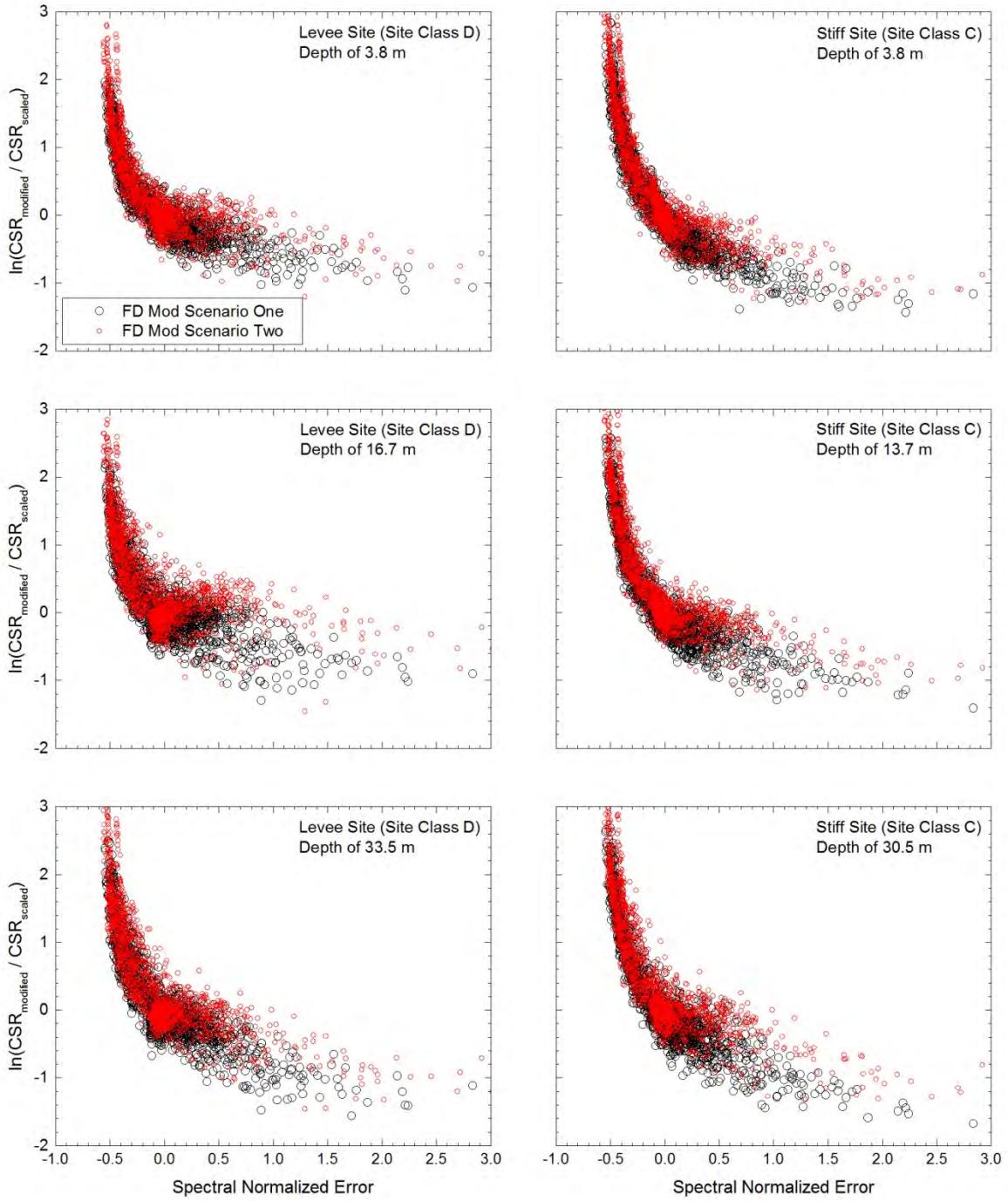

Figure 6.70. Logarithmic ratios of the modified-to-scaled cyclic stress ratios (*CSR*) of the FD-modified motions in scenarios I and II for both sites at all three depths plotted versus spectral mismatch, quantified by NE_s.

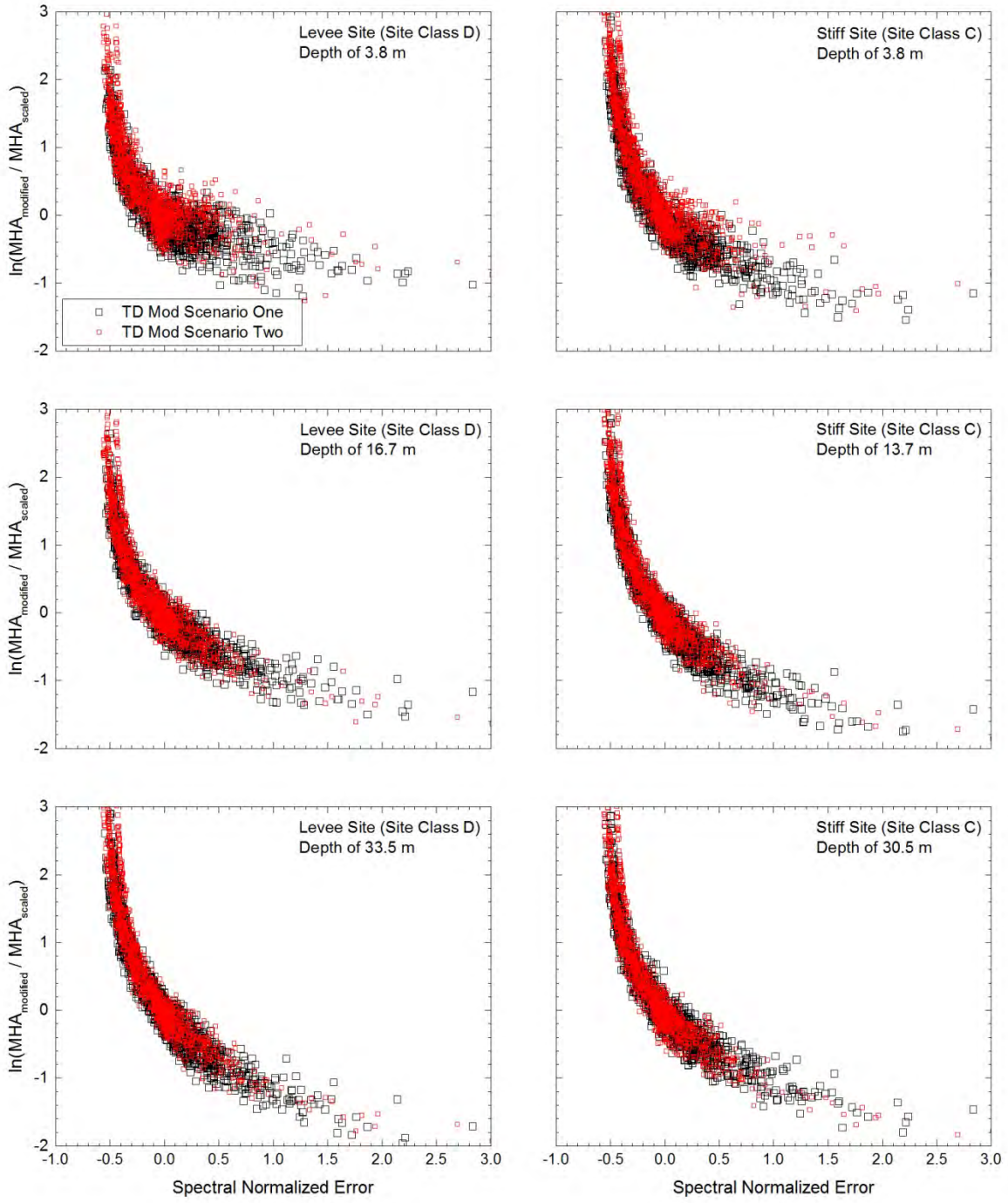

Figure 6.71. Logarithmic modified-to-scaled maximum horizontal acceleration (*MHA*) ratios of the TD-modified motions in scenarios I and II for both sites at all three depths plotted versus spectral mismatch, quantified by NE_s.

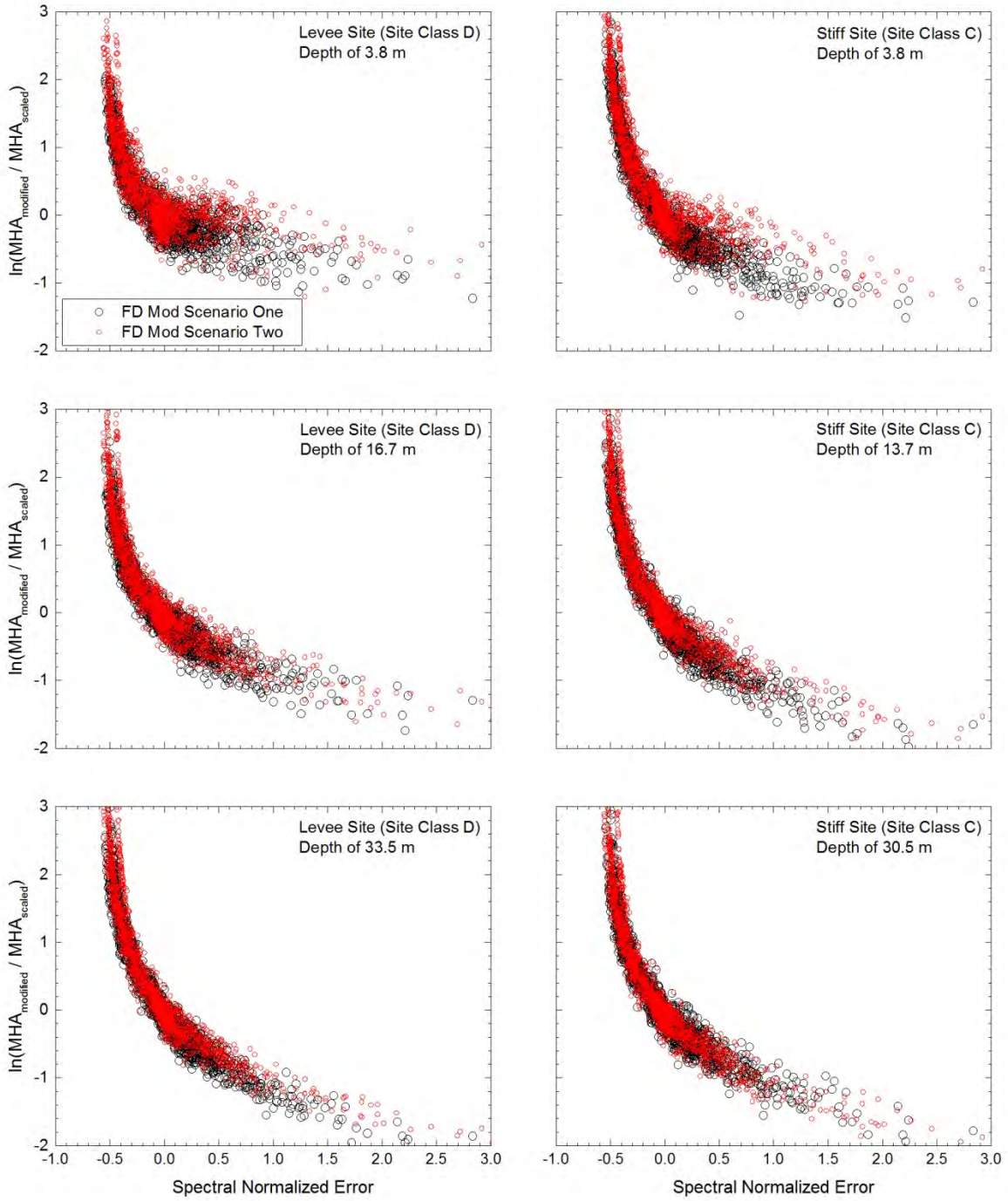

Figure 6.72. Logarithmic modified-to-scaled maximum horizontal acceleration (*MHA*) ratios of the FD-modified motions in scenarios I and II for both sites at all three depths plotted versus spectral mismatch, quantified by NE_s.

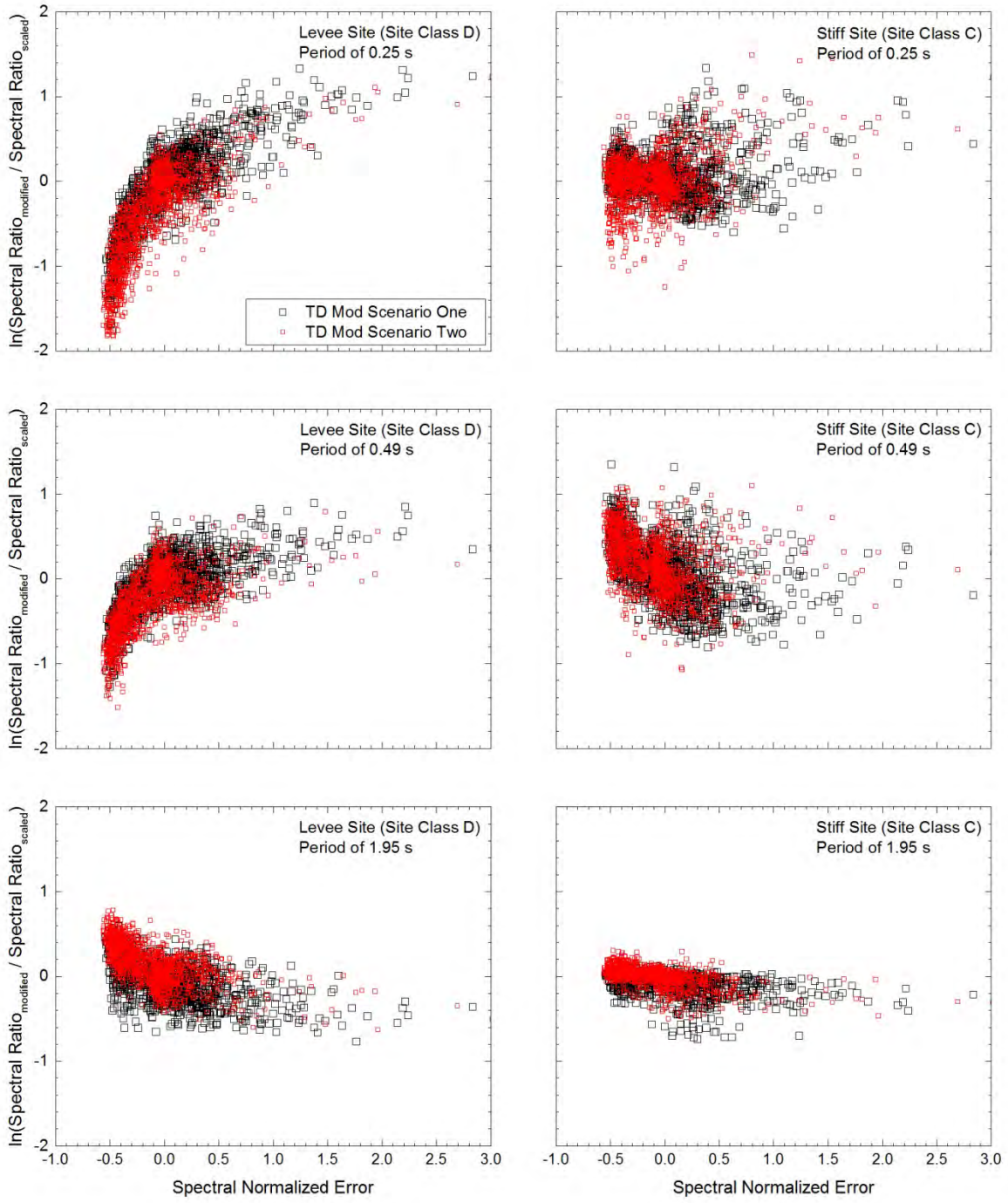

Figure 6.73. Logarithmic ratios of the modified-to-scaled spectral ratios of the TD-modified motions in scenarios I and II for both sites at all three periods plotted versus spectral mismatch, quantified by NE_s.

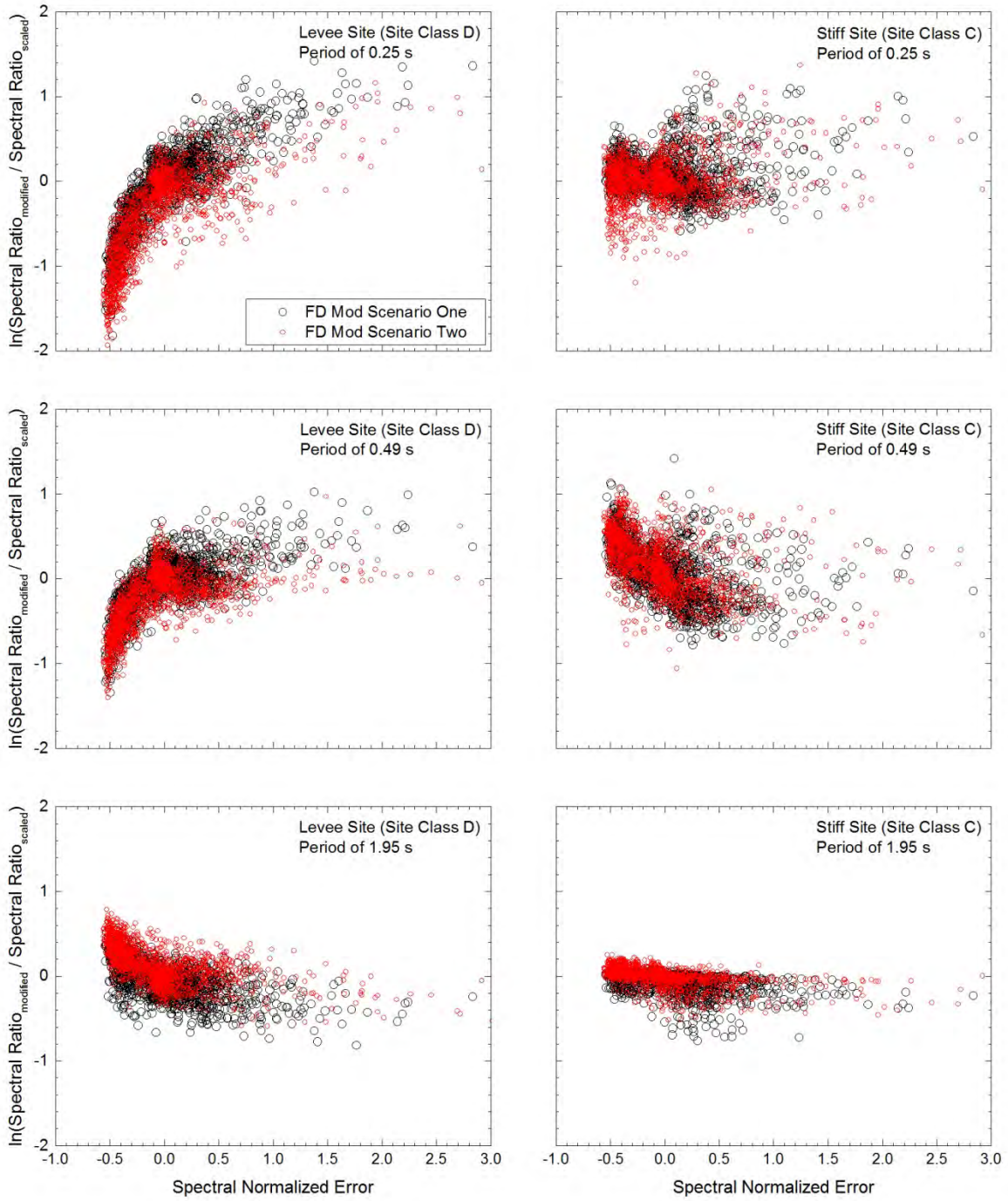

Figure 6.74. Logarithmic ratios of the modified-to-scaled spectral ratios of the FD-modified motions in scenarios I and II for both sites at all three periods plotted versus spectral mismatch, quantified by NE_s.

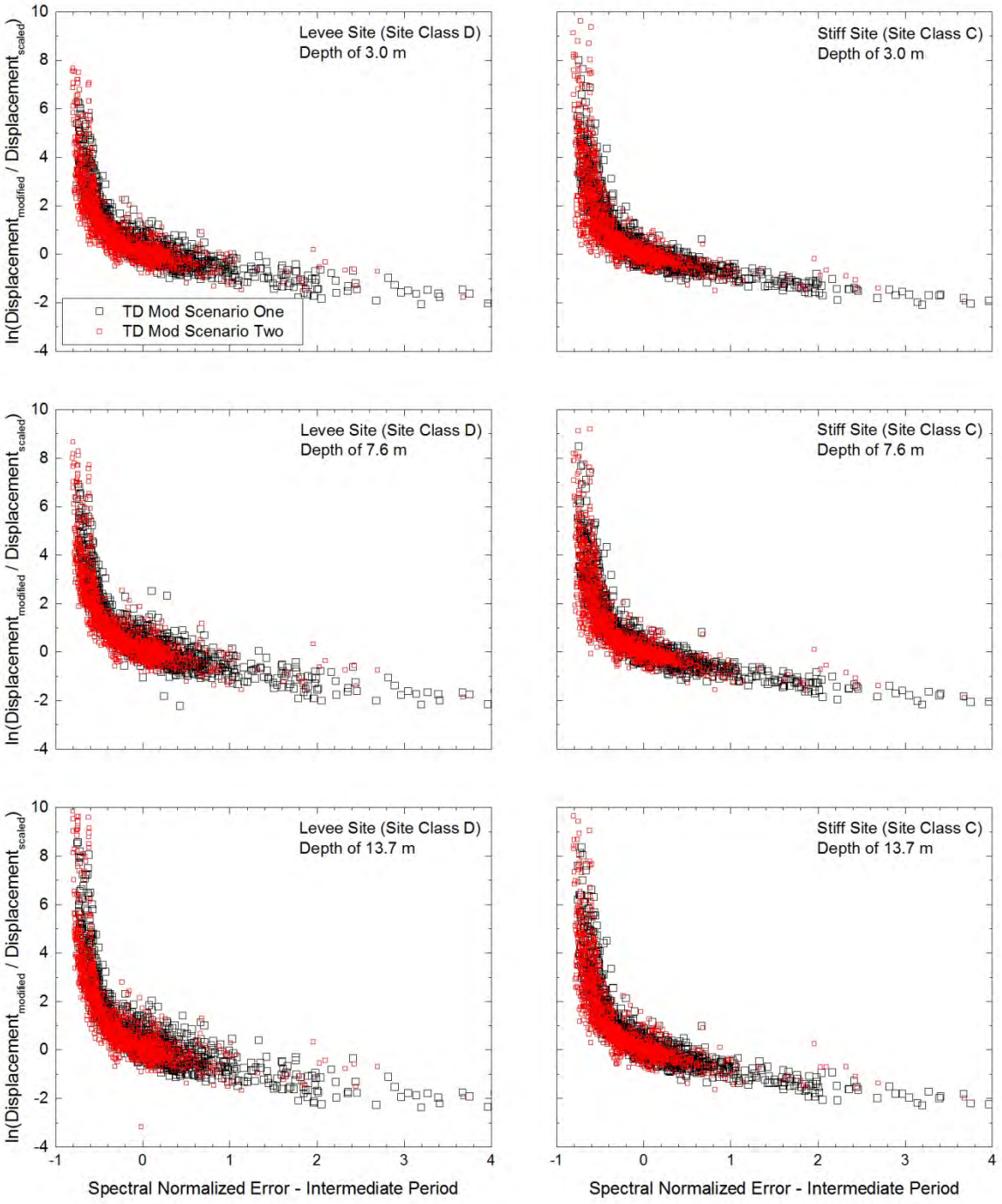

Figure 6.75. Logarithmic modified-to-scaled Newmark-type slope displacement ratios of the TD-modified motions in scenarios I and II for both sites, all three depths, and a k_y / k_{max} value of 0.05 plotted versus spectral mismatch in the intermediate period range, quantified by $NE_{s,IP}$.

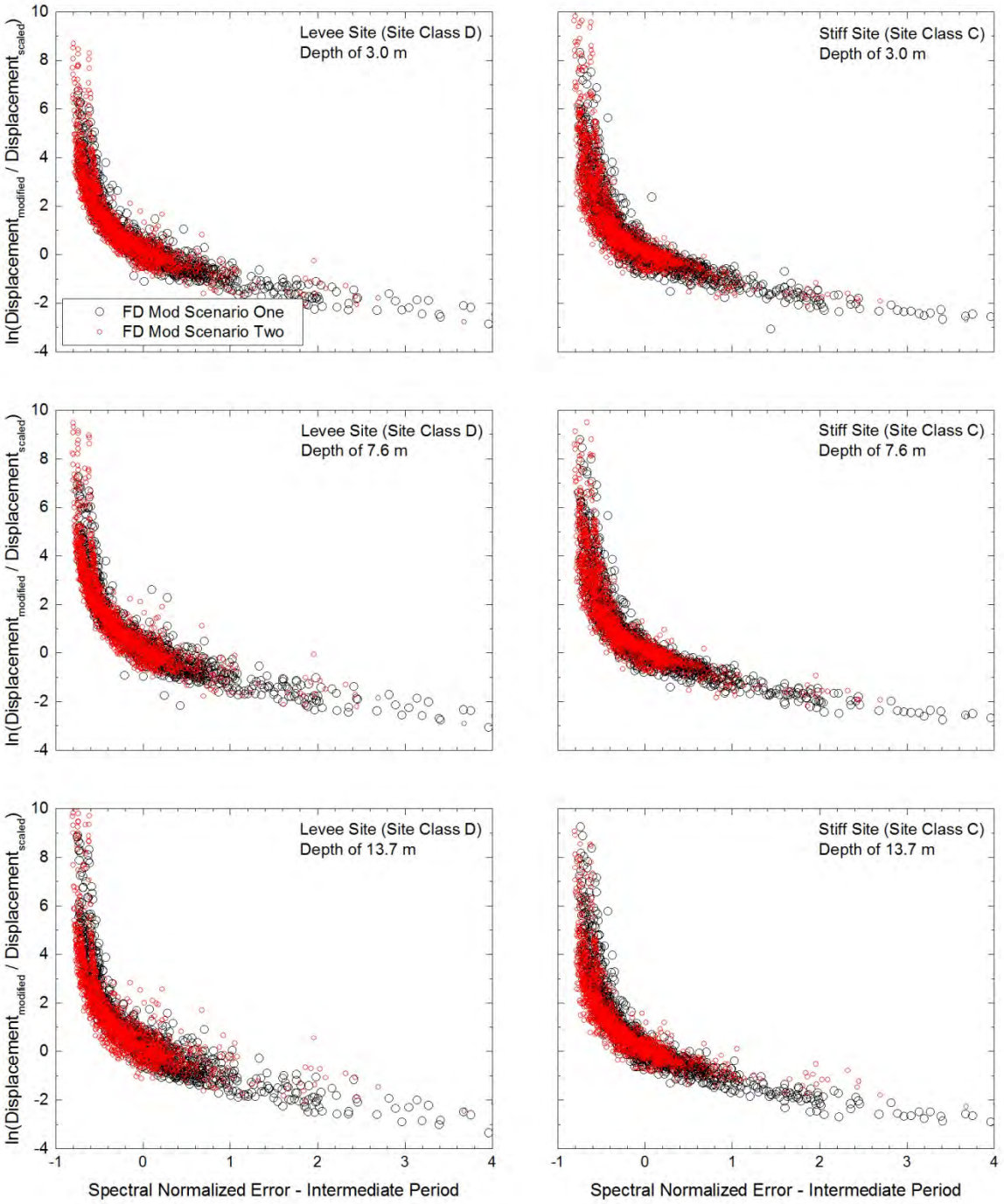

Figure 6.76. Logarithmic modified-to-scaled Newmark-type slope displacement ratios of the FD-modified motions in scenarios I and II for both sites, all three depths, and a k_y / k_{max} value of 0.05 plotted versus spectral mismatch in the intermediate period range, quantified by $NE_{s,IP}$.

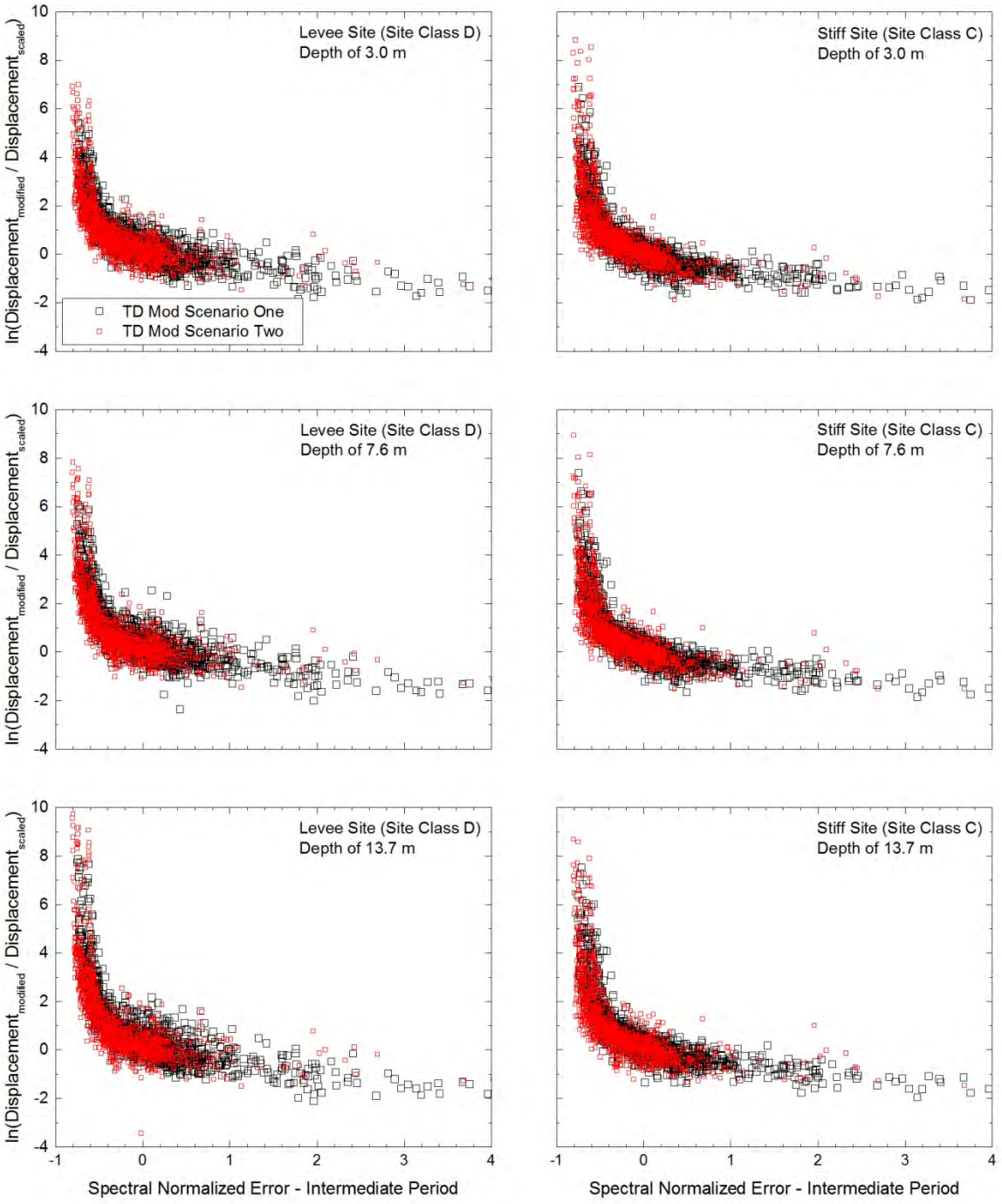

Figure 6.77. Logarithmic modified-to-scaled Newmark-type slope displacement ratios of the TD-modified motions in scenarios I and II for both sites, all three depths, and a k_y / k_{max} value of 0.15 plotted versus spectral mismatch in the intermediate period range, quantified by $NE_{s,IP}$.

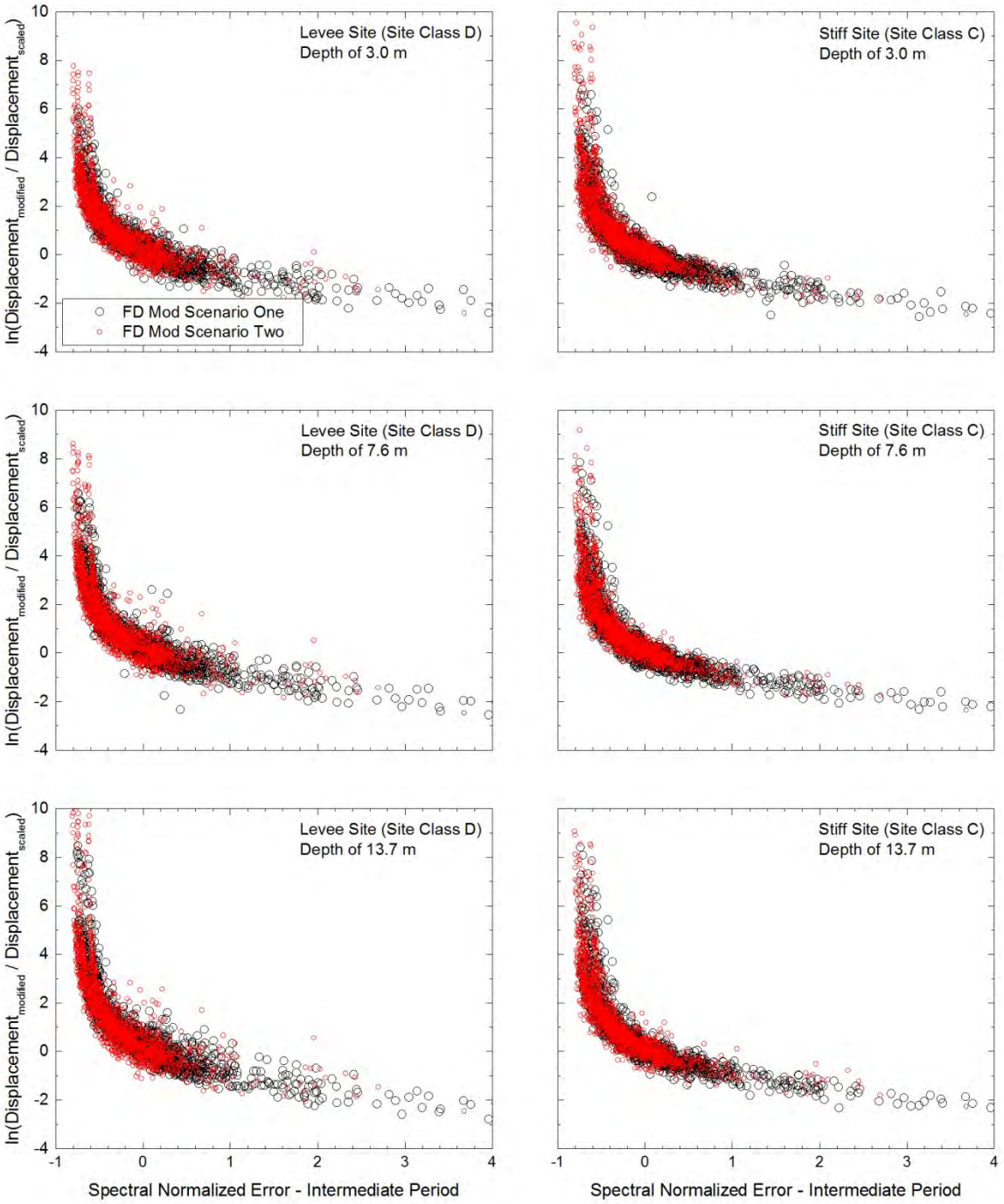

Figure 6.78. Logarithmic modified-to-scaled Newmark-type slope displacement ratios of the FD-modified motions in scenarios I and II for both sites, all three depths, and a k_y / k_{max} value of 0.15 plotted versus spectral mismatch in the intermediate period range, quantified by $NE_{s,IP}$.

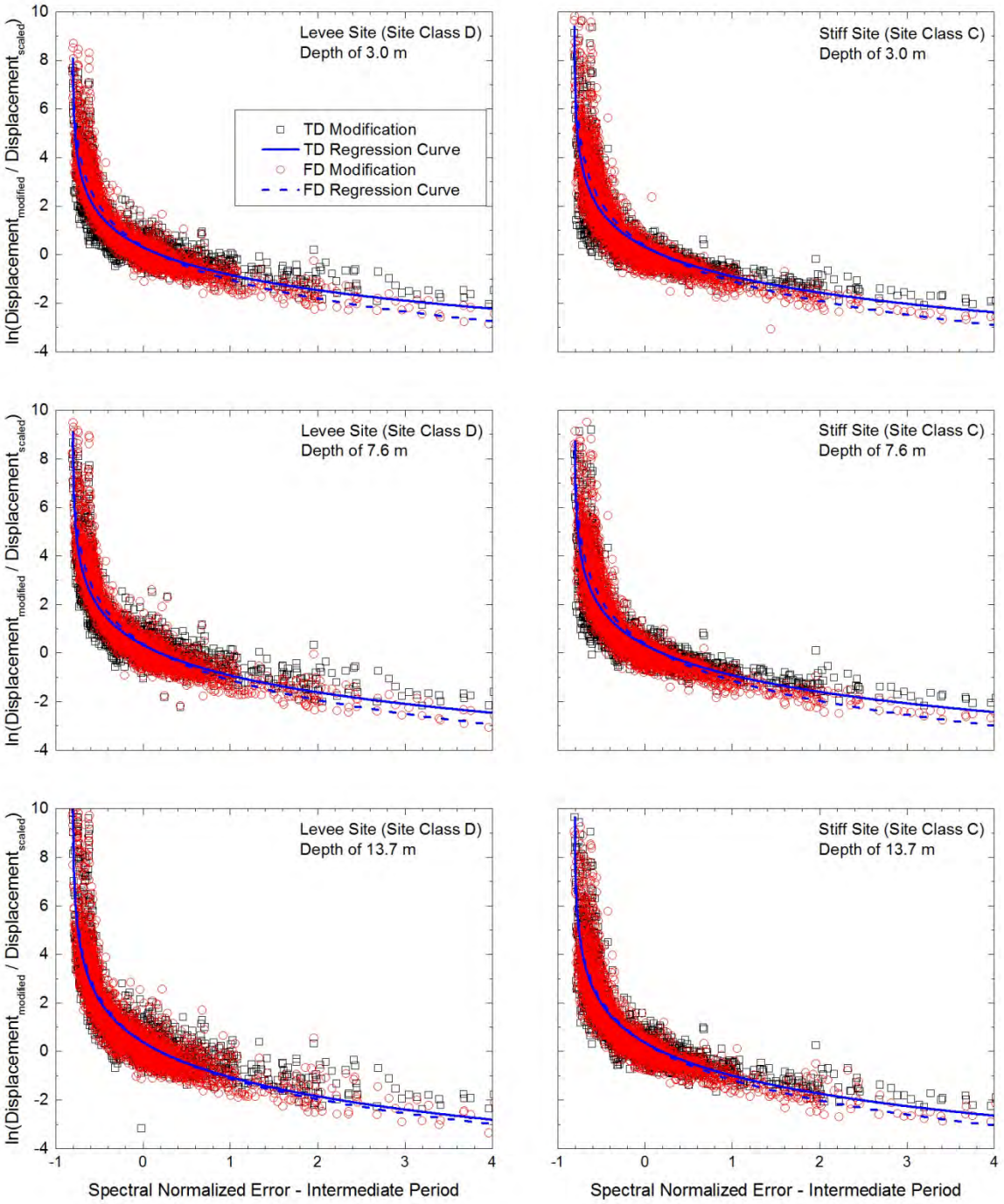

Figure 6.79. Regression curves developed for the relationship between the logarithmic modified-to-scaled Newmark-type displacement ratios and spectral mismatch for both sites at all three depths for a k_y / k_{max} value of 0.05 using the motions from scenarios I and II.

CHAPTER 7
Conclusions

7.1 Summary of Research

The purpose of this study was to systematically examine the effects of time (TD) and frequency domain (FD) modification techniques on the ground motion characteristics and time histories of the seed ground motion and the subsequent response metrics of geotechnical dynamic analyses. Given the relatively unknown impact of ground motion modification on the stationary (e.g., peak ground displacement) and non-stationary (e.g., displacement time history) characteristics of the seed ground motions and the subsequent seismic response analyses, it was important that this study provided a quantitative assessment of the impacts of spectral matching on the characteristics and seismic response.

The first part of this study included the development of a computer program that executed time and frequency domain modification to match suites of scaled ground motions to multiple target spectra.

Ground motion characteristics of scaled and modified motions calculated by the program were used to quantify the impact of modification on the characteristics of the original motions. The ground motion characteristics (e.g., peak ground velocity) were studied for two sets of approximately 100 ground motions selected for two very different earthquake scenarios that were scaled using three different scaling factors and matched to five alternative target spectra. Regression equations were developed for the combined set of motions from these two scenarios relating the mismatch between the response spectrum of the recorded ground motion and the target spectrum (i.e., spectral mismatch) to the modified-to-scaled ground motion characteristics. The modified-to-scaled ground motion characteristics for a set of ground motions from a third scenario were then compared to the developed regression curves to validate the general applicability of the regression equations for all earthquake scenarios.

The effects of ground motion modification on the time histories of the seed ground motions, as quantified by the goodness-of-fit (*GOF*) between the scaled and modified time histories, were then examined. This was achieved by correlating spectral mismatch to *GOF* metrics. Threshold values for *GOF* were established based on a visual examination of the scaled and modified time histories and the relationship between *GOF* and the modified-to-scaled ground motion characteristic ratios.

The effects of modification on the geotechnical seismic response analyses for two different soil profiles were also examined for scenarios I and II. This portion of the study examined whether modification introduced any bias in the responses of geotechnical dynamic analyses relative to the responses produced by the scaled motions. Spectral mismatch was also examined to study its impact on the effects of ground motion modification on the response metrics of geotechnical dynamic analyses.

7.2 Findings and Recommendations

7.2.1 Development of GMM Program

A major outcome of this study is the development of GMM, a computer program that scales and matches a suite of ground motions using both TD and FD modification techniques to multiple target spectra. One-page output summaries are generated by GMM for each ground motion to aid the engineer in selecting the appropriate ground motions and modification technique for a specific scenario. Values for the *GOF* between the scaled and modified time histories are also output by GMM to quantify the effects of modification on the non-stationary characteristics of the ground motions. GMM is not yet ready to be used in engineering practice, but can be made available after incorporating the improvements listed in **Section 3.6**.

7.2.2 Impact of Modification on Ground Motion Characteristics

- Well-defined relationship between the effects of modification on certain ground motion characteristics and spectral mismatch was established: The modified-to-scaled ratios for *PGV*, *PGD*, I_a, and *CAV* appear to be strongly correlated to spectral mismatch, as quantified by normalized error (NE_s), for different ranges of periods. Effects of modification on $D_{5\text{-}95}$ and T_m also appear to be related to NE_s; however, these relationships are not as strong. The

effects of modification on *PGV* and *PGD* correlate well with NE_s over intermediate ($NE_{s,IP}$) and long ($NE_{s,LP}$) periods, respectively ($NE_{s,IP}$ is calculated for 0.5 s $\leq T_i \leq$ 3.0 s and $NE_{s,LP}$ is calculated for 3.0 s$\leq T_i \leq$ 5.0 s). NE_s over the entire range of periods (0.01 s$\leq T_i \leq$ 5.0 s) is strongly correlated with the effects of modification on I_a and *CAV*. These observations were made for thousands of matched ground motions for two very different earthquake scenarios then validated using a third scenario for which the selection criteria were greatly relaxed (note some deviations from developed regression equations were observed in the third scenario for *PGV* and *PGD* for large, negative $NE_{s,IP}$ and $NE_{s,LP}$, respectively). This finding signifies that the effects of modification on the ground motion characteristics can be accurately predicted by spectral mismatch prior to performing modification. The regression equations provided in **Section 4.2.2** are recommended to predict the *PGV*, *PGD*, I_a, and *CAV* of the modified ground motions for NE_s, $NE_{s,IP}$, and $NE_{s,LP}$ between -0.4 and 1.

- TD and FD modification have similar effects on the ground motion characteristics for values of NE_s within ± 0.1 of 0: Overall, the effects of the TD and FD modification techniques on the ground motion characteristics are similar for values of NE_s close to 0. Therefore, depending on the ground motion characteristic and value of NE_s, it may be suitable to use either modification technique. It is also observed that values of NE_s close to 0 generally lead to limited changes in the ground motion characteristics during modification. This finding supports the empirical recommendation that engineers should scale ground motions to minimize the spectral mismatch, quantified by NE_s in this study, and then perform modification. **Table 4.16** provides ranges of NE_s for the different ground motion characteristics and modification techniques for which the impact of modification on the ground motion characteristics is relatively small (i.e., changes of less than 25% in the ground motion characteristics during the modification process).
- Ground motion characteristics of ground motions with negative NE_s are more sensitive to changes in NE_s: The modified-to-scaled ground motion characteristic ratios, for the most part, are more sensitive for motions with negative NE_s. This finding signifies that the characteristics of the modified motion are less likely to be significantly affected when response spectra are decreased (i.e., positive NE_s) to match the target spectrum instead of increased (i.e., negative NE_s). For this reason, it is recommended that ground motions with

positive NE_s are selected and modified to match the target spectrum in an attempt to reduce the impact of modification on the ground motion characteristics.

7.2.3 Impact of Modification on Ground Motion Time Histories

- A strong relationship was established between the *GOF* for the $v(t)$ and $d(t)$ and qualitative rankings assigned to these time histories based on a visual assessment: This contribution allows quantitative threshold *GOF* values to be established that can be used when deciding to accept or reject the modified motions in place of the current practice of accepting or rejecting modified motions based on a visual examination of the time histories. Since motions with positive $NE_{s,LP}$ are affected differently by modification than motions with negative $NE_{s,LP}$, threshold *GOF* values are established separately for motions with positive $NE_{s,LP}$ and motions with negative $NE_{s,LP}$. Based on observations in **Chapter 4**, it is recommended that motions with positive $NE_{s,LP}$ and corresponding threshold *GOF* values are used. For motions with positive $NE_{s,LP}$, acceptable modified motions should have $v(t)$ with *GOF* values, as quantified by $imRMSE_t$, greater than 0.50 and 0.595 for TD and FD modification, respectively, and $d(t)$ with *GOF* values greater than 0.585 and 0.565 for TD and FD modification, respectively.
- A well-defined relationship between the effects of modification on the time histories and the ground motion characteristics was established: The *GOF* between the modified and scaled $a(t)$, *FAS*, $v(t)$, and $d(t)$ are clearly related to the modified-to-scaled ground motion characteristic ratios of the motions. Specifically, *GOF* for $a(t)$ and *FAS* are related to modified-to-scaled *PGA* ratios while $v(t)$ and $d(t)$ are related to modified-to-scaled *PGV* and *PGD* ratios, respectively. Acceptable limits for the change in the characteristics of the modified motion relative to the scaled motion can be set based on the project requirements (e.g., 25% increase in *PGV* modification or modified-to-scaled *PGV* ratio of 1.25). Then, the regression equations developed for the relationships between *GOF* and the modified-to-scaled ground motion characteristic ratios (see **Section 5.2.2.2** and **Table 5.7**), can be used to establish acceptable *GOF* values for the modified motions.

7.2.4 Impact of Modification on the Results of Site Response Analyses

- No significant differences were observed between the median geotechnical seismic responses produced by the TD-modified motions and those produced by the FD-modified motions: Generally, differences between the median γ_{max}, *CSR*, *MHA*, and spectral ratios produced by the TD-modified motions and those produced by the FD-modified motions are less than 10%. Although notable differences are observed between the median Newmark-type displacements produced by the TD- and FD-modified motions for certain target spectra, these differences are likely the result of differences in the I_a for the TD- and FD-modified motions. These observations are made for the optimally scaled ground motions matched to the target spectra, further supporting the recommendation that ground motions should be scaled to reduce spectral mismatch. This finding suggests that either modification technique may be appropriate for performing geotechnical seismic response analyses.
- Impact of modification on the geotechnical seismic responses appears to be influenced by the ground motion characteristics and response spectra of the scaled and modified motions: This finding suggests that inherent mathematical manipulations of the modification techniques are not producing biases, but rather the effects of modification on the ground motion characteristics are leading to observed biases. The differences between the median γ_{max}, *CSR*, and *MHA* produced by the scaled motions and those produced by the modified motions are likely caused by differences between the median *PGA* and I_a of the scaled and modified motions (see **Tables 6.1** and **6.2**) and differences between the median spectra of the scaled motions and the target spectra (see **Figures 6.7** and **6.8**). Median Newmark-type displacements caused by the modified motions are generally larger than the median Newmark-type displacements caused by the scaled motions when the target spectra, to which the modified motions are matched, are larger than the response spectra of the scaled motions for intermediate and long periods. Conversely, the scaled motions caused larger Newmark-type displacements than the modified motions when the response spectra of the scaled motions were larger than the target spectra for intermediate and long periods.
- Well-defined relationships were observed between the effects of modification on the geotechnical seismic responses and spectral mismatch, as quantified by normalized error (NE_s): This observation is generally made for the different seismic response parameters, modification techniques, sites, and sliding masses (or k_y / k_{max} values) investigated. The

effects of TD and FD modification on the seismic responses with respect to spectral mismatch are very similar, further supporting the recommendation that either technique is appropriate for geotechnical seismic response analyses. Based on this study, the impact of the site condition and sliding mass (or k_y / k_{max} value) on the modified-to-scaled seismic response ratio appear to be minor relative to the impact of spectral mismatch. The relationships between the modified-to-scaled geotechnical seismic response ratios and spectral mismatch for scenarios I and II are very similar, which means these trends may generally apply to any earthquake scenario. This observation potentially means that the effect of modification on the geotechnical seismic responses can be predicted using spectral mismatch, quantified by NE_s or $NE_{s,IP}$, prior to performing ground motion modification.

7.3 Recommendations for Future Research

The following items should be studied in future research:

- The effects of only partially matching the target spectrum during modification: In this study, all motions were matched to the target spectrum from 0.01 to 5 seconds. The effects of modification on the ground motion and subsequent dynamic analyses should also be investigated when only a portion of the target spectrum is matched. The results for matching the target spectrum for the entire period range and a smaller period range should be compared to understand if the trends presented in this research are dependent on the range of periods matched. Additionally, the effect of changing the periods used to define the different ranges for spectral mismatch should be studied as part of this investigation.
- Develop comprehensive regression equations for the relationship between the modified-to-scaled seismic response ratios and spectral mismatch: Although regression equations are presented in this research for the relationship between the modified-to-scaled Newmark-type displacement ratios and spectral mismatch, very few depths and sites are considered. Additional sites with different V_{S30}, more depths, and more k_y / k_{max} values must be examined in the future before the developed regression equations can be recommended for use in practice. Multivariate regression equations may be necessary if it is observed that parameters such as depth also affect the modified-to-scaled seismic response ratios in addition to spectral

mismatch. These regression equations can also be extended to other response metrics (e.g., cyclic stress ratio).

- Impact of modification on the results of structural seismic response analyses: Although the effects of modification on the seismic response of structural systems have been studied more extensively (e.g., Heo et al. 2011, Grant and Diaferia 2013, Seifried 2013), no comprehensive study has been performed to understand the effects of FD modification or impact of spectral mismatch on the responses for structural dynamic analyses. A similar methodology to the one used in this study for the site response analyses can be used. This includes: examining the median structural responses produced by the optimally scaled and modified motions, examining the ratio of the modified-to-scaled median responses, and examining the relationship between the modified-to-scaled structural seismic responses and spectral mismatch. The structures initially examined should be simplified in nature (e.g., single degree-of-freedom system elastic, perfectly plastic behavior) in order to isolate the effects of modification.
- Effects of modification on more complex geotechnical and structural systems: Similar studies to the one presented in this research for the geotechnical seismic responses can examine the effects of modification on seismic responses for increasingly complex models for structural (e.g., strength reduction or collapse) and geotechnical systems (e.g., sites susceptible to liquefaction). These studies will provide a better understanding of the effects of ground motion modification on the responses of other realistic systems.
- Improvements to GMM program: As mentioned in **Section 3.6**, there are several improvements that should be made to GMM before it can be made available for use in practice. These improvements include the addition of recommendations from this study, a faster run time, a graphical user interface, and additional error checks.